The Dissertation Committee for Jie Xu certifies that this is the approved version of the following dissertation:

Source-to-sink analysis of the lower Miocene strata in the Gulf of Mexico Basin

Committee:

John W. Snedden, Supervisor

Craig S. Fulthorpe, Co-Supervisor

Daniel F. Stockli

Ronald J. Steel

Wonsuck Kim

Michael D. Blum

Source-to-sink analysis of the lower Miocene strata in the Gulf of Mexico Basin

by

Jie Xu, B.E.; M.E.

Dissertation

Presented to the Faculty of the Graduate School of

The University of Texas at Austin

in Partial Fulfillment

of the Requirements

for the Degree of

Doctor of Philosophy

The University of Texas at Austin

May 2017

Dedication

I dedicate this dissertation to my grandmother, parents and wife, who have always loved me, and provided abundant support for my study and research.

Acknowledgements

I would like to acknowledge my supervisor, Dr. John Snedden, for his patient teaching and sharing so many insights from his entire career with me. John always pushed me to think beyond my current progress, and suggested I make a detailed research plan and stick to it. I want to thank my co-supervisor, Dr. Craig Fulthorpe, who is always there listening to me, supporting me, and providing numerous and generous help. I really enjoyed the daily conversion, research discussion, and field trip with him. I am grateful for the help from Dr. Daniel Stockli, for his help with detrital zircon U-Pb and (U-Th)/He training and great scientific input on research. I would like also thank the insightful suggestions from Drs. Ron Steel, Wonsuck Kim and Mike Blum, which greatly improved my dissertation.

I want to especially thank Dr. William Galloway. Although he is not on my PhD program committee, I benefited so much from his knowledge of the Gulf of Mexico depositional history, sedimentology, and sedimentary source-to-sink system. The conversion with him is always inspiring and enjoyable. I appreciate the help of Patty Ganey-Curry, the project manager of the Gulf Basin Depositional Systems project (GBDS), for making me to feel at home in GBDS, even I am thousand miles away from my country. She is so nice, not only caring for our study and research progress, but also is concerned about our health and future. I am so glad I have the opportunity to work with her for five years.

I would like to thank the GIS expertise of GBDS, Tim Whiteaker and Jon Virdell, for their help with my ArcGIS project. They are also good friends, sharing me their life experiences and food choices in Austin. Thank GBDS graduate students, Jason Sanford, Ann Caroline Bovay, Luciana de la Rocha, Enrique Arce, and Mario A Gutierrez. I enjoy

the working time in room 3.110H. I would like also thank numerous GBDS undergraduate students for their contribution to the GBDS project, which helped my research directly.

Thank you to Hilary Olson for giving me the opportunity to work with her as a Teaching Assistant for two basic Geological classes. I learned a lot from the way she teaches students. It is a very important experience for my future career, as I am going to be a faculty member in the China University of Geosciences and teaching will be an important part of my life.

I owe to my thanks to Philip A. Guerrero, who is the graduate coordinator, for processing my application materials and always answering my questions and helping me deal with numerous forms. I thank Dr. John Lassiter, the chair of my qualify exam, and appreciate his input to my research program.

Thank you to my friends here at the Jackson School. I have enjoyed learning from you.

Lastly but most importantly, thank you my wife Ruohan, for supporting me each day. You light my life at UT and in future.

Source-to-sink analysis of the lower Miocene strata in the Gulf of Mexico Basin

Jie Xu, Ph.D.

The University of Texas at Austin, 2017

Supervisor: John W. Snedden

Co-supervisor: Craig S. Fulthorpe

The sedimentary archive of the Gulf of Mexico Basin provides an opportunity to study sediment routing from continental highlands to basin sinks for a large passive margin system. This dissertation focuses on the source-to-sink analysis of the lower Miocene system, a major siliciclastic unit. Much remains unknown about sediment routing within this system. In this work, detrital zircon U-Pb and (U-Th)/He double dating and channel-belt scaling relationship are used for source-to-sink analysis.

Zircon U-Pb age data from 19 samples across the northern Gulf of Mexico margin indicate that continental-scale sediment sources shift across the northern Gulf of Mexico from highlands in western North America to the Appalachian Mountains and foreland basin in eastern North America during the early Miocene. Sediment associated with the paleo–Rio Bravo, Rio Grande, Brazos, Red, Mississippi, Tombigbee, and Apalachicola rivers can be differentiated, improving definition of sediment transport pathways from upland sources to basin sinks.

Combined U-Pb and (U-Th)/He double dating on single zircon grains documents both crystallization and exhumation histories of source terranes and have the ability to differentiate first-cycle volcanic and plutonic zircons from multi-cycle zircons. Many

Mesozoic zircons yield roughly identical U-Pb and (U-Th)/He ages, indicating that large volumes of sediments were eroded from various Cretaceous-Oligocene volcanic fields in western North America. A large proportion of older Proterozoic zircons, including those from Grenville, Mid-Continent and Yavapai-Mazatzal provinces, yield several phases of exhumation, providing clues for tracing intermediate sediment sources. This work shows that recycled sedimentary strata are important sediment contributors to the Gulf of Mexico Basin.

We also estimate the drainage areas of lower Miocene systems by using scaling relationships, developed in source-to-sink studies, between drainage area and fluvial channel depth. Single-storey channel-belt thicknesses were measured from a well log database in this well-explored basin and used to estimate paleo-drainage areas of five differentiated early Miocene fluvial systems. The predicted drainage areas show good agreement with the paleo-drainage areas reconstructed independently from detrital zircon provenance analyses and continental geomorphic synthesis. Therefore, knowledge of fluvial deposit dimensions provides a first-order estimate of drainage basin area and a plausible assessment of a continental geomorphology.

Table of Contents

List of Tables

List of Figures

Chapter 1: Introduction

1.1 Background

Sediment source-to-sink (S2S) analysis for large passive margin basins involves studying sediment production in mountainous source terranes, transportation through rivers, deposition on the basin margin and, where applicable, delivery to the deep-water basin floor (Fig. 1.1). S2S analyses are important for understanding earth surface processes, landscape development, the carbon cycle, sediment mass partitioning along S2S transects, and the associated driving processes (Allen, 2008a; Sømme et al., 2009a; Bhattacharya et al., 2016; Leithold et al., 2016; Walsh et al., 2016). Most S2S studies focus on modern or Quaternary systems (e.g., Sømme et al., 2009a, 2011; Covault et al., 2010, 2011; Romans et al., 2016), where components of the S2S system are preserved, or on closed or semi-closed basins (Allen, 2008b), where sediment loss is minimal during the transit from source to sink.

Application to ancient passive margin basins is challenging because onshore components of the S2S system, such as sediment source terranes and drainage basin area, can be modified by subsequent tectonism and erosional processes. In addition, the limited amount of drilling and seismic data commonly available for analysis of deep basinal settings hinders detailed measurement of sediment mass partitioning in the basinal sink. As a result, few studies have applied the S2S concept to deep-time stratigraphic records (e.g., Bhattacharya and Tye, 2004; Sømme et al., 2009b, 2013; Bentley et al., 2016; Bhattacharya et al., 2016).

Although the Gulf of Mexico Basin is probably one of world's most important hydrocarbon basins and has undergone decades of drilling, knowledge of sediment routing from continental highland to basin margin remains limited. The Lower Miocene unit (LM;

23 - 15Ma), in particular, has been less well studied than both the overlying Middle Miocene and underlying Oligocene. It is marked by high rates of sediment supply and continental margin outbuilding that followed the Anahuac transgression (Fig. 1.2). The interval is capped by the major transgressive Amphistegina shale (Galloway et al., 1986). The lower Miocene can be further divided into two subunits, lower Miocene 1 (LM1) and lower Miocene 2 (LM2), separated by a transgression at about 18 Ma that is continuously developed in the northwest Gulf of Mexico.

The lower Miocene unit was deposited during a transitional period of tectonic reorganization and climatic change in North America. Paleogeography changed dramatically as a result of major tectonic reorganization during the middle Cenozoic (Galloway et al. 2011). The late Eocene to Oligocene was characterized by widespread volcanism in the southwestern United States and deposition of voluminous amounts of volcanic ash on the Gulf of Mexico coastal plain (Galloway, 1977, 1981; Galloway et al., 2011). The mid-Cenozoic volcanism waned in the early Miocene, but mantle upwelling and dynamic surface uplift continued to induce deep erosion in the late Oligocene–early Miocene on the southern Great Plains, the southern Colorado Plateau, part of northeastern Mexico, and in central-western Texas (Cather, 2011; Cather et al., 2012). Simultaneously, the Rio Grande Rift created N-S–trending fault blocks and extensional basins in the late Oligocene that both trapped sediment and played an important role in reshaping topography, drainage basin configuration, and sediment routing in the southwest United States (e.g., Chapin and Cather, 1994; Galloway et al., 2011). As a result, the pre-established Eocene paleodrainage system in the southwestern United States was profoundly reorganized during the late Oligocene–early Miocene (Cather et al., 2008, 2012). The middle–late Miocene was dominated by Basin and Range extension in the western United States and northern Mexico (e.g., Stewart, 1998). Hence, the early Miocene

was a critical transitional period that involved changes in regional tectonics, paleogeography and paleodrainage across the North American Cordillera. Arid climatic conditions were prevalent in the western United States (Cather et al., 2008; Chapin, 2008; Fan et al., 2014) and extended to the northwestern Gulf of Mexico (Galloway et al., 1982). Locally, the Llano uplift and Edwards Plateau were uplifted and began to contribute sediment to the Gulf of Mexico. Given these profound changes, there is a critical need to understand influence of these evolving tectonic, paleogeographic, and climatic conditions in the continental interior and sediment routing from hinterlands to basinal sinks.

In addition, the voluminous lower Miocene sediments deposited in coastal plain, shorezone, deltaic and, in particular, submarine fan environments constitute a major hydrocarbon producing unit in the Gulf of Mexico. However, much of the lower Miocene deep-water sediment lies beneath the salt canopy and is difficult to correlate to onshore counterparts. The widespread salt canopy (Fig. 1.3) significantly reduces seismic data quality, making it difficult to map sediments located beneath the canopy. The high costs of deep-water drilling, as well as of wide azimuth (WAZ) and full azimuth (FAZ) seismic data necessary to image beneath the salt, make it challenging to map the distribution of sediment at basin scale. Therefore, other approaches are needed to build regional and basin-scale relationships between morphological elements and sedimentological parameters in order to improve prediction of sediment distribution within the deep-water Gulf of Mexico sink. In this work we apply U-Pb and (U-Th)/He dating together with scaling relationships to understand the lower Miocene S2S system of the northern Gulf of Mexico.

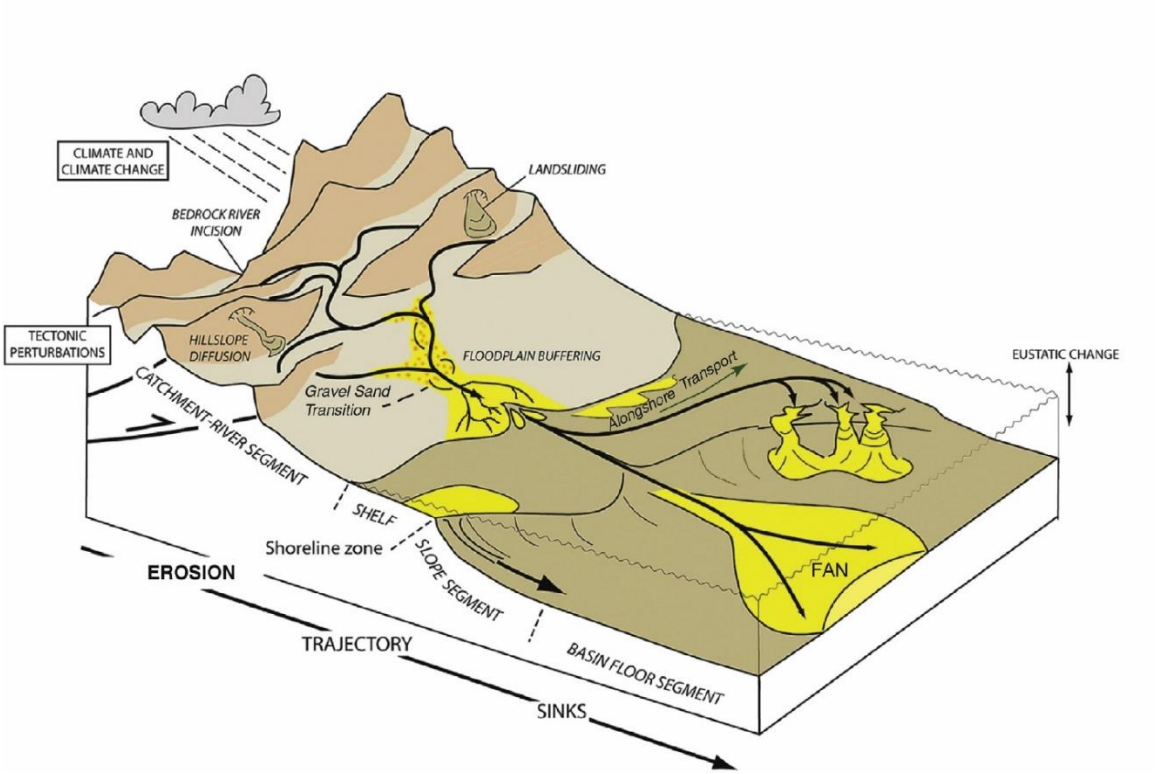

Figure 1.1: Simplified source-to-sink components and processes.

The figure is adapted from Bhattacharya et al. (2016).

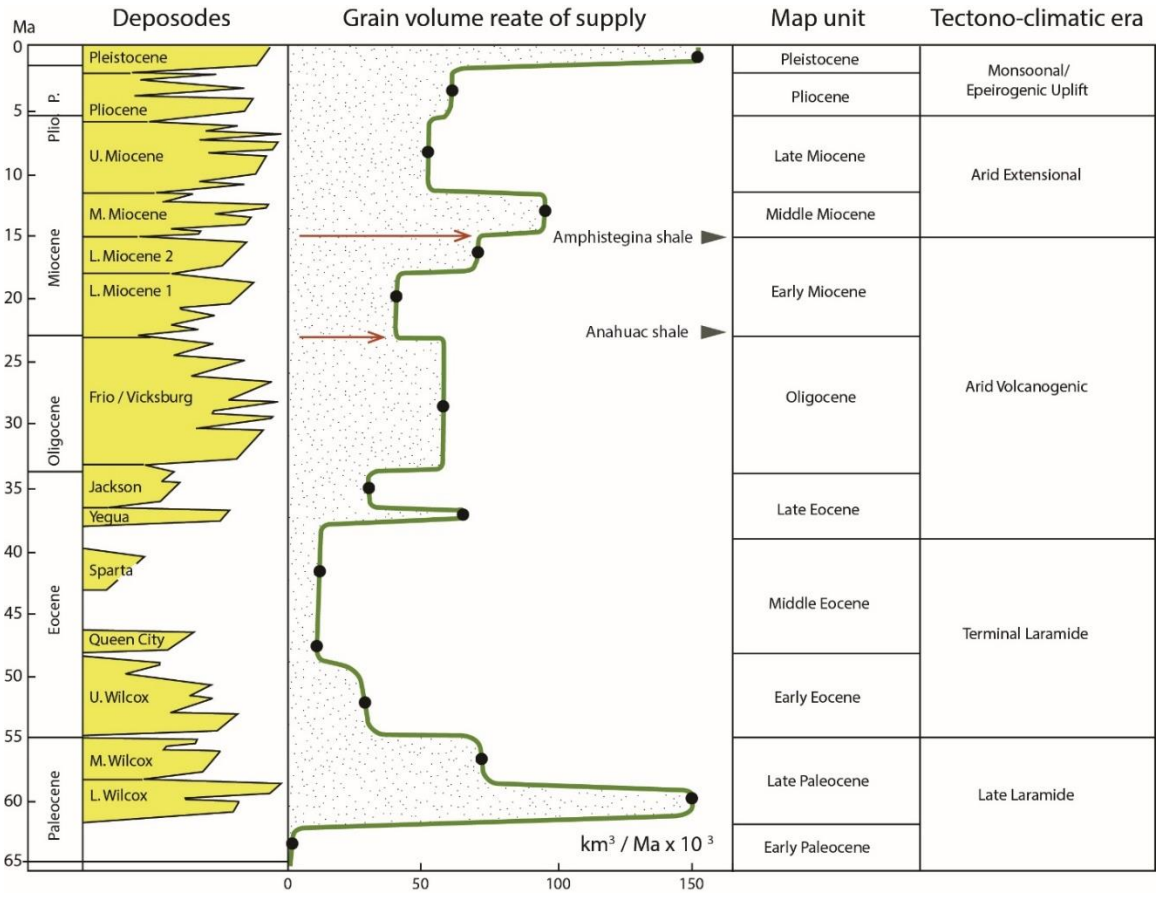

Figure 1.2: Chronology of Cenozoic depositional episodes.

Chronology of Cenozoic depositional episodes (deposodes) showing changing grain volume of sediment supply rate through time. Sediment input rates increase during the lower Miocene (arrows) toward the middle Miocene peak. Modified from Galloway et al. (2011).

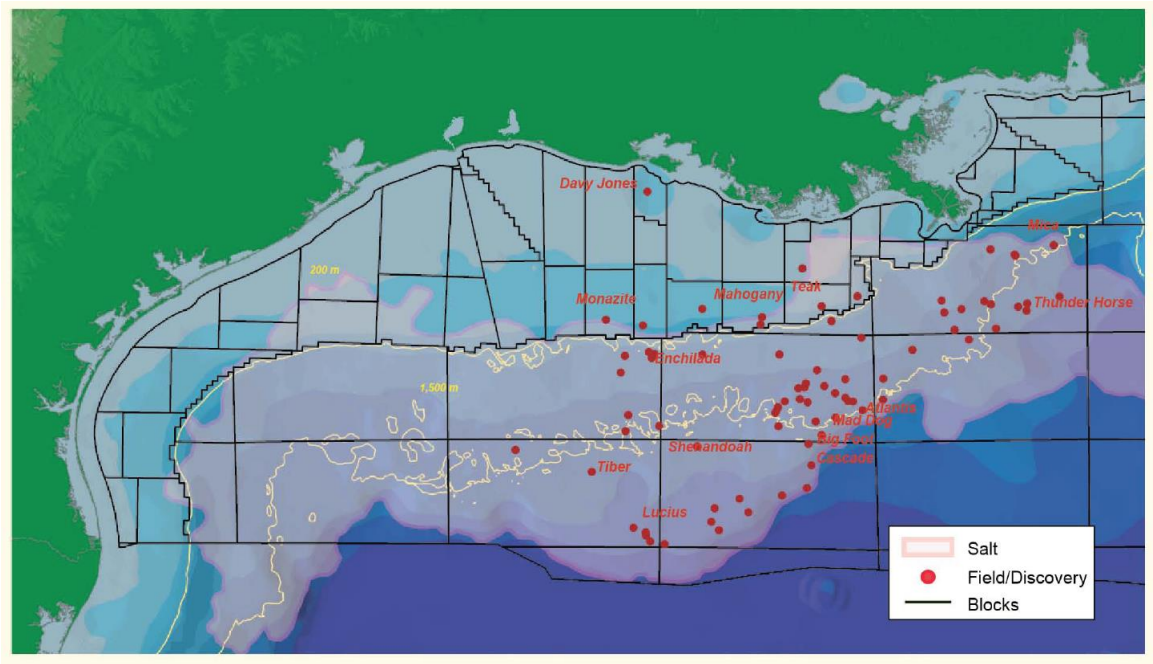

Figure 1.3: Location of sub-salt hydrocarbon fields and discoveries.

Location of sub-salt hydrocarbon fields and discoveries, offshore US Gulf of Mexico. From Arbouille et al. (2013).

1.2 Research Objective and Scope

The objective of this study is to understand the entire S2S system of the lower Miocene interval in the Gulf of Mexico Basin. Because the early Miocene upstream drainage basins have been modified by subsequently tectonism and erosion and the deep-marine fans are beneath the salt canopy, this dissertation focuses on extracting provenance information and paleo-river dimensions from sedimentary strata in the basin margin to reconstruct the S2S system. The sedimentary strata that archived in basinal margin are highly influenced by tectonic and climatic changes in source terranes and by drainage basin evolution and therefore preserve a record of sediment flux from hinterland to ocean that can be used for S2S analyses (Allen, 2008a; Covault et al., 2010; Romans et al., 2016).

This dissertation contains three chapters (1–3) written as stand-alone manuscripts submitted for publication in peer-reviewed journals. Chapter 2 presents 2192 new detrital zircon U-Pb analyses from 19 lower Miocene samples spanning the entire northern Gulf of Mexico margin and which are used to elucidate early Miocene sediment provenance and paleodrainage systems. This work documents continental-scale drainage basin and provenance changes from western to eastern North America. This chapter was submitted to the Geological Society of America Bulletin and published online on August 2016.

Chapter 3 employs combined U-Pb and (U-Th)/He dating on individual zircon grains from lower Miocene strata to reveal both crystallization and cooling histories of source terranes. This work demonstrates the ability to differentiate volcanic, plutonic, and multi-cycled zircon sources, which allows much greater understanding of the complex sediment-source evolution for large passive margin basins such as the Gulf of Mexico Basin. This chapter will be submitted to Earth and Planetary Science Letters in October 2016.

Chapter 4 explores the potential of using ancient channel-belt dimensions measured from geophysical well logs to predict paleo drainage basin area. Data from modern and Quaternary fluvial systems suggest a strong correlation between channel depth and both drainage basin area and water discharge rate. As a data-rich basin having well-preserved fluvial coastal plain deposits along its northern margin, the Gulf of Mexico provides an opportunity to test such scaling relationships using large, reconstructed lower Miocene fluvial systems. The drainage basin analysis using detrital zircon U-Pb data (Chapter 2; Xu et al., 2017) was used as an independent test for the reliability of the prediction. Chapter 4 was submitted to Geosphere and accepted pending minor revision in August 2016.

Chapter 2: Early Miocene continental-scale sediment supply to the Gulf of Mexico Basin based on detrital zircon analysis[1]

ABSTRACT

The early Miocene was a period of major continental margin progradation in the Gulf of Mexico Basin that accompanied prominent tectonic and climatic changes in North America. However, sediment pathways from continental upland sources to deep basinal sinks remain poorly constrained. This study presents 2192 new detrital zircon U-Pb analyses from 19 Lower Miocene samples spanning the entire northern Gulf of Mexico margin to elucidate early Miocene sediment provenance and paleodrainage systems. The U-Pb age patterns indicate that the Great Plains, southern Rocky Mountains, and mid-Cenozoic volcanic field were the major source terranes for the western-central Gulf of Mexico coast, whereas the Appalachian foreland basin and Appalachian Mountains mainly contributed sediment to the eastern Gulf of Mexico coast. Local source terranes included the Llano uplift and Edwards Plateau in central Texas and the Ouachita Mountains and foreland basin in Oklahoma and Arkansas. A comparison to previous detrital zircon studies around the Gulf of Mexico indicates that sediment recycling was important during the early Miocene.

Sediment associated with major paleorivers, including the Rio Bravo, Rio Grande, Houston-Brazos, Red, Mississippi, Tombigbee, and Apalachicola Rivers, can be differentiated using the detrital zircon U-Pb analyses. These data help to better define the early Miocene source-to-sink system in the northern Gulf of Mexico, by relating the basin fill to hinterland tectonic and geological evolution. In comparison to the Paleocene–Eocene

[1]This chapter was published. Xu, J., Snedden, J.W., Stockli, D.F., Fulthorpe, C.S., and Galloway, W.E., 2016, Early Miocene continental-scale sediment supply to the Gulf of Mexico Basin based on detrital zircon analysis: Geological Society of America Bulletin, v. 129; no. 1/2; p. 3–22. Jie Xu is the main author conducting the majority of the research, writing and drawing figures.

Wilcox drainage system, the early Miocene drainage system of the northern Gulf of Mexico was smaller and received less input from western Mexico arc terranes and Archean basement in Wyoming. This drainage area reduction, related to regional thermal uplift and Basin and Range–Rio Grande rifting, likely explains the reduced sediment volume of the Lower Miocene strata in the Gulf of Mexico relative to the Paleocene–Eocene Wilcox Group.

2.1 INTRODUCTION

Early Miocene (ca. 15–23 Ma) sediment input to the Gulf of Mexico, derived from erosion of North American interior highlands, formed deep-water reservoirs. Many studies have investigated sediment accumulation and depositional facies in this terminal basin sink (Galloway et al., 2000; Zeng and Hentz, 2004; Galloway, 2008; Loucks et al., 2011). However, few provenance analyses have been performed on the Lower Miocene strata of the Gulf of Mexico, and there is much to be learned about the linkage between the deep-water sedimentary record and the evolution of the sediment source terranes.

Previous provenance studies of the Lower Miocene strata in the Gulf of Mexico were largely carried out using petrographic methods applied to sandstones (McBride et al., 1988; Dutton et al., 2012). Resulting ternary diagrams of sandstone components (QFL, QmFLt) allow for discrimination among arc, low-grade metamorphic, high-grade metamorphic, and sedimentary sources (e.g., Dickinson and Suczek, 1979). However, subsurface diagenetic alteration of detrital feldspars and heavy minerals affects such provenance interpretations (Milliken, 1988, 2007). Furthermore, enhanced weathering and attrition under relatively humid conditions as well as limited resolution power can prevent standard sandstone petrography from illuminating complex source terrane histories (Mackey et al., 2012).

By contrast, the mineral zircon is highly resistant to both chemical and physical weathering and is ubiquitous in sandstones. Detrital zircon grains are therefore ideal for providing provenance information by relating zircon crystallization age to potential source terranes (e.g., Carrapa, 2010; Gehrels, 2014). The detrital zircon U-Pb analytical method has been proven to be a useful tool for provenance and paleodrainage analysis (e.g., Dickinson and Gehrels, 2003, 2008; Lawton et al., 2009; Dickinson et al., 2009, 2010; Saylor et al., 2012; Benyon et al., 2014; Blum and Pecha, 2014).

Previous detrital zircon work on the Cretaceous Cenomanian and Paleocene–Eocene Wilcox Group strata in the northern Gulf of Mexico indicated that a continental-scale drainage reorganization occurred in the Mid-Cretaceous in response to the tectonic formation of the western U.S. Cordillera. This reorganization changed the pre-established westward sediment routing (from the Appalachians to the western United States) to the southward sediment delivery pattern that persists today (Blum and Pecha, 2014). Mackey et al. (2012) documented a sediment source contribution from the western Mexico arc terranes by examining detrital zircon age spectra on the Paleocene–Eocene Wilcox Group strata in south Texas. Craddock and Kylander-Clark (2013) suggested that the majority of sediment supply to the Cenozoic Mississippi River Delta in Louisiana originated from the Sevier-Laramide region of the western United States.

However, the routing of Lower Miocene siliciclastic sediment from hinterland source to basinal Gulf of Mexico sink has received little attention, and there have been no systematic detrital zircon analyses on these important strata at a regional basin scale, despite major tectonic reorganization occurring in the late Oligocene–early Miocene. The late Eocene to Oligocene was characterized by widespread volcanism in the southwestern United States and deposition of voluminous amounts of volcanic ash on the Gulf of Mexico coastal plain (Galloway, 1977, 1981; Galloway et al., 2011). While the mid-Cenozoic

volcanism waned in the early Miocene, mantle upwelling and dynamic surface uplift continued to induce deep erosion in the late Oligocene–early Miocene on the southern Great Plains, the southern Colorado Plateau, part of northeastern Mexico, and in central-western Texas (Cather, 2011; Cather et al., 2012). Simultaneously, the Rio Grande Rift created N–S–trending fault blocks and extensional basins in the late Oligocene that both trapped sediment and played an important role in reshaping the topography, drainage basin configuration, and sediment routing in the southwest United States (e.g., Chapin and Cather, 1994; Galloway et al., 2011). As a result, the pre-established Eocene paleodrainage system in the southwestern United States was profoundly reorganized during the late Oligocene–early Miocene (Cather et al., 2008, 2012). The middle–late Miocene was dominated by Basin and Range extension in the western United States and northern Mexico (e.g., Stewart, 1998). Hence, the early Miocene was a critical transitional period that involved changes in regional tectonics, paleogeography, and paleodrainage across the North American Cordillera. Arid climatic conditions were prevalent in the western United States (Cather et al., 2008; Chapin, 2008; Fan et al., 2014) and extended to the northwestern Gulf of Mexico (Galloway et al., 1982). Locally, the Llano uplift and Edwards Plateau were uplifted and began to contribute sediment to the Gulf of Mexico. Given these profound changes, there is a critical need for systematic detrital zircon analyses from the Lower Miocene sedimentary strata of the Gulf of Mexico basin in order to understand the influence of these evolving tectonic, paleogeographic, and climatic conditions in the continental interior and the sediment routing from hinterlands to the basinal sinks.

The Gulf of Mexico is one of most important hydrocarbon-producing basins in the world. Sediment eroded from an enormous portion of the continental United States prograded across the continental shelf and was transported into this deep-water sink during the Miocene. However, much of the Lower Miocene deep-water sediment lies beneath the

salt canopy and is difficult to correlate seismically to source areas. Therefore, detrital zircon work on the Lower Miocene rocks of the Gulf of Mexico coastal plain can provide a critical link between paleogeographic evolution in the source area and sediment stored in the basinal sink. This work also provides new insights into the evolution of the regional drainage system of North America from the Paleocene to early Miocene.

This study presents 2192 new detrital zircon U-Pb analyses from 19 sample locations along the northern margin of the Gulf of Mexico with the objective of understanding the complex sediment sources and delivery pathways in the critical Lower Miocene strata (Fig. 2.1). We also integrated these new results with published detrital zircon age spectra from: (1) the Cordillera foreland basin (Dickinson and Gehrels, 2009), (2) Paleocene–Eocene Wilcox Group strata from the Gulf Coast (Mackey et al., 2012; Blum and Pecha, 2014), (3) Upper Cretaceous–Paleogene Difunta strata in Laramide foreland basins in Mexico (Lawton et al., 2009), and (4) Paleozoic strata in the Appalachian foreland basin (Park et al., 2010). Detrital zircon U-Pb age spectra from these various strata and areas are important for understanding pre-Miocene paleogeography and paleodrainage systems and the shifts that occurred during the Miocene. Comparison of detrital zircon age spectra between these published data and our Lower Miocene data allows examination of the influence of tectonism and drainage organization on the evolution of sediment routing to the northern Gulf of Mexico.

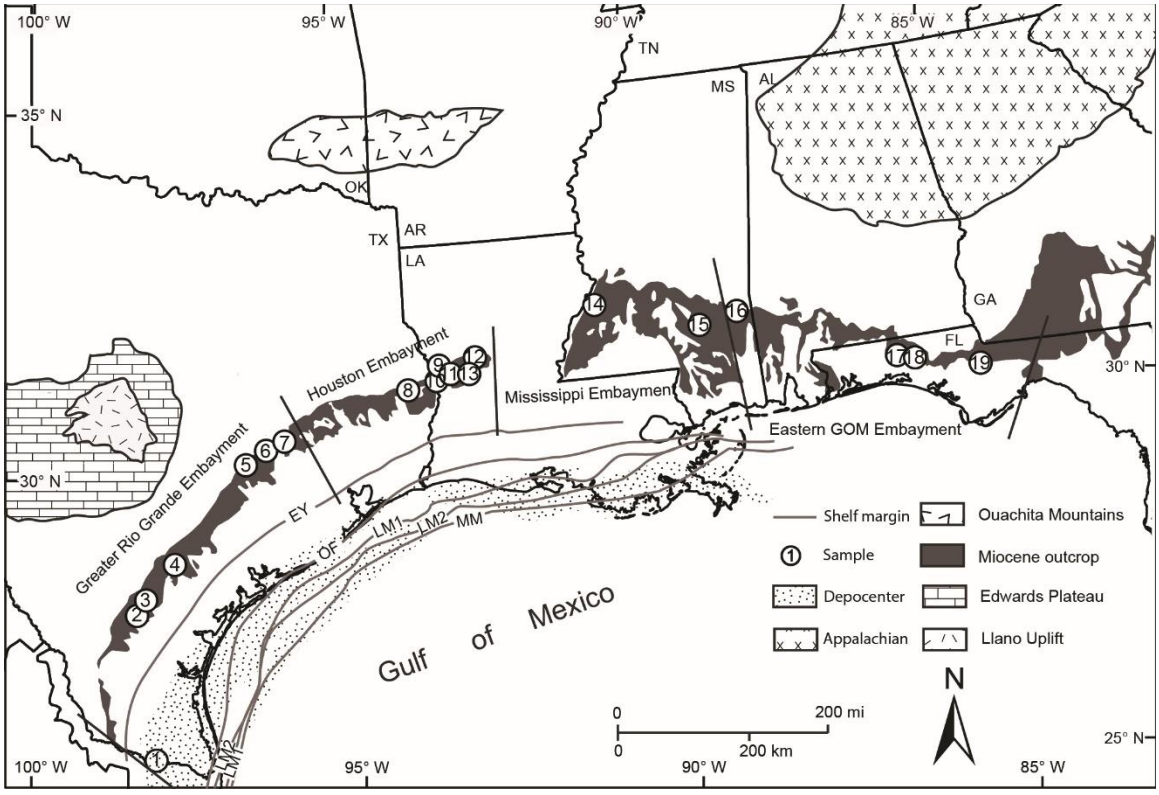

Figure 2.1: Lower Miocene sample location.

Geological map of U.S. Gulf Coast showing Lower Miocene sample locations, Oligocene–Miocene depocenters, and major highlands. Map is adapted from Garrity and Soller (2009). The samples are widely distributed across the northern Gulf of Mexico (GOM) margin. Shelf margins and depocenters are from Galloway (2005). Shelf margin abbreviations: EY—Eocene Yegua; OF—Oligocene Frio; LM1—Lower Miocene 1; LM2—Lower Miocene 2; MM—Middle Miocene. State abbreviations: OK—Oklahoma; TX—Texas; AR—Arkansas; LA—Louisiana; TN—Tennessee; MS—Mississippi; AL—Alabama; FL—Florida; GA—Georgia.

2.2 GEOLOGICAL BACKGROUND

The Gulf of Mexico is a small oceanic basin created by rifting within Pangea (e.g., Pindell, 1985; Stern and Dickinson, 2010; Van Avendonk et al., 2015). The basin was initially filled with thick salt prior to, and during, Late Jurassic seafloor spreading as seawater filled the restricted basin, and then accumulated both carbonate and siliciclastic sediment through the rest of the Mesozoic (Galloway, 2008; Hudec et al., 2013). High sea level during the mid-Late Cretaceous across the Western Interior Seaway limited siliciclastic input to the basin (Galloway, 2008). In contrast, the Cenozoic history of the Gulf of Mexico was marked by a dramatic increase in siliciclastic influx, including episodes of high sediment supply in the Paleocene–Eocene (Wilcox Group), Oligocene (Frio/Vicksburg Group), early Miocene, middle Miocene, and Pleistocene (Galloway, 2008; Galloway et al., 2011; Fig. 2.2).

The Paleogene Wilcox Group was largely fed from the central-southern Rocky Mountains, Cordillera arc terranes, and western Mexico basement terranes (Hutto et al., 2009; Mackey et al., 2012; Blum and Pecha, 2014). Oligocene Frio/Vicksburg Group strata are enriched in volcanic materials, mainly derived from southwestern U.S. and northern Mexico volcanic centers (Winker, 1982; Galloway et al., 2011). Therefore, western U.S. terranes were the dominant sediment sources for the Paleogene strata.

The early Miocene was a transitional period involving tectonic reorganization, climate change, and sediment redistribution in North America. Paleogeography in the western United States changed as a result of major tectonic events during the middle Cenozoic (Galloway et al., 2011). Regional crustal heating, uplift, and volcanism during the Oligocene were followed by Basin and Range extension in the middle Miocene (Stewart, 1998; Mack, 2004; Cather et al., 2012), leading to changes in sediment source provinces in western North America. Simultaneously, arid weather conditions extended to

the northwest Gulf of Mexico margin, whereas a warm and humid climate began to characterize the eastern Gulf of Mexico coastal plain and Appalachian uplands (Galloway et al., 2011).

Lower Miocene strata in the northern Gulf of Mexico are marked by continental margin progradation that followed the Anahuac transgression (Fig. 2.2). These strata are capped by the major transgressive Amphistegina Shale. The Lower Miocene strata can be divided into two subunits, Lower Miocene 1 (LM1) and Lower Miocene 2 (LM2), separated by a transgressive shale dated at ca. 18 Ma that is continuously developed in the northwestern Gulf of Mexico (Galloway et al., 1986).

At the beginning of the early Miocene, sediment supply rate decreased relative to the underlying Oligocene Frio/Vicksburg strata (Fig. 2.2). However, by the late early Miocene, the rate of sediment supply began to increase in response to an increasing contribution from the Appalachians (Galloway, 2008; Galloway et al., 2011). During the middle Miocene, this eastern contribution peaked as rejuvenation of the Appalachians and consequent rapid erosion caused thick sediment accumulations to be deposited in both the eastern Gulf of Mexico and the western Atlantic (Poag and Sevon, 1989; Boettcher and Milliken, 1994; Galloway et al., 2011; Liu, 2014).

There are few provenance studies of the Lower Miocene sandstones in the Gulf of Mexico (McBride et al., 1988; Dutton et al., 2012). Published provenance work suggests a transition from volcanic-rock-fragment–rich Oligocene strata to more quartz-dominated Lower Miocene sandstone in the central Gulf of Mexico (Dutton et al., 2012). Petrographic analyses of sandstones from offshore Louisiana indicate a provenance similar to sediment carried by the modern Mississippi River, with source terranes from the Rocky Mountain, Appalachian, and Ouachita orogenic belts (McBride et al., 1988; Dutton et al., 2012).

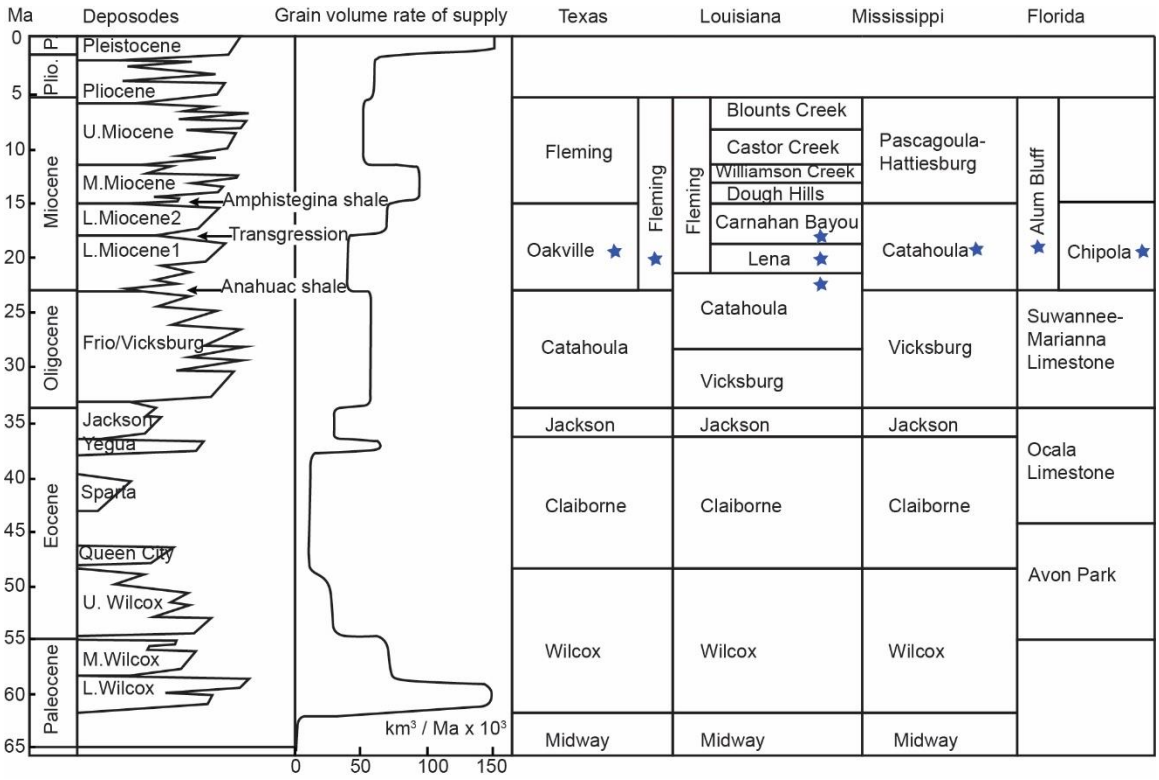

Figure 2.2: Stratigraphic context of samples.

Cenozoic Gulf of Mexico stratigraphy with emphasis on the Lower Miocene strata. Depositional episodes (deposodes) and grain volume rate of sediment supply are from Galloway et al. (2011). The Lower Miocene strata have various formation names around the northern Gulf of Mexico. The local formation nomenclature is after Johnston et al. (2000), Scott et al. (2001), and DeWitt et al. (2010). Stars mark the stratigraphic intervals where samples were collected.

2.3 STRATIGRAPHIC CONTEXT OF SAMPLES

Samples were collected from 16 outcrop exposures across the northern margin of the Gulf of Mexico (Fig. 2.1; Table A2.1 in Appendix). In addition, three subsurface core samples were obtained from the core repositories of the Bureau of Economic Geology, University of Texas at Austin, and the Florida Geological Survey (Fig. 2.1; Table A2.2). Most of our well samples have limited biostratigraphic or geochronological control, but geophysical log correlations permit stratigraphic age assignments to sampled core intervals.

The stratigraphic ages of outcrop samples are constrained by published studies. Samples GOM2–7 (where GOM stands for Gulf of Mexico; Fig. 2.2) are from the Lower Miocene Oakville Formation of the Texas coastal plain, which was described by Galloway et al. (1982). GOM8 is from the basal part of the undifferentiated Miocene Fleming Formation that overlies the Oligocene Catahoula Formation in Jasper County, east Texas (Singleton, 2008). GOM9–13 are from the Miocene Catahoula, Lena, and Carnahan Bayou Formations in Louisiana. The Catahoula Formation in Louisiana is described as partly late Oligocene and early Miocene in age (Fig. 2.2), but our sample locations are mainly indicated as Lower Miocene by the Geological Map of Louisiana (Louisiana Geological Survey staff, 2008). GOM14–16 are from outcrops in Mississippi and are identified as belonging to the Lower Miocene Catahoula Formation based on published lithostratigraphies (Kolb and Durham, 1967; Dockery and May, 1981). Core samples GOM17 and 18 from the eastern Gulf of Mexico coast have been assigned to the undifferentiated Miocene Alum Bluff Group by the Florida Geological Survey. Samples were collected from the basal part of the Alum Bluff Group where it overlies the Oligocene Suwannee Limestone. The ages of these two samples are uncertain, and they could be middle Miocene. However, their zircon age spectra are similar to that of sample GOM19,

obtained from the Chipola Formation along the modern Apalachicola River. GOM19 is the most precisely dated sample, with biostratigraphy and isotopic data indicating an early Miocene age, ca. 18.3 Ma (Bryant et al., 1992).

In total, 3 to 4 kg of material were collected from each outcrop, whereas 500–800 g were selected from subsurface cores. Core samples were obtained by cutting a 2.5-cm-wide longitudinal slice of core over a distance of several meters. Samples are from fluvial strata, mostly medium- to coarse-grained sandstones, with lesser fine-grained sandstones deposited in overbank environments. The samples collected from the northwestern Florida coastal plain are highly fossiliferous sandstones interbedded with limestone.

2.4 Geochronology Methodology

Standard mineral separation techniques, including heavy mineral and magnetic separation, were employed to extract zircon from surface and subsurface rock samples (see Data Repository for detailed procedures [footnote 1]). Separated zircon grains were sprinkled-mounted onto double-sided tape on 1 in. (2.54 cm) acrylic discs and analyzed at random using depth-profiling laser-ablation–inductively coupled plasma–mass spectrometry (LA-ICP-MS) U-Pb geochronology. For each sample, at least 120 grains were analyzed to obtain a statistically robust provenance data set (Vermeesch, 2004). The analyses were completed using a PhotonMachine Analyte G.2 Excimer laser (30 mm laser spot size) with a large-volume Helex sample cell and a Thermo Element2 ICP-MS. GJ1 was used as the primary reference standard (Jackson et al., 2004), and Pak1 was used as a secondary zircon standard (thermal ionization mass spectrometry [TIMS] $^{206}Pb/^{238}U$ age of 43.0 Ma). Depth profiling of nonpolished, tape-mounted zircon grains enables the resolution of multiple zircon growth zones evident from core and rim ages (Stockli and Stockli, 2013). For analyzed detrital zircon grains, the $^{206}Pb/^{238}U$ age is used for grains

younger than 1000 Ma, and $^{207}Pb/^{206}Pb$ age is used for grains older than 1000 Ma. For zircon U-Pb ages older than 1000 Ma, the discordance was calculated based on $^{206}Pb/^{238}U$ and $^{207}Pb/^{206}Pb$ ages. For zircon ages younger than 1000 Ma, the discordance was calculated based on $^{206}Pb/^{238}U$ and $^{207}Pb/^{235}U$ ages. All grains older than 1000 Ma with >20% discordance and grains younger than 1000 Ma with >10% discordance were discarded, as well as grains with >10% analytical error. The detailed analytical methods and raw data are incorporated in the ancillary Data Repository files (see footnote 1). All detrital zircon U-Pb geochronology analyses were carried out at the UTChron Geo- and Thermochronometry Laboratory at the University of Texas at Austin.

2.5 Detrital Zircon Results

This study presents 2192 new detrital zircon U-Pb results from 19 samples. The data display large age variability, ranging from late Oligocene (ca. 24 Ma) to Archean (ca. 3600 Ma; Fig. 2.3). The spectra are divided into seven age components, based on a combination of ages of major basement provinces and magmatic events in North America and age peaks in our data (Fig. 2.3): Cordillera Magmatic Province (A; 24–280 Ma), Appalachian-Ouachita Province (B; 280–500 Ma), Pan-Africa Province (C; 500–700 Ma), Grenville Province (D; 950–1300 Ma), Midcontinent Province (E; 1300–1500 Ma), Yavapai-Mazatzal Province (F; 1600–1800 Ma), and Shield Province (G; >1800 Ma). Although the nomenclature for each group is interpretive, we do not necessarily make the assumption that zircon grains of the appropriate ages are from these provinces, but we simply use the province nomenclature to designate zircon age groups.

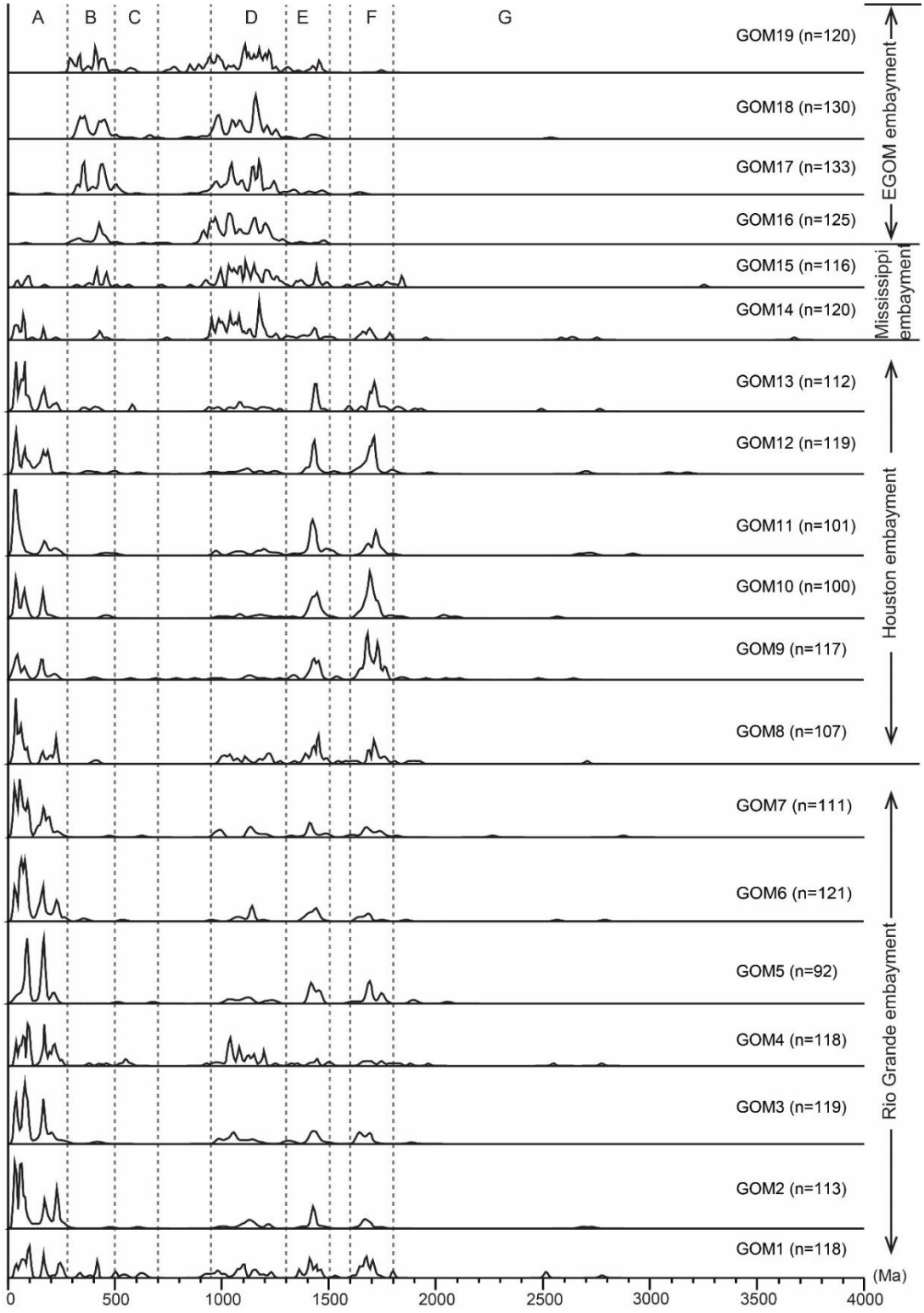

Figure 2.3: Continued next page

Figure 2.3: Normalized U-Pb age spectra of 19 Lower Miocene samples.

Normalized detrital zircon U-Pb age distribution curves for 19 Lower Miocene samples from the northern Gulf of Mexico (GOM). Samples are organized from west at the base to east at the top. Age data were plotted using Kernel Density Estimator software, developed by Vermeesch (2012). A bandwidth of 5 m.y. was used to construct the curves; n—number of zircons analyzed for U-Pb age from each sample; EGOM—eastern Gulf of Mexico. A–G represents components defined by clusters of ages: A—Cordillera Magmatic Province (24–280 Ma); B—Appalachian-Ouachita Province (280–500 Ma); C—Pan-Africa Province (500–700 Ma); D—Grenville Province (950–1300 Ma); E—Midcontinent Province (1300–1500 Ma); F—Yavapai-Mazatzal (1600–1800 Ma); G—Shield Province (>1800 Ma).

Sample Name	Province A < 280 Ma (%)	Province B 280-500 Ma (%)	Province C 500-700 Ma (%)	Province D 950-1300 (%)	Province E 1300-1500 Ma (%)	Province F 1600-1800 (%)	Province G >1800 Ma (%)	Others (%)
GOM1	31	7	5	19	14	19	3	3
GOM2	68	0	2	12	10	7	2	0
GOM3	60	2	0	15	12	11	1	0
GOM4	46	3	3	29	7	8	4	1
GOM5	52	0	2	12	14	16	3	0
GOM6	68	2	1	10	11	7	2	0
GOM7	61	1	1	13	10	12	3	0
GOM8	39	2	0	19	19	16	5	1
GOM9	26	2	2	7	17	38	6	3
GOM10	29	2	0	9	20	33	5	2
GOM11	40	2	1	13	22	17	4	2
GOM12	38	3	2	10	15	26	5	1
GOM13	41	4	2	16	11	20	6	0
GOM14	15	4	1	52	11	11	5	2
GOM15	07	10	3	52	13	7	4	4
GOM16	1	17	2	69	5	0	0	6
GOM17	2	31	5	53	7	2	0	1
GOM18	0	30	5	58	5	0	1	1
GOM19	0	24	3	53	8	0	1	10

Table 2.1: Percentage of zircon U-Pb age component in each sample.

Cordillera Magmatic Province (component A) is composed of late Paleozoic to Cenozoic zircon grains and makes up 31.8% of the total population in all samples. It is the largest component for samples from the western Gulf of Mexico (GOM1–13; Fig. 2.3; Table 2.1). However, the percentage of Cordillera Magmatic Province grains gradually decreases eastward, and it constitutes only a minor component in samples GOM14–19. The Cordillera Magmatic Province component can be further subdivided into six subgroups, A1–A6 (Fig. 2.4). Middle Permian to Late Triassic zircon grains (subgroup A6; 270–210 Ma) account for 10.3% of total Cordillera Magmatic Province grains and have age peaks around 230 Ma in samples GOM1, 2, 6, and 7, and peaks around 214 Ma in samples GOM4 and 5 (Fig. 2.4). Jurassic grains (subgroup A5; 180–150 Ma) are relatively abundant in samples GOM1–13 with several peaks around 160 Ma, 165 Ma, and 173 Ma. Zircon ages from 140 to 110 Ma are rare (3.7%), resulting in a significant age gap between subgroups A5 and A4 (Fig. 2.4). Early Late Cretaceous zircon grains (subgroup A4; 110–85 Ma) are an important component in samples GOM1, 4, 5, and 7, with peaks around 95 Ma. Late Cretaceous zircon grains (subgroup A3; 85–65 Ma) show a common age peak around 75 Ma, while Paleogene zircon grains (subgroup A2; 65–40 Ma) show age peaks around 57 Ma and 46 Ma. Late Eocene to Oligocene zircon grains (subgroup A1; 40–24 Ma) are represented by ages peaks around 35 Ma and 27 Ma (Fig. 2.4).

Appalachian-Ouachita Province (B; 280–500 Ma) constitutes 8.3% of the total population in all samples. It is an important component for samples GOM15–19 from the eastern Gulf of Mexico (Fig. 2.3; Table 2.1). The Pan-Africa Province (C; 500–700 Ma) is a minor component in all samples (Table 2.1). The Grenville Province (D; 950–1300 Ma) is prevalent in all samples and features multiple age peaks; it accounts for 28% of the total population in all samples. Grenville-age zircon grains are most abundant in samples GOM14–19 from the eastern Gulf of Mexico. It is also an important component of several

samples from the western Gulf of Mexico; e.g., GOM4 contains 29% Grenville-age zircon grains (Table 2.1). However, the proportion of Grenville-age zircon grains in western Gulf of Mexico samples is much lower than in samples from the eastern Gulf of Mexico. Midcontinent (E; 1300–1500 Ma) and Yavapai-Mazatzal (F; 1600–1800 Ma) zircon grains are present in most samples. They are most abundant in GOM8–13 from the central Gulf of Mexico and less abundant in samples from both the eastern and western Gulf of Mexico. Shield Province (G; >1800 Ma) zircon grains are a minor component, and few zircon grains display this age (<6% of each sample).

The multidimensional scaling (MDS) approach was used to detect dissimilarity between the U-Pb age spectra of the samples. The MDS method is based on the widely used Kolmogorov-Smirnov (K-S) test, but it provides better visualization of the similarity or dissimilarity between samples (Vermeesch, 2013). As indicated by the MDS plot (Fig. 2.5), 19 samples fall within four main groups. These groups correlate with the geographic positions of samples in known depocenters (Fig. 2.1) and are assigned the following names: Greater Rio Grande Embayment, Houston Embayment, Mississippi Embayment, and Eastern Gulf of Mexico Embayment. Samples GOM1 and GOM4 plot outside the Greater Rio Grande Embayment group (Fig. 2.5). This is because of differences in their components of Appalachian-Ouachita (GOM1), Pan-Africa (GOM1), and Grenville (GOM4; Fig. 2.3; Table 2.1) Provinces. However, given the geographic locations of these samples and high similarity of Cordillera Magmatic Province, Midcontinent, and Yavapai-Mazatzal components to other Great Rio Grande Embayment samples (Fig. 2.3; Table 2.1), we regard all of samples GOM1–7 as a single group. The dissimilarities of GOM1 and 4 are discussed in the following.

The Greater Rio Grande Embayment samples are characterized by high proportions of Cordillera Magmatic Province zircon grains and moderate proportions of Grenville,

Midcontinent, and Yavapai-Mazatzal components (Fig. 2.3; Table 2.1). The Houston Embayment group includes six samples (GOM8–13) and shows a similar age pattern to the Greater Rio Grande Embayment group, but it shows a trend of decreasing Cordillera Magmatic Province component and increasing content of Midcontinent and Yavapai-Mazatzal components from west to east (Fig. 2.3; Table 2.1).

Significant changes occur between the Houston Embayment and Mississippi Embayment groups. The Mississippi Embayment consists of two samples (GOM14–15), showing a rapid increase of Grenville component and decrease of Cordillera Magmatic Province component relative to the Houston Embayment (Fig. 2.3; Table 2.1). In comparison to both the Greater Rio Grande and Houston Embayment, the Cordillera Magmatic Province becomes only a moderate or even minor component. Midcontinent and Yavapai-Mazatzal inputs still play important roles, but they lose importance eastward. The Eastern Gulf of Mexico Embayment consists of samples GOM16–19 and is dominated by Appalachian-Ouachita and Grenville components (Fig. 2.3; Table 2.1).

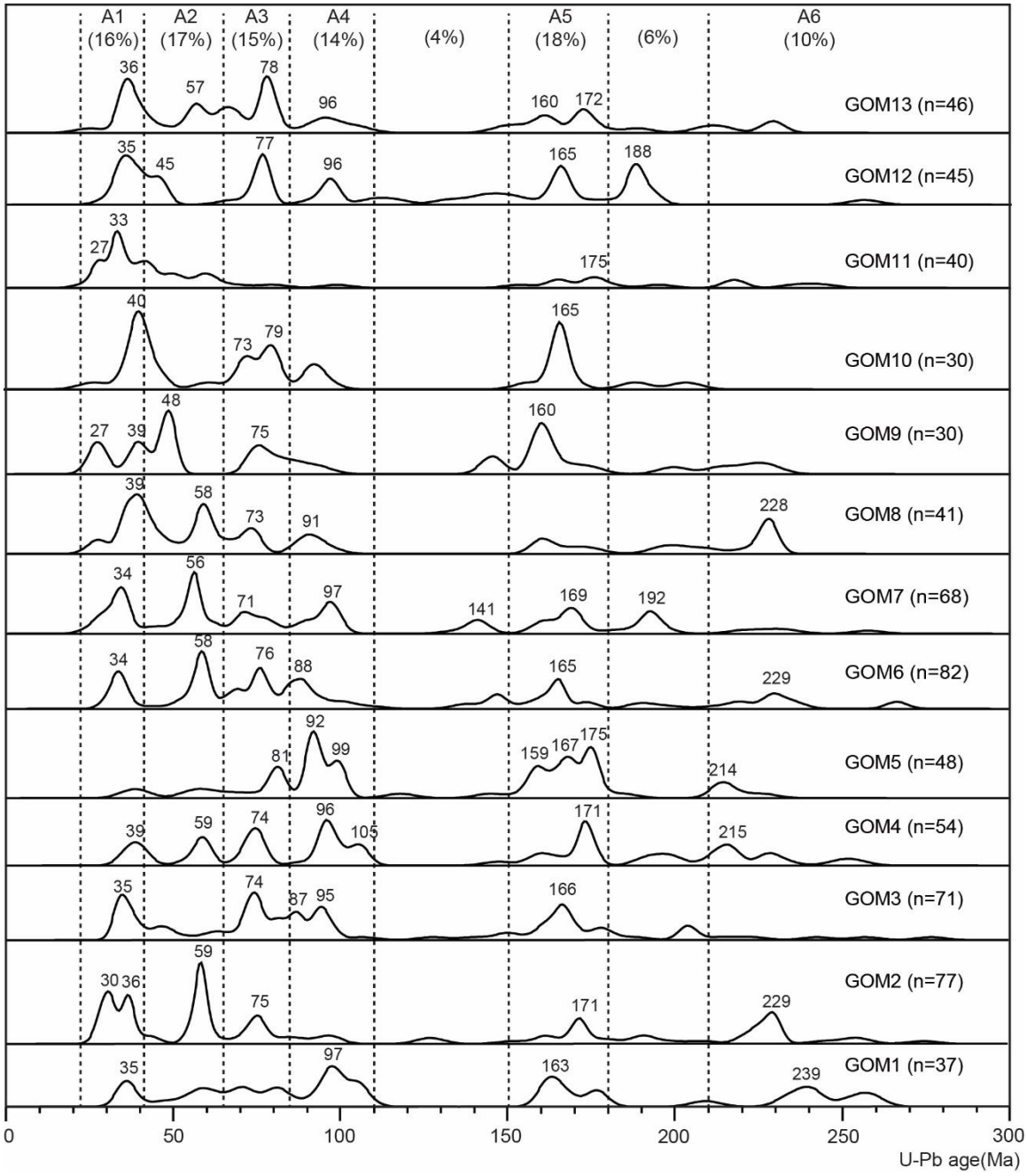

Figure 2.4: Continued next page.

Figure 2.4: Normalized U-Pb age spectra (<300 Ma) of 19 Lower Miocene samples.

Normalized detrital zircon U-Pb age (<300 Ma) distribution curves for 13 Lower Miocene samples from the western-central Gulf of Mexico (GOM). Samples GOM14–19 from the eastern Gulf of Mexico have low proportions of grains <300 Ma and are therefore not plotted here. Samples are organized from west at the base to east at the top. Age data were plotted using Kernel Density Estimator software. A bandwidth of 2 m.y. was used to visually enhance the variability of each curve. Six subgroups are identified based on the distribution of peaks and troughs; n—number of zircon grains analyzed for U-Pb age from each sample. The percentages at top represent proportion of each subgroup in all 13 samples.

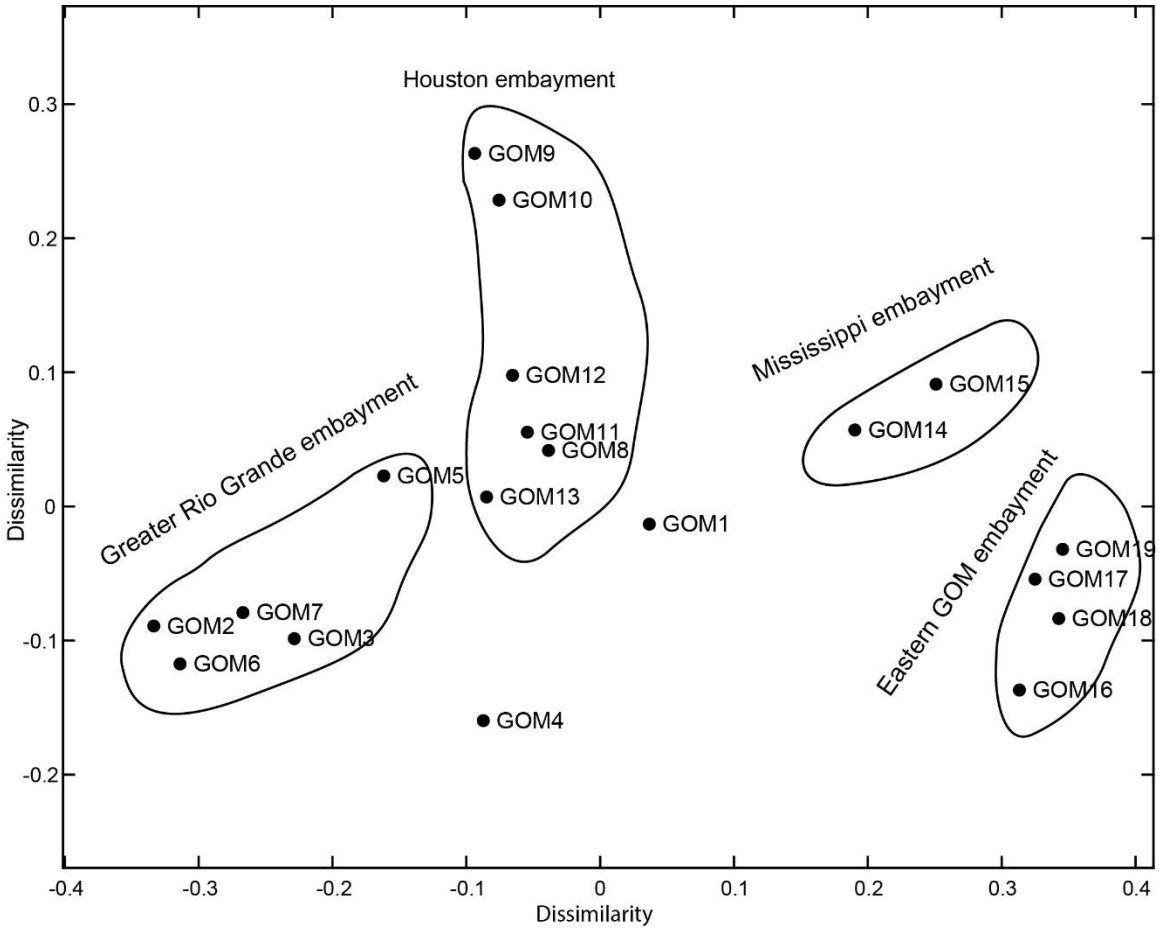

Figure 2.5: Multidimensional scaling (MDS) plots of the 19 detrital zircon samples.

The axes are dissimilarities measured between samples. GOM—Gulf of Mexico.

2.6 GEOCHRONOLOGICAL PROVINCES

2.6.1 Cordillera Magmatic Province (A; 24–280 Ma)

Late Paleozoic to middle Cenozoic zircon grains (24–280 Ma) coincide with documented magmatic activity in the Western Cordillera arc and its predecessors (Chen and Moore, 1982; Ducea, 2001; DeCelles, 2004; DeCelles et al., 2009; Fig. 2.6). The oldest igneous activity (245–280 Ma, corresponding to subgroup A6) is recorded in isolated Permian igneous centers across northern Sonora in Mexico and plutons in the East Mexico arc (Fig. 2.7; Torres et al., 1999; Dickinson et al., 2010). Two younger peaks of magmatic activity at 150–160 Ma (subgroup A5) and 85–100 Ma (subgroup A4) are documented in the Sierra Nevada Batholith (Fig. 2.7; Chen and Moore, 1982; Ducea, 2001; DeCelles et al., 2009).

The Coast Mountains Batholith in the northwestern United States reflects magmatism in the Late Jurassic (150–160 Ma), Early to Late Cretaceous (85–110 Ma), and Late Cretaceous to Paleogene (50–80 Ma), encompassing subgroups A2–A5 (DeCelles et al., 2009; Paterson et al., 2011). Early Cretaceous (110–150 Ma) igneous activity mainly occurred in southernmost California and northern Baja Peninsula (Fig. 2.7; Dickinson and Lawton, 2001), but it is not common in the southwestern United States. Late Cretaceous (80–100 Ma) magmatism can be also found in the Baja Peninsula (Mackey et al., 2012, and references therein).

Late Cretaceous to middle Eocene (40–80 Ma, subgroups A2 and A3) zircon grains are related to the Laramide orogeny, coinciding with rapidly increasing convergence between the North American and Farallon plates (DeCelles, 2004). Magmatic intrusions (dated at 40–75 Ma) are documented in the Laramide porphyry copper province in southern Arizona, southwestern New Mexico, northern Mexico, and the Colorado mineral belt (Fig. 2.7; Tweto and Sims, 1963; Cunningham et al., 1994; Chapin et al., 2004; Barra et al.,

2005; Chapin, 2012). The youngest subgroup (A1; 24–40 Ma) corresponds to the mid-Cenozoic ignimbrite flare-up that extends from Trans-Pecos Texas to central Colorado, including the San Juan, Mogollon-Datil, Trans-Pecos, and Sierra Madre Occidental volcanic fields (Ferrari et al., 1999; Chapin et al., 2004; Ferrari et al., 2007; Fig. 2.7).

2.6.2 Appalachian-Ouachita Province (B; 280–500 Ma)

Paleozoic zircon grains (280–500 Ma) correspond to the Appalachian-Ouachita orogeny along the eastern margin of North America, which formed during assembly of the supercontinent Pangea (Fig. 2.6). The age peaks in the Appalachian-Ouachita Province correspond to three major tectonic accretion events, including the Taconic orogeny (440–465 Ma), Acadian orogeny (350–380Ma), and Alleghanian orogeny (265–327 Ma; Eriksson et al., 2003; Thomas et al., 2004; Hatcher, 1987, 2010; Park et al., 2010; Thomas, 2011). Although the Appalachian-Ouachita terranes are widely distributed, extensive exposures only occur in the Central and Southern Appalachian Mountains, whereas more restricted exposures can be found in the Ouachita Mountains in Oklahoma and Marathon uplift in west Texas.

2.6.3 Pan-Africa Province (C; 500–700 Ma)

Late Proterozoic to early Paleozoic zircon grains (500–700 Ma) may be derived from Iapetan rifting, magmatism along the eastern Laurentia margin, and/or the Pan-African orogeny, which built supercontinent Gondwana (Hoffman, 1989; Park et al., 2010). Zircon grains originating from these tectonic processes are usually from the Suwannee, Carolina, and Avalon terranes in the eastern United States (Park et al., 2010). Another possible source of component C is the Amarillo-Wichita uplift, which features a sharp Cambrian age peak at ca. 516 Ma (Riggs et al., 1996; Dickinson et al., 2010).

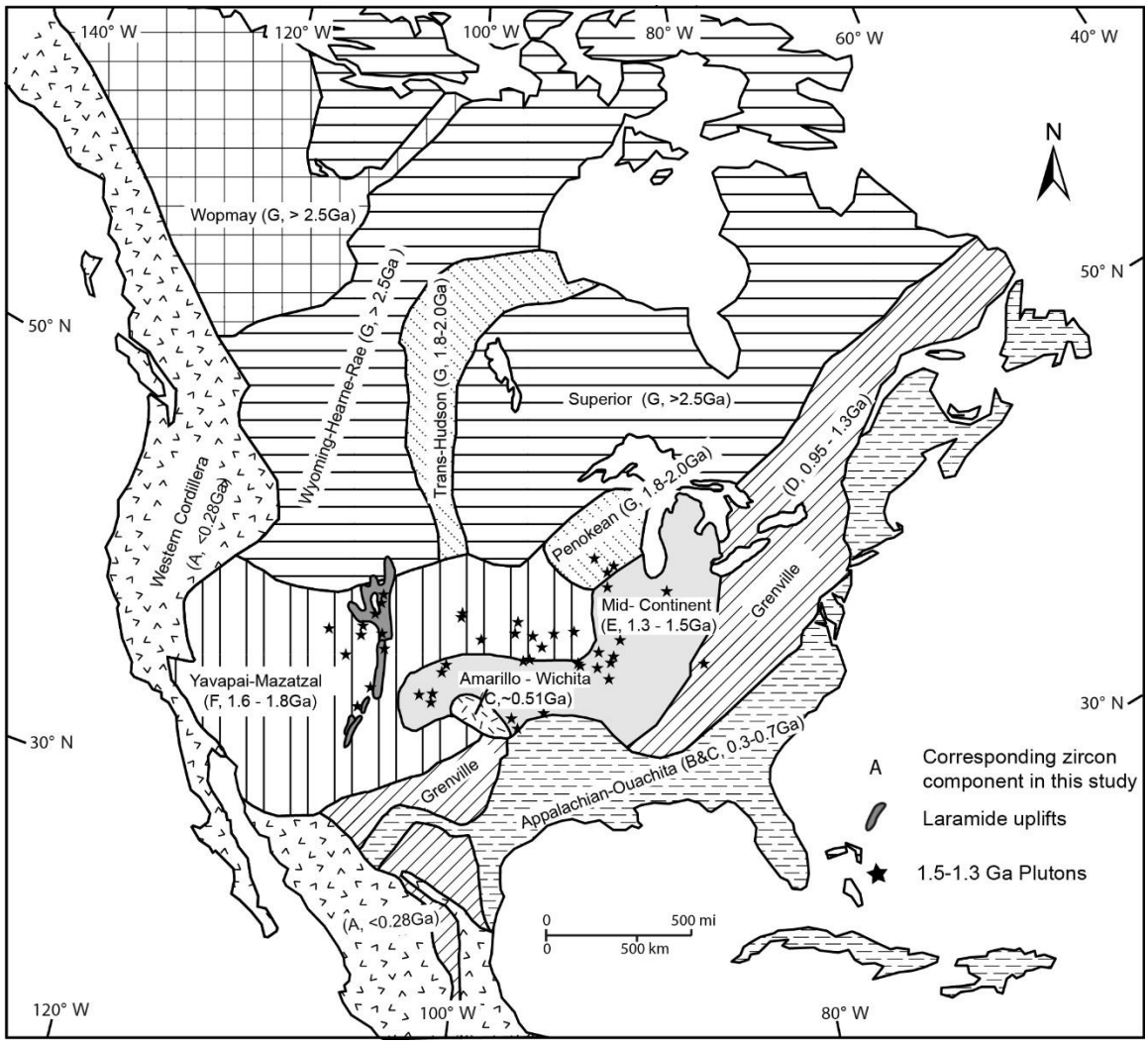

Figure 2.6: Geochronological provinces of North America.

Distribution of basement provinces of North America. Appalachian-Ouachita terranes incorporate Paleozoic Taconic, Acadian, Alleghanian, and Ouachita orogenies (280–500 Ma), together with Gondwanan terranes (500–700 Ma). Figure is adapted from Hoffman (1989), Gehrels et al. (2011), and Blum and Pecha (2014). Midcontinent plutons are after Bickford et al. (1986); Laramide uplifts are from Galloway et al. (2011).

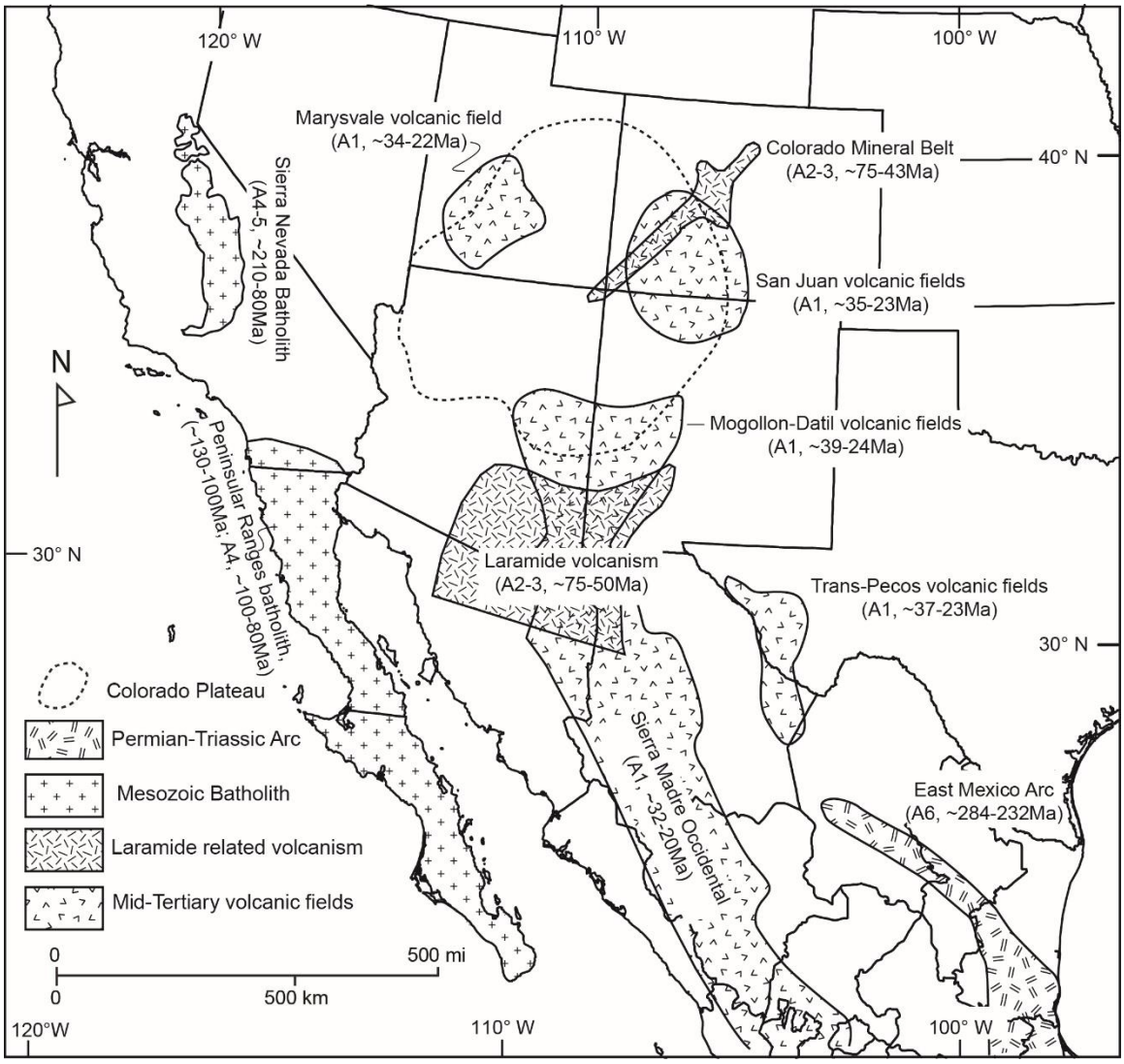

Figure 2.7: Major Late Permian–early Miocene magmatism in southwestern North America.

East Mexico arc is after Dickinson and Gehrels (2009); Mesozoic batholiths are after Mackey et al. (2012) and Laskowski et al. (2013); Laramide-related magmatism is after Cather et al. (2012); mid-Cenozoic volcanism is after Galloway et al. (2011).

2.6.4 Grenville Province (D; 950–1300 Ma)

Middle Mesoproterozoic to early Neoproterozoic zircon grains (D; 950–1300 Ma) are derived from Grenville basement in southern and eastern Laurentia (Fig. 2.6), formed during a Mesoproterozoic orogeny, contemporary with the assemblage of supercontinent Rodinia (Hoffman, 1989; Dickinson and Gehrels, 2009). The Appalachian terranes in the eastern United States have exposures of Grenville basement. Zircon grains from this area usually feature two major age peaks at 1020–1090 Ma and 1140–1190 Ma, which correspond to the Ottawan orogeny and Shawinigan orogeny, respectively (Rivers et al., 2002; Rivers, 2008).

In addition, the Llano uplift in Texas is a major Grenville basement exposure in southern Laurentia with three major phases of magmatic activity: 1232–1288 Ma, 1120–1150 Ma, and 1070–1120 Ma (Mosher, 1998). There are also limited exposures of Grenville basement in the Franklin Mountains in west Texas (Amato and Mack, 2012).

2.6.5 Midcontinent Province (E; 1300–1500 Ma)

Zircon grains of 1300–1500 Ma represent Mesoproterozoic A-type granite-rhyolite in midcontinental North America (Fig. 2.6; Bickford et al., 1986; Van Schmus et al., 1996). However, Phanerozoic cover buried most of the basement except for an exposure in the St. Francois Mountains (Bickford et al., 1986). Therefore, more likely sources for zircon grains of this age are the numerous granitic intrusions in the southwestern United States (Fig. 2.6; Bickford et., 1986; Hoffman, 1989; Karlstrom et al., 1997, 2004).

2.6.6 Yavapai-Mazatzal Province (F; 1600–1800 Ma)

Yavapai-Mazatzal Province corresponds to Yavapai (1700–1800 Ma) and Mazatzal (1600–1700 Ma) basement in southwestern Laurentia (Hoffman, 1989; Karlstrom et al., 2004; Whitmeyer and Karlstrom, 2007). Yavapai-Mazatzal basement was elevated during

the Laramide orogeny and formed the core of the southern Rocky Mountains, which are therefore the most likely direct source for zircon grains with this age range. Alternative sources of Yavapai-Mazatzal grains would be recycling from older sedimentary strata in the western United States, e.g., Carboniferous–Permian (Gehrels and Pecha, 2014) and Permian–Jurassic (Dickinson and Gehrels, 2003) rocks, which had originally received zircon grains from the local Ancestral Rocky Mountains province during the late Paleozoic.

2.6.7 Shield Province (G; >1800 Ma)

Pre–1800 Ma zircon grains were formed by Trans-Hudson, Wyoming, and Superior orogenic events that formed the Precambrian Canadian Shield and the North American craton (Whitmeyer and Karlstrom, 2007; Fig. 2.6). Modern exposures of these Proterozoic and Archean basements are in the northern United States and Canadian Shield region (Laskowski et al., 2013). Uplifts in Wyoming, such as the Wind River Range (2500–2700 Ma; Frost et al., 2000), could be possible sources for zircon grains in this age range, because the adjacent Wind River Basin records rapid uplift and erosion of these highlands in the Paleocene–early Eocene (Fan et al., 2011).

2.7 DISCUSSION

2.7.1 Provenance interpretation

Detrital zircon U-Pb age spectra of 19 Lower Miocene samples from the Gulf of Mexico display high west-to-east variability. The geochronological data show that each of the four distinct groups (Greater Rio Grande Embayment, Houston Embayment, Mississippi Embayment, and Eastern Gulf of Mexico Embayment) represents a unique provenance and thus provides key insights into drainage system development and sediment routing.

2.7.1.1 Greater Rio Grande Embayment Provenance

Detrital zircon U-Pb data for the Greater Rio Grande Embayment consist of seven samples from the south-central Texas coastal plain and are characterized by a high proportion of Cordillera Magmatic Province component and moderate proportions of Grenville, Midcontinent, and Yavapai-Mazatzal components (Fig. 2.3; Table 2.1). Zircon grains of 24–40 Ma (subgroup A1) correspond to the period of mid-Cenozoic magmatism in the southwestern United States. Volcanic fields, including the San Juan volcanic field in southwestern Colorado, Mogollon-Datil volcanic field in western New Mexico, Trans-Pecos volcanic field in western Texas and northern central Mexico, and Sierra Madre Occidental in western Mexico, are the likely ultimate sources (Chapin et al., 2004; Ferrari et al., 2007; Cather et al., 2008). However, the Rio Grande Rift extension developed since the late Oligocene would have precluded large volumes of volcanic materials from volcanic fields to the west entering the Gulf of Mexico. Only the Trans-Pecos volcanic field is a likely direct volcanic zircon source (Fig. 2.8). However, some older zircon grains within this component might be derived from Eocene–Oligocene strata on the Great Plains and Texas coastal plain, to which large volumes of volcanic ash were transported by northeastward-blowing winds (e.g., Larson and Evanoff, 1998). The presence of mid-Cenozoic volcanic zircon grains is also evident by the abundance of volcanic rock fragments in sediment deposited in the Rio Grande Embayment (Galloway et al., 1982, 2000, 2011; Dutton et al., 2012).

Pre–40 Ma Cordillera Magmatic Province zircon grains correspond to major Permian–Triassic arc, Sierra Nevada Batholith, and Laramide-related magmatic centers to the west of Laramide uplifts. However, the uplifted mid-Cenozoic volcanic fields along the eastern Colorado Plateau margin formed a topographic barrier to eastward sediment transportation (Cather et al., 2008, 2012). Consequently, the drainage systems, which

previously carried sediment eastward to the Gulf of Mexico in the Paleocene and Eocene, were reorganized by the mid-Cenozoic volcanism, resulting in a relatively closed drainage system with a fluvial outlet only to the Pacific Northwest (Cather, 2011; Galloway et al., 2011; Cather et al., 2012; Fig. 2.8). In addition, the initiation of the Rio Grande Rift in the late Oligocene–early Miocene created series of extensional basins, which stored sediment eroded from the southern Colorado Plateau (Chapin and Cather, 1994). Although the volume of Lower Miocene sediment stored in the Rio Grande Rift basin is limited (Chapin and Cather, 1994), it is likely that large volumes of sediment eroded from various Cordillera arc terranes were no longer able to reach the Gulf of Mexico as result of the rift-related drainage basin dismemberment.

All of these factors suggest that the late Paleozoic to Paleogene zircon grains (40–280 Ma; subgroups A2–A6) in Lower Miocene Gulf of Mexico strata were probably not directly sourced from western Cordillera arc terranes. This interpretation is supported by dramatic differences in detrital zircon U-Pb age spectra between the Lower Miocene Gulf of Mexico coastal plain strata and Mesozoic eolian strata on the Colorado Plateau (Dickinson and Gehrels, 2009; Fig. 2.9A). Major differences exist in several age components, especially for the 300–700 Ma component, which is abundant in Colorado Plateau Mesozoic strata but nearly absent on the Gulf of Mexico coast. Therefore, it is unlikely that a large volume of sediment reached the Gulf of Mexico from the Colorado Plateau region.

The zircon grains with 40–280 Ma ages are instead more likely recycled from strata previously deposited on the southern Great Plains, western and central Texas, and northeastern Mexico. These strata are Cretaceous–Early Cenozoic erosional products that were derived from the Permian–Triassic arc, Sierra Nevada Batholith, and Laramide-related magmatic terranes and transported by eastward-flowing paleorivers (Dickinson et

al., 1988; Cather et al., 2012). Deep erosion occurred on the southern Great Plains and southern Rocky Mountains during the late Oligocene–early Miocene in response to increased mantle buoyancy induced by the mid-Cenozoic volcanism in southwestern North America (Roy et al., 2004; Eaton, 2008; Cather, 2011; Cather et al., 2012). This deep erosion removed ~1.5 km of Upper Cretaceous–Paleogene strata on the southern Great Plains of Texas, New Mexico, and northeastern Mexico (Kelley and Chapin, 1995; Cather et al., 2012, and references therein). Sediment eroded from such older strata probably comprise an important component of the Lower Miocene strata along the Texas coastal plain, because of the high similarity between U-Pb age spectra of the Lower Miocene strata and Paleocene–Eocene Wilcox Group strata (Fig. 2.9B).

This similarity is most marked in central Texas, although Yavapai-Mazatzal Province and Shield Province components are more abundant in the Wilcox strata (Fig. 2.9B). In contrast, detrital zircon age spectra of the Wilcox strata in southwestern Texas (Mackey et al., 2012) are dissimilar to those of the Lower Miocene strata (Fig. 2.9C). For example, the Wilcox strata U-Pb data from Mackey et al. (2012) show a continuous pattern from 50 Ma to 280 Ma without significant age gaps, while 110–150 Ma grains are almost entirely missing from the Lower Miocene strata. In addition, the Grenville Province component is much less common in the Wilcox strata of southwestern Texas (Fig. 2.9C). Large differences also exist between the Upper Cretaceous–Paleogene Difunta strata in the foreland basin of the Sierra Madre Oriental (Lawton et al., 2009) and the Lower Miocene strata (Fig. 2.9D). The former contains abundant 110–150 Ma and 230 Ma zircon grains, whereas the Lower Miocene strata have rare zircon grains in those ranges. Therefore, the Lower Miocene strata may be partially recycled from the Wilcox Group strata in central Texas (Fig. 2.9B), but the Laramide foreland basins in Mexico and the Wilcox Group of southwestern Texas are unlikely to be significant sources (Figs. 2.9C and 2.9D).

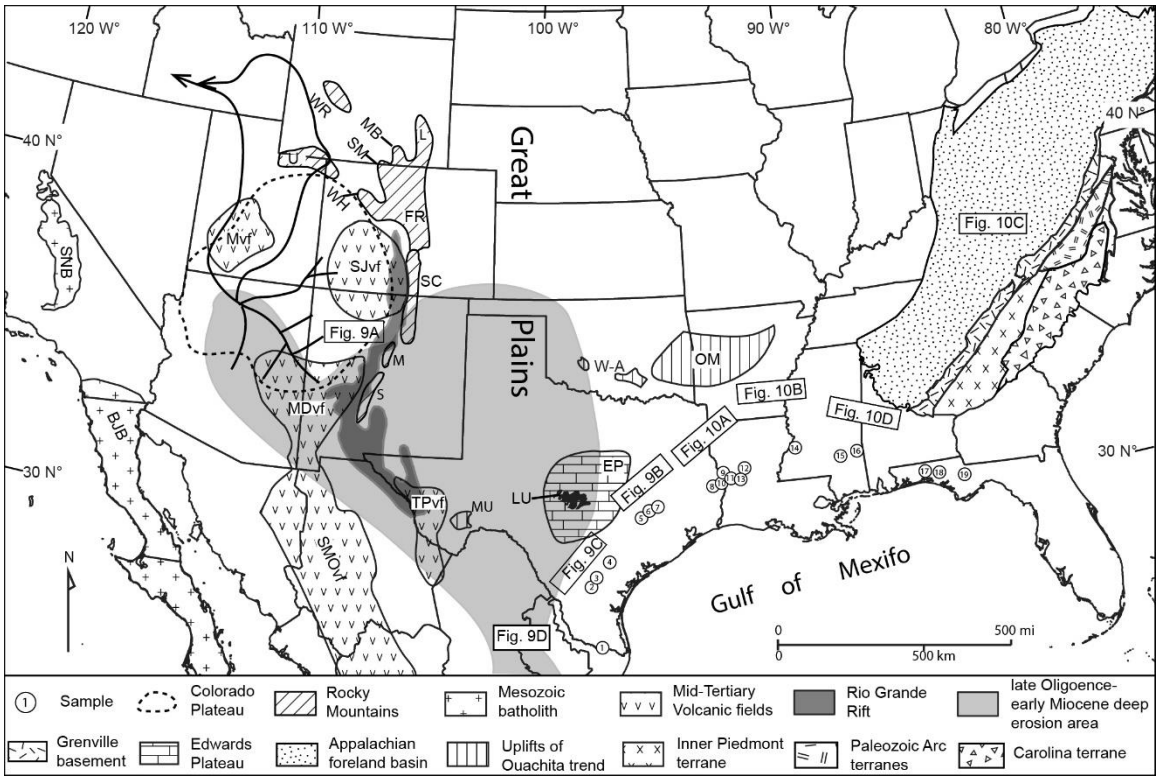

Figure 2.8: Paleogeographic map for the Lower Miocene strata of the northern Gulf of Mexico coastal plain.

The drainage systems are not depicted here and are covered in detail in Figure 2.12. Laramide uplift abbreviations: FR—Front Range; L—Laramie; M—Montosa; MB—Medicine Bow; S—Sierra; SC—San Luis and Sangre de Cristo; SM—Sierra Madre; U—Uinta; WH—White River; WR—Wind River. Mid-Cenozoic volcanic field abbreviations: MDvf—Mogollon-Datil volcanic field; Mvf—Marysvale volcanic field; SJvf— San Juan volcanic field; SMOvf—Sierra Madre Occidental volcanic field; TPvf—Trans-Pecos volcanic field. Major Mesozoic batholith abbreviations: SNB—Sierra Nevada Batholith; BJB—Baja California Batholith. Highlands for Gulf of Mexico region abbreviations: LU—Llano uplift; EP—Edwards Plateau; OM—Ouachita Mountains; MU—Marathon uplift; W-A—Wichita and Arbuckle Mountains. Area of the Appalachian foreland basin is

adapted from Park et al. (2010), and major Appalachian terranes are from Eriksson et al. (2003). Rivers are adapted from Cather et al. (2012). Laramide uplift and mid-Cenozoic volcanic fields are from Galloway et al. (2011). Mesozoic batholiths are from Mackey et al. (2012) and Laskowski et al. (2013).

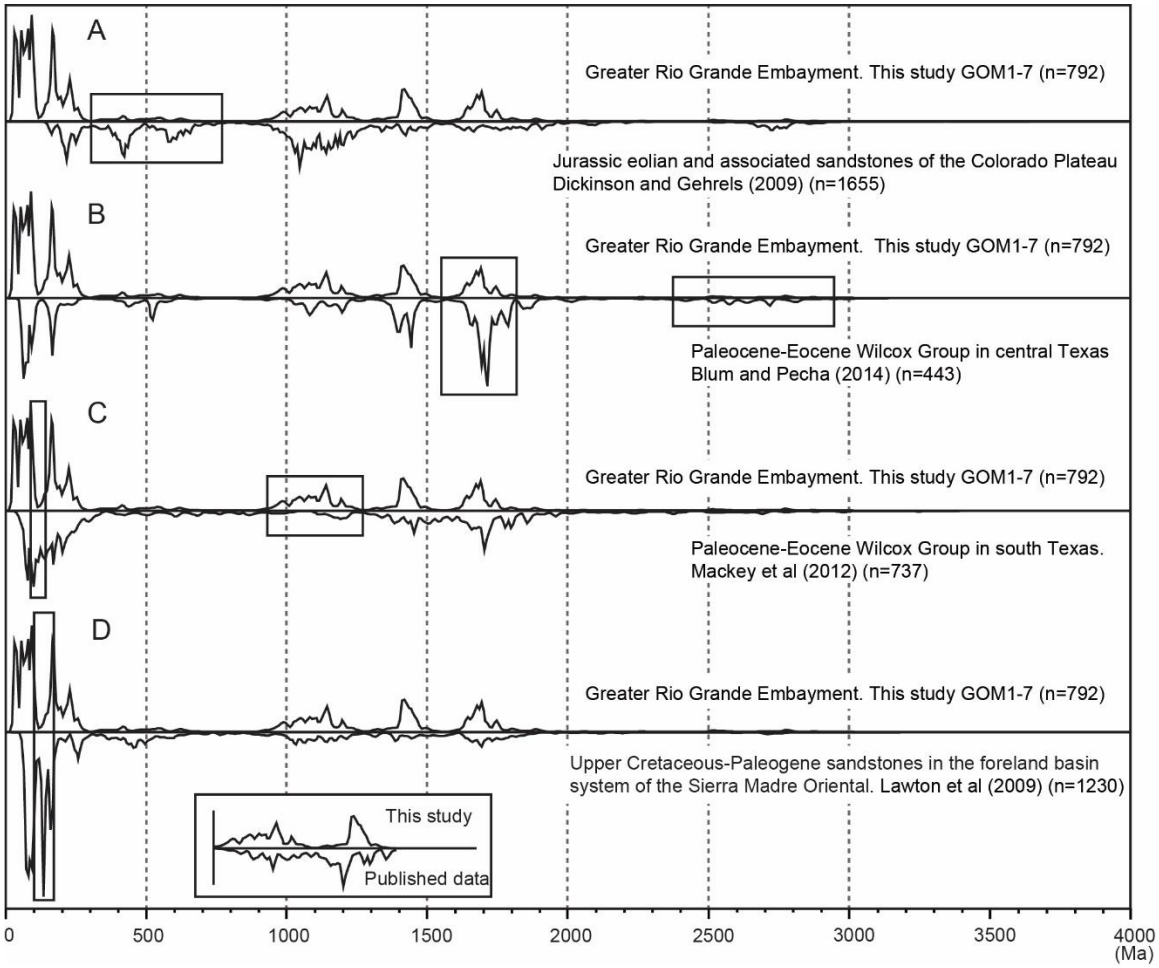

Figure 2.9: Comparison of Lower Miocene U-Pb data of samples in Greater Rio Grande Embayment and published strata.

Comparison of normalized U-Pb age plots for the Lower Miocene strata from the Texas coastal plain and potential recycled sources (see Fig. 2.8 for locations). The rectangles emphasize the major differences between sets of U-Pb age spectra being compared; n—number of zircon grains analyzed in each data set; GOM—Gulf of Mexico.

The original source of 110–150 Ma zircon grains is most likely the Peninsular Ranges Batholith in southernmost part of California, northern Baja Peninsula, and north-central Sonora (Dickinson and Lawton, 2001; Lawton et al., 2009; Mackey et al., 2012). Magmatism in this age interval is not common in other terranes in the southwestern United States. Therefore, the absence of zircon grains of 110–150 Ma age in the Lower Miocene strata suggests a reduced catchment size compared to the Paleogene Wilcox Group, with cutoff of sediment supply from southernmost California, northern Baja Peninsula, and western Mexico (Fig. 2.8).

Grenville zircon grains (D; 9500–1300 Ma) in the Greater Rio Grande Embayment probably indicate a recycled source. Although Grenville basement exposures in the southwestern United States are limited, Grenville-affinity grains are commonly found in several sedimentary basins, e.g., the Late Jurassic to Early Cretaceous Bisbee and McCoy basins (Dickinson et al., 2009), Mesozoic eolian basins on the Colorado Plateau (Dickinson and Gehrels, 2003, 2008, 2009), and Paleocene–Eocene Wilcox Group in the Gulf of Mexico (Blum and Pecha, 2014). Most Rio Grande Embayment samples (GOM1–3 and 5–7) do not show a prominent increase of Grenville zircon grains in the Lower Miocene strata relative to the Paleogene Wilcox Group (Blum and Pecha, 2014; Fig. 2.9B), suggesting that their Grenville-component zircon grains are possibly recycled from these strata. Only sample GOM4 displays a high proportion of Grenville component (Fig. 2.3; Table 2.1), indicating local input of Grenville grains. The main such primary contributor of Grenville grains in Texas was the Llano uplift. About 1.3 km of the Llano uplift and Edwards Plateau were unroofed starting in the early Miocene (Corrigan et al., 1998; Ewing, 2005).

Midcontinent (E; 1300–1500 Ma) and Yavapai-Mazatzal (F; 1600–1800 Ma) are additional important components in the Greater Rio Grande Embayment samples. They can either come from Yavapai-Mazatzal basement exposed by the southern Laramide

uplift, or be recycled from sedimentary strata such as the Mississippian–Permian (Gehrels and Pecha, 2014), Permian–Jurassic (Dickinson and Gehrels, 2003), and Paleocene–Eocene Wilcox Group strata (Blum and Pecha, 2014). Compared to the Paleogene Wilcox Group strata (Blum and Pecha, 2014; Fig. 2.9B), the Yavapai-Mazatzal and Shield components in the Lower Miocene samples are smaller. This contrast probably indicates that the Lower Miocene and Paleocene–Eocene Wilcox Group strata shared similar sediment source terranes, but with a decreased sediment supply from Laramide uplifts and Archean basement exposures in Wyoming. It is also possible that the Lower Miocene strata are largely recycled from the Paleocene–Eocene Wilcox strata, with an extra input of younger grains that dilutes the Yavapai-Mazatzal and Shield components.

Few zircon grains are present from the Appalachian-Ouachita Province (B; 300–500 Ma), Pan-Africa Province (C; 500–700 Ma), and Shield Province (G; >1800 Ma). No basement sources are available nearby for direct supply of these grains. Therefore, those present are probably partially recycled from older strata, e.g., the Wilcox Group (Blum and Pecha, 2014). Sample GOM1 has a small U-Pb age peak around 413 Ma, which might be recycled from the Marathon region in west Texas, where this peak is recorded in the Pennsylvanian Haymond Formation (Gleason et al., 2007). Therefore, it is possible that sample GOM1 records slightly different source terranes, perhaps including a tributary from the Marathon uplift in west Texas.

In summary, the Lower Miocene samples from the Greater Rio Grande Embayment record large volumes of zircon grains that were likely recycled from older strata on the southern Great Plains, western and central Texas, and northeastern Mexico. The mid-Cenozoic volcanic fields, particularly the Trans-Pecos volcanic field, probably provided the majority of first cycle volcanic zircon grains. The Llano uplift in central Texas contributed sediment in a limited area. By comparison with two previous studies (Lawton

et al., 2009; Mackey et al., 2012) on the Paleogene strata in the Gulf of Mexico region, the lack of 110–150 Ma zircon grains indicates that sediment sourced from western Mexico arc terranes was cut off by the early Miocene (Figs. 2.9C and 2.9D). Compared to the Paleocene–Eocene Wilcox strata deposited on the central Texas coastal plain (Fig. 2.9B; Blum and Pecha, 2014), the Lower Miocene strata have fewer grains from Yavapai-Mazatzal and Wyoming-Superior terranes, indicating either that sediment supply from the Rocky Mountains and Wyoming-Superior terranes had decreased or that Lower Miocene strata were largely recycled from older strata on the southern Great Plains (Fig. 2.9B). Future application of detrital zircon U-Pb and (U-Th)/He double dating to individual zircon crystals may help to resolve this uncertainty.

2.7.1.2 Houston Embayment Provenance

The Houston Embayment (samples GOM8–13), centered near the Texas-Louisiana boundary, is distinguished from the Greater Rio Grande Embayment by a decrease of Cordillera Magmatic Province zircon grains and a marked increase of Midcontinent and Yavapai-Mazatzal zircon grains (Fig. 2.3; Table 2.1). Cordillera Magmatic Province zircon grains are still an important component of the Houston Embayment group, indicating similar sources to those of the Greater Rio Grande Embayment. However, the influence of these sources is reduced in the Houston Embayment.

Midcontinent and Yavapai-Mazatzal zircon grains become pronounced components of the Houston Embayment group (Fig. 2.3; Table 2.1). Midcontinent and Yavapai-Mazatzal zircon grains are most likely derived from Laramide basement uplifts in the southwestern United States (Bickford et al., 1986; Hoffman, 1989; Karlstrom et al., 1997, 2004; Fig. 2.6). A significant increase of Yavapai-Mazatzal grains relative to the Greater Rio Grande Embayment indicates that source terranes for the Lower Miocene strata

may have shifted northward to the major southern Laramide uplifts where the Paleozoic and Mesozoic cover strata had been eroded and Precambrian Yavapai-Mazatzal basement core exposed (Tweto, 1975).

Similarity exists between the Lower Miocene strata and the Paleogene Wilcox Group in the Houston Embayment (Fig. 2.10A). This indicates that the Lower Miocene strata are either recycled from the Wilcox strata or that they come from similar source terranes to those of the Wilcox. However, the proportion of Yavapai-Mazatzal zircon grains in the Lower Miocene strata (24.8%) is larger than the proportion of Yavapai-Mazatzal component in the Wilcox Group (19.5%). The Proterozoic basement cores of Laramide uplifts were exposed during the late Paleocene to Eocene, as indicated by the Precambrian igneous and metamorphic clasts preserved in adjacent lacustrine basins (e.g., Tweto, 1980; Carroll et al., 2006). Apatite fission-track thermochronology studies on the southern Rocky Mountains indicate that >2 km of material were eroded during the late Oligocene–early Miocene from the Sangre de Cristo Mountains in New Mexico (Kelley and Chapin, 1995; Pazzaglia and Kelley, 1998). These observations suggest that erosion of uplifted Laramide cores, particularly the Sangre de Cristo Mountains, added increasing amounts of Yavapai-Mazatzal zircon grains to the Lower Miocene strata relative to the Paleocene–Eocene Wilcox strata.

However, differences in Yavapai-Mazatzal components between the Wilcox and Lower Miocene strata are not great, and resulting interpretations should be treated with caution. For example, the variation could be caused by the limited data set (i.e., ~100 grains in each sample). Yavapai-Mazatzal component zircon grains may be derived from a mixed source that included both Laramide basement and sedimentary strata in the western United States.

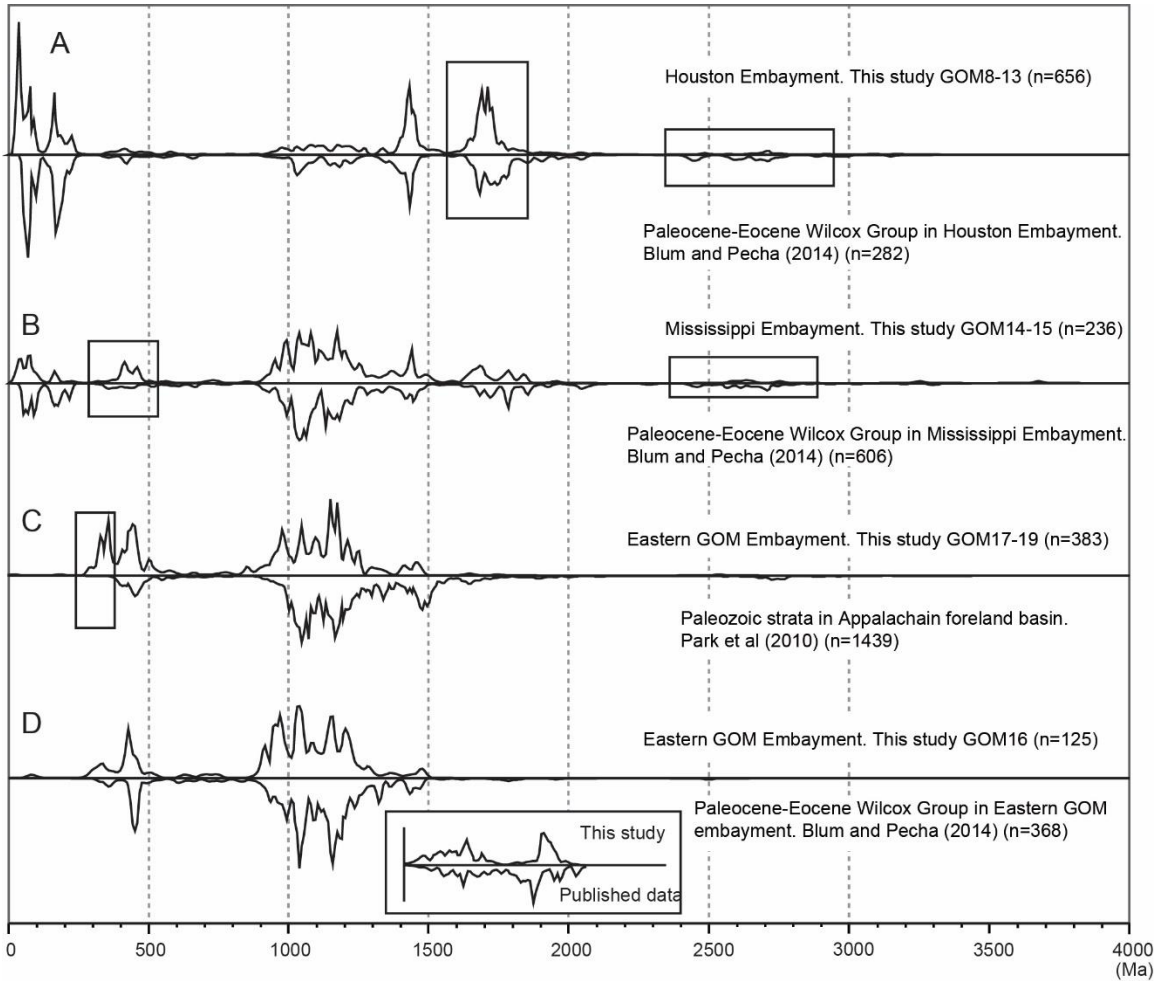

Figure 2.10: Comparison of Lower Miocene U-Pb data of samples in central-eastern Gulf of Mexico and published strata.

Comparison of normalized U-Pb age plots for the Lower Miocene strata from the Houston–eastern Gulf of Mexico embayment and potential recycled sources (see Fig. 2.8 for locations). The rectangles emphasize the major differences between sets of U-Pb age spectra being compared; n—number of zircon grains analyzed in each data set; GOM—Gulf of Mexico.

The Shield component is an important portion (13.5%) of the Paleocene–Eocene Wilcox strata, indicating a sediment contribution from basement uplifts in Wyoming. In contrast, the Lower Miocene strata lack a large Shield component (Fig. 2.10A; Table 2.1).

Generally, the Houston Embayment records a decrease in the impact of sources from the southern Great Plains, western and central Texas, northeasternmost Mexico, and the Trans-Pecos volcanic field. The Houston Embayment source terranes extended to the major southern Laramide uplifts, as reflected by the large component of Yavapai-Mazatzal zircon grains contained in samples GOM8–13. Compared to the Wilcox Group, the Houston Embayment contains fewer zircon grains from basement uplifts in Wyoming.

2.7.1.3 Mississippi Embayment Provenance

The Mississippi Embayment group shows a dramatic difference in U-Pb age patterns with respect to the Houston Embayment, with a sharp increase in the Grenville component and decrease in the Cordillera Magmatic Province component (Fig. 2.3; Table 2.1), indicating a large contribution from the Appalachian terranes in the east and reduced contribution from the western U.S. terranes. Although Grenville zircon grains are common in Mesozoic–Cenozoic basins in western North America (e.g., Patchett et al., 1999; Dickinson and Gehrels, 2008, 2009; Leier and Gehrels, 2011; Blum and Pecha, 2014), dominance to the degree found in the Mississippi Embayment (>50%) is mostly found in the Appalachian regions (e.g., Eriksson et al., 2003, 2004; Park et al., 2010).

This change is coupled with an increase in the Appalachian-Ouachita component (300–500 Ma), which is likely derived from exposures of the Paleozoic fold-and-thrust belt in the Appalachian terranes. Exposure of the Appalachian-Ouachita terranes in the Ouachita Mountains could be an alternative source for these grains. Detrital zircon studies on the Cenomanian Woodbine-Tuscaloosa Formation in the Gulf of Mexico region (Blum

and Pecha, 2014) and the Cenomanian Dakota Formation in western Iowa and eastern Nebraska (Finzel, 2014) suggest that the Ouachita Mountains and foreland basin are potential major sources for both Appalachian-Ouachita and Grenville zircon grains. Previous petrographic studies on the Lower Miocene strata also indicate the Ouachita Mountains as an important local source terrane (e.g., Galloway et al., 2000, 2011; Dutton et al., 2012).

Midcontinent and Yavapai-Mazatzal components in the Mississippi Embayment are also reduced relative to the Houston Embayment (Fig. 2.3; Table 2.1). However, Cordillera Magmatic Province, Midcontinent, and Yavapai-Mazatzal components still make up ~30% of the total detrital zircon population in the Mississippi Embayment, indicating a continued strong western U.S. influence. Paleostream and sub-Ogallala paleovalley trend (as discussed in next section) studies indicate fluvial transport of such sediment from Laramide uplift regions eastward to the Great Plains (Bart, 1975; Scott, 1975; Fig. 2.11), where it was finally collected by the paleo–Mississippi River (Galloway et al., 2011).

A comparison of the Mississippi Embayment of the Lower Miocene strata to the Wilcox Group strata located to the north (updip; Blum and Pecha, 2014; Figs. 2.8 and 2.10B) shows them to be very similar, indicating that the Lower Miocene strata were probably either sourced from recycled Paleocene–Eocene Wilcox strata or originated from the same drainage area. The Shield component is more abundant in the Wilcox Group strata, possibly indicating a stronger connection to Wyoming basement uplifts in the Paleocene–Eocene than during the early Miocene. This can be partially explained by climatic changes. Paleostream analysis of Miocene Arikaree strata of the High Plains of western Nebraska and eastern Wyoming suggests that paleorivers carried sediment from the Laramie Range (Archean basement) eastward to the Great Plains (Bart, 1975).

However, it is probable that the arid climate that prevailed in the western United States during the late Oligocene and early Miocene diminished the capacity for fluvial sediment transport (Galloway et al., 2011).

In summary, the Lower Miocene strata in the Mississippi Embayment record a sharp increase in sediment delivered from the Appalachian terranes relative to the Houston Embayment (Fig. 2.8), but Great Plains and Laramide uplifts were still important contributors of sediment. Lower Miocene strata might also include recycled Wilcox strata, but probably with less contribution from the Archean basements uplifts of the northern Rocky Mountains than is the case for the Wilcox Group strata.

2.7.1.4 Eastern Gulf of Mexico Embayment Provenance

The Appalachian-Ouachita and Grenville components (Fig. 2.3; Table 2.1) dominate the Eastern Gulf of Mexico Embayment samples, with only minor Pan-Africa, Midcontinent, Yavapai-Mazatzal, and Shield components, and Cordillera Magmatic Province zircon grains are completely absent. The predominance of the Appalachian-Ouachita and Grenville components indicates a proximal source from the Grenville basement and Paleozoic fold-and-thrust belt in the Appalachian terranes (Fig. 2.8).

Our Grenville age spectra basically match the four pulses of orogeny in the Appalachian terranes: Elzeverian (1190–1250 Ma), Shawinigan (1140–1190 Ma), Ottawan (1020–1080 Ma), and Rigolet (980–1010 Ma; Rivers et al., 2002; Rivers, 2008). Eriksson et al. (2004) suggested that Grenville zircon grains in Neoproterozoic through Pennsylvanian sedimentary rocks of the Central Appalachian Basin have a bimodal distribution with distinct age peaks between 1020 and 1080 Ma (Ottawan) and 1140–1190 Ma (Shawinigan). This age pattern can also be seen in Paleozoic strata in the Appalachian foreland basin (Park et al., 2010) and the Paleogene Wilcox Group strata on the eastern

Gulf of Mexico coastal plain (Blum and Pecha, 2014). These major Ottawan and Shawinigan peaks are also present in our data, and the overall patterns are similar (Figs. 2.3, 2.10C, and 2.10D).

Paleozoic grains are the second important component in samples from the Eastern Gulf of Mexico Embayment and constitute 17%–31% of each sample (Table 2.1). Sample GOM16 has a single prominent age peak corresponding to the Taconic orogeny (ca. 430–500 Ma), while GOM17–19 record two additional peaks related to the Acadian (ca. 350–400 Ma) and Alleghanian (ca. 265–325 Ma) orogenies. Taconic plutons are mainly exposed in the Chopawamsic and Milton terranes of the Central Appalachians, while Acadian and Alleghanian rocks are widely developed in the Inner Piedmont of the Southern Appalachian terranes (Eriksson et al., 2003). The increase of Acadian and Alleghanian components in GOM17–19 indicates more materials sourced from the proximal Southern Appalachian terranes.

Marked similarity can be observed between the Eastern Gulf of Mexico Embayment Lower Miocene and Paleozoic strata of the Appalachian foreland basin (Park et al., 2010; Fig. 2.10C) and the Wilcox samples from the eastern Gulf of Mexico coastal plain (Blum and Pecha, 2014; Fig. 2.10D). These similarities likely indicate multiple recycling events of older strata. However, the two high peaks exhibited by samples GOM17–19 and corresponding to the Acadian and Alleghanian orogenies indicate a proximal source from the Southern Appalachian terranes (Fig. 2.8). Because the Pan-Africa component (C; 500–700 Ma) is rare, the peri-Gondwanan terranes (e.g., Carolina terrane) are excluded as a possible source of the Lower Miocene strata in the Eastern Gulf of Mexico Embayment.

2.7.2 Drainage Systems of the Early Miocene in the Gulf of Mexico Basin

The early Miocene was an important transitional interval of tectonic reorganization in North America for which the drainage systems are not well known (Cather et al., 2012). Major drainage reorganization occurred on the Colorado Plateau as the mid-Cenozoic volcanism disrupted the preexisting eastward-flowing Eocene drainage system and reversed the flow direction to northwestward toward the Pacific Northwest (Spencer et al., 2008; Cather et al., 2008, 2012). The Rio Grande Rift probably also played a role in preventing western rivers from entering the northern Gulf of Mexico (Fig. 2.12). However, the continental drainage divide was probably west of the rift, along the axis of volcanic centers in southwestern North America during the earliest early Miocene (LM1; Fig. 2.12; Galloway et al., 2011). As a result, volcaniclastic detritus from the mid-Cenozoic volcanic fields to the west of the Rio Grande Rift (e.g., San Juan volcanic field and Mogollon-Datil volcanic field) could still reach the Rio Grande Embayment in the Gulf of Mexico during this period, as indicated by the presence of abundant volcanic-rock-fragment–rich sediment stored in the Rio Grande Embayment (Galloway, 1981; Galloway et al., 1982). Rapid progradation of the Rio Grande Embayment shelf margin in LM1 indicates a continuity of sediment input to the Gulf of Mexico from the Oligocene to early Miocene. In contrast, retrogradation of the shelf margin in the late early Miocene (LM2) suggests a decline of sediment influx associated with increased sequestering of sediment by the Rio Grande Rift and disruption of the regional drainage basin by extensional tectonics (Fig. 2.1; Galloway, 2005). Other studies have suggested that sedimentation in the Rio Grande Rift began in the early Miocene, but that rapid basin subsidence and sediment accumulation in the rift clearly occurred in the middle–late Miocene (Chapin and Cather, 1994; Cather et al., 1994; Connell, 2004; Chapin, 2008). Therefore, it is probable that there was a connection between volcanic fields in New Mexico and southern Colorado and the Gulf of Mexico in the

earliest early Miocene. As volcanic activity waned and Rio Grande Rift extension accelerated, transport of sediment from these sources to the Greater Rio Grande Embayment began to decline (Fig. 2.12).

The paleo–Missouri and Ohio Rivers were probably not fully integrated into a southward flowing system until the Pliocene–Pleistocene (Galloway et al., 2011; Blum and Roberts, 2012). Instead, the paleo–Ohio River, which drained the Appalachian foreland basin, flowed northeastward in the early Miocene as a tributary to the preglacial St. Lawrence River (Hoagstrom et al., 2014, and reference therein). Similarly, the Miocene upper Missouri River flowed northward and joined the preglaciation "Bell River" in Canada (Howard, 1958; Sears, 2013). The size of the early Miocene drainage system feeding the Gulf of Mexico was therefore much smaller than the modern system, and this is reflected in the contrast between the sediment volumes reaching the Gulf of Mexico in the early Miocene and in the Pleistocene (Fig. 2.2).

Analysis of the early Miocene drainage systems is helpful for understanding how bulk sediment was transported from upland source terranes to basinal sinks. Previous paleodrainage analyses have been mainly constrained by petrographic data and logical deduction where the sedimentary record was limited (Galloway et al., 1982, 2011). Detrital zircon U-Pb analysis greatly enhances our understanding of paleodrainage systems supplying the northern Gulf of Mexico by allowing us to distinguish individual fluvial systems.

2.7.2.1 Early Miocene Drainage on the Great Plains

Our detrital zircon analysis strongly suggests a major sediment source from the Great Plains and southern Rocky Mountains. Large paleorivers carried the bulk of sediment to the Gulf of Mexico. However, the courses of these rivers across the Great Plains are

difficult to define because their sedimentary records were mostly eroded during the late Cenozoic. Major erosion occurred before the deposition of the Middle to Upper Miocene Ogallala Group, cutting deeply into Permian, Triassic, Jurassic, and Lower Cretaceous rocks on the southern Great Plains, and less deeply into Upper Cretaceous–Cenozoic rocks on the northern Great Plains (Fig. 2.11). In contrast to poor preservation of Lower Miocene strata on the southern Great Plains, the aquifer made up of the Middle-Upper Miocene Ogallala Group is well preserved and studied. The contours of the base of this aquifer from Weeks and Gutentag (1981) guide reconstruction of the ancestral drainage pattern. The courses of the major early Miocene rivers can be interpreted based on the trend and configuration of these contours (Fig. 2.11).

Some Lower Miocene strata are preserved on the northern Great Plains where erosion was shallow. Paleostream analysis based on heavy mineral assemblages and cross-bedding in the Lower Miocene strata of the Arikaree Formation in western Nebraska and southeastern Wyoming suggests that northeastward-flowing streams carried materials eastward from the Laramie Mountains and Front Range (Bart, 1975). Condon (2005) also documented paleocurrents on the northern Great Plains oriented east-northeastward from a major source in the Front Range. This flow pattern might be related to regional structural tilting to the northeast induced by mantle buoyancy (Roy et al., 2004; Condon, 2005). The trend of basal Ogallala aquifer contours also displays a similar east-northeast trend (Fig. 2.11).

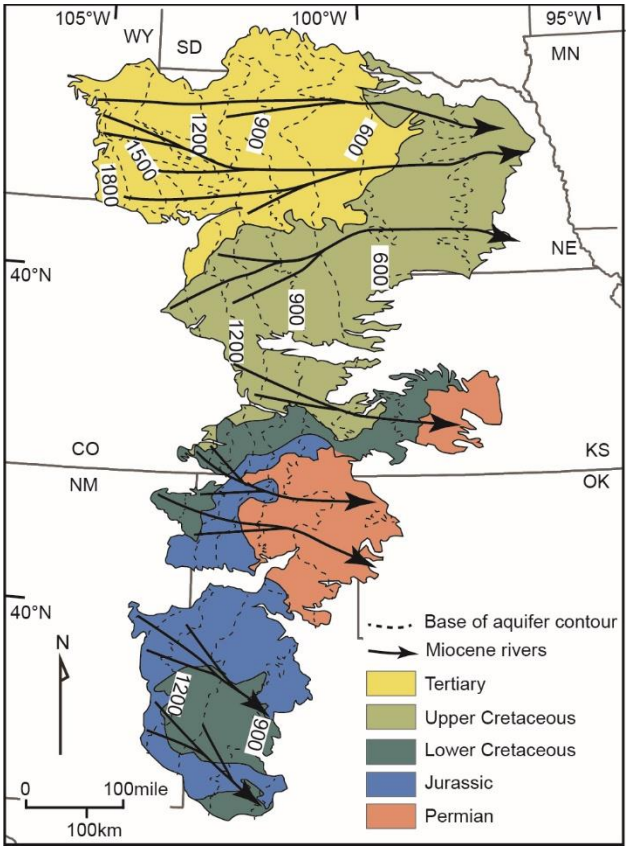

Figure 2.11: Paleodrainage map of the Great Plains aquifer.

Paleodrainage map of the Great Plains aquifer. Bedrock geology and altitude contours of the base of the Ogallala aquifer (in m) are from Weeks and Gutentag (1981). Faults and sinkholes that can influence the base-of-aquifer contours are not shown here. State abbreviations: CO—Colorado; NM—New Mexico; KS—Kansas; OK—Oklahoma; NE—Nebraska; MN—Minnesota; SD—South Dakota; WY—Wyoming.

There are few records of the early Miocene paleodrainage trends on the southern Great Plains. Basal Ogallala aquifer contours suggest that the early Miocene rivers generally flowed east-southeastward (Fig. 2.11; Weeks and Gutentag, 1981; Fallin, 1988; Chapin, 2008). The sediment derived from the Great Plains was deposited in the Rio Grande, Houston, and Mississippi Embayment depocenters of the Gulf of Mexico (Galloway et al., 2011).

2.7.2.2 Paleo–Rio Bravo, Rio Grande, and Houston-Brazos Drainage Systems

While detrital zircon U-Pb age spectra of GOM1–7 display similar overall age patterns, indicating a shared common source terrane, these samples represent three different drainage systems influenced by local structures. These drainage systems can be differentiated by both sample petrographic features and detailed analysis of the detrital zircon age spectra. Samples GOM1–4 lie in the Rio Grande Embayment (Fig. 2.1). However, the U-Pb age pattern of GOM1 differs from those of samples GOM2–4, which are presumed to reflect paleo–Rio Grande delivery. Sample GOM1 has an age peak around 412 Ma that is reduced or absent in samples GOM2–4 (Fig. 2.3; Table 2.1). Sample GOM1 may have collected tributary contributions from the Marathon uplift by recycling strata from Pennsylvanian Haymond Formation, where zircon grains of Paleozoic age are well documented (Gleason et al., 2007). We interpret sample GOM1 to indicate a distinct fluvial system, paleo–Rio Bravo, rather than the paleo–Rio Grande (Fig. 2.12).

Although detrital zircon U-Pb signals of samples GOM2–7 are similar (Fig. 2.3), they are from two different fluvial systems, separated by local structures (e.g., the San Marcos Arch). The paleo–Rio Grande fluvial system (GOM2–4) south of the San Marcos Arch is thought to have been a coarse-grained bed-load river system, whereas intrabasinal fluvial systems (GOM5–7; named paleo–Houston-Brazos here) to the north of the arch

were considered more mixed-load fluvial (Galloway et al., 1982). In addition, the paleo–Rio Grande was enriched in volcanic rock fragments that were delivered by an extrabasinal river from the southern Laramide uplifts and southern Great Plains, whereas the paleo–Houston-Brazos was more carbonate-rock-fragment–rich because of proximity to the Edwards Plateau in central Texas (Galloway et al., 1982, 2011; Dutton et al., 2012; Fig. 2.12).

Major fluvial rerouting occurred in the paleo–Houston-Brazos system to the northeast during this period. The paleo–Houston-Brazos was a large extrabasinal fluvial system in Eocene–Oligocene time, but the river discharge diminished during the early Miocene, and it became a minor sediment contributor to the Gulf of Mexico with no large deltaic depocenter formed in front of the fluvial axis (Spradlin, 1980; Galloway et al., 1986, 2011). This change may have been related to uplift of the Edwards Plateau in the early Miocene. This uplift deflected a paleoriver from the southern Great Plains, which had previously flowed southeast to join the Houston-Brazos, eastward to merge with the paleo–Red River instead (Galloway et al., 2011; Fig. 2.12).

2.7.2.3 Paleo–Red River and Mississippi Drainage System

The paleo–Red River had not yet been integrated with the Mississippi River in the early Miocene and was thus a separate major fluvial system delivering sediment to the deep-water Gulf of Mexico (Galloway et al., 2000, 2011). Two major deltaic depocenters were mapped by Galloway et al. (2000, 2011): one in eastern Texas (paleo–Red River) and the other in Louisiana (paleo–Mississippi River). The paleo–Red river and paleo–Mississippi River axes have similar mineral compositions: only mapping at the Gulf of Mexico margin differentiates the two. However, detrital zircon U-Pb age spectra from the

two systems (GOM8–13 and GOM14) differ significantly and help to differentiate these fluvial systems (Fig. 2.3; Table 2.1).

Samples in the Houston Embayment have a reduced component of Cordillera Magmatic Province zircon grains and a high percentage of Yavapai-Mazatzal grains, indicating major southern Rocky Mountains and southern Great Plains sources (Fig. 2.12). Mineral assemblages (e.g., chert pebbles, garnet, and chromite) in Lower Miocene paleochannel deposits indicate that tributaries draining the southern Ouachita Mountains flowed southward to join the Red River in the early Miocene (McBride et al., 1988). In addition, Permian–Cretaceous vertebrate fossils were reworked from southwestern Oklahoma to paleochannel deposits in eastern Texas and western Louisiana by the paleo–Red River (Manning, 1990). The Red River may also have collected tributaries that earlier connected to the Houston-Brazos paleoriver in central Texas, as noted above.

In contrast, sample GOM14, near the Louisiana-Mississippi state boundary, strongly suggests transport by the paleo–Mississippi River (Fig. 2.12), because its U-Pb age data consist of large numbers of zircon grains from both the Appalachian terranes to the east (Grenville and Appalachian-Ouachita grains) and western U.S. sources (Western Cordillera arc, Yavapai-Mazatzal, and Midcontinent grains).

However, the early Miocene paleo–Mississippi River drainage area was much smaller than that of the Paleocene–Eocene, as well as that of the modern Mississippi River, because the paleo–upper Missouri and Ohio Rivers did not drain to the south until diverted by continental glaciation in the Pliocene–Pleistocene (Fig. 2.12; Galloway et al., 2011; Blum and Roberts, 2012). This is also evidenced by the lack of Archean aged zircon grains from northern Wyoming or the Canadian Shield in Lower Miocene strata (Figs. 2.3 and 2.12; Table 2.1). In contrast, Archean aged zircon grains are an important component of both the Paleocene–Eocene Wilcox Group (Fig. 2.10B; Blum and Pecha, 2014) and modern

samples (Iizuka et al., 2005). Sample GOM15, from central-eastern Mississippi, is a fine-grained coastal and shelf sandstone and does not represent direct fluvial axis deposition. It displays a similar detrital zircon U-Pb age pattern as sample GOM14, suggesting eastward longshore current reworking of the paleo–Mississippi River deposits to the west.

2.7.2.4 Paleo–Tombigbee River and Apalachicola Drainage System

Lower Miocene strata from the eastern Gulf of Mexico margin are mainly thin marine carbonates and barrier island and beach sand deposits (Galloway et al., 2000; Galloway 2008). The river that preceded the middle Miocene Tennessee River was relatively small, and sediment was reworked into coastal and shelf sand bodies. The onshore fluvial deposits identified here are local intrabasinal fluvial systems, which provided limited sediment influx to the Gulf of Mexico.

We interpret sample GOM16 as representative of the proximal, intrabasinal paleo–Tombigbee River. Sample GOM16 contains high proportions of Grenville- and Appalachian-Ouachita aged zircon grains with no grains younger than 280 Ma. Zircon grains derived from western U.S. sources were collected by the paleo–Mississippi River to the west and could not pass eastward of this barrier. Most of the paleo–Tombigbee River sediment was recycled from the Paleocene–Eocene Wilcox Group located to the north (updip) or Paleozoic strata from the Appalachian foreland basin (Figs. 2.8, 2.10C, and 2.10D). Overall, the sediment influx rate in this region was low, and only in the middle Miocene did the emerging paleo–Tennessee River begin to carry large volumes of sediment to the Gulf of Mexico continental shelf and basin (Galloway et al., 2000, 2011). Boettcher and Milliken (1994) suggested a change of exhumation rate in the Southern Appalachians from only 0.4 ± 0.2 km eroded within 60 m.y. before 20 Ma, to 1.5 ± 0.5 km eroded from 20 Ma to present. The increase in sediment erosion rate was postulated to be principally

related to epeirogenic uplift of the Appalachians induced by dynamic mantle activity (Gallen et al., 2013; Miller et al., 2013; Liu, 2014).

We also interpret a paleo–Apalachicola River based on distinct detrital zircon U-Pb age spectra of samples GOM17–19 and their locations near the modern Apalachicola Embayment. The zircon components of the Eastern Gulf of Mexico Embayment provenance are dominated by the Grenville and Appalachian orogeny terranes, suggesting that the paleo–Apalachicola River drained the eastern Blue Ridge and Inner Piedmont of the Southern Appalachian terranes that were similar to those seen today. At the GOM19 outcrop, the fossiliferous quartz sand (ca. 18.3 Ma; Bryant et al., 1992) directly overlies Oligocene Suwanee Limestone, suggesting a pronounced early Miocene transition from a Paleogene carbonate environment to a Neogene siliciclastic environment.

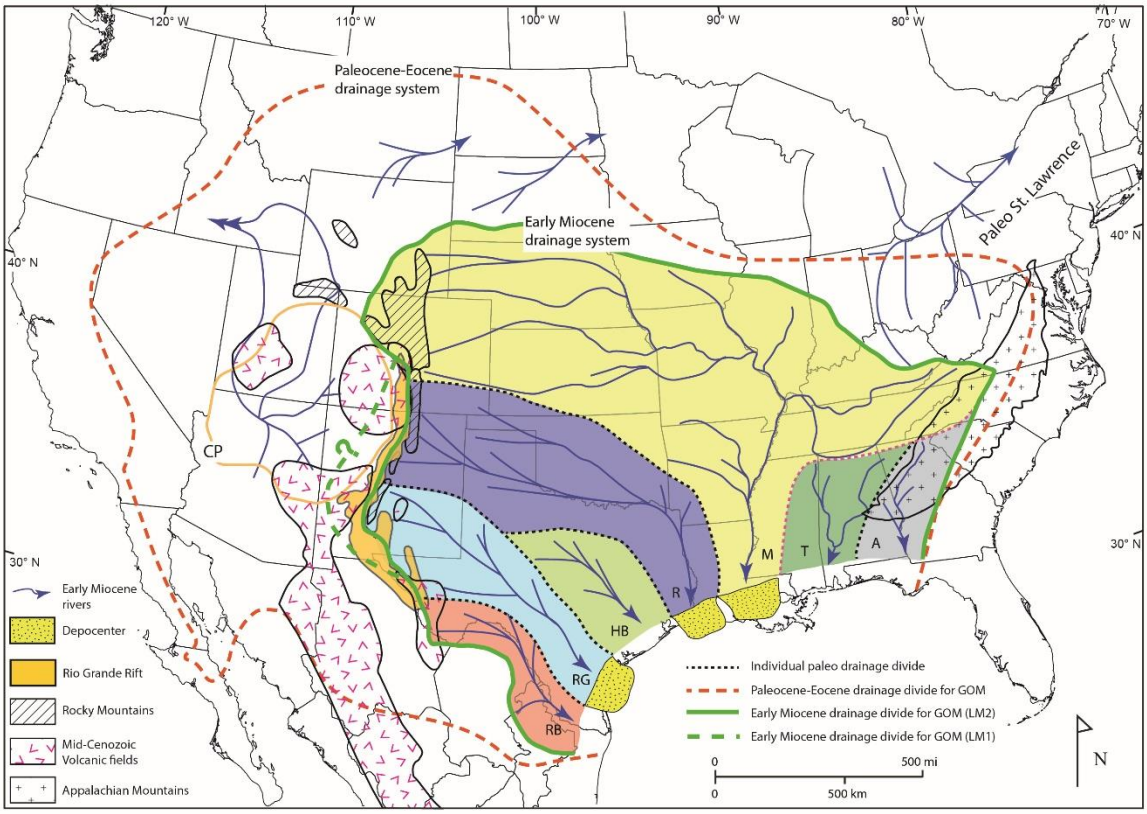

Figure 2.12: Early Miocene paleodrainage systems of the northern Gulf of Mexico (GOM) coast.

The configurations of early Miocene paleodrainage patterns on the Great Plains are drawn with reference to modern rivers, the sub-Ogallala paleovalley trend (see Fig. 2.11), and previous mineralogical studies (Bart, 1975; Weeks and Gutentag, 1981; Fallin, 1988; Condon, 2005; Cather et al., 2012). Only major structural features are shown. Paleocene–Eocene drainage system is adapted from Mackey et al. (2012) and Blum and Pecha (2014). Paleo–St. Lawrence River is adapted from Hoagstrom et al. (2014). CP—Colorado Plateau. Fluvial abbreviations: RB—Rio Bravo; RG—Rio Grande; HB—Houston-Brazos; R—Red; M—Mississippi; T—Tombigbee; A—Apalachicola.

2.8 SUMMARY AND CONCLUSIONS

Nineteen Lower Miocene samples were collected from the northern Gulf of Mexico margin, and 2192 reliable detrital zircon U-Pb ages were obtained. The detrital zircon data display large variability in age distributions, ranging from late Oligocene (ca. 24 Ma) to Archean (ca. 3600 Ma). Major zircon components include Cordillera Magmatic Province (24–280 Ma), Appalachian-Ouachita Province (300–500 Ma), Grenville Province (950–1300 Ma), Midcontinent Province (1300–1500 Ma), and Yavapai-Mazatzal Province (1600–1800 Ma). Only a few grains appear to come from the Pan-Africa (500–700 Ma) and Shield (>1800 Ma) Provinces.

Detrital zircon age data from the 19 samples generally cluster into four regional components: Greater Rio Grande Embayment, Houston Embayment, Mississippi Embayment, and Eastern Gulf of Mexico Embayment. Each of these groups represents a distinct provenance. The Greater Rio Grande Embayment strata were mainly derived from the southern Great Plains and Trans-Pecos volcanic field. Local source terranes include the Llano uplift and Edwards Plateau in central Texas, both of which were uplifted and exhumed during the early Miocene. The Houston Embayment strata were likely derived from the southern Rocky Mountains and the southern Great Plains, where deep erosion occurred during the late Oligocene–early Miocene. The Mississippi Embayment on the central Gulf of Mexico coast contains sediment sourced from both western (mainly Great Plains and southern-central Rocky Mountains) and eastern U.S. terranes (Appalachian foreland basin and Paleozoic Appalachian orogenic terranes). Locally, the Ouachita Mountains and Ouachita foreland basin could have been sediment contributors. The Eastern Gulf of Mexico Embayment suggests a locally proximal source from the eastern Blue Ridge and Inner Piedmont of the Southern Appalachian terranes. Therefore, the detrital zircon age spectra document a continental-scale sediment provenance shift across

the northern Gulf of Mexico from highlands in the western United States to the Appalachian Mountains and foreland basin in the eastern United States.

The sediment associated with the paleo–Rio Bravo, Rio Grande, Brazos, Red, Mississippi, Tombigbee, and Apalachicola Rivers can be differentiated based on detrital zircon analysis, improving definition of sediment transport pathways from upland sources to basin sinks (Fig. 2.12). Future detrital zircon U-Pb dating of deepwater samples could provide a complete sediment routing pathway from hinterland source terranes to basin terminal sinks. Complementary onshore and deep-water detrital zircon analyses that reveal sediment pathways from fluvial sources to basinal sinks would also aid in prediction of petroleum reservoir quality in the deep basin.

Comparison with published detrital zircon provenance studies yields improved understanding of drainage system evolution through time. The absence of zircon grains with ages of 110–140 Ma in the Lower Miocene strata indicates a cutoff of drainage from western Mexico terranes at this time. A smaller component of grains older than 1800 Ma in the Lower Miocene, compared to the Paleogene Wilcox strata, probably indicates a reduced contribution from the central-northern Rocky Mountains, if the contrast is not biased by the limited detrital zircon age data (~100 grains in each sample). Finally, a reduced Lower Miocene drainage area compared to that of the Paleogene Wilcox Group can be inferred (Fig. 2.12). This may partially explain the decreased volume of sediment in the Lower Miocene Gulf of Mexico strata relative to the Wilcox Group (Galloway et al., 2011; Fig. 2.2). This decrease in sediment volume may also have been related to arid conditions in the western United States, which reduced water discharge and thus the capacity of rivers to deliver sediment to the Gulf of Mexico.

A comparison with published detrital zircon provenance studies also suggests that recycling is common in Lower Miocene strata. The prominent Cordilleran Magmatic

Province component is probably a product of erosion of earlier Mesozoic–Cenozoic strata rather than sourced directly from arc terranes to the west of the Rio Grande Rift. Other important components, like Appalachian-Ouachita, Grenville, Midcontinent, and Yavapai-Mazatzal grains, might have been partially recycled from the Paleocene–Eocene Wilcox Group strata. These recycling events may have been highly responsive to tectonic and paleodrainage evolution, e.g., thermal uplift and development of the Rio Grande Rift in the late Oligocene–early Miocene in the southwestern United States. Future application of combined detrital zircon U-Pb and (U-Th)/He analyses on single zircon crystals would further refine sediment provenance and help to resolve remaining uncertainties surrounding sediment sources and routing.

ACKNOWLEDGMENTS

We would like to thank the members of the Gulf Basin Depositional Synthesis Project (GBDS) industrial associate program and GBDS Project Manager Patricia Ganey-Curry. This research was also funded by an internal Jackson School of Geosciences Energy Theme seed grant to Stockli and Snedden. We are grateful for an Ed Picou Fellowship from the Gulf Coast Section of the Society for Sedimentary Geology, which helped fund the field work. We also thank the Institute for Geophysics, The University of Texas at Austin, for providing a Ewing-Worzel Graduate Fellowship. Field sample collection was facilitated by Gary Kinsland and Robert Hatcher. The Florida Geological Survey and Bureau of Economic Geology allowed us to sample subsurface cores. We also thank Lisa Stockli and Spencer Seman for assistance with U-Pb dating, and Daniel Arnost, Timothy Shin, and Shanping Liu for their help with mineral separation. Constructive comments by reviewers Mike Blum and Andrew Leier and Editors Timothy Lawton and Aaron Cavosie are appreciated and helped to greatly improve this manuscript.

Chapter 3: Enhanced provenance interpretation using combined U–Pb and (U–Th)/He double dating on detrital zircon grains from lower Miocene strata, Gulf of Mexico Basin, North America [2]

ABSTRACT

Detrital zircon U–Pb analysis is an effective approach for studying sediment provenance by relating crystallization age to potential crystalline terranes, but it reveals little information about tectonic exhumation events that ultimately control basin evolution and sediment dispersal. Investigations of large passive margin basins, such as the Gulf of Mexico Basin, that have received sediment from multiple terranes with indistinguishable crystallization ages or sedimentary strata, require additional information to constrain provenance interpretation. In this study, combined U–Pb and (U–Th)/He analyses on single zircons from the Lower Miocene sandstones in the northern Gulf of Mexico Basin reveal a complicated history of sediment source evolution. Single U–Pb age data indicate that most sediment sources came from five major crystalline terranes, including the Western Cordillera Arc (<250 Ma), the Appalachian–Ouachita (500–260 Ma), the Grenville (1300–950 Ma), the Mid–Continent Granite–Rhyolite (1500–1300 Ma), and the Yavapai–Mazatzal (1800–1600 Ma) terranes. A few are from Pan–African (700–500 Ma) and Canadian Shield (>1800 Ma) terranes. Zircon (U–Th)/He analyses record multiple exhumation (paleotemperature cooling) events in each terrane, including Grenville (1300–950 Ma), Appalachian–Ouachita (500–300 Ma), Ancestral Rockies (~310 Ma), Pangea rifting (250–150 Ma), Sevier–Nevadan (170–80 Ma) and Laramide (80–40 Ma) tectonism and mid–Cenozoic volcanism (40–24 Ma). The revealed crystallization and cooling ages for a single zircon provide dual constraints for sediment provenance interpretation, and thus can differentiate volcanic and plutonic zircon source, as well as multi–recycled

[2]This chapter was submitted to Earth and Planetary Science Letters and under review.

sedimentary sources (e.g., Grenville zircons). This double dating method allows much greater understanding of the complex sediment source evolution for large passive margin basins such as the Gulf of Mexico Basin.

3.1 INTRODUCTION

Detrital U–Pb geochronology has become one of the most powerful and widely applied tools for provenance analyses elucidating sediment origin, sediment dispersal patterns, drainage basin evolution, and characterization of source terranes as well as providing constraints on maximum depositional age (e.g., Fedo et al., 2003; Dickerson and Gehrels, 2009; Lawton et al., 2009; Carrapa, 2010; Leier and Gehrels, 2011; Gehrels, 2014). This methodology has been increasingly applied to the understanding of Cenozoic sediment delivery into the Gulf of Mexico Basin (e.g., Mackey et al., 2012; Craddock and Kylander–Clark, 2013; Blum and Pecha, 2014; Wahl et al., 2016; Xu et al., 2017).

However, detrital zircon U–Pb geochronology has inherent limitation to resolve sediment provenance precisely as a result of non–diagnostic age signatures. Although zircon U–Pb ages are useful to trace sediment to their ultimate crystalline terranes, they provide little information to differentiate multiple potential source terranes with roughly similar crystallization ages (e.g., Howard et al., 2009; Fig. 3.1). For example, the northern African continental crust is dominated by Pan–African orogenic signals, resulting zircon U–Pb pattern with little to no variation as exemplified by the Nile or Niger River drained the Pan–Africa and Archean crust (Rino et al., 2008; Iizuka et al., 2013). Similarly, Grenville basements, which were extended from northeastern Canada to Mexico and have high zircon fertility (Moecher and Samson, 2006; Dickinson, 2008), dominate zircon U–Pb age signals in sedimentary basins both in eastern (e.g., Park et al., 2010) and western North America (e.g., Dickinson and Gehrels, 2003, 2009). In addition, zircon can survive

multiple erosion–deposition cycles, due to its durability despite physical and chemical weathering. Zircons either can be from multi–cycle sedimentary strata or derived from primary crystalline source, but yielding a similar pattern of U–Pb age spectra, hindering detailed provenance interpretations (e.g., Grenville zircons in North America; Thomas, 2011).

The limitations of zircon U–Pb dating can be overcome by combined use of Hf–isotope analyses (e.g., Iizuka et al., 2005; Gerdes and Zeh, 2006; Clements et al., 2012; Gehrels and Pecha, 2014), trace elements (Stockli and Stockli, 2013), and low–temperature thermochronology dating, such as zircon fission–track (ZFT) and zircon (U–Th)/He (ZHe) analysis, on a single zircon crystal (Reiners et al., 2005; Lawton, 2014; Painter et al., 2014). Hf–isotopic analyses could provide genesis character of zircon's parental magma and thus are able to distinguish multiple source rocks of similar crystallization age but with different geological histories (Howard et al., 2009; Clements et al., 2012). Trace element measured from zircon crystal by depth–profile laser–ablation–split–stream ICP–MS analysis provides petrologic growth environment and crystallization temperatures. However, both analyses do not reveal the exhumation/cooling event of highlands, which is particularly important for understanding the intensity of tectonic events, unroofing rate, and timing of sediment exhumation in the source areas that determine sediment dispersal from source to sink. This problem can be solved by the combination of of U–Pb and (U–Th)/He (U–Pb–He) dating on single zircon crystal (Fig. 3.1).

The ZHe dating of the same zircon provides additionally independent constraints on the basis of cooling age information (Fig. 3.1). This detrital zircon U–Pb–He double dating approach has a number of advantages as it allows for the differentiation of individual DZ U–Pb age components, a more definitive assignment of provenance, a more robust maximum depositional age (MDA), interpretation of volcanic grains (U–Pb age = ZHe age)

as well as a better understanding of the hinterland tectonic or erosional history that is controlling the sediment supply (Rahl et al., 2003; Campbell et al., 2005; Reiners et al., 2005; Saylor et al., 2012). Several previous studies have successfully applied zircon U–Pb–He double dating to describe sediment–routing systems and basin evolutions (Rahl et al., 2003; Campbell et al., 2005; Reiners et al., 2005; Filleaudeau et al., 2012; Saylor et al., 2012).

The Cenozoic drainage basin feeding sediment into the GOM is particularly well suited for this potent U–Pb–He double–dating approach as the United States in characterized by a plethora of U–Pb age provinces as well as a number of Phanerozoic tectonic belts with specific tectonic and exhumation histories. Only two zircon U–Pb–He double dating were carried on modern the Mississippi river sand (Reiners et al., 2005) and Pleistocene Mississippi fan deposits (Fildani et al., 2016), and no U–Pb–He double dating was applied to understand the complicated drainage system of the lower Miocene system in the Gulf of Mexico Basin. In this work, 2303 zircon U–Pb ages and 144 ZHe ages from same zircon are used to reconstruct sediment routing from continental hinters to depositional sink.

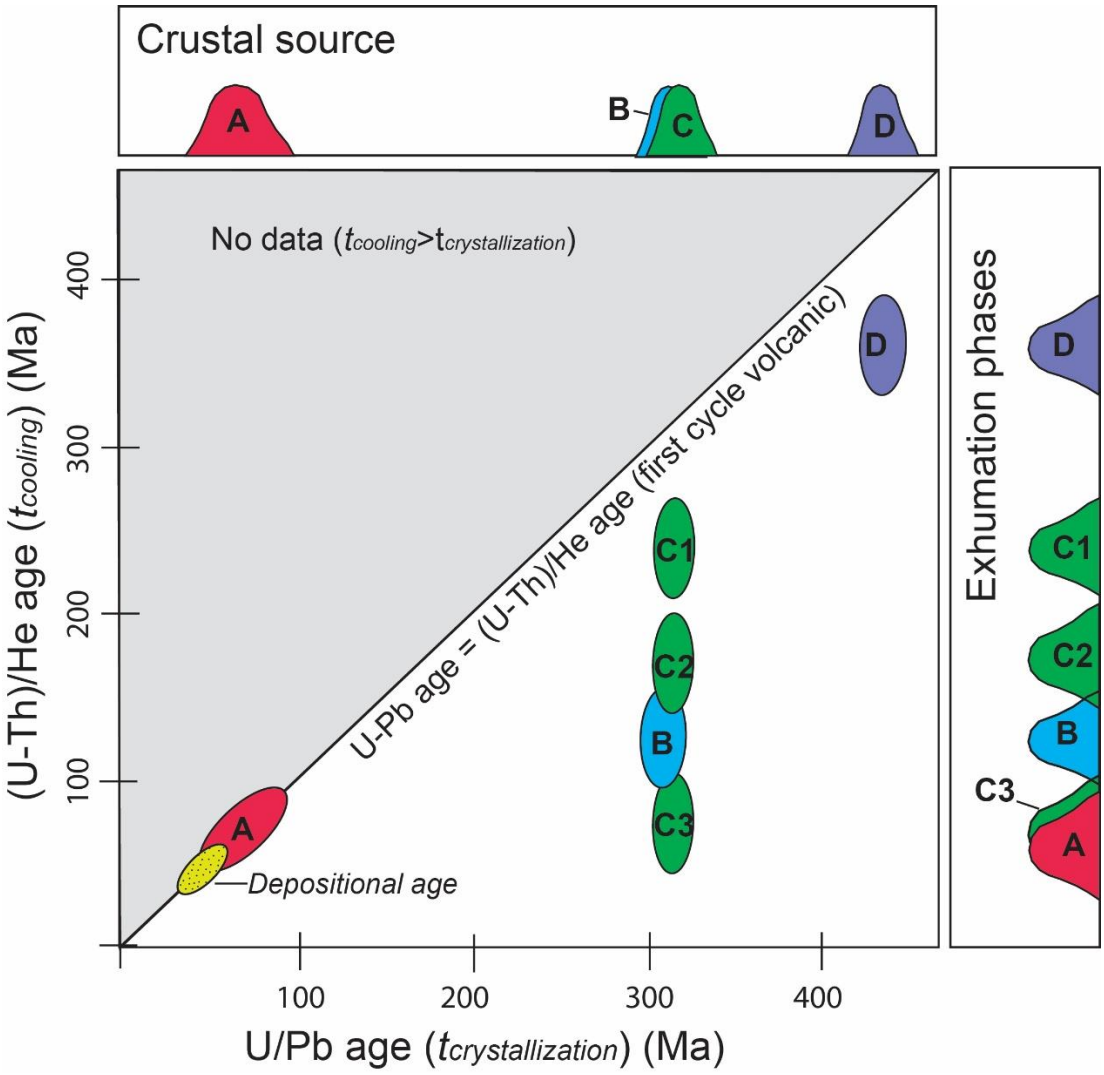

Figure 3.1: The principle of zircon double dating for differentiating sediment source areas.

Same source terrane (same U–Pb age; C) with different cooling histories (C1, C2, and C3) or different source terranes crystallized during a similar time interval (B and C) cannot be distinguished by U–Pb dating alone. Detrital zircon double dating provides much higher resolution for resolving complicated sediment sources. In addition, the minimum ZHe age can be used to constrain maximum depositional age. Modified from Reiners et al. (2005).

3.2 GEOLOGIC BACKGROUND

Many previous studies suggest that the northern Gulf of Mexico in the Cenozoic included continental–scale drainage system delivering sediment from much of North America's hinterland (e.g., Winker, 1982; Galloway et al., 2000, 2011; Galloway, 2008). Therefore, the continental crustal growth and tectonic exhumation history of North America should be understood before correlating zircon U–Pb age and ZHe age to the potential sediment source terranes.

3.2.1 Crustal assembly of North America

The cratonic core of North America is mainly composed of various Archean basements (e.g., Wyoming and Superior) which were assembled by the continent–to–continent collision during the Trans–Hudson Orogeny (2.0–1.8 Ga; Hoffman, 1988; Fig. 3.2). After assembly, the Yavapai (1.8–1.7 Ga) and Mazatzal (1.7–1.65 Ga) provinces, which are dominantly juvenile arc crust, accreted the Laurentia core to the north. An A–type granite intrusion ensued, between 1.48 and 1.35 Ga (here termed Mid–Continent; Bickford et al., 1986; Whitmeyer and Karlstrom, 2007; Fig. 3.2). A protracted period of tectonism (1.3–0.95 Ga) in eastern and southern Laurentia followed, forming the supercontinent of Rodinia. Laurentia was dominated by a rifted margin in 0.95–0.5 Ga and was followed in the Paleozoic (500–250 Ma; Hatcher, 2010; Fig. 3.2) by a series of compressional events termed the Appalachian–Ouachita Orogeny. From the Late Paleozoic to the Cenozoic, a series of Cordilleran orogenies took place in western Laurentia; by contrast, eastern Laurentia remained relatively stable after Pangean rifting in the Mesozoic.

3.2.2 Tectonic evolution and exhumation of the United States

Before the Mesozoic, the Appalachian Mountains in eastern and southeastern Laurentia was the most tectonically active highland in North America (Fig. 3.2). This

terrane was first elevated by the Grenville orogeny (1.3–0.95 Ga), providing sediment to paleorivers that flowed more than 3000 km across the Laurentian craton to the Neoproterozoic Shaler Group in northwestern Canada (Rainbird et al., 1992). The Appalachian Mountains were subsequently rejuvenated in the Paleozoic Appalachian–Ouachita Orogeny (500–250 Ma), creating a second strong exhumation phase and delivering sediment to the nearby foreland basin (e.g., Thomas et al., 2004; Park et al., 2010) and the sedimentary basins of western Laurentia (e.g., Dickinson and Gehrels, 2003, 2009). Meanwhile, the Ancestral Rockies tectonism occurred in the western U.S. was related to the Appalachian–Ouachita Orogeny to the south (Kluth and Coney, 1981; Kluth, 1986) and exhumed the local Yavapai–Mazatzal crystalline terranes and 1340 –1480 Ma Mesoproterozoic plutonic rocks (Dickinson and Gehrels, 2003). In the Late Paleozoic to Cenozoic, major erosional events shifted to the western North American highlands, due to Western Cordillera Arc activity. Major tectonic events, including the Sevier–Nevadan and Laramide orogenies and mid–Cenozoic volcanism, strongly affected highland erosion, sediment dispersal, and deposition in the northern Gulf of Mexico Basin throughout the Cenozoic (Galloway et al., 2011).

3.2.3 Depositional history of the Gulf of Mexico Basin

The Gulf of Mexico is a large passive margin basin formed as a part of Pangea rifting in the early Mesozoic (e.g., Pindell, 1985; Stern and Dickinson, 2010). During the Mesozoic it was predominantly a carbonate shelf–ramp to platform margin system that provided a few minor pulses of siliciclastic influx into the western deep–water basin (Galloway, 2008). Contributions from eastern Appalachian and Peninsular Florida basement sources were limited to coeval shelf basins of onshore areas, with the notable exception of the Ceno–Turonian siliciclastic input to the Alaminos and Keathley Canyon

deep–water protraction blocks (Weislogel et al. 2015; Snedden et al. 2016; Snedden et al. in review).

During the Cenozoic, siliciclastic sediment influx to the western Gulf of Mexico greatly increased because of the effects of the Laramide Orogeny in the Western Interior, ranging in age from 80 through 40 Ma (Galloway et al., 2011; Blum and Pecha, 2014). The Laramide event was followed by the late Eocene–Oligocene deep crustal heating in the southwestern U.S., producing widespread volcanism and volcaniclastic sedimentation in the northern Gulf of Mexico (Galloway, 1977; Galloway et al., 2000; Fig. 3.3). In the early Miocene, the mid–Cenozoic volcanism waned, but continued thermal uplift induced by magmatism caused deep erosion on the southern Great Plains, the southern Colorado Plateau, part of northeastern Mexico, and central to western Texas (Cather et al., 2012). The middle to late Miocene was characterized by the Basin and Range extension in western interior, trapping sediment derived from west getting into the northern Gulf of Mexico (e.g., Chapin and Cather, 1994; Galloway et al., 2011). In the eastern Gulf of Mexico, rejuvenation of Appalachians in the middle Miocene combined with wetter climatic conditions to increase discharge to the central and eastern Gulf of Mexico, thus increasing the sediment supply rate compared to that in lower Miocene strata (Galloway et al., 2011; Liu, 2014; Fig. 3.3).

In the Paleogene, the major depocenters of the Gulf of Mexico Basin were located in the northwestern basin margin, whereas in the Neogene, Basin and Range extension coupled with Appalachian rejuvenation shifted the axes of deposition to the central and eastern parts of the basin. Therefore, the early Miocene was a transitional period of tectonic and drainage reorganization in the U.S., and the preserved strata in the northern Gulf of Mexico document this profound change.

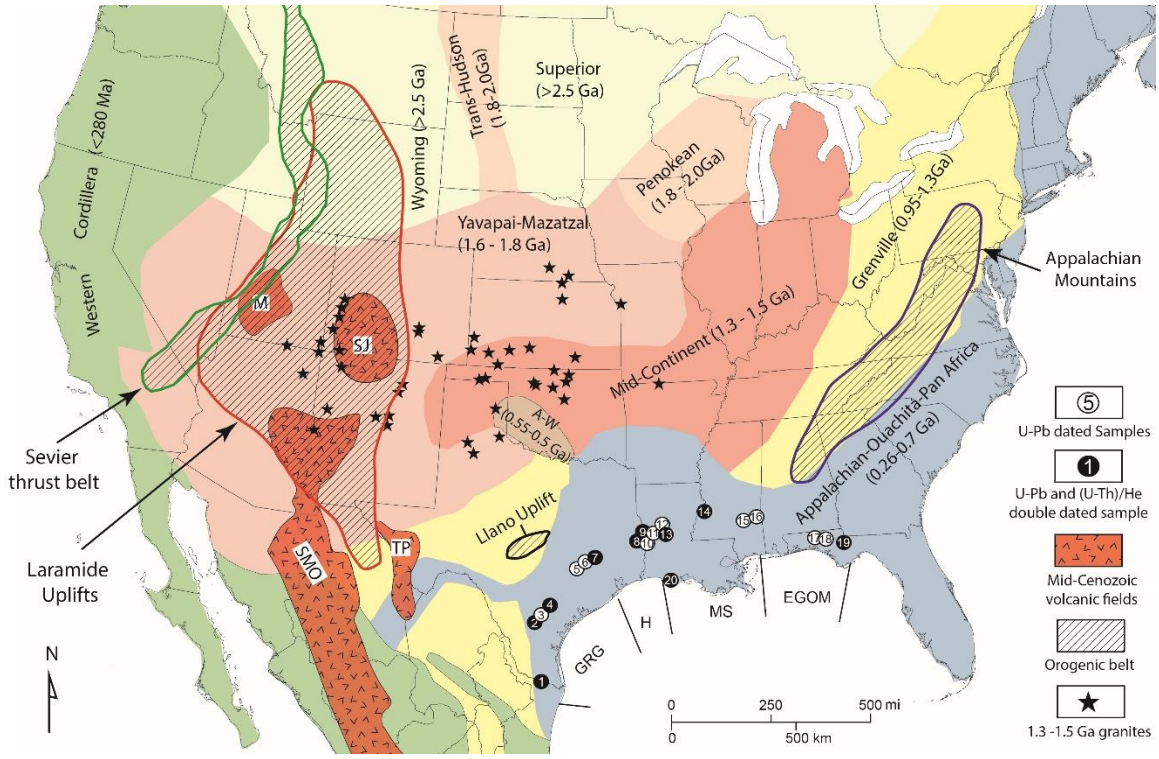

Figure 3.2: North American crustal terrains, orogenic belts, and sample locations in the northern Gulf of Mexico Basin.

The map is adapted from Gehrels et al. (2011), Blum and Pacha (2014), and Fildani et al. (2016). The term "Western Cordillera" as used here is not restricted to various batholiths (e.g., Sierra Nevada Batholith and Idaho batholith) in the Western Interior; it also includes Laramide magmatism and widespread mid–Cenozoic volcanism in southwestern North America. Abbreviations: GRG–Greater Rio Grande Embayment; H–Houston Embayment; MS–Mississippi Embayment; EGOM–Eastern Gulf of Mexico Embayment; M–Marysvale volcanic field; SJ – San Juan volcanic field; TP–Trans–Pecos volcanic field; SMO – Sierra Madre Occidental volcanic field; A–W–Amarillo–Wichita.

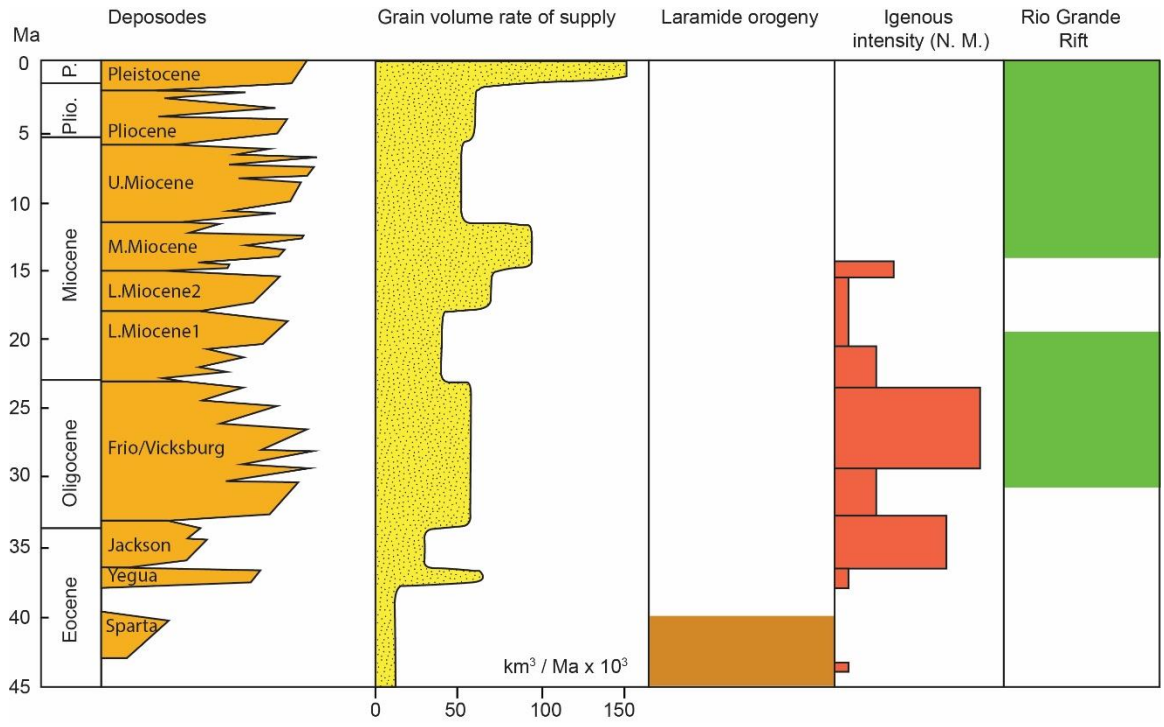

Figure 3.3: Major tectonic and depositional evolution of the Gulf of Mexico in the Cenozoic.

Columns show principal depositional episodes, tectonostratigraphic phases, and grain volume rate of sediment supply rate. Modified from Galloway et al. (2011). Abbreviations: L.–lower; M.–Middle; U.–Upper; Plio.–Pliocene; P.–Pleistocene; N.M.–New Mexico.

3.3 METHODOLOGY

For this study, 20 samples were selected from Miocene–aged strata from the entire US expanse of the GOM. For each sample, 20–25 zircons were selected for ZHe dating as to represent the entire U–Pb age signature. On average 4–5 zircons (unfractured, euhedral, >70 microns in width) were selected from each major U–Pb age component for each samples for double dating. All analyzes were conducted at the UTChron Geo– and Thermochronometry Laboratories at the University of Texas at Austin.

After conventional heavy mineral separation, detrital zircons were mounted on double–sided adhesive tape without polishing and at least 120 zircons were randomly chosen to be analyzed using laser ablation–inductively coupled plasma–mass spectrometry (LA–ICP–MS) U–Pb geochronology to obtain a statistically representative provenance dataset (Vermeesch, 2004). The analyses were completed using a PhotonMachine Analyte G.2 Excimer laser with a large–volume Helex sample cell and a Thermo Element2 ICP–MS. GJ1 was used as the primary reference standard (Jackson et al., 2004) and Pak1 (in–house 42 Ma zircon from Pakistan) as secondary reference standard. A 30 μm laser spot was used to ablate ~16 μm deep pits on the flat prism plane of the non–polished, tape–mounted zircons, providing a depth profile of each analyzed grain. This technique enables the resolution of multiple zircon growth zones evident from core and rim ages and also preserves most of the zircon for subsequent conventional ZHe dating (Stockli and Stockli, 2013). The data from the analyses were then reduced using the Iolite data reduction software and VizualAge (Paton et al., 2011; Petrus and Kamber, 2012). For increased precision and not artificially divide a cluster of analyses, the ages presented are $^{206}Pb/^{238}U$ ages for zircons younger than 850 Ma and $^{207}Pb/^{206}Pb$ ages for zircons older than 850 Ma. All ages reported use 2σ absolute propagated uncertainties, $^{207}Pb/^{206}Pb$ ages are less than 30% discordant, and $^{206}Pb/^{238}U$ ages are less than 10% discordant (Gehrels, 2011). The

discordance reported is calculated with the $^{206}Pb/^{238}U$ and $^{207}Pb/^{235}U$ ages if < 850 Ma and the $^{206}Pb/^{238}U$ and $^{207}Pb/^{206}Pb$ ages if > 850 Ma.

After depth–profile U–Pb analysis, zircons representative of each sample's major U–Pb age components, were selected for ZHe analysis following the laboratory procedures of Wolfe and Stockli (2010). Unfractured, euhedral, non–metamict zircons with a width >70 μm were morphometrically measured for alpha ejection correction and packed into 1 mm platinum tubes. Each single grain aliquot was diode laser heated for 10 minutes at ~1300°C to extract 4He and reheated for 10 minutes at ~1300°C until 4He yield dropped to <1%. Degassed zircons, unpacked from platinum foil, were dissolved using a two–step HF–HNO3 and HCl pressure–vessel digestion procedure and analyzed for U, Th ID–ICP–MS analysis using a Thermo Element2 ICP–MS. Reported ages are alpha ejection corrected (FT) and errors are standard errors (~8%, 2σ) on the basis of intra–laboratory reproducibility of the Fish Canyon Tuff standard.

The obtained zircon U–Pb–He ages are not only used to identify the crystallization and exhumation history of each source terrane, but also their age differences, Δt = U–Pb age – ZHe age, is used in this study to differentiate volcanic, plutonic, and multi–cycling zircons. Volcanic zircons will have a nearly identical U–Pb–He age within errors (Δt ~ 0) due to eruption, whereas plutonic zircons will cool gradually after crystallization and thus produce a large Δt.

3.4 RESULTS

In order to demonstrate the utility of the double–dating approach for enhanced provenance interpretation, this work presents 144 new ZHe ages from 10 samples collected from the northern Gulf of Mexico (Fig. 3.2; Table B2.1). Previously published U–Pb ages from 19 samples (GOM1–19, n = 2192; Xu et al., 2017) and 112 new U–Pb ages from one

offshore sample (GOM20; Table B1.1) were combined with ZHe ages to analyze sediment provenance (Figs. 3.2 and 3.4). The zircon U–Pb data show a broad spread of ages, but they form five major age groups: (1) 250–24 Ma, (2) 500–250 Ma, (3) 1300–950 Ma, (4) 1500–1300 Ma, and (5) 1800–1600 Ma (Fig. 3.4). A few zircons have U–Pb age of 700–500 Ma or greater than1800 Ma. Based on zircon U–Pb age clusters and sample geographic locations, the samples can be divided into four groups: (1) Greater Rio Grande Embayment, (2) Houston Embayment, (3) Mississippi Embayment, and (4) Eastern Gulf of Mexico Embayment (Figs. 3.2, and 3.4). The zircon U–Pb ages display a compositional shift from the western to eastern Gulf of Mexico, as shown in the probability curve and cumulative percentage plot (Figs. 3.4A and 3.4B).

Zircon grains analyzed for ZHe age were selected from major U–Pb age peaks from each sample. In total, 144 ZHe age were obtained to reveal the cooling history of source terranes. ZHe data display a wide spectrum of cooling (exhumation) ages ranging from Archean to Cenozoic, with the majority scattering between 500–24 Ma (Fig. 3.5).

Paleoproterozoic zircons (U–Pb age: 1800–1600 Ma) are an important component in most samples (Fig. 3.4) and 28 grains were selected for ZHe analyses. Overall, ~80% of ZHe ages are from 210–55 Ma (n=22), 10% are 400–250 Ma (n=3) and the remaining 10% are 1000–600 Ma (n=3) (Fig. 3.5). Analyses of 22 Mesoproterozoic zircons (U–Pb: 1500–1300 Ma) yield similar ZHe age populations, of which 70% are 220–40 Ma (n=16), 15% are 400–250 Ma (n=3) and the remaining 15% are 1100–600 Ma (n=3) (Fig. 3.5).

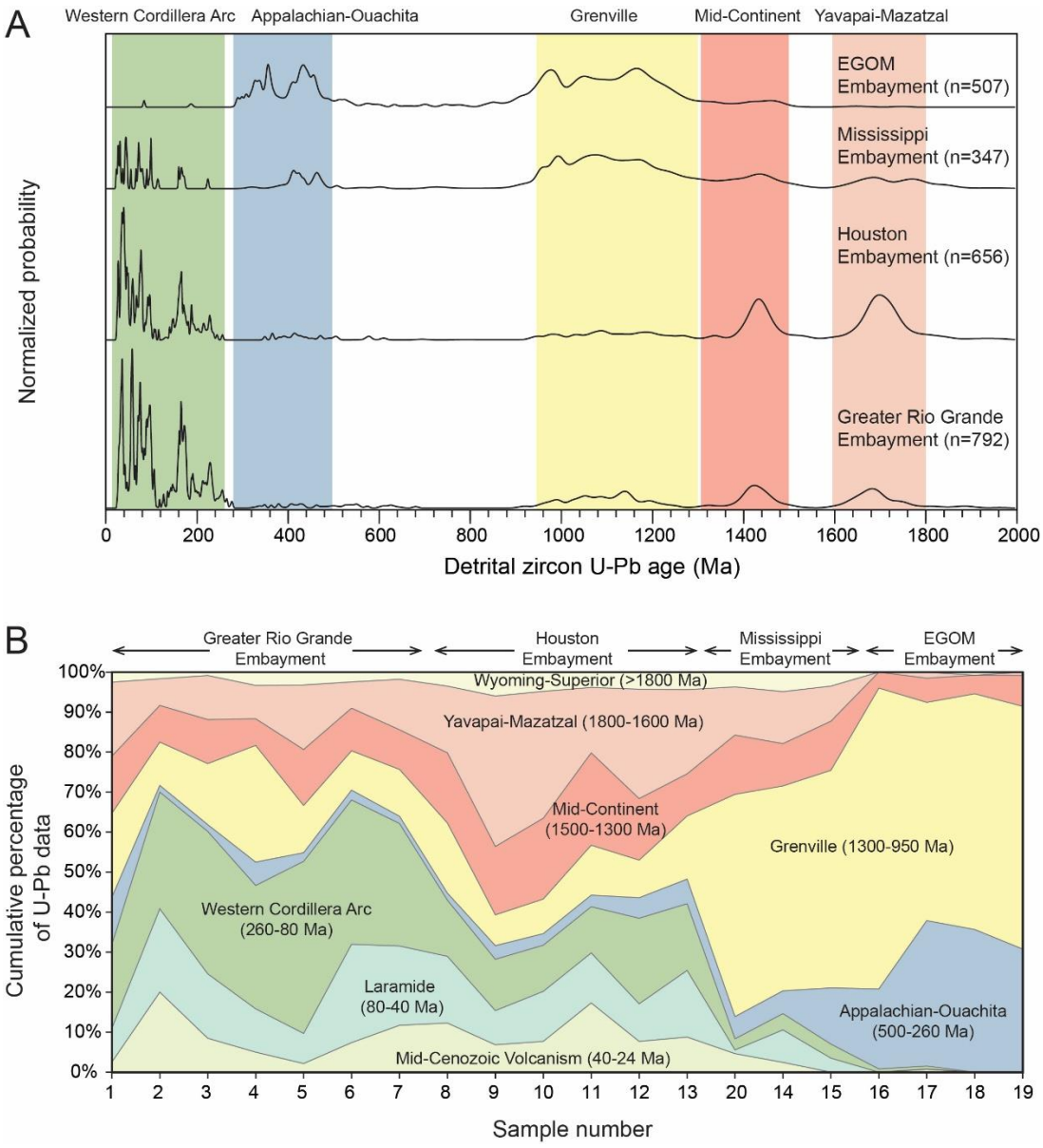

Figure 3.4: Detrital zircon U–Pb age data of 20 lower Miocene samples, northern Gulf of Mexico.

(A) Normalized probability plot of composited zircon U–Pb ages in each embayment. Only limited grains have U–Pb ages older than 2000 Ma (<5%); thus, they are omitted here. (B) Cumulative percentage plot of zircon U–Pb ages of each sample. n = number of analyses. Sample locations are shown in figure 3.2.

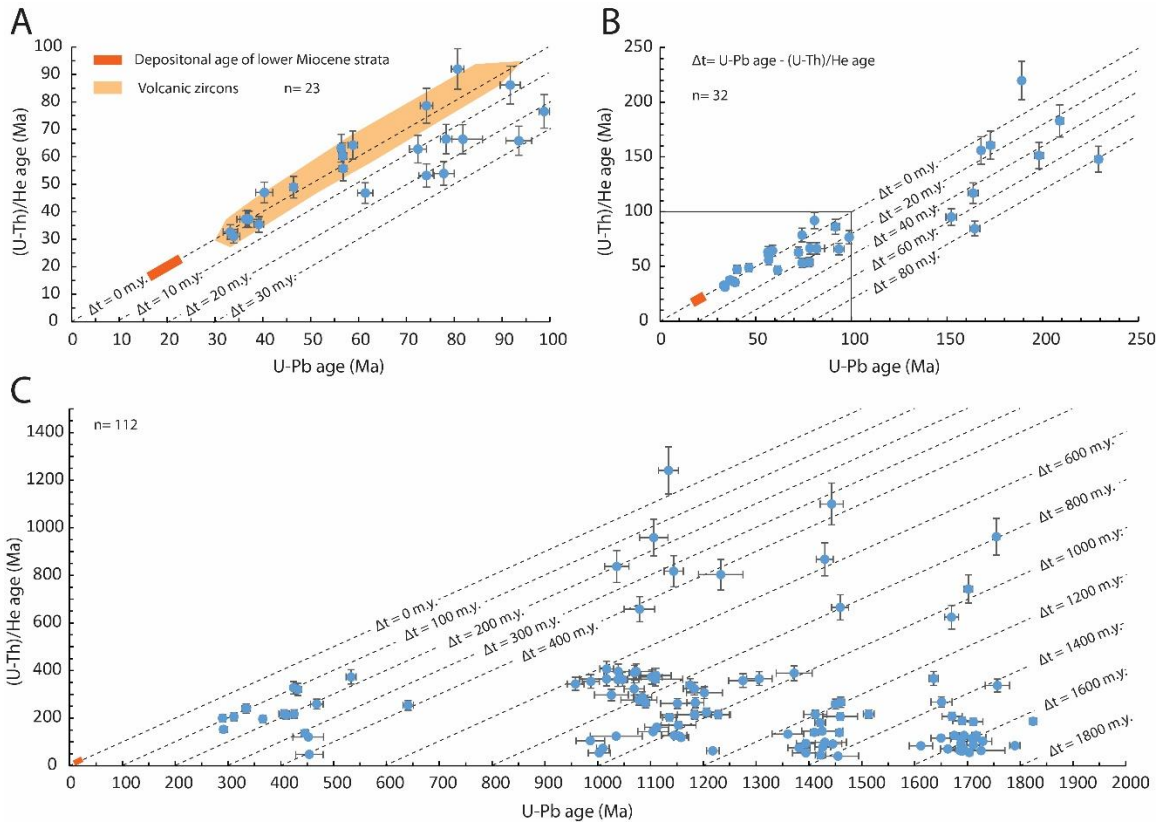

Figure 3.5: Detrital zircon U–Pb and (U–Th)/He age of the lower Miocene strata in the northern Gulf of Mexico Basin.

(A) Plot of U–Pb age (<100 Ma) versus their corresponding (U–Th)/He age. (B) Plot of U–Pb age (<250 Ma) versus their corresponding (U–Th)/He age. (C) Plot of U–Pb age (>250 Ma) versus their corresponding (U–Th)/He age.

Mesoproterozoic to Neoproterozoic zircons (U–Pb age: 1300–950 Ma) form the dominant component in samples from the Mississippi and Eastern Gulf of Mexico embayments (Fig. 3.4). Forty–six zircons from these groups were selected for ZHe analyses (Fig. 3.5). More than half of the grains (n=24; 52%) have Paleozoic ZHe ages (500–260 Ma; Fig. 3.5). Another 35% zircons yield Mesozoic ZHe ages (n=15; 230–50 Ma). The rest zircons yield Precambrian (1250–600 Ma; n=6) ZHe ages.

Only two grains were selected for ZHe dating from the 700–500 Ma group, which yield late Paleozoic ZHe ages (Fig. 3.5). Paleozoic (U–Pb age: 500–260 Ma) zircon is an important component in the Mississippi and Eastern Gulf of Mexico Embayment samples (Fig. 3.4) and 14 grains were picked to obtain ZHe ages. Three grains yield late Paleozoic ZHe age, and most of the ZHe ages are Mesozoic (n=10). Only one grain has a Cenozoic ZHe age (Fig. 3.5; Table B2.1).

Mesozoic to Cenozoic zircon (U–Pb age: <250 Ma) is the most prevalent component of samples in the Greater Rio Grande Embayment and Houston Embayment (Fig. 3.4). Thirty–two grains were analyzed for ZHe age. Most of the zircons yield ZHe ages that are within errors of their U–Pb ages (Fig. 3.5A). Only a few grains yielded ZHe ages 80–20 Myr younger than the U–Pb age (Fig. 3.5 and Table B2.1).

3.5 Interpretation and Discussion

Continental–scale drainage systems, such as the Mississippi River, drain vast continent hinterland and transport sediments derived from various crystalline terranes as well as recycled sedimentary cover sequences which conventional zircon U–Pb approach cannot distinguish from a primary source. Multiple terranes with indistinguishable crystallization ages in the drainage system (e.g., Grenville basement in Laurentia) further complicated the interpretation, as these zircons cannot be spatial attributed. However,

zircon U–Pb–He double dating has the potential not only to identify first cycle volcanic and plutonic zircons, but also to differentiate and better spatially attribute multi–cycle zircons from different parts of the drainage basin. Grenville basement is exposed from eastern Canada to southern Mexico, but given its abundance and zircon fertility (Moecher and Samson, 2006; Dickinson, 2008), is usually ignored as they are regarded as not very diagnostic. This work demonstrates how the combination of U–Pb–He double dating exploit this Grenville signal and provide more provenance information. This is illustrated by an enhanced provenance interpretation for the continental–scale sediment routing of the Gulf of Mexico basin. Subsequent section discusses the U–Pb and U–Pb–He data and their implication for Miocene drainage in the Gulf of Mexico.

3.5.1 U–Pb provenance analysis

Zircon U–Pb age spectra in the Greater Rio Grande Embayment samples are dominantly Mesozoic to Cenozoic (260–24 Ma; Fig. 3.4), corresponding to Cordilleran magmatic activity, Laramide–related magmatism, and mid–Cenozoic volcanism in western North America (Chen and Moore, 1982; Ducea, 2001; DeCelles, 2004; Chapin et al., 2004). Grenville (1300–950 Ma), Mid–Continent (1500–1300 Ma), and Yavapai–Mazatzal (1800–1600 Ma) zircons are secondary components, indicating a strong influence from these earlier source terranes.

Zircon U–Pb age spectra in the Houston Embayment samples show prominent peaks of Mid–Continent and Yavapai–Mazatzal components, indicating increased sediment sourcing from Laramide uplifts. These Mid–Continent and Yavapai–Mazatzal basements formed the core of the southern Rocky Mountains, becoming exhumed during the Cenozoic (Tweto, 1975). The Western Cordillera component was still influential, but it decreased eastward.

The U–Pb age spectra of the Mississippi Embayment samples differ distinctly from the age spectra of Houston Embayment samples. The Mississippi Embayment samples show the predominance of Grenville zircon. The Western Cordillera component is secondary, but combined with the Mid–Continent and Yavapai–Mazatzal components, it still constitutes about 30% of the total U–Pb age population in the Mississippi Embayment samples. The U–Pb age spectra indicate a strong sediment supply from both highlands in the western U.S. and Appalachian terranes in eastern North America (Xu et al., 2017). The Eastern Gulf of Mexico Embayment samples are dominated by the Appalachian–Ouachita (500–260 Ma) component and the Grenville component, indicating a major source from the proximal southern Appalachian Mountains.

Zircon U–Pb dating revels an ultimate sediment source from the Yavapai–Mazatzal, Mid–Continent, Grenville, Appalachian–Ouachita, and Western Cordillera Arc terranes. The intermediate sediment storage along the source–to–sink transect could be remobilized and become important sediment contributor, however, is below the resolution of U–Pb dating and bias true provenance interpretation. Yavapai–Mazatzal, Mid–Continent, and Grenville zircons are both documented in many sedimentary basins of North America and lower Miocene samples, making provenance interpretation ambiguous.

3.5.2 Zircon U–Pb–He double dating

3.5.2.1 Differentiating volcanic zircon from plutonic zircon

Zircons can be from volcanic, plutonic, or sedimentary rocks by recycling, but single U–Pb provides only the crystallization time and thus has no ability to differentiate these sources. Zircon U–Pb–He double dating offers additional constraints for differentiating volcanic from plutonic zircon, by comparing the age difference (defines as Δt) between crystallization and cooling events (Reiners et al., 2005; Campbell et al., 2005;

Saylor et al., 2012; Fig. 3.5). Volcanic originated zircon is characterized by a very short time difference between crystallization and eruption and thus has U–Pb ages and ZHe ages within errors ($\Delta t \sim 0$).

All zircons with U–Pb ages of 40–30 Ma (n=8) have ZHe ages within errors, suggesting that these grains represent first–cycle zircon from volcanic or hypabyssal rocks (Fig. 3.5A). The prevalent Eocene–Oligocene volcanic fields in the southwestern U.S. are the likely source of these zircons (Chapin et al., 2004; Reiner et al., 2005). However, the Rio Grande Rift, initiated in the late Oligocene–early Miocene, has acted as a sediment barrier and prevented a large volume of material from volcanic fields to the west (e.g., the San Juan and Mogollon–Datil volcanic fields) from entering into the northern Gulf of Mexico (Chapin and Cather, 1994; Galloway et al., 2011; Xu et al., 2017). The Trans–Pecos volcanic fields in West Texas are a major contributor of volcanic zircons. An alternative source could be the volcanic–rich Eocene–Oligocene strata on the southern Greater Plains, where deep erosion (> 1 km) occurred during the early Miocene (Reiners et al., 2005; Cather et al., 2012). The volcanic–source hypothesis is also supported by the abundance of volcanic rock fragments in the lower Miocene Oakville Formation of the Texas coastal plain (Dutton et al., 2012).

A few grains (n=6) showing an 80–40 Ma crystallization and eruption event (Fig. 3.5A) appear to be related to Laramide magmatism in the western U.S., indicating a likely source from the Colorado Mineral Belt (Chapin, 2012) or the Laramide porphyry copper province in southwestern New Mexico and northern Mexico (Chapin et al., 2004; Barra et al., 2005). One grain has ~90 Ma and two grains have ~180–160 Ma U–Pb–He ages that are possibly eroded from the Sierra Nevada batholith (Chen and Moore, 1982; Ducea, 2001; DeCelles et al., 2009). A zircon with U–Pb age of 1134 Ma yielded a Proterozoic

ZHe age (~1241 ± 99 Ma) that suggests a rapidly cooled zircon from the Grenville orogeny (Fig. 3.5C).

Only in the rare case of extremely rapid exhumation would the non–volcanic ZHe age approach the U–Pb age (Saylor et al., 2012). Plutonic zircons are generally slowly cooled and unroofed with Δt commonly longer than 10 Myr (Fig. 3.5). Most plutonic zircons of Western Cordillera Arc (U–Pb age < 260 Ma) has Δt between 0 and 40 Myr (n=11) with three grains yield Δt from 40 to 80 Myr. The relative short Δt of these zircons agree with the active Mesozoic–Cenozoic continental assembly in the western North America.

3.5.2.2 Differentiation of Grenville zircons by U–Pb–He double dating

Grenville zircons appear in all samples and constitute an important component (Fig. 3.4). However, provenance for these zircons is hard to assign to a particular source, because multiple Grenville aged terranes located adjacent to the Gulf of Mexico Basin, including Appalachian Mountains in eastern North America, the Llano Uplift in Central Texas, and the Grenville basement in Mexico, which all could be possible source terranes. In addition, many sedimentary basins of North America were documented to contain abundant Grenville zircons, for example Appalachian foreland basin (Park et al., 2010), Western Canada Sedimentary Basin (Leier and Gehgrels, 2011; Blum and Pecha, 2014) and Permian–Jurassic sandstones on the Colorado Plateau (Dickinson and Gehrels, 2003, 2009; Rahl et al., 2003), and they all likely contribute multi–cycled zircons to the Gulf of Mexico basin. Using U–Pb ages alone is insufficient in detecting these differences and obscures detailed provenance interpretation (Fig. 3.1).

In total, 46 Grenville zircons are selected for ZHe analyses. The generated ZHe data display a wide range from Mesoproterozoic to Paleocene (~1300–50 Ma) and large

variety in geography from western to eastern Gulf of Mexico (Fig. 3.6A). A few Grenville zircons (n=6) contain ZHe age between 1200 and 600 Ma (Fig. 3.6A), probably exhumed during the ancient Grenville orogenies that assembly of supercontinent Rodinia in eastern Laurentia. Previous zircon U–Pb work on the Neoproterozoic Shaler Group in northwestern Canada documented an abundance of Grenville zircons, suggesting that most of the detritus was derived from the Grenville orogenic belt in eastern North America and was carried by transcontinental rivers (Rainbird et al., 1992). Therefore, one possible source of these Grenville grains with Proterozoic ZHe ages is recycled from the Precambrian strata that deposited along the paleo–sediment transport pathway. The Llano Uplift in Central Texas could be an alternative Grenville zircon source (Mosher, 1998). The Grenville basement in the Llano Uplift was buried during most of the Phanerozoic and was not experienced intensive erosion until in the early Miocene (Corrigan et al., 1998; Ewing, 2005). Zircons may reside in the shallow crustal for a protracted time and retain the Proterozoic ZHe age until exhumation occurred during the Miocene (Fig. 3.6B).

Twenty–four or 53% of doubly dated Grenville grains yielded a Paleozoic ZHe age (500–260 Ma; Fig. 3.6A), corresponding to the Appalachian–Ouachita orogeny; this strongly suggests an ultimate origin from the Appalachian terranes in eastern North America. For the samples in the Mississippi Embayment, this is consistent with the paleogeographic reconstruction that the paleo–Mississippi River taped the Appalachian–Ouachita Mountains and foreland basin in early Miocene (Galloway et al., 2011). However, it is unlikely that the sediment derived from the Appalachian areas crossed the paleo–Mississippi river and reached the Greater Rio Grande and Houston embayments in the early Miocene. Previous zircon work on the Upper Cretaceous and Paleogene Wilcox strata in the northern Gulf of Mexico suggests that the paleo–Mississippi River formed during the early Paleocene, carrying sediment from the Appalachian Mountains southward to the Gulf

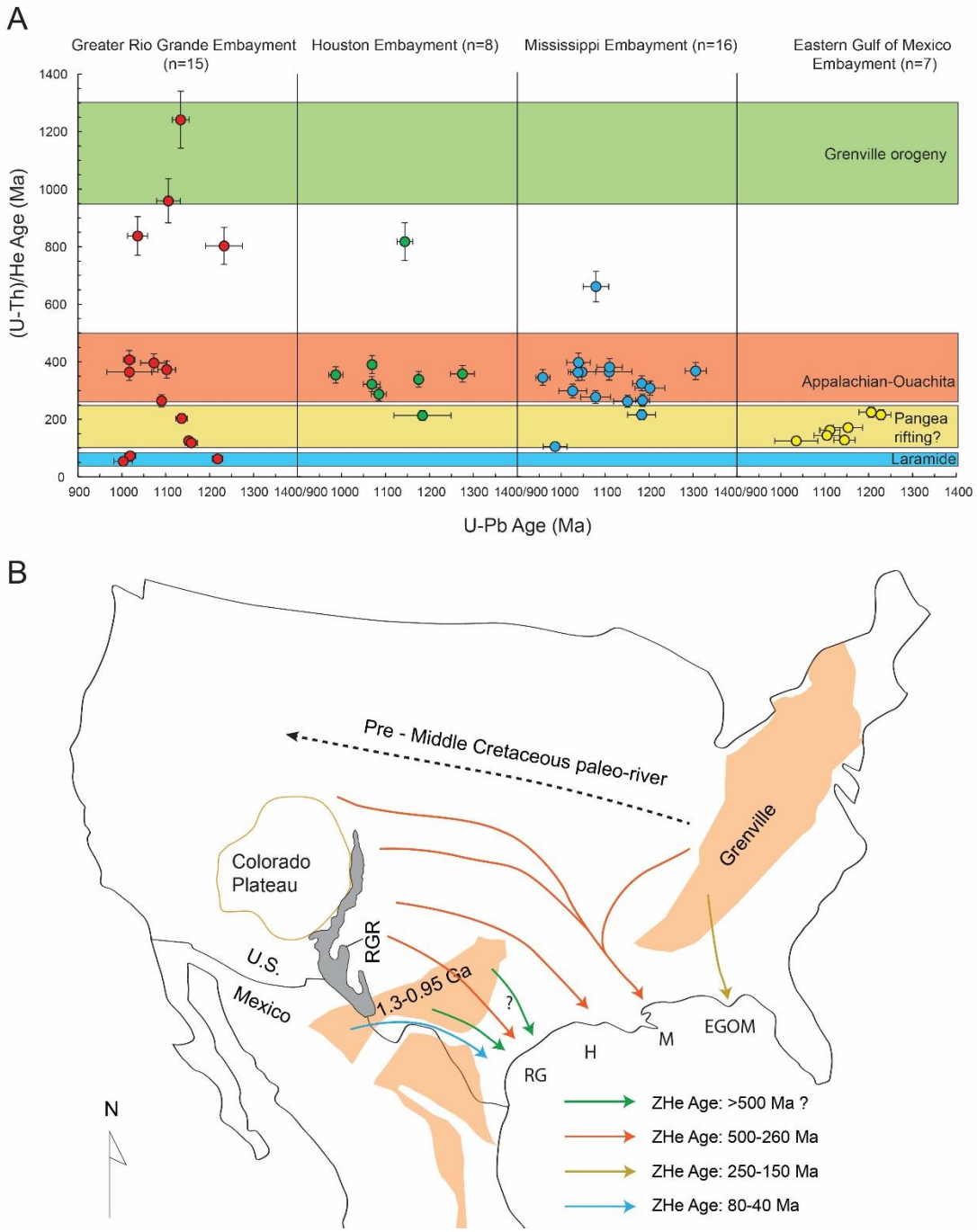

Figure 3.6: Continued next page.

Figure 3.6: U–Pb–He ages and routing of Grenville zircons.

(A) U–Pb–He ages of Grenville zircons in the lower Miocene strata of the Gulf of Mexico basin, (B) Sediment routing of Grenville grains. Pre–Middle Cretaceous paleoriver was proposed by Rahl et al. (2003), Dickinson and Gehrels (2009), and Blum and Pecha (2014). RGR – Rio Grande Rift. n = number of analyses. Color bars indicate different orogenic events.

of Mexico (Blum and Pecha, 2014). More likely, these grains are an erosional product of older strata deposited in the western United States. Pre–Cenozoic strata, e.g., Cenomanian strata in the northern Gulf of Mexico (Blum and Pecha, 2014) and Triassic fluvial sandstone on the Colorado Plateau (Dickinson and Gehrels, 2009) all contain a high percentage of Grenville zircon that were brought from the Appalachian terranes by westward–flowing paleorivers (Fig. 3.6B). Zircon double dating on the Lower Jurassic Navajo Sandstone of southwestern Utah has documented a combination of Grenville crystallization and Appalachian–Ouachita exhumation ages that similar to the U–Pb–He age combination in the lower Miocene strata in this study (Rahl et al., 2003). Therefore, zircons with combined 1300–950 crystallization age and 500–260 Ma cooling age in western Gulf of Mexico are more likely from multi–cycled sedimentary strata, instead of being directly derived from the Appalachian terranes in eastern North America (Fig. 3.6B).

All Grenville zircons (n=7) observed in the Eastern Gulf of Mexico Embayment display much younger Mesozoic ZHe ages (230–100 Ma; Fig. 3.6A), indicating erosions of the southern Appalachian Mountains after the Alleghenian orogeny. The Pangean rifting in the eastern U.S. is the likely mechanism that created topographic highs of Grenville basement for increased exhumation during the Mesozoic (Weislogel et al., 2015). Three Grenville zircons from the Greater Rio Grande Embayment and one zircon from the Houston Embayment also contain similar Mesozoic ZHe ages (Fig. 3.6A), but are not related to any known tectonism within Grenville terranes in the western North America. Zircon U–Pb analysis of the Cenomanian Woodbine–Tuscaloosa Formation (ca. 100–94 Ma) in the Gulf of Mexico suggests a drainage connection between the Appalachian highlands and western U.S. prior to 100 Ma (Blum and Pecha, 2014). It is likely that these

grains are recycled from Mesozoic strata deposited in the western U.S. (e.g., the Great Plains), with their ultimate source having been the Appalachian Mountains in the east (Fig. 3.6B). Two zircons cooled through Mesozoic time in the Mississippi Embayment can be either recycled from sedimentary strata or from eroding the southern Appalachian Mountains (Figs. 3.6A and 3.6B).

Three Grenville zircons from the Greater Rio Grande Embayment yielded ZHe ages of 73 Ma, 63 Ma and 54 Ma, respectively (Fig. 3.6A), corresponding to the Laramide Orogeny in the western U.S. The likely source could be the Grenville exposure in western Texas (such as the Franklin Mountains) and northern Mexico, which were affected by the Laramide Orogeny of 80–40 Ma (Figs. 3.6A and 3.6B).

3.5.2.3 Differentiation of older Meso– and Paleoproterozoic zircons

Doubly dated Yavapai–Mazatzal (n=28) display a wide range of ZHe ages (1100–55 Ma; Fig. 3.7A), indicating a protracted history of erosion. Three grains contain Precambrian cooling age (1100–624 Ma) that might be related to the assembly of Rodina to the southern Laurentia, with the older grain (ZHe = 1100 Ma) exhumed during the Grenville orogeny and two slightly younger grains (624 and 742 Ma) cooled long time after orogeny. Rahl et al. (2003) observed a similar U–Pb and ZHe age combination in the Jurassic Navajo Sandstone and suggested that the grains were elevated to the shallow crust and resided there for a long time before the exhumation occurred during the Ancestral Rockies tectonism in Pennsylvanian time. Three Paleozoic–Triassic ZHe ages (366–267 Ma) roughly correlate with the Ancestral Rockies orogeny and are exhumed in Ancestral Rockies province and deposited in adjacent basins, e.g., Carboniferous–Permian (Gehrels and Pecha, 2014) and Permian–Jurassic rocks (Dickinson and Gehrels, 2003). These above zircons are possibly incorporated into the lower Miocene strata by recycling. Triassic to

Early Cretaceous ZHe ages (n=16) could be derived from Sevier–Nevada orogenic terranes, and Late Cretaceous to Paleogene ZHe ages (n=6) are from the Laramide Uplifts (Fig. 3.7).

Mid–Continent Granite–Rhyolite zircons (n=22) shows a similar ZHe pattern to that of Yavapai–Mazatzal zircons, with cooling ages from 1100 to 40 Ma (Fig. 3.7A). Precambrian ZHe ages only constitutes ~15% of doubly dated Granite–Rhyolite zircons (n=3), with one zircon (ZHe=1100 Ma) cooled during Grenville orogeny and another two grains cooled 100–300 Myr after the orogeny (Fig. 3.7A). Three Paleozoic cooled zircons (390–250 Ma) are possibly exhumed during the Ancestral Rockies, as the ZHe age only a few millions year predate or postdate the orogeny. Most of zircons are cooled from Late Triassic–Late Cretaceous (220–90 Ma; n=11) and Late Cretaceous–Paleogene (80–40 Ma; n=5), corresponding to Sevier–Nevadan and Laramide orogenies in western North America.

Both Mid–Continent and Yavapai–Mazatzal grains have large numbers of ZHe ages related to the Sevier–Nevada Orogeny (Fig. 3.7A), indicating an original source from the Nevada and Sevier thrust belts. However, paleostreams that collected materials from the Sevier–Nevada terranes probably carried the sediment to the Pacific Northwest rather than to the Gulf of Mexico in the late Oligocene–early Miocene (Cather et al., 2012). Previous work suggests a drainage connection between the Cordillera thrust terranes and the Gulf of Mexico from latest Cretaceous to Eocene time (Lawton, 2008). The Upper Cretaceous–Paleogene strata on the Great Plains, which received these zircons were remobilized in early Miocene, could be a more likely intermediate source (Cather et al., 2012; Xu et al., 2017).

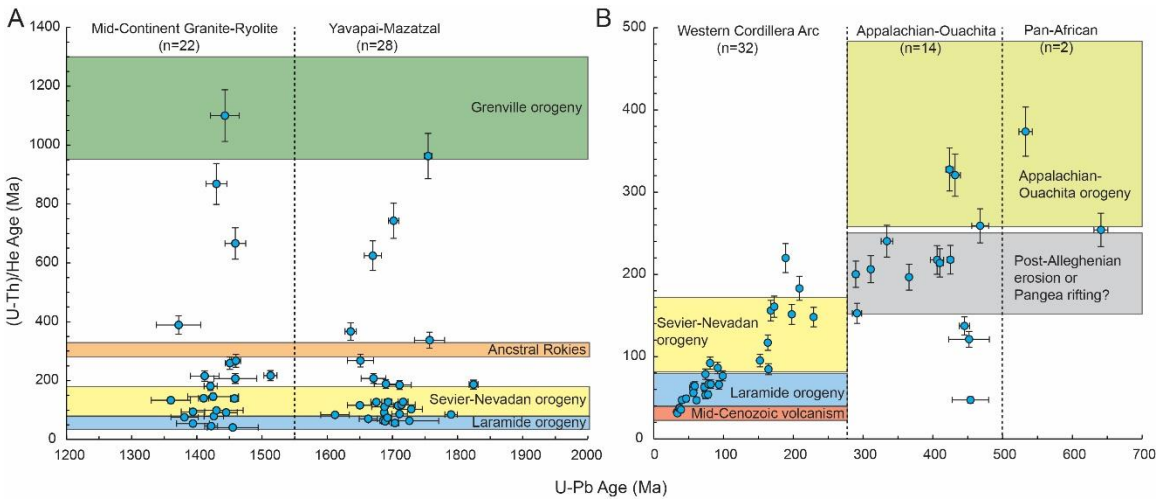

Figure 3.7: U–Pb–He ages of Neoproterozoic–Cenozoic zircons.

(A) U–Pb–He ages of Yavapai–Mazatzal and Mid–Continent Granite–Rhyolite zircons. (B) U–Pb–He ages of Pan–African, Appalachian–Ouachita, and Western Cordillera Arc zircons. n = number of analyses. Color bars indicate different orogenic events.

3.5.2.4 Differentiation of Neoproterozoic–Cenozoic zircons

Two Neoproterozoic zircons (U–Pb age: 700–500 Ma) from the Greater Rio Grande Embayment yield Paleozoic Appalachian–Ouachita cooling ages (500–260 Ma; Hatcher, 2010; Fig. 3.7B), indicating an origin from the peri–Gondwanan terranes (e.g., Carolina terrane) in eastern North America. For nonwestern Gulf of Mexico margin in the early Miocene, arrival of these Gondwanan–Affinity sources from eastern North America would be implausible, but previous zircon work on Permian–Jurassic sandstone on the Colorado Plateau documented U–Pb peaks of 500–700 Ma and 1000–1300 Ma, suggesting a sediment flux from the residual highlands of the Appalachian terranes before Jurassic (Dickinson and Gehrels, 2003). Neoproterozoic zircons are therefore likely eroded from the older sedimentary strata in western United States, with ultimately source from the eastern Larentia.

Paleozoic zircons (U–Pb age: 500–260 Ma) have only three synorogenic grains that cooled during the Alleghenian orogeny (ZHe age: 327–259 Ma; Fig. 3.7B). A few grains with slightly younger ZHe age (240–190 Ma; n=7) could be post–Alleghenian erosion or related to the Pangea rifting that rejuvenated the topography and increased exhumation rate (Weislogel et al., 2015; Pazzaglia et al., 2015). Late Jurassic– Early Cretaceous cooling ages (160–120 Ma; n=3) are not related to any orogenic event in eastern North America, but were reflected by relative high sediment flux both to Atlantic margin and Gulf of Mexico basins (Poag and Sevon, 1989; Galloway, 2008; Snedden et al., 2016). Only one grain yields ZHe age in Eocene (Fig. 3.7B), this is consistent with the tectonic quiescence, slow sedimentation rate and widespread carbonate deposition in eastern Gulf of Mexico margin (Galloway, 2008).

Thirty–two Mesozoic–Cenozoic zircons (U–Pb age: 230–24 Ma) contain most of ZHe ages falling in groups of 170–80, 80–40, and 40–24 Ma, corresponding to cooling

events of Sevier–Nevadan, Laramide, and mid–Cenozoic volcanism, respectively (Fig. 3.7B). As discussed above, many of these grains are first–cycle zircons eroded from Cretaceous–Cenozoic volcanic fields in the western United States (Reiners et al., 2005; Fildani et al., 2016). A few grains cooled during 80–40 Ma are from Laramide magmatism in northern Mexico and southwestern New Mexico or Colorado Mineral Belt, whereas the grains cooled during 170–80 Ma are probably derived from igneous rocks in the Sevier–Nevada Thrust Belt. However, the Rio Grande Rift, initiated in the late Oligocene to early Miocene, prevented large volumes of western sediment from reaching the northern Gulf of Mexico. It is likely that some zircons are from easily eroded sedimentary strata that temporally stored on the Great Plains.

3.5.3 Enhanced provenance interpretation for Miocene in Gulf of Mexico Basin

Low–temperature thermochronology ZHe analysis provides the cooling history of source terranes, adding another dimension for resolving sediment sources when combined with zircon U–Pb dating. A multi–component analysis of zircon U–Pb–He double dating is therefore developed as a workflow to interpret the complicated sediment sources of the lower Miocene strata in each embayment (Fig. 3.8). Take the Greater Rio Grande Embayment for example, 13 cooling histories from 4 major zircon U–Pb components could be identified (Fig. 3.8; will be discussed below), greatly improving our understanding of the complicated sediment source history for a large passive margin basins like the Gulf of Mexico.

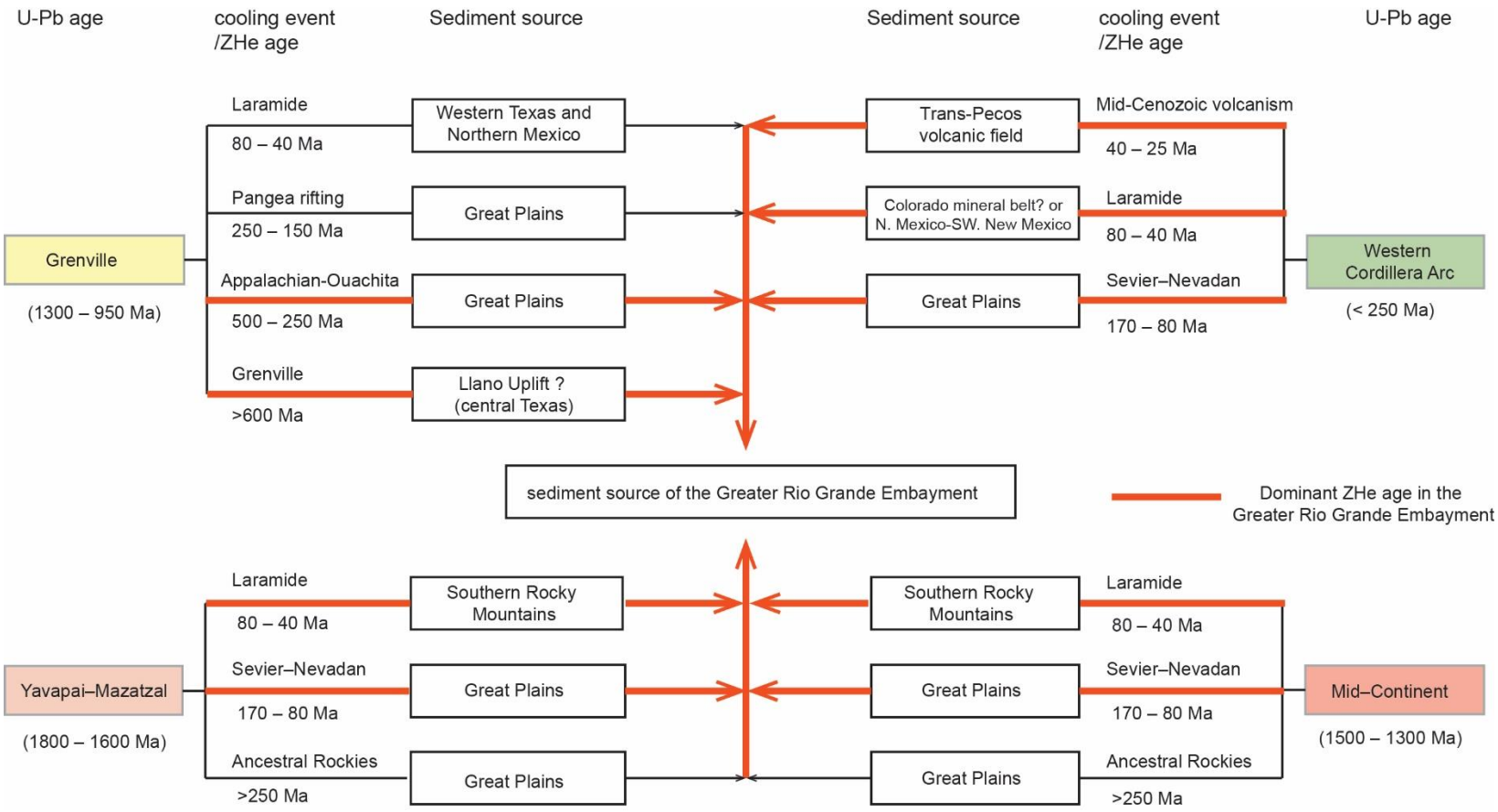

Figure 3.8: Provenance interpretation using U–Pb–He double dating.

Multicomponent analysis of the U–Pb and (U–Th)/He data from samples in the Greater Rio Grande Embayment, illustrating the complicated sediment source history in the northwestern Gulf of Mexico.

3.5.3.1 Greater Rio Grande Embayment provenance

Zircon U–Pb–He dating on the samples in the Greater Rio Grande Embayment show strong sediment flux of Western Cordillera Arc terranes, as characterized by young crystallization ages (<260 Ma) and cooling ages of Sevier–Nevadan and Laramide orogenies and mid–Cenozoic volcanism (Fig. 3.9). However, the Rio Grande Rift, initiated in the late Oligocene–early Miocene, has acted as a sediment barrier and prevented a large volume of material from highlands to the west of Rio Grande Rift (e.g., Sevier–Nevada–thrust–belt, San Juan and Mogollon–Datil volcanic fields) from entering into the northern Gulf of Mexico (Chapin and Cather, 1994; Galloway et al., 2011; Xu et al., 2017). Instead, zircons with cooling ages corresponding to the Sevier–Nevadan orogeny are probably eroded from the Cretaceous–Paleogene sedimentary strata of the Great Plains. Trans–Pecos volcanic field in West Texas and Colorado Mineral Belt are likely primary igneous source (Fig. 3.8).

A few Meso– and Neoproterozoic Grenville and Pan–African zircons (U–Pb: 1300–500 Ma) that cooled during or after Appalachian–Ouachita orogenic (500–150 Ma) are multi–cycling zircons from eroding sedimentary strata in western U.S. (e.g., Great Plains), but ultimately derived from eastern North America (Figs. 3.8 and 3.9A). Precambrian ZHe age for Grenville zircons probably indicate a source from the Llano uplift in central Texas, whereas much younger ZHe ages (80–40 Ma) suggest a likely source from Grenville basement in westernmost Texas and northern Mexico (Figs. 3.6B and 3.9A).

Paleo– and Mesoproterozoic Yavapai–Mazatzal and Granite–Rhyolite zircons that exhumed during the Laramide orogeny (80–40 Ma) strongly indicate a primary source from the southern Rocky Mountains (Figs. 3.8 and 3.9A). Mesozoic cooled zircons are derived from the Sevier–Nevada–Thrust–Belt, but due to the Rio Grande rifting in early Miocene

the intermediate source could be from sedimentary strata on the Great Plains where deep erosion occurred in late Oligocene–early Miocene (Cather et al., 2012). Yavapai–Mazatzal and Granite–Rhyolite zircons with ZHe ages of 400–300 Ma (n=2) are likely erosional products of Ancestral Rockies in Paleozoic and entering the Gulf of Mexico by recycling. The remaining two grains have yielded older Precambrian ZHe age (700–600 Ma), might be elevated during the Grenville orogeny, but reside at the shallow crust prior to next orogenic event (Rahl et al., 2003). The intermediate source is hard to define for these Precambrian cooled zircons, but possibly eroded from sedimentary strata in western North America (e.g., Great Plains; Fig. 3.8).

3.5.3.2 Houston Embayment provenance

Zircon U–Pb–He double dating on the Houston Embayment samples yields a pattern similar to that of the Greater Rio Grande Embayment samples. However, the Grenville grains have fewer Precambrian ZHe ages (Fig. 3.9B) and no grains have Laramide orogeny (80–40 Ma) ZHe ages. This indicates a weak drainage connection to the Grenville exposures in the Llano Uplift and in western Texas and northern Mexico, which is consistent with previous paleogeographic work (Galloway et al., 2011; Xu et al., 2017; Fig. 3.6B). The Paleozoic ZHe ages (500–260 Ma) become more dominant among Grenville grains (Fig. 3.9B), indicating that the sediment recycled from the older strata on the Great Plains is increased (Figs. 3.6B and 3.8). Increased amounts of Mid–Continent and Yavapai–Mazatzal zircons in the Houston Embayment (Fig. 3.4), coupled with associated ZHe ages that fall in the time range of the Laramide Orogeny (Fig. 3.9B), indicate an increasing sediment supply from the southern Rocky Mountains.

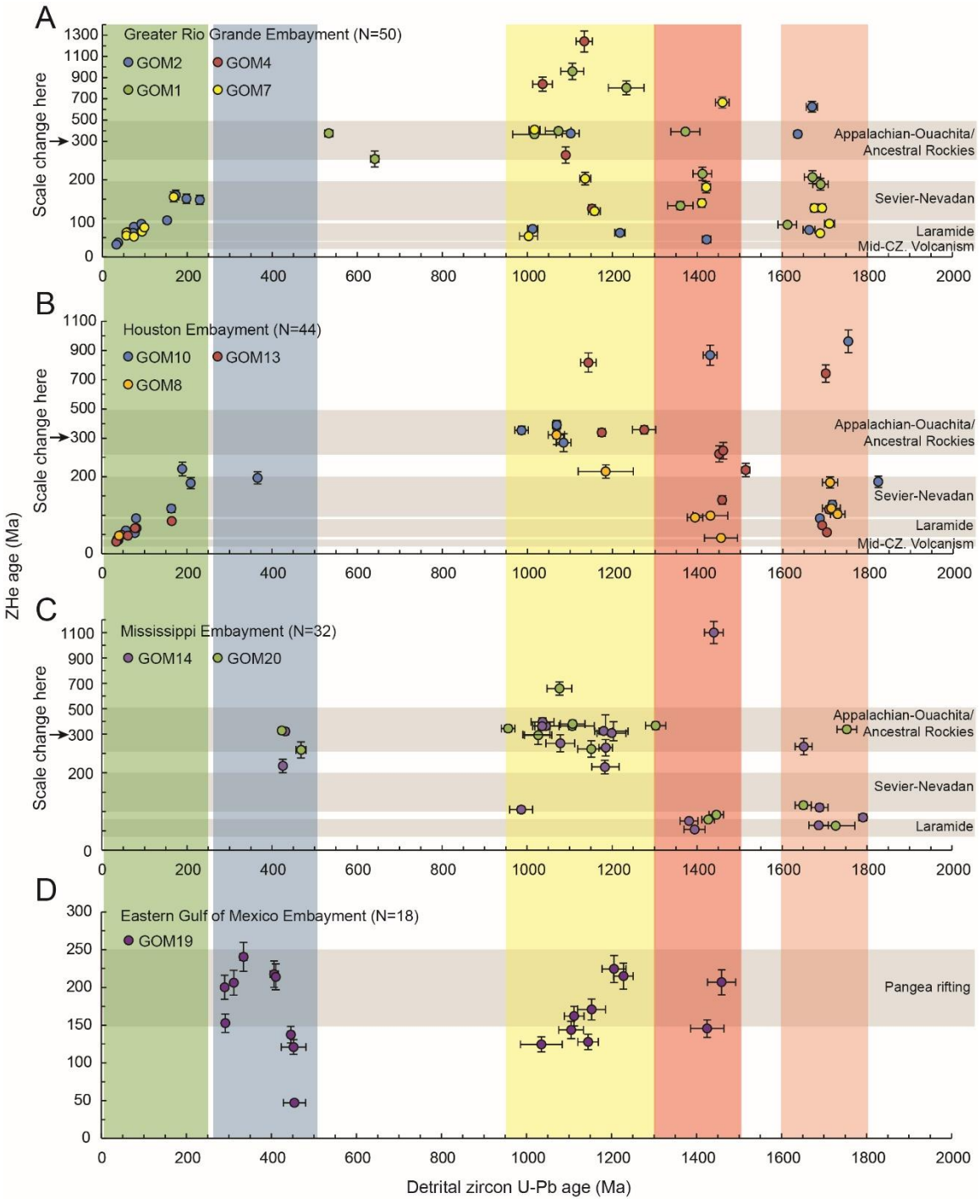

Figure 3.9: Continued next page.

Figure 3.9: Sedimentary provenance interpretation of lower Miocene strata.

Sedimentary provenance interpretation of lower Miocene strata, northern Gulf of Mexico, based on detrital zircon U–Pb and (U–Th)/He double dating. Sample locations are shown in figure 3.2. The color bar highlights major crustal crystallization and cooling events of source terranes in North America. CZ – Cenozoic.

3.5.3.3 Mississippi Embayment provenance

The Mississippi Embayment samples have different U–Pb–He age combination compared to samples in the Greater Rio Grande and Houston embayments (Fig. 3.9C). Most of the cooling ages extracted from Grenville grains are in the range of 500–260 Ma, corresponding to the Appalachian–Ouachita orogeny. Such a combination of Grenville U–Pb age and Appalachian–Ouachita ZHe age (Fig. 3.9C) strongly suggests a primary source from the Appalachian Mountains and foreland basins. Additional evidence was provided by the high abundance of Grenville zircon (>50%; Fig. 3.4), which is commonly observed in strata of eastern North America (Park et al., 2010; Blum and Pecha, 2014). However, a few of these grains might be recycled from various sedimentary strata in the western U.S. (e.g., Navajo sandstone; Rahl et al., 2003), but with the ultimate source from the Appalachian terranes (Fig. 3.6B).

The Yavapai–Mazatzal and Mid–Continent grains have yielded ZHe ages mainly corresponding to the Ancestral Rockies, Sevier–Nevadan, and Laramide orogenies in the western U.S. If the limited data are broadly representative, it seems the Laramide Orogeny provided most of the Yavapai–Mazatzal and Mid–Continent grains, whereas the Ancestral Rockies and Sevier–Nevada orogenies provided fewer grains for the sediment transported to the Mississippi Embayment.

3.5.3.4 Eastern Gulf of Mexico Embayment provenance

Because of the dominance of Grenville and Appalachian–Ouachita U–Pb ages in the Eastern Gulf of Mexico Embayment samples (Fig. 3.4), ZHe dating was mainly performed on these grains (Fig. 3.9D). The ZHe age from sample GOM19 displayed a dramatically different age pattern comparing to that of the Mississippi Embayment (Fig. 3.9D). Eastern Gulf of Mexico Embayment samples have much younger ZHe ages, mainly ranging from 250 to 150 Ma. This exhumation event is possibly related to the Mesozoic

reactivation of the Appalachian orogenic terranes by the rifting of Pangea (Weislogel et al., 2015). Several sediment flux episodes were recorded by relatively high sedimentation in the Mesozoic both in the Gulf of Mexico and in the Atlantic margins (Poag and Sevon, 1989; Galloway, 2008; Snedden et al., 2016).

3.6 CONCLUSIONS

Zircon U–Pb–He double dating has only been carried on modern Mississippi River delta and Pleistocene fans in the Gulf of Mexico Basin. This work presents the first regional provenance study using U–Pb–He double dating to unravel the sediment routing from both the ultimate and intermediate source to the depositional sink for the Miocene system.

Detrital zircon U–Pb analyses of 20 lower Miocene samples indicate that the Gulf of Mexico is a natural sedimentary archive of the North America crustal basement history. The lower Miocene strata mainly include zircons from the Yavapai–Mazatzal, Mid–Continent, Grenville, Appalachian–Ouachita, and Western Cordillera Arc terranes. They also record a few sediments sourced from Wyoming–Superior and Pan–African terranes.

ZHe analyses reveal the exhumation history of North America since the Mesoproterozoic. As indicated by the ZHe data, Proterozoic Grenville, Paleozoic Appalachian–Ouachita and Ancestral Rockies, Mesozoic Sevier–Nevada, Mesozoic–Cenozoic Laramide orogenies, and mid–Cenozoic volcanism have significantly influenced sediment erosion and distribution in North America.

Difference between crystallization and cooling age (Δt) is used to differentiate between first–cycle volcanic and plutonic zircons. Many grains are identified as first–cycle volcanic zircon and are likely eroded from Cretaceous–Cenozoic volcanic fields or the volcanic–fragment–rich Eocene–Oligocene strata on the Great Plains. This is consistent with the presence of volcanic rock fragments in the northwestern Gulf of Mexico.

For a large passive margin basin, both the first cycle and multi–cycle zircons could be in the drainage system, where zircon U–Pb analyses alone cannot recognize the intermediate sedimentary source. Zircon U–Pb–He double dating in this study demonstrates the ability to identify different sources for first cycle and multi–cycle zircons, especially to differentiate the different sources of Grenville zircons. Four distinct U–Pb–He age combinations were recognized for Grenville zircons. Primary first cycle sources include the Llano Uplift in central Texas (ZHe age>600 Ma), Grenville exposures in western Texas and northern Mexico (ZHe age: 80–40 Ma), and Appalachian terranes (ZHe age: 250–150 Ma). Multi–cycled zircons were eroded from the sedimentary strata on the Great Plains, which originated from the Grenville exposures in eastern North America and exhumed during either Appalachian–Ouachita orogeny or Pangean rifting.

A combined U–Pb–He approach provides both the crystallization and the cooling ages of source areas, adding another dimension for provenance analysis. An example illustrated by zircon U–Pb–He analysis on samples in the Greater Rio Grande Embayment demonstrates that 13 exhumation events can be identified from four major zircon U–Pb components. Multiple recycled sedimentary sources, as well as the first–cycle primary source from crystalline terranes were identified, greatly increasing our understanding of the complicated sediment source in large passive margin basins like the Gulf of Mexico Basin.

ACKNOWLEDGMENTS

This research was funded in part by an internal Jackson School of Geosciences Energy Theme Seed Grant to Stockli and Snedden. We are grateful for an Ed Picou Fellowship from Gulf Coast Section SEPM (GCSSEPM), which helped fund our

fieldwork. We also thank the Institute for Geophysics at The University of Texas at Austin, for providing an Ewing–Worzel Graduate Fellowship. Field sample collection was facilitated by Drs. Gary Kinsland and Robert Hatcher. The Florida Geological Survey and UT's Bureau of Economic Geology allowed us to sample subsurface cores. We also appreciate the assistance of Lisa Stockli, Spencer Seman, Daniel Arnost, Adam Goldsmith, Edgardo J Pujols, and Shanping Liu for their help with U–Pb and (U–Th)/He double dating analyses.

We thank the members of the Gulf Basin Depositional Synthesis (GBDS) Industrial Associates Program which includes Anadarko Petroleum Corporation, Apache Corporation, BHP Billiton Petroleum (Americas) Inc., BP America, Inc., Chesapeake Operating LLC, Chevron Corporation, Cobalt International Energy Inc., ConocoPhillips Inc., Devon Energy Corporation, Ecopetrol America Inc., ENI Petoleum Co., Inc., ExxonMobil Exploration Company, Freeport–McMoRan Oil and Gas LLC, GulfSlope Energy, Hess Corporation, INPEX Corporation, Lukoil, Maersk Oil Houston Inc., Marathon Oil Company, Murphy Oil Company, Nexen Petroleum U.S.A. Inc., Noble Energy Inc., Petrobras America, Repsol E&P USA Inc., Ridgewood Energy, Samson Energy Company, LLC, Shell Exploration and Production Co., Statoil Gulf of Mexico, Stone Energy Corp., Suncor Energy, Total E&P USA Inc., Venari Resources. The GBDS principal investigator is John Snedden and GBDS project manager is Patricia Ganey–Curry.

Chapter 4: Channel-belt scaling relationship and application to lower Miocene source-to-sink systems in the Gulf of Mexico basin[3]

ABSTRACT

In past decades, numerous studies have focused on the alluvial sedimentary record of basin fill. Paleo-drainage-basin characteristics, such as drainage area or axial river length, have received little attention, mostly because the paleo-drainage system underwent erosion or bypass, and its record is commonly modified and overprinted by subsequent tectonism or erosional processes. In this work, we estimate the drainage areas of lower Miocene systems in the Gulf of Mexico basin by using scaling relationships between drainage area and river channel dimensions (e.g., depth) developed in Source-to-Sink (S2S) studies. Channel-belt thickness was used to estimate channel depth and was measured from numerous geophysical well logs. Both lower channel-belt thickness and bankfull thickness were measured to estimate the paleo-water depth at low and bankfull stages.

Previous paleogeographic reconstruction using detrital zircon and petrographic provenance analysis and continental geomorphic synthesis constrains independent estimates of drainage basin extent. Comparison of results generated by the two independent approaches indicates that drainage basin areas predicted from channel-belt thickness are reasonable and suggests that bankfull thickness correlates best with drainage basin area. The channel bankfull thickness also correlates with reconstructed submarine fan dimension. This work demonstrates application to the deep-time stratigraphic archive, where records of drainage basin characteristics are often modified or lost.

[3]This chapter was published. Xu, J., Snedden, J.W., Galloway, W.E., Milliken, K.T., and Blum, M.D., 2017, Channel-belt scaling relationship and application to early Miocene source-to-sink systems in the Gulf of Mexico basin: Geosphere, v. 13, no. 1, p. 179–200. Jie Xu is the main author conducting the majority of the research, writing and drawing figures.

4.1 INTRODUCTION

Drainage basin area, which controls sediment supply and water discharge to sedimentary basins, has a strong influence on sediment distribution and rock architecture in the basin (Sømme et al., 2009a; Davidson and Hartley, 2014). A quantitative analysis of paleo-drainage area for a specific unit would also provide a better understanding of sediment provenance and paleoclimate at the source terranes. However, such work on reconstructing paleo-drainage area has received less attention, compared to the numerous studies focused on the alluvial sedimentary record of basin fill.

Recent advances in Source-to-Sink (S2S) analysis provide a method for calculating paleo-drainage basin area by examining the dimensions of sedimentary strata in the basin. The S2S analysis considers whole-sediment erosional-depositional processes as a contemporaneous and genetically linked system (Allen, 2008a; Sømme et al., 2009a, b; Fig. 4.1). Among the components of the S2S system, tectonics and climate, acting on the drainage basin area, determine sediment supply and water discharge (Fig. 4.2A; Matthai, 1990; Milliman and Syvitski, 1992; Syvitski and Milliman, 2007; Allen, 2008b; Sømme et al., 2009a). Although fluvial deposits are volumetrically minor in most basin fills, the majority of the basin fills transits from source to sink through fluvial channels (Galloway, 1981; Hovius, 1998), and channel flow is thus a key link between upstream drainage basin and depositional sinks. Therefore, sediments deposited in fluvial settings should preserve critical signals that could be used to estimate the key parameters of S2S systems (Blum and Törnqvist, 2000; Blum and Womack, 2009). In this study, the term “channel-belt” is used to mean both the channels defined by two adjacent river cutbanks and fluvial deposits that preserved in 3-D stratigraphic record.

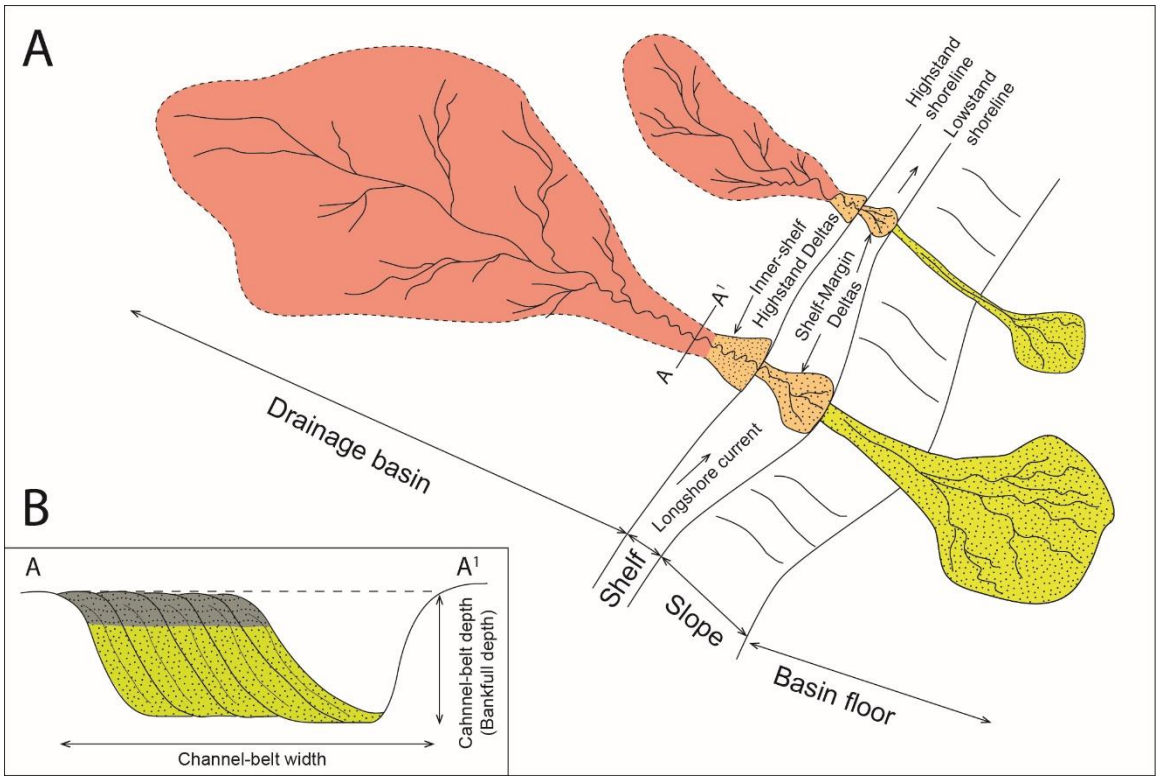

Figure 4.1: A simplified S2S system model and channel-belt profile.

(A) Large drainage systems usually produce greater sediment flux and water discharge, and thereby produce a larger delta and submarine fan systems than do smaller ones. (B) Idealized cross-section of fluvial channel deposits on a low-gradient coastal plain. Channel deposits are the stratigraphic record of the key linking pathway connecting sediment production in the source drainage basin and deposition in the deep basin.

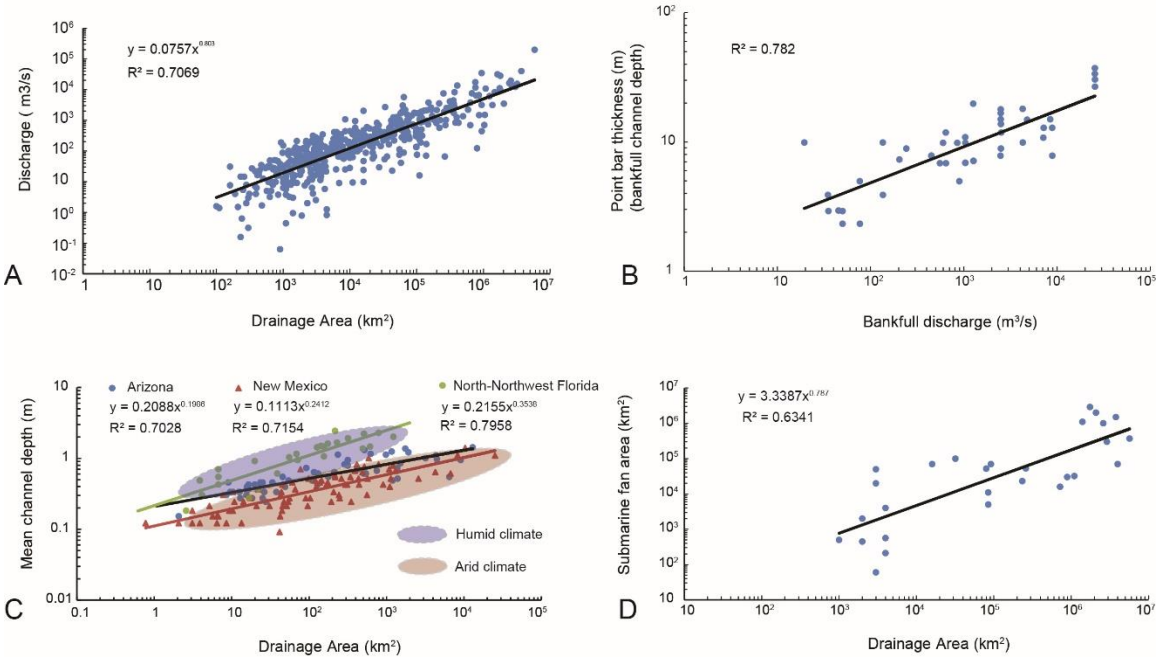

Figure 4.2: Scaling relationships between different components of S2S system.

Correlations between A) river discharge and drainage area, B) bankfull discharge and channel-belt thickness, C) drainage area and mean channel bankfull depth, and D) drainage area and submarine fan area. Fig. 2A to 2D are replotted from Syvitski and Milliman (2007), Blum et al. (2013), Moddy et al. (2003) and Metcalf (2004), and Sømme et al. (2009), respectively.

Studies of modern and Quaternary fluvial systems have explored the relationships among channel-belt dimensions, drainage area, and water discharge (e.g., Leopold and Maddock, 1953; Ethridge and Schumm, 1977; Matthai, 1990; Davidson and North, 2009; Blum et al., 2013). Investigation of 488 modern rivers by Syvitski and Milliman (2007), covering 63% of the global land surface, suggests a strong correlation between drainage area and river discharge (Fig. 4.2A). Blum et al. (2013) measured Quaternary fluvial systems in different tectono-climatic regions and found that channel bankfull depth (or channel-belt thickness) has a positive correlation with bankfull discharge (Fig. 4.2B). Anderson et al. (2004, 2016) documented a strong correlation between river sediment flux and drainage basin area in the late Quaternary glacioeustatic cycles in the northern Gulf of Mexico (GOM) margin.

In addition, climate has greatly affected river discharge, which a humid climate could generate a relatively deep channel depth with a small water-contributing area (Feldman et al., 2005; Gibling, 2006; Davidson and North, 2009; Davidson and Hartley, 2014; Bhattacharya et al., 2016). Local studies of drainage within a specific climatic, lithologic, and hydrologic region (called geomorphological regional curves) indicate a strong correlation among drainage area, mean channel depth, and climate (Fig. 4.2C; Davidson and North, 2009).

To estimate the drainage basin area of an ancient system, the key is to extract correct paleo-fluvial dimensions from outcrop or subsurface data. Miall (2006) pointed out that the vertical dimension of channel (depth) is more easily measured from well logs, cores, or outcrops and that these measurements more reliably reflect features of ancient rivers than do river width and length estimated from limited outcrops. Some studies report that channel-belt deposits formed in bends of meandering rivers provide a good proxy estimate of paleo-channel depth (e.g., Leeder, 1973; Ethridge and Schumm, 1977; Willis, 1989).

Therefore, channel depth can be estimated by measuring a completely preserved channel-bar-deposit package (Lorenz et al., 1985; Bridge and Tye, 2000; Bhattacharya and Tye, 2004; Miall, 2006; Holbrook and Wanas, 2014).

Some studies have attempted to recover drainage basin area from preserved channel deposits (e.g., Bhattacharya and Tye, 2004; Davidson and North, 2009; Davidson and Hartley, 2014). For example, Davidson and North (2009) used maximum preserved channel depth to calculate drainage area of an ancient rock unit by applying the scaling relationships derived from modern regional geomorphological curves. Knowledge of tectonic and climatic conditions in ancient system is required for guiding the selection of suitable modern systems having similar settings. Most previous studies have proven useful in a relatively small basin within a uniform tectonic and climatic region; this scaling relationship has not been tested in large, passive margin basins that have diverse climatic, tectonic, topographic, lithologic, and geomorphic zones.

In this work, we statistically characterize several channel-belt dimensions using well logs and then use these results to calculate paleo-drainage area, by employing the scaling relationship established on modern and Quaternary fluvial system. As a data-rich basin having well-preserved fluvial coastal plain deposits along its northern margin, the GOM provides an opportunity to test such scaling relationships using large, reconstructed lower Miocene fluvial systems. Previous drainage basin analysis using detrital zircon U-Pb analysis (Xu et al., 2017) was used as an independent test for the reliability of the prediction. We extend our analysis to the deep basin and test the correlation between the drainage basin area, basin length, and submarine fan area and length proposed by Sømme et al. (2009a; Figs. 4.1 and 4.2D).

Our results have implications for deep-water exploration in the GOM, as lower Miocene sediment slope and basinal sandstones are one of the major deep-water reservoirs

in the basin. However, fan distributions and areas are commonly masked by a structurally complex salt canopy that developed during and after Miocene deposition. Therefore, channel belt dimensional data obtained from onshore fluvial deposits could be a useful predictor of axial length of submarine channel sands.

4.2 BACKGROUND

The Cenozoic GOM is characterized by voluminous siliciclastic sediment influx from the North American hinterland to the basin. Major tectono-stratigraphic phases, including Laramide, Mid-Cenozoic Thermal, Basin and Range, and Neogene Glacier, produced four distinct sediment-routing and basin-filling histories (Fig. 4.3; Galloway, 2008; Galloway et al., 2011). The resulting depositional units, Paleocene–Eocene Wilcox, Oligocene Frio/Vicksburg, Miocene, and Pleistocene, are the major hydrocarbon production units in the Gulf (Fig. 4.3).

The early Miocene (ca. 23–15 Ma) was a transitional period of tectonic reorganization in North America, changing from arid volcanogenic in the late Eocene to early Miocene to arid extensional in the middle-to-late Miocene (Fig. 4.3). Arid climatic conditions extended from the Western Interior to the northwest Gulf margin, whereas a humid climate prevailed in the eastern Gulf coastal plain and Appalachian uplands (Galloway et al., 2011). The arid climate and Rio Grande extension in the Western Interior combined to be a major cause of the decreased sediment input in early Miocene time (Fig. 4.3). Rejuvenation of Appalachians in the middle Miocene combined with the wet climate increased the delivery of sediment to the east-central GOM through the paleo-Tennessee River. Together with the Mississippi, the Tennessee formed a large deltaic depocenter. Consequently, the lower Miocene interval records both sediment-routing and linked depocenters shifting from the western GOM in the Paleogene to the central Gulf in the

Neogene (Galloway et al., 2011; Bentley et al., 2016; Fig. 4.3). Recent exploration success in deep-water drilling suggests Miocene submarine fans ran out hundreds of kilometers onto the abyssal plain.

Two major transgressive shales bound the lower Miocene depositional sequence, the Amphistegina B shales at the top and the Anahuac shales at the base (Fig. 4.3). Lower Miocene strata can be separated into two subunits, informally termed lower Miocene 1 (LM1) and lower Miocene 2 (LM2), by a transgressive shale dated as ~ 18 Ma (Galloway et al., 1986).

The paleogeography constructed by Galloway et al. (2011) is based upon previous studies of the Cenozoic tectono-climatic history of the North American interior (source) and the depositional record in the GOM basin (sink). This compilation indicates that in the early Miocene, the northern GOM had multiple synchronous fluvial systems, ranging from large extra-basinal rivers to local intra-basinal streams (Galloway, 1981; Galloway et al., 2011; Figs. 4.3, 4.4, and 4.5). A few large rivers, including the paleo-Mississippi and Red rivers and the Rio Grande, carried voluminous sediments and deposited thick fluvial-deltaic deposits onto the coastal plain and shelf and linked submarine fans in the abyssal plain (Galloway et al., 2000, 2011; Galloway, 2008; Figs. 4.3, 4.4, and 4.5). Smaller intrabasinal streams, including the paleo-Guadalupe and Houston-Brazos rivers, were minor sediment conveyers that only built small bay-head deltas and shore zones in the northwestern GOM (Anderson et al., 2014; Figs. 4.3, 4.4, and 4.5).

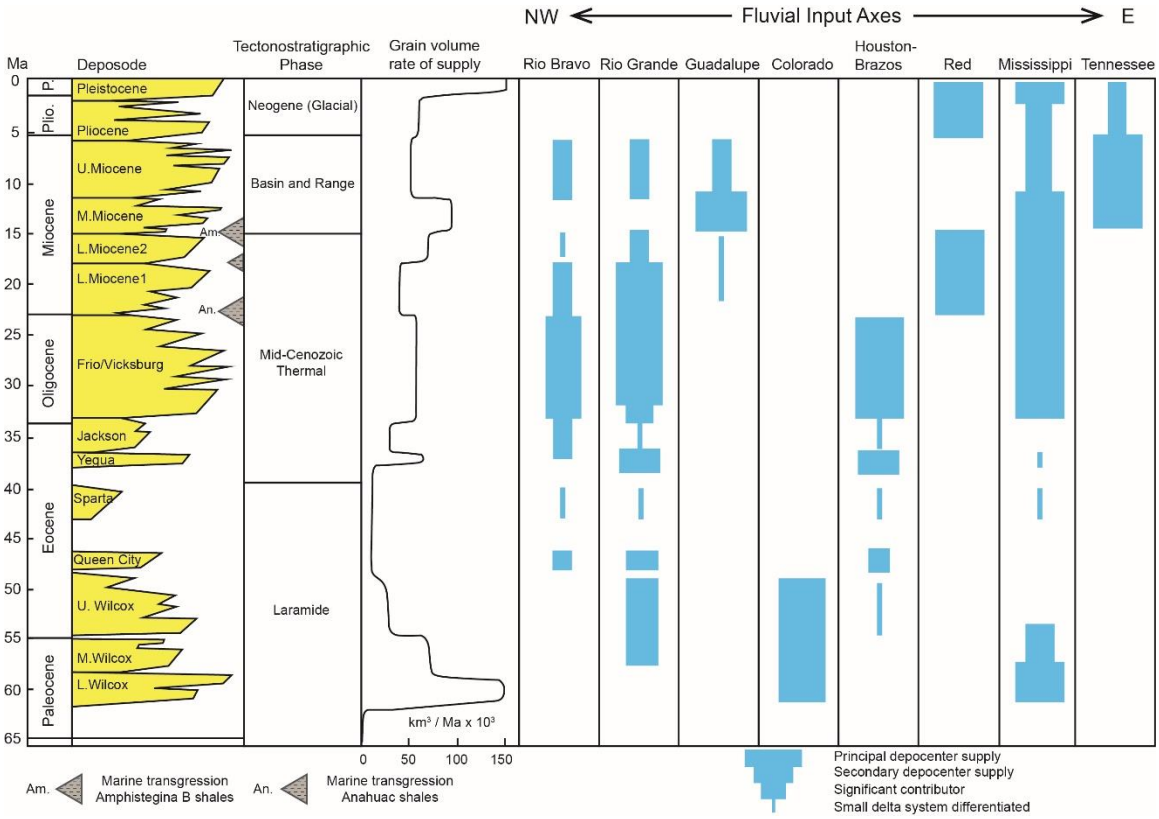

Figure 4.3: Depositional evolution history of the principal Cenozoic northern Gulf of Mexico fluvial axes.

Columns show principal depositional episodes, major tectonostratigraphic phases, grain volume rate of sediment supply rate, and changing rates of supply through each fluvial input axis. Modified from Galloway et al. (2011).

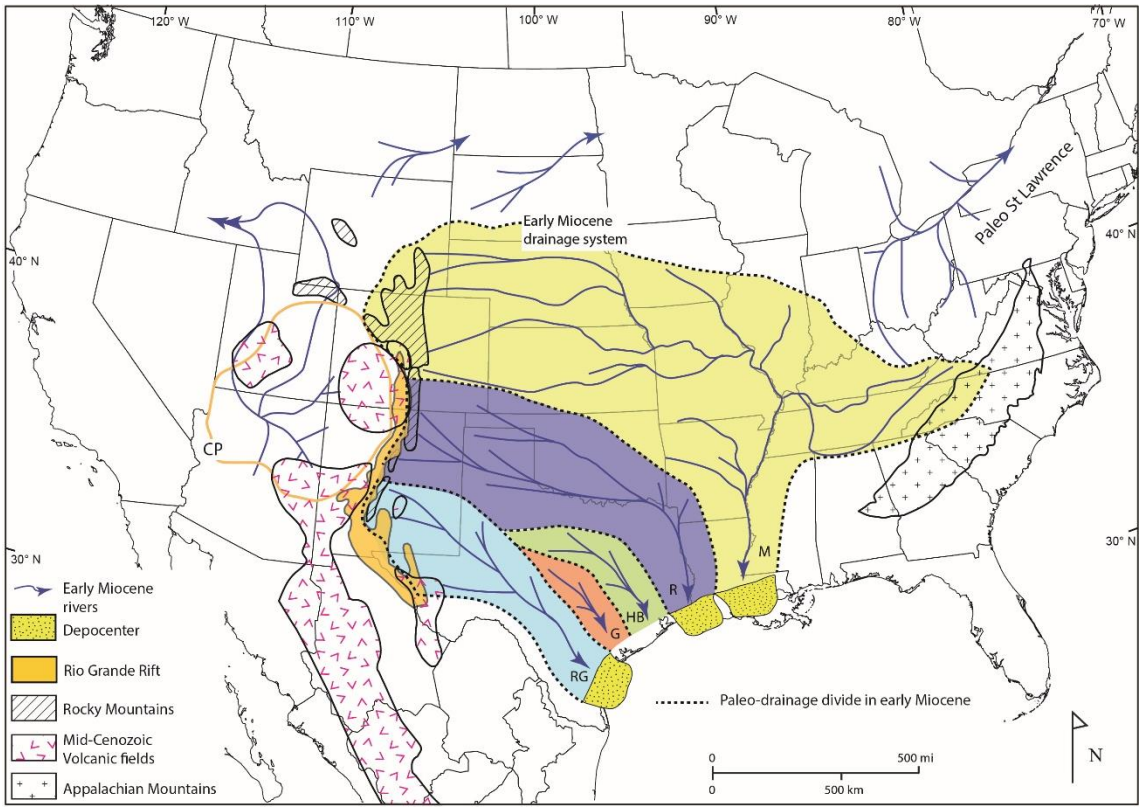

Figure 4.4: Paleo-drainage map of the five major fluvial axes of the early Miocene Gulf of Mexico.

Modified from Galloway et al. (2011) and Xu et al. (2017). Abbreviations: RG – Rio Grande; G – Guadalupe; HB – Houston-Brazos; R – Red; M – Mississippi.

Several differences exist between the drainage systems in the early Miocene and their modern counterparts. Detrital zircon provenance analysis of lower Miocene sediments suggests the presence of very limited amounts of Archean aged zircons from corresponding basements in northern Wyoming and in Canadian shields; thus, the drainage connection between the GOM and northern Wyoming, Montana, and Canada was weak (Xu et al., 2017; Fig. 4.4). The paleo-Upper Missouri and the paleo-Ohio River might have not fully integrated into a southward-flowing system until the Pliocene–Pleistocene (Galloway et al., 2011; Blum and Roberts, 2012; Bentley et al., 2016). Alternatively, the paleo-Ohio River flowed northeastward and joined the pre-glacial St. Lawrence River in the early Miocene (Hoagstrom et al., 2014, and references therein), whereas the Miocene Upper Missouri River flowed northward and merged with the pre-glaciation "Bell River" in Canada (Howard, 1958; Sears, 2013; Fig. 4.4). The Red River drained the southern Rocky Mountains (Galloway et al., 2011; Dutton et al., 2012; Xu et al., 2017) and fed the large Calcasieu Delta in western Louisiana through eastern Texas (Fig. 4.5). Sediments deposited in this deltaic depocenter, as much as about 2500 m thick, imply that the Red River was one of the largest fluvial systems during early Miocene time. The Red River did not merge with the Mississippi River; it was a separate fluvial system for the GOM until the Holocene (Saucier, 1994; Galloway et al., 2011).

4.3 Database and Methodology

4.3.1 Database

A complete succession of point bar deposits in outcrop can be used to estimate channel depth. However, lower Miocene outcrop exposures are few and generally small, and they rarely display a complete channel-belt succession. Measurement of channel-belt thickness in this study is therefore based on subsurface well logs. Logs from 94 wells were

used to measure the channel-belt thickness of five major early Miocene rivers on the Gulf Coast: the paleo-Mississippi, Red, Houston-Brazos, and Guadalupe rivers, and the Rio Grande (Figs. 4.4 and 4.5; Table C1.1).

These well logs were extracted from several publications (Spradlin, 1980; Dodge and Posey, 1981; Bebout and Gutierrez, 1983; Eversull, 1984; Galloway et al., 1986; Foote et al., 1990; Baker, 1995; Young et al., 2010, 2012). The lower Miocene boundaries are well constrained in previous publications by biostratigraphic data or by detailed well correlation based on key depositional surfaces (e.g., erosional unconformities and marine flooding surfaces) in the GOM region. Paleogeographic maps interpreted from numerous well logs, along with seismic interpretation by Gulf of Mexico Basin Depositional Synthesis (GBDS) project researchers, provide a well-defined reconstruction of the Gulf coastal plain (Fig. 4.5). The shoreline position defined by GBDS researchers delineates the approximate boundary between fluvial and delta-marine environments (Fig. 4.5). Wells are located on the fluvial-coastal plain regions, landward of the paleo-shoreline. A few wells are located near the paleo-shoreline and display both marine deposits formed during high sea-level stage and fluvial features in lowstand. Criteria for recognition of fluvial channel-belt facies and thickness measurements are discussed below.

4.3.2 Single-storey channel-belt recognition

A river is a dynamic conduit that carries sediments from the hinterland to build coastal plains and deltas along the basin margin and in some cases even feed submarine fans on the abyssal plain. Major fluvial sediments deposited in coastal plains usually consist of channel-belt fills (lateral accretion deposits), crevasse splay, floodplain, and lake deposits (Fig. 4.6). Recognition of each fluvial-coastal plain depositional facies has been well established by previous works (e.g., Bernard et al., 1970; Galloway, 1981, 1982;

Bridge and Tye, 2000). One effective way to differentiate these facies is by using well logs patterns, e.g., spontaneous (SP), gamma ray (GR), or resistivity (RT) curves. Different sedimentary facies have distinct depositional processes, producing differing lithological assemblages, grain size trends, and mineral composition, thereby revealing different responses on geophysical well logs (e.g., Galloway, 1981; Galloway et al., 1982, 1986; Snedden, 1984; Fig. 4.6; Figs. S3.1, 2, 3 and 4).

Channel-belt deposits, which form from migration of an active channel, are major repositories of sediments within fluvial systems. The channel filling and bar aggrading usually result from reducing flow and decreasing water depth (Miall, 2010). Therefore, a fluvial channel- belt deposit is typically characterized by a sharply defined erosional base and an upward-fining succession, due to the decline in fluvial strength and consequent decreasing grain size upward (Fielding and Crane, 1987; Bridge and Tye, 2000; Miall, 2010; Hubbard et al., 2011; Figs. 4.6 and 4.7). Channel-belt deposits can be divided into two subunits–the lower channel-belt, characterized by coarse-grained sandstone and large-scale trough cross-bedding at the base, and an upper channel-belt, characterized by fine-grained sandstone/silt/mudstone, horizontal lamination and ripple cross bedding at the top (Bernard et al., 1970; Bridge and Tye, 2000; Figs. 4.7A and B). It is easy to differentiate channels and bars from floodplain, levee, and splay deposits as the latter are mostly muddy and may display upward-coarsening textural trends (Galloway, 1981; Galloway and Hobday, 1996; Ambrose et al., 2009; Fig. 4.6). Coastal deltaic deposits usually show an upward-coarsening well log motif and are easy to differentiate from channel-belt deposits (Olariu and Bhattacharya, 2006).

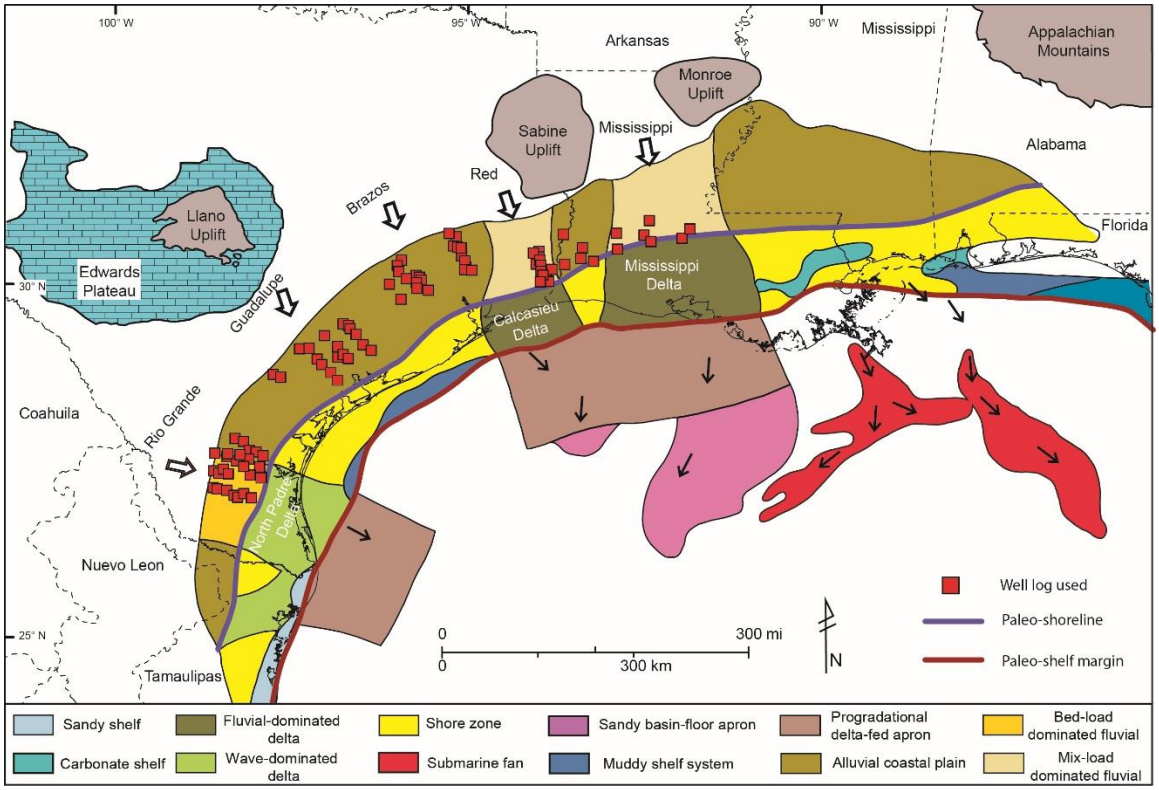

Figure 4.5: Well log dataset used to measure the channel-belt thickness.

Well log dataset used to measure the channel-belt thickness of five major fluvial systems in the northern Gulf of Mexico. The paleogeography map of lower Miocene interval is updated from Galloway et al. (2000) and unpublished maps of the GBDS (Gulf of Mexico Basin Depositional Synthesis) project atlas.

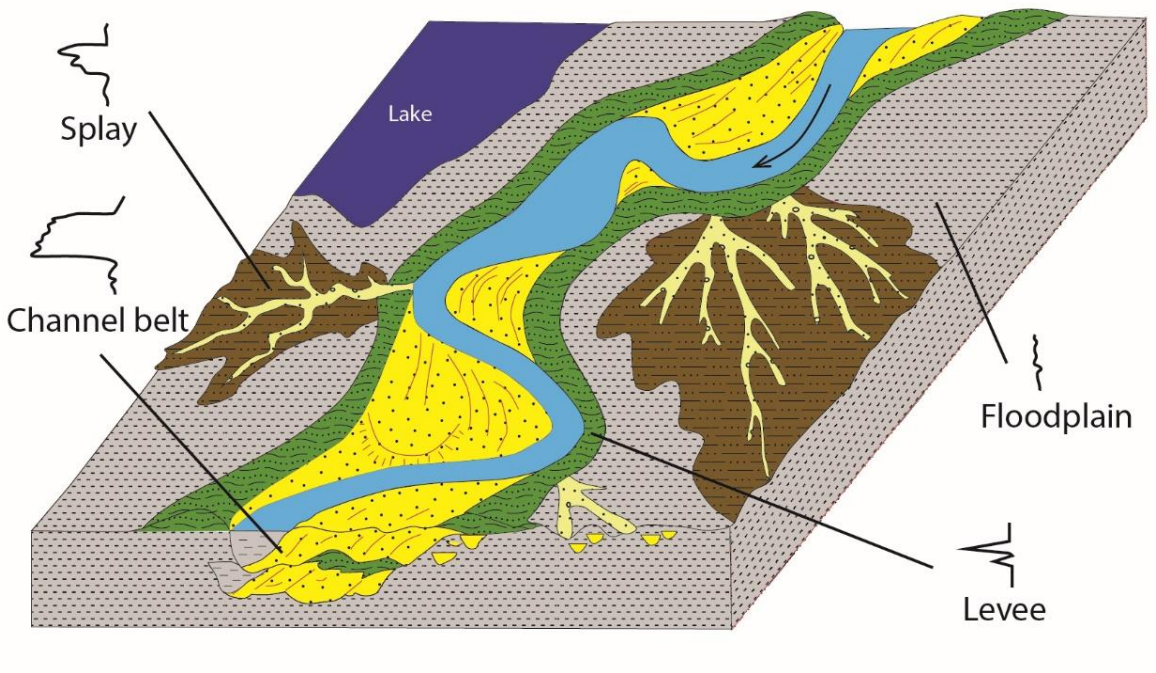

Figure 4.6: Schematic features of a meandering fluvial system.

Schematic features of a meandering fluvial system characteristic of the early Miocene Gulf Coast. Each sedimentary facies has distinct well log patterns. Modified from Galloway (1981).

Channel-belts in fluvial systems can deposit sediment by either lateral expansion or downstream translation (Bridge and Tye, 2000; Bridge, 2003; Willis and Tang, 2009; Smith et al., 2009, 2011; Ghinassi and Ielpi, 2015, 2016). The upstream channel-belt deposited by lateral accretion has a higher net- sandstone content (Fig. 4.7C). The downstream channel-belt is formed by downstream translation and is characterized by a heterogeneous package of sands and muds and a serrate, upward-fining log motif (Willis, 1989; Smith et al., 2009, 2011; Willis and Tang, 2010; Hubbard et al., 2011; Durkin et al., 2015; Fig. 4.7C). The lithological heterogeneity is likely caused by deposition of clay derived from the undercut bank by caving during flood stages, or by clay drapes deposited in channel-belt swales during flooding (Bernard et al., 1970; Davies et al., 1993). Seasonal sediment flux can also result in a heterogeneous package of sands and muds in channel-belt deposits (e.g., Labrecque et al., 2011).

When a channel is abandoned by single meander loop neck-cutoff or by avulsion, the remaining accommodation space is usually filled by fine-grained sediments in response to resultant reduced flow energy (Bernard et al., 1970; Bridge and Tye, 2000; Blum et al., 2013). The channel fills can be either sand rich in upstream areas where the channel remains connected to the new active channel or very muddy in downstream regions located away from the active channel. Overall, the well log SP/GR curve of channel fills is characterized by a relatively thin, blocky or bell-shaped sandstone at the base and a thick, flat shale baseline on the top (Fig. 4.7C).

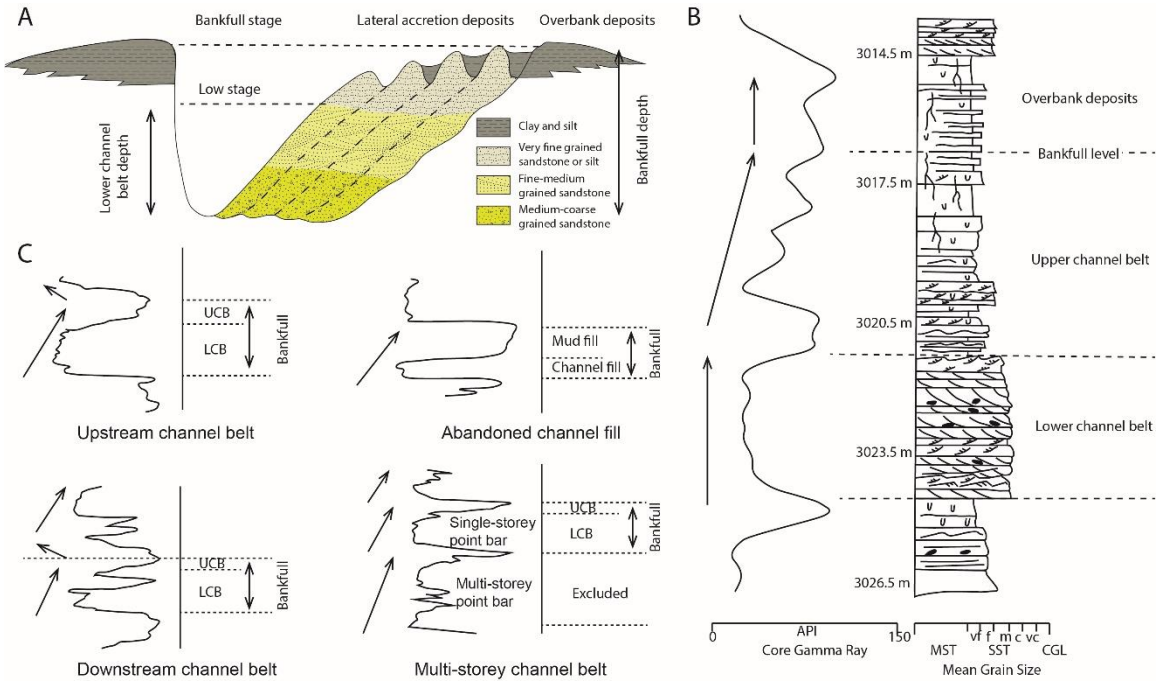

Figure 4.7: Sedimentological and wireline-log features of channel-belt deposits.

(A) Cross-section of channel-belt deposits. Modified from Saucier (1994). (B) Sedimentological and wireline-log features of channel-belt deposits. Modified from Tye (1991) and Bridge and Tye (2000). (C) Typical well log response patterns of early Miocene channel-belt deposits observed in the northern Gulf of Mexico, including upstream channel-belt, downstream channel-belt, abandoned channel fill, and multi-storey channel-belt. Facies recognition criteria on the well log are adapted from Bernard et al. (1970) and Bridge and Tye (2000). Abbreviations: LCB – lower channel-belt; UCB – upper channel-belt.

4.3.3 Multi-storey channel-belt deposits

The stratigraphic record is usually incomplete (Strauss and Sadler, 1989; Sadler and Jerolmack, 2015), and preservation of a complete succession of channel deposits is always a critical issue to consider when using channel-belt thickness to estimate channel depth in the deep-time stratigraphic setting (Lorenz et al., 1985; Bridge and Tye, 2000; Miall, 2010; Holbrook and Wanas, 2014; Nicholas et al., 2016). Preservation of channel-belt succession is highly dependent on sediment supply and accommodation space (Bridge, 2003; Gibling, 2006). The fluvial deposits tend to become amalgamated and to form multi-storey sandbodies in low- accommodation settings. River avulsions usually reoccupy the previous river course by eroding and stacking upon earlier channel deposits (Blum et al., 2013). This process can sometimes make it hard to differentiate multi-storey from single-storey channel-belt deposits. In a rapidly subsiding basin, such as the GOM during the Cenozoic, the high accommodation rate favors a more complete preservation of channel deposits (Bridge, 2003; Gibling, 2006; Miall, 2010).

Amalgamated channel deposits usually display blocky, over-thickened, multi-storey sandbodies with some embedded, thin, laminated mud layers (Fig. 7C). Thin mud layers are either the basal, mud-clast-rich channel-lag deposits of an overlying channel-belt or the upper, muddy part of underlying channel-belt that have not been fully eroded. The mud bed can cause SP/GR curves deflect to a shale baseline between two stacking channel-belt deposits. In our analyses, we try to avoid measuring channel-belt thickness from multi-storey channel-belts and instead focus upon single-storey channel-belts.

4.3.4 Channel-belt thickness measurement

A complete channel-belt deposit incorporating both sandy lower part and muddy upper part represents a bankfull stage of river discharge that forms the channel (Wolman and Miller, 1960; Bridge and Tye, 2000; Gibling, 2006; Miall, 2014; Fig. 4.7A). Bridge

and Tye (2000) suggested that complete preservation of a channel-fill sequence is a useful proxy for estimation of paleo-channel depth. The thickness of sandy lower channel-belt deposits (Fig. 4.7A) indicates the minimum constructional depth of the channels and only preserves a fraction of channel-forming discharge (Frazier and Osanik, 1961; Bridge and Tye, 2000; Miall, 2014). The lower channel-belt deposits are relatively easily recognized on SP, GR, and RT logs, because the sandy lower channel-belt and the muddy upper channel-belt have markedly different clay contents and thus have different a response on well log curves (Figs. 4.7B and C). Bankfull thickness (a complete succession of channel-belt thickness) is relatively more difficult to measure, because the top boundary of the muddy upper channel-belt is not easily distinguished from subsequent overbank deposits by grain size and clay content. Thus, uncertainty is associated with this measurement. Upper channel-belt thickness can be either underestimated, if part of the top deposit was truncated by an overlying channel, or overestimated if the near-channel overbank deposit is not differentiated.

We measure both the thickness of lower channel-belt (sand body) and bankfull deposits in this work (in a complete upward-fining succession). We define the top of bankfull deposits by observing the maximum deflection to the shale baseline on well log curves (SP, GR, or RT; Fig. 4.7C). In summary, the lower channel-belt thickness, which is easier to measure but only preserves a fraction of channel-forming water discharge, whereas bankfull deposit thickness, which is interpretive but is reflective of paleo-channel depth at high flow discharge. In this work, we use both measured mean lower channel-belt and interpreted mean bankfull thicknesses to estimate the paleo-drainage area, but we do separate them in our analysis.

4.3.5 Drainage basin area calculation

Blum et al. (2013) collected data on modern and Quaternary channel-belt thickness, river discharge, and drainage basin area from 61 rivers worldwide to establish a scaling relationship between channel depth and drainage basin area. Their work suggests that drainage basin area has a first-order control on river discharge and channel-belt dimension, and that climate plays a secondary role. In this work, we use the scaling relationship dataset from Blum et al. (2013) to calculate the drainage basin area of lower Miocene systems. Previous paleogeographic reconstruction using detrital zircon and petrographic provenance analysis and continental geomorphic synthesis provides independent estimates of drainage basin areas (Galloway et al., 2011; Xu et al., 2017; Fig. 4.4) and helps determine whether the calculated drainage basin areas calculated from channel-belt thickness were geologically reasonable.

4.3.6 Fan dimension measurement

We also measure submarine fan dimension in the GOM to explore the relationship between sediment deposited in the basinal sink, river dimension, and drainage basin area. Data used to map Miocene submarine fan distribution in the deep-water basin were maintained in an ArcGIS database, and all measurements in this work were made using ArcGIS tools (Figs. 4.4 and 4.8). The term “apron” is used here to describe the poorly organized, line-sourced submarine slope system that fronted much of the ancient GOM shelf margins (Galloway, 1998; Figs. 4.4 and 4.8). In this work, the fan run-out length is calculated from the shelf margin to termination of the distal submarine fan or apron lobe, as appropriate to the slope system type. Submarine-fan area is measured from the maximum mapped fan or apron-facies distribution. The submarine fan systems in the eastern GOM were not measured, as they do not connect directly to any fluvial-deltaic

axes; rather they received sediment reworked along the coast or shelf edge by longshore currents before being diverted into deep water (Fig. 4.8; Snedden et al., 2012).

4.4 RESULTS

We measured 489 lower channel-belt and 552 bankfull thicknesses from 94 subsurface well logs that cover the major fluvial axes of the paleo-Mississippi, Red, Brazos, and Guadalupe rivers, and the Rio Grande (Fig. 4.5; Table C3.1). Both the lower channel-belt and bankfull thicknesses from each river show a different frequency modal in histogram (Figs. 4.9 and 4.10). Thickness data of each river show a wide range, from few meters to >50 m (Table C1.1; Figs. 4.9 and 4.10). We here apply a 20% filter to separate outliers, removing both the thinnest and the thickest 10% values. The thinnest 10% parts of the channel-belt thicknesses are probably deposits of local intra-basinal rivers or side rivers near these large fluvial axes. The thickest 10% of channel-belt thicknesses are probably multi-storey channel deposits or valley-fill deposits. These outliers would not represent true paleo-channel depths. The remaining 80% channel-belt data should be more characteristic of the time-averaged fluvial channel-belts recorded in deep-time archives. In this study, we present both the raw data and truncated data to give a better view of channel-belt thicknesses of the five major river systems in the northern GOM (Figs. 4.9 and 4.10).

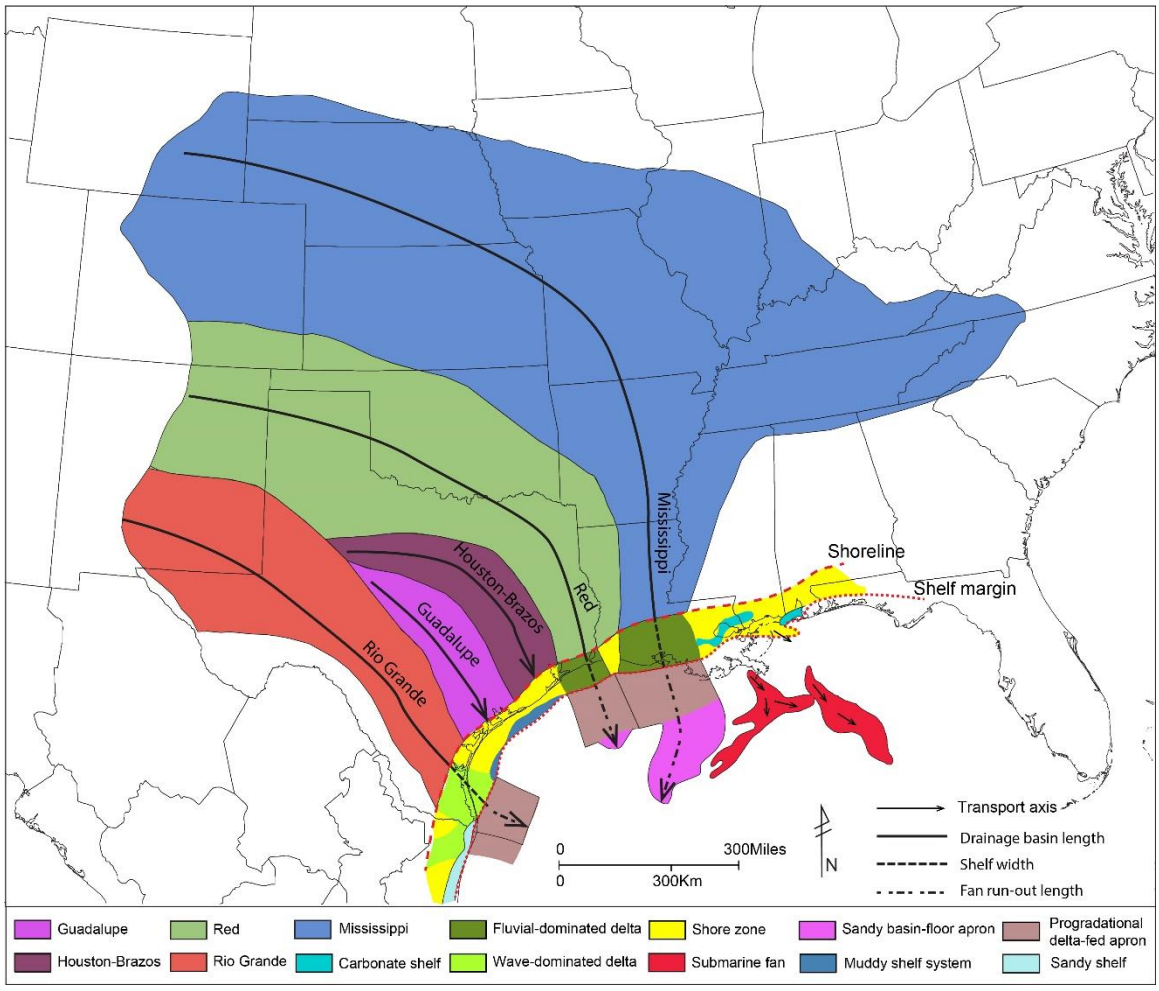

Figure 4.8: Measurement of S2S components in early Miocene Gulf of Mexico.

Paleogeographic parameters of the five early Miocene sediment-routing systems used to explore the relationships among different S2S components. Fan areas were measured from the extent of slope and basin-floor apron. Modified from Galloway et al. (2000, 2011) and Xu et al. (2017).

4.4.1 Lower Channel-belt Thickness

Thicknesses of lower channel-belts show a wide range, 3 to 40 m (Fig. 4.9; Table 4.1). Each river shows a distinct channel-belt-thickness distribution. The paleo-Mississippi River data have multiple peaks, including a major peak at approximately 15–21 m and three secondary peaks at 24–27, 30–33, and 39–42 m (Fig. 4.9). The paleo-Red River data display a similar range of lower channel-belt thicknesses, in comparison to the paleo-Mississippi River. However, the lower channel-belt thicknesses of the paleo-Red River are more clustered at 12–24 m, with only a few channel-belts thicker than 30 m. In contrast, the paleo-Rio Grande and paleo-Brazos and paleo-Guadalupe rivers show a narrower range of channel-belt thicknesses, from 3 to 24 m (Fig. 4.9; Table 4.1). The paleo-Rio Grande shows a slightly skewed normal distribution peaking at 9–18 m, whereas the paleo-Brazos and paleo-Guadalupe rivers show a strong right-skewed pattern, with most of the lower channel-belt data peaking at approximately 6–15 m (Fig. 4.9).

Truncated thickness data have removed the highest and lowest values, which make the mean thickness not be affected by extreme values. The paleo-Mississippi has the largest lower channel-belts ranging from 10 to 35 m, whereas most of the paleo-Red River lower channel-belts are thinner, about 9 to 26 m. Lower channel-belts of the paleo-Rio Grande and the paleo-Brazos and Guadalupe rivers are mostly thinner than 18 m (Fig. 4.9).

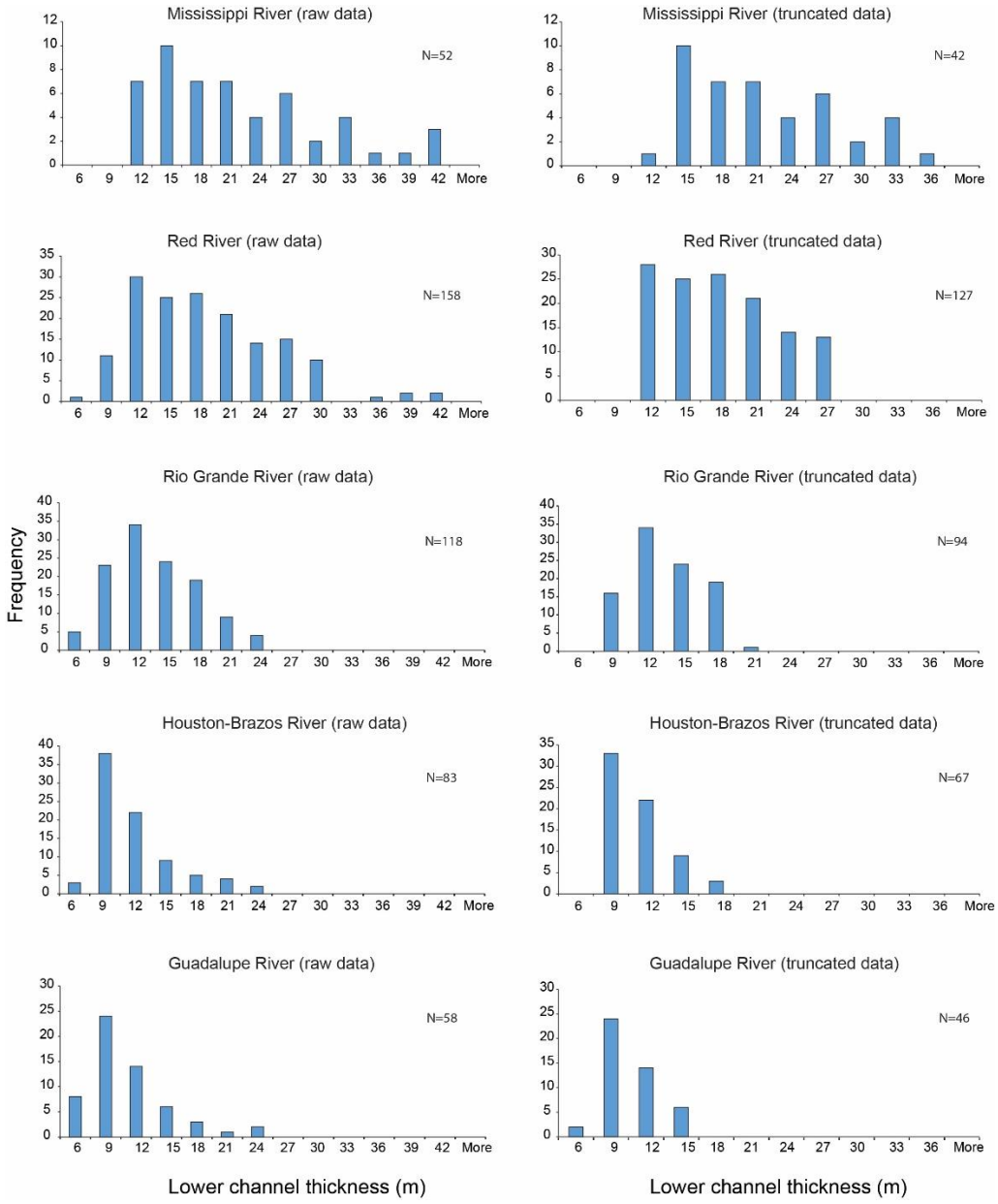

Figure 4.9: Histograms of lower channel-belt thickness in the five Miocene fluvial systems.

Truncated data remove the highest and lowest 10% values. N is the number of measurements.

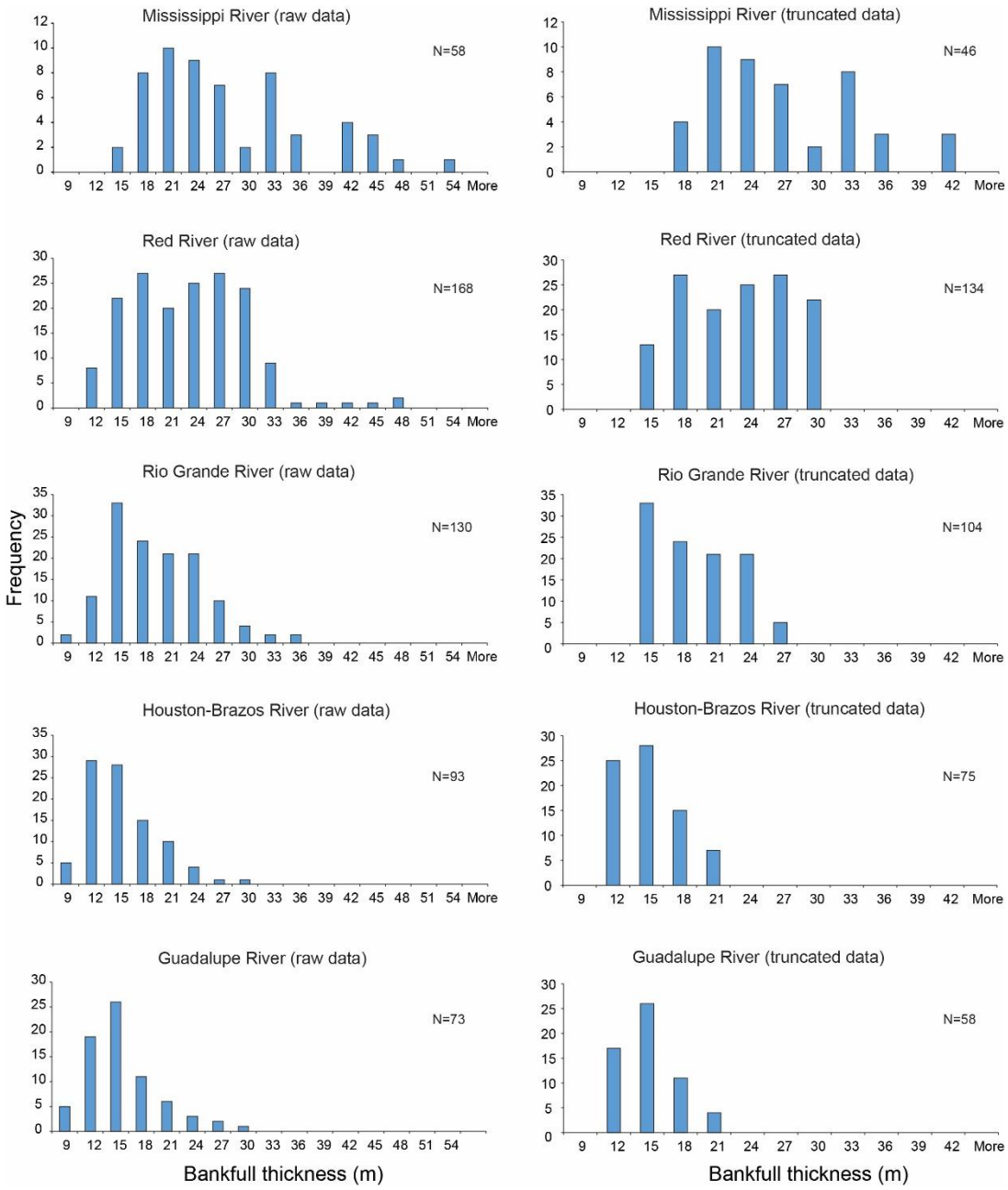

Figure 4.10: Histograms of bankfull thickness in the five Miocene fluvial systems.

Truncated data remove the highest and lowest 10% values. N is the number of measurements.

River system	Lower channel-belt thickness Range (m)	Filtered lower channel-belt thickness Range (m)	Filtered lower channel-belt thickness Mean ± Std. (m)	Bankfull thickness Range (m)	Filtered bankfull thickness Range (m)	Filtered bankfull thickness Mean ± Std.* (m)
Mississippi	9 - 40	10 - 35	19.7 ± 6.4	12 - 52	15 - 40	25.0 ± 6.6
Red	4 - 40	9 - 26	16.1 ± 4.9	9 - 46	13.5 - 29	21.1 ± 4.8
Rio Grande	4 - 23	6 - 18	11.2 ± 3.2	6 - 34	12 - 24.5	17.0 ± 3.8
Houston-Brazos	3 - 22	6 - 16	9.1 ± 2.4	6 - 28	9 - 18.5	13.0 ± 2.8
Guadalupe	3 - 23	5 - 13	8.4 ± 2.2	6 - 29	9 - 18.5	12.8 ± 2.6

Std.* = Standard deviation

Table 4.1: Parameters of measured channel belt deposits.

Parameters of measured channel belt deposits measured from five major fluvial systems in the northern Gulf of Mexico.

4.4.2 Bankfull Thickness

In the paleo-Mississippi River, the bankfull thickness plot displays a major peak at 15–27 m and two minor peaks at 30–36 m and 39–48 m (Fig. 4.10). Bankfull thicknesses of the paleo-Red River show a broad distribution in thickness ranging from 9–33 m (Fig. 4.10). The bankfull thickness of the paleo-Rio Grande has a narrower range relative to the paleo-Red River and paleo-Mississippi River, with most data peaking at 12–24 m (Fig. 4.10). The paleo-Brazos and Guadalupe rivers have a slightly right-skewed distribution, with most data clustering at 9–15 m and a few data ranging from 21 to 30 m in the tail of the distribution (Fig. 4.10). Truncated data display a narrower range but distribution patterns that are still similar to those of the raw data (Fig. 4.10).

4.4.3 Comparison of Channel-belt Thickness

Truncated lower channel-belt thickness data of each river show significant differences in statistics and on cumulative frequency plots (Fig. 4.11A; Table 4.1). The paleo-Mississippi River yielded a relatively gentle slope in its cumulative percentage plot; lower channel-belt thickness ranges from 9 to 40 m. Truncated data have an average lower channel-belt thickness of 19.7 m, with a standard deviation of 6.4 m (Table 4.1). The paleo-Red River displays a similar pattern, but the data from thinner lower channel-belts range from 9 to 27 m. The paleo-Red River has an average lower channel-belt thickness of 16.1 ± 4.9 m (Table 4.1). In contrast to the paleo-Mississippi and Red rivers, the paleo-Brazos and Guadalupe rivers are dominated by lower channel-belt thicknesses ranging from 6 to 18 m (Fig. 4.11A). They have an average lower channel-belt thickness of 9.1 ± 2.4 m and 8.4 ± 2.2 m, respectively (Table 4.1). The paleo-Rio Grande is intermediate between the large paleo-Mississippi and Red rivers and intrabasinal paleo-Guadalupe and Brazos rivers,

with lower channel-belt thicknesses ranging from 6 to 21 m and an average lower channel-belt thickness of 11.2 ± 3.2 m (Fig. 4.11A; Table 4.1).

The truncated bankfull thickness of each river displays a pattern similar to that of lower channel-belt thickness in statistics and in the cumulative frequency plot (Fig. 4.11B; Table 4.1). The paleo-Mississippi River has an average thickness of 25.0 ± 6.6 m, characterized by a gentle slope on a cumulative frequency plot (Fig. 4.11B). Compared to the paleo-Mississippi River, the paleo-Red River and Rio Grande have thinner bankfull thicknesses, averaging 21.1 ± 4.8 m and 17.0 ± 3.8 m, respectively (Table 4.1). The paleo-Houston-Brazos and Guadalupe rivers have steep slopes on their cumulative frequency plots, their average thicknesses being 13.0 ± 2.8 m and 12.8 ± 2.6 m, respectively (Fig. 4.11B; Table 4.1). Similar patterns are reproduced on the histogram plots of bankfull thickness of each river (Figs. 4.9 and 4.10).

The distinct mean and range of channel-belt thickness of each river (Figs. 4.9, 4.10, and 4.11; Table 4.1), together with previous work on fluvial input axes (Fig. 4.3), suggest three scales of river dimension. We categorize these river systems into three classes: continental-scale river with mean bankfull thickness of > 25 m or mean lower channel-belt thickness of >20 m (e.g., the paleo-Mississippi Rriver), large-scale river with mean bankfull thickness of 15–25 m or mean lower channel-belt thickness of 10–20 m (e.g., the paleo-Red River and Rio Grande), and moderate-scale river with mean bankfull thickness < 15 m or mean lower channel-belt thickness < 10 m (e.g., paleo-Brazos and Guadalupe rivers). Features of each class are discussed in the next section.

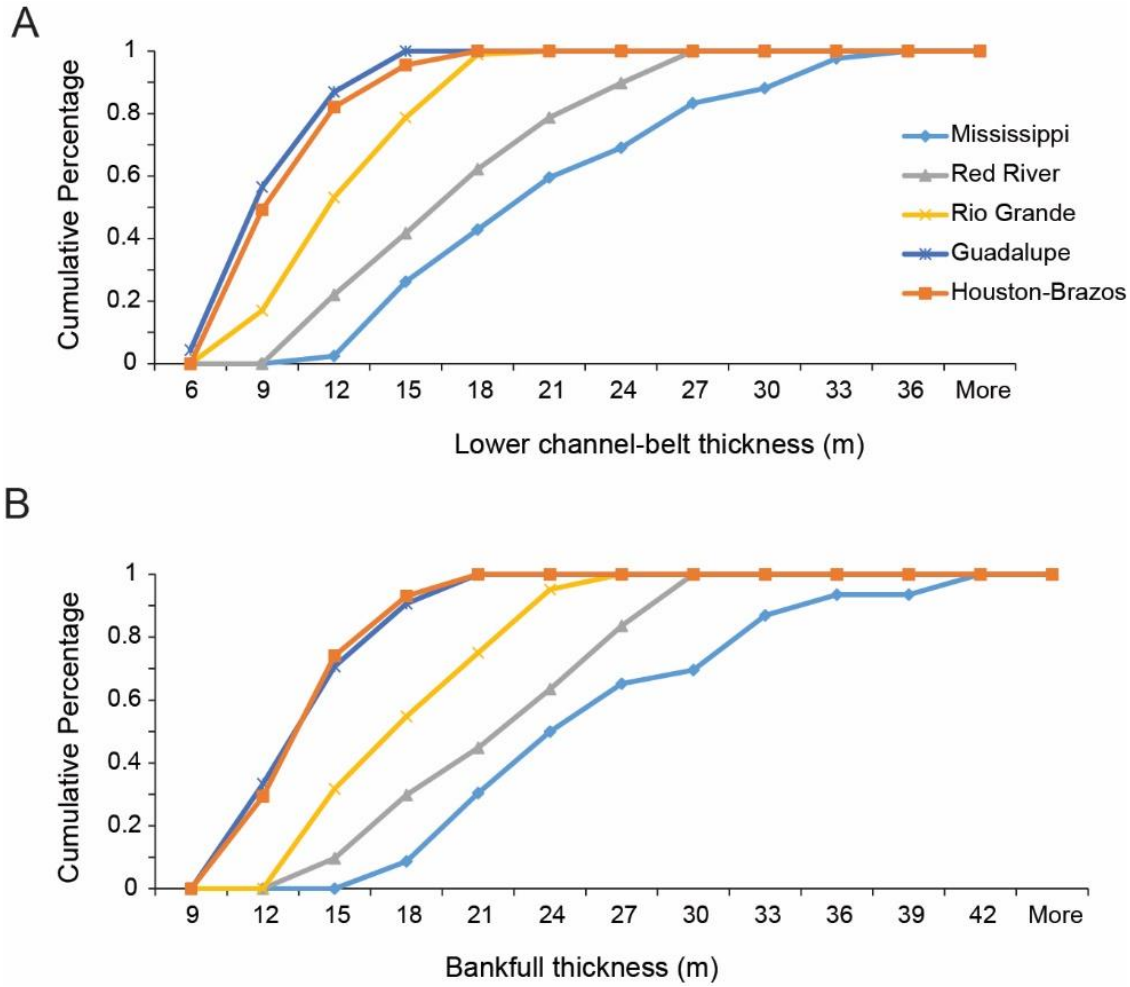

Figure 4.11: Comparative cumulative frequency plots of five early Miocene fluvial systems.

Comparative cumulative frequency plots of lower channel-belt thickness and bankfull thickness in five fluvial systems in the northern Gulf of Mexico. (A) and (B) Cumulative frequency plots of lower channel-belt and bankfull thickness reveal distinct thickness distribution patterns in the five fluvial systems.

4.5 DISCUSSION

4.5.1 Channel-belt thickness related to drainage basin area

Fluvial geomorphological data collected from modern and Quaternary systems suggest a strong correlation between drainage area and channel depth (Blum et al., 2013). In our work, we also used modern and Quaternary data to constrain predicted drainage area (Fig. 4.12). Both mean lower channel thickness and mean bankfull thickness data were used to calculate drainage basin area (Fig. 4.12; Table 4.2). The drainage area predicted from the mean lower channel-belt thickness is much smaller than the prediction from the mean bankfull thickness. The maximum predicted drainage area is about 30 times larger than the minimum prediction, e.g., the paleo-Mississippi River (1880 $*10^3$ km^2 versus 66 $*10^3$ km^2; Table 4.2).

The mapped drainage basin areas from paleogeographic reconstructions of Galloway et al. (2011) and Xu et al. (2017) lie within the range of the drainage basin areas predicted from both mean lower channel-belt and mean bankfull thicknesses (Fig. 4.12 and Table 4.2), indicating that such prediction is geologically reasonable. In addition, the correlation between channel dimension and reconstructed drainage area agrees with the trend of modern and Quaternary rivers (Fig. 4.12). However, the reconstructed drainage basin areas show large deviations from the median trend of modern and Quaternary systems when plotted with mean lower channel-belt thickness, whereas it shows a better correlation with mean bankfull thickness (Fig. 4.12). In addition, the difference between reconstructed drainage area and median predicted value from mean lower channel-belt thickness (41%–354%) is much larger than that of mean bankfull thickness (19%–159%; Table 4.2).

These results indicate that mean bankfull thickness better reflects drainage basin area. The sandy lower channel-belt, although easily identified from subsurface well logs and outcrops, only preserves a fraction of bankfull channel depth that scales with water

discharge through channel. In addition, the sandy lower channel-belt thickness varies from upstream to downstream (Fig. 4.7C), while bankfull thickness are relatively consistent in different parts of river system. Wolman and Leopold (1957) and Wolman and Miller (1960) defined bankfull flow depth as the most effective flow stage that maintains channel dimensions and profiles over time. Therefore, bankfull thickness that incorporates both sandy lower and muddy upper channel-belt, although sometimes more difficult to define on well logs, appears to be more sensitive to water discharge and thus drainage basin area. Therefore, in this work we focus on using mean bankfull thickness to predict drainage basin area.

4.5.1.1 Continental-scale river (paleo-Mississippi)

The paleo-Mississippi River was the most important sediment routing system in the early Miocene GOM (Fig. 4.3; Galloway et al., 2000, 2011). The paleo-Mississippi River bankfull thickness ranges from 15 to 40 m and has an average thickness of 25 m (Fig. 4.10; Table 4.1). The maximum bankfull thickness, 40 m, is close to the modern Mississippi channel depth. The bankfull depth of the modern Mississippi River ranges from 30 to 40 m (Frazier and Osanik, 1962; Saucier, 1994). Cox et al. (2014) interpreted the paleo-depth of the lower Mississippi River valley of Pliocene age as 35 m. Early Miocene Mississippi bankfull thickness is thus about 60–70% that of the Pliocene and modern Mississippi rivers.

The maximum drainage-basin area calculated from mean bankfull thickness using global modern and Quaternary river data is about 3000 $*10^3$ km^2, which is close to the area of the modern Mississippi River, whereas the minimum prediction, about 120 $*10^3$ km^2, approximates the modern Brazos River (Fig. 4.12; Table 4.2). The maximum prediction is about 30 times larger than the minimum prediction. The median predicted drainage area lies between minimum and maximum, 580 $*10^3$ km^2 (Fig. 4.12; Table 4.2).

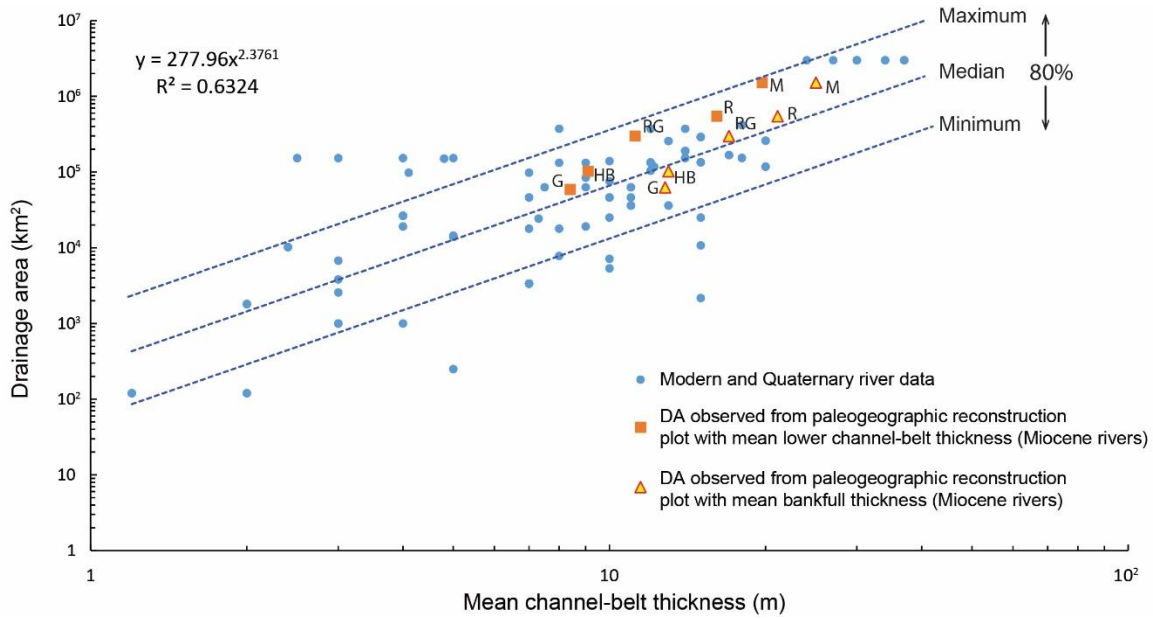

Figure 4.12: Comparison of early Miocene data and global modern-Quaternary data.

Correlation of early Miocene drainage basin area (DA) with mean channel-belt thickness compared to the global scaling relationship established for modern and Quaternary systems. Previous paleogeographic work by Galloway et al. (2011) and Xu et al. (2017) provides an additional constraint on drainage basin area to test predictions. The modern and Quaternary systems data are from Blum et al. (2013). The median regression line is generated by the whole dataset of modern and Quaternary systems. The maximum and minimum lines incorporate 80% of data that concentrate toward the median line. The early Miocene dataset fit well with the trend of modern-Quaternary river systems. Abbreviations: RG – Rio Grande; G – Guadalupe; HB – Houston-Brazos; R – Red; M – Mississippi.

River system	Thickness (m)	Minimum predicted *DA (10^3 km^2)	Maximum predicted *DA (10^3 km^2)	Median predicted *DA (10^3 km^2)	Paleogeographic reconstruction *DA (10^3 km^2)	Difference† (%)
Lower channel-belt						
Mississippi	19.7	66	1880	330	1500	354
Red	16.1	41	1160	200	540	170
Rio Grande	11.2	17	490	86	300	249
Houston-Brazos	9.1	10	300	53	100	89
Guadalupe	8.4	9	250	44	62	41
Channel-belt bankfull						
Mississippi	25.0	120	3310	580	1500	159
Red	21.1	80	2210	390	540	39
Rio Grande	17.0	50	1320	230	300	30
Houston-Brazos	13.0	25	700	123	100	19
Guadalupe	12.8	24	670	119	62	48

*DA = Drainage area. Difference† is calculated based on DA predicted from mean channel depth and observed from paleogeographic reconstruction.

Table 4.2: Drainage basin area estimated from mean channel bankfull thickness and paleogeographic reconstruction.

The continental reconstruction combined with detrital zircon U-Pb ages suggests that the lower Miocene Mississippi sediments were primarily sourced from the Rocky Mountains and Great Plains in the west, Ouachita Mountains, and Appalachian Mountains and foreland basin in the east (Galloway et al., 2011; Xu et al., 2017; Figs. 4.4 and 4.8). The paleo-drainage was similar to that of the modern Mississippi River. However, the upper Missouri River and Ohio River were not integrated into the Mississippi River until the Pliocene (Blum and Robert, 2012; Bentley et al., 2015). Absence of an Upper Missouri River draining northern Wyoming and southern Canada is supported by the rarity of Archean zircons in lower Miocene sediment deposited in the coastal plain (Xu et al., 2017). Therefore, the reconstructed drainage area of the paleo-Mississippi is approximately $1{,}500*10^3$ km^2 (Table 4.2).

The reconstructed drainage area of the paleo-Mississippi lies between the median and maximum predicted drainage area from mean bankfull thickness, validating that such prediction is reasonable; however, the uncertainty is more than an order of magnitude. The mean bankfull thickness of the early Miocene Mississippi River is about 60–80% of the modern Mississippi (25 m versus 30–40 m), and consequently the drainage area of the early Miocene Mississippi River is about 50% of its modern counterpart ($1500 *10^3$ km^2 versus $3300 *10^3$ km^2). The consistent relationship between channel depth and drainage area in early Miocene and modern system also supports the use of the modern dataset to predict the ancient, unmappable drainage basin area. The general agreement between two independent approaches increases the confidence level of current understanding of the paleo-Mississippi drainage basin.

4.5.1.2 Large-scale River (Paleo-Red River and Rio Grande)

The paleo-Red River was a major sediment carrier in the early Miocene. It built the Calcasieu delta near the Texas–Louisiana state boundary (Galloway et al., 2000, 2011; Fig. 4.5). The bankfull thickness of the paleo-Red River ranges from 14 to 29 m, with an average thickness of 21 m (Fig. 4.10; Table 4.1). The paleo-Red River has the second thickest channel-belt deposit in the northern GOM coastal plain (Figs. 4.9, 4.10, and 4.11). The bankfull thickness of the paleo-Red River, now a tributary of the modern Mississippi River system, is much thicker than that of the modern Red River (8 – 18 m). The drainage area calculated from mean bankfull thickness ranges from 78 $*10^3$ km^2 to 2,210 $*10^3$ km^2, with median value of 390 $*10^3$ km^2 (Table 4.2).

Detrital zircon provenance analyses show that most paleo-Red River sediment was derived from the southern Rocky Mountains, southern Great Plains, eastern margins of volcanic fields in southwestern North America, and the Ouachita Mountains (Xu et al., 2017; Fig. 4.4). The reconstructed paleo-Red provenance suggested a drainage basin area of 540 $*10^3$ km^2 (Fig. 4.12; Table 4.2).

The geologically mapped paleo-Red drainage area lies between the median and maximum predicted drainage area, and the difference between median predicted drainage area and reconstructed drainage area is 39% (Fig. 4.12; Table 4.2). The general agreement between two independent approaches indicates that the scaling relationship built for modern and Quaternary data applies well to this ancient system.

The paleo-Rio Grande River was a bedload-dominated extra-basinal river that drained lithologically diverse source terranes with abundant volcanic rocks (Galloway, 1981; Galloway et al., 1982; Galloway et al., 2011). It prograded across the shelf, built a large North Padre delta, and fed sediments into a deep-water basin (Fig. 4.4), indicating a large sediment influx and drainage basin area. The paleo-Rio Grande has a medium

channel-belt dimension among river systems on the northern GOM coastal plain (Figs. 4.9, 4.10, and 4.11). Bankfull thickness ranges from 12 to 24.5 m and has an average thickness of 17 m. The calculated drainage basin area is from 47 $*10^3$ km^2 to 1320 $*10^3$ km^2, with a median value of 230 $*10^3$ km^2 (Fig. 4.12; Table 4.2).

Detrital zircon analyses of lower Miocene sediments on the South Texas coastal plain suggest that most zircons were sourced from volcanic fields from southwestern North America (Xu et al., 2017). This conclusion is also supported by petrographic analyses that show that volcanic fragments are the dominant rock fragments (Dutton et al., 2012). Reconstructed paleogeographic maps show a possible a drainage basin area of 300 $*10^3$ km^2 (Fig. 4.4). The mapped drainage area is within the range of maximum and minimum predicted drainage basin areas (Fig. 4.12; Table 4.2). The drainage area difference between the two independent methods is 30% (Table 4.2), indicating that the predicted drainage area is reasonable.

4.5.1.3 Moderate-scale Rivers (Paleo-Houston-Brazos and Guadalupe)

The paleo-Houston-Brazos and Guadalupe rivers were two moderate-scale river systems in the early Miocene paleo-drainage network. No large deltas were built outboard of the coastal plain (Fig. 4.4). Mean bankfull thicknesses of the paleo Houston-Brazos and Guadalupe rivers are about 13 m. On cumulative frequency plots, they clustered on the left side and decreased rapidly from 21 to 9 m (Fig. 4.11B).

The drainage area calculated from mean bankfull thickness of 13 m is from approximately 25 $*10^3$ km^2 to 700 $*10^3$ km^2, with a median value of 120 $*10^3$ km^2 (Fig. 4.12; Table 4.2). Galloway (1981) defined the paleo-Brazos-Houston and Guadalupe rivers as basin-fringe to intra-basinal streams. Sandstones in the eastern Texas coastal plain contain abundant carbonate rock fragments provided by a proximal sediment source from

the elevated Edwards Plateau (Galloway et al., 1982; Galloway et al., 2011; Dutton et al., 2012). The paleo-Brazos drainage basin is about 100 *10^3 km^2, according to provenance analysis (Figs. 4.4 and 4.8; Table 4.2). The paleo-Guadalupe system has mixed sediments, sourced from carbonate material from the Edwards Plateau and reworked volcanic materials, and it has a drainage basin area of 60 *10^3 km^2 (Figs. 4.4 and 4.8; Table 4.2).

Reconstructed drainage areas of the paleo-Houston-Brazos (100 *10^3 km^2) and paleo-Guadalupe (60 *10^3 km^2) lie within the range of the calculated drainage areas (25–700 *10^3 km^2 ;Table 4.2; Fig. 4.12) and the difference between calculated median drainage area and reconstructed area is 19–48% (Table 4.2; Fig. 4.12). These agreements suggest that the scaling correlation between channel depth and drainage area from global river data is applicable to moderate-scale ancient river systems. In addition, the modern Brazos River has recorded a deeper channel depth (17–20 m; Bernard et al., 1970) and larger associated drainage area (116*10^3 km^2) than those of early Miocene Brazos River, displaying a consistent correlation from Miocene to modern systems.

4.5.2 Scaling Relationships among S2S Components

All components in S2S systems are thought to be genetically linked, and the dimension of one component should scale to other components if the whole system is in equilibrium (Sømme et al., 2009a; Romans and Graham, 2013; Bentley et al., 2016; Bhattacharya et al., 2016; Romans et al., 2016; Fig. 4.1). Sediment volume transferred by rivers is significantly influenced by area, relief, lithology, and climate of catchment, and in turn it also affects the dimensions of depositional components in the basinal sink, such as submarine fan dimensions (Hovius and Leeder, 1998; Syvitski and Milliman, 2007; Covault et al., 2012; Holbrook and Wanas, 2014; Bhattacharya et al., 2016). In this work, we also measured additional components of S2S systems, including submarine fan run-out

length and area, and drainage basin length, to explore the relationships among these different components in S2S systems (Fig. 4.8).

A correlation exists between mean bankfull thickness and drainage basin area of the five lower Miocene fluvial systems (Fig. 3.13B). Sømme et al. (2009a) suggested that length of the longest river channel increases with expanding drainage basin area. However, in an ancient system, it is difficult to measure the river length directly. Alternatively, it is more practical to measure the drainage basin length as a proxy for the longest river length (Figs. 4.8 and 3.13A). Drainage basin length should scale to the water discharge of the entire basin and thus relate to the bankfull thickness. The drainage basin length of five lower Miocene systems displays a linear correlation with mean bankfull thickness (Fig. 3.13C). More data collected from ancient systems in the GOM would further test and refine this relationship.

Submarine fan run-out length and area were calculated for three mapped lower Miocene fan or apron systems, corresponding to the paleo-Mississippi River, Red River, and Rio Grande (Fig. 4.8). These three systems are characterized by progradation of shelf margin and deposition in the deep-water basin by turbidity flows. Although the distribution of these basin-floor fans was mapped by GBDS project researchers by using well log and seismic data, uncertainties remain about the exact fan run-out length and fan area in the deep-water basin. Due to the presence of a complicated salt canopy in the GOM, even after decades of explorations of lower Miocene deep-water reservoirs, the dimensions of lower Miocene submarine fan beneath salt canopy are still being mapped. No submarine fans are observed in front of paleo-Houston-Brazos and Guadalupe fluvial systems. This can be a product of their relatively low sediment supply rate, to storage of most sediment as shoreface, shelf, and growth-faulted upper slope deposits (Fig. 4.5), or to masking of fan deposits beneath the complicated salt canopy.

Dimensions of the fan systems show correlation with the mean bankfull thickness (Table 4.3; Figs. 3.13 D and E). The paleo-Mississippi fan system extends across the abyssal plain 380 km from the coeval shelf margin and covers an area of 64,000 km^2. The early Miocene Mississippi fan length is shorter than the modern system, which has a fan run-out length of 655 km. The fan length difference is consistent with the observed channel-belt thickness of the early Miocene Mississippi fluvial system, which was approximately 60–80% of the thickness of the modern system (25 m versus 30–40 m), and an early Miocene drainage area that was about 50% of modern system (1,500 * 10^3 km^2 versus 3,000 * 10^3 km^2). In addition, the area of the early Miocene Mississippi fan is about 64,000 km^2 (this work; Table 4.3), much smaller than the modern system, which has an area of 300,000 km^2 (Sømme et al., 2009a). The fan run-out distance of the paleo-Red River system is about a half-length of the paleo-Mississippi system (190 km), whereas the paleo-Rio Grande has a submarine fan run-out length of only 130 km, which is about one-third of the paleo-Mississippi fan run-out length (Table 4.3). The paleo-Red River and Rio Grande systems have smaller fluvial and fan dimensions compared to the paleo-Mississippi, due to their smaller drainage areas. Therefore, the dimension of the lower Miocene and modern submarine fans in the GOM scale with their onshore river dimension and drainage area, which is consistent with the mass-balance assumption in S2S, provided there is no significant intermediate storage or loss of sediment mass.

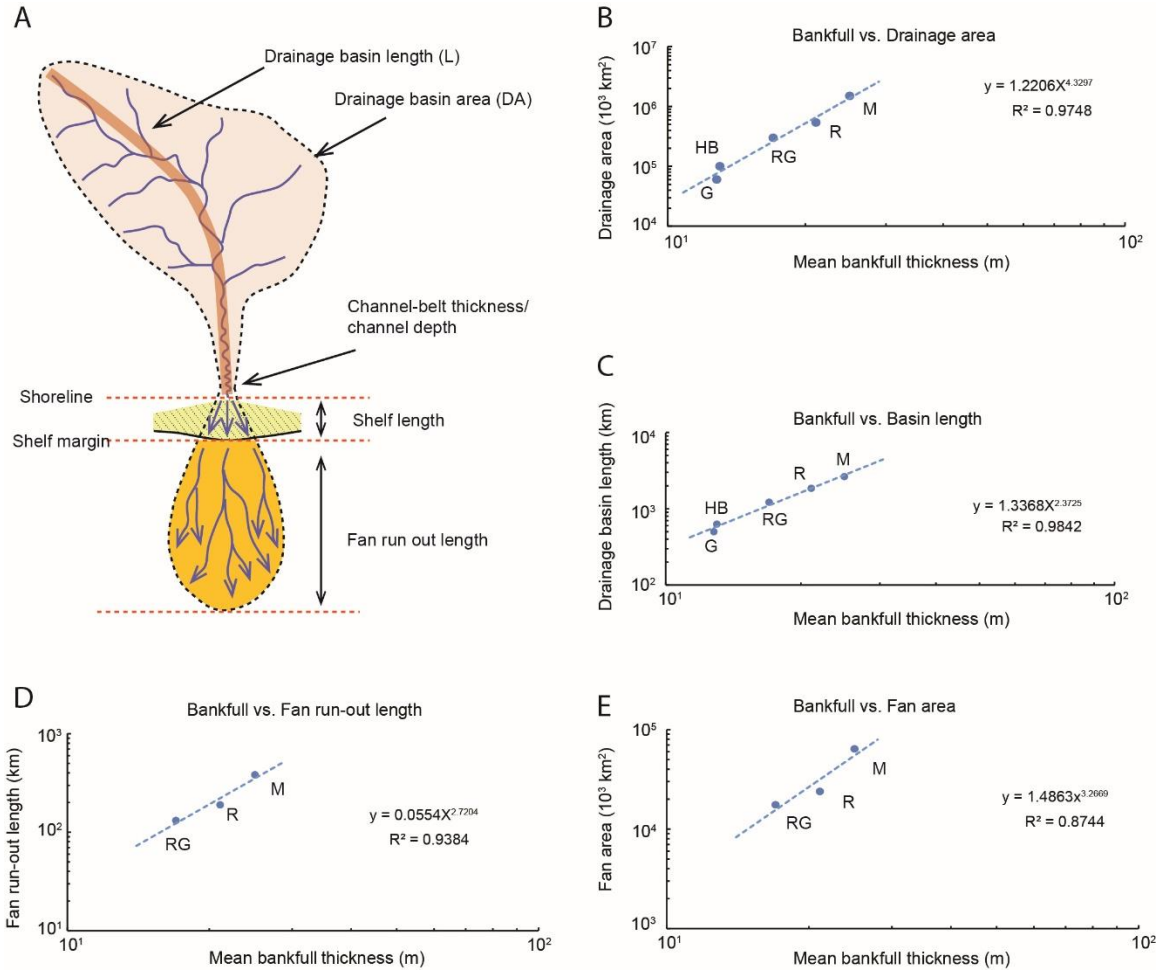

Figure 4.13: Relationship between mean bankfull thickness and different lower Miocene S2S components.

(A) A simplified S2S model illuminates the scaling parameters for different components of the system. (B) and (C) Correlations among mean bankfull thickness, drainage basin length, and drainage basin area. (D) and (E) Correlations among mean bankfull thickness, submarine fan run-out length and submarine fan area. The correlations are based on few dataset and more data collected from ancient systems will refine this relationship. Abbreviations: RG – Rio Grande; G – Guadalupe; HB – Houston-Brazos; R – Red; M – Mississippi.

River system	Lower channel belt thickness (m)	Mean bankfull thickness (m)	Shelf width (m)	Drainage basin length (km)	Drainage basin size (10^3 km^2)	Submarine fan run-out length (km)	Submarine fan size (km^2)
Mississippi	19.7	25	142	2650	1500	380	64000
Red	16.1	21.1	92	1860	540	190	24000
Rio Grande	11.2	17	115	1220	300	130	17600
Houston-Brazos	9.1	13	75	450	100	N/A	N/A
Guadalupe	8.4	12.8	77	470	60	N/A	N/A

Table 4.3: Parameters of source-to-sink system of lower Miocene interval in the northern Gulf of Mexico.

4.5.3 Uncertainties and limitations

Most quantitative or semi-quantitative S2S studies were based on modern or Quaternary data (e.g., Wetzel, 1993; Sømme et al., 2009a, b), with few current applications to deep-time stratigraphy. When applying a scaling relationship derived from modern systems to rock records, several uncertainties and limitations are associated with the method.

Uncertainties can arise from morphological variations in a single channel. A single channel-belt can have high variations in thickness by at least a factor of two during channel-forming processes (Bridge and Tye, 2000). For example, the thalweg depth can be significantly thicker than the thickness of the channel-belt that was deposited on the depositional bank (e.g., Fisk, 1944; Willis and Tang, 2010).

The measurement of a complete succession of channel-belt deposits to estimate paleo-channel depth is difficult to do by using well logs alone, because the upper channel deposit can be either partially truncated by an overlying channel or mixed with overbank deposits (e.g., Lorenz et al., 1985). Combing of outcrop and core data would increase the precision of measurement. The lower channel-belt is sand and gravel rich and easier to identify from outcrop, core, and well log data. However, it underestimates the paleo-flow depth (Bridge and Tye, 2000).

Climatic variations in time and space can induce a large variation in channel-belt thickness in rivers (Figs. 4.9, 4.10, and 4.11) of similar drainage basin area and statistical overlap of values for rivers with much different areas. The maximum channel-belt thickness of the paleo-Houston-Brazos and Guadalupe rivers can be equal to the minimum channel-belt thickness of the paleo-Mississippi River. This overlap can result from measuring channel-belt thickness in different locations within a channel landform (e.g.,

thalweg versus depositional bank), or from periodic climate changes during the history of the river system. For small drainage systems, the peak water discharge can be several orders of magnitude higher than the long-term average rate (Mulder and Syvitski, 1995). Therefore, the flood stage of small systems can have a temporary channel-flow depth similar to that of much larger systems. In this work, we use average bankfull thickness to average these variations and use it to represent the long-term flow depth for the entire early Miocene period (~ 8 Ma).

Additional uncertainty comes from burial compaction of channel-belt sediments. The compaction is complicated by many factors, including grain roundness, sorting, mineral composition, and size grading (Allen and Chilingarian, 1975). Ethridge and Schumm (1977) suggested a reduction of 10% of original bankfull depth by subsurface compaction. Our channel- belt data were compiled from various well log data from the Texas-Louisiana coastal plain. Most channel-belt data were measured from units that are now lying between 100 m and 1000 m deep; a few channel-belt deposits are buried to a depth of 1500 m. It is not easy to give a simple decompaction correction for our channel-belt measurement because they experienced different compaction histories. Overly simple correction for compaction may introduce extra uncertainties into system. Given that uncertainties in the statistical predictions lie in the range of one to two orders of magnitude, we conclude that compacted variability will not affect the predictions measurably; thus, we do not apply corrections.

In summary, natural S2S systems are complex (e.g., thickness variations in a single channel), and many uncertainties are associated with the measurements. Variations in tectonics and climate in catchment areas complicate the correlation between channel depth and drainage- basin area, resulting in uncertainties of more than an order of magnitude. However, these uncertainties are part of natural systems and are not flaws in methodology.

Given these uncertainties, it may be hard to differentiate a continental-scale drainage system from a large-scale drainage system by using channel-belt thickness alone. However, continental-scale systems rarely share the same channel dimensions with moderate-scale rivers or smaller systems (Fig. 4.11). Alternatively, detrital zircon U-Pb age spectra have been proven to be a useful approach for conducting provenance analyses and reconstructing paleogeography. However, detrital zircons can survive multiply recycling events, blurring or complicating the definition of specific source terranes, and they may sometimes fail to track intermediate source terranes. Combining detrital zircon provenance analysis and channel-belt measurement provides a better constraint on paleo-drainage basin area than does either technique alone.

4.6 CONCLUSIONS

Single-storey channel-belt thicknesses were measured from an extensive well log database in the well-explored Gulf of Mexico basin and used to calculate paleo-drainage areas of several differentiated early Miocene fluvial systems. Mean channel-belt thicknesses shows a strong correlation with paleo-drainage areas that were reconstructed independently from petrographic and detrital zircon provenance analyses and continental geomorphic synthesis (Fig. 3.13B).

Drainage areas were calculated from both mean lower channel-belt and mean bankfull-thickness data, using scaling relationships that built on a global modern and Quaternary river database. Drainage basin areas calculated from mean bankfull thickness show good agreement with independently mapped drainage basin areas (Table 4.2), although the measurement of bankfull thickness has high interpretive uncertainties when based on well log data alone. Sandy lower channel-belt thickness, which is easy to identify from well log response, resulted in smaller predicted areas that depart significantly from

the independently mapped drainage basin areas and from the trend line of modern and Quaternary river data (Fig. 4.12; Table 4.2). Therefore, bankfull thickness is the better proxy for estimating paleo-channel depths and calculation of drainage basin area.

Drainage basin area predicted from mean bankfull thickness shows a wide range of more than an order of magnitude. However, the reconstructed drainage area of each well-studied lower Miocene system lies between the minimum and maximum values of this scaling relationship, supporting the use of the modern dataset to predict ancient, less easily mappable drainage basin areas. Combining detrital zircon provenance analyses and channel-belt measurements constrains paleo-drainage basin area better than does either technique alone.

Extrapolating the scaling relationship established from modern and Quaternary data into deep-time stratigraphy involves many uncertainties, including natural internal channel-belt thickness variation, incomplete channel preservation, subjective interpretation and measurement of channel-belt thickness, compaction overprints, and climatic and tectonic variability in catchment areas. However, these uncertainties do not negate the power of this scaling relationship. Knowledge of fluvial deposit dimensions, such as channel-belt thickness, provides a first-order estimate of drainage basin area and a plausible assessment of continental geomorphology.

Mean channel-belt bankfull depth also correlates with drainage-basin length and area and submarine-fan length and area in lower Miocene S2S systems. This correlation indicates a mass balance between sediment supply from catchment, sediment transport through fluvial channels, and sediment ultimately deposited in the basin. Therefore, knowledge of channel dimensions onshore also has implications for prediction of the dimensions of fan run-out length and area in the deep-water basin.

ACKNOWLEDGMENT

We would like to thank the members of the Gulf Basin Depositional Synthesis Project (GBDS) industrial associate program and GBDS project manager Patricia Ganey-Curry. We thank the Institute for Geophysics, University of Texas at Austin, for providing a Ewing-Worzel Graduate Fellowship. Constructive comments by an anonymous reviewer and Peter Sadler are appreciated and helped greatly to improve this manuscript.

Chapter 5: Conclusions

This work is the first regional study to analyze the source-to-sink system of the lower Miocene strata in the northern Gulf of Mexico Basin by using detrital zircon U-Pb and (U-Th)/He double dating. The detrital zircon U-Pb age data obtained from 19 lower Miocene samples spanning the northern Gulf of Mexico margin document a continental-scale sediment provenance shift across the northern Gulf of Mexico from highlands in the western United States to the Appalachian Mountains and foreland basin in the eastern United States. The sediment associated with the paleo–Rio Bravo, Rio Grande, Brazos, Red, Mississippi, Tombigbee, and Apalachicola Rivers can be differentiated based on detrital zircon analyses, improving definition of sediment transport pathways from upland sources to basinal sinks.

Compared to published detrital zircon work on Paleogene Wilcox Group, the absence of zircon grains with Mesozoic ages (110–140 Ma) and smaller numbers of Archean-Paleoproterozoic (>1800 Ma) zircons in lower Miocene strata indicate reduced sediment contribution from the central-northern Rocky Mountains and western Mexico terranes. The resulting smaller drainage basin area may partially explain the decreased volume of sediment in lower Miocene strata relative to the Wilcox Group (Galloway et al., 2011). This decrease in sediment volume may also have been related to arid conditions in the western United States, which reduced fluvial discharge and thus the capacity of rivers to deliver sediment to the Gulf of Mexico.

Combined zircon U-Pb and (U-Th)/He double dating of detrital zircon grains is used to reveal both crystallization and exhumation histories of source terranes and to differentiate first-cycle volcanic and plutonic zircons from multi-cycle zircon sources. Many grains are identified as first–cycle volcanic zircons and are likely eroded from

Cretaceous–Cenozoic volcanic fields or the volcanic–fragment–rich Eocene–Oligocene strata on the Great Plains, consistent with the presence of volcanic rock fragments in the northwestern Gulf of Mexico.

Zircon U-Pb and (U-Th)/He double dating provides the ability to identify different sources for first cycle and multi–cycle zircons, especially to differentiate the various sources of Grenville zircons. Grenville zircons from the Llano Uplift in central Texas, exposures in western Texas, northern Mexico and the southern Appalachian Mountains, as well as multi–cycled zircons from the sedimentary strata on the Great Plains and Appalachian foreland basin, can all be identified and differentiated. Multiple recycled sedimentary sources, as well as first–cycle primary sources from crystalline terranes can be identified using these techniques, greatly increasing our ability to understand the complex system of sediment sources in large passive margin basins like the Gulf of Mexico Basin.

This work also explores the potential for applying the scaling relationship between channel-belt thickness and drainage basin area, which was established for modern-Quaternary systems, to deep-time stratigraphy. Single-storey channel-belt thicknesses were measured from an extensive well log database in the well-explored Gulf of Mexico basin and used to calculate paleo-drainage areas of several differentiated early Miocene fluvial systems. The predicted drainage areas from channel-belt thickness show good agreement with the paleo-drainage areas that were reconstructed independently from petrographic and detrital zircon provenance analyses and a continental geomorphic synthesis. Therefore, knowledge of fluvial deposit dimensions, such as channel-belt thickness, provides a first-order estimate of drainage basin area and a plausible assessment of continental geomorphology.

Mean channel-belt bankfull depth correlates with drainage-basin length and area and submarine-fan length and area in lower Miocene S2S systems. This correlation indicates a mass balance between sediment supply from catchment, sediment transport through fluvial channels, and sediment ultimately deposited in the basin. Therefore, knowledge of channel dimension onshore also has implications for prediction of the dimensions of fan run-out length and area in the deep-water basin.

Appendices

APPENDIX A: SUPPLEMENTARY FILE FOR CHAPTER 2

Appendix A1 Zircon U-Pb LA-ICP-MS methodology

Zircon U-Pb geochronology was conducted at the laser ablation high-resolution inductively coupled plasma mass spectrometry (LA-HR-ICP-MS) laboratory at the University of Texas at Austin (UTChron Laboratory, Department of Geological Sciences). Nineteen samples from the northern Gulf of Mexico coast were selected for study. Each sample was crushed and pulverized. All grains were passed through a Wilfley water table for hydrodynamic separation of relative high-density minerals from low density ones. Heavy liquids with densities of 2.84 g/cc (Bromoform) and 3.3 g/cc (methylene iodide, MEI) were used to further separate minerals by density. Frantz, a kind of magnetic mineral separator, was performed on mineral separation based on magnetic susceptibility. This step was followed by visual selection of barite, pyrite and rutile under a binocular microscope to remove non-zircon grains. Zircons from each sample are randomly selected for isotopic analysis to avoid bias. Zircons were sprinkled onto double-sided tape and depth-profiled, which allows for detection of thin (≤5 μm) rims.

The LA-ICP-MS system consisted of a PhotonMachines Analyte.G2 ArF excimer 193nm laser, equipped with a two-volume Helex 9 sample cell, coupled to a ThermoFisher Element 2 double-focusing magnetic sector ICP-MS. Helium was used as the carrier gas and mixed with Argon before entering the ICPMS. All analyses were conducted in static mode with a laser beam diameter of 30μm, operated with an energy density of 1.43 J/cm2, and a pulse rate of 10 Hz. Zircon analysis consisted of 6 cleaning shots, 25 seconds of baseline data collection, 30 seconds of laser dwell time, and 35 seconds of washout.

Ablation rates of ~0.5μm/second mean that only the outer 15-17μm of zircons are typically sampled by this technique.

Elemental and isotopic fractionation of Pb/U and Pb isotopes, respectively, is correct by interspersed analysis of primary zircon standard GJ1 ($^{206}Pb/^{238}U$ 601.7 ± 1.3 Ma; Jackson et al., 2004). The common unknown to standard measurement ratio is generally 4:1 at UTChron. Uncertainty resulting from calibration correction is generally 1-2% for both $^{206}Pb/^{207}Pb$ and $^{206}Pb/^{238}U$. An internal lab zircon standard (Pak 1 and Plesovice) is used as a secondary reference. Age calculation was performed using Iolite (Igor Pro) and VizualAge (Petrus and Kamber, 2012), based on ISOPLOT V3 formulas (Ludwig, 2003) from baseline-subtracted intensities. No correction was applied for common Pb due to interferences in measurement of 204Pb; however, common Pb was evaluated graphically and high Pbc zones usually rejected. Errors for isotopic ratios are presented at 2-sigma absolute error.

Appendix A2 Rock sample information

A2.1 Outcrop sample information

Outcrop sample	Local formation name	Latitude	Longitude	Sedimentary facies
GOM2	Oakville	28.104964	-98.390381	Fluvial channel
GOM3	Oakville	28.324192	-98.232987	Fluvial channel
GOM4	Oakville	28.803502	-97.798488	Fluvial channel
GOM5	Oakville	30.146861	-96.640822	Fluvial channel
GOM6	Oakville	30.330725	-96.314522	Fluvial channel
GOM7	Oakville	30.451781	-96.026872	Fluvial channel
GOM8	Oakville	31.055100	-94.028200	Fluvial channel
GOM9	Lena	31.196412	-93.564165	Fluvial channel
GOM10	Carnahan Bayou	31.196412	-93.564165	Fluvial channel
GOM11	Carnahan Bayou	31.239455	-93.378590	Fluvial channel
GOM12	Catahoula	31.512663	-93.031941	Fluvial channel
GOM13	Lena	31.440175	-92.949738	Sheet splay
GOM14	Catahoula	31.999614	-90.964758	Fluvial channel
GOM15	Catahoula	31.551700	-89.321842	Shallow marine*
GOM16	Catahoula	31.682821	-88.683854	Fluvial channel
GOM19	Chipola	30.469205	-84.982084	Shallow marine

* Uncertainty of sedimentary facies due to very limited exposure.

Table A1: Outcrop samples information.

A2.2 Subsurface core information

Core sample	Lease name	Formation	Depth (ft)	Latitude	Longitude	Sedimentary Facies
GOM1	Sorenson Gu #2	Lower Miocene	3877-3877.5	26.108090	-98.119870	Fluvial channel
GOM17	Gavin #1	Basal undifferential Miocene Alum Bluff	232.0-264.0	30.759199	-86.199996	Fluvial channel
GOM18	Kohler #1	Basal undifferential Miocene Alum Bluff	238.0-263.0	30.702800	-86.035598	Fluvial channel

Table A2: Subsurface cores information.

Appendix A3 Zircon U-Pb database

Sample: GOM1	Isotopic Ratios							Isotopic ages (Ma)								
Analysis	[U] ppm	U/Th	207/235	2σ err.	206/238	2σ err.	RHO	207/235	2σ err.	206/238	2σ err.	207/206	2σ err.	Best age	2σ err.	% Dis.
GOM1_106	85.3	0.87	0.0358	0.0058	0.0055	0.0004	0.2250	35.5	5.7	35.3	2.4	10	310	35.3	2.4	0.6
GOM1_37	95.3	1.20	0.0377	0.0034	0.0055	0.0003	0.0671	37.5	3.3	35.6	1.9	260	210	35.6	1.9	5.1
GOM1_53	274	0.50	0.0399	0.0023	0.0058	0.0002	0.2748	39.7	2.3	37.2	1.4	220	130	37.2	1.4	6.3
GOM1_97	932	5.32	0.0478	0.0012	0.0074	0.0002	0.1004	47.4	1.1	47.2	1.0	116	63	47.2	1.0	0.3
GOM1_29	231.2	1.00	0.0569	0.0037	0.0087	0.0003	0.1642	56.1	3.5	55.6	1.7	80	130	55.6	1.7	0.9
GOM1_82	187	1.71	0.0578	0.0036	0.0091	0.0003	0.0715	57.4	3.3	58.4	1.8	80	130	58.4	1.8	1.7
GOM1_95	138.9	13.20	0.0634	0.0045	0.0096	0.0003	0.1903	62.3	4.3	61.4	1.9	90	130	61.4	1.9	1.4
GOM1_114	790	1.05	0.0661	0.0020	0.0103	0.0002	0.0539	65.0	1.9	65.9	1.3	69	77	65.9	1.3	1.4
GOM1_38	78.8	0.79	0.0751	0.0052	0.0110	0.0004	0.1256	74.1	5.1	70.4	2.3	260	150	70.4	2.3	5.0
GOM1_117	890	2.65	0.0734	0.0018	0.0112	0.0002	0.3573	71.9	1.7	71.5	1.2	113	52	71.5	1.2	0.6
GOM1_79	170	1.32	0.0824	0.0075	0.0121	0.0005	0.0474	80.2	7.0	77.7	3.2	180	190	77.7	3.2	3.1
GOM1_4	122.2	1.09	0.0835	0.0043	0.0126	0.0004	0.0682	81.3	4.0	80.9	2.4	150	120	80.9	2.4	0.5
GOM1_98	354	0.80	0.0832	0.0071	0.0129	0.0006	0.1141	81.0	6.6	82.7	3.9	70	190	82.7	3.9	2.1
GOM1_19	467	1.53	0.0933	0.0029	0.0142	0.0003	0.1861	90.5	2.7	90.8	1.9	90	73	90.8	1.9	0.3
GOM1_18	153	1.07	0.0989	0.0052	0.0148	0.0005	0.1512	95.6	4.8	94.7	3.2	100	110	94.7	3.2	0.9
GOM1_12	249	0.32	0.1022	0.0071	0.0150	0.0006	0.3209	100.2	6.9	96.2	3.7	180	150	96.2	3.7	4.0
GOM1_93	463	0.88	0.1000	0.0031	0.0152	0.0004	0.3675	96.7	2.9	97.4	2.4	64	59	97.4	2.4	0.7
GOM1_122	884	3.38	0.1018	0.0065	0.0155	0.0010	0.6709	98.4	6.0	99.1	6.5	100	110	99.1	6.5	0.7
GOM1_120	500	0.85	0.1035	0.0031	0.0156	0.0003	0.2590	100.4	2.7	100.0	1.9	134	68	100.0	1.9	0.4
GOM1_83	214	0.89	0.1114	0.0043	0.0163	0.0004	0.0087	107.1	3.9	104.4	2.5	146	82	104.4	2.5	2.5
GOM1_81	227.9	1.12	0.1106	0.0035	0.0164	0.0003	0.2577	106.4	3.2	105.1	1.9	155	72	105.1	1.9	1.2
GOM1_103	35.1	0.93	0.1190	0.0140	0.0168	0.0009	0.1682	113.0	13.0	107.4	5.4	200	240	107.4	5.4	5.0
GOM1_56	311.2	0.82	0.1731	0.0042	0.0253	0.0003	0.4413	162.0	3.6	160.9	2.1	175	46	160.9	2.1	0.7
GOM1_108	153	0.34	0.1698	0.0082	0.0254	0.0011	0.0618	159.1	7.1	161.7	6.7	140	120	161.7	6.7	1.6
GOM1_87	196.8	0.98	0.1783	0.0077	0.0258	0.0008	0.2924	166.4	6.7	163.9	5.1	219	89	163.9	5.1	1.5
GOM1_44	127	0.32	0.1797	0.0063	0.0261	0.0007	0.3272	167.6	5.4	166.0	4.1	239	82	166.0	4.1	1.0
GOM1_111	314	0.50	0.1817	0.0056	0.0265	0.0006	0.1448	169.5	4.8	168.8	3.7	168	86	168.8	3.7	0.4

GOM1_73	259	1.60	0.1974	0.0069	0.0278	0.0006	0.3997	182.6	5.9	176.8	3.7	286	69	176.8	3.7	3.2
GOM1_59	226	1.58	0.1896	0.0053	0.0278	0.0005	0.1000	176.1	4.5	177.0	3.3	177	70	177.0	3.3	0.5
GOM1_70	187.7	0.47	0.2243	0.0054	0.0330	0.0006	0.2055	205.3	4.5	209.2	3.9	201	58	209.2	3.9	1.9
GOM1_41	210	0.96	0.2639	0.0063	0.0369	0.0005	0.2285	237.6	5.1	233.5	3.3	302	57	233.5	3.3	1.7
GOM1_124	153.4	1.10	0.2630	0.0110	0.0374	0.0010	0.3487	236.6	8.5	236.5	6.3	249	88	236.5	6.3	0.0
GOM1_91	65	1.26	0.2700	0.0140	0.0380	0.0011	0.0825	242.0	11.0	240.4	7.1	270	110	240.4	7.1	0.7
GOM1_31	39.3	0.86	0.2730	0.0170	0.0382	0.0017	0.3940	244.0	13.0	242.0	10.0	360	150	242.0	10.0	0.8
GOM1_49	333	1.06	0.2841	0.0065	0.0398	0.0008	0.2370	254.3	5.0	251.6	4.7	292	68	251.6	4.7	1.1
GOM1_119	601	6.31	0.2914	0.0059	0.0406	0.0006	0.3146	259.5	4.6	256.6	3.6	266	50	256.6	3.6	1.1
GOM1_76	316	1.80	0.2893	0.0082	0.0411	0.0007	0.1224	257.6	6.5	259.8	4.5	241	67	259.8	4.5	0.9
GOM1_85	370.3	0.71	0.3920	0.0170	0.0527	0.0016	0.2325	335.0	13.0	331.0	10.0	328	94	331.0	10.0	1.2
GOM1_63	186	1.32	0.3928	0.0091	0.0540	0.0010	0.2546	336.0	6.6	339.6	6.0	353	54	339.6	6.0	1.1
GOM1_3	442	1.02	0.5100	0.0100	0.0610	0.0011	0.4420	418.1	6.7	381.9	6.7	599	38	381.9	6.7	8.7
GOM1_77	240	1.04	0.5020	0.0140	0.0661	0.0016	0.5056	414.6	9.5	412.6	9.4	432	57	412.6	9.4	0.5
GOM1_5	165	2.46	0.4980	0.0300	0.0667	0.0040	0.4806	414.0	18.0	416.0	24.0	410	140	416.0	24.0	0.5
GOM1_11	511	1.11	0.5230	0.0110	0.0669	0.0013	0.1535	426.6	7.4	417.3	8.0	493	43	417.3	8.0	2.2
GOM1_16	113.6	0.63	0.5120	0.0230	0.0671	0.0021	0.4855	418.0	16.0	418.0	13.0	440	89	418.0	13.0	0.0
GOM1_78	226	1.57	0.6410	0.0120	0.0803	0.0014	0.4553	502.8	7.5	498.1	8.2	522	44	498.1	8.2	0.9
GOM1_105	125.5	0.84	0.6370	0.0270	0.0812	0.0020	0.4075	503.0	16.0	503.0	12.0	492	84	503.0	12.0	0.0
GOM1_67	80.3	1.01	0.7010	0.0170	0.0862	0.0016	0.1848	540.0	10.0	533.0	9.5	576	59	533.0	9.5	1.3
GOM1_32	108.9	1.26	0.7380	0.0170	0.0895	0.0017	0.3634	560.5	9.8	552.5	9.8	600	48	552.5	9.8	1.4
GOM1_20	306	1.77	0.8280	0.0160	0.0999	0.0018	0.5833	611.9	8.9	614.0	11.0	610	34	614.0	11.0	0.3
GOM1_102	78	1.45	0.8480	0.0260	0.1019	0.0020	0.1158	622.0	14.0	626.0	12.0	590	72	626.0	12.0	0.6
GOM1_6	87.4	1.09	0.8660	0.0140	0.1046	0.0018	0.1952	632.7	7.9	641.0	10.0	596	48	641.0	10.0	1.3
GOM1_45	149	2.13	1.4850	0.0210	0.1526	0.0018	0.4215	924.5	8.7	915.0	10.0	934	28	915.0	10.0	1.0
GOM1_57	163.3	1.00	1.5580	0.0430	0.1554	0.0041	0.4831	953.0	17.0	931.0	23.0	1002	46	931.0	23.0	2.3
GOM1_121	85.8	1.43	1.5550	0.0390	0.1589	0.0032	0.2500	951.0	15.0	950.0	18.0	934	57	950.0	18.0	0.1
GOM1_96	19.4	1.43	1.6240	0.0580	0.1614	0.0031	0.2139	978.0	22.0	964.0	17.0	1011	71	964.0	17.0	1.4
GOM1_104	469	5.03	1.6150	0.0190	0.1641	0.0021	0.6843	975.6	7.5	979.0	12.0	980	18	979.0	12.0	0.3
GOM1_72	82.2	1.40	1.6490	0.0300	0.1644	0.0025	0.3166	988.0	11.0	983.0	14.0	1007	36	983.0	14.0	0.5
GOM1_34	44.3	1.03	1.7850	0.0420	0.1762	0.0034	0.4321	1040.0	15.0	1046.0	18.0	1001	43	1001.0	43.0	4.5
GOM1_23	47	2.14	1.7410	0.0440	0.1724	0.0041	0.5216	1024.0	16.0	1027.0	22.0	1017	51	1017.0	51.0	1.0
GOM1_26	153.9	1.00	1.7840	0.0290	0.1733	0.0023	0.3057	1039.0	11.0	1030.0	13.0	1056	33	1056.0	33.0	2.5

GOM1_60	254	0.71	1.8540	0.0190	0.1814	0.0025	0.5483	1064.4	6.9	1074.0	13.0	1072	22	1072.0	22.0	0.2
GOM1_36	110.5	1.49	1.7500	0.0290	0.1681	0.0030	0.4907	1026.0	11.0	1001.0	17.0	1073	30	1073.0	30.0	6.7
GOM1_14	28.54	0.80	1.7640	0.0440	0.1689	0.0040	0.3701	1030.0	16.0	1005.0	22.0	1085	49	1085.0	49.0	7.4
GOM1_107	53.9	1.01	1.9750	0.0700	0.1863	0.0047	0.1909	1106.0	24.0	1101.0	26.0	1091	92	1091.0	92.0	0.9
GOM1_2	129.3	1.26	1.9110	0.0240	0.1837	0.0028	0.4105	1086.8	8.5	1087.0	15.0	1096	32	1096.0	32.0	0.8
GOM1_66	88.8	0.75	1.8980	0.0330	0.1813	0.0026	0.3540	1079.0	11.0	1074.0	14.0	1101	33	1101.0	33.0	2.5
GOM1_116	132.7	1.31	1.9110	0.0250	0.1788	0.0023	0.4364	1084.4	8.6	1060.0	13.0	1106	27	1106.0	27.0	4.2
GOM1_17	88.5	1.13	1.9020	0.0380	0.1810	0.0029	0.5172	1082.0	13.0	1072.0	16.0	1109	34	1109.0	34.0	3.3
GOM1_22	117.2	1.99	2.0960	0.0280	0.1955	0.0030	0.5069	1148.2	9.0	1151.0	16.0	1142	29	1142.0	29.0	0.8
GOM1_43	147	1.16	2.0930	0.0370	0.1932	0.0037	0.4682	1147.0	12.0	1138.0	20.0	1145	38	1145.0	38.0	0.6
GOM1_48	216	1.57	2.0510	0.0360	0.1918	0.0042	0.6960	1131.0	12.0	1131.0	23.0	1158	31	1158.0	31.0	2.3
GOM1_90	211	1.48	1.8370	0.0350	0.1697	0.0028	0.6399	1059.0	13.0	1010.0	15.0	1161	28	1161.0	28.0	13.0
GOM1_58	73	0.93	2.1470	0.0640	0.1984	0.0059	0.5121	1161.0	21.0	1170.0	31.0	1182	54	1182.0	54.0	1.0
GOM1_30	44.7	1.25	2.3440	0.0570	0.2094	0.0041	0.3993	1223.0	17.0	1225.0	22.0	1199	45	1199.0	45.0	2.2
GOM1_88	442	1.70	2.2530	0.0280	0.2023	0.0026	0.5624	1197.1	8.7	1187.0	14.0	1227	21	1227.0	21.0	3.3
GOM1_42	56.7	2.12	2.4150	0.0780	0.2142	0.0046	0.7781	1242.0	23.0	1250.0	25.0	1233	42	1233.0	42.0	1.4
GOM1_54	45.79	2.07	2.3600	0.1200	0.1966	0.0076	0.4868	1236.0	34.0	1156.0	41.0	1360	93	1360.0	93.0	15.0
GOM1_71	73.8	2.37	2.8540	0.0730	0.2379	0.0058	0.9107	1366.0	20.0	1374.0	30.0	1360	30	1360.0	30.0	1.0
GOM1_109	52.8	1.14	2.8680	0.0510	0.2393	0.0046	0.4492	1372.0	13.0	1382.0	24.0	1372	34	1372.0	34.0	0.7
GOM1_1	353	0.88	2.9430	0.0280	0.2403	0.0017	0.5718	1392.5	7.1	1388.0	9.1	1396	15	1396.0	15.0	0.6
GOM1_25	193	1.73	3.0810	0.0390	0.2502	0.0041	0.7535	1427.2	9.8	1445.0	21.0	1404	21	1404.0	21.0	2.9
GOM1_75	44.2	1.78	2.9250	0.0650	0.2343	0.0050	0.6512	1388.0	17.0	1356.0	26.0	1410	35	1410.0	35.0	3.8
GOM1_100	186	1.50	2.9860	0.0480	0.2448	0.0042	0.3203	1403.0	12.0	1411.0	22.0	1411	27	1411.0	27.0	0.0
GOM1_123	179.7	1.17	3.0270	0.0360	0.2440	0.0034	0.5756	1413.9	9.0	1407.0	18.0	1412	22	1412.0	22.0	0.4
GOM1_13	41.6	0.93	2.9580	0.0660	0.2374	0.0048	0.4504	1395.0	17.0	1373.0	25.0	1419	43	1419.0	43.0	3.2
GOM1_52	328	1.06	3.0520	0.0490	0.2461	0.0042	0.7225	1420.0	12.0	1418.0	22.0	1422	22	1422.0	22.0	0.3
GOM1_24	78.3	0.95	3.0390	0.0440	0.2438	0.0037	0.4773	1418.0	11.0	1406.0	19.0	1437	27	1437.0	27.0	2.2
GOM1_113	183	0.98	3.1220	0.0470	0.2532	0.0042	0.7631	1437.0	12.0	1454.0	22.0	1438	21	1438.0	21.0	1.1
GOM1_99	139.8	1.28	3.1390	0.0560	0.2527	0.0051	0.5520	1441.0	14.0	1451.0	26.0	1439	26	1439.0	26.0	0.8
GOM1_28	51.2	1.65	3.1960	0.0690	0.2541	0.0041	0.4002	1459.0	17.0	1459.0	21.0	1455	41	1455.0	41.0	0.3
GOM1_39	192.1	2.19	3.0970	0.0640	0.2455	0.0052	0.7661	1431.0	16.0	1415.0	27.0	1461	26	1461.0	26.0	3.1
GOM1_50	64.9	0.85	3.1170	0.0580	0.2465	0.0048	0.3807	1436.0	14.0	1420.0	25.0	1466	41	1466.0	41.0	3.1
GOM1_84	90.8	1.42	3.5060	0.0560	0.2705	0.0042	0.6276	1527.0	13.0	1543.0	21.0	1530	26	1530.0	26.0	0.8

GOM1_115	206	4.25	4.0460	0.0600	0.2918	0.0045	0.7048	1642.0	12.0	1650.0	23.0	1612	22	1612.0	22.0	2.4
GOM1_10	271	1.33	3.9480	0.0570	0.2829	0.0047	0.8049	1624.0	12.0	1608.0	24.0	1638	18	1638.0	18.0	1.8
GOM1_21	74.9	1.20	3.9200	0.0570	0.2825	0.0053	0.4929	1620.0	12.0	1603.0	27.0	1645	32	1645.0	32.0	2.6
GOM1_101	327	1.57	4.0960	0.0810	0.2904	0.0046	0.7465	1653.0	16.0	1643.0	23.0	1645	25	1645.0	25.0	0.1
GOM1_110	94.9	1.38	3.7980	0.0680	0.2701	0.0052	0.4884	1593.0	15.0	1541.0	26.0	1657	40	1657.0	40.0	7.0
GOM1_55	50.1	1.00	4.1900	0.0780	0.2984	0.0051	0.5013	1670.0	15.0	1683.0	25.0	1658	35	1658.0	35.0	1.5
GOM1_62	109	0.68	3.9540	0.0530	0.2825	0.0042	0.7007	1624.0	11.0	1603.0	21.0	1667	23	1667.0	23.0	3.8
GOM1_68	159	1.05	4.2140	0.0450	0.2990	0.0039	0.6005	1677.4	9.0	1686.0	20.0	1670	22	1670.0	22.0	1.0
GOM1_27	130	0.88	4.0850	0.0430	0.2879	0.0031	0.5446	1652.8	8.5	1631.0	15.0	1671	19	1671.0	19.0	2.4
GOM1_86	78.8	1.20	4.2140	0.0900	0.2955	0.0055	0.4236	1678.0	18.0	1672.0	27.0	1675	26	1675.0	26.0	0.2
GOM1_94	332	2.20	4.1050	0.0530	0.2913	0.0041	0.6501	1654.0	10.0	1647.0	21.0	1679	22	1679.0	22.0	1.9
GOM1_112	200	2.33	4.2300	0.1400	0.2964	0.0088	0.8559	1678.0	26.0	1673.0	44.0	1680	30	1680.0	30.0	0.4
GOM1_15	319	1.31	4.1250	0.0430	0.2892	0.0044	0.7278	1658.6	8.4	1637.0	22.0	1690	18	1690.0	18.0	3.1
GOM1_46	161.9	1.79	4.3590	0.0470	0.3055	0.0036	0.5843	1705.0	8.7	1718.0	18.0	1698	18	1698.0	18.0	1.2
GOM1_47	201	1.05	4.3050	0.0640	0.3004	0.0052	0.6838	1693.0	12.0	1692.0	26.0	1700	22	1700.0	22.0	0.5
GOM1_118	180	1.03	4.4800	0.0580	0.3133	0.0048	0.7179	1728.0	11.0	1756.0	24.0	1704	17	1704.0	17.0	3.1
GOM1_92	84.7	1.64	4.4670	0.0910	0.3094	0.0064	0.7186	1722.0	17.0	1736.0	31.0	1707	33	1707.0	33.0	1.7
GOM1_61	408	2.59	4.4610	0.0730	0.3097	0.0062	0.7550	1722.0	14.0	1742.0	30.0	1713	25	1713.0	25.0	1.7
GOM1_69	422	3.66	4.3800	0.0770	0.3058	0.0082	0.8752	1708.0	15.0	1719.0	40.0	1715	23	1715.0	23.0	0.2
GOM1_9	222	1.73	4.5220	0.0590	0.3070	0.0046	0.7718	1735.0	11.0	1728.0	23.0	1736	17	1736.0	17.0	0.5
GOM1_7	58.6	0.65	4.4510	0.0980	0.2960	0.0062	0.4965	1721.0	18.0	1671.0	31.0	1799	45	1799.0	45.0	7.1
GOM1_40	322	5.49	5.1290	0.0720	0.3386	0.0054	0.7094	1840.0	12.0	1880.0	26.0	1801	22	1801.0	22.0	4.4
GOM1_80	69.1	0.69	11.0400	0.1600	0.4826	0.0074	0.6652	2526.0	13.0	2537.0	32.0	2512	20	2512.0	20.0	1.0
GOM1_65	402	1.31	10.4700	0.1200	0.4586	0.0065	0.7456	2478.0	11.0	2433.0	29.0	2517	14	2517.0	14.0	3.3
GOM1_8	88.8	1.18	13.6500	0.3300	0.5150	0.0130	0.6376	2725.0	23.0	2676.0	54.0	2776	43	2776.0	43.0	3.6

Sample: GOM2	Isotopic Ratios							Isotopic ages (Ma)								
Analysis	[U] ppm	U/Th	207/235	2σ err.	206/238	2σ err.	RHO	207/235	2σ err.	206/238	2σ err.	207/206	2σ err.	Best age	2σ err.	% Dis.
GOM2_96	29.29	0.30	0.0273	0.0048	0.0042	0.0003	0.0000	27.2	4.8	27.2	1.6	680	150	27.2	1.6	0.0
GOM2_99	50.6	0.25	0.0289	0.0033	0.0044	0.0002	0.0000	28.8	3.3	28.6	1.2	580	120	28.6	1.2	0.7
GOM2_80	163.7	0.36	0.0290	0.0012	0.0045	0.0001	0.0000	29.0	1.2	28.6	0.6	262	56	28.6	0.6	1.3

GOM2_102	130.4	0.49	0.0317	0.0020	0.0045	0.0001	0.0000	31.7	1.9	28.9	0.8	497	76	28.9	0.8	9.0
GOM2_76	83	0.88	0.0306	0.0032	0.0047	0.0002	0.0000	30.5	3.1	29.9	1.2	510	110	29.9	1.2	2.0
GOM2_49	157	1.13	0.0315	0.0016	0.0048	0.0001	0.0000	31.4	1.6	30.7	0.8	289	65	30.7	0.8	2.1
GOM2_20	258	1.86	0.0309	0.0010	0.0048	0.0001	0.0000	30.9	0.9	30.9	0.6	157	39	30.9	0.6	0.1
GOM2_11	295	1.05	0.0330	0.0013	0.0049	0.0001	0.0000	32.9	1.3	31.5	0.6	304	57	31.5	0.6	4.3
GOM2_79	193.9	1.22	0.0327	0.0015	0.0050	0.0001	0.0000	32.7	1.4	31.9	0.6	278	52	31.9	0.6	2.4
GOM2_32	59.7	1.05	0.0329	0.0034	0.0050	0.0003	0.0000	32.8	3.4	32.3	1.9	411	99	32.3	1.9	1.5
GOM2_95	152.7	0.41	0.0325	0.0013	0.0052	0.0001	0.0000	32.4	1.3	33.5	0.8	224	50	33.5	0.8	3.4
GOM2_108	97.4	0.93	0.0377	0.0031	0.0056	0.0002	0.0000	37.6	3.1	36.0	1.4	490	130	36.0	1.4	4.3
GOM2_42	114	0.83	0.0389	0.0032	0.0056	0.0001	0.0000	38.6	3.1	36.2	0.9	450	100	36.2	0.9	6.3
GOM2_90	81.7	0.67	0.0358	0.0028	0.0057	0.0002	0.0000	35.7	2.7	36.5	1.4	352	79	36.5	1.4	2.2
GOM2_19	112	0.66	0.0409	0.0024	0.0057	0.0002	0.0000	40.6	2.3	36.8	1.1	299	80	36.8	1.1	9.4
GOM2_115	145.9	1.01	0.0378	0.0016	0.0057	0.0001	0.0000	37.6	1.6	36.8	0.7	290	53	36.8	0.7	2.0
GOM2_12	478	14.40	0.0410	0.0041	0.0058	0.0004	0.0000	40.8	4.0	37.1	2.5	248	84	37.1	2.5	9.1
GOM2_117	82.3	0.63	0.0401	0.0035	0.0059	0.0002	0.0000	39.9	3.4	38.2	1.2	264	54	38.2	1.2	4.3
GOM2_48	21.57	0.59	0.0421	0.0064	0.0067	0.0003	0.0000	41.5	6.2	42.8	1.9	670	130	42.8	1.9	3.1
GOM2_39	17.8	0.63	0.0406	0.0075	0.0068	0.0004	0.0000	39.9	7.3	43.4	2.3	760	170	43.4	2.3	8.8
GOM2_24	206.4	1.43	0.0554	0.0016	0.0086	0.0002	0.0000	54.8	1.6	55.0	1.0	181	33	55.0	1.0	0.4
GOM2_93	36.4	0.91	0.0547	0.0096	0.0086	0.0008	0.0000	53.8	9.2	55.3	5.1	510	180	55.3	5.1	2.8
GOM2_40	215	1.08	0.0564	0.0019	0.0088	0.0001	0.0000	55.6	1.8	56.7	0.8	179	35	56.7	0.8	2.0
GOM2_72	486	0.99	0.0573	0.0013	0.0089	0.0001	0.0000	56.6	1.2	57.0	0.8	117	26	57.0	0.8	0.6
GOM2_5	158	1.07	0.0585	0.0021	0.0090	0.0002	0.0000	57.7	2.0	57.7	1.0	181	32	57.7	1.0	0.0
GOM2_55	136	1.05	0.0610	0.0023	0.0091	0.0003	0.0000	60.5	2.3	58.1	1.6	335	70	58.1	1.6	4.0
GOM2_35	137	1.13	0.0568	0.0027	0.0091	0.0003	0.0000	56.0	2.6	58.5	2.0	141	41	58.5	2.0	4.5
GOM2_58	83.9	1.93	0.0624	0.0032	0.0091	0.0003	0.0000	61.4	3.0	58.6	1.7	294	56	58.6	1.7	4.6
GOM2_33	190	1.25	0.0616	0.0020	0.0092	0.0002	0.0000	60.9	2.0	58.8	1.0	207	41	58.8	1.0	3.4
GOM2_29	179	1.57	0.0600	0.0018	0.0092	0.0002	0.0000	59.2	1.7	58.9	1.1	187	32	58.9	1.1	0.5
GOM2_70	158	1.62	0.0599	0.0023	0.0092	0.0002	0.0000	59.0	2.2	59.2	1.2	226	45	59.2	1.2	0.3
GOM2_54	177.3	1.07	0.0579	0.0018	0.0093	0.0002	0.0000	57.1	1.7	59.6	1.2	164	37	59.6	1.2	4.4
GOM2_77	356	4.99	0.0606	0.0013	0.0094	0.0002	0.0000	59.8	1.3	60.2	0.9	156	26	60.2	0.9	0.7
GOM2_38	186.9	1.31	0.0638	0.0020	0.0096	0.0002	0.0000	62.8	1.9	61.7	1.0	192	29	61.7	1.0	1.8
GOM2_21	273	3.35	0.0665	0.0021	0.0100	0.0004	0.0000	65.4	2.0	64.2	2.4	181	49	64.2	2.4	1.8
GOM2_83	272.2	2.79	0.0706	0.0017	0.0110	0.0002	0.0000	69.3	1.6	70.7	1.3	122	29	70.7	1.3	2.0

GOM2_97	85.4	0.52	0.0734	0.0033	0.0113	0.0003	0.0000	71.8	3.1	72.4	1.8	248	44	72.4	1.8	0.8
GOM2_52	83.8	2.32	0.0830	0.0034	0.0116	0.0002	0.0000	80.9	3.2	74.2	1.3	340	45	74.2	1.3	8.3
GOM2_22	203.4	5.28	0.0799	0.0024	0.0117	0.0002	0.0000	78.0	2.3	75.0	1.0	257	37	75.0	1.0	3.8
GOM2_73	277	5.54	0.0777	0.0016	0.0119	0.0002	0.0000	76.0	1.5	76.1	1.0	126	23	76.1	1.0	0.1
GOM2_45	90.9	0.76	0.0808	0.0072	0.0119	0.0004	0.0000	78.7	6.7	76.2	2.7	510	220	76.2	2.7	3.2
GOM2_60	430	3.04	0.0797	0.0020	0.0121	0.0002	0.0000	77.8	1.9	77.6	1.2	163	29	77.6	1.2	0.3
GOM2_86	164.4	0.94	0.0839	0.0031	0.0130	0.0003	0.0000	82.5	2.9	83.0	1.6	181	34	83.0	1.6	0.6
GOM2_71	125	1.14	0.0881	0.0031	0.0134	0.0003	0.0000	85.7	2.8	85.6	1.7	214	39	85.6	1.7	0.1
GOM2_69	175.4	1.14	0.0968	0.0032	0.0143	0.0003	0.0000	93.8	3.0	91.7	2.1	226	41	91.7	2.1	2.2
GOM2_107	176	1.88	0.0986	0.0025	0.0151	0.0003	0.0000	95.4	2.3	96.7	1.7	152	24	96.7	1.7	1.4
GOM2_53	236	1.25	0.1010	0.0029	0.0154	0.0003	0.0000	97.7	2.7	98.2	1.6	139	29	98.2	1.6	0.5
GOM2_106	120	0.66	0.1307	0.0041	0.0197	0.0004	0.0000	124.6	3.7	125.8	2.6	222	43	125.8	2.6	1.0
GOM2_112	47.2	0.66	0.1398	0.0065	0.0202	0.0005	0.0000	132.5	5.7	128.6	3.0	339	57	128.6	3.0	2.9
GOM2_26	152	0.68	0.1604	0.0040	0.0239	0.0004	0.0000	151.0	3.5	152.2	2.8	175	26	152.2	2.8	0.8
GOM2_59	100.1	0.72	0.1729	0.0053	0.0254	0.0004	0.0000	162.5	4.7	161.8	2.6	237	34	161.8	2.6	0.4
GOM2_103	285.1	0.61	0.1710	0.0026	0.0254	0.0002	0.0000	160.3	2.3	161.8	1.5	163	22	161.8	1.5	0.9
GOM2_37	230	0.65	0.1838	0.0051	0.0266	0.0005	0.0000	171.3	4.4	169.0	2.9	195	32	169.0	2.9	1.3
GOM2_98	375.4	1.27	0.1835	0.0026	0.0270	0.0003	0.0000	171.0	2.3	171.5	1.7	179	20	171.5	1.7	0.3
GOM2_63	256	0.63	0.1860	0.0032	0.0270	0.0003	0.0000	173.2	2.8	171.8	2.0	177	27	171.8	2.0	0.8
GOM2_109	305.3	0.87	0.1871	0.0036	0.0270	0.0003	0.0000	174.1	3.1	171.8	2.1	208	32	171.8	2.1	1.3
GOM2_4	324.1	0.88	0.1830	0.0060	0.0272	0.0003	0.0000	170.6	5.1	172.7	2.1	192	43	172.7	2.1	1.2
GOM2_92	239.9	1.14	0.1899	0.0028	0.0278	0.0003	0.0000	176.5	2.4	177.0	1.8	188	21	177.0	1.8	0.3
GOM2_101	84.4	14.10	0.2052	0.0098	0.0286	0.0007	0.0000	189.2	8.3	181.8	4.1	279	56	181.8	4.1	3.9
GOM2_87	1086	1.00	0.2135	0.0032	0.0300	0.0004	0.0000	196.4	2.7	190.6	2.5	268	21	190.6	2.5	3.0
GOM2_105	254	0.89	0.2073	0.0027	0.0301	0.0002	0.0000	191.2	2.3	191.3	1.4	191	18	191.3	1.4	0.1
GOM2_85	118	1.86	0.2127	0.0056	0.0312	0.0004	0.0000	195.6	4.7	198.0	2.3	215	29	198.0	2.3	1.2
GOM2_64	290	2.14	0.2294	0.0030	0.0329	0.0003	0.0000	209.6	2.5	208.9	1.7	209	17	208.9	1.7	0.3
GOM2_94	111	0.89	0.2473	0.0066	0.0350	0.0005	0.0000	224.2	5.4	221.5	2.9	275	30	221.5	2.9	1.2
GOM2_110	121.1	1.88	0.2452	0.0055	0.0351	0.0005	0.0000	222.5	4.5	222.2	3.0	265	31	222.2	3.0	0.1
GOM2_67	103.1	0.99	0.2434	0.0074	0.0356	0.0004	0.0000	219.2	4.9	225.3	2.4	236	40	225.3	2.4	2.8
GOM2_6	1121	1.90	0.2505	0.0023	0.0357	0.0002	0.0000	227.0	1.8	225.9	1.4	242	12	225.9	1.4	0.5
GOM2_46	140	0.92	0.2492	0.0045	0.0359	0.0004	0.0000	225.8	3.6	227.4	2.2	274	30	227.4	2.2	0.7
GOM2_7	474.5	3.07	0.2536	0.0022	0.0362	0.0003	0.0000	229.5	1.8	229.1	2.0	236	12	229.1	2.0	0.2

GOM2_120	130.1	0.90	0.2544	0.0045	0.0363	0.0004	0.0000	230.0	3.6	229.5	2.7	244	27	229.5	2.7	0.2
GOM2_89	570	1.51	0.2577	0.0029	0.0364	0.0004	0.0000	232.8	2.3	230.7	2.4	251	17	230.7	2.4	0.9
GOM2_2	550	1.96	0.2581	0.0045	0.0365	0.0005	0.0000	233.0	3.6	231.0	3.3	261	17	231.0	3.3	0.9
GOM2_74	243	1.76	0.2579	0.0035	0.0365	0.0004	0.0000	233.3	2.7	231.3	2.3	236	18	231.3	2.3	0.9
GOM2_51	140.2	0.98	0.2732	0.0047	0.0388	0.0004	0.0000	246.0	3.8	245.3	2.2	257	19	245.3	2.2	0.3
GOM2_43	79.1	0.89	0.2865	0.0069	0.0401	0.0006	0.0000	255.6	5.4	253.5	3.9	252	33	253.5	3.9	0.8
GOM2_1	150	1.08	0.2829	0.0058	0.0406	0.0004	0.0000	252.8	4.6	256.5	2.4	246	22	256.5	2.4	1.5
GOM2_8	221.7	2.99	0.3079	0.0038	0.0436	0.0005	0.0000	272.5	2.9	275.0	3.1	261	20	275.0	3.1	0.9
GOM2_62	330	1.03	0.5960	0.0140	0.0770	0.0019	0.0000	474.6	9.2	478.0	12.0	450	16	478.0	12.0	0.7
GOM2_9	92.1	0.93	0.8280	0.0170	0.0989	0.0013	0.0000	612.3	9.4	607.7	7.6	624	30	607.7	7.6	0.8
GOM2_111	195.7	2.85	1.6670	0.0120	0.1660	0.0010	0.0000	995.9	4.7	990.1	5.6	1008	9	990.1	5.6	0.6
GOM2_62	153	2.13	1.7340	0.0250	0.1723	0.0026	0.0000	1020.8	9.3	1025.0	14.0	1019	13	1019.0	13.0	0.6
GOM2_84	154	1.95	1.8470	0.0180	0.1792	0.0019	0.0000	1064.4	6.6	1062.0	10.0	1075	13	1075.0	13.0	1.2
GOM2_100	73.2	1.30	1.8860	0.0240	0.1805	0.0022	0.0000	1075.6	8.4	1069.0	12.0	1098	13	1098.0	13.0	2.6
GOM2_104	25.2	1.05	1.8710	0.0410	0.1797	0.0029	0.0000	1076.0	14.0	1065.0	16.0	1102	20	1102.0	20.0	3.4
GOM2_23	13.21	0.84	1.8280	0.0940	0.1749	0.0056	0.0000	1053.0	34.0	1039.0	31.0	1123	45	1123.0	45.0	7.5
GOM2_27	69.6	6.03	2.0660	0.0290	0.1939	0.0025	0.0000	1136.8	9.6	1144.0	13.0	1127	11	1127.0	11.0	1.5
GOM2_17	41.2	0.72	2.0100	0.0250	0.1900	0.0022	0.0000	1118.4	8.3	1121.0	12.0	1130	19	1130.0	19.0	0.8
GOM2_81	50.5	1.79	1.9860	0.0280	0.1845	0.0021	0.0000	1109.9	9.6	1091.0	11.0	1148	13	1148.0	13.0	5.0
GOM2_13	75.1	1.14	2.0280	0.0370	0.1903	0.0030	0.0000	1123.0	13.0	1122.0	16.0	1148	11	1148.0	11.0	2.3
GOM2_68	34.7	0.70	2.0900	0.0450	0.1913	0.0035	0.0000	1145.0	15.0	1128.0	19.0	1171	25	1171.0	25.0	3.7
GOM2_93	52.6	0.94	2.2480	0.0280	0.2012	0.0016	0.0000	1195.9	8.9	1181.5	8.8	1218	12	1218.0	12.0	3.0
GOM2_61	60.3	0.77	2.2140	0.0230	0.1992	0.0020	0.0000	1186.0	7.5	1171.0	11.0	1219	13	1219.0	13.0	3.9
GOM2_18	162.2	1.01	2.8820	0.0190	0.2399	0.0015	0.0000	1376.9	5.0	1386.0	8.0	1374	7	1373.5	7.1	0.9
GOM2_91	51.1	0.88	3.0760	0.0380	0.2484	0.0026	0.0000	1425.8	9.5	1430.0	13.0	1409	14	1409.0	14.0	1.5
GOM2_16	185	1.77	2.9720	0.0200	0.2406	0.0019	0.0000	1402.3	5.1	1389.5	9.7	1422	6	1421.9	6.2	2.3
GOM2_10	69.9	0.98	3.1250	0.0630	0.2543	0.0050	0.0000	1437.0	16.0	1460.0	26.0	1422	10	1422.0	10.0	2.7
GOM2_30	207	1.50	3.0620	0.0330	0.2469	0.0027	0.0000	1422.7	8.3	1422.0	14.0	1425	6	1425.2	6.3	0.2
GOM2_57	1087	3.51	2.8710	0.0200	0.2314	0.0019	0.0000	1374.9	5.5	1341.0	10.0	1426	6	1426.1	6.4	6.0
GOM2_3	233	1.63	3.0110	0.0300	0.2412	0.0029	0.0000	1410.0	7.6	1393.0	15.0	1427	12	1427.0	12.0	2.4
GOM2_118	726	2.60	2.9800	0.0280	0.2403	0.0033	0.0000	1402.3	7.3	1388.0	17.0	1432	14	1432.0	14.0	3.1
GOM2_50	340	1.82	2.8520	0.0260	0.2285	0.0022	0.0000	1369.1	6.9	1328.0	12.0	1435	5	1435.4	4.5	7.5
GOM2_12	148	0.64	2.7960	0.0410	0.2222	0.0030	0.0000	1354.0	11.0	1293.0	16.0	1452	13	1452.0	13.0	11.0

GOM2_31	535	2.71	3.0330	0.0260	0.2365	0.0019	0.0000	1415.6	6.5	1368.1	9.9	1479	5	1478.7	4.7	7.5
GOM2_41	94.9	0.92	4.0560	0.0320	0.2901	0.0021	0.0000	1645.9	6.2	1642.0	11.0	1636	9	1636.0	8.5	0.4
GOM2_56	330	3.41	3.8750	0.0640	0.2743	0.0063	0.0000	1608.0	13.0	1562.0	32.0	1663	14	1663.0	14.0	6.1
GOM2_114	301	1.73	3.9430	0.0460	0.2836	0.0033	0.0000	1622.2	9.5	1609.0	17.0	1664	10	1664.0	10.0	3.3
GOM2_25	107.5	0.65	3.8820	0.0350	0.2755	0.0034	0.0000	1609.6	7.2	1568.0	17.0	1670	13	1670.0	13.0	6.1
GOM2_14	42	0.87	4.0800	0.0340	0.2912	0.0026	0.0000	1650.8	7.1	1649.0	13.0	1677	12	1677.0	12.0	1.7
GOM2_88	187	1.49	4.3590	0.0470	0.3053	0.0033	0.0000	1705.4	8.7	1717.0	16.0	1691	9	1691.4	9.2	1.5
GOM2_82	184	1.22	4.3070	0.0260	0.3026	0.0023	0.0000	1694.5	5.0	1704.0	11.0	1693	5	1693.1	4.5	0.6
GOM2_116	235	1.71	4.5860	0.0330	0.3134	0.0027	0.0000	1747.2	6.2	1757.0	13.0	1742	6	1741.6	5.9	0.9
GOM2_28	175.9	1.62	12.6900	0.1900	0.4994	0.0058	0.0000	2655.0	14.0	2610.0	25.0	2685	11	2685.0	11.0	2.8
GOM2_119	59.8	0.89	13.2800	0.0980	0.5125	0.0038	0.0000	2699.4	7.0	2667.0	16.0	2730	6	2729.5	5.7	2.3

Sample: GOM3	Isotopic Ratios							Isotopic ages (Ma)								
Analysis	[U] ppm	U/Th	207/235	2σ err.	206/238	2σ err.	RHO	207/235	2σ err.	206/238	2σ err.	207/206	2σ err.	Best age	2σ err.	% Dis.
GOM3__32	237	1.13	0.0326	0.0012	0.0051	0.0001	-0.0888	32.6	1.2	33.0	0.5	205	49	33.0	0.5	1.1
GOM3_3	1616	1.41	0.0352	0.0007	0.0052	0.0001	0.4383	35.1	0.7	33.4	0.6	109	20	33.4	0.6	4.9
GOM3_57	77.9	1.18	0.0348	0.0026	0.0053	0.0001	0.0675	34.7	2.5	33.9	0.9	418	84	33.9	0.9	2.4
GOM3_14	185	1.33	0.0353	0.0016	0.0054	0.0002	0.2123	35.2	1.6	34.7	1.0	218	54	34.7	1.0	1.4
GOM3_109	115.6	0.77	0.0362	0.0025	0.0054	0.0001	0.4252	36.4	2.3	34.8	0.8	329	64	34.8	0.8	4.4
GOM3_39	136.6	1.27	0.0363	0.0020	0.0055	0.0002	0.2294	36.1	2.0	35.5	1.0	259	55	35.5	1.0	1.7
GOM3_34	193	0.95	0.0372	0.0018	0.0058	0.0001	0.0528	37.1	1.8	37.2	0.8	177	68	37.2	0.8	0.2
GOM3_82	194.6	0.81	0.0366	0.0031	0.0058	0.0003	0.0938	36.5	3.0	37.3	1.8	440	210	37.3	1.8	2.2
GOM3_119	352	0.74	0.0399	0.0016	0.0060	0.0001	0.1491	39.7	1.6	38.8	0.9	179	32	38.8	0.9	2.3
GOM3_97	173.3	0.98	0.0398	0.0021	0.0062	0.0002	0.0135	39.6	2.0	39.6	1.0	149	54	39.6	1.0	0.0
GOM3_100	382	0.78	0.0437	0.0016	0.0067	0.0001	-0.0508	43.4	1.5	42.8	0.7	198	51	42.8	0.7	1.3
GOM3_31	603	1.34	0.0473	0.0010	0.0072	0.0001	0.3143	46.9	1.0	46.2	0.6	107	24	46.2	0.6	1.6
GOM3_60	356	1.75	0.0470	0.0012	0.0074	0.0001	-0.0359	46.6	1.1	47.2	0.6	102	25	47.2	0.6	1.3
GOM3_44	440	0.98	0.0502	0.0009	0.0077	0.0001	-0.0034	49.8	0.8	49.6	0.5	119	19	49.6	0.5	0.4
GOM3_38	362	1.17	0.0566	0.0011	0.0087	0.0001	0.2674	55.9	1.1	55.8	0.7	143	27	55.8	0.7	0.1
GOM3_7	284	1.80	0.0641	0.0014	0.0098	0.0001	-0.0900	63.0	1.3	62.6	0.6	170	28	62.6	0.6	0.6
GOM3_26	268	1.54	0.0652	0.0014	0.0100	0.0001	0.1806	64.1	1.3	64.1	0.8	126	25	64.1	0.8	0.0

GOM3_108	107	1.24	0.0679	0.0027	0.0108	0.0002	0.1876	66.7	2.6	69.5	1.1	234	63	69.5	1.1	4.2
GOM3_25	146	2.56	0.0743	0.0019	0.0112	0.0001	-0.0715	72.7	1.8	71.6	0.9	156	32	71.6	0.9	1.5
GOM3_76	278	1.48	0.0755	0.0012	0.0114	0.0002	0.1346	73.9	1.1	72.7	1.0	141	17	72.7	1.0	1.6
GOM3_63	183.7	0.62	0.0733	0.0030	0.0114	0.0002	0.0438	71.8	2.8	72.8	1.2	126	30	72.8	1.2	1.4
GOM3_22	206.2	1.11	0.0748	0.0019	0.0115	0.0002	0.2778	73.2	1.8	73.5	1.2	130	29	73.5	1.2	0.4
GOM3_29	514	1.79	0.0762	0.0014	0.0116	0.0001	0.1308	74.6	1.4	74.6	0.5	130	23	74.6	0.5	0.1
GOM3_95	103.6	2.60	0.0738	0.0040	0.0117	0.0003	-0.0269	72.3	3.7	75.0	2.0	77	62	75.0	2.0	3.7
GOM3_96	157.6	0.98	0.0760	0.0026	0.0118	0.0002	0.0350	74.3	2.4	75.8	1.3	143	42	75.8	1.3	2.0
GOM3_85	628	1.84	0.0777	0.0017	0.0119	0.0003	0.5790	76.0	1.6	76.2	1.7	79	23	76.2	1.7	0.3
GOM3_23	28.19	0.95	0.0763	0.0086	0.0120	0.0004	0.0745	74.4	8.1	76.6	2.8	346	82	76.6	2.8	3.0
GOM3_54	636	0.95	0.0823	0.0017	0.0125	0.0002	0.6298	80.3	1.6	80.1	1.1	106	20	80.1	1.1	0.2
GOM3_17	417.6	1.69	0.0857	0.0045	0.0126	0.0007	0.2871	83.5	4.2	80.8	4.2	70	57	80.8	4.2	3.2
GOM3_106	198	0.48	0.0921	0.0030	0.0128	0.0003	0.4541	89.4	2.8	82.0	1.9	325	46	82.0	1.9	8.3
GOM3_72	338	1.30	0.0838	0.0014	0.0129	0.0001	0.0074	81.7	1.3	82.5	0.9	142	25	82.5	0.9	1.0
GOM3_9	219.5	1.99	0.0887	0.0021	0.0135	0.0002	0.3636	86.2	2.0	86.2	1.2	183	34	86.2	1.2	0.0
GOM3_52	193.1	1.27	0.0856	0.0021	0.0136	0.0002	0.2365	83.4	2.0	87.1	1.2	84	29	87.1	1.2	4.4
GOM3_73	520	0.73	0.0895	0.0019	0.0136	0.0002	0.2375	87.0	1.8	87.1	1.4	129	23	87.1	1.4	0.1
GOM3_105	124.6	0.91	0.0905	0.0030	0.0136	0.0002	0.0259	87.9	2.8	87.2	1.1	232	39	87.2	1.1	0.8
GOM3_81	130.6	1.99	0.0917	0.0029	0.0141	0.0002	0.0984	89.0	2.7	90.0	1.1	126	26	90.0	1.1	1.1
GOM3_19	162.3	2.14	0.0960	0.0026	0.0144	0.0002	0.1103	93.0	2.4	92.3	1.5	160	33	92.3	1.5	0.8
GOM3_71	187	1.79	0.0970	0.0024	0.0147	0.0002	0.1130	94.0	2.2	93.7	1.1	151	26	93.7	1.1	0.3
GOM3_101	333.4	1.22	0.0974	0.0023	0.0147	0.0002	-0.0539	94.4	2.1	94.0	1.2	183	25	94.0	1.2	0.4
GOM3_87	249.1	0.52	0.0945	0.0034	0.0148	0.0004	0.1664	91.7	3.1	94.5	2.2	100	31	94.5	2.2	3.1
GOM3_51	1015	2.11	0.0994	0.0017	0.0150	0.0001	0.2733	96.2	1.6	95.9	0.8	108	18	95.9	0.8	0.4
GOM3_65	332.1	1.82	0.0993	0.0019	0.0152	0.0002	0.1083	96.1	1.8	97.1	1.2	107	21	97.1	1.2	1.0
GOM3_115	345	1.35	0.1073	0.0020	0.0153	0.0002	0.4849	103.4	1.8	97.9	1.2	173	21	97.9	1.2	5.3
GOM3_35	395	1.77	0.1102	0.0018	0.0167	0.0002	0.1973	106.1	1.7	106.9	1.2	137	21	106.9	1.2	0.8
GOM3_56	284.4	1.46	0.1344	0.0021	0.0200	0.0002	0.3704	128.0	1.9	127.8	1.3	141	18	127.8	1.3	0.2
GOM3_10	64.7	0.63	0.1588	0.0058	0.0220	0.0003	0.1791	149.6	5.1	140.5	2.0	291	36	140.5	2.0	6.1
GOM3_83	351	1.39	0.1580	0.0021	0.0235	0.0002	-0.3185	148.9	1.8	149.4	1.3	143	16	149.4	1.3	0.3
GOM3_53	57.5	0.78	0.1583	0.0058	0.0238	0.0004	-0.2250	149.0	5.1	151.5	2.4	249	44	151.5	2.4	1.7
GOM3_79	704	1.25	0.1693	0.0015	0.0250	0.0002	0.4087	158.8	1.3	159.0	1.0	158	13	159.0	1.0	0.1
GOM3_62	266	0.82	0.1712	0.0023	0.0253	0.0002	0.2661	160.4	2.0	161.2	1.3	168	18	161.2	1.3	0.5

GOM3_116	83	0.51	0.1814	0.0047	0.0254	0.0004	0.1547	169.1	4.0	161.7	2.3	295	37	161.7	2.3	4.4
GOM3_78	174	0.54	0.1771	0.0049	0.0258	0.0004	0.1965	165.5	4.2	164.1	2.5	188	25	164.1	2.5	0.8
GOM3_67	176	0.67	0.1800	0.0042	0.0259	0.0005	-0.0117	168.0	3.6	165.0	3.1	263	32	165.0	3.1	1.8
GOM3_30	183.8	1.18	0.1776	0.0031	0.0262	0.0003	0.2567	166.0	2.7	166.7	1.6	173	27	166.7	1.6	0.4
GOM3_70	454	1.05	0.1789	0.0028	0.0262	0.0004	0.5930	167.0	2.4	166.8	2.3	162	18	166.8	2.3	0.1
GOM3_80	291.6	0.75	0.1851	0.0035	0.0262	0.0003	-0.1019	172.4	3.0	166.9	1.7	235	28	166.9	1.7	3.2
GOM3_117	120.9	1.12	0.1787	0.0037	0.0265	0.0004	0.3808	166.8	3.2	168.8	2.3	168	25	168.8	2.3	1.2
GOM3_1	363	1.26	0.1831	0.0051	0.0267	0.0005	0.4521	170.7	4.4	169.8	3.1	174	39	169.8	3.1	0.5
GOM3_46	36.05	0.36	0.1827	0.0072	0.0270	0.0007	0.3140	170.3	6.2	171.5	4.1	176	36	171.5	4.1	0.7
GOM3_4	267	0.75	0.1897	0.0040	0.0279	0.0005	0.1425	176.3	3.4	177.5	2.9	171	32	177.5	2.9	0.7
GOM3_37	121.9	1.09	0.1904	0.0075	0.0280	0.0006	0.1912	176.9	6.4	177.9	4.0	177	43	177.9	4.0	0.6
GOM3_64	457	1.24	0.1968	0.0064	0.0284	0.0008	0.2793	182.4	5.4	180.4	5.3	182	68	180.4	5.3	1.1
GOM3_5	200	3.85	0.2028	0.0025	0.0296	0.0002	0.2683	187.5	2.1	188.3	1.5	183	18	188.3	1.5	0.4
GOM3_75	186.3	0.76	0.2223	0.0029	0.0321	0.0003	0.0996	203.8	2.4	203.4	1.6	200	16	203.4	1.6	0.2
GOM3_48	812	2.49	0.2236	0.0035	0.0322	0.0003	0.4602	204.9	2.9	204.4	1.8	216	15	204.4	1.8	0.2
GOM3_8	436	4.02	0.2243	0.0029	0.0323	0.0003	0.6024	205.4	2.4	204.7	1.8	212	17	204.7	1.8	0.3
GOM3_84	88	0.99	0.2336	0.0059	0.0337	0.0004	-0.0850	213.0	4.9	213.6	2.8	225	35	213.6	2.8	0.3
GOM3_36	123.9	0.93	0.2465	0.0051	0.0353	0.0004	0.0787	223.6	4.2	223.5	2.7	217	33	223.5	2.7	0.0
GOM3_28	194	1.10	0.2732	0.0049	0.0384	0.0004	0.2540	245.2	3.9	242.7	2.4	259	23	242.7	2.4	1.0
GOM3_88	104.5	0.88	0.2905	0.0085	0.0407	0.0009	0.4706	258.9	6.7	257.4	5.5	265	49	257.4	5.5	0.6
GOM3_11	464	0.55	0.3135	0.0029	0.0439	0.0003	0.5760	276.8	2.2	277.0	2.1	292	9	277.0	2.1	0.1
GOM3_33	127.3	1.10	0.4916	0.0075	0.0650	0.0005	0.2650	405.9	5.1	406.1	2.8	393	21	406.1	2.8	0.0
GOM3_120	75.8	1.30	0.5389	0.0095	0.0697	0.0005	0.4144	437.4	6.3	434.4	3.2	454	21	434.4	3.2	0.7
GOM3_107	28.29	1.50	1.6310	0.0260	0.1648	0.0019	0.2814	981.4	9.9	983.0	10.0	981	18	983.0	10.0	0.2
GOM3_61	195	2.11	1.6410	0.0110	0.1651	0.0011	0.4811	985.8	4.3	984.8	5.8	993	7	984.8	5.8	0.1
GOM3_103	88.4	1.69	1.6970	0.0180	0.1678	0.0013	0.4727	1007.0	6.8	999.7	7.4	1028	12	999.7	7.4	0.7
GOM3_110	181	1.52	1.8050	0.0160	0.1786	0.0019	0.6411	1047.0	5.7	1059.0	10.0	1022	11	1022.0	11.0	3.6
GOM3_58	52	0.88	1.7250	0.0170	0.1709	0.0013	0.2263	1017.5	6.3	1017.2	7.2	1027	14	1027.0	14.0	1.0
GOM3_6	104	3.00	1.7990	0.0180	0.1759	0.0021	0.4684	1045.0	6.4	1044.0	12.0	1044	15	1044.0	15.0	0.0
GOM3_102	246.1	0.64	1.7290	0.0150	0.1686	0.0020	0.6027	1019.0	5.5	1005.0	11.0	1052	13	1052.0	13.0	4.5
GOM3_40	105.6	1.51	1.8550	0.0250	0.1794	0.0025	0.5236	1064.7	9.0	1063.0	14.0	1053	13	1053.0	13.0	0.9
GOM3_93	94.6	0.70	1.8110	0.0150	0.1761	0.0013	0.4048	1049.2	5.4	1045.4	7.0	1059	9	1058.7	8.8	1.3
GOM3_16	152.7	1.13	1.8440	0.0200	0.1787	0.0013	0.3266	1061.1	7.3	1060.1	7.3	1061	10	1061.0	10.0	0.1

GOM3_15	74.8	1.24	1.9140	0.0220	0.1830	0.0012	0.1535	1086.0	7.6	1083.1	6.6	1078	12	1078.0	12.0	0.5
GOM3_50	373	1.83	1.8180	0.0130	0.1743	0.0012	0.4407	1052.7	4.7	1036.0	6.3	1095	8	1094.6	8.0	5.4
GOM3_42	23.9	1.19	1.9650	0.0420	0.1871	0.0030	0.6968	1102.0	14.0	1105.0	16.0	1106	21	1106.0	21.0	0.1
GOM3_66	83.4	1.39	2.0350	0.0210	0.1910	0.0023	0.5858	1126.9	6.9	1127.0	12.0	1132	9	1131.6	9.0	0.4
GOM3_94	140.1	2.36	1.9890	0.0250	0.1866	0.0019	0.7754	1114.6	8.7	1103.0	10.0	1144	10	1144.0	10.0	3.6
GOM3_59	150	1.89	2.0120	0.0130	0.1877	0.0010	0.3843	1119.5	4.4	1108.6	5.3	1153	6	1152.6	6.4	3.8
GOM3_91	212.5	1.98	2.1680	0.0200	0.1980	0.0019	0.7099	1170.4	6.5	1165.0	10.0	1186	7	1186.2	6.9	1.8
GOM3_68	51.7	0.61	2.5230	0.0230	0.2172	0.0019	0.0238	1279.4	6.4	1267.0	10.0	1298	15	1298.0	15.0	2.4
GOM3_69	295	1.04	2.5320	0.0160	0.2178	0.0014	0.6716	1282.3	4.6	1270.0	7.2	1312	5	1312.4	5.0	3.2
GOM3_90	205	1.14	2.7220	0.0160	0.2301	0.0017	0.6759	1334.2	4.4	1334.7	8.9	1336	7	1335.6	6.7	0.1
GOM3_27	131	1.50	2.9730	0.0310	0.2426	0.0027	0.6394	1400.1	7.9	1400.0	14.0	1404	11	1404.0	11.0	0.3
GOM3_86	103	0.47	2.7980	0.0270	0.2276	0.0021	0.7415	1354.7	7.3	1322.0	11.0	1412	11	1412.0	11.0	6.4
GOM3_24	93.7	0.59	3.0300	0.0230	0.2454	0.0014	0.2953	1415.1	5.7	1414.8	7.2	1419	8	1418.7	8.1	0.3
GOM3_47	101.6	1.91	2.9020	0.0240	0.2347	0.0013	0.5143	1382.1	6.2	1358.8	6.9	1420	7	1420.1	7.3	4.3
GOM3_43	312	2.56	3.0320	0.0180	0.2456	0.0017	0.6400	1415.5	4.6	1415.6	9.0	1425	6	1424.7	6.4	0.6
GOM3_55	111.7	0.86	2.9090	0.0220	0.2298	0.0019	0.5543	1384.1	5.6	1333.1	9.8	1432	7	1432.4	7.0	6.9
GOM3_13	269	1.72	2.9460	0.0350	0.2350	0.0028	0.8495	1393.4	9.0	1360.0	15.0	1439	7	1438.5	7.3	5.5
GOM3_111	117	1.00	3.0870	0.0210	0.2457	0.0014	0.5214	1429.1	5.1	1416.0	7.4	1443	7	1443.3	7.1	1.9
GOM3_113	111.5	1.07	3.1670	0.0370	0.2518	0.0026	0.6754	1450.8	9.6	1448.0	13.0	1446	13	1446.0	13.0	0.1
GOM3_89	110.5	1.51	3.1860	0.0260	0.2532	0.0017	0.4189	1453.4	6.3	1454.9	8.7	1454	9	1453.6	9.1	0.1
GOM3_74	47.9	0.85	2.8370	0.0300	0.2251	0.0016	0.3832	1364.8	8.0	1308.8	8.4	1465	13	1465.0	13.0	10.7
GOM3_64	89	1.51	3.2180	0.0630	0.2493	0.0034	0.7699	1466.0	17.0	1435.0	17.0	1499	15	1499.0	15.0	4.3
GOM3_112	59	0.70	3.8870	0.0280	0.2817	0.0019	0.3724	1610.6	5.8	1599.7	9.3	1629	8	1629.2	7.9	1.8
GOM3_104	178	1.69	3.9890	0.0250	0.2875	0.0021	0.5000	1632.8	4.9	1629.0	10.0	1636	6	1636.0	6.3	0.4
GOM3_49	204.9	1.57	3.9310	0.0220	0.2853	0.0016	0.6647	1620.0	4.5	1617.9	8.1	1642	6	1641.6	6.3	1.4
GOM3_20	99	1.95	3.9730	0.0320	0.2867	0.0023	0.5937	1628.4	6.4	1625.0	12.0	1643	6	1643.4	5.5	1.1
GOM3_21	78.9	1.24	3.8690	0.0290	0.2767	0.0019	0.5123	1606.9	6.0	1574.4	9.6	1652	8	1651.5	7.5	4.7
GOM3_12	76.4	0.96	3.8120	0.0320	0.2730	0.0021	0.7252	1595.0	6.8	1556.0	11.0	1655	5	1655.0	5.4	6.0
GOM3_92	1798	32.42	4.1320	0.0230	0.2935	0.0014	0.5021	1660.5	4.5	1659.1	7.2	1665	7	1665.0	6.5	0.4
GOM3_77	96.3	1.21	4.1020	0.0310	0.2895	0.0019	0.5918	1655.0	6.0	1638.7	9.7	1678	7	1677.9	6.8	2.3
GOM3_118	169.8	3.80	4.2900	0.0700	0.2996	0.0033	0.7241	1690.0	13.0	1692.0	16.0	1679	16	1679.0	16.0	0.8
GOM3_98	191.4	1.10	4.2080	0.0330	0.2961	0.0019	0.5425	1675.5	6.4	1671.8	9.6	1693	9	1692.6	9.0	1.2
GOM3_99	211.1	1.16	4.2610	0.0390	0.2979	0.0023	0.6588	1685.6	7.6	1681.0	11.0	1694	8	1693.9	7.8	0.8

GOM3_2	152.4	1.74	4.2720	0.0330	0.2988	0.0027	0.7727	1687.7	6.4	1685.0	13.0	1694	6	1694.3	6.1	0.5
GOM3_18	132	1.28	4.4180	0.0380	0.3055	0.0027	0.7468	1715.3	7.1	1718.0	13.0	1718	6	1717.6	6.2	0.0
GOM3_41	386	12.10	5.3680	0.0630	0.3390	0.0040	0.9327	1881.0	11.0	1881.0	19.0	1886	6	1886.4	6.3	0.3

Sample: GOM4	Isotopic Ratios							Isotopic ages (Ma)								
Analysis	[U] ppm	U/Th	207/235	2σ err.	206/238	2σ err.	RHO	207/235	2σ err.	206/238	2σ err.	207/206	2σ err.	Best age	2σ err.	% Dis.
GOM4_25	82	0.66	0.0364	0.0023	0.0056	0.0002	0.0994	36.2	2.2	35.7	1	355	59	35.7	1.0	1.4
GOM4_120	80.9	0.50	0.0377	0.0024	0.0057	0.0002	-0.0375	37.5	2.4	36.8	1.1	366	58	36.8	1.1	1.9
GOM4_8	21.1	0.38	0.0418	0.0067	0.0060	0.0003	-0.0935	42	6.4	38.7	1.6	850	140	38.7	1.6	7.9
GOM4_116	24.2	0.73	0.0440	0.0051	0.0063	0.0003	0.1231	43.5	5	40.6	2.1	660	110	40.6	2.1	6.7
GOM4_44	53.6	0.89	0.0447	0.0031	0.0065	0.0002	0.0019	44.3	3.1	41.6	1.3	610	100	41.6	1.3	6.1
GOM4_56	613	1.62	0.0559	0.0008	0.0085	0.0001	0.3643	55.21	0.79	54.61	0.69	103	14	54.6	0.7	1.1
GOM4_53	74	2.03	0.0583	0.0031	0.0090	0.0002	-0.1128	57.4	2.9	57.7	1.4	293	63	57.7	1.4	0.5
GOM4_63	231	3.60	0.0607	0.0019	0.0092	0.0001	0.0303	59.8	1.8	59.01	0.75	203	31	59.0	0.8	1.3
GOM4_97	286	1.11	0.0607	0.0014	0.0092	0.0001	-0.1633	59.8	1.3	59.3	0.67	181	30	59.3	0.7	0.8
GOM4_26	529	0.70	0.0618	0.0014	0.0094	0.0001	-0.1058	60.9	1.3	60.43	0.74	161	30	60.4	0.7	0.8
GOM4_52	1170	0.99	0.0784	0.0012	0.0109	0.0003	0.6035	76.6	1.2	70.2	1.8	328	32	70.2	1.8	8.4
GOM4_23	75	2.80	0.0748	0.0038	0.0113	0.0003	-0.1783	73.2	3.6	72.4	1.7	157	51	72.4	1.7	1.1
GOM4_13	620	1.03	0.0749	0.0010	0.0114	0.0001	0.5764	73.3	0.93	73.07	0.87	97	15	73.1	0.9	0.3
GOM4_27	354	1.24	0.0764	0.0014	0.0116	0.0002	0.3595	74.8	1.3	74.2	1.2	132	19	74.2	1.2	0.8
GOM4_55	216	2.17	0.0776	0.0022	0.0118	0.0002	0.2505	75.8	2	75.8	1.2	145	26	75.8	1.2	0.0
GOM4_103	162	1.20	0.0771	0.0022	0.0119	0.0002	0.1321	75.4	2.1	76.31	0.99	202	32	76.3	1.0	1.2
GOM4_59	129.7	1.19	0.0810	0.0038	0.0120	0.0002	0.3570	78.9	3.5	77	1.2	313	90	77.0	1.2	2.4
GOM4_46	93.7	2.00	0.0929	0.0030	0.0140	0.0002	-0.0195	90.2	2.7	89.7	1.5	252	39	89.7	1.5	0.6
GOM4_42	302	0.75	0.0978	0.0017	0.0148	0.0002	0.1737	94.7	1.6	94.6	1.1	166	24	94.6	1.1	0.1
GOM4_82	162.6	1.53	0.0970	0.0026	0.0148	0.0002	-0.0323	94	2.4	94.7	1.4	191	38	94.7	1.4	0.7
GOM4_66	107.1	2.02	0.0981	0.0029	0.0149	0.0002	0.1564	95	2.7	95.1	1.4	176	30	95.1	1.4	0.1
GOM4_71	239.1	0.76	0.1022	0.0022	0.0151	0.0002	0.0302	98.8	2	96.4	1	180	29	96.4	1.0	2.4
GOM4_93	86.6	1.37	0.1037	0.0030	0.0151	0.0002	0.0475	100.5	2.8	96.8	1.4	237	36	96.8	1.4	3.7
GOM4_106	362	1.30	0.1061	0.0022	0.0154	0.0002	0.2542	102.4	2	98.5	1.5	214	27	98.5	1.5	3.8
GOM4_105	127.7	0.55	0.1139	0.0042	0.0155	0.0003	0.0036	109.5	3.8	99.3	2	403	64	99.3	2.0	9.3

GOM4_54	362	0.65	0.1051	0.0017	0.0160	0.0002	0.0753	101.5	1.6	102.24	0.95	124	16	102.2	1.0	0.7
GOM4_3	392	1.40	0.1105	0.0020	0.0164	0.0002	0.1297	106.4	1.9	105.1	1.3	170	29	105.1	1.3	1.2
GOM4_43	244	1.28	0.1102	0.0017	0.0166	0.0002	-0.0425	106.1	1.6	106.2	1.1	157	23	106.2	1.1	0.1
GOM4_20	147	1.16	0.1181	0.0031	0.0168	0.0003	0.0650	113.3	2.9	107.1	1.9	276	40	107.1	1.9	5.5
GOM4_119	150	0.88	0.1565	0.0027	0.0232	0.0003	0.1343	147.6	2.4	147.5	1.9	173	22	147.5	1.9	0.1
GOM4_57	67.5	0.48	0.1697	0.0049	0.0249	0.0004	0.1594	159	4.3	158.7	2.2	221	43	158.7	2.2	0.2
GOM4_86	34.8	0.48	0.1646	0.0086	0.0252	0.0006	0.1751	154.3	7.5	160.2	3.4	262	65	160.2	3.4	3.8
GOM4_58	223	0.42	0.1739	0.0027	0.0259	0.0003	-0.0150	163.1	2.3	164.8	1.6	161	21	164.8	1.6	1.0
GOM4_81	320	0.46	0.1792	0.0020	0.0265	0.0002	0.1546	167.4	1.7	168.6	1.4	158	17	168.6	1.4	0.7
GOM4_98	640	0.99	0.1831	0.0018	0.0271	0.0002	0.3903	170.7	1.5	172.6	1.3	167	17	172.6	1.3	1.1
GOM4_5	215	1.42	0.1902	0.0038	0.0272	0.0005	0.4876	176.7	3.2	173.2	2.9	209	21	173.2	2.9	2.0
GOM4_11	132	0.74	0.1860	0.0036	0.0272	0.0003	-0.0534	173.1	3.1	173.2	1.9	188	25	173.2	1.9	0.1
GOM4_96	328	0.79	0.1827	0.0023	0.0272	0.0002	0.2527	170.6	2	173.2	1.4	154	15	173.2	1.4	1.5
GOM4_12	349	0.86	0.1883	0.0030	0.0276	0.0003	0.3396	175.1	2.6	175.5	1.7	175	18	175.5	1.7	0.2
GOM4_34	239	0.70	0.1896	0.0034	0.0277	0.0003	0.1799	176.2	2.9	175.9	1.8	190	23	175.9	1.8	0.2
GOM4_47	233	4.72	0.2096	0.0039	0.0300	0.0003	0.3214	193.2	3.3	190.7	2.1	208	33	190.7	2.1	1.3
GOM4_10	205.1	0.91	0.2103	0.0054	0.0305	0.0006	0.3155	193.7	4.6	193.6	3.6	193	36	193.6	3.6	0.1
GOM4_48	224	1.68	0.2190	0.0110	0.0312	0.0008	0.5935	200.7	9.3	198	4.7	242	67	198.0	4.7	1.3
GOM4_22	189	0.73	0.2214	0.0036	0.0316	0.0003	-0.0072	203	3	200.5	1.6	226	18	200.5	1.6	1.2
GOM4_2	64.4	0.54	0.2335	0.0057	0.0333	0.0004	0.1701	212.8	4.7	211	2.7	263	31	211.0	2.7	0.8
GOM4_87	168	0.96	0.2316	0.0084	0.0336	0.0006	0.2696	211.4	6.9	212.9	3.8	216	44	212.9	3.8	0.7
GOM4_92	133.8	1.04	0.2341	0.0044	0.0340	0.0003	0.2078	213.4	3.6	215.5	1.9	200	24	215.5	1.9	1.0
GOM4_110	111.9	0.74	0.2403	0.0045	0.0343	0.0005	0.1553	218.5	3.7	217.1	3.2	281	28	217.1	3.2	0.6
GOM4_102	83.2	0.47	0.2540	0.0100	0.0345	0.0005	0.4010	229.1	8.2	218.4	3.2	411	87	218.4	3.2	4.7
GOM4_91	170	1.57	0.2523	0.0036	0.0359	0.0003	0.1525	228.4	2.9	227.2	2	247	24	227.2	2.0	0.5
GOM4_19	236	0.68	0.2517	0.0076	0.0361	0.0008	0.8200	227.8	6.2	228.6	5	209	22	228.6	5.0	0.4
GOM4_41	235	0.83	0.2613	0.0042	0.0368	0.0004	0.5283	235.6	3.4	232.7	2.3	269	23	232.7	2.3	1.2
GOM4_24	161.3	1.07	0.2810	0.0048	0.0395	0.0004	0.2986	251.8	3.7	249.6	2.7	248	25	249.6	2.7	0.9
GOM4_64	85	1.49	0.2770	0.0082	0.0403	0.0007	0.1840	248.8	6.8	254.4	4.3	263	35	254.4	4.3	2.3
GOM4_21	380	1.19	0.4592	0.0043	0.0607	0.0005	0.6396	383.6	3	379.8	2.9	394.3	9.5	379.8	2.9	1.0
GOM4_78	140.4	0.82	0.5271	0.0066	0.0686	0.0006	0.0322	429.8	4.4	427.6	3.5	444	22	427.6	3.5	0.5
GOM4_107	558	0.72	0.5662	0.0038	0.0743	0.0005	0.5454	455.5	2.5	462.1	2.9	447.7	8.3	462.1	2.9	1.4
GOM4_36	190.8	1.31	0.6843	0.0056	0.0851	0.0005	0.3367	529.3	3.3	526.3	2.8	532	12	526.3	2.8	0.6

GOM4_38	41.3	1.65	0.7130	0.0130	0.0890	0.0011	0.2397	546.8	8.1	549.6	6.3	535	24	549.6	6.3	0.5
GOM4_77	29.5	1.70	0.7380	0.0150	0.0895	0.0010	0.1647	561.9	9.2	552.6	6	582	29	552.6	6.0	1.7
GOM4_30	79.8	1.18	0.7544	0.0088	0.0931	0.0009	0.3920	570.6	5.1	574	5.5	561	13	574.0	5.5	0.6
GOM4_118	77.6	1.76	1.4230	0.0140	0.1472	0.0013	0.2847	898.2	5.7	885	7.5	927	15	927.0	15.0	4.5
GOM4_7	83.6	2.02	1.5420	0.0120	0.1572	0.0011	0.2661	947.1	4.7	942.1	6.3	959.7	9.8	959.7	9.8	1.8
GOM4_1	130	2.27	1.6180	0.0170	0.1633	0.0018	0.5196	976.7	6.6	975	10	978	15	978.0	15.0	0.3
GOM4_16	93.8	1.22	1.5750	0.0170	0.1575	0.0012	0.4044	960.2	6.6	942.9	6.5	997	13	997.0	13.0	5.4
GOM4_95	145	0.94	1.7290	0.0170	0.1730	0.0013	0.5331	1019.8	6.4	1028.6	7	1022.3	9.7	1022.3	9.7	0.6
GOM4_101	135.9	1.85	1.6710	0.0270	0.1669	0.0025	0.8386	998	11	994	14	1028	10	1028.0	10.0	3.3
GOM4_84	47	0.96	1.7790	0.0200	0.1759	0.0013	0.2638	1037.2	7.3	1044.2	7.2	1029	15	1029.0	15.0	1.5
GOM4_28	27.76	0.87	1.6380	0.0440	0.1621	0.0037	0.5437	984	17	968	20	1036	34	1036.0	34.0	6.6
GOM4_72	16.05	1.00	1.8570	0.0310	0.1818	0.0021	0.1858	1065	11	1078	12	1036	23	1036.0	23.0	4.1
GOM4_40	33.5	0.75	1.7500	0.0230	0.1715	0.0018	0.4166	1027.5	8.5	1020	10	1039	14	1039.0	14.0	1.8
GOM4_4	32.8	0.60	1.7990	0.0230	0.1764	0.0015	0.2948	1045.3	8.4	1046.9	8.3	1040	13	1040.0	13.0	0.7
GOM4_111	112.1	1.30	1.7680	0.0140	0.1733	0.0014	0.4554	1033.6	5.1	1029.9	7.5	1042.9	9.7	1042.9	9.7	1.2
GOM4_114	215	0.64	1.7680	0.0150	0.1733	0.0016	0.6881	1033.4	5.6	1030	8.7	1046.8	8.2	1046.8	8.2	1.6
GOM4_75	84.6	1.22	1.8490	0.0130	0.1793	0.0012	0.2526	1062.8	4.6	1063.3	6.7	1051	11	1051.0	11.0	1.2
GOM4_85	191.8	1.80	1.7770	0.0130	0.1738	0.0014	0.6140	1036.9	4.6	1032.9	7.4	1051	8	1051.0	8.0	1.7
GOM4_83	57.3	0.95	1.8290	0.0180	0.1761	0.0014	0.1336	1056.3	6.6	1045.5	7.9	1068	15	1068.0	15.0	2.1
GOM4_117	74.9	1.25	1.8260	0.0310	0.1748	0.0023	0.7325	1054	11	1039	13	1076	17	1076.0	17.0	3.4
GOM4_45	45.1	1.06	1.8900	0.0190	0.1818	0.0013	0.1895	1077.1	6.7	1076.9	7.1	1079	15	1079.0	15.0	0.2
GOM4_94	83	0.93	1.8260	0.0200	0.1771	0.0014	0.4885	1054.4	7.2	1051.1	7.6	1082	12	1082.0	12.0	2.9
GOM4_90	52.8	0.87	1.8390	0.0230	0.1775	0.0018	0.4826	1059.8	8.2	1053	10	1084	13	1084.0	13.0	2.9
GOM4_108	228	0.85	1.9057	0.0098	0.1836	0.0010	0.3117	1083	3.4	1086.7	5.7	1090.4	7	1090.4	7.0	0.3
GOM4_89	83.2	0.93	1.8890	0.0210	0.1807	0.0013	0.2276	1076.6	7.3	1070.5	7.1	1104	16	1104.0	16.0	3.0
GOM4_112	151.1	1.91	1.9570	0.0140	0.1861	0.0013	0.5963	1101.3	4.7	1100	6.8	1116.3	9	1116.3	9.0	1.5
GOM4_67	203	2.72	2.1020	0.0530	0.1954	0.0036	0.8582	1147	17	1150	20	1123	18	1123.0	18.0	2.4
GOM4_50	143	1.60	2.0400	0.0140	0.1919	0.0012	0.3707	1128.9	4.6	1131.5	6.2	1127.1	8.5	1127.1	8.5	0.4
GOM4_70	35.5	1.03	1.9540	0.0270	0.1829	0.0018	0.2919	1099.3	9.2	1082.5	9.8	1134	19	1134.0	19.0	4.5
GOM4_49	34.6	0.86	2.1460	0.0360	0.1977	0.0023	-0.0010	1165	11	1163	12	1147	20	1147.0	20.0	1.4
GOM4_51	89.2	1.13	2.0970	0.0190	0.1951	0.0014	0.3556	1148.3	6	1149.1	7.4	1151	13	1151.0	13.0	0.2
GOM4_69	258.3	3.18	2.0140	0.0210	0.1856	0.0020	0.7158	1119.9	7.2	1098	11	1152.1	7	1152.1	7.0	4.7
GOM4_33	51.4	2.24	2.1550	0.0200	0.1972	0.0017	0.3468	1168.2	6.6	1160	9.2	1179	11	1179.0	11.0	1.6

GOM4_17	51.3	1.22	2.2400	0.0200	0.2038	0.0015	0.4172	1195.2	6.3	1195.8	8.1	1189.6	9.3	1189.6	9.3	0.5
GOM4_15	66.5	1.02	2.2300	0.0210	0.2012	0.0016	0.6020	1190	6.5	1181.5	8.5	1198.3	8.5	1198.3	8.5	1.4
GOM4_99	224.1	1.86	2.2530	0.0110	0.2059	0.0012	0.4238	1197.5	3.6	1206.9	6.2	1199.1	7.1	1199.1	7.1	0.7
GOM4_31	10.95	1.16	2.1050	0.0400	0.1889	0.0032	0.5302	1149	13	1115	17	1200	21	1200.0	21.0	7.1
GOM4_37	67.9	1.26	2.4030	0.0260	0.2129	0.0017	0.5590	1242.9	7.7	1244.3	9	1250	9.2	1250.0	9.2	0.5
GOM4_68	75.6	1.13	2.7010	0.0280	0.2281	0.0023	0.5251	1328.2	7.6	1324	12	1324	10	1324.0	10.0	0.0
GOM4_113	42.3	1.02	2.6900	0.0260	0.2263	0.0017	0.3596	1325.2	7.2	1315	9	1354.2	9.1	1354.2	9.1	2.9
GOM4_35	88	1.76	3.0290	0.0230	0.2455	0.0017	0.2763	1414.6	5.7	1415.2	8.8	1410	10	1410.0	10.0	0.4
GOM4_62	206	2.30	3.0570	0.0220	0.2451	0.0023	0.7146	1422.4	5.6	1413	12	1428.7	8.5	1428.7	8.5	1.1
GOM4_60	56.81	0.83	3.1490	0.0280	0.2494	0.0015	0.3322	1444.4	6.8	1435.5	8	1445	11	1445.0	11.0	0.7
GOM4_104	122	1.10	3.1350	0.0240	0.2516	0.0018	0.5386	1441	6	1446.8	9.3	1447.3	8.4	1447.3	8.4	0.0
GOM4_109	129	1.73	3.2030	0.0310	0.2500	0.0021	0.4888	1457.5	7.4	1438	11	1493.6	9.4	1493.6	9.4	3.7
GOM4_80	62.4	0.67	3.3750	0.0280	0.2583	0.0022	0.4496	1499.2	6.5	1482	11	1508	10	1508.0	10.0	1.7
GOM4_48	114.6	1.86	4.0180	0.0750	0.2870	0.0036	0.8525	1637	15	1626	18	1652	16	1652.0	16.0	1.6
GOM4_29	204	2.05	4.3170	0.0230	0.3047	0.0018	0.7192	1696.5	4.5	1714.3	8.9	1666.1	4.1	1666.1	4.1	2.9
GOM4_6	71.1	0.88	4.1570	0.0320	0.2934	0.0021	0.6914	1666	6.2	1658	11	1680.6	6.8	1680.6	6.8	1.3
GOM4_73	175	1.15	4.2800	0.0240	0.2975	0.0015	0.6315	1689.4	4.6	1678.8	7.3	1693.9	4.9	1693.9	4.9	0.9
GOM4_32	274	1.34	4.3250	0.0320	0.2995	0.0019	0.6684	1698.6	5.9	1688.8	9.4	1708.4	6	1708.4	6.0	1.1
GOM4_61	103.3	1.20	4.5530	0.0290	0.3093	0.0022	0.5568	1740.4	5.3	1737	11	1740.7	7.3	1740.7	7.3	0.2
GOM4_100	260	1.16	4.6400	0.0290	0.3170	0.0023	0.8810	1756.2	5.2	1775	11	1750	5.7	1750.0	5.7	1.4
GOM4_9	71.4	1.63	4.8070	0.0340	0.3192	0.0027	0.6030	1785.8	5.9	1785	13	1780.9	7.6	1780.9	7.6	0.2
GOM4_65	26.25	1.15	4.6430	0.0510	0.3043	0.0027	0.0944	1756.3	9.1	1712	14	1806	13	1806.0	13.0	5.2
GOM4_88	38.4	0.33	4.9820	0.0500	0.3245	0.0024	0.4431	1815.8	8.5	1812	12	1831	10	1831.0	10.0	1.0
GOM4_74	122.1	0.50	4.8000	0.0370	0.3016	0.0024	0.6938	1784.6	6.5	1701	11	1880.6	8.1	1880.6	8.1	9.6
GOM4_39	60.7	0.46	5.4830	0.0590	0.3290	0.0035	0.6727	1898.7	9	1833	17	1963.9	9.5	1963.9	9.5	6.7
GOM4_79	73.6	1.38	11.1060	0.0780	0.4754	0.0032	0.6856	2531.7	6.5	2509	14	2548.2	5.1	2548.2	5.1	1.5
GOM4_76	331	3.99	12.2900	0.2300	0.4577	0.0078	0.9872	2627	17	2428	35	2774.4	4.8	2774.4	4.8	12.5

Sample:GOM5	Isotopic Ratios							Isotopic ages (Ma)								
Analysis	[U] ppm	U/Th	207/235	2σ err.	206/238	2σ err.	RHO	207/235	2σ err.	206/238	2σ err.	207/206	2σ err.	Best age	2σ err.	% Dis.
GOM5_35	94.6	0.82	0.0393	0.0026	0.0058	0.0003	0.0769	39.1	2.6	37.2	1.6	314	54	37.2	1.6	4.9

GOM5_89	78.8	0.79	0.0436	0.0025	0.0063	0.0002	0.0102	43.3	2.5	40.4	1.0	408	71	40.4	1.0	6.7
GOM5_23	328	1.00	0.0575	0.0013	0.0087	0.0001	-0.0530	56.8	1.2	55.5	0.7	211	33	55.5	0.7	2.3
GOM5_88	272	0.95	0.0628	0.0026	0.0092	0.0002	0.4614	61.8	2.4	59.2	1.4	190	45	59.2	1.4	4.2
GOM5_61	144.2	0.95	0.0689	0.0024	0.0103	0.0002	0.1067	67.6	2.3	66.2	1.1	211	35	66.2	1.1	2.1
GOM5_82	168	1.42	0.0818	0.0045	0.0116	0.0004	0.2606	79.8	4.2	74.4	2.2	307	61	74.4	2.2	6.8
GOM5_60	254.3	1.58	0.0828	0.0022	0.0125	0.0002	0.1292	80.7	2.0	80.3	1.2	159	34	80.3	1.2	0.5
GOM5_16	123.6	1.76	0.0857	0.0027	0.0127	0.0002	0.2757	83.5	2.5	81.2	1.2	199	33	81.2	1.2	2.8
GOM5_12	95.8	2.03	0.0834	0.0040	0.0127	0.0004	0.3696	81.3	3.7	81.6	2.6	172	32	81.6	2.6	0.4
GOM5_49	63.6	1.19	0.0870	0.0038	0.0129	0.0003	-0.0335	85.2	3.4	82.6	2.0	275	37	82.6	2.0	3.1
GOM5_90	296	2.43	0.0906	0.0019	0.0140	0.0002	-0.0386	88.3	1.8	89.8	1.0	141	28	89.8	1.0	1.7
GOM5_113	225	2.45	0.0917	0.0024	0.0142	0.0003	0.1651	89.1	2.3	90.7	1.6	119	24	90.7	1.6	1.8
GOM5_9	293	0.97	0.0929	0.0021	0.0143	0.0002	0.0085	90.1	1.9	91.4	1.0	141	27	91.4	1.0	1.4
GOM5_13	42.8	1.17	0.0984	0.0059	0.0143	0.0004	-0.0357	95.1	5.5	91.4	2.2	383	72	91.4	2.2	3.9
GOM5_34	85.2	0.93	0.0979	0.0039	0.0144	0.0003	-0.1326	94.7	3.6	92.4	1.8	270	42	92.4	1.8	2.4
GOM5_37	274	1.55	0.0974	0.0022	0.0145	0.0002	-0.0014	94.3	2.0	92.6	1.0	184	26	92.6	1.0	1.8
GOM5_93	630	1.86	0.1032	0.0023	0.0147	0.0002	-0.0271	99.7	2.1	94.0	1.0	254	31	94.0	1.0	5.7
GOM5_1	50.5	0.86	0.1004	0.0073	0.0147	0.0004	-0.1112	96.9	6.7	94.1	2.4	318	81	94.1	2.4	2.9
GOM5_94	129.5	1.85	0.1010	0.0022	0.0152	0.0002	0.0121	97.7	2.0	97.0	1.4	175	27	97.0	1.4	0.7
GOM5_21	375.9	0.97	0.1021	0.0016	0.0154	0.0002	0.0794	98.7	1.5	98.5	1.1	136	20	98.5	1.1	0.2
GOM5_112	133.5	1.59	0.1141	0.0034	0.0156	0.0002	0.1099	110.0	3.0	99.5	1.5	348	46	99.5	1.5	9.5
GOM5_119	465	3.87	0.1022	0.0021	0.0157	0.0003	0.4598	98.8	1.9	100.3	1.8	120	23	100.3	1.8	1.5
GOM5_51	95.4	1.33	0.1042	0.0063	0.0157	0.0004	0.0511	100.6	5.8	100.5	2.5	147	50	100.5	2.5	0.1
GOM5_38	403	1.47	0.1251	0.0020	0.0185	0.0002	0.2610	119.6	1.8	118.0	1.2	155	19	118.0	1.2	1.3
GOM5_14	126.9	0.89	0.1534	0.0035	0.0227	0.0003	0.0086	144.8	3.1	144.9	2.1	198	30	144.9	2.1	0.1
GOM5_115	11.33	0.32	0.1710	0.0160	0.0244	0.0009	0.0013	161.0	13.0	155.4	5.5	467	79	155.4	5.5	3.5
GOM5_87	28.19	0.42	0.1680	0.0076	0.0249	0.0006	0.0171	157.2	6.7	158.4	3.5	335	55	158.4	3.5	0.8
GOM5_72	21.2	1.10	0.1790	0.0110	0.0249	0.0008	0.1042	166.4	9.5	158.7	4.8	444	68	158.7	4.8	4.6
GOM5_32	93.1	0.50	0.1750	0.0051	0.0250	0.0006	0.3060	163.7	4.4	158.8	4.0	269	56	158.8	4.0	3.0
GOM5_11	202	1.52	0.1747	0.0030	0.0255	0.0003	0.3039	163.7	2.6	162.2	1.7	188	20	162.2	1.7	0.9
GOM5_69	333	0.88	0.1756	0.0039	0.0257	0.0003	0.4832	164.8	3.3	163.6	2.0	202	22	163.6	2.0	0.7
GOM5_20	112.5	0.60	0.1784	0.0037	0.0260	0.0004	0.0304	166.6	3.1	165.2	2.2	227	31	165.2	2.2	0.8
GOM5_75	236	0.96	0.1762	0.0033	0.0262	0.0003	0.3864	164.8	2.8	166.6	1.9	158	21	166.6	1.9	1.1
GOM5_44	72.4	0.79	0.1836	0.0042	0.0264	0.0004	0.0994	171.0	3.6	168.2	2.7	264	31	168.2	2.7	1.6

GOM5_104	193.3	0.47	0.1818	0.0038	0.0265	0.0004	0.1466	169.5	3.3	168.5	2.2	190	27	168.5	2.2	0.6
GOM5_100	213	1.61	0.1813	0.0036	0.0267	0.0003	0.0673	169.1	3.1	169.7	2.1	172	26	169.7	2.1	0.4
GOM5_15	353	1.65	0.1824	0.0024	0.0269	0.0003	0.2782	170.1	2.0	171.0	1.9	167	20	171.0	1.9	0.5
GOM5_80	348	0.88	0.1875	0.0025	0.0273	0.0003	0.3260	174.4	2.2	173.5	1.9	186	15	173.5	1.9	0.5
GOM5_55	330	1.00	0.1855	0.0030	0.0274	0.0003	0.3953	172.7	2.6	174.5	1.7	182	18	174.5	1.7	1.0
GOM5_52	319	0.88	0.1892	0.0032	0.0275	0.0003	0.3108	175.9	2.7	175.0	2.0	198	20	175.0	2.0	0.5
GOM5_103	427	0.49	0.1875	0.0018	0.0276	0.0002	0.1041	174.7	1.6	175.5	1.3	182	15	175.5	1.3	0.5
GOM5_99	200.7	0.91	0.1908	0.0056	0.0277	0.0005	0.4096	177.2	4.7	176.0	2.8	207	30	176.0	2.8	0.7
GOM5_41	590	1.40	0.1945	0.0023	0.0280	0.0003	0.4780	180.4	1.9	177.7	1.6	201	11	177.7	1.6	1.5
GOM5_31	190.7	0.82	0.2050	0.0120	0.0290	0.0005	0.9561	189.3	9.5	184.3	3.4	232	47	184.3	3.4	2.6
GOM5_111	146.1	0.96	0.2332	0.0040	0.0336	0.0003	-0.0497	212.8	3.3	212.9	2.1	224	24	212.9	2.1	0.0
GOM5_25	170.8	1.40	0.2359	0.0045	0.0338	0.0003	0.2918	215.5	3.8	214.3	2.1	216	22	214.3	2.1	0.6
GOM5_30	133	0.65	0.2407	0.0046	0.0342	0.0004	0.2380	218.8	3.8	217.0	2.3	236	21	217.0	2.3	0.8
GOM5_76	251	1.32	0.2471	0.0041	0.0357	0.0004	0.3908	224.1	3.3	225.9	2.5	225	22	225.9	2.5	0.8
GOM5_78	100	4.50	0.6630	0.0210	0.0830	0.0020	0.6470	516.0	13.0	514.0	12.0	547	30	514.0	12.0	0.4
GOM5_36	61.6	0.47	0.9640	0.0170	0.1113	0.0011	0.2521	685.0	8.7	680.4	6.6	698	20	680.4	6.6	0.7
GOM5_62	116.6	0.93	1.7090	0.0160	0.1704	0.0013	0.4624	1012.5	6.2	1014.5	7.1	1021	9	1020.7	8.6	0.6
GOM5_77	133.8	106.20	1.7620	0.0190	0.1729	0.0014	0.5436	1031.2	6.9	1028.2	7.6	1038	11	1038.0	11.0	0.9
GOM5_47	158	1.86	1.7660	0.0160	0.1720	0.0014	0.5699	1033.4	6.0	1023.1	7.9	1054	10	1054.0	10.0	2.9
GOM5_106	75.7	0.84	1.8270	0.0170	0.1748	0.0015	0.3517	1054.8	6.3	1038.2	8.3	1083	12	1083.0	12.0	4.1
GOM5_8	115.5	1.97	1.8340	0.0250	0.1752	0.0024	0.7811	1058.2	9.2	1040.0	13.0	1106	10	1106.0	10.0	6.0
GOM5_71	50.8	0.61	1.8560	0.0230	0.1756	0.0020	0.4567	1066.1	8.4	1043.0	11.0	1114	13	1114.0	13.0	6.4
GOM5_84	153.2	0.80	2.0060	0.0180	0.1886	0.0019	0.6171	1117.9	6.1	1114.0	10.0	1134	9	1133.9	8.7	1.8
GOM5_24	239	1.85	1.9830	0.0150	0.1849	0.0014	0.7357	1110.3	5.3	1094.3	7.6	1140	6	1140.0	5.5	4.0
GOM5_108	264	1.12	2.2850	0.0170	0.2063	0.0017	0.6723	1207.5	5.1	1208.8	8.9	1201	8	1200.8	7.6	0.7
GOM5_95	182.7	1.45	2.4070	0.0210	0.2160	0.0016	0.7089	1244.5	6.1	1260.7	8.7	1230	6	1229.7	5.9	2.5
GOM5_26	118	1.21	2.3180	0.0210	0.2042	0.0019	0.6594	1218.1	6.5	1198.0	10.0	1250	8	1249.8	8.0	4.1
GOM5_59	425	1.66	2.9020	0.0270	0.2375	0.0021	0.7703	1382.0	7.0	1375.0	11.0	1407	7	1406.7	7.2	2.3
GOM5_81	190.2	2.70	2.7330	0.0390	0.2233	0.0027	0.8635	1338.0	11.0	1299.0	14.0	1408	8	1408.3	7.5	7.8
GOM5_91	242	0.98	3.0360	0.0170	0.2460	0.0017	0.5090	1416.5	4.4	1417.7	8.7	1415	7	1414.5	6.8	0.2
GOM5_48	195	1.73	3.0510	0.0200	0.2468	0.0018	0.6330	1420.3	4.9	1421.7	9.2	1418	7	1417.8	6.8	0.3
GOM5_57	319	1.68	2.8320	0.0430	0.2303	0.0036	0.9406	1363.0	12.0	1335.0	19.0	1419	8	1419.0	7.6	5.9
GOM5_43	250	2.07	2.9950	0.0210	0.2415	0.0021	0.7440	1406.0	5.2	1395.0	11.0	1421	7	1421.0	7.2	1.8

GOM5_107	173	1.27	3.0240	0.0240	0.2424	0.0017	0.6395	1413.3	6.1	1398.9	8.9	1434	6	1433.5	6.1	2.4
GOM5_120	76.4	0.76	3.0760	0.0290	0.2470	0.0026	0.6252	1426.3	7.3	1423.0	13.0	1434	9	1434.4	8.9	0.8
GOM5_70	241.7	1.19	3.0250	0.0230	0.2412	0.0022	0.7581	1414.8	5.5	1393.0	11.0	1446	5	1446.4	5.3	3.7
GOM5_3	289	1.14	2.7470	0.0170	0.2197	0.0017	0.7241	1341.0	4.6	1280.1	9.1	1447	6	1447.2	6.0	11.5
GOM5_27	315.1	1.31	3.0850	0.0270	0.2446	0.0025	0.7714	1429.4	6.6	1410.0	13.0	1460	7	1460.3	7.3	3.4
GOM5_68	102.8	1.83	3.2100	0.0360	0.2538	0.0028	0.8502	1459.0	8.7	1458.0	14.0	1463	9	1462.5	9.1	0.3
GOM5_45	463	1.73	2.8240	0.0430	0.2227	0.0035	0.9638	1361.0	12.0	1296.0	19.0	1464	5	1463.8	5.1	11.5
GOM5_85	96.5	2.52	3.5970	0.0370	0.2643	0.0024	0.7359	1548.3	8.1	1512.0	12.0	1605	7	1605.0	7.1	5.8
GOM5_40	87.4	0.79	3.3980	0.0340	0.2450	0.0032	0.7886	1503.5	7.8	1415.0	16.0	1642	8	1642.1	8.3	13.8
GOM5_86	27.2	0.44	4.1050	0.0530	0.2891	0.0035	0.4346	1654.0	10.0	1639.0	18.0	1676	13	1676.0	13.0	2.2
GOM5_18	105.9	1.01	4.0650	0.0280	0.2855	0.0023	0.6035	1647.8	5.8	1619.0	12.0	1681	7	1680.6	7.0	3.7
GOM5_5	172	0.96	3.8750	0.0550	0.2727	0.0031	0.8810	1609.0	11.0	1554.0	16.0	1684	7	1684.4	6.8	7.7
GOM5_114	36.76	0.69	4.1170	0.0410	0.2889	0.0031	0.5322	1657.0	8.2	1636.0	16.0	1687	11	1687.0	11.0	3.0
GOM5_2	326	1.20	4.3020	0.0450	0.3004	0.0032	0.9044	1694.2	8.7	1693.0	16.0	1689	5	1688.7	5.2	0.3
GOM5_64	319	1.43	4.0240	0.0390	0.2821	0.0031	0.8591	1638.5	7.8	1601.0	16.0	1695	6	1695.4	6.1	5.6
GOM5_110	166.6	1.37	4.0680	0.0370	0.2827	0.0025	0.7014	1647.5	7.3	1605.0	13.0	1697	7	1696.7	7.0	5.4
GOM5_92	189	1.49	4.1300	0.0460	0.2886	0.0030	0.6118	1659.8	9.0	1634.0	15.0	1700	11	1700.0	11.0	3.9
GOM5_7	183.3	1.78	4.3140	0.0320	0.2984	0.0022	0.7008	1695.8	6.2	1685.0	11.0	1713	7	1712.5	6.7	1.6
GOM5_102	557	1.52	4.4160	0.0360	0.3000	0.0032	0.8703	1714.9	6.9	1691.0	16.0	1746	6	1745.6	6.1	3.1
GOM5_63	313	2.07	4.4900	0.0490	0.3051	0.0030	0.8666	1730.7	9.0	1716.0	15.0	1746	6	1746.2	6.0	1.7
GOM5_6	725	9.85	4.4100	0.0260	0.2984	0.0017	0.8259	1715.1	4.8	1683.4	8.7	1750	3	1750.1	3.3	3.8
GOM5_105	695	1.29	4.4350	0.0350	0.2984	0.0025	0.8309	1719.5	6.7	1685.0	12.0	1764	5	1764.2	4.5	4.5
GOM5_58	169.4	0.78	5.2550	0.0510	0.3294	0.0035	0.7232	1861.1	8.4	1835.0	17.0	1890	5	1890.3	5.4	2.9
GOM5_56	12.8	1.36	5.4080	0.0850	0.3394	0.0050	0.4599	1885.0	13.0	1883.0	24.0	1903	13	1903.0	13.0	1.1
GOM5_96	73.4	0.88	6.6480	0.0470	0.3813	0.0026	0.6545	2066.3	6.3	2082.0	12.0	2056	6	2055.5	5.5	1.3

Sample:GOM6	Isotopic Ratios							Isotopic ages (Ma)								
Analysis	[U] ppm	U/Th	207/235	2σ err.	206/238	2σ err.	RHO	207/235	2σ err.	206/238	2σ err.	207/206	2σ err.	Best age	2σ err.	% Dis.
GOM6_107	27.2	0.83	0.0291	0.0032	0.0047	0.0002	0.1222	29.1	3.1	30.3	1.3	640	140	30.3	1.3	4.1
GOM6_97	174.2	1.02	0.0348	0.0015	0.0048	0.0001	-0.0214	34.7	1.5	31.1	0.5	390	51	31.1	0.5	10.3
GOM6_113	42.2	0.71	0.0347	0.0031	0.0050	0.0002	0.0050	34.5	3.0	32.4	1.2	512	77	32.4	1.2	6.1

GOM6_20	128.4	0.60	0.0340	0.0021	0.0052	0.0002	0.4940	33.9	2.0	33.3	1.3	275	93	33.3	1.3	1.8
GOM6_50	47	0.88	0.0372	0.0050	0.0053	0.0002	0.1766	37.0	4.9	34.0	1.6	400	120	34.0	1.6	8.1
GOM6_39	114.7	1.10	0.0360	0.0016	0.0054	0.0001	-0.0363	36.2	1.6	34.4	0.8	283	50	34.4	0.8	5.1
GOM6_58	333.1	1.06	0.0355	0.0011	0.0053	0.0001	0.1299	35.4	1.1	34.4	0.5	185	31	34.4	0.5	2.9
GOM6_23	170	0.70	0.0373	0.0013	0.0057	0.0001	0.0950	37.2	1.2	36.4	0.5	239	45	36.4	0.5	2.2
GOM6_32	42.49	0.77	0.0395	0.0038	0.0057	0.0002	0.0664	39.3	3.7	36.4	1.3	350	89	36.4	1.3	7.4
GOM6_57	83	0.49	0.0462	0.0021	0.0068	0.0002	-0.0696	45.8	2.1	43.8	1.1	342	69	43.8	1.1	4.4
GOM6_76	107.8	1.31	0.0547	0.0023	0.0082	0.0002	0.0027	54.1	2.2	52.4	1.4	231	53	52.4	1.4	3.1
GOM6_13	227	0.82	0.0541	0.0014	0.0083	0.0001	0.0454	53.5	1.3	53.1	0.8	141	28	53.1	0.8	0.8
GOM6_117	88.5	0.72	0.0553	0.0025	0.0087	0.0002	0.1419	54.6	2.4	55.8	1.1	282	70	55.8	1.1	2.2
GOM6_21	359.4	1.16	0.0585	0.0015	0.0088	0.0002	0.1996	57.7	1.4	56.7	1.1	109	22	56.7	1.1	1.7
GOM6_74	123.8	0.85	0.0584	0.0019	0.0089	0.0002	-0.0300	57.6	1.9	57.3	1.3	181	38	57.3	1.3	0.5
GOM6_48	232	1.41	0.0580	0.0012	0.0089	0.0001	0.0700	57.3	1.1	57.4	0.8	128	24	57.4	0.8	0.1
GOM6_59	192.2	1.97	0.0595	0.0015	0.0091	0.0002	-0.0852	58.7	1.4	58.7	0.9	172	30	58.7	0.9	0.0
GOM6_84	76.3	0.66	0.0594	0.0025	0.0092	0.0002	0.1079	58.5	2.4	58.8	1.4	271	54	58.8	1.4	0.5
GOM6_16	183	0.96	0.0602	0.0017	0.0092	0.0001	-0.1459	59.3	1.7	59.0	0.9	157	36	59.0	0.9	0.6
GOM6_124	159.9	1.31	0.0603	0.0020	0.0093	0.0002	0.1708	59.4	1.9	59.7	1.1	185	38	59.7	1.1	0.5
GOM6_18	282.6	0.91	0.0625	0.0014	0.0093	0.0002	0.1539	61.5	1.4	59.8	0.9	156	23	59.8	0.9	2.8
GOM6_90	233	1.37	0.0605	0.0015	0.0094	0.0002	0.1114	59.7	1.5	60.0	0.9	151	31	60.0	0.9	0.5
GOM6_94	41.78	0.76	0.0636	0.0038	0.0095	0.0003	-0.1818	62.5	3.6	61.1	1.9	405	79	61.1	1.9	2.2
GOM6_100	169	1.11	0.0647	0.0021	0.0100	0.0001	-0.0070	63.6	2.0	64.1	0.7	224	41	64.1	0.7	0.8
GOM6_128	318	3.36	0.0673	0.0015	0.0104	0.0002	0.2270	66.2	1.5	66.4	1.3	147	30	66.4	1.3	0.3
GOM6_60	43.8	0.68	0.0746	0.0072	0.0106	0.0003	0.1146	72.7	6.4	68.0	1.8	431	93	68.0	1.8	6.5
GOM6_103	239.8	0.79	0.0714	0.0036	0.0109	0.0003	0.0727	70.0	3.4	69.7	1.6	158	54	69.7	1.6	0.4
GOM6_26	133.5	1.07	0.0720	0.0025	0.0110	0.0002	0.2250	71.0	2.3	70.2	1.2	187	46	70.2	1.2	1.1
GOM6_118	472	0.81	0.0766	0.0015	0.0111	0.0002	0.3608	74.9	1.4	71.2	1.4	189	24	71.2	1.4	4.9
GOM6_66	234.3	1.25	0.0773	0.0018	0.0117	0.0001	0.2142	75.6	1.7	74.7	0.8	185	30	74.7	0.8	1.2
GOM6_22	106.5	1.22	0.0730	0.0043	0.0117	0.0004	0.1195	71.5	4.1	75.2	2.3	142	26	75.2	2.3	5.2
GOM6_65	567	1.13	0.0797	0.0018	0.0118	0.0001	0.0161	77.8	1.7	75.5	0.9	152	28	75.5	0.9	3.0
GOM6_15	302.6	1.61	0.0778	0.0019	0.0118	0.0002	0.3001	76.1	1.8	75.6	1.1	160	32	75.6	1.1	0.7
GOM6_112	156	0.99	0.0775	0.0021	0.0119	0.0002	-0.0342	75.7	1.9	76.0	1.1	161	30	76.0	1.1	0.4
GOM6_87	93.9	2.65	0.0801	0.0035	0.0121	0.0003	-0.1938	78.2	3.3	77.5	1.7	234	53	77.5	1.7	0.9
GOM6_3	88.9	1.10	0.0798	0.0035	0.0121	0.0002	0.1267	78.0	3.3	77.8	1.5	164	45	77.8	1.5	0.3

GOM6_55	22.5	0.39	0.0838	0.0080	0.0123	0.0005	0.0136	81.4	7.4	79.1	3.3	446	87	79.1	3.3	2.8
GOM6_40	69.1	0.73	0.0863	0.0027	0.0125	0.0003	0.2178	84.4	2.6	80.1	1.6	265	35	80.1	1.6	5.1
GOM6_106	860	1.25	0.0860	0.0016	0.0132	0.0002	0.5623	83.8	1.5	84.3	1.2	107	22	84.3	1.2	0.6
GOM6_123	97	1.09	0.0880	0.0030	0.0132	0.0002	0.1711	85.6	2.8	84.7	1.3	213	32	84.7	1.3	1.1
GOM6_14	199.4	1.50	0.0891	0.0022	0.0133	0.0002	-0.0408	86.7	2.1	85.3	1.2	141	32	85.3	1.2	1.6
GOM6_95	277.7	1.64	0.0874	0.0017	0.0134	0.0001	0.0983	85.1	1.6	85.6	0.9	137	24	85.6	0.9	0.6
GOM6_1	205	3.12	0.0902	0.0019	0.0138	0.0002	-0.0011	87.7	1.8	88.2	1.3	105	24	88.2	1.3	0.6
GOM6_125	232.2	0.92	0.0869	0.0031	0.0138	0.0003	0.4129	84.6	2.9	88.5	1.6	92	31	88.5	1.6	4.6
GOM6_28	167.3	1.97	0.0926	0.0027	0.0139	0.0002	0.1047	90.3	2.6	89.0	1.2	191	28	89.0	1.2	1.4
GOM6_72	355	1.06	0.0910	0.0029	0.0140	0.0002	-0.0305	88.4	2.7	89.8	1.4	75	20	89.8	1.4	1.6
GOM6_108	142	1.32	0.0932	0.0028	0.0143	0.0002	-0.0986	90.8	2.5	91.5	1.3	250	43	91.5	1.3	0.8
GOM6_34	181.9	2.49	0.0956	0.0025	0.0146	0.0002	-0.0632	92.7	2.3	93.7	1.0	125	28	93.7	1.0	1.1
GOM6_127	166	2.43	0.0933	0.0029	0.0148	0.0003	0.0963	90.5	2.7	94.8	2.2	91	43	94.8	2.2	4.8
GOM6_70	426	1.77	0.1028	0.0014	0.0157	0.0002	0.4705	99.4	1.3	100.1	1.1	101	13	100.1	1.1	0.7
GOM6_96	404	1.20	0.1044	0.0032	0.0159	0.0004	0.4065	100.7	3.0	101.7	2.8	136	34	101.7	2.8	1.0
GOM6_86	328.2	1.78	0.1129	0.0017	0.0170	0.0001	0.2197	108.6	1.5	109.0	0.9	119	17	109.0	0.9	0.3
GOM6_10	694	0.71	0.1479	0.0017	0.0214	0.0002	0.5278	140.1	1.5	136.5	1.5	199	16	136.5	1.5	2.6
GOM6_104	91.9	1.08	0.1517	0.0078	0.0220	0.0007	0.0870	143.4	6.9	140.2	4.2	180	72	140.2	4.2	2.2
GOM6_99	338.2	1.08	0.1529	0.0019	0.0230	0.0002	0.1846	144.4	1.7	146.6	1.4	134	16	146.6	1.4	1.5
GOM6_98	71.7	0.91	0.1585	0.0079	0.0231	0.0006	0.1824	149.3	6.9	147.1	3.5	245	51	147.1	3.5	1.5
GOM6_122	124.9	0.52	0.1557	0.0060	0.0231	0.0005	0.2259	146.8	5.3	147.1	3.1	180	53	147.1	3.1	0.2
GOM6_9	52.3	0.37	0.1662	0.0048	0.0241	0.0004	0.0322	156.5	4.1	153.5	2.7	274	44	153.5	2.7	1.9
GOM6_44	212	0.84	0.1719	0.0026	0.0248	0.0003	0.3071	161.1	2.2	157.7	1.7	166	20	157.7	1.7	2.1
GOM6_81	559	1.38	0.1727	0.0023	0.0253	0.0003	0.7207	161.7	2.0	160.8	1.8	171	10	160.8	1.8	0.6
GOM6_30	211.4	0.38	0.1702	0.0021	0.0253	0.0002	0.3107	159.8	1.8	161.1	1.3	131	13	161.1	1.3	0.8
GOM6_105	761	0.91	0.1748	0.0018	0.0258	0.0002	0.2841	163.5	1.6	164.3	1.5	166	17	164.3	1.5	0.5
GOM6_116	357	0.53	0.1771	0.0019	0.0260	0.0002	0.2124	165.8	1.6	165.3	1.3	176	15	165.3	1.3	0.3
GOM6_4	337	0.51	0.1740	0.0035	0.0260	0.0003	0.3251	162.8	3.1	165.4	1.9	161	24	165.4	1.9	1.6
GOM6_88	349	0.67	0.1783	0.0019	0.0260	0.0003	0.4049	166.6	1.6	165.7	1.6	166	13	165.7	1.6	0.5
GOM6_119	217	0.89	0.1771	0.0025	0.0261	0.0002	0.3145	165.5	2.1	165.9	1.4	172	19	165.9	1.4	0.2
GOM6_83	305	1.14	0.1841	0.0026	0.0272	0.0003	0.4993	171.6	2.2	173.0	2.0	176	17	173.0	2.0	0.8
GOM6_79	276	0.98	0.1880	0.0030	0.0274	0.0003	0.2938	174.9	2.6	174.1	2.0	169	20	174.1	2.0	0.5
GOM6_120	480	0.74	0.2024	0.0043	0.0296	0.0004	0.4593	187.1	3.6	188.3	2.6	196	28	188.3	2.6	0.6

GOM6_8	103	1.79	0.2088	0.0036	0.0301	0.0004	0.0127	192.4	3.0	191.3	2.2	210	22	191.3	2.2	0.6
GOM6_25	209	0.90	0.2185	0.0052	0.0313	0.0005	0.6467	200.6	4.3	198.5	3.1	207	26	198.5	3.1	1.0
GOM6_12	622	1.83	0.2326	0.0023	0.0334	0.0003	0.4666	212.3	1.9	212.0	2.0	230	16	212.0	2.0	0.1
GOM6_41	143.7	0.50	0.2491	0.0043	0.0345	0.0005	0.2717	225.8	3.5	218.7	2.9	265	27	218.7	2.9	3.1
GOM6_91	86.6	1.18	0.2416	0.0046	0.0348	0.0005	0.1685	219.6	3.8	220.3	2.8	241	28	220.3	2.8	0.3
GOM6_35	334	2.02	0.2501	0.0029	0.0358	0.0003	0.4904	226.6	2.3	226.9	1.9	234	15	226.9	1.9	0.1
GOM6_6	166	1.36	0.2555	0.0045	0.0362	0.0004	0.2448	230.9	3.7	229.0	2.4	261	26	229.0	2.4	0.8
GOM6_54	223	1.30	0.2567	0.0035	0.0362	0.0004	0.1357	232.0	2.8	229.4	2.6	244	21	229.4	2.6	1.1
GOM6_78	252	1.24	0.2548	0.0031	0.0366	0.0003	0.1264	230.4	2.5	231.6	2.0	227	15	231.6	2.0	0.5
GOM6_77	425.3	1.21	0.2598	0.0039	0.0371	0.0005	0.4124	234.5	3.1	234.8	3.3	248	18	234.8	3.3	0.1
GOM6_7	295	1.71	0.2630	0.0028	0.0374	0.0003	0.2223	237.0	2.3	236.9	1.8	236	15	236.9	1.8	0.0
GOM6_92	167	1.12	0.2952	0.0041	0.0421	0.0004	0.1755	262.6	3.2	265.9	2.2	249	18	265.9	2.2	1.3
GOM6_69	354	2.70	0.3028	0.0037	0.0423	0.0003	0.2026	268.5	2.9	266.7	2.1	282	14	266.7	2.1	0.7
GOM6_53	511	2.03	0.4121	0.0047	0.0558	0.0007	0.5075	350.3	3.4	349.8	3.9	360	15	349.8	3.9	0.1
GOM6_73	240	0.71	0.4389	0.0051	0.0579	0.0005	0.4294	369.4	3.6	363.1	2.9	397	14	363.1	2.9	1.7
GOM6_109	322	1.49	0.6910	0.0051	0.0870	0.0004	0.1987	533.7	3.1	537.6	2.6	525	9	537.6	2.6	0.7
GOM6_56	78.9	0.98	1.5790	0.0140	0.1595	0.0011	0.4586	961.8	5.4	953.9	6.2	989	10	953.9	6.2	0.8
GOM6_52	33.8	0.79	1.8560	0.0240	0.1797	0.0016	0.3130	1065.0	8.6	1065.0	8.6	1061	15	1061.0	15.0	0.4
GOM6_111	34.1	1.05	1.8470	0.0250	0.1782	0.0015	0.3902	1062.7	8.8	1056.9	8.1	1070	15	1070.0	15.0	1.2
GOM6_61	76.5	1.73	1.9180	0.0220	0.1830	0.0017	0.6181	1087.9	7.3	1083.3	9.5	1085	13	1085.0	13.0	0.2
GOM6_27	66.3	1.03	1.7980	0.0600	0.1714	0.0058	0.6925	1044.0	22.0	1020.0	32.0	1097	27	1097.0	27.0	7.0
GOM6_5	23.1	1.12	2.0660	0.0270	0.1949	0.0018	0.3347	1137.9	8.9	1147.5	9.7	1132	18	1132.0	18.0	1.4
GOM6_67	54.4	1.24	2.0060	0.0200	0.1875	0.0016	0.2352	1117.0	6.8	1107.9	8.7	1140	12	1140.0	12.0	2.8
GOM6_114	52.4	1.47	2.0870	0.0230	0.1946	0.0018	0.3321	1144.1	7.4	1147.2	9.5	1140	12	1140.0	12.0	0.6
GOM6_89	83.3	1.19	2.0750	0.0200	0.1941	0.0014	0.5150	1140.2	6.5	1143.4	7.5	1142	10	1142.1	9.9	0.1
GOM6_64	22.6	0.96	1.9810	0.0330	0.1846	0.0025	0.2564	1108.0	11.0	1092.0	13.0	1145	22	1145.0	22.0	4.6
GOM6_47	193.5	1.29	2.0800	0.0170	0.1929	0.0014	0.6049	1141.9	5.6	1137.2	7.6	1148	7	1147.6	7.0	0.9
GOM6_51	127	1.05	2.1910	0.0200	0.1982	0.0014	0.5780	1177.9	6.2	1165.8	7.6	1195	8	1194.5	8.3	2.4
GOM6_49	32.4	0.41	2.8170	0.0380	0.2329	0.0021	0.1106	1359.0	10.0	1350.0	11.0	1384	14	1384.0	14.0	2.5
GOM6_42	120	0.65	2.9230	0.0240	0.2383	0.0020	0.6291	1387.4	6.3	1378.0	10.0	1392	8	1392.0	7.8	1.0
GOM6_63	80.1	0.85	2.8390	0.0210	0.2303	0.0015	0.3795	1365.6	5.5	1335.9	8.0	1404	7	1403.9	7.3	4.8
GOM6_46	156.2	1.02	2.9140	0.0160	0.2374	0.0012	0.2829	1385.5	4.1	1373.1	6.4	1409	7	1409.4	7.4	2.6
GOM6_102	180.3	2.15	2.8950	0.0240	0.2357	0.0018	0.8189	1381.4	6.5	1364.1	9.4	1416	7	1415.5	7.0	3.6

GOM6_19	387	1.54	2.9260	0.0250	0.2371	0.0018	0.7512	1389.0	6.3	1371.4	9.5	1422	6	1422.0	5.9	3.6
GOM6_110	177.1	0.88	2.8640	0.0280	0.2297	0.0015	0.8151	1372.1	7.4	1332.6	7.7	1432	6	1432.2	6.1	7.0
GOM6_126	457	0.84	2.8340	0.0220	0.2301	0.0022	0.7834	1364.2	5.9	1335.0	12.0	1437	5	1436.8	4.6	7.1
GOM6_45	532	3.71	2.9940	0.0260	0.2381	0.0020	0.7213	1406.6	6.5	1377.0	11.0	1439	8	1438.8	8.4	4.3
GOM6_85	114.1	0.95	3.0720	0.0250	0.2440	0.0015	0.5006	1425.4	6.2	1407.5	7.5	1446	7	1445.6	7.3	2.6
GOM6_43	25.8	0.65	3.1240	0.0320	0.2469	0.0019	0.1815	1439.0	7.6	1422.0	10.0	1450	12	1450.0	12.0	1.9
GOM6_62	274	2.22	3.0500	0.0370	0.2428	0.0023	0.8279	1419.3	9.3	1401.0	12.0	1452	7	1452.1	6.9	3.5
GOM6_37	321	0.87	3.1000	0.0240	0.2431	0.0021	0.7678	1432.4	5.9	1403.0	11.0	1469	5	1469.1	5.2	4.5
GOM6_101	9.11	0.62	4.0050	0.0610	0.2876	0.0043	0.3820	1639.0	13.0	1631.0	21.0	1636	17	1636.0	17.0	0.3
GOM6_68	73.2	0.86	3.9490	0.0250	0.2833	0.0021	0.7264	1623.5	5.1	1606.0	10.0	1643	7	1643.2	7.4	2.3
GOM6_82	163	2.02	4.1170	0.0560	0.2912	0.0028	0.8780	1656.0	11.0	1647.0	14.0	1657	14	1657.0	14.0	0.6
GOM6_38	98	0.52	4.2030	0.0340	0.2937	0.0021	0.6312	1674.2	6.5	1660.0	10.0	1675	7	1674.5	7.4	0.9
GOM6_93	118.1	1.40	4.2220	0.0460	0.2982	0.0047	0.7250	1678.8	9.2	1682.0	23.0	1682	13	1682.0	13.0	0.0
GOM6_11	133	1.51	4.2660	0.0230	0.2984	0.0016	0.5559	1686.7	4.5	1683.1	8.0	1689	6	1688.5	6.4	0.3
GOM6_17	31.32	2.12	4.1110	0.0400	0.2901	0.0032	0.5708	1655.8	8.1	1642.0	16.0	1691	10	1691.0	10.0	2.9
GOM6_2	219	1.74	4.6450	0.0250	0.3154	0.0018	0.6539	1757.7	4.5	1766.9	8.6	1750	5	1750.0	4.6	1.0
GOM6_31	150.1	2.67	5.2650	0.0320	0.3353	0.0020	0.5877	1862.9	5.1	1864.0	9.7	1862	6	1862.3	5.7	0.1
GOM6_75	123.5	1.41	10.7370	0.0900	0.4538	0.0040	0.6763	2500.3	7.8	2412.0	18.0	2569	6	2568.5	6.1	6.1
GOM6_29	38.3	0.50	14.2000	0.1000	0.5250	0.0038	0.6806	2763.8	6.6	2720.0	16.0	2791	6	2790.6	5.5	2.5

Sample:GOM7	Isotopic Ratios							Isotopic ages (Ma)								
Analysis	[U] ppm	U/Th	207/235	2σ err.	206/238	2σ err.	RHO	207/235	2σ err.	206/238	2σ err.	207/206	2σ err.	Best age	2σ err.	% Dis.
GOM7_618	76.6	0.51	0.0270	0.0021	0.0040	0.0001	-0.0150	27.0	2.1	25.5	0.7	552	92	25.5	0.7	5.7
GOM7_94	220	1.15	0.0277	0.0012	0.0043	0.0001	0.0371	27.7	1.2	27.5	0.6	263	47	27.5	0.6	0.9
GOM7_89	162.4	0.90	0.0326	0.0019	0.0046	0.0001	0.3548	32.5	1.9	29.4	0.7	315	61	29.4	0.7	9.5
GOM7_102	214	0.90	0.0301	0.0013	0.0046	0.0001	0.1777	30.1	1.3	29.9	0.6	202	52	29.9	0.6	0.7
GOM7_615	173.5	1.29	0.0339	0.0014	0.0050	0.0001	-0.0440	33.9	1.4	32.0	0.9	267	38	32.0	0.9	5.5
GOM7_644	146.9	0.81	0.0345	0.0023	0.0051	0.0001	0.0190	34.4	2.3	32.9	0.8	236	68	32.9	0.8	4.4
GOM7_61	191.8	0.77	0.0340	0.0012	0.0053	0.0001	-0.0088	33.9	1.2	33.9	0.6	184	52	33.9	0.6	0.1
GOM7_64	1132	0.12	0.0343	0.0006	0.0054	0.0000	0.0984	34.2	0.6	34.6	0.3	84	18	34.6	0.3	1.2
GOM7_111	225	1.06	0.0346	0.0012	0.0054	0.0001	-0.0533	34.5	1.2	35.0	0.5	200	50	35.0	0.5	1.4

GOM7_638	68.3	0.56	0.0368	0.0050	0.0056	0.0003	0.2066	36.7	4.8	35.8	2.1	630	280	35.8	2.1	2.5
GOM7_68	86	0.60	0.0368	0.0025	0.0056	0.0002	0.0115	36.7	2.4	36.0	1.0	418	74	36.0	1.0	1.9
GOM7_62	393	1.02	0.0365	0.0011	0.0057	0.0001	0.0396	36.4	1.1	36.9	0.6	155	35	36.9	0.6	1.3
GOM7_657	158.3	0.84	0.0437	0.0018	0.0066	0.0001	-0.0044	43.4	1.8	42.6	0.9	330	62	42.6	0.9	1.8
GOM7_70	43.2	0.64	0.0493	0.0042	0.0071	0.0003	0.1235	49.2	4.0	45.3	1.7	517	79	45.3	1.7	7.9
GOM7_71	214.2	1.50	0.0520	0.0014	0.0079	0.0001	0.1027	51.4	1.3	50.7	0.9	140	30	50.7	0.9	1.4
GOM7_63	189.8	1.59	0.0528	0.0013	0.0082	0.0001	-0.0894	52.2	1.3	52.8	0.8	206	40	52.8	0.8	1.1
GOM7_2	89.3	0.72	0.0550	0.0030	0.0084	0.0002	-0.1296	54.3	2.9	53.7	1.1	207	49	53.7	1.1	1.1
GOM7_96	206.8	1.56	0.0568	0.0015	0.0087	0.0001	0.1230	56.0	1.5	55.8	0.7	186	41	55.8	0.7	0.3
GOM7_58	212	0.85	0.0574	0.0015	0.0088	0.0001	0.1363	56.6	1.5	56.2	0.7	187	36	56.2	0.7	0.7
GOM7_607	200	0.76	0.0557	0.0015	0.0088	0.0002	-0.0459	55.0	1.4	56.3	1.0	137	27	56.3	1.0	2.3
GOM7_1	248.6	1.58	0.0574	0.0016	0.0088	0.0001	0.0210	56.6	1.5	56.4	0.7	191	38	56.4	0.7	0.4
GOM7_4	260	0.91	0.0589	0.0018	0.0089	0.0001	-0.0282	58.1	1.8	56.8	0.8	167	31	56.8	0.8	2.3
GOM7_633	342	0.87	0.0596	0.0017	0.0089	0.0002	0.2597	58.7	1.6	57.1	1.2	143	30	57.1	1.2	2.7
GOM7_3	375	1.19	0.0587	0.0014	0.0090	0.0001	0.0895	57.9	1.3	57.6	0.8	158	26	57.6	0.8	0.6
GOM7_113	791	1.37	0.0618	0.0007	0.0095	0.0001	0.2712	60.9	0.7	60.8	0.6	93	15	60.8	0.6	0.1
GOM7_6	94.7	2.61	0.0624	0.0044	0.0096	0.0004	-0.2821	61.4	4.2	61.6	2.3	273	94	61.6	2.3	0.3
GOM7_635	510	3.16	0.0711	0.0015	0.0103	0.0001	0.1641	69.7	1.4	65.8	0.8	185	25	65.8	0.8	5.7
GOM7_117	86.3	2.82	0.0702	0.0031	0.0110	0.0002	0.0747	68.8	2.9	70.7	1.2	215	44	70.7	1.2	2.8
GOM7_95	208	2.01	0.0724	0.0017	0.0111	0.0001	0.1147	70.9	1.6	70.9	0.8	147	24	70.9	0.8	0.0
GOM7_626	106.9	1.10	0.0728	0.0028	0.0111	0.0002	0.0297	71.3	2.7	71.2	1.3	280	48	71.2	1.3	0.1
GOM7_658	230	1.07	0.0756	0.0028	0.0116	0.0003	0.1968	74.0	2.7	74.2	1.6	176	51	74.2	1.6	0.3
GOM7_67	262	1.40	0.0794	0.0020	0.0119	0.0002	0.0326	77.6	1.9	76.2	0.9	170	28	76.2	0.9	1.8
GOM7_59	443	0.76	0.0824	0.0017	0.0122	0.0002	0.1775	80.4	1.6	78.3	0.9	154	29	78.3	0.9	2.6
GOM7_617	315	0.62	0.0820	0.0018	0.0124	0.0002	0.2830	80.0	1.7	79.4	1.0	166	27	79.4	1.0	0.7
GOM7_104	210	1.18	0.0916	0.0020	0.0134	0.0002	0.0843	88.9	1.8	85.8	1.0	191	29	85.8	1.0	3.5
GOM7_5	278	0.96	0.0928	0.0030	0.0140	0.0003	0.1939	90.0	2.8	89.6	1.6	147	30	89.6	1.6	0.4
GOM7_97	118.2	0.96	0.0909	0.0031	0.0140	0.0003	-0.1237	88.3	2.9	90.1	1.7	164	39	90.1	1.7	2.0
GOM7_621	132.8	1.48	0.1057	0.0056	0.0146	0.0004	-0.2015	101.9	5.2	93.5	2.7	275	86	93.5	2.7	8.2
GOM7_60	42.1	0.67	0.1035	0.0057	0.0150	0.0003	-0.0996	99.8	5.2	95.9	2.0	355	57	95.9	2.0	3.9
GOM7_614	212	0.91	0.0996	0.0025	0.0151	0.0002	0.0345	96.4	2.3	96.4	1.3	124	20	96.4	1.3	0.0
GOM7_73	304	1.03	0.0993	0.0017	0.0151	0.0002	0.0716	96.1	1.6	96.6	1.0	156	22	96.6	1.0	0.5
GOM7_610	396.4	1.17	0.1018	0.0024	0.0154	0.0002	0.3590	98.9	2.4	98.8	1.3	129	33	98.8	1.3	0.1

GOM7_92	485	1.46	0.1019	0.0016	0.0154	0.0002	0.2009	98.5	1.4	98.8	1.1	123	21	98.8	1.1	0.3
GOM7_103	498	1.37	0.1050	0.0019	0.0157	0.0002	0.4368	101.4	1.8	100.3	1.2	144	24	100.3	1.2	1.1
GOM7_99	438	1.27	0.1432	0.0016	0.0212	0.0002	0.3514	135.9	1.4	135.1	1.1	148	16	135.1	1.1	0.6
GOM7_76	188	1.75	0.1480	0.0047	0.0221	0.0003	0.0904	140.1	4.2	140.7	2.0	161	36	140.7	2.0	0.4
GOM7_625	126.1	0.92	0.1441	0.0030	0.0221	0.0003	0.1050	136.6	2.7	140.8	2.1	162	30	140.8	2.1	3.1
GOM7_101	224	1.38	0.1499	0.0024	0.0225	0.0002	0.0538	141.8	2.2	143.4	1.4	141	21	143.4	1.4	1.1
GOM7_112	323	0.63	0.1677	0.0021	0.0249	0.0002	0.3121	157.4	1.8	158.3	1.1	165	15	158.3	1.1	0.6
GOM7_651	70.1	0.27	0.1742	0.0059	0.0252	0.0005	0.1894	162.9	5.1	160.4	3.3	277	44	160.4	3.3	1.5
GOM7_627	709	0.69	0.1759	0.0027	0.0255	0.0003	0.6239	164.9	2.2	162.3	1.9	184	12	162.3	1.9	1.6
GOM7_7	428	1.56	0.1773	0.0019	0.0260	0.0002	0.2851	165.7	1.6	165.2	1.3	177	15	165.2	1.3	0.3
GOM7_606	316	0.92	0.1804	0.0032	0.0264	0.0003	0.3827	168.7	2.8	167.8	1.6	183	19	167.8	1.6	0.5
GOM7_93	305	0.90	0.1807	0.0026	0.0265	0.0004	0.5321	168.6	2.3	168.4	2.3	173	22	168.4	2.3	0.1
GOM7_641	328.9	1.20	0.1817	0.0029	0.0266	0.0003	0.2787	169.8	2.5	169.5	1.7	168	20	169.5	1.7	0.2
GOM7_90	154	0.76	0.1825	0.0031	0.0269	0.0003	0.2861	170.1	2.7	171.2	1.5	174	22	171.2	1.5	0.6
GOM7_640	459	0.97	0.1856	0.0051	0.0270	0.0005	0.1777	172.9	4.4	171.7	3.0	190	42	171.7	3.0	0.7
GOM7_629	334.2	1.28	0.1982	0.0074	0.0284	0.0006	0.6612	183.5	6.2	180.3	3.5	230	38	180.3	3.5	1.7
GOM7_120	226.3	1.19	0.2033	0.0028	0.0296	0.0003	0.3421	187.9	2.3	187.9	1.6	197	18	187.9	1.6	0.0
GOM7_100	161	1.45	0.2074	0.0043	0.0301	0.0005	0.2327	191.3	3.6	191.2	2.8	223	27	191.2	2.8	0.1
GOM7_605	210.1	0.98	0.2113	0.0040	0.0303	0.0004	0.3777	194.5	3.3	192.3	2.6	238	22	192.3	2.6	1.1
GOM7_110	208.3	2.65	0.2110	0.0140	0.0304	0.0011	0.8763	194.0	11.0	193.0	6.7	172	52	193.0	6.7	0.5
GOM7_74	167.9	1.55	0.2127	0.0036	0.0307	0.0003	0.1974	195.7	3.0	194.8	1.7	204	24	194.8	1.7	0.5
GOM7_107	399	1.24	0.2163	0.0030	0.0311	0.0004	0.6782	198.7	2.5	197.4	2.3	211	15	197.4	2.3	0.7
GOM7_620	259	9.60	0.2410	0.0059	0.0347	0.0004	0.2265	219.1	4.8	219.8	2.7	224	20	219.8	2.7	0.3
GOM7_636	686	0.83	0.2531	0.0026	0.0360	0.0003	0.3717	229.0	2.1	227.8	1.7	243	16	227.8	1.7	0.5
GOM7_611	168.4	2.18	0.2594	0.0049	0.0370	0.0004	0.3853	234.1	3.9	234.2	2.4	243	28	234.2	2.4	0.0
GOM7_660	163	1.26	0.2888	0.0056	0.0408	0.0006	0.1758	257.4	4.4	257.8	3.8	262	28	257.8	3.8	0.2
GOM7_630	34.1	1.35	0.5970	0.0160	0.0763	0.0019	0.4618	474.0	10.0	474.0	11.0	508	35	474.0	11.0	0.0
GOM7_622	171.5	0.75	0.8620	0.0110	0.1021	0.0009	0.5218	630.8	5.8	626.4	5.0	658	17	626.4	5.0	0.7
GOM7_654	40.8	1.83	1.6180	0.0270	0.1622	0.0015	0.2729	976.0	10.0	969.0	8.3	1003	21	969.0	8.3	0.7
GOM7_91	285	2.26	1.6430	0.0110	0.1626	0.0011	0.6429	986.9	4.2	971.3	6.1	1032	6	971.3	6.1	1.6
GOM7_110	178.9	1.63	2.0050	0.0130	0.1660	0.0016	0.4957	1117.0	4.4	990.0	8.8	1372	12	990.0	8.8	11.4
GOM7_72	52.6	1.05	1.7360	0.0200	0.1670	0.0015	0.3218	1021.3	7.6	995.4	8.5	1069	13	995.4	8.5	2.5
GOM7_106	137.2	1.23	1.6760	0.0180	0.1674	0.0019	0.5985	999.3	6.9	998.0	10.0	1017	13	998.0	10.0	0.1

GOM7_613	65.8	0.96	1.9960	0.0290	0.1881	0.0019	0.1545	1116.0	10.0	1111.0	11.0	1122	22	1122.0	22.0	1.0
GOM7_639	238	1.59	1.9150	0.0220	0.1805	0.0028	0.5705	1086.0	7.8	1070.0	15.0	1123	15	1123.0	15.0	4.7
GOM7_69	101.7	0.73	1.9780	0.0170	0.1853	0.0012	0.1489	1108.6	5.6	1095.8	6.3	1135	10	1135.0	10.0	3.5
GOM7_78	258.3	2.30	1.8700	0.0320	0.1751	0.0028	0.8472	1070.0	11.0	1040.0	15.0	1136	13	1136.0	13.0	8.5
GOM7_628	100.8	3.17	1.9640	0.0220	0.1831	0.0019	0.6858	1103.7	7.8	1084.0	11.0	1142	10	1141.6	9.5	5.0
GOM7_653	37.6	1.18	2.0750	0.0290	0.1924	0.0021	0.3113	1139.7	9.4	1134.0	11.0	1158	14	1158.0	14.0	2.1
GOM7_609	236	2.26	1.9510	0.0300	0.1781	0.0022	0.9109	1098.0	10.0	1056.0	12.0	1169	12	1169.0	12.0	9.7
GOM7_632	121	1.25	2.2410	0.0320	0.2034	0.0033	0.3973	1193.4	9.9	1193.0	18.0	1199	19	1199.0	19.0	0.5
GOM7_66	9.7	2.31	2.2260	0.0700	0.2044	0.0041	0.0342	1187.0	22.0	1199.0	22.0	1210	31	1210.0	31.0	0.9
GOM7_619	73.6	0.95	2.5290	0.0290	0.2149	0.0019	0.5606	1280.1	8.4	1255.0	10.0	1324	12	1324.0	12.0	5.2
GOM7_608	110.7	0.84	2.9150	0.0330	0.2389	0.0029	0.7350	1387.2	8.9	1381.0	15.0	1387	11	1387.0	11.0	0.4
GOM7_116	283	1.02	2.8630	0.0150	0.2338	0.0013	0.5948	1372.0	4.0	1354.2	6.7	1407	6	1406.9	5.6	3.7
GOM7_98	130.5	1.77	2.9240	0.0190	0.2385	0.0019	0.5410	1388.0	4.8	1378.9	9.8	1410	8	1410.4	7.8	2.2
GOM7_655	184.4	2.46	2.9670	0.0230	0.2405	0.0021	0.5177	1398.9	5.8	1389.0	11.0	1412	8	1412.1	7.6	1.6
GOM7_115	162.4	1.64	2.9630	0.0200	0.2408	0.0016	0.5548	1398.0	5.2	1390.6	8.4	1413	7	1412.5	6.6	1.6
GOM7_648	92.9	1.28	2.9750	0.0250	0.2395	0.0018	0.4475	1400.8	6.3	1383.7	9.6	1421	10	1421.0	10.0	2.6
GOM7_649	102.9	1.92	2.9900	0.0440	0.2390	0.0040	0.5063	1404.0	11.0	1381.0	21.0	1429	18	1429.0	18.0	3.4
GOM7_108	25.1	1.57	2.9400	0.0450	0.2333	0.0030	0.3927	1393.0	12.0	1351.0	16.0	1459	16	1459.0	16.0	7.4
GOM7_616	196	1.85	3.1250	0.0350	0.2441	0.0027	0.6758	1439.2	8.7	1408.0	14.0	1486	9	1486.1	9.0	5.3
GOM7_604	58.3	2.57	3.1500	0.0800	0.2432	0.0065	0.6144	1444.0	20.0	1406.0	33.0	1495	26	1495.0	26.0	6.0
GOM7_623	98.2	3.46	3.6520	0.0430	0.2708	0.0028	0.4003	1560.3	9.3	1544.0	14.0	1595	15	1595.0	15.0	3.2
GOM7_642	188.1	2.78	3.9970	0.0290	0.2905	0.0021	0.5473	1633.3	5.9	1644.0	10.0	1619	9	1619.4	8.8	1.5
GOM7_105	188	10.90	3.6640	0.0330	0.2615	0.0024	0.7663	1563.2	7.1	1498.0	12.0	1659	6	1659.0	5.9	9.7
GOM7_114	194	1.60	3.9390	0.0380	0.2792	0.0027	0.8163	1621.4	7.7	1587.0	14.0	1669	5	1668.6	5.3	4.9
GOM7_601	100.4	0.59	4.1340	0.0290	0.2915	0.0021	0.4546	1660.8	5.6	1649.0	10.0	1671	7	1670.9	7.0	1.3
GOM7_602	288	3.60	3.7590	0.0620	0.2643	0.0050	0.8983	1584.0	13.0	1511.0	26.0	1675	8	1675.3	8.4	9.8
GOM7_652	309.4	1.83	4.1060	0.0320	0.2875	0.0026	0.7348	1656.3	6.1	1629.0	13.0	1689	6	1689.1	6.0	3.6
GOM7_659	283	2.51	4.1200	0.0280	0.2893	0.0022	0.6154	1658.1	5.6	1638.0	11.0	1693	6	1693.4	6.1	3.3
GOM7_634	187.6	2.05	4.2800	0.0930	0.2925	0.0057	0.1785	1688.0	17.0	1654.0	28.0	1711	12	1711.0	12.0	3.3
GOM7_624	186.6	2.11	4.1020	0.0490	0.2826	0.0030	0.6722	1654.3	9.7	1604.0	15.0	1724	10	1724.0	10.0	7.0
GOM7_109	276	1.25	4.5160	0.0320	0.3073	0.0022	0.7294	1733.5	5.9	1727.0	11.0	1738	6	1738.2	6.4	0.6
GOM7_650	80.8	2.48	4.4930	0.0310	0.3047	0.0026	0.4852	1729.3	5.7	1714.0	13.0	1743	9	1742.8	9.0	1.7
GOM7_631	82.4	1.70	4.0910	0.0560	0.2763	0.0030	0.7891	1652.0	11.0	1573.0	15.0	1761	8	1760.9	7.9	10.7

GOM7_75	316	3.82	4.6050	0.0260	0.3024	0.0018	0.7460	1750.6	4.5	1703.0	9.1	1816	4	1816.3	4.3	6.2
GOM7_643	236	2.22	7.9000	0.1400	0.3995	0.0045	0.7991	2217.0	16.0	2166.0	21.0	2265	17	2265.0	17.0	4.4
GOM7_656	461	1.88	14.7800	0.1400	0.5212	0.0050	0.8267	2801.0	8.8	2704.0	21.0	2876	4	2875.5	4.4	6.0

Sample:GOM8	Isotopic Ratios							Isotopic ages (Ma)								
Analysis	[U] ppm	U/Th	207/235	2σ err.	206/238	2σ err.	RHO	207/235	2σ err.	206/238	2σ err.	207/206	2σ err.	Best age	2σ err.	% Dis.
GOM8_15	94.2	1.32	0.0308	0.0053	0.0043	0.0004	0.0064	30.7	5.2	27.5	2.4	340	340	27.5	2.4	10.4
GOM8_28	168.8	1.56	0.0306	0.0029	0.0044	0.0002	0.1500	30.5	2.8	28.1	1.0	220	180	28.1	1.0	7.9
GOM8_110	132.3	0.91	0.0358	0.0043	0.0055	0.0004	0.0892	35.6	4.2	35.2	2.3	90	240	35.2	2.3	1.1
GOM8_59	384	0.27	0.0372	0.0018	0.0056	0.0001	0.0356	37.1	1.8	36.1	0.9	130	100	36.1	0.9	2.6
GOM8_64	106.5	0.34	0.0373	0.0043	0.0057	0.0004	0.0991	37.1	4.2	36.4	2.3	80	220	36.4	2.3	1.9
GOM8_38	127.4	1.28	0.0384	0.0037	0.0057	0.0003	0.1580	38.2	3.6	36.8	1.6	140	190	36.8	1.6	3.7
GOM8_58	95.4	0.59	0.0417	0.0051	0.0061	0.0006	0.1900	41.5	5.0	39.2	3.8	280	220	39.2	3.8	5.5
GOM8_73	507	1.16	0.0403	0.0023	0.0062	0.0002	0.0276	40.1	2.2	39.8	1.1	100	130	39.8	1.1	0.7
GOM8_122	140	1.10	0.0432	0.0052	0.0063	0.0003	0.0690	42.8	5.1	40.3	1.8	190	260	40.3	1.8	5.8
GOM8_79	71	0.47	0.0470	0.0100	0.0064	0.0006	0.0888	46.0	10.0	41.2	3.9	280	450	41.2	3.9	10.4
GOM8_11	65.5	1.24	0.0473	0.0061	0.0066	0.0005	0.1285	46.8	5.9	42.4	3.0	300	250	42.4	3.0	9.4
GOM8_112	47.4	1.07	0.0506	0.0094	0.0070	0.0006	0.0303	49.8	9.1	45.1	3.5	160	330	45.1	3.5	9.4
GOM8_86	113.5	0.63	0.0512	0.0071	0.0071	0.0004	0.0778	50.5	6.9	45.3	2.2	290	290	45.3	2.2	10.3
GOM8_10	456	21.90	0.0533	0.0028	0.0079	0.0003	0.5790	53.2	2.8	50.4	2.1	139	86	50.4	2.1	5.3
GOM8_49	64.9	1.31	0.0607	0.0060	0.0085	0.0005	0.0678	59.6	5.7	54.3	3.2	360	220	54.3	3.2	8.9
GOM8_89	104.5	0.97	0.0612	0.0092	0.0091	0.0006	0.0596	62.4	9.5	58.2	3.7	130	270	58.2	3.7	6.7
GOM8_62	184	1.32	0.0621	0.0049	0.0092	0.0003	0.0347	61.1	4.7	58.8	1.9	160	160	58.8	1.9	3.8
GOM8_13	648	0.67	0.0605	0.0018	0.0092	0.0002	0.0610	59.6	1.7	59.2	1.2	73	68	59.2	1.2	0.7
GOM8_61	324	4.16	0.0615	0.0053	0.0094	0.0003	0.0432	60.5	5.0	60.1	1.7	60	180	60.1	1.7	0.7
GOM8_55	90	0.84	0.0623	0.0066	0.0096	0.0004	0.1679	61.1	6.2	61.3	2.4	180	230	61.3	2.4	0.3
GOM8_8	140.2	0.69	0.0656	0.0056	0.0103	0.0005	0.1625	64.4	5.3	65.7	3.1	70	170	65.7	3.1	2.0
GOM8_113	170.3	1.09	0.0707	0.0044	0.0105	0.0003	0.1652	69.3	4.2	67.5	1.7	110	120	67.5	1.7	2.6
GOM8_97	201	1.72	0.0780	0.0077	0.0114	0.0006	0.0807	76.1	7.3	72.9	3.7	310	210	72.9	3.7	4.2
GOM8_85	238.4	4.78	0.0794	0.0050	0.0116	0.0003	0.0689	77.5	4.7	74.2	2.1	170	140	74.2	2.1	4.3
GOM8_9	79.3	0.70	0.0800	0.0100	0.0116	0.0006	0.0585	77.6	9.4	74.4	3.8	250	270	74.4	3.8	4.1

GOM8_77	169.3	1.32	0.0924	0.0057	0.0137	0.0004	0.2757	92.2	5.4	88.0	2.4	150	110	88.0	2.4	4.6
GOM8_103	48.1	1.71	0.0942	0.0097	0.0141	0.0013	0.2449	91.3	9.0	90.2	8.1	140	190	90.2	8.1	1.2
GOM8_92	153	1.02	0.0953	0.0050	0.0145	0.0004	0.0685	92.2	4.6	92.7	2.6	110	120	92.7	2.6	0.5
GOM8_115	100.7	1.44	0.1050	0.0110	0.0151	0.0011	0.1000	101.0	10.0	96.5	6.9	190	260	96.5	6.9	4.5
GOM8_23	104.8	1.23	0.1770	0.0210	0.0251	0.0020	0.0685	166.0	18.0	160.0	12.0	350	330	160.0	12.0	3.6
GOM8_42	76	0.47	0.1680	0.0110	0.0252	0.0008	0.3774	157.0	10.0	160.7	5.0	170	140	160.7	5.0	2.4
GOM8_83	38.4	0.35	0.1860	0.0130	0.0264	0.0013	0.3793	173.0	11.0	167.9	7.9	320	150	167.9	7.9	2.9
GOM8_52	63.1	1.19	0.1950	0.0092	0.0275	0.0011	0.1388	180.5	7.8	175.0	6.7	250	130	175.0	6.7	3.0
GOM8_21	88.3	0.63	0.2220	0.0150	0.0309	0.0009	0.2193	203.0	12.0	196.1	5.3	290	120	196.1	5.3	3.4
GOM8_76	177.6	2.09	0.2212	0.0067	0.0317	0.0006	0.0788	202.8	5.6	201.4	3.5	212	80	201.4	3.5	0.7
GOM8_14	128.7	2.12	0.2330	0.0160	0.0331	0.0016	0.0037	212.0	13.0	209.8	9.8	220	160	209.8	9.8	1.0
GOM8_35	142.6	0.82	0.2510	0.0170	0.0352	0.0014	0.2813	231.0	13.0	222.7	8.5	330	150	222.7	8.5	3.6
GOM8_57	194.2	0.70	0.2488	0.0078	0.0358	0.0009	0.5326	225.5	6.4	226.9	5.4	240	64	226.9	5.4	0.6
GOM8_40	710	28.90	0.2515	0.0047	0.0360	0.0006	0.4988	228.3	3.9	228.1	3.7	226	42	228.1	3.7	0.1
GOM8_119	218	0.83	0.2590	0.0110	0.0361	0.0011	0.4767	233.7	8.5	228.8	6.9	242	81	228.8	6.9	2.1
GOM8_48	244	1.46	0.2559	0.0071	0.0363	0.0006	0.0289	231.1	5.7	229.9	3.5	241	63	229.9	3.5	0.5
GOM8_22	856	0.96	0.5000	0.0190	0.0646	0.0022	0.7284	412.0	13.0	403.0	13.0	482	64	403.0	13.0	2.2
GOM8_105	129.2	1.10	0.5230	0.0180	0.0680	0.0009	0.1576	428.2	9.3	423.9	5.5	429	69	423.9	5.5	1.0
GOM8_12	212.5	2.31	1.6800	0.0230	0.1669	0.0020	0.4498	1003.3	8.0	995.0	11.0	1026	24	995.0	11.0	0.8
GOM8_99	36	0.83	1.7880	0.0470	0.1770	0.0028	0.1446	1038.0	17.0	1050.0	15.0	1002	59	1002.0	59.0	4.8
GOM8_121	136.8	2.78	1.7450	0.0350	0.1709	0.0020	0.1463	1024.0	13.0	1017.0	11.0	1013	34	1013.0	34.0	0.4
GOM8_16	92	1.33	1.7570	0.0290	0.1715	0.0023	0.2901	1029.0	11.0	1020.0	13.0	1020	36	1020.0	36.0	0.0
GOM8_80	252.9	2.42	1.7840	0.0230	0.1761	0.0018	0.4823	1038.9	8.5	1046.0	10.0	1031	19	1031.0	19.0	1.5
GOM8_5	17.53	1.03	1.7920	0.0640	0.1748	0.0052	0.0883	1044.0	22.0	1038.0	29.0	1042	94	1042.0	94.0	0.4
GOM8_101	85	1.68	1.8910	0.0350	0.1851	0.0026	0.1054	1077.0	12.0	1095.0	14.0	1044	43	1044.0	43.0	4.9
GOM8_2	310.6	1.69	1.8420	0.0230	0.1780	0.0023	0.6839	1059.9	8.4	1056.0	12.0	1069	19	1069.0	19.0	1.2
GOM8_118	92.4	1.01	1.9340	0.0390	0.1845	0.0027	0.4665	1091.0	13.0	1091.0	15.0	1078	34	1078.0	34.0	1.2
GOM8_72	55	0.85	2.0060	0.0450	0.1894	0.0032	0.3281	1115.0	15.0	1118.0	17.0	1109	40	1109.0	40.0	0.8
GOM8_114	50.7	0.79	1.8590	0.0460	0.1761	0.0034	0.3876	1067.0	16.0	1045.0	19.0	1113	52	1113.0	52.0	6.1
GOM8_63	22.54	1.19	2.0730	0.0710	0.1986	0.0050	0.0715	1146.0	24.0	1167.0	27.0	1131	89	1131.0	89.0	3.2
GOM8_47	99.5	2.13	2.0860	0.0390	0.1927	0.0026	0.3774	1145.0	13.0	1136.0	14.0	1173	35	1173.0	35.0	3.2
GOM8_60	34.6	1.05	2.2270	0.0680	0.2017	0.0040	0.1270	1185.0	21.0	1184.0	22.0	1184	65	1184.0	65.0	0.0
GOM8_82	47.1	1.42	2.2670	0.0470	0.2013	0.0032	0.0406	1200.0	14.0	1182.0	17.0	1207	43	1207.0	43.0	2.1

GOM8_31	40.7	1.16	2.1930	0.0570	0.1973	0.0034	0.0224	1176.0	18.0	1160.0	18.0	1215	60	1215.0	60.0	4.5
GOM8_43	61.6	8.36	2.2490	0.0450	0.2013	0.0027	0.1076	1195.0	14.0	1182.0	15.0	1220	43	1220.0	43.0	3.1
GOM8_122	9.7	0.99	2.5500	0.3000	0.2230	0.0100	0.1613	1281.0	88.0	1296.0	55.0	1230	210	1230.0	210.0	5.4
GOM8_69	15.6	1.32	2.3120	0.0660	0.2052	0.0047	0.2448	1212.0	20.0	1202.0	25.0	1233	66	1233.0	66.0	2.5
GOM8_71	55.6	0.79	2.4140	0.0530	0.2138	0.0045	0.4056	1245.0	16.0	1248.0	24.0	1274	50	1274.0	50.0	2.0
GOM8_32	97.3	1.08	2.6940	0.0420	0.2284	0.0021	0.1148	1327.0	11.0	1326.0	11.0	1341	36	1341.0	36.0	1.1
GOM8_6	16.09	0.56	2.9500	0.1000	0.2418	0.0060	0.3723	1394.0	25.0	1395.0	31.0	1383	69	1383.0	69.0	0.9
GOM8_27	171	1.06	2.8900	0.0230	0.2368	0.0019	0.2779	1379.0	6.1	1369.8	9.9	1394	18	1394.0	18.0	1.7
GOM8_33	204.6	1.22	2.8720	0.0240	0.2348	0.0017	0.3881	1375.0	6.1	1360.6	9.2	1396	16	1396.0	16.0	2.5
GOM8_107	26.9	0.91	2.4380	0.0920	0.1983	0.0043	0.2282	1253.0	26.0	1166.0	23.0	1408	67	1408.0	67.0	17.2
GOM8_67	67.3	1.28	3.1300	0.0470	0.2555	0.0032	0.4472	1442.0	12.0	1468.0	17.0	1421	24	1421.0	24.0	3.3
GOM8_18	59.5	1.02	2.9970	0.0500	0.2429	0.0028	0.2427	1407.0	13.0	1401.0	15.0	1424	35	1424.0	35.0	1.6
GOM8_90	65.9	0.77	3.0090	0.0550	0.2433	0.0038	0.2358	1408.0	14.0	1403.0	20.0	1430	41	1430.0	41.0	1.9
GOM8_66	25.72	0.65	3.1500	0.1400	0.2525	0.0062	0.2971	1441.0	34.0	1451.0	32.0	1432	78	1432.0	78.0	1.3
GOM8_98	154.6	0.62	3.0840	0.0330	0.2490	0.0019	0.2642	1428.1	8.3	1433.0	10.0	1434	22	1434.0	22.0	0.1
GOM8_123	110.1	1.09	3.1340	0.0370	0.2473	0.0026	0.2479	1440.3	9.2	1424.0	13.0	1446	27	1446.0	27.0	1.5
GOM8_29	232	7.90	3.0260	0.0430	0.2432	0.0036	0.6656	1413.0	11.0	1403.0	18.0	1448	22	1448.0	22.0	3.1
GOM8_7	48.63	1.16	3.1270	0.0760	0.2485	0.0034	0.2340	1438.0	19.0	1431.0	18.0	1452	43	1452.0	43.0	1.4
GOM8_106	102.5	0.85	3.1490	0.0400	0.2506	0.0034	0.5719	1443.8	9.9	1441.0	18.0	1454	26	1454.0	26.0	0.9
GOM8_108	677	1.50	2.9700	0.1200	0.2357	0.0093	0.8583	1400.0	30.0	1364.0	48.0	1455	39	1455.0	39.0	6.3
GOM8_117	53.3	1.16	3.2980	0.0900	0.2567	0.0035	0.5485	1472.0	18.0	1473.0	18.0	1455	43	1455.0	43.0	1.2
GOM8_70	46.54	1.01	3.4370	0.0860	0.2692	0.0045	0.2778	1511.0	20.0	1536.0	23.0	1463	45	1463.0	45.0	5.0
GOM8_109	20.5	0.69	3.0990	0.0730	0.2455	0.0051	0.2110	1434.0	18.0	1417.0	27.0	1467	51	1467.0	51.0	3.4
GOM8_37	86.7	0.73	3.1260	0.0740	0.2453	0.0031	0.2775	1436.0	17.0	1416.0	15.0	1487	45	1487.0	45.0	4.8
GOM8_54	49.2	0.71	3.3910	0.0860	0.2625	0.0052	0.2334	1499.0	20.0	1505.0	26.0	1495	45	1495.0	45.0	0.7
GOM8_93	10.63	1.84	3.3900	0.1200	0.2615	0.0070	0.1273	1495.0	29.0	1496.0	36.0	1547	80	1547.0	80.0	3.3
GOM8_51	45.7	4.44	3.5900	0.1200	0.2670	0.0067	0.6805	1544.0	28.0	1524.0	34.0	1581	43	1581.0	43.0	3.6
GOM8_96	107.6	1.21	3.7220	0.0430	0.2742	0.0032	0.2817	1575.3	9.2	1562.0	16.0	1610	27	1610.0	27.0	3.0
GOM8_94	82.6	2.53	3.6000	0.1200	0.2626	0.0075	0.7469	1548.0	26.0	1503.0	38.0	1635	47	1635.0	47.0	8.1
GOM8_104	218	1.58	4.2280	0.0330	0.2972	0.0026	0.7143	1679.1	6.5	1677.0	13.0	1684	14	1684.0	14.0	0.4
GOM8_75	104.2	1.27	4.3190	0.0510	0.3025	0.0034	0.4086	1698.0	10.0	1703.0	17.0	1685	22	1685.0	22.0	1.1
GOM8_88	76.5	1.84	4.3830	0.0640	0.3049	0.0049	0.4631	1709.0	12.0	1715.0	24.0	1689	30	1689.0	30.0	1.5
GOM8_3	257	1.34	4.1220	0.0710	0.2893	0.0036	0.8375	1660.0	14.0	1638.0	18.0	1694	15	1694.0	15.0	3.3

GOM8_74	426.8	1.14	4.0010	0.0470	0.2763	0.0037	0.6853	1634.0	9.6	1572.0	19.0	1711	19	1711.0	19.0	8.1
GOM8_95	246	1.19	4.4320	0.0540	0.3064	0.0033	0.6645	1719.0	10.0	1723.0	16.0	1711	18	1711.0	18.0	0.7
GOM8_45	105	0.90	4.3020	0.0500	0.2983	0.0029	0.4420	1692.9	9.5	1683.0	15.0	1714	21	1714.0	21.0	1.8
GOM8_68	84.2	0.99	4.1940	0.0670	0.2927	0.0046	0.6014	1671.0	13.0	1654.0	23.0	1715	25	1715.0	25.0	3.6
GOM8_65	27.2	0.55	4.2100	0.1100	0.2946	0.0070	0.2352	1673.0	22.0	1664.0	35.0	1722	60	1722.0	60.0	3.4
GOM8_50	177.9	0.40	4.3100	0.0680	0.2984	0.0053	0.6502	1694.0	13.0	1683.0	26.0	1725	25	1725.0	25.0	2.4
GOM8_120	177.3	1.05	4.5420	0.0450	0.3096	0.0032	0.6126	1738.1	8.4	1738.0	16.0	1729	17	1729.0	17.0	0.5
GOM8_25	33.6	2.90	4.2460	0.0700	0.2942	0.0044	0.3302	1685.0	14.0	1662.0	22.0	1740	31	1740.0	31.0	4.5
GOM8_44	28.5	1.25	4.4400	0.1000	0.2992	0.0046	0.2790	1717.0	19.0	1687.0	23.0	1754	42	1754.0	42.0	3.8
GOM8_41	210	2.85	4.5870	0.0420	0.3094	0.0028	0.3885	1746.3	7.6	1737.0	14.0	1762	19	1762.0	19.0	1.4
GOM8_53	126.4	0.92	4.5470	0.0670	0.3070	0.0046	0.6772	1742.0	12.0	1725.0	23.0	1773	24	1773.0	24.0	2.7
GOM8_4	180.3	1.64	5.0430	0.0500	0.3283	0.0038	0.6678	1827.0	8.2	1830.0	18.0	1810	16	1810.0	16.0	1.1
GOM8_20	55.62	2.55	5.1640	0.0820	0.3289	0.0049	0.4849	1848.0	13.0	1832.0	24.0	1873	26	1873.0	26.0	2.2
GOM8_56	129.4	0.79	4.9100	0.2300	0.3080	0.0140	0.3584	1803.0	40.0	1730.0	67.0	1899	96	1899.0	96.0	8.9
GOM8_1	54.4	0.55	5.5570	0.0600	0.3423	0.0041	0.3932	1909.9	9.5	1897.0	20.0	1925	24	1925.0	24.0	1.5
GOM8_116	108.8	0.63	13.4700	0.1700	0.5211	0.0064	0.7114	2712.0	12.0	2707.0	28.0	2709	15	2709.0	15.0	0.1

Sample:GOM9	Isotopic Ratios							Isotopic ages (Ma)								
Analysis	[U] ppm	U/Th	207/235	2σ err.	206/238	2σ err.	RHO	207/235	2σ err.	206/238	2σ err.	207/206	2σ err.	Best age	2σ err.	% Dis.
GOM9_114	178.4	1.04	0.0269	0.0013	0.0041	0.0001	0.0930	26.9	1.3	26.6	0.7	311	63	26.6	0.7	1.3
GOM9_53	313	0.48	0.0277	0.0016	0.0043	0.0001	-0.0701	27.7	1.6	27.7	0.8	210	120	27.7	0.8	0.1
GOM9_78	170.2	1.16	0.0297	0.0015	0.0044	0.0001	0.2086	29.7	1.4	28.5	0.8	335	59	28.5	0.8	4.2
GOM9_43	1016	0.69	0.0384	0.0013	0.0060	0.0001	0.2219	38.2	1.3	38.6	0.8	60	20	38.6	0.8	0.9
GOM9_94	191.7	0.89	0.0403	0.0016	0.0062	0.0002	0.1640	40.1	1.5	39.7	1.0	264	53	39.7	1.0	1.0
GOM9_34	628	1.16	0.0421	0.0012	0.0063	0.0001	0.1234	41.9	1.2	40.6	0.5	151	34	40.6	0.5	3.2
GOM9_57	145	0.61	0.0465	0.0021	0.0072	0.0002	0.0587	46.1	2.1	46.4	1.0	339	73	46.4	1.0	0.7
GOM9_11	463	1.00	0.0469	0.0013	0.0075	0.0001	-0.0281	46.5	1.2	48.3	0.9	112	32	48.3	0.9	3.9
GOM9_1	540.1	0.82	0.0478	0.0016	0.0076	0.0001	0.3559	47.4	1.5	48.9	0.5	49	26	48.9	0.5	3.2
GOM9_36	107	0.69	0.0498	0.0041	0.0077	0.0003	0.0224	49.3	4.0	49.2	1.8	244	68	49.2	1.8	0.2
GOM9_39	210	0.79	0.0501	0.0018	0.0077	0.0002	0.2452	49.6	1.7	49.4	1.1	156	37	49.4	1.1	0.4
GOM9_120	92.5	0.98	0.0806	0.0035	0.0116	0.0002	0.1765	78.6	3.3	74.5	1.4	317	47	74.5	1.4	5.2

GOM9_12	81.6	3.04	0.0746	0.0037	0.0117	0.0002	-0.0986	72.9	3.5	74.8	1.4	251	49	74.8	1.4	2.6
GOM9_62	493	1.61	0.0802	0.0019	0.0122	0.0001	0.1795	78.3	1.8	77.9	0.9	126	24	77.9	0.9	0.5
GOM9_93	200.9	1.46	0.0844	0.0065	0.0128	0.0003	-0.0947	82.2	6.1	82.2	2.0	86	42	82.2	2.0	0.0
GOM9_86	238	1.64	0.0902	0.0030	0.0135	0.0003	0.0138	87.6	2.8	86.5	1.6	157	43	86.5	1.6	1.3
GOM9_23	685	0.97	0.1067	0.0048	0.0146	0.0003	0.3077	102.9	4.4	93.6	1.8	334	54	93.6	1.8	9.0
GOM9_82	148	0.85	0.1539	0.0056	0.0227	0.0004	0.3616	145.2	4.9	144.7	2.4	197	39	144.7	2.4	0.3
GOM9_67	266	0.89	0.1526	0.0028	0.0229	0.0003	0.1679	144.2	2.4	146.2	1.8	154	21	146.2	1.8	1.4
GOM9_72	279.8	0.43	0.1695	0.0033	0.0248	0.0004	0.5224	158.9	2.8	158.0	2.4	159	22	158.0	2.4	0.6
GOM9_50	178.8	0.39	0.1730	0.0046	0.0249	0.0003	0.4107	162.5	4.1	158.2	2.1	195	29	158.2	2.1	2.6
GOM9_131	250	1.12	0.1805	0.0036	0.0252	0.0004	-0.1089	168.4	3.1	160.3	2.4	269	41	160.3	2.4	4.8
GOM9_85	269.9	0.44	0.1783	0.0027	0.0253	0.0003	-0.0553	166.5	2.4	161.1	1.8	258	22	161.1	1.8	3.2
GOM9_64	210.8	0.97	0.1763	0.0043	0.0256	0.0005	0.5050	164.8	3.7	162.7	2.8	193	21	162.7	2.8	1.3
GOM9_29	250	0.61	0.1894	0.0084	0.0262	0.0004	0.4711	176.0	7.1	166.8	2.7	309	71	166.8	2.7	5.2
GOM9_118	324	1.23	0.1874	0.0038	0.0274	0.0004	0.3694	174.4	3.2	174.4	2.4	195	24	174.4	2.4	0.0
GOM9_27	172	2.91	0.2185	0.0080	0.0314	0.0011	0.4464	200.6	6.7	199.4	7.0	228	41	199.4	7.0	0.6
GOM9_14	159	2.26	0.2460	0.0048	0.0337	0.0004	0.3157	223.2	3.9	213.5	2.5	321	29	213.5	2.5	4.3
GOM9_2	230.8	0.70	0.2510	0.0047	0.0351	0.0006	-0.0288	227.3	3.8	222.6	3.5	278	38	222.6	3.5	2.1
GOM9_5	194.6	0.93	0.2488	0.0036	0.0361	0.0003	0.0721	225.5	2.9	228.4	2.0	206	21	228.4	2.0	1.3
GOM9_32	84.8	1.31	0.4750	0.0100	0.0625	0.0007	-0.0888	394.7	7.1	390.9	4.1	424	32	390.9	4.1	1.0
GOM9_97	705	4.40	0.5650	0.0110	0.0670	0.0011	0.2950	454.8	7.2	418.3	6.4	632	17	418.3	6.4	8.0
GOM9_109	338	1.29	0.7750	0.0100	0.0932	0.0011	0.3458	582.8	5.8	574.4	6.3	621	19	574.4	6.3	1.4
GOM9_106	57.7	1.25	1.0070	0.0250	0.1137	0.0024	-0.0510	706.0	13.0	694.0	14.0	747	24	694.0	14.0	1.7
GOM9_126	91.8	1.78	1.2230	0.0610	0.1306	0.0046	0.8859	811.0	28.0	791.0	26.0	929	38	791.0	26.0	2.5
GOM9_58	31.3	0.63	1.4460	0.0870	0.1459	0.0062	0.6806	906.0	36.0	877.0	35.0	954	50	877.0	35.0	3.2
GOM9_107	96.1	1.24	1.6230	0.0170	0.1599	0.0015	0.4867	979.5	6.5	956.3	8.1	1028	14	956.3	8.1	2.4
GOM9_84	79.8	1.43	1.7110	0.0220	0.1673	0.0017	0.4735	1012.2	8.3	997.3	9.4	1051	18	997.3	9.4	1.5
GOM9_31	31.7	1.74	1.8370	0.0670	0.1746	0.0037	0.5058	1057.0	24.0	1037.0	20.0	1109	22	1109.0	22.0	6.5
GOM9_92	177	3.50	1.8140	0.0340	0.1717	0.0025	0.8554	1050.0	12.0	1022.0	14.0	1129	18	1129.0	18.0	9.5
GOM9_61	40.4	0.73	2.0600	0.0270	0.1926	0.0021	0.7099	1136.2	9.5	1135.0	11.0	1136	20	1136.0	20.0	0.1
GOM9_26	93.4	0.89	2.0720	0.0280	0.1919	0.0016	0.0165	1141.1	8.8	1131.4	8.8	1159	19	1159.0	19.0	2.4
GOM9_52	210.2	1.60	2.1040	0.0200	0.1910	0.0017	0.7956	1149.6	6.7	1126.9	9.4	1203	7	1203.4	7.2	6.4
GOM9_69	83.3	1.64	2.4950	0.0510	0.2158	0.0030	0.8394	1272.0	15.0	1260.0	16.0	1271	19	1271.0	19.0	0.9
GOM9_25	27.1	1.85	2.5420	0.0480	0.2179	0.0024	0.2366	1285.0	14.0	1271.0	12.0	1329	21	1329.0	21.0	4.4

GOM9_63	70.6	1.08	2.6870	0.0250	0.2263	0.0020	0.4283	1324.4	6.8	1315.0	10.0	1337	9	1337.3	8.8	1.7
GOM9_3	139	1.65	2.6820	0.0250	0.2255	0.0015	0.4901	1323.2	6.8	1311.0	8.1	1345	10	1345.0	10.0	2.5
GOM9_66	175.2	0.95	2.8730	0.0220	0.2336	0.0020	0.5893	1374.5	5.7	1353.0	10.0	1406	9	1406.0	8.8	3.8
GOM9_104	54.3	1.61	2.6900	0.0440	0.2202	0.0029	0.3808	1325.0	12.0	1283.0	15.0	1407	14	1407.0	14.0	8.8
GOM9_40	35.8	1.38	3.1110	0.0350	0.2534	0.0023	0.2005	1435.9	8.9	1456.0	12.0	1416	17	1416.0	17.0	2.8
GOM9_59	171	1.65	2.9480	0.0250	0.2385	0.0019	0.7428	1393.9	6.5	1378.6	9.7	1422	9	1421.5	8.8	3.0
GOM9_102	56.7	0.63	2.9680	0.0330	0.2402	0.0025	0.5408	1398.8	8.4	1387.0	13.0	1425	10	1425.0	10.0	2.7
GOM9_98	122.1	1.13	2.9720	0.0280	0.2388	0.0025	0.6921	1400.1	7.1	1382.0	13.0	1430	9	1429.9	9.3	3.3
GOM9_90	120.3	1.34	2.9170	0.0220	0.2341	0.0014	0.6687	1386.0	5.7	1355.7	7.2	1432	7	1431.5	6.5	5.3
GOM9_89	64.1	1.11	2.9470	0.0360	0.2367	0.0026	0.4962	1393.3	9.4	1369.0	13.0	1432	13	1432.0	13.0	4.4
GOM9_132	94.4	1.50	2.9300	0.0310	0.2361	0.0022	0.5976	1389.0	8.1	1366.0	11.0	1432	9	1432.3	9.3	4.6
GOM9_88	102.3	0.97	3.1110	0.0210	0.2492	0.0019	0.5274	1435.9	5.0	1434.2	9.6	1438	7	1438.1	7.0	0.3
GOM9_24	252.5	2.50	3.0980	0.0220	0.2466	0.0017	0.6827	1432.0	5.5	1420.6	8.6	1451	7	1450.5	6.8	2.1
GOM9_7	117.9	0.96	3.1000	0.0250	0.2470	0.0017	0.4413	1432.2	6.1	1422.8	8.9	1453	9	1452.6	9.0	2.1
GOM9_4	97.8	1.07	3.0130	0.0270	0.2415	0.0024	0.6814	1411.7	6.5	1394.0	12.0	1453	12	1453.0	12.0	4.1
GOM9_33	98	1.39	3.2250	0.0260	0.2567	0.0021	0.3605	1462.8	6.2	1473.0	11.0	1455	9	1455.1	9.1	1.2
GOM9_75	161.6	0.93	2.8940	0.0290	0.2269	0.0025	0.2166	1380.2	7.6	1318.0	13.0	1460	15	1460.0	15.0	9.7
GOM9_105	55	0.61	3.0600	0.0290	0.2433	0.0019	0.4952	1422.2	7.3	1404.0	10.0	1460	13	1460.0	13.0	3.8
GOM9_42	262	1.89	3.1300	0.0180	0.2465	0.0013	0.4904	1440.0	4.4	1420.3	6.6	1470	6	1469.8	6.3	3.4
GOM9_113	95.7	1.35	3.3080	0.0300	0.2503	0.0027	0.4757	1482.4	7.2	1440.0	14.0	1536	11	1536.0	11.0	6.3
GOM9_13	65	1.74	3.2600	0.1400	0.2479	0.0043	0.4696	1468.0	33.0	1428.0	22.0	1543	62	1543.0	62.0	7.5
GOM9_112	139.2	2.73	3.6200	0.1800	0.2630	0.0110	0.9323	1552.0	39.0	1504.0	57.0	1627	16	1627.0	16.0	7.6
GOM9_49	126	2.46	3.7100	0.1200	0.2647	0.0093	0.7741	1581.0	22.0	1513.0	47.0	1646	38	1646.0	38.0	8.1
GOM9_74	48	2.75	4.0870	0.0480	0.2902	0.0027	0.3736	1651.2	9.6	1642.0	13.0	1646	16	1646.0	16.0	0.2
GOM9_17	279	2.47	3.9450	0.0890	0.2826	0.0039	0.8650	1621.0	19.0	1604.0	20.0	1651	25	1651.0	25.0	2.8
GOM9_9	345	4.27	4.1290	0.0220	0.2947	0.0020	0.6337	1660.0	4.4	1665.0	10.0	1658	5	1657.8	5.1	0.4
GOM9_16	222.4	1.54	4.0280	0.0320	0.2862	0.0022	0.8424	1639.5	6.4	1622.0	11.0	1661	5	1660.7	5.4	2.3
GOM9_20	34.77	1.02	3.7570	0.0540	0.2678	0.0031	0.3929	1583.0	12.0	1530.0	16.0	1670	23	1670.0	23.0	8.4
GOM9_110	140	1.40	4.1580	0.0410	0.2948	0.0032	0.3715	1665.1	8.1	1665.0	16.0	1674	15	1674.0	15.0	0.5
GOM9_8	250.1	1.61	3.9060	0.0520	0.2767	0.0040	0.8581	1615.0	11.0	1575.0	20.0	1675	8	1675.0	8.0	6.0
GOM9_21	164	1.19	4.3070	0.0280	0.3043	0.0022	0.6441	1694.4	5.3	1712.0	11.0	1677	7	1676.8	6.8	2.1
GOM9_22	330	154.00	3.5590	0.0390	0.2513	0.0028	0.7874	1540.1	8.6	1445.0	14.0	1677	6	1676.9	6.3	13.8
GOM9_76	46.1	0.65	3.8860	0.0480	0.2735	0.0035	0.4841	1612.0	9.5	1561.0	17.0	1678	14	1678.0	14.0	7.0

GOM9_116	70.5	0.67	3.9500	0.0520	0.2779	0.0035	0.4479	1624.0	11.0	1580.0	18.0	1679	16	1679.0	16.0	5.9
GOM9_127	105.3	0.91	4.0100	0.0400	0.2822	0.0031	0.6640	1635.6	8.1	1602.0	15.0	1681	8	1681.3	7.5	4.7
GOM9_122	149.3	1.57	3.9690	0.0520	0.2787	0.0037	0.5766	1627.0	11.0	1585.0	18.0	1682	16	1682.0	16.0	5.8
GOM9_65	50.3	0.64	4.1030	0.0410	0.2884	0.0032	0.3902	1655.4	8.0	1633.0	16.0	1683	13	1683.0	13.0	3.0
GOM9_46	155	1.17	4.0600	0.0280	0.2850	0.0019	0.6644	1646.9	5.4	1616.4	9.4	1684	7	1683.7	6.7	4.0
GOM9_45	91.6	0.89	3.9300	0.0350	0.2759	0.0029	0.6912	1620.4	7.4	1570.0	15.0	1685	7	1684.7	7.1	6.8
GOM9_68	92.1	1.08	4.0250	0.0430	0.2826	0.0034	0.7389	1638.5	8.8	1606.0	17.0	1685	9	1685.1	8.5	4.7
GOM9_28	140.6	4.50	4.2690	0.0440	0.2977	0.0034	0.6800	1686.8	8.5	1679.0	17.0	1696	10	1696.0	10.0	1.0
GOM9_99	161.3	1.64	4.1590	0.0330	0.2909	0.0022	0.6862	1667.3	6.8	1646.0	11.0	1696	7	1696.3	7.0	3.0
GOM9_119	76.9	1.74	4.1170	0.0300	0.2887	0.0026	0.6256	1657.3	6.0	1635.0	13.0	1697	9	1697.3	9.1	3.7
GOM9_130	299	5.80	4.2510	0.0390	0.2958	0.0024	0.9235	1683.4	7.6	1670.0	12.0	1699	8	1698.6	7.9	1.7
GOM9_124	202.5	1.29	4.1000	0.0430	0.2837	0.0029	0.6685	1654.1	8.6	1610.0	15.0	1704	9	1704.1	8.6	5.5
GOM9_48	574	4.39	4.3800	0.0300	0.3039	0.0029	0.8536	1709.2	5.8	1710.0	14.0	1705	7	1704.9	6.5	0.3
GOM9_71	162	1.15	4.1350	0.0580	0.2867	0.0044	0.7617	1660.0	12.0	1624.0	22.0	1712	13	1712.0	13.0	5.1
GOM9_44	214.6	0.62	4.0760	0.0360	0.2801	0.0028	0.5515	1649.4	7.3	1595.0	13.0	1716	8	1716.2	8.3	7.1
GOM9_37	535	1.95	4.2190	0.0320	0.2921	0.0022	0.7029	1678.1	6.0	1652.0	11.0	1718	6	1717.7	6.2	3.8
GOM9_54	39.7	0.68	4.1770	0.0410	0.2865	0.0025	0.2888	1670.0	7.8	1624.0	13.0	1723	15	1723.0	15.0	5.7
GOM9_95	682	11.60	4.2630	0.0700	0.2952	0.0096	0.9737	1686.0	13.0	1667.0	47.0	1725	16	1725.0	16.0	3.4
GOM9_15	78.2	1.12	4.2510	0.0490	0.2920	0.0029	0.4736	1683.1	9.4	1651.0	14.0	1729	12	1729.0	12.0	4.5
GOM9_77	86.2	1.41	4.3030	0.0440	0.2933	0.0035	0.6064	1695.0	8.1	1658.0	17.0	1730	11	1730.0	11.0	4.2
GOM9_101	97.6	2.25	4.2200	0.0520	0.2888	0.0037	0.5458	1677.0	10.0	1635.0	19.0	1732	12	1732.0	12.0	5.6
GOM9_87	223	2.66	4.3810	0.0450	0.3005	0.0032	0.6535	1708.4	8.5	1694.0	16.0	1734	8	1733.6	7.5	2.3
GOM9_83	348	1.59	4.4190	0.0310	0.3011	0.0024	0.8289	1717.1	5.8	1696.0	12.0	1734	4	1733.8	4.4	2.2
GOM9_123	306	4.42	4.2700	0.1300	0.2910	0.0130	0.7772	1686.0	24.0	1646.0	63.0	1734	23	1734.0	23.0	5.1
GOM9_35	217	0.84	3.5720	0.0730	0.2421	0.0050	0.9176	1542.0	16.0	1397.0	26.0	1735	11	1735.0	11.0	19.5
GOM9_70	270	2.73	4.3280	0.0260	0.2952	0.0014	0.5890	1698.4	4.9	1667.6	6.9	1737	6	1737.3	5.9	4.0
GOM9_10	229	2.39	4.6810	0.0590	0.3182	0.0035	0.7903	1763.0	11.0	1781.0	17.0	1742	10	1741.5	9.7	2.3
GOM9_115	225	1.03	4.3770	0.0430	0.2967	0.0034	0.6573	1707.5	8.1	1675.0	17.0	1759	9	1758.9	8.9	4.8
GOM9_125	102	1.93	4.2970	0.0810	0.2877	0.0037	0.3802	1692.0	15.0	1630.0	19.0	1763	29	1763.0	29.0	7.5
GOM9_30	217.3	1.58	4.6690	0.0530	0.3142	0.0035	0.9089	1761.1	9.5	1761.0	17.0	1764	5	1763.5	4.5	0.1
GOM9_108	146	2.11	4.4950	0.0370	0.3034	0.0036	0.5251	1729.7	6.8	1708.0	18.0	1767	10	1767.0	10.0	3.3
GOM9_96	279	2.08	4.3000	0.1700	0.2990	0.0140	0.7005	1690.0	33.0	1687.0	68.0	1768	26	1768.0	26.0	4.6
GOM9_111	66.3	1.66	4.1930	0.0600	0.2742	0.0040	0.6062	1672.0	12.0	1562.0	20.0	1834	11	1834.0	11.0	14.8

GOM9_121	329	3.37	4.6350	0.0450	0.2972	0.0034	0.8338	1755.4	8.0	1677.0	17.0	1854	8	1853.6	7.5	9.5
GOM9_79	191.4	2.45	5.0690	0.0360	0.3054	0.0023	0.6470	1831.5	6.1	1718.0	11.0	1957	6	1957.2	6.0	12.2
GOM9_117	118	1.98	5.9260	0.0640	0.3404	0.0041	0.7646	1966.7	8.8	1888.0	20.0	2050	7	2049.9	6.9	7.9
GOM9_91	43.78	1.28	6.5170	0.0930	0.3616	0.0048	0.6927	2047.0	13.0	1989.0	23.0	2112	11	2112.0	11.0	5.8
GOM9_55	119.4	2.21	9.1220	0.0950	0.4069	0.0034	0.6704	2349.7	9.5	2200.0	16.0	2484	11	2484.0	11.0	11.4
GOM9_80	127.3	1.21	11.3200	0.2700	0.4560	0.0130	0.7377	2549.0	22.0	2421.0	55.0	2645	16	2645.0	16.0	8.5

Sample:GOM10	Isotopic Ratios							Isotopic ages (Ma)								
Analysis	[U] ppm	U/Th	207/235	2σ err.	206/238	2σ err.	RHO	207/235	2σ err.	206/238	2σ err.	207/206	2σ err.	Best age	2σ err.	% Dis.
GOM10_48	494	0.96	0.0276	0.0010	0.0042	0.0001	-0.0105	27.6	0.9	27.0	0.4	215	47	27.0	0.4	2.0
GOM10_21	140.5	0.96	0.0386	0.0022	0.0057	0.0002	0.0326	38.4	2.1	36.4	1.2	288	61	36.4	1.2	5.2
GOM10_118	2590	1.59	0.0373	0.0005	0.0059	0.0001	0.3699	37.2	0.5	37.9	0.4	49	13	37.9	0.4	1.8
GOM10_18	598	1.29	0.0396	0.0010	0.0060	0.0001	0.0264	39.4	1.0	38.9	0.6	187	35	38.9	0.6	1.3
GOM10_8	245	0.87	0.0402	0.0012	0.0062	0.0001	0.0123	40.0	1.2	40.1	0.6	176	31	40.1	0.6	0.3
GOM10_28	178	2.32	0.0416	0.0017	0.0063	0.0001	-0.0479	41.3	1.6	40.5	0.6	206	43	40.5	0.6	1.9
GOM10_45	182	1.12	0.0469	0.0024	0.0065	0.0002	-0.0300	46.5	2.3	41.9	0.9	273	60	41.9	0.9	9.8
GOM10_62	497	0.82	0.0442	0.0014	0.0066	0.0001	0.0891	43.9	1.4	42.2	0.8	163	31	42.2	0.8	3.9
GOM10_86	164	1.14	0.0467	0.0020	0.0070	0.0001	-0.0344	46.3	2.0	45.0	0.8	279	48	45.0	0.8	2.8
GOM10_119	545	1.09	0.0476	0.0011	0.0072	0.0001	0.1845	47.2	1.0	46.4	0.7	140	30	46.4	0.7	1.7
GOM10_19	353	1.81	0.0645	0.0042	0.0096	0.0003	0.2654	63.4	4.0	61.4	1.6	220	100	61.4	1.6	3.2
GOM10_116	91	0.96	0.0720	0.0038	0.0111	0.0003	0.0584	70.5	3.6	71.4	1.7	254	49	71.4	1.7	1.3
GOM10_37	94.1	0.73	0.0803	0.0055	0.0113	0.0005	0.0576	78.3	5.1	72.2	2.9	296	82	72.2	2.9	7.8
GOM10_99	103.5	0.56	0.0757	0.0032	0.0115	0.0002	0.2061	74.0	3.1	73.5	1.5	243	49	73.5	1.5	0.7
GOM10_84	338.5	1.78	0.0791	0.0022	0.0122	0.0002	-0.0191	77.3	2.0	78.3	1.2	88	25	78.3	1.2	1.3
GOM10_34	284	0.90	0.0790	0.0022	0.0124	0.0002	0.2837	77.2	2.1	79.6	1.4	87	27	79.6	1.4	3.1
GOM10_107	214.5	1.10	0.0828	0.0023	0.0125	0.0002	0.3383	80.7	2.2	80.2	1.4	130	30	80.2	1.4	0.6
GOM10_117	312	1.45	0.0842	0.0045	0.0128	0.0006	0.9039	83.0	4.6	81.8	4.1	157	34	81.8	4.1	1.4
GOM10_60	1460	4.79	0.0961	0.0012	0.0144	0.0002	0.1872	93.2	1.1	91.8	1.0	146	14	91.8	1.0	1.5
GOM10_113	201	1.30	0.0943	0.0031	0.0144	0.0003	-0.0702	91.4	2.9	92.4	1.8	176	39	92.4	1.8	1.1
GOM10_111	489	0.89	0.0996	0.0023	0.0150	0.0003	-0.0819	96.4	2.1	95.9	1.6	145	29	95.9	1.6	0.5
GOM10_78	103	2.14	0.1621	0.0056	0.0246	0.0005	0.1728	152.4	4.9	156.9	2.9	160	35	156.9	2.9	3.0

GOM10_105	539	0.81	0.1757	0.0022	0.0258	0.0002	0.2931	164.3	1.9	164.1	1.4	176	18	164.1	1.4	0.1
GOM10_3	204.7	0.79	0.1762	0.0044	0.0259	0.0004	0.2539	165.5	3.6	164.5	2.6	173	27	164.5	2.6	0.6
GOM10_13	85.9	0.46	0.1779	0.0082	0.0261	0.0004	0.3129	166.1	7.0	166.2	2.4	173	60	166.2	2.4	0.1
GOM10_89	63.8	0.25	0.1794	0.0087	0.0262	0.0008	0.1397	167.3	7.5	166.4	4.9	215	51	166.4	4.9	0.5
GOM10_88	217.1	1.44	0.1825	0.0061	0.0262	0.0003	0.2084	170.1	5.3	166.7	1.9	222	39	166.7	1.9	2.0
GOM10_91	159.5	0.41	0.1842	0.0045	0.0267	0.0004	0.2349	171.6	3.9	169.8	2.4	226	26	169.8	2.4	1.0
GOM10_30	137.4	0.53	0.2080	0.0120	0.0296	0.0012	0.2798	192.0	10.0	188.3	7.2	250	79	188.3	7.2	1.9
GOM10_61	266	1.60	0.2229	0.0032	0.0321	0.0003	0.3640	204.2	2.7	203.5	1.9	195	21	203.5	1.9	0.3
GOM10_58	452	1.86	0.5800	0.0240	0.0727	0.0010	0.5767	464.0	15.0	452.2	6.2	526	87	452.2	6.2	2.5
GOM10_73	332	0.18	0.6115	0.0062	0.0759	0.0007	0.3637	484.4	3.9	471.5	4.3	546	13	471.5	4.3	2.7
GOM10_1	284.8	1.91	1.6692	0.0095	0.1655	0.0008	0.4801	996.8	3.6	987.0	4.2	1020	6	987.0	4.2	1.0
GOM10_6	517	3.35	1.7180	0.0140	0.1695	0.0014	0.8104	1014.9	5.2	1009.3	7.6	1029	6	1028.7	6.2	1.9
GOM10_4	121.6	1.19	1.8880	0.0160	0.1823	0.0012	0.3877	1076.7	5.6	1079.2	6.7	1081	10	1081.0	10.0	0.2
GOM10_59	61.6	0.80	1.9260	0.0200	0.1823	0.0014	0.2463	1089.5	7.1	1079.6	7.8	1088	15	1088.0	15.0	0.8
GOM10_22	28.2	2.08	2.0250	0.0360	0.1891	0.0019	0.4296	1126.0	12.0	1116.0	10.0	1144	18	1144.0	18.0	2.4
GOM10_81	289	2.65	2.1660	0.0150	0.1969	0.0012	0.6485	1170.1	4.8	1158.6	6.7	1175	8	1175.3	7.9	1.4
GOM10_75	164	1.21	2.1080	0.0180	0.1911	0.0013	0.5204	1151.2	6.0	1127.3	6.9	1190	8	1189.9	8.4	5.3
GOM9_1_121	73.4	0.64	2.3190	0.0270	0.2085	0.0019	0.5479	1217.5	8.2	1220.5	9.9	1224	11	1224.0	11.0	0.3
GOM10_93	43.1	0.80	2.2250	0.0440	0.1973	0.0036	0.0961	1188.0	14.0	1160.0	19.0	1275	27	1275.0	27.0	9.0
GOM10_96	26.1	0.35	2.4830	0.0340	0.2122	0.0023	0.4022	1266.0	10.0	1240.0	12.0	1332	13	1332.0	13.0	6.9
GOM10_76	253.8	0.93	2.8770	0.0170	0.2331	0.0020	0.5551	1375.7	4.4	1351.0	10.0	1400	8	1399.7	7.8	3.5
GOM10_7	112.1	0.94	2.9100	0.0170	0.2372	0.0016	0.3133	1385.7	4.5	1371.9	8.3	1406	9	1405.6	8.9	2.4
GOM10_82	134.5	1.88	2.9490	0.0200	0.2388	0.0017	0.4456	1394.4	5.2	1380.5	8.6	1413	8	1412.5	8.0	2.3
GOM10_14	100.8	1.79	2.9840	0.0220	0.2417	0.0015	0.3317	1403.3	5.7	1395.2	7.7	1416	8	1416.3	8.2	1.5
GOM10_20	97.3	1.97	3.1200	0.0270	0.2519	0.0026	0.5241	1437.4	6.8	1448.0	13.0	1419	12	1419.0	12.0	2.0
GOM10_41	48	0.86	3.0500	0.0470	0.2456	0.0035	0.5584	1419.0	12.0	1417.0	18.0	1425	15	1425.0	15.0	0.6
GOM9_1_123	253	1.36	2.9310	0.0180	0.2367	0.0017	0.5598	1389.6	4.6	1369.3	9.0	1428	9	1427.8	8.8	4.1
GOM10_74	610	2.14	3.0030	0.0910	0.2403	0.0079	0.9698	1407.0	23.0	1387.0	41.0	1428	11	1428.0	11.0	2.9
GOM10_50	250	1.78	2.9950	0.0190	0.2393	0.0015	0.5908	1406.9	4.9	1383.2	7.8	1433	5	1433.2	5.4	3.5
GOM10_35	128.5	1.69	3.0930	0.0210	0.2461	0.0016	0.5058	1430.7	5.2	1418.3	8.1	1441	7	1440.8	7.4	1.6
GOM10_2	89	0.98	3.0120	0.0210	0.2411	0.0020	0.6448	1411.1	5.5	1392.0	11.0	1443	8	1442.6	8.0	3.5
GOM10_92	122	1.27	2.9330	0.0250	0.2347	0.0021	0.6505	1390.9	6.5	1359.0	11.0	1444	9	1444.1	8.5	5.9
GOM9_1_126	35.4	0.68	2.9730	0.0350	0.2390	0.0028	0.4404	1400.1	8.8	1381.0	15.0	1450	13	1450.0	13.0	4.8

GOM10_109	348	1.65	3.0060	0.0230	0.2392	0.0020	0.6870	1409.9	6.0	1382.0	10.0	1450	8	1450.3	7.6	4.7
GOM10_94	185	1.10	3.0880	0.0250	0.2451	0.0018	0.5128	1429.4	6.2	1413.0	9.4	1451	7	1450.6	7.2	2.6
GOM10_25	139	1.44	3.1850	0.0250	0.2517	0.0018	0.5664	1453.2	6.0	1447.1	9.2	1458	6	1457.7	6.3	0.7
GOM10_9	323	1.83	3.1320	0.0460	0.2481	0.0042	0.9256	1440.0	12.0	1428.0	22.0	1460	7	1460.0	7.1	2.2
GOM10_53	396.5	1.68	3.1580	0.0130	0.2464	0.0014	0.5168	1446.8	3.2	1419.8	7.5	1474	6	1474.3	6.2	3.7
GOM10_51	33.2	0.42	2.9990	0.0310	0.2341	0.0026	0.3828	1406.8	7.8	1358.0	14.0	1477	13	1477.0	13.0	8.1
GOM9_1_124	56.1	0.55	3.3820	0.0330	0.2612	0.0020	0.4243	1500.7	7.8	1496.0	10.0	1513	10	1513.0	10.0	1.1
GOM10_67	127	1.10	3.8690	0.0270	0.2778	0.0023	0.5374	1608.5	5.8	1580.0	11.0	1634	7	1633.8	7.1	3.3
GOM10_102	110	1.29	4.1140	0.0360	0.2951	0.0021	0.6896	1656.6	7.1	1667.0	11.0	1646	7	1646.0	7.4	1.3
GOM10_26	143	1.22	3.9450	0.0240	0.2826	0.0017	0.6538	1622.6	5.0	1604.1	8.5	1649	5	1649.0	5.1	2.7
GOM10_56	187	9.00	4.2890	0.0950	0.3017	0.0048	0.9652	1688.0	19.0	1699.0	24.0	1665	16	1665.0	16.0	2.0
GOM10_98	31.1	0.66	4.0400	0.0440	0.2870	0.0027	0.3128	1641.6	8.9	1626.0	14.0	1667	11	1667.0	11.0	2.5
GOM10_44	91.3	1.06	4.1500	0.0490	0.2929	0.0038	0.6374	1663.8	9.6	1656.0	19.0	1673	11	1673.0	11.0	1.0
GOM10_97	134.4	1.15	3.9390	0.0520	0.2765	0.0039	0.6867	1621.0	11.0	1574.0	20.0	1675	13	1675.0	13.0	6.0
GOM10_120	151	1.63	4.2080	0.0300	0.2970	0.0026	0.6665	1675.3	5.9	1676.0	13.0	1676	6	1676.3	6.2	0.0
GOM10_40	155	1.55	4.0970	0.0260	0.2886	0.0017	0.6731	1653.4	5.2	1634.4	8.7	1677	5	1676.7	4.6	2.5
GOM10_11	141	2.24	4.0090	0.0270	0.2801	0.0019	0.6975	1636.5	5.5	1591.7	9.6	1686	6	1686.2	6.0	5.6
GOM10_87	110.3	1.36	4.4060	0.0340	0.3054	0.0028	0.5715	1713.2	6.4	1718.0	14.0	1690	10	1689.5	9.9	1.7
GOM10_15	332	1.56	4.0070	0.0270	0.2803	0.0019	0.7440	1636.8	5.7	1592.9	9.6	1690	6	1689.6	5.7	5.7
GOM10_42	179.8	2.21	4.0700	0.0380	0.2828	0.0023	0.6181	1648.0	7.7	1607.0	11.0	1690	9	1690.0	9.0	4.9
GOM10_70	363.8	2.33	3.9000	0.0540	0.2710	0.0037	0.8120	1613.0	11.0	1546.0	19.0	1691	9	1690.6	9.1	8.6
GOM10_33	162	2.31	4.0690	0.0250	0.2838	0.0016	0.6079	1647.9	5.0	1611.5	8.2	1691	6	1691.3	5.8	4.7
GOM10_95	267	1.73	4.2770	0.0480	0.3003	0.0032	0.9091	1688.2	9.5	1692.0	16.0	1692	6	1692.4	6.3	0.0
GOM10_85	161	9.50	3.8000	0.2600	0.2660	0.0140	0.9880	1592.0	63.0	1537.0	62.0	1694	47	1694.0	47.0	9.3
GOM9_1_127	208.5	1.22	4.0960	0.0820	0.2899	0.0046	0.8871	1652.0	17.0	1641.0	23.0	1700	11	1700.0	11.0	3.5
GOM10_38	94	0.84	4.3690	0.0270	0.3035	0.0016	0.3872	1706.9	5.2	1708.5	8.1	1702	8	1701.8	7.9	0.4
GOM10_115	193.5	4.21	4.0820	0.0260	0.2858	0.0019	0.6935	1651.9	5.4	1620.2	9.6	1703	7	1703.0	6.6	4.9
GOM10_80	192	1.69	4.2400	0.0260	0.2926	0.0017	0.6057	1682.3	4.9	1654.2	8.5	1704	6	1703.8	5.9	2.9
GOM10_55	201	1.28	4.0900	0.0420	0.2834	0.0040	0.8611	1652.0	8.4	1608.0	20.0	1708	8	1708.0	7.9	5.9
GOM10_31	72.7	0.75	4.1670	0.0380	0.2881	0.0025	0.6006	1667.1	7.4	1632.0	12.0	1709	7	1708.7	7.1	4.5
GOM10_46	277.1	1.35	4.0080	0.0660	0.2767	0.0052	0.7858	1635.0	14.0	1575.0	26.0	1710	20	1710.0	20.0	7.9
GOM9_1_122	83.2	1.14	4.3290	0.0310	0.2998	0.0023	0.4947	1698.6	5.9	1690.0	11.0	1715	8	1715.4	7.7	1.5
GOM10_24	184	1.19	4.1740	0.0280	0.2887	0.0020	0.5481	1669.3	5.7	1634.8	9.8	1716	7	1715.5	6.8	4.7

GOM10_101	353	0.96	4.4800	0.0460	0.3082	0.0032	0.9445	1726.5	8.7	1732.0	16.0	1726	6	1725.7	5.7	0.4
GOM10_36	329	0.97	4.0150	0.0590	0.2740	0.0033	0.0291	1637.0	12.0	1561.0	17.0	1731	29	1731.0	29.0	9.8
GOM10_83	284	1.13	4.0370	0.0290	0.2757	0.0029	0.6271	1641.5	5.8	1570.0	14.0	1731	9	1731.2	8.6	9.3
GOM10_100	101	1.00	4.5290	0.0340	0.3091	0.0026	0.4915	1736.8	6.4	1736.0	13.0	1733	9	1732.7	8.5	0.2
GOM9_1_128	990	2.17	4.2670	0.0500	0.2922	0.0038	0.8453	1686.5	9.6	1652.0	19.0	1738	6	1738.3	5.9	5.0
GOM10_114	64.7	4.79	4.6940	0.0380	0.3143	0.0026	0.5499	1765.8	6.8	1761.0	13.0	1781	9	1780.8	8.9	1.1
GOM10_65	590.4	10.83	4.5290	0.0850	0.2971	0.0072	0.8349	1736.0	16.0	1677.0	36.0	1799	10	1799.0	10.0	6.8
GOM10_66	120.4	1.16	4.8880	0.0350	0.3137	0.0020	0.3279	1800.0	6.1	1759.0	9.9	1841	8	1841.2	8.2	4.5
GOM10_57	256.1	2.11	5.1130	0.0360	0.2940	0.0018	0.6870	1838.1	5.9	1661.2	9.0	2033	6	2032.8	5.8	18.3
GOM10_112	225	1.60	6.3140	0.0340	0.3646	0.0024	0.6079	2020.1	4.7	2004.0	11.0	2045	4	2044.9	4.1	2.0
GOM10_103	99.2	0.87	6.9030	0.0380	0.3856	0.0025	0.6436	2098.9	4.8	2102.0	11.0	2094	5	2094.4	4.7	0.4
GOM10_23	1300	11.76	10.6500	0.1200	0.4515	0.0070	0.8359	2495.1	9.5	2401.0	31.0	2569	10	2569.4	9.7	6.6

Sample:GOM11	Isotopic Ratios							Isotopic ages (Ma)								
Analysis	[U] ppm	U/Th	207/235	2σ err.	206/238	2σ err.	RHO	207/235	2σ err.	206/238	2σ err.	207/206	2σ err.	Best age	2σ err.	% Dis.
GOM11_21	91.4	1.08	0.0262	0.0031	0.0038	0.0002	-0.1408	26.2	3.1	24.1	1.1	500	130	24.1	1.1	8.0
GOM11_39	448	0.59	0.0300	0.0011	0.0043	0.0001	-0.2393	30.0	1.1	27.4	0.5	276	39	27.4	0.5	8.6
GOM11_101	68.5	0.62	0.0298	0.0045	0.0043	0.0003	0.0773	29.7	4.4	27.8	1.8	550	160	27.8	1.8	6.4
GOM11_41	229.7	1.29	0.0294	0.0012	0.0044	0.0001	0.0508	29.4	1.2	28.4	0.5	247	56	28.4	0.5	3.6
GOM11_32	189.7	0.83	0.0315	0.0017	0.0044	0.0001	-0.0255	31.5	1.7	28.4	0.7	369	80	28.4	0.7	10.0
GOM11_88	272	0.61	0.0333	0.0023	0.0051	0.0001	0.2724	33.2	2.3	32.6	0.7	214	60	32.6	0.7	2.0
GOM11_2	96.7	0.66	0.0358	0.0021	0.0051	0.0002	0.1213	35.7	2.0	32.6	1.0	371	59	32.6	1.0	8.7
GOM11_116	93.9	0.81	0.0342	0.0018	0.0051	0.0001	-0.0004	34.1	1.7	32.9	0.8	421	95	32.9	0.8	3.6
GOM11_105	294.4	0.88	0.0359	0.0041	0.0052	0.0001	0.1128	35.8	4.0	33.2	0.9	710	260	33.2	0.9	7.3
GOM11_34	34.6	0.38	0.0371	0.0041	0.0052	0.0003	-0.1693	36.9	4.1	33.2	1.7	611	95	33.2	1.7	10.0
GOM11_96	686	0.75	0.0353	0.0019	0.0053	0.0002	0.3494	35.2	1.9	34.0	1.2	216	65	34.0	1.2	3.4
GOM11_15	109.9	0.53	0.0389	0.0025	0.0054	0.0001	-0.0906	38.7	2.5	34.9	0.8	510	110	34.9	0.8	9.9
GOM11_47	72.4	1.04	0.0407	0.0073	0.0056	0.0003	0.1835	40.4	7.1	36.3	2.1	340	140	36.3	2.1	10.1
GOM11_109	162	0.89	0.0392	0.0022	0.0058	0.0002	-0.0101	39.0	2.1	37.5	1.0	268	67	37.5	1.0	3.9
GOM11_14	155	1.14	0.0393	0.0016	0.0061	0.0002	0.1681	39.1	1.6	39.1	0.9	189	38	39.1	0.9	0.0
GOM11_29	249	3.22	0.0454	0.0046	0.0063	0.0002	0.4297	44.9	4.2	40.5	1.1	520	150	40.5	1.1	9.8

GOM11_123	116	0.68	0.0427	0.0032	0.0065	0.0002	0.0461	42.4	3.1	42.0	1.1	290	96	42.0	1.1	0.9
GOM11_16	71.2	1.68	0.0446	0.0028	0.0067	0.0002	-0.0236	44.2	2.7	43.0	1.3	430	100	43.0	1.3	2.7
GOM11_127	400	3.84	0.0450	0.0014	0.0067	0.0001	0.1229	44.6	1.4	43.1	0.7	177	41	43.1	0.7	3.5
GOM11_75	566	3.05	0.0489	0.0015	0.0073	0.0001	-0.0306	48.4	1.5	47.1	0.6	193	43	47.1	0.6	2.7
GOM11_72	98.4	1.09	0.0538	0.0034	0.0077	0.0002	0.0327	53.1	3.3	49.3	1.1	402	68	49.3	1.1	7.2
GOM11_84	154	0.83	0.0513	0.0032	0.0079	0.0002	0.1337	50.8	3.1	50.9	1.4	276	66	50.9	1.4	0.2
GOM11_121	300	1.93	0.0548	0.0012	0.0084	0.0001	0.0689	54.1	1.2	53.7	0.8	154	38	53.7	0.8	0.7
GOM11_36	160.1	1.40	0.0579	0.0033	0.0092	0.0002	0.1619	57.1	3.2	58.9	1.1	123	35	58.9	1.1	3.2
GOM11_63	557	0.69	0.0614	0.0014	0.0093	0.0001	0.4120	60.5	1.4	59.7	0.8	130	24	59.7	0.8	1.3
GOM11_120	88.1	1.00	0.0644	0.0033	0.0096	0.0003	0.3061	63.3	3.1	61.8	1.7	239	54	61.8	1.7	2.4
GOM11_23	49.6	0.71	0.0743	0.0070	0.0106	0.0003	-0.0104	72.6	6.6	67.9	1.8	342	92	67.9	1.8	6.5
GOM11_98	186	0.48	0.0828	0.0033	0.0125	0.0003	-0.2028	80.8	3.1	79.8	2.1	254	71	79.8	2.1	1.2
GOM11_1	167.9	1.74	0.1024	0.0027	0.0155	0.0003	-0.1671	98.9	2.5	98.8	1.7	172	33	98.8	1.7	0.1
GOM11_67	830	1.42	0.1613	0.0049	0.0241	0.0005	0.6256	152.9	4.7	153.4	3.4	147	27	153.4	3.4	0.3
GOM11_92	51.8	0.31	0.1797	0.0072	0.0259	0.0006	-0.0498	167.5	6.1	164.7	3.5	242	52	164.7	3.5	1.7
GOM11_50	191.1	1.26	0.1786	0.0049	0.0260	0.0004	0.4113	166.8	4.3	165.7	2.8	177	31	165.7	2.8	0.7
GOM11_111	381	0.96	0.1860	0.0067	0.0275	0.0006	-0.1331	173.1	5.7	174.6	3.9	198	71	174.6	3.9	0.9
GOM11_99	50.17	0.51	0.1900	0.0110	0.0276	0.0005	-0.0407	176.2	9.1	175.7	3.2	244	54	175.7	3.2	0.3
GOM11_80	274	0.83	0.1941	0.0038	0.0282	0.0003	0.3059	180.0	3.2	179.5	2.0	191	26	179.5	2.0	0.3
GOM11_71	106.7	1.16	0.2136	0.0069	0.0307	0.0006	0.0807	197.6	6.0	195.0	3.4	253	50	195.0	3.4	1.3
GOM11_53	123.2	0.99	0.2411	0.0063	0.0342	0.0003	0.2775	219.2	5.1	216.8	2.1	268	28	216.8	2.1	1.1
GOM11_69	155.3	0.99	0.2512	0.0058	0.0344	0.0006	0.4174	227.4	4.7	218.2	3.4	348	23	218.2	3.4	4.0
GOM11_106	437	3.74	0.2647	0.0035	0.0373	0.0003	0.0628	238.4	2.8	236.1	2.0	265	18	236.1	2.0	1.0
GOM11_91	156.5	1.72	0.2704	0.0051	0.0386	0.0004	0.1504	242.9	4.0	244.0	2.4	241	28	244.0	2.4	0.5
GOM11_95	88.1	2.09	0.5474	0.0081	0.0706	0.0008	0.1310	443.0	5.3	439.5	4.9	459	22	439.5	4.9	0.8
GOM11_33	126	1.33	0.6050	0.0110	0.0759	0.0012	0.2969	480.5	6.9	471.8	6.9	504	23	471.8	6.9	1.8
GOM11_56	212.4	0.89	0.6454	0.0056	0.0818	0.0008	0.2626	505.6	3.5	506.6	4.6	492	16	506.6	4.6	0.2
GOM11_52	104	46.00	1.6520	0.0180	0.1628	0.0016	0.6032	989.7	6.9	972.4	8.9	1037	14	972.4	8.9	1.7
GOM11_104	29.04	0.66	1.6060	0.0270	0.1634	0.0017	0.1599	972.0	11.0	975.5	9.4	970	23	975.5	9.4	0.4
GOM11_42	88.2	1.70	1.8180	0.0220	0.1768	0.0014	0.2200	1051.2	8.1	1049.2	7.4	1053	16	1053.0	16.0	0.4
GOM11_48	76.4	0.50	1.7680	0.0200	0.1693	0.0014	0.0823	1033.2	7.5	1008.0	7.5	1070	15	1070.0	15.0	5.8
GOM11_61	104.3	1.04	1.9240	0.0200	0.1839	0.0015	0.4926	1089.0	7.0	1089.1	8.3	1091	10	1091.0	10.0	0.2
GOM11_45	25.76	2.05	1.8520	0.0610	0.1761	0.0031	0.5850	1063.0	22.0	1045.0	17.0	1107	26	1107.0	26.0	5.6

GOM11_110	233	1.81	2.1850	0.0140	0.2010	0.0012	0.2891	1177.0	4.6	1180.9	6.4	1165	7	1164.5	7.1	1.4
GOM11_126	47.7	1.06	2.0930	0.0300	0.1910	0.0019	0.0791	1145.7	9.6	1127.0	10.0	1170	15	1170.0	15.0	3.7
GOM11_20	19.22	0.82	2.2910	0.0490	0.2052	0.0041	-0.2434	1209.0	15.0	1203.0	22.0	1198	36	1198.0	36.0	0.4
GOM11_78	244	0.93	2.2190	0.0150	0.2016	0.0012	0.6547	1186.9	4.7	1183.9	6.4	1199	7	1199.2	7.4	1.3
GOM11_46	21.18	1.13	2.1240	0.0530	0.1890	0.0032	0.2099	1155.0	17.0	1116.0	17.0	1216	30	1216.0	30.0	8.2
GOM11_103	11.53	0.95	2.3220	0.0530	0.2092	0.0026	0.0596	1217.0	16.0	1225.0	14.0	1243	37	1243.0	37.0	1.4
GOM11_102	214	1.71	2.5250	0.0250	0.2233	0.0018	0.5843	1278.9	7.3	1298.9	9.4	1268	7	1267.5	7.2	2.5
GOM11_118	106	1.51	2.7250	0.0220	0.2296	0.0018	0.3597	1334.9	6.1	1332.1	9.5	1336	11	1336.0	11.0	0.3
GOM11_49	71	0.55	2.7560	0.0300	0.2255	0.0022	0.0071	1343.0	8.1	1312.0	11.0	1379	13	1379.0	13.0	4.9
GOM11_22	104	0.86	2.9410	0.0230	0.2381	0.0017	0.6722	1392.2	6.0	1376.8	8.7	1405	7	1404.7	7.4	2.0
GOM11_55	46.8	0.56	2.9380	0.0360	0.2376	0.0023	0.3936	1390.9	9.3	1374.0	12.0	1408	13	1408.0	13.0	2.4
GOM11_30	109.6	1.83	2.8020	0.0320	0.2283	0.0018	0.0432	1355.5	8.4	1325.7	9.3	1417	18	1417.0	18.0	6.4
GOM11_122	101.5	0.69	2.9180	0.0200	0.2361	0.0018	0.5654	1386.4	5.0	1367.6	9.6	1417	9	1417.2	8.7	3.5
GOM11_107	122	0.78	2.9170	0.0220	0.2367	0.0015	0.4465	1385.9	5.7	1369.4	7.8	1418	8	1418.4	8.4	3.5
GOM11_17	79.7	0.99	3.1070	0.0280	0.2512	0.0019	0.6612	1434.1	6.9	1444.7	9.7	1420	9	1420.2	9.0	1.7
GOM11_38	57.2	0.90	3.1310	0.0290	0.2512	0.0026	0.2718	1440.0	7.0	1445.0	13.0	1421	13	1421.0	13.0	1.7
GOM11_124	294	2.22	3.1030	0.0300	0.2494	0.0026	0.7533	1432.9	7.5	1435.0	13.0	1423	7	1423.1	7.1	0.8
GOM11_62	166.3	1.81	2.9020	0.0230	0.2332	0.0020	0.5727	1382.1	5.9	1351.0	10.0	1427	6	1426.9	6.4	5.3
GOM11_112	50.7	1.75	3.1380	0.0360	0.2526	0.0025	0.3696	1441.4	8.9	1452.0	13.0	1428	14	1428.0	14.0	1.7
GOM11_125	70.1	1.04	3.2230	0.0270	0.2561	0.0018	0.3903	1462.3	6.5	1469.9	9.5	1433	11	1433.0	11.0	2.6
GOM11_24	125	1.34	3.1060	0.0220	0.2478	0.0015	0.5504	1433.8	5.3	1428.1	7.7	1435	7	1435.0	6.7	0.5
GOM11_65	68.4	1.10	3.1050	0.0290	0.2480	0.0019	0.5158	1433.6	7.1	1428.0	10.0	1439	8	1438.6	7.7	0.7
GOM11_60	103.6	1.31	2.9960	0.0230	0.2399	0.0020	0.3872	1406.3	5.9	1386.0	10.0	1439	12	1439.0	12.0	3.7
GOM11_6	147.6	0.84	2.9990	0.0250	0.2407	0.0019	0.5883	1407.0	6.3	1390.0	10.0	1440	10	1440.0	10.0	3.5
GOM11_97	12.74	0.13	3.1300	0.0790	0.2475	0.0033	0.0263	1438.0	20.0	1426.0	17.0	1447	27	1447.0	27.0	1.5
GOM11_51	114.1	0.79	3.0710	0.0200	0.2456	0.0014	0.4587	1425.2	5.0	1416.7	7.2	1451	7	1450.6	6.9	2.3
GOM11_94	137.6	1.38	3.1750	0.0270	0.2488	0.0030	0.5773	1452.4	6.6	1434.0	15.0	1483	14	1483.0	14.0	3.3
GOM11_85	9.72	0.51	3.4440	0.0910	0.2662	0.0049	0.0640	1512.0	20.0	1521.0	25.0	1487	29	1487.0	29.0	2.3
GOM11_90	167.3	1.29	3.3000	0.0290	0.2555	0.0019	0.8112	1480.7	6.8	1467.0	10.0	1498	6	1498.1	6.3	2.1
GOM11_79	21.4	0.58	3.5690	0.0920	0.2732	0.0045	0.4734	1541.0	20.0	1557.0	23.0	1516	34	1516.0	34.0	2.7
GOM11_108	133	0.95	3.3450	0.0380	0.2568	0.0020	0.4243	1490.8	8.9	1473.0	10.0	1525	17	1525.0	17.0	3.4
GOM11_54	68.1	1.63	4.1140	0.0450	0.2919	0.0026	0.8394	1654.6	9.5	1651.0	13.0	1660	9	1659.5	9.3	0.5
GOM11_57	83.1	1.32	4.0160	0.0350	0.2835	0.0027	0.6892	1637.0	7.0	1609.0	14.0	1675	7	1675.1	7.4	3.9

GOM11_9	16.13	0.88	3.8930	0.0820	0.2748	0.0044	0.4399	1614.0	16.0	1565.0	22.0	1678	16	1678.0	16.0	6.7
GOM11_117	219.2	2.87	3.7190	0.0290	0.2666	0.0021	0.7146	1575.2	6.3	1523.0	11.0	1686	6	1685.8	6.2	9.7
GOM11_76	174	0.92	4.2310	0.0310	0.2978	0.0017	0.3054	1679.8	5.9	1680.1	8.6	1690	8	1690.3	8.0	0.6
GOM11_18	72	0.77	4.1070	0.0340	0.2875	0.0024	0.4233	1655.2	6.8	1629.0	12.0	1693	7	1693.1	7.2	3.8
GOM11_10	155.2	1.59	4.3220	0.0240	0.2980	0.0015	0.5786	1697.4	4.6	1681.1	7.7	1717	6	1717.1	6.2	2.1
GOM11_74	131.3	0.81	4.4750	0.0250	0.3103	0.0016	0.2187	1726.1	4.6	1742.0	7.8	1718	7	1718.3	6.7	1.4
GOM11_40	274	2.14	4.3280	0.0280	0.2979	0.0023	0.6781	1698.5	5.2	1681.0	11.0	1720	5	1720.4	4.8	2.3
GOM11_27	132.1	0.89	4.2210	0.0230	0.2892	0.0022	0.4372	1678.0	4.6	1639.0	11.0	1721	8	1721.3	7.8	4.8
GOM11_12	513	2.26	4.1970	0.0390	0.2892	0.0027	0.7834	1674.8	7.7	1637.0	14.0	1725	7	1724.6	7.4	5.1
GOM11_28	184	1.31	4.4150	0.0380	0.3008	0.0029	0.7554	1714.9	7.1	1695.0	14.0	1728	5	1728.0	5.4	1.9
GOM11_68	84.7	0.77	4.2400	0.1100	0.2951	0.0058	0.7377	1684.0	23.0	1666.0	29.0	1729	25	1729.0	25.0	3.6
GOM11_66	150.6	0.60	4.4940	0.0450	0.3073	0.0024	0.5249	1729.3	8.2	1727.0	12.0	1741	13	1741.0	13.0	0.8
GOM11_119	152	2.49	4.8490	0.0260	0.3264	0.0023	0.5518	1793.3	4.6	1822.0	11.0	1749	6	1748.6	6.4	4.2
GOM11_3	202	1.61	4.4510	0.0330	0.3039	0.0022	0.8182	1721.6	6.2	1712.0	11.0	1753	7	1753.4	7.3	2.4
GOM11_35	207.6	2.56	4.7710	0.0270	0.3160	0.0020	0.6298	1779.6	4.8	1770.0	10.0	1802	6	1801.5	6.0	1.7
GOM11_73	61.7	0.49	11.7400	0.3800	0.4630	0.0140	0.9338	2581.0	31.0	2452.0	62.0	2674	13	2674.0	13.0	8.3
GOM11_8	75.1	1.38	13.3540	0.0890	0.5191	0.0034	0.6656	2705.4	6.4	2695.0	15.0	2712	5	2711.5	5.2	0.6
GOM11_113	40.6	0.58	14.0300	0.1200	0.5329	0.0043	0.6931	2751.0	8.3	2753.0	18.0	2738	7	2737.9	7.1	0.6
GOM11_7	251.1	1.88	16.0500	0.1100	0.5469	0.0040	0.8730	2879.7	6.6	2812.0	17.0	2923	3	2923.4	3.2	3.8

Sample:GOM12	Isotopic Ratios							Isotopic ages (Ma)								
Analysis	[U] ppm	U/Th	207/235	2σ err.	206/238	2σ err.	RHO	207/235	2σ err.	206/238	2σ err.	207/206	2σ err.	Best age	2σ err.	% Dis.
GOM12_98	352.1	1.53	0.0321	0.0013	0.0048	0.0001	0.0575	32.0	1.3	30.7	0.7	224	50	30.7	0.7	3.9
GOM12_14	217	0.59	0.0336	0.0017	0.0052	0.0001	0.0274	33.6	1.7	33.5	0.7	163	46	33.5	0.7	0.3
GOM12_67	117.3	0.57	0.0372	0.0024	0.0053	0.0002	0.2374	37.0	2.4	34.1	1.4	266	57	34.1	1.4	7.8
GOM12_10	189.1	0.78	0.0352	0.0011	0.0054	0.0001	0.2983	35.1	1.1	35.0	0.6	180	30	35.0	0.6	0.2
GOM12_41	103.4	0.48	0.0391	0.0029	0.0056	0.0001	-0.0205	38.9	2.8	36.2	0.8	500	120	36.2	0.8	7.0
GOM12_107	135	0.55	0.0364	0.0017	0.0057	0.0001	0.1828	36.3	1.6	36.6	0.8	216	48	36.6	0.8	0.8
GOM12_60	172	0.75	0.0384	0.0016	0.0061	0.0001	-0.0720	38.3	1.5	39.0	0.8	285	58	39.0	0.8	1.8
GOM12_16	254.4	1.10	0.0392	0.0020	0.0061	0.0002	0.1893	39.0	2.0	39.3	1.2	191	43	39.3	1.2	0.8
GOM12_80	374	0.50	0.0411	0.0010	0.0063	0.0001	0.1426	40.8	0.9	40.7	0.6	158	39	40.7	0.6	0.5

GOM12_119	38.6	1.06	0.0419	0.0041	0.0066	0.0003	-0.1857	41.5	4.0	42.3	1.6	680	130	42.3	1.6	1.9
GOM12_120	90.7	1.31	0.0500	0.0027	0.0072	0.0002	0.2542	49.4	2.6	46.0	1.2	302	43	46.0	1.2	6.9
GOM12_76	401.7	1.07	0.0461	0.0014	0.0072	0.0001	-0.3277	45.8	1.4	46.1	0.7	129	32	46.1	0.7	0.7
GOM12_32	64.5	0.88	0.0481	0.0041	0.0072	0.0003	-0.1840	47.6	4.0	46.5	2.0	405	77	46.5	2.0	2.3
GOM12_92	939	1.13	0.0696	0.0013	0.0106	0.0001	0.0799	68.3	1.2	68.1	0.7	103	22	68.1	0.7	0.3
GOM12_82	126.6	1.43	0.0741	0.0028	0.0116	0.0002	-0.0452	72.5	2.6	74.5	1.5	202	66	74.5	1.5	2.8
GOM12_84	66.5	0.95	0.0762	0.0040	0.0118	0.0003	0.1389	74.5	3.8	75.6	2.0	204	68	75.6	2.0	1.5
GOM12_94	399	1.48	0.0806	0.0024	0.0119	0.0004	0.0968	78.7	2.3	76.3	2.3	146	55	76.3	2.3	3.0
GOM12_89	170.2	2.64	0.0797	0.0037	0.0121	0.0002	0.1681	77.8	3.5	77.6	1.4	168	40	77.6	1.4	0.3
GOM12_111	357	0.76	0.0813	0.0014	0.0121	0.0001	0.0663	79.3	1.3	77.8	0.9	172	24	77.8	0.9	1.9
GOM12_34	202	0.72	0.0806	0.0040	0.0122	0.0004	0.6534	78.7	3.7	77.9	2.4	199	32	77.9	2.4	1.0
GOM12_46	296	1.10	0.0961	0.0024	0.0144	0.0003	0.7036	93.1	2.3	92.1	1.6	157	26	92.1	1.6	1.1
GOM12_102	736	1.09	0.1017	0.0017	0.0151	0.0002	0.1816	98.3	1.6	96.7	1.0	156	25	96.7	1.0	1.6
GOM12_79	1010.7	0.71	0.1027	0.0015	0.0152	0.0001	0.0008	99.2	1.4	97.3	0.8	147	25	97.3	0.8	1.9
GOM12_5	300.2	1.05	0.1034	0.0026	0.0152	0.0002	0.2850	99.9	2.3	97.4	1.4	166	35	97.4	1.4	2.5
GOM12_47	418	1.54	0.1163	0.0017	0.0171	0.0002	0.3499	111.7	1.5	109.1	1.1	181	18	109.1	1.1	2.3
GOM12_12	57.9	1.42	0.1262	0.0045	0.0182	0.0003	0.1883	120.6	4.1	116.0	1.9	270	50	116.0	1.9	3.8
GOM12_69	16.4	2.09	0.1470	0.0110	0.0207	0.0008	-0.0414	138.0	10.0	132.0	4.8	516	83	132.0	4.8	4.3
GOM12_17	266	0.94	0.1468	0.0028	0.0220	0.0002	0.0737	139.0	2.4	140.3	1.4	149	23	140.3	1.4	0.9
GOM12_115	65.4	0.41	0.1518	0.0071	0.0227	0.0007	-0.0704	143.4	6.2	144.8	4.2	246	70	144.8	4.2	1.0
GOM12_61	126.6	0.50	0.1572	0.0061	0.0234	0.0005	0.0822	148.2	5.3	149.2	2.9	143	35	149.2	2.9	0.7
GOM12_113	69.3	0.37	0.1621	0.0070	0.0242	0.0006	0.0152	152.4	6.2	154.4	3.6	222	48	154.4	3.6	1.3
GOM12_38	860	1.07	0.1745	0.0029	0.0256	0.0003	0.5956	163.3	2.5	162.9	1.9	178	19	162.9	1.9	0.2
GOM12_88	397	0.74	0.1799	0.0039	0.0259	0.0004	0.4840	167.9	3.4	164.8	2.5	199	28	164.8	2.5	1.8
GOM12_40	90.9	0.77	0.1748	0.0056	0.0259	0.0003	0.2206	163.4	4.8	165.5	2.1	169	36	165.5	2.1	1.3
GOM12_117	295.5	0.42	0.1789	0.0026	0.0262	0.0002	0.2568	167.1	2.3	166.7	1.2	173	19	166.7	1.2	0.2
GOM12_23	274	0.57	0.1791	0.0023	0.0263	0.0002	0.3218	167.3	2.0	167.0	1.4	163	16	167.0	1.4	0.2
GOM12_18	154	0.78	0.1877	0.0048	0.0270	0.0005	-0.0424	174.6	4.1	171.9	3.2	203	39	171.9	3.2	1.5
GOM12_72	516	1.10	0.1940	0.0017	0.0286	0.0002	0.2641	180.0	1.5	181.8	1.4	161	12	181.8	1.4	1.0
GOM12_63	410	1.33	0.2018	0.0040	0.0295	0.0005	0.0561	186.7	3.4	187.1	2.9	195	25	187.1	2.9	0.2
GOM12_20	159.3	1.98	0.2010	0.0035	0.0295	0.0002	0.1331	185.9	3.0	187.4	1.5	182	24	187.4	1.5	0.8
GOM12_54	325.1	1.07	0.2068	0.0042	0.0296	0.0003	0.5261	190.9	3.6	188.3	1.6	230	25	188.3	1.6	1.4
GOM12_45	119.1	1.03	0.2068	0.0061	0.0297	0.0005	0.3140	190.7	5.1	188.5	3.1	270	37	188.5	3.1	1.2

GOM12_44	171.5	1.43	0.2073	0.0039	0.0303	0.0003	0.2154	191.2	3.3	192.1	2.2	195	20	192.1	2.2	0.5
GOM12_1	168	1.72	0.2095	0.0075	0.0304	0.0006	-0.1832	193.1	6.3	193.0	3.9	211	65	193.0	3.9	0.1
GOM12_2	448	2.73	0.2920	0.0026	0.0405	0.0003	0.3461	260.4	2.1	256.2	1.9	287	11	256.2	1.9	1.6
GOM12_116	209	1.72	0.4373	0.0047	0.0583	0.0005	0.1343	368.7	3.4	365.3	2.9	376	18	365.3	2.9	0.9
GOM12_108	966	3.40	0.4641	0.0059	0.0609	0.0007	0.7954	387.6	4.0	380.9	4.2	419	10	380.9	4.2	1.7
GOM12_71	201.1	0.73	0.5092	0.0061	0.0666	0.0005	0.2625	417.7	4.1	415.4	3.1	442	15	415.4	3.1	0.6
GOM12_33	320	5.50	0.6300	0.0140	0.0789	0.0011	0.5225	495.1	8.6	489.6	6.4	508	16	489.6	6.4	1.1
GOM12_85	49.2	0.68	0.6410	0.0100	0.0812	0.0010	0.1790	502.6	6.2	503.0	6.1	523	23	503.0	6.1	0.1
GOM12_110	221	0.88	0.8236	0.0067	0.0993	0.0007	0.3631	610.4	3.8	610.4	4.3	612	10	610.4	4.3	0.0
GOM12_31	144.5	1.88	1.5900	0.0140	0.1579	0.0011	0.5607	966.0	5.6	945.0	6.2	1006	8	945.0	6.2	2.2
GOM12_105	269	0.60	1.9230	0.0520	0.1635	0.0060	0.8928	1088.0	18.0	976.0	34.0	1268	24	976.0	34.0	10.3
GOM12_77	148	2.48	1.7170	0.0250	0.1687	0.0017	0.4301	1014.7	9.2	1004.9	9.5	1032	13	1032.0	13.0	2.6
GOM12_43	167.8	1.69	1.8260	0.0140	0.1776	0.0013	0.4564	1054.5	4.8	1054.0	7.2	1067	10	1066.9	9.5	1.2
GOM12_25	157	0.94	1.8880	0.0140	0.1793	0.0012	0.4376	1076.5	4.8	1063.9	6.7	1096	9	1095.9	9.0	2.9
GOM12_103	88	0.63	1.8520	0.0150	0.1758	0.0011	0.3403	1064.1	5.3	1044.2	6.2	1104	12	1104.0	12.0	5.4
GOM12_50	12.92	0.51	1.9440	0.0630	0.1831	0.0043	0.2417	1101.0	23.0	1083.0	23.0	1126	39	1126.0	39.0	3.8
GOM12_112	115.2	1.14	1.8450	0.0380	0.1730	0.0029	0.7494	1064.0	13.0	1028.0	16.0	1126	17	1126.0	17.0	8.7
GOM12_29	37.7	0.74	2.1540	0.0230	0.1956	0.0017	0.3312	1165.8	7.5	1151.6	9.0	1174	14	1174.0	14.0	1.9
GOM12_62	55	1.07	2.2380	0.0570	0.2030	0.0046	0.8566	1192.0	18.0	1191.0	25.0	1186	14	1186.0	14.0	0.4
GOM12_74	109.2	0.78	2.1940	0.0250	0.1936	0.0019	0.6317	1181.7	8.0	1140.0	10.0	1241	9	1241.4	9.2	8.2
GOM12_22	12.87	0.99	2.2750	0.0490	0.2027	0.0024	0.1926	1202.0	15.0	1189.0	13.0	1254	30	1254.0	30.0	5.2
GOM12_65	75	0.82	2.9140	0.0320	0.2387	0.0019	0.7248	1384.8	8.4	1379.6	9.8	1395	10	1395.0	10.0	1.1
GOM12_78	73.2	1.05	2.9030	0.0230	0.2377	0.0018	0.5628	1383.2	5.7	1374.4	9.4	1398	8	1398.0	8.3	1.7
GOM12_37	75.4	1.07	2.7940	0.0360	0.2284	0.0027	0.7747	1353.1	9.7	1326.0	14.0	1403	9	1402.9	8.9	5.5
GOM12_53	860	2.16	2.8690	0.0130	0.2323	0.0011	0.6126	1374.0	3.4	1346.3	5.8	1422	5	1422.3	5.2	5.3
GOM12_36	137.3	1.27	2.9860	0.0170	0.2407	0.0013	0.3099	1404.0	4.4	1390.1	6.8	1424	8	1423.9	7.7	2.4
GOM12_101	104	1.64	3.1210	0.0210	0.2521	0.0016	0.4882	1437.6	5.2	1449.1	8.3	1424	8	1424.1	8.4	1.8
GOM12_114	194	1.70	2.9560	0.0210	0.2385	0.0015	0.7502	1396.1	5.3	1379.0	7.9	1426	6	1425.8	5.5	3.3
GOM12_118	147	1.09	3.1250	0.0230	0.2502	0.0017	0.6421	1438.5	5.7	1439.4	8.8	1430	8	1429.5	8.4	0.7
GOM12_57	58.9	2.23	3.0090	0.0230	0.2405	0.0021	0.2381	1409.8	5.7	1389.0	11.0	1430	12	1430.0	12.0	2.9
GOM12_97	41.2	0.87	3.1470	0.0370	0.2524	0.0028	0.4888	1443.8	9.0	1451.0	14.0	1431	13	1431.0	13.0	1.4
GOM12_73	77.4	0.71	3.0590	0.0220	0.2447	0.0017	0.4185	1422.8	5.5	1411.2	8.9	1432	8	1432.4	7.8	1.5
GOM12_66	72.8	1.03	2.9960	0.0280	0.2416	0.0020	0.5270	1407.0	7.0	1395.0	10.0	1436	11	1436.0	11.0	2.9

GOM12_48	80.3	0.63	2.9930	0.0300	0.2404	0.0016	0.3951	1405.5	7.5	1388.9	8.1	1436	9	1436.2	9.0	3.3
GOM12_83	156.9	1.18	3.0460	0.0180	0.2444	0.0016	0.6441	1419.1	4.4	1409.6	8.5	1441	6	1440.5	5.9	2.1
GOM12_58	158	1.00	3.1590	0.0220	0.2522	0.0015	0.4769	1446.8	5.3	1449.5	7.9	1444	7	1443.9	7.4	0.4
GOM12_21	88.1	0.96	3.1130	0.0230	0.2465	0.0023	0.4595	1435.7	5.8	1420.0	12.0	1454	11	1454.0	11.0	2.3
GOM12_30	173.5	1.75	3.1010	0.0260	0.2458	0.0019	0.5573	1432.4	6.5	1416.9	9.9	1462	8	1461.6	8.0	3.1
GOM12_7	535	3.44	3.4190	0.0190	0.2644	0.0017	0.8002	1509.2	4.3	1512.4	8.8	1515	5	1514.7	5.1	0.2
GOM12_16	437	2.30	2.9080	0.0930	0.2192	0.0059	0.9491	1383.0	24.0	1277.0	31.0	1537	13	1537.0	13.0	16.9
GOM12_24	218	3.30	3.9400	0.1000	0.2862	0.0050	0.9186	1619.0	21.0	1621.0	25.0	1614	18	1614.0	18.0	0.4
GOM12_6	147	2.78	4.0660	0.0740	0.2908	0.0034	0.8513	1645.0	15.0	1645.0	17.0	1629	22	1629.0	22.0	1.0
GOM12_109	113	1.06	3.8990	0.0360	0.2802	0.0021	0.4686	1615.2	7.1	1592.0	11.0	1643	9	1643.4	9.0	3.1
GOM12_35	854	19.50	3.2940	0.0410	0.2328	0.0022	0.8864	1478.9	9.7	1349.0	12.0	1648	8	1648.0	8.2	18.1
GOM12_99	168	1.03	4.0720	0.0250	0.2891	0.0014	0.4298	1648.5	5.0	1637.2	7.0	1661	7	1660.9	7.1	1.4
GOM12_39	28.1	0.53	4.0430	0.0410	0.2857	0.0026	0.2604	1643.2	8.4	1620.0	13.0	1667	12	1667.0	12.0	2.8
GOM12_93	89.4	1.02	4.1670	0.0280	0.2941	0.0020	0.4676	1667.3	5.6	1662.0	10.0	1670	8	1670.4	8.2	0.5
GOM12_9	99.7	1.07	4.1980	0.0310	0.2960	0.0018	0.6106	1674.1	6.1	1671.4	9.2	1674	7	1673.5	7.0	0.1
GOM12_4	176	4.19	4.3970	0.0460	0.3073	0.0033	0.8542	1711.1	8.6	1727.0	16.0	1682	5	1682.4	4.8	2.7
GOM12_63	342	0.91	4.2980	0.0720	0.2978	0.0051	0.9579	1692.0	14.0	1680.0	25.0	1686	8	1686.4	7.6	0.4
GOM12_90	188	2.00	4.3170	0.0310	0.3026	0.0023	0.7515	1697.0	5.7	1704.0	11.0	1687	6	1687.1	5.6	1.0
GOM12_15	40.7	0.68	4.3700	0.0530	0.3048	0.0029	0.1737	1708.0	10.0	1715.0	14.0	1689	13	1689.0	13.0	1.5
GOM12_56	81.2	1.35	4.2610	0.0400	0.2985	0.0022	0.6066	1687.3	7.7	1684.0	11.0	1692	9	1691.7	8.9	0.5
GOM12_42	293	0.97	4.0890	0.0240	0.2864	0.0020	0.5071	1652.0	4.9	1623.0	10.0	1695	9	1694.6	8.7	4.2
GOM12_75	450	1.51	4.2200	0.0280	0.2950	0.0020	0.8022	1677.7	5.5	1666.4	9.8	1696	4	1695.6	4.4	1.7
GOM12_51	208	1.70	4.2460	0.0230	0.2967	0.0016	0.6630	1682.7	4.5	1675.0	8.0	1699	5	1698.7	4.5	1.4
GOM12_8	236	2.53	4.3530	0.0210	0.3044	0.0019	0.6084	1704.1	3.9	1712.8	9.4	1700	5	1699.9	5.0	0.8
GOM12_68	306	2.95	4.0400	0.0190	0.2814	0.0015	0.6308	1642.2	3.8	1598.4	7.6	1702	5	1702.1	4.7	6.1
GOM12_86	145.4	2.11	4.0740	0.0300	0.2830	0.0021	0.6207	1649.0	5.9	1606.0	11.0	1707	8	1706.5	8.1	5.9
GOM12_19	152	1.58	4.2310	0.0440	0.2939	0.0022	0.2941	1679.6	8.5	1661.0	11.0	1711	11	1711.0	11.0	2.9
GOM12_59	250	1.43	4.4170	0.0310	0.3064	0.0027	0.6203	1715.4	5.8	1723.0	13.0	1713	8	1712.5	8.2	0.6
GOM12_64	167.3	2.14	4.2670	0.0250	0.2950	0.0018	0.6284	1686.8	4.9	1666.2	9.2	1713	5	1712.5	5.2	2.7
GOM12_11	36.62	1.19	4.4180	0.0560	0.3043	0.0037	0.4936	1715.0	10.0	1715.0	19.0	1713	12	1713.0	12.0	0.1
GOM12_27	31.32	0.55	4.6100	0.0790	0.3167	0.0032	0.4962	1749.0	14.0	1773.0	16.0	1713	22	1713.0	22.0	3.5
GOM12_91	185	0.74	4.4300	0.0330	0.3060	0.0018	0.5967	1717.7	6.1	1720.9	8.9	1713	6	1713.4	6.4	0.4
GOM12_28	140.4	0.87	4.3510	0.0280	0.3003	0.0021	0.6248	1703.5	5.3	1693.0	10.0	1716	6	1715.9	5.6	1.3

GOM12_106	294	2.06	4.3820	0.0330	0.3038	0.0023	0.7883	1708.6	6.2	1710.0	11.0	1719	6	1718.6	6.2	0.5
GOM12_55	228.4	0.78	4.4710	0.0310	0.3060	0.0027	0.6015	1725.4	5.7	1721.0	13.0	1727	6	1726.8	6.2	0.3
GOM12_13	65.9	1.36	4.5850	0.0340	0.3135	0.0025	0.5487	1746.2	6.2	1758.0	12.0	1734	8	1733.7	7.7	1.4
GOM12_26	329	2.53	4.6490	0.0460	0.3079	0.0025	0.8703	1759.5	8.6	1730.0	13.0	1789	6	1788.7	5.6	3.3
GOM12_3	108.6	1.32	4.8070	0.0330	0.3166	0.0016	0.5952	1785.9	5.8	1773.2	7.7	1796	6	1796.0	6.2	1.3
GOM12_52	85.8	1.43	4.9200	0.0360	0.3212	0.0019	0.3967	1805.3	6.2	1795.2	9.2	1816	6	1816.4	6.3	1.2
GOM12_49	348.3	0.82	5.6810	0.0330	0.3417	0.0020	0.8379	1928.3	4.9	1894.9	9.6	1971	4	1970.8	4.0	3.9
GOM12_81	189	0.76	13.4810	0.0600	0.5302	0.0026	0.6349	2713.8	4.2	2742.0	11.0	2695	4	2694.7	3.6	1.8
GOM12_104	90	0.58	12.0500	0.2100	0.4742	0.0082	0.8574	2607.0	16.0	2501.0	36.0	2712	9	2712.0	9.3	7.8
GOM12_70	19.38	4.67	18.9000	0.2300	0.5770	0.0110	0.3940	3037.0	11.0	2938.0	43.0	3092	21	3092.0	21.0	5.0
GOM12_70	25.1	3.99	21.8600	0.3200	0.6355	0.0078	0.5179	3179.0	14.0	3176.0	30.0	3178	19	3178.0	19.0	0.1

Sample:GOM13	Isotopic Ratios							Isotopic ages (Ma)								
Analysis	[U] ppm	U/Th	207/235	2σ err.	206/238	2σ err.	RHO	207/235	2σ err.	206/238	2σ err.	207/206	2σ err.	Best age	2σ err.	% Dis.
GOM13_46	166.3	0.79	0.0277	0.0017	0.0040	0.0001	0.1426	27.7	1.7	25.5	0.7	338	66	25.5	0.7	8.1
GOM13_77	125	0.69	0.0359	0.0030	0.0054	0.0002	0.2760	35.8	2.9	34.6	1.1	295	69	34.6	1.1	3.4
GOM13_96	371	0.88	0.0344	0.0012	0.0054	0.0001	0.3285	34.3	1.2	34.7	0.7	120	30	34.7	0.7	1.3
GOM13_39	177.3	0.54	0.0365	0.0011	0.0055	0.0001	0.0898	36.3	1.1	35.6	0.6	179	39	35.6	0.6	2.1
GOM13_86	82	0.93	0.0360	0.0024	0.0057	0.0002	-0.0747	35.8	2.4	36.4	1.0	374	92	36.4	1.0	1.7
GOM13_92	332	0.95	0.0374	0.0011	0.0057	0.0001	0.1282	37.2	1.1	36.8	0.6	189	35	36.8	0.6	1.2
GOM13_26	197.7	0.41	0.0398	0.0014	0.0060	0.0001	0.2595	39.6	1.4	38.8	0.9	192	40	38.8	0.9	2.1
GOM13_67	125	0.60	0.0381	0.0018	0.0061	0.0002	-0.0796	37.9	1.8	39.2	1.0	327	94	39.2	1.0	3.3
GOM13_100	304	1.73	0.0424	0.0014	0.0064	0.0001	0.0909	42.2	1.4	41.3	0.8	205	55	41.3	0.8	2.1
GOM13_85	333	0.76	0.0453	0.0015	0.0068	0.0001	0.4062	45.0	1.4	43.6	0.7	178	29	43.6	0.7	3.2
GOM13_84	127	0.93	0.0551	0.0023	0.0078	0.0001	0.0484	54.4	2.2	50.3	0.9	332	54	50.3	0.9	7.5
GOM13_28	146.3	1.01	0.0553	0.0024	0.0087	0.0002	-0.0192	54.6	2.3	56.1	1.1	173	45	56.1	1.1	2.7
GOM13_24	206	1.49	0.0592	0.0015	0.0088	0.0001	0.2994	58.4	1.5	56.7	0.8	168	26	56.7	0.8	3.0
GOM13_62	331	1.12	0.0583	0.0018	0.0090	0.0002	0.0093	57.5	1.7	57.5	1.0	125	35	57.5	1.0	0.0
GOM13_119	174	1.08	0.0607	0.0018	0.0093	0.0002	0.0709	59.8	1.8	59.7	1.0	194	48	59.7	1.0	0.1
GOM13_115	363	2.06	0.0663	0.0016	0.0100	0.0001	0.2239	65.3	1.5	64.3	0.8	172	27	64.3	0.8	1.5
GOM13_13	185	1.06	0.0653	0.0017	0.0102	0.0002	0.1363	64.4	1.7	65.1	0.9	129	30	65.1	0.9	1.1

GOM13_7	267.3	1.37	0.0696	0.0023	0.0104	0.0002	0.0724	68.3	2.2	67.0	1.3	181	37	67.0	1.3	1.9
GOM13_34	48.9	1.92	0.0734	0.0049	0.0109	0.0003	0.0539	71.7	4.7	69.6	1.6	393	69	69.6	1.6	2.9
GOM13_6	245.2	1.32	0.0715	0.0013	0.0110	0.0001	0.1465	70.1	1.3	70.7	0.9	124	24	70.7	0.9	0.9
GOM13_87	1350	2.83	0.0791	0.0017	0.0120	0.0002	0.1510	77.3	1.6	76.7	1.4	151	24	76.7	1.4	0.8
GOM13_103	95.5	1.63	0.0795	0.0024	0.0120	0.0002	0.1645	77.6	2.3	76.9	1.3	216	40	76.9	1.3	0.9
GOM13_23	1060	4.30	0.0826	0.0028	0.0122	0.0004	0.3775	80.6	2.6	77.8	2.2	214	33	77.8	2.2	3.5
GOM13_19	141	1.47	0.0847	0.0032	0.0122	0.0003	0.2344	82.5	3.0	78.2	1.6	251	46	78.2	1.6	5.2
GOM13_21	231	1.00	0.0821	0.0030	0.0123	0.0003	0.5267	80.1	2.8	78.9	2.1	185	39	78.9	2.1	1.5
GOM13_74	134.7	0.69	0.0829	0.0025	0.0126	0.0002	-0.1366	80.9	2.3	80.4	1.2	213	30	80.4	1.2	0.6
GOM13_120	370	0.87	0.0821	0.0017	0.0126	0.0002	-0.0222	80.1	1.6	80.7	1.3	149	31	80.7	1.3	0.7
GOM13_109	372	2.20	0.0921	0.0020	0.0140	0.0002	0.2035	89.4	1.9	89.4	1.0	145	25	89.4	1.0	0.0
GOM13_45	595	1.81	0.0985	0.0020	0.0148	0.0002	0.4163	95.3	1.9	94.4	1.4	99	23	94.4	1.4	0.9
GOM13_31	315	0.81	0.0985	0.0022	0.0151	0.0002	0.3656	95.4	2.1	96.4	1.5	120	25	96.4	1.5	1.0
GOM13_82	537	0.40	0.1059	0.0022	0.0158	0.0002	0.4899	102.1	2.0	100.8	1.5	164	24	100.8	1.5	1.3
GOM13_20	109.6	0.79	0.1115	0.0035	0.0166	0.0003	0.2662	107.3	3.2	106.0	1.9	185	36	106.0	1.9	1.2
GOM13_73	120.5	0.28	0.1585	0.0042	0.0233	0.0003	0.0500	149.3	3.7	148.6	1.7	208	40	148.6	1.7	0.5
GOM13_111	188	0.59	0.1630	0.0042	0.0241	0.0005	0.3746	153.3	3.7	153.5	3.0	163	33	153.5	3.0	0.1
GOM13_1	411	0.50	0.1719	0.0022	0.0251	0.0002	0.5186	161.0	1.9	159.6	1.1	168	14	159.6	1.1	0.9
GOM13_47	409	0.65	0.1738	0.0027	0.0254	0.0004	0.5887	162.7	2.3	161.6	2.3	162	18	161.6	2.3	0.7
GOM13_52	450	0.55	0.1744	0.0031	0.0257	0.0004	0.4895	163.2	2.7	163.6	2.6	188	21	163.6	2.6	0.2
GOM13_98	510	2.46	0.1885	0.0018	0.0270	0.0002	0.2148	175.3	1.5	171.9	1.3	201	12	171.9	1.3	1.9
GOM13_37	448	1.15	0.1855	0.0031	0.0270	0.0004	0.4564	172.7	2.6	172.0	2.5	184	22	172.0	2.5	0.4
GOM13_57	61.5	0.71	0.1859	0.0056	0.0273	0.0006	-0.0372	173.0	4.8	173.7	3.6	226	45	173.7	3.6	0.4
GOM13_60	159	1.22	0.1922	0.0049	0.0279	0.0005	0.2319	178.4	4.2	177.1	3.3	223	37	177.1	3.3	0.7
GOM13_61	255	1.17	0.2032	0.0034	0.0298	0.0002	0.0756	187.7	2.9	189.0	1.5	186	21	189.0	1.5	0.7
GOM13_5	485.5	4.83	0.2299	0.0025	0.0329	0.0003	0.6111	210.1	2.0	208.9	1.9	237	15	208.9	1.9	0.6
GOM13_83	227	1.23	0.2351	0.0035	0.0338	0.0003	0.0236	214.4	2.8	214.4	2.0	207	26	214.4	2.0	0.0
GOM13_93	215	1.06	0.2529	0.0048	0.0361	0.0004	0.0422	228.9	3.9	228.7	2.5	242	23	228.7	2.5	0.1
GOM13_12	149.5	1.06	0.2570	0.0083	0.0363	0.0005	0.0176	232.1	6.7	230.1	3.2	248	32	230.1	3.2	0.9
GOM13_22	344	0.86	0.4212	0.0053	0.0556	0.0006	0.6544	356.8	3.8	349.1	3.6	410	12	349.1	3.6	2.2
GOM13_106	316.6	1.22	0.4331	0.0059	0.0584	0.0006	0.3185	365.3	4.2	366.0	3.7	366	16	366.0	3.7	0.2
GOM13_107	93.4	294.00	0.4910	0.0130	0.0638	0.0011	0.0407	405.6	8.7	398.9	6.5	452	32	398.9	6.5	1.7
GOM13_99	249.4	0.68	0.5032	0.0067	0.0660	0.0008	0.5161	413.8	4.5	411.8	4.5	429	12	411.8	4.5	0.5

GOM13_29	109	0.79	0.5360	0.0110	0.0690	0.0007	0.1114	435.7	7.2	430.2	4.1	468	25	430.2	4.1	1.3
GOM13_32	159.2	0.84	0.7859	0.0070	0.0941	0.0007	0.0682	588.7	4.0	579.7	3.9	627	15	579.7	3.9	1.5
GOM13_17	76.7	4.56	1.1490	0.0710	0.0981	0.0049	0.7475	613.0	28.0	582.0	28.0	820	32	582.0	28.0	5.1
GOM13_72	118	1.50	1.5420	0.0180	0.1587	0.0018	0.7107	946.8	7.3	949.0	10.0	935	9	949.0	10.0	0.2
GOM13_55	68.5	1.87	1.5500	0.0180	0.1559	0.0012	0.5205	950.1	7.2	934.7	7.1	978	13	934.7	7.1	1.6
GOM13_54	30.2	0.86	1.6370	0.0250	0.1658	0.0020	0.2668	985.1	9.8	989.0	11.0	987	16	989.0	11.0	0.4
GOM13_117	90.8	2.19	1.7720	0.0150	0.1747	0.0012	0.3469	1035.1	5.4	1037.8	6.6	1030	9	1029.7	9.0	0.8
GOM13_68	195.3	0.94	1.7650	0.0110	0.1736	0.0012	0.1318	1032.5	4.1	1031.9	6.8	1046	12	1046.0	12.0	1.3
GOM13_35	666	1.45	1.6810	0.0120	0.1631	0.0013	0.7955	1001.0	4.4	974.1	7.2	1060	7	974.1	7.2	2.7
GOM13_63	74.89	0.90	1.8270	0.0170	0.1773	0.0013	0.2847	1055.0	6.2	1052.4	7.0	1069	10	1069.4	9.8	1.6
GOM13_64	75.8	0.85	1.8220	0.0140	0.1762	0.0014	0.4689	1053.1	5.0	1045.9	7.5	1080	10	1080.0	10.0	3.2
GOM13_90	19.68	0.73	1.8800	0.0270	0.1790	0.0024	0.1975	1074.4	9.8	1062.0	13.0	1085	17	1085.0	17.0	2.1
GOM13_102	142	1.10	1.9320	0.0120	0.1842	0.0013	0.3794	1092.1	4.2	1089.6	6.8	1092	9	1092.2	8.8	0.2
GOM13_76	130.8	1.32	1.8920	0.0210	0.1797	0.0016	0.2900	1078.1	7.5	1065.2	8.7	1112	20	1112.0	20.0	4.2
GOM13_16	256	1.55	1.9250	0.0110	0.1813	0.0011	0.4268	1089.6	3.8	1073.8	6.2	1125	8	1125.1	7.6	4.6
GOM13_15	87	0.82	2.0570	0.0170	0.1919	0.0013	0.4520	1134.2	5.6	1131.6	6.9	1145	10	1145.0	10.0	1.2
GOM13_94	135.8	1.53	2.0900	0.0220	0.1896	0.0013	0.3019	1145.2	7.1	1119.1	7.2	1176	14	1176.0	14.0	4.8
GOM13_97	112.5	0.89	2.2410	0.0190	0.2027	0.0018	0.5565	1194.9	6.3	1189.7	9.7	1191	9	1191.0	9.3	0.1
GOM13_95	62.6	0.85	2.2390	0.0240	0.2016	0.0016	0.6086	1192.8	7.5	1184.0	8.7	1208	10	1208.1	9.7	2.0
GOM13_42	46	1.94	2.3230	0.0330	0.2049	0.0024	0.6621	1219.0	10.0	1201.0	13.0	1228	18	1228.0	18.0	2.2
GOM13_8	51	1.05	2.3540	0.0520	0.2059	0.0036	0.8556	1230.0	15.0	1207.0	19.0	1270	12	1270.0	12.0	5.0
GOM13_80	161	1.47	3.0880	0.0180	0.2485	0.0015	0.4249	1429.5	4.4	1430.8	7.8	1427	7	1427.3	6.8	0.2
GOM13_118	50.53	1.20	3.0850	0.0430	0.2458	0.0021	0.3560	1429.0	11.0	1417.0	11.0	1430	16	1430.0	16.0	0.9
GOM13_79	107.6	1.87	3.0990	0.0360	0.2492	0.0032	0.7963	1431.6	8.9	1434.0	16.0	1430	8	1430.4	8.0	0.3
GOM13_113	246.9	1.52	3.0840	0.0130	0.2471	0.0010	0.5091	1429.1	3.3	1423.3	5.3	1432	4	1431.5	4.4	0.6
GOM13_65	372	1.91	3.0670	0.0370	0.2471	0.0028	0.9336	1424.0	9.1	1423.0	15.0	1435	5	1435.4	5.4	0.9
GOM13_30	64.4	0.76	3.0230	0.0240	0.2413	0.0021	0.5511	1413.1	6.1	1393.0	11.0	1441	8	1440.8	8.3	3.3
GOM13_108	206.4	1.25	3.0120	0.0230	0.2396	0.0016	0.5712	1410.4	5.8	1384.6	8.1	1441	7	1440.9	7.3	3.9
GOM13_101	106	1.90	3.0550	0.0190	0.2433	0.0016	0.4592	1421.4	4.9	1403.9	8.4	1443	10	1442.8	9.6	2.7
GOM13_58	242	2.98	3.1260	0.0220	0.2489	0.0023	0.9826	1439.0	5.4	1433.0	12.0	1446	7	1446.0	6.6	0.9
GOM13_27	315	2.22	3.0700	0.0170	0.2453	0.0015	0.6965	1425.1	4.2	1414.0	7.8	1450	5	1449.9	5.2	2.5
GOM13_17	919	7.55	2.8170	0.0140	0.2247	0.0014	0.8136	1360.0	3.8	1306.4	7.4	1453	4	1453.0	4.3	10.1
GOM13_112	91.7	0.75	2.9620	0.0370	0.2320	0.0025	0.7868	1397.4	9.5	1345.0	13.0	1477	11	1477.0	11.0	8.9

GOM13_62	54.1	1.40	3.6360	0.0670	0.2679	0.0051	0.9060	1557.0	15.0	1530.0	26.0	1590	24	1590.0	24.0	3.8
GOM13_105	50.2	0.98	3.7220	0.0340	0.2740	0.0025	0.0952	1575.7	7.3	1561.0	12.0	1597	11	1597.0	11.0	2.3
GOM13_25	275.4	3.85	3.9230	0.0180	0.2821	0.0015	0.6199	1618.3	3.8	1601.8	7.8	1648	5	1648.4	5.2	2.8
GOM13_71	144.8	0.73	4.0430	0.0250	0.2892	0.0021	0.7153	1643.4	4.8	1639.0	11.0	1658	5	1657.8	5.4	1.1
GOM13_49	144	4.60	3.8570	0.0390	0.2683	0.0027	0.7879	1605.6	8.0	1532.0	14.0	1687	4	1687.3	4.4	9.2
GOM13_59	266	1.36	4.1520	0.0310	0.2901	0.0022	0.8167	1664.2	6.0	1642.0	11.0	1688	4	1688.1	4.4	2.7
GOM13_40	191	2.62	4.3340	0.0510	0.3028	0.0037	0.8105	1700.0	10.0	1707.0	19.0	1689	8	1688.5	7.5	1.1
GOM13_9	291	1.91	4.1620	0.0250	0.2916	0.0021	0.6546	1666.3	4.9	1649.0	10.0	1694	5	1693.8	5.1	2.6
GOM13_41	40	0.71	4.1170	0.0400	0.2844	0.0029	0.2656	1657.2	7.9	1613.0	15.0	1700	12	1700.0	12.0	5.1
GOM13_18	39.3	1.81	4.1120	0.0410	0.2860	0.0029	0.3284	1656.2	8.1	1621.0	14.0	1701	11	1701.0	11.0	4.7
GOM13_51	54.6	1.34	4.2110	0.0370	0.2928	0.0025	0.2812	1675.9	7.2	1655.0	12.0	1706	9	1706.1	8.7	3.0
GOM13_11	707	2.19	3.5390	0.0320	0.2451	0.0026	0.9008	1535.7	7.3	1413.0	13.0	1708	6	1707.8	5.7	17.3
GOM13_91	176.3	1.20	4.0180	0.0230	0.2778	0.0021	0.5471	1637.7	4.6	1580.0	11.0	1712	6	1712.2	5.9	7.7
GOM13_69	947	4.55	4.0630	0.0270	0.2806	0.0023	0.8073	1646.8	5.5	1595.0	12.0	1714	7	1713.9	6.7	6.9
GOM13_48	106	0.65	4.4480	0.0310	0.3075	0.0022	0.5712	1721.0	5.7	1728.0	11.0	1716	8	1716.4	7.7	0.7
GOM13_78	59.71	0.89	4.2100	0.0610	0.2921	0.0033	0.2101	1676.0	12.0	1652.0	17.0	1717	24	1717.0	24.0	3.8
GOM13_110	187	0.96	4.4840	0.0270	0.3074	0.0017	0.5745	1727.8	5.0	1727.7	8.5	1723	5	1722.8	5.4	0.3
GOM13_33	212	2.68	4.1530	0.0460	0.2855	0.0036	0.8694	1664.2	8.9	1619.0	18.0	1723	7	1723.2	7.4	6.0
GOM13_44	117	1.36	4.1360	0.0340	0.2846	0.0023	0.4576	1661.3	6.8	1614.0	12.0	1728	10	1728.0	10.0	6.6
GOM13_66	110.2	1.51	4.6600	0.0410	0.3175	0.0030	0.6083	1759.8	7.3	1777.0	15.0	1743	7	1743.0	7.3	2.0
GOM13_10	136.3	1.74	4.4260	0.0270	0.3004	0.0019	0.5926	1717.6	4.9	1693.2	9.6	1755	6	1754.8	5.9	3.5
GOM13_50	93	0.73	4.3100	0.1400	0.2886	0.0083	0.9360	1693.0	27.0	1634.0	42.0	1770	10	1770.0	10.0	7.7
GOM13_70	366	3.34	4.8110	0.0300	0.3166	0.0021	0.7185	1786.6	5.2	1773.0	10.0	1811	5	1811.2	5.4	2.1
GOM13_36	78.7	1.20	4.7030	0.0330	0.3062	0.0022	0.4445	1767.5	5.9	1722.0	11.0	1825	7	1824.5	6.7	5.6
GOM13_81	84.8	0.94	4.9780	0.0280	0.3204	0.0017	0.2786	1816.1	5.0	1791.7	8.5	1841	9	1841.2	8.7	2.7
GOM13_56	320.8	1.84	5.0740	0.0380	0.3139	0.0028	0.6202	1831.7	6.4	1760.0	14.0	1902	7	1901.6	6.8	7.4
GOM13_75	206	2.29	5.6710	0.0450	0.3470	0.0029	0.7550	1926.7	6.8	1920.0	14.0	1931	7	1930.8	6.9	0.6
GOM13_88	40.3	1.45	10.5030	0.0610	0.4644	0.0032	0.3397	2480.0	5.4	2459.0	14.0	2494	9	2493.7	8.5	1.4
GOM13_89	36.46	0.69	13.9600	0.2300	0.5240	0.0120	0.7571	2747.0	16.0	2714.0	51.0	2766	16	2766.0	16.0	1.9

Sample:GOM14	Isotopic Ratios	Isotopic ages (Ma)

Analysis	[U] ppm	U/Th	207/235	2σ err.	206/238	2σ err.	RHO	207/235	2σ err.	206/238	2σ err.	207/206	2σ err.	Best age	2σ err.	% Dis.
GOM14_119	356	1.86	0.0312	0.0027	0.0049	0.0002	0.0404	31.2	2.6	31.5	1.0	40	170	31.5	1.0	1.0
GOM14_3	243	0.88	0.0307	0.0019	0.0050	0.0002	0.0815	30.6	1.9	32.0	1.0	20	130	32.0	1.0	4.5
GOM14_123	45.4	0.94	0.0331	0.0058	0.0051	0.0004	0.0197	32.8	5.7	32.6	2.4	40	320	32.6	2.4	0.6
GOM14_107	362	1.97	0.0430	0.0036	0.0068	0.0003	0.0370	42.8	3.5	43.5	2.1	40	180	43.5	2.1	1.6
GOM14_113	68.1	0.68	0.0468	0.0042	0.0069	0.0003	0.2331	46.9	4.0	44.5	2.1	190	190	44.5	2.1	5.1
GOM14_72	348	0.95	0.0485	0.0015	0.0074	0.0001	0.2286	48.1	1.5	47.7	0.9	102	84	47.7	0.9	0.9
GOM14_59	3090	6.20	0.0577	0.0035	0.0086	0.0003	0.4372	57.0	3.4	55.2	1.6	130	130	55.2	1.6	3.2
GOM14_79	316.5	2.29	0.0680	0.0026	0.0104	0.0002	0.0157	66.8	2.5	66.4	1.5	91	93	66.4	1.5	0.6
GOM14_64	109	1.06	0.0748	0.0050	0.0112	0.0003	0.2881	73.1	4.7	71.6	2.2	110	120	71.6	2.2	2.1
GOM14_117	589	1.47	0.0761	0.0046	0.0113	0.0004	0.4269	74.5	4.3	72.3	2.8	160	120	72.3	2.8	3.0
GOM14_58	1332.8	1.87	0.0746	0.0011	0.0113	0.0001	0.0550	73.2	1.0	72.7	0.6	109	40	72.7	0.6	0.7
GOM14_15	74	1.69	0.0746	0.0051	0.0117	0.0005	0.0017	73.0	4.8	74.9	2.9	100	170	74.9	2.9	2.6
GOM14_120	1390	1.67	0.0805	0.0062	0.0120	0.0005	0.9737	78.6	5.8	76.6	3.3	220	170	76.6	3.3	2.5
GOM14_62	148.8	2.26	0.1184	0.0043	0.0178	0.0004	0.2300	113.5	3.9	114.0	2.4	120	94	114.0	2.4	0.4
GOM14_83	388	1.95	0.1859	0.0047	0.0262	0.0006	0.6080	173.0	4.0	166.8	4.0	232	53	166.8	4.0	3.6
GOM14_85	289	0.84	0.1811	0.0046	0.0262	0.0004	0.1101	168.9	3.9	166.9	2.5	186	63	166.9	2.5	1.2
GOM14_13	210.9	0.72	0.1819	0.0048	0.0262	0.0006	0.0345	169.6	4.1	166.9	3.7	163	78	166.9	3.7	1.6
GOM14_77	340	1.02	0.2489	0.0053	0.0354	0.0004	0.2928	226.1	4.2	224.0	2.5	251	47	224.0	2.5	0.9
GOM14_48	134.3	1.79	0.4990	0.0130	0.0656	0.0009	0.1943	410.9	8.7	409.4	5.7	425	55	409.4	5.7	0.4
GOM14_101	238.1	1.36	0.5201	0.0084	0.0682	0.0008	0.1267	424.9	5.6	425.1	4.5	422	41	425.1	4.5	0.0
GOM14_54	576	1.65	0.6000	0.0110	0.0693	0.0013	0.5371	477.0	6.9	432.1	7.6	682	31	432.1	7.6	9.4
GOM14_124	253.3	0.51	0.5410	0.0110	0.0699	0.0008	0.3569	439.5	7.5	435.8	4.5	457	37	435.8	4.5	0.8
GOM14_22	214	1.25	0.5810	0.0100	0.0745	0.0009	0.4004	464.7	6.4	463.0	5.1	462	39	463.0	5.1	0.4
GOM14_89	28.7	1.08	1.0890	0.0590	0.1222	0.0040	0.1933	754.0	32.0	743.0	23.0	740	130	743.0	23.0	1.5
GOM14_95	248.5	2.03	1.6180	0.0240	0.1559	0.0021	0.5967	976.6	9.1	934.0	12.0	1059	26	934.0	12.0	4.4
GOM14_49	139.5	1.31	1.6320	0.0170	0.1592	0.0014	0.3169	982.3	6.5	952.5	7.8	1046	23	952.5	7.8	3.0
GOM14_50	599	26.30	1.6020	0.0310	0.1595	0.0023	0.8878	973.0	12.0	954.0	13.0	996	18	954.0	13.0	2.0
GOM14_26	110.1	1.16	1.5730	0.0190	0.1596	0.0017	0.3029	959.1	7.4	954.4	9.6	986	27	954.4	9.6	0.5
GOM14_100	504	2.49	1.7750	0.0150	0.1597	0.0013	0.6994	1036.3	5.6	955.1	7.4	1199	15	955.1	7.4	7.8
GOM14_110	428	2.82	1.6130	0.0160	0.1614	0.0013	0.6634	975.0	6.3	964.6	7.1	1007	16	964.6	7.1	1.1
GOM14_36	65.9	1.41	1.6540	0.0350	0.1627	0.0022	0.0651	992.0	13.0	971.0	12.0	1027	49	971.0	12.0	2.1
GOM14_51	348	2.17	1.6750	0.0270	0.1643	0.0024	0.7704	998.0	10.0	981.0	13.0	1020	21	981.0	13.0	1.7

GOM14_90	45.5	0.85	1.6760	0.0350	0.1648	0.0020	0.0478	998.0	13.0	983.0	11.0	1003	49	983.0	11.0	1.5
GOM14_39	313.6	2.48	1.6750	0.0170	0.1648	0.0013	0.2974	998.8	6.3	983.5	7.2	1038	20	983.5	7.2	1.5
GOM14_97	360	1.25	1.6950	0.0170	0.1654	0.0018	0.7031	1007.2	6.6	986.7	9.8	1038	17	986.7	9.8	2.0
GOM14_111	42.2	2.47	1.7000	0.0480	0.1665	0.0034	0.2025	1007.0	18.0	992.0	19.0	1054	73	992.0	19.0	1.5
GOM14_80	80	1.42	1.6690	0.0180	0.1671	0.0014	0.2982	996.3	6.8	996.2	7.6	1003	27	996.2	7.6	0.0
GOM14_16	188	6.29	1.6910	0.0310	0.1675	0.0017	0.0141	1005.0	12.0	998.4	9.4	1039	41	998.4	9.4	0.7
GOM14_18	118.1	2.61	1.7000	0.0240	0.1697	0.0020	0.3003	1008.1	9.0	1010.0	11.0	1005	32	1005.0	32.0	0.5
GOM14_88	247	3.07	1.7310	0.0180	0.1718	0.0019	0.5590	1019.7	6.6	1022.0	10.0	1005	20	1005.0	20.0	1.7
GOM14_34	92.7	1.68	1.6880	0.0190	0.1686	0.0015	0.2929	1004.7	6.8	1004.3	8.0	1009	25	1009.0	25.0	0.5
GOM14_66	168	1.76	1.7640	0.0230	0.1757	0.0015	0.5569	1033.8	8.4	1043.1	8.4	1018	22	1018.0	22.0	2.5
GOM14_23	126.3	2.86	1.7270	0.0200	0.1708	0.0014	0.1724	1018.1	7.3	1016.6	7.9	1022	26	1022.0	26.0	0.5
GOM14_1	156	1.83	1.7690	0.0210	0.1744	0.0014	0.1076	1034.6	7.4	1036.3	7.9	1033	26	1033.0	26.0	0.3
GOM14_28	102.5	1.97	1.7750	0.0240	0.1753	0.0014	0.2359	1035.8	8.7	1040.9	7.6	1038	30	1038.0	30.0	0.3
GOM14_47	87.3	1.93	1.6990	0.0200	0.1679	0.0017	0.2295	1008.9	7.5	1000.5	9.2	1039	27	1039.0	27.0	3.7
GOM14_70	86.5	1.72	1.7780	0.0750	0.1735	0.0041	0.0931	1037.0	28.0	1031.0	23.0	1040	110	1040.0	110.0	0.9
GOM14_81	146.5	1.47	1.7350	0.0180	0.1702	0.0013	0.3590	1022.1	6.9	1013.1	7.3	1043	23	1043.0	23.0	2.9
GOM14_42	70.25	0.54	1.7860	0.0290	0.1740	0.0018	0.4379	1041.0	11.0	1036.0	10.0	1047	31	1047.0	31.0	1.1
GOM14_60	171.3	3.71	1.8250	0.0190	0.1777	0.0017	0.3955	1054.8	7.0	1054.1	9.1	1049	22	1049.0	22.0	0.5
GOM14_99	114	0.86	1.7440	0.0370	0.1711	0.0024	0.5737	1026.0	14.0	1018.0	13.0	1058	36	1058.0	36.0	3.8
GOM14_30	116.6	2.36	1.8030	0.0210	0.1743	0.0015	0.2154	1046.0	7.5	1035.7	8.3	1059	27	1059.0	27.0	2.2
GOM14_91	33.7	1.06	1.8620	0.0360	0.1809	0.0023	0.0332	1066.0	13.0	1072.0	13.0	1065	47	1065.0	47.0	0.7
GOM14_44	87.6	2.27	1.7780	0.0270	0.1726	0.0020	0.3665	1038.4	9.6	1026.0	11.0	1065	32	1065.0	32.0	3.7
GOM14_41	11.58	1.02	1.7800	0.1000	0.1739	0.0081	0.2276	1034.0	36.0	1033.0	45.0	1070	140	1070.0	140.0	3.5
GOM14_68	64.6	1.25	1.8930	0.0360	0.1817	0.0026	0.3929	1079.0	12.0	1076.0	14.0	1078	34	1078.0	34.0	0.2
GOM14_25	220	1.33	1.8610	0.0220	0.1793	0.0019	0.3462	1067.0	7.8	1063.0	10.0	1079	26	1079.0	26.0	1.5
GOM14_118	23.9	0.97	1.8970	0.0530	0.1828	0.0032	0.1061	1088.0	19.0	1087.0	17.0	1081	67	1081.0	67.0	0.6
GOM14_84	295	8.10	1.8200	0.0160	0.1749	0.0025	0.3537	1052.6	5.7	1039.0	14.0	1083	24	1083.0	24.0	4.1
GOM14_112	297	9.89	1.7940	0.0180	0.1722	0.0016	0.6516	1043.0	6.4	1023.9	8.6	1085	16	1085.0	16.0	5.6
GOM14_108	464	1.69	1.8610	0.0120	0.1781	0.0012	0.5157	1067.3	4.1	1056.6	6.7	1094	14	1094.0	14.0	3.4
GOM14_14	106.8	1.08	1.9490	0.0610	0.1845	0.0031	0.2568	1097.0	21.0	1092.0	17.0	1102	58	1102.0	58.0	0.9
GOM14_24	105.7	2.15	1.8760	0.0250	0.1776	0.0017	0.2720	1072.1	8.6	1053.7	9.5	1107	26	1107.0	26.0	4.8
GOM14_37	155	2.02	1.9160	0.0290	0.1826	0.0023	0.6865	1086.0	10.0	1081.0	12.0	1119	26	1119.0	26.0	3.4
GOM14_35	177	2.12	2.0350	0.0270	0.1906	0.0023	0.6974	1127.9	9.2	1124.0	13.0	1129	22	1129.0	22.0	0.4

GOM14_11	380	1.93	2.0070	0.0170	0.1880	0.0012	0.4177	1117.4	5.8	1110.4	6.7	1132	17	1132.0	17.0	1.9
GOM14_86	164.2	1.67	2.0160	0.0260	0.1878	0.0015	0.1483	1120.4	8.6	1109.3	8.4	1136	26	1136.0	26.0	2.4
GOM14_116	43.9	1.11	2.1050	0.0410	0.1966	0.0026	0.2844	1149.0	13.0	1157.0	14.0	1156	42	1156.0	42.0	0.1
GOM14_65	115.2	2.10	2.0580	0.0220	0.1894	0.0016	0.3471	1134.5	7.3	1117.8	8.6	1169	21	1169.0	21.0	4.4
GOM14_61	333	3.32	2.0150	0.0300	0.1845	0.0074	0.4426	1121.0	10.0	1092.0	40.0	1169	73	1169.0	73.0	6.6
GOM14_33	200	1.95	2.1240	0.0220	0.1940	0.0015	0.2628	1156.3	7.0	1143.1	8.0	1172	22	1172.0	22.0	2.5
GOM14_56	92	1.94	2.0940	0.0330	0.1916	0.0026	0.4773	1146.0	11.0	1130.0	14.0	1173	33	1173.0	33.0	3.7
GOM14_105	54.9	2.86	2.0260	0.0800	0.1884	0.0047	0.2560	1123.0	27.0	1112.0	26.0	1173	93	1173.0	93.0	5.2
GOM14_98	60	1.42	2.2040	0.0380	0.2038	0.0030	0.3001	1181.0	12.0	1195.0	16.0	1175	40	1175.0	40.0	1.7
GOM14_6	465	2.56	2.0240	0.0140	0.1853	0.0015	0.5728	1124.2	4.8	1095.7	8.0	1176	13	1176.0	13.0	6.8
GOM14_20	60.5	0.77	2.1510	0.0330	0.1974	0.0021	0.1645	1165.0	11.0	1161.0	11.0	1183	32	1183.0	32.0	1.9
GOM14_12	222.3	1.42	2.0790	0.0190	0.1903	0.0015	0.2722	1141.7	6.4	1122.9	7.9	1183	21	1183.0	21.0	5.1
GOM14_5	244	8.07	2.2360	0.0210	0.2036	0.0014	0.5570	1192.8	6.5	1194.3	7.8	1185	16	1185.0	16.0	0.8
GOM14_31	143	1.18	2.1290	0.0240	0.1949	0.0018	0.4986	1158.6	7.5	1147.8	9.8	1187	19	1187.0	19.0	3.3
GOM14_103	245	2.32	2.0510	0.0380	0.1862	0.0028	0.7135	1132.0	13.0	1100.0	15.0	1197	27	1197.0	27.0	8.1
GOM14_73	156.9	1.19	2.0450	0.0300	0.1849	0.0018	0.2140	1130.2	9.9	1094.0	10.0	1199	33	1199.0	33.0	8.8
GOM14_74	41.5	0.69	2.1450	0.0380	0.1941	0.0029	0.4049	1166.0	12.0	1143.0	15.0	1202	34	1202.0	34.0	4.9
GOM14_87	52.6	1.65	2.2970	0.0730	0.2067	0.0046	0.6994	1215.0	22.0	1213.0	25.0	1212	41	1212.0	41.0	0.1
GOM14_63	66.7	1.21	2.2030	0.0360	0.1946	0.0021	0.2800	1183.0	11.0	1146.0	12.0	1231	35	1231.0	35.0	6.9
GOM14_21	122.2	0.96	2.2650	0.0300	0.2001	0.0027	0.3398	1200.8	9.3	1176.0	14.0	1252	31	1252.0	31.0	6.1
GOM14_19	88.2	1.48	2.4820	0.0540	0.2182	0.0039	0.7443	1265.0	16.0	1272.0	20.0	1256	29	1256.0	29.0	1.3
GOM14_55	80.4	1.21	2.6050	0.0600	0.2233	0.0050	0.6164	1301.0	17.0	1299.0	26.0	1300	37	1300.0	37.0	0.1
GOM14_94	169.4	2.45	2.4310	0.0470	0.2069	0.0028	0.4131	1254.0	15.0	1212.0	15.0	1316	33	1316.0	33.0	7.9
GOM14_7	110	1.34	2.7590	0.0340	0.2319	0.0022	0.4690	1347.1	9.2	1344.0	12.0	1336	25	1336.0	25.0	0.6
GOM14_82	61	1.60	2.8190	0.0390	0.2338	0.0024	0.3039	1360.0	10.0	1354.0	12.0	1365	28	1365.0	28.0	0.8
GOM14_40	165	2.41	2.8810	0.0610	0.2375	0.0049	0.8691	1379.0	16.0	1373.0	25.0	1381	21	1381.0	21.0	0.6
GOM14_27	74.4	0.64	2.9240	0.0420	0.2394	0.0032	0.4405	1389.0	10.0	1383.0	16.0	1394	25	1394.0	25.0	0.8
GOM14_115	161.8	0.90	2.8350	0.0220	0.2313	0.0018	0.3239	1364.5	5.9	1341.0	9.6	1412	17	1412.0	17.0	5.0
GOM14_114	29	1.05	3.1950	0.0640	0.2551	0.0036	0.1247	1456.0	15.0	1464.0	18.0	1422	44	1422.0	44.0	3.0
GOM14_92	98.9	3.19	3.1190	0.0370	0.2498	0.0024	0.5191	1437.1	9.2	1437.0	13.0	1431	23	1431.0	23.0	0.4
GOM14_29	107	0.96	3.0910	0.0280	0.2485	0.0023	0.2697	1430.9	7.2	1430.0	12.0	1432	23	1432.0	23.0	0.1
GOM14_57	72.9	0.76	3.1640	0.0430	0.2518	0.0025	0.5480	1449.0	10.0	1448.0	13.0	1442	23	1442.0	23.0	0.4
GOM14_9	52.7	1.47	3.1030	0.0380	0.2489	0.0032	0.4455	1432.7	9.4	1432.0	17.0	1443	22	1443.0	22.0	0.8

GOM14_69	178.8	0.91	3.0380	0.0610	0.2358	0.0036	0.4511	1420.0	14.0	1365.0	19.0	1478	38	1478.0	38.0	7.6
GOM14_4	132.1	1.39	3.1970	0.0280	0.2481	0.0022	0.2330	1456.1	6.7	1428.0	11.0	1498	19	1498.0	19.0	4.7
GOM14_122	115.7	1.12	3.1370	0.0410	0.2427	0.0026	0.4099	1441.2	9.9	1400.0	14.0	1520	25	1520.0	25.0	7.9
GOM14_59	151.3	2.99	4.0570	0.0780	0.2884	0.0027	0.4484	1645.0	16.0	1633.0	14.0	1640	33	1640.0	33.0	0.4
GOM14_38	102	0.98	3.8590	0.0480	0.2766	0.0027	0.4489	1605.6	9.7	1576.0	14.0	1651	20	1651.0	20.0	4.5
GOM14_2	272	1.34	4.1070	0.0260	0.2917	0.0017	0.5734	1655.5	5.2	1650.1	8.3	1663	12	1663.0	12.0	0.8
GOM14_70	27.26	0.87	4.2080	0.0580	0.2959	0.0040	0.3427	1675.0	11.0	1671.0	20.0	1664	29	1664.0	29.0	0.4
GOM14_106	244	1.42	4.2190	0.0300	0.2974	0.0023	0.7845	1677.4	5.9	1678.0	12.0	1681	12	1681.0	12.0	0.2
GOM14_75	179.4	0.74	4.2670	0.0370	0.2983	0.0028	0.2837	1686.7	7.0	1683.0	14.0	1688	20	1688.0	20.0	0.3
GOM14_109	486	0.73	4.0190	0.0330	0.2822	0.0020	0.7067	1639.5	6.6	1602.0	10.0	1689	10	1689.0	10.0	5.2
GOM14_17	316.7	2.29	4.0200	0.0290	0.2814	0.0022	0.7056	1638.6	6.0	1598.0	11.0	1699	11	1699.0	11.0	5.9
GOM14_32	336	2.22	4.1310	0.0270	0.2868	0.0025	0.5949	1660.2	5.4	1625.0	12.0	1705	13	1705.0	13.0	4.7
GOM14_46	91	1.45	4.3290	0.0460	0.2979	0.0034	0.4312	1699.6	9.1	1680.0	17.0	1713	24	1713.0	24.0	1.9
GOM14_104	190.9	2.47	4.6410	0.0420	0.3111	0.0027	0.3804	1756.3	7.5	1746.0	13.0	1776	14	1776.0	14.0	1.7
GOM14_43	79.6	1.79	4.7370	0.0470	0.3144	0.0026	0.2412	1773.2	8.3	1762.0	13.0	1790	22	1790.0	22.0	1.6
GOM14_8	351	3.20	5.0100	0.0450	0.3311	0.0029	0.7641	1822.6	7.7	1843.0	14.0	1790	10	1790.0	9.7	3.0
GOM14_120	103.7	0.96	5.9200	0.1100	0.3560	0.0065	0.8908	1964.0	16.0	1963.0	31.0	1955	30	1955.0	30.0	0.4
GOM14_121	185.2	1.66	11.0890	0.0700	0.4646	0.0029	0.7548	2530.3	5.8	2460.0	13.0	2589	8	2589.1	7.8	5.0
GOM14_52	106.6	0.55	11.7730	0.0750	0.4774	0.0036	0.7326	2586.2	5.9	2516.0	16.0	2630	9	2630.4	9.1	4.3
GOM14_78	53.9	0.35	12.2300	0.1100	0.4915	0.0054	0.5215	2622.5	8.7	2580.0	24.0	2652	17	2652.0	17.0	2.7
GOM14_96	9.81	2.34	13.2800	0.2100	0.4984	0.0097	0.4906	2698.0	15.0	2610.0	41.0	2755	29	2755.0	29.0	5.3
GOM14_93	318	1.66	34.2100	0.2400	0.7215	0.0053	0.7784	3615.7	7.0	3501.0	20.0	3679	7	3678.7	7.1	4.8

Sample: GOM15	Isotopic Ratios							Isotopic ages (Ma)								
Analysis	[U] ppm	U/Th	207/235	2σ err.	206/238	2σ err.	RHO	207/235	2σ err.	206/238	2σ err.	207/206	2σ err.	Best age	2σ err.	% Dis.
GOM15_124	1610	0.72	0.0461	0.0015	0.0068	0.0002	0.4521	45.8	1.4	43.6	1.5	157	79	43.6	1.5	4.8
GOM15_28	268	0.45	0.0449	0.0044	0.0070	0.0005	0.3359	44.5	4.2	44.8	2.9	40	180	44.8	2.9	0.7
GOM15_120	671	0.79	0.0819	0.0026	0.0125	0.0004	0.1017	79.9	2.4	79.9	2.2	74	74	79.9	2.2	0.0
GOM15_83	2550	6.57	0.0830	0.0027	0.0127	0.0005	0.5207	81.0	2.5	81.3	2.9	71	57	81.3	2.9	0.4
GOM15_114	1180	1.30	0.1001	0.0021	0.0150	0.0003	0.3783	96.9	2.0	96.2	2.0	104	52	96.2	2.0	0.7
GOM15_12	553	2.70	0.1030	0.0028	0.0155	0.0003	0.1389	99.8	2.6	99.3	1.9	125	66	99.3	1.9	0.5

GOM15_123	2288	1.13	0.1031	0.0019	0.0157	0.0003	0.3025	99.6	1.8	100.1	2.0	99	50	100.1	2.0	0.5
GOM15_125	529	0.63	0.1884	0.0036	0.0271	0.0005	0.3707	175.6	3.1	172.3	2.9	174	46	172.3	2.9	1.9
GOM15_8	805	62.70	0.3730	0.0130	0.0511	0.0019	0.6972	322.0	9.5	321.0	12.0	343	79	321.0	12.0	0.3
GOM15_73	1410	4.57	0.4600	0.0180	0.0595	0.0025	0.5207	384.0	13.0	373.0	15.0	435	55	373.0	15.0	2.9
GOM15_127	1406	1.39	0.4840	0.0140	0.0621	0.0018	0.6327	400.3	9.9	388.0	11.0	432	51	388.0	11.0	3.1
GOM15_78	255.6	0.86	0.5120	0.0340	0.0658	0.0018	0.4215	419.0	22.0	411.0	11.0	430	130	411.0	11.0	1.9
GOM15_57	260	0.57	0.5040	0.0120	0.0660	0.0017	0.6070	415.4	8.0	412.0	10.0	420	52	412.0	10.0	0.8
GOM15_6	557	0.59	0.5058	0.0080	0.0663	0.0010	0.5355	415.3	5.4	413.8	6.1	427	35	413.8	6.1	0.4
GOM15_7	452	1.19	0.5150	0.0120	0.0666	0.0014	0.5598	421.3	7.9	415.3	8.7	450	42	415.3	8.7	1.4
GOM15_91	299	15.50	0.5480	0.0210	0.0695	0.0025	0.4799	443.0	14.0	433.0	15.0	435	87	433.0	15.0	2.3
GOM15_24	541	6.10	0.5650	0.0130	0.0736	0.0015	0.7611	454.1	8.4	457.9	8.8	448	39	457.9	8.8	0.8
GOM15_59	231.5	0.57	0.5850	0.0150	0.0739	0.0016	0.5281	467.0	9.4	459.4	9.8	494	58	459.4	9.8	1.6
GOM15_88	280.4	1.27	0.5780	0.0200	0.0742	0.0015	0.2458	465.0	13.0	461.3	8.7	471	75	461.3	8.7	0.8
GOM15_104	314.3	1.43	0.6080	0.0160	0.0754	0.0014	0.4613	482.1	9.9	468.6	8.6	505	59	468.6	8.6	2.8
GOM15_105	300.6	0.83	0.6550	0.0110	0.0819	0.0012	0.3512	512.2	6.7	507.2	7.4	535	40	507.2	7.4	1.0
GOM15_1	101.8	2.31	0.7740	0.0260	0.0914	0.0032	0.6373	581.0	15.0	563.0	19.0	614	67	563.0	19.0	3.1
GOM15_87	218	1.15	1.0340	0.0250	0.1178	0.0031	0.7167	720.0	12.0	718.0	18.0	760	45	718.0	18.0	0.3
GOM15_30	1087	11.10	1.3400	0.1500	0.1420	0.0120	0.5328	861.0	65.0	853.0	68.0	860	200	853.0	68.0	0.9
GOM15_19	218	2.24	1.4770	0.0240	0.1527	0.0027	0.6092	921.2	9.8	916.0	15.0	938	28	916.0	15.0	0.6
GOM15_85	996	1.69	1.7090	0.0770	0.1541	0.0058	0.7514	1011.0	29.0	924.0	32.0	1178	63	924.0	32.0	8.6
GOM15_48	1071	2.47	1.6500	0.1000	0.1556	0.0097	0.8241	986.0	39.0	932.0	54.0	1050	100	932.0	54.0	5.5
GOM15_117	218	1.50	1.5850	0.0200	0.1594	0.0022	0.4529	963.8	7.8	953.0	12.0	972	28	953.0	12.0	1.1
GOM15_101	301.6	1.29	1.6920	0.0270	0.1643	0.0035	0.4326	1005.0	10.0	980.0	19.0	1049	38	980.0	19.0	2.5
GOM15_79	187.9	1.83	1.6790	0.0300	0.1649	0.0026	0.4619	1002.0	12.0	984.0	14.0	1029	35	984.0	14.0	1.8
GOM15_42	110.2	1.43	1.6840	0.0230	0.1662	0.0020	0.5004	1003.1	8.9	991.0	11.0	1025	29	991.0	11.0	1.2
GOM15_46	136.5	1.47	1.6810	0.0480	0.1668	0.0037	0.6419	1003.0	19.0	994.0	20.0	1017	45	994.0	20.0	0.9
GOM15_26	426	1.24	1.6940	0.0210	0.1670	0.0021	0.7064	1006.0	7.9	996.0	12.0	1051	21	996.0	12.0	1.0
GOM15_115	130.2	0.77	1.7310	0.0280	0.1676	0.0021	0.2943	1022.4	9.9	999.0	12.0	1051	36	999.0	12.0	2.3
GOM15_116	129.8	1.67	1.7400	0.0420	0.1716	0.0044	0.7217	1026.0	16.0	1020.0	24.0	1029	37	1029.0	37.0	0.9
GOM15_119	250	1.46	1.7730	0.0340	0.1730	0.0027	0.6494	1037.0	12.0	1028.0	15.0	1031	28	1031.0	28.0	0.3
GOM15_56	153.9	1.35	1.7380	0.0270	0.1683	0.0027	0.4361	1023.6	9.5	1003.0	15.0	1032	39	1032.0	39.0	2.8
GOM15_4	122.3	1.83	1.7870	0.0360	0.1761	0.0031	0.6013	1039.0	13.0	1045.0	17.0	1036	33	1036.0	33.0	0.9
GOM15_35	387	0.98	1.7740	0.0200	0.1727	0.0020	0.5559	1035.5	7.2	1027.0	11.0	1039	22	1039.0	22.0	1.2

GOM15_109	214	2.33	1.8000	0.0280	0.1747	0.0027	0.5536	1044.0	10.0	1038.0	15.0	1043	34	1043.0	34.0	0.5
GOM15_45	266.6	2.23	1.7380	0.0560	0.1726	0.0063	0.7151	1027.0	23.0	1026.0	35.0	1049	54	1049.0	54.0	2.2
GOM15_122	458	1.55	1.8320	0.0790	0.1779	0.0076	0.9224	1054.0	28.0	1053.0	41.0	1052	37	1052.0	37.0	0.1
GOM15_44	410	1.05	1.7650	0.0310	0.1728	0.0037	0.7554	1032.0	11.0	1027.0	21.0	1058	31	1058.0	31.0	2.9
GOM15_92	564	5.39	1.7660	0.0250	0.1701	0.0024	0.8175	1032.4	9.4	1013.0	13.0	1058	20	1058.0	20.0	4.3
GOM15_94	871	1.53	1.7850	0.0170	0.1727	0.0019	0.4873	1039.8	6.1	1027.0	11.0	1063	21	1063.0	21.0	3.4
GOM15_16	272.4	1.61	1.8780	0.0360	0.1811	0.0038	0.7384	1076.0	12.0	1073.0	21.0	1068	30	1068.0	30.0	0.5
GOM15_126	443	1.50	1.8600	0.0230	0.1780	0.0026	0.5853	1066.6	8.2	1055.0	14.0	1074	24	1074.0	24.0	1.8
GOM15_70	779	2.28	1.8420	0.0240	0.1761	0.0030	0.7040	1060.0	8.7	1046.0	16.0	1077	26	1077.0	26.0	2.9
GOM15_33	312.9	1.65	1.7690	0.0330	0.1690	0.0035	0.6312	1033.0	12.0	1006.0	19.0	1084	36	1084.0	36.0	7.2
GOM15_18	381	1.61	1.7930	0.0220	0.1719	0.0025	0.6600	1042.4	8.1	1024.0	14.0	1085	26	1085.0	26.0	5.6
GOM15_40	271	1.79	1.8250	0.0280	0.1754	0.0030	0.5662	1055.0	9.9	1042.0	16.0	1085	32	1085.0	32.0	4.0
GOM15_89	129	1.33	1.9140	0.0290	0.1832	0.0026	0.5521	1085.0	10.0	1084.0	14.0	1088	28	1088.0	28.0	0.4
GOM15_11	255	0.95	1.8990	0.0470	0.1820	0.0054	0.6185	1082.0	16.0	1077.0	29.0	1096	49	1096.0	49.0	1.7
GOM15_72	243.1	0.94	1.8960	0.0360	0.1803	0.0042	0.5376	1079.0	13.0	1068.0	23.0	1110	44	1110.0	44.0	3.8
GOM15_106	558	1.16	1.9270	0.0240	0.1837	0.0023	0.8712	1091.2	7.9	1087.0	13.0	1110	14	1110.0	14.0	2.1
GOM15_113	475	1.60	1.8560	0.0560	0.1770	0.0100	0.2644	1065.0	20.0	1051.0	55.0	1110	110	1110.0	110.0	5.3
GOM15_66	328	1.85	1.9930	0.0410	0.1868	0.0047	0.6055	1112.0	14.0	1107.0	25.0	1113	43	1113.0	43.0	0.5
GOM15_69	431	1.35	1.9700	0.1700	0.1840	0.0140	0.8166	1102.0	58.0	1089.0	76.0	1116	98	1116.0	98.0	2.4
GOM15_37	313	1.73	2.0120	0.0600	0.1900	0.0052	0.8597	1119.0	21.0	1121.0	28.0	1122	31	1122.0	31.0	0.1
GOM15_63	34.7	0.78	1.8490	0.0760	0.1798	0.0047	0.3076	1061.0	27.0	1066.0	26.0	1125	88	1125.0	88.0	5.2
GOM15_13	125	0.76	2.0510	0.0520	0.1925	0.0049	0.6577	1136.0	18.0	1134.0	27.0	1127	45	1127.0	45.0	0.6
GOM15_84	320	3.23	2.0770	0.0380	0.1928	0.0036	0.7471	1141.0	13.0	1136.0	19.0	1134	25	1134.0	25.0	0.2
GOM15_121	416	2.17	1.9690	0.0640	0.1822	0.0058	0.6865	1103.0	22.0	1078.0	31.0	1145	56	1145.0	56.0	5.9
GOM15_3	649	2.15	1.9630	0.0300	0.1813	0.0033	0.7321	1102.0	10.0	1074.0	18.0	1147	24	1147.0	24.0	6.4
GOM15_47	382	2.05	2.0640	0.0280	0.1913	0.0026	0.4256	1136.3	9.4	1128.0	14.0	1148	30	1148.0	30.0	1.7
GOM15_91	340	1.94	2.1100	0.0420	0.1954	0.0037	0.6901	1152.0	14.0	1150.0	20.0	1151	44	1151.0	44.0	0.1
GOM15_81	244	1.37	2.0990	0.0270	0.1939	0.0026	0.7010	1148.0	8.7	1142.0	14.0	1155	20	1155.0	20.0	1.1
GOM15_128	247	1.33	2.1800	0.0270	0.1984	0.0025	0.4858	1176.0	8.4	1167.0	13.0	1159	24	1159.0	24.0	0.7
GOM15_65	312	1.73	2.1540	0.0460	0.1990	0.0055	0.6631	1171.0	14.0	1169.0	30.0	1167	39	1167.0	39.0	0.2
GOM15_67	301.2	2.00	2.0830	0.0230	0.1905	0.0024	0.6620	1142.8	7.7	1124.0	13.0	1169	23	1169.0	23.0	3.8
GOM15_77	475	2.14	2.0580	0.0350	0.1870	0.0035	0.5995	1134.0	12.0	1105.0	19.0	1175	32	1175.0	32.0	6.0
GOM15_53	738	1.18	2.0360	0.0460	0.1849	0.0041	0.8002	1127.0	15.0	1093.0	22.0	1191	31	1191.0	31.0	8.2

GOM15_110	240.7	1.59	2.0150	0.0330	0.1828	0.0032	0.6734	1123.0	11.0	1082.0	17.0	1202	30	1202.0	30.0	10.0
GOM15_112	293.6	0.48	2.1420	0.0460	0.1974	0.0056	0.7791	1173.0	18.0	1161.0	30.0	1202	39	1202.0	39.0	3.4
GOM15_111	227	1.53	2.1860	0.0480	0.1993	0.0036	0.6144	1176.0	15.0	1172.0	19.0	1203	35	1203.0	35.0	2.6
GOM15_25	111.2	1.68	2.2660	0.0500	0.2047	0.0042	0.5267	1200.0	15.0	1200.0	22.0	1212	42	1212.0	42.0	1.0
GOM15_54	152	1.38	2.1330	0.0480	0.1936	0.0041	0.6267	1158.0	16.0	1141.0	22.0	1215	34	1215.0	34.0	6.1
GOM15_107	212	2.26	2.3460	0.0370	0.2114	0.0035	0.5939	1228.0	12.0	1239.0	18.0	1218	26	1218.0	26.0	1.7
GOM15_21	255.6	1.33	2.2470	0.0270	0.2020	0.0026	0.5992	1195.4	8.4	1186.0	14.0	1222	21	1222.0	21.0	2.9
GOM15_32	222	1.83	2.2450	0.0410	0.2021	0.0036	0.7308	1197.0	13.0	1186.0	19.0	1227	29	1227.0	29.0	3.3
GOM15_80	354	1.79	2.3360	0.0310	0.2062	0.0029	0.6389	1222.7	9.3	1208.0	16.0	1235	22	1235.0	22.0	2.2
GOM15_49	1181	1.64	2.2570	0.0240	0.1993	0.0024	0.6531	1198.5	7.5	1172.0	13.0	1241	17	1241.0	17.0	5.6
GOM15_93	363	1.82	2.2480	0.0410	0.1977	0.0030	0.7016	1197.0	13.0	1163.0	16.0	1254	25	1254.0	25.0	7.3
GOM15_76	149.1	0.55	2.3370	0.0640	0.2045	0.0050	0.6127	1222.0	19.0	1199.0	27.0	1256	45	1256.0	45.0	4.5
GOM15_9	485	4.68	2.3730	0.0360	0.2070	0.0031	0.6609	1234.0	11.0	1212.0	17.0	1261	23	1261.0	23.0	3.9
GOM15_68	406	2.06	2.3890	0.0270	0.2087	0.0026	0.5246	1240.3	8.4	1222.0	14.0	1276	23	1276.0	23.0	4.2
GOM15_86	400	5.05	2.4930	0.0630	0.2138	0.0051	0.7905	1267.0	18.0	1252.0	28.0	1283	25	1283.0	25.0	2.4
GOM15_118	397	1.62	2.6140	0.0460	0.2242	0.0044	0.8186	1306.0	13.0	1303.0	23.0	1304	23	1304.0	23.0	0.1
GOM15_52	92.8	1.41	2.9000	0.1400	0.2419	0.0082	0.4706	1380.0	36.0	1396.0	42.0	1345	66	1345.0	66.0	3.8
GOM15_103	123.7	0.95	2.5870	0.0680	0.2166	0.0051	0.5048	1296.0	19.0	1263.0	27.0	1350	50	1350.0	50.0	6.4
GOM15_2	184	1.31	2.7680	0.0840	0.2259	0.0071	0.2423	1345.0	23.0	1312.0	37.0	1369	52	1369.0	52.0	4.2
GOM15_29	96.3	1.70	2.8020	0.0490	0.2322	0.0048	0.5727	1355.0	13.0	1345.0	25.0	1373	32	1373.0	32.0	2.0
GOM15_39	501	4.09	2.7840	0.0530	0.2284	0.0054	0.7429	1353.0	14.0	1325.0	28.0	1388	34	1388.0	34.0	4.5
GOM15_55	867	36.00	2.8800	0.1300	0.2287	0.0087	0.8247	1379.0	32.0	1338.0	50.0	1423	52	1423.0	52.0	6.0
GOM15_58	270	1.35	3.1250	0.0390	0.2503	0.0036	0.5162	1438.3	9.6	1440.0	19.0	1439	24	1439.0	24.0	0.1
GOM15_90	977	1.06	2.9390	0.0250	0.2324	0.0024	0.3336	1392.0	6.5	1347.0	13.0	1440	27	1440.0	27.0	6.5
GOM15_75	260	1.48	3.1960	0.0570	0.2490	0.0052	0.6275	1454.0	14.0	1432.0	27.0	1442	31	1442.0	31.0	0.7
GOM15_23	124.1	1.44	2.9750	0.0640	0.2359	0.0056	0.4502	1400.0	16.0	1365.0	29.0	1444	50	1444.0	50.0	5.5
GOM15_41	321	1.67	3.0110	0.0560	0.2376	0.0056	0.7963	1410.0	14.0	1373.0	29.0	1451	25	1451.0	25.0	5.4
GOM15_27	446	1.02	3.0210	0.0380	0.2409	0.0034	0.6415	1412.2	9.4	1391.0	17.0	1458	23	1458.0	23.0	4.6
GOM15_64	348	1.32	3.0700	0.0600	0.2346	0.0043	0.4415	1424.0	15.0	1358.0	23.0	1486	37	1486.0	37.0	8.6
GOM15_71	224	1.62	3.2200	0.0710	0.2485	0.0057	0.7090	1461.0	17.0	1430.0	29.0	1494	34	1494.0	34.0	4.3
GOM15_83	817	3.09	3.2100	0.2900	0.2390	0.0190	0.8644	1459.0	70.0	1381.0	98.0	1585	64	1585.0	64.0	12.9
GOM15_95	96	1.15	3.8440	0.0750	0.2740	0.0063	0.6043	1601.0	16.0	1560.0	32.0	1637	37	1637.0	37.0	4.7
GOM15_5	135.5	0.88	3.9620	0.0560	0.2817	0.0035	0.5169	1626.0	11.0	1600.0	18.0	1659	25	1659.0	25.0	3.6

GOM15_50	186	1.21	4.2480	0.0630	0.2974	0.0052	0.6809	1683.0	12.0	1678.0	26.0	1676	26	1676.0	26.0	0.1
GOM15_10	140.6	0.85	4.0840	0.0630	0.2872	0.0047	0.6888	1652.0	12.0	1627.0	23.0	1685	23	1685.0	23.0	3.4
GOM15_14	206	1.04	4.5030	0.0970	0.3055	0.0080	0.7863	1729.0	18.0	1723.0	40.0	1732	32	1732.0	32.0	0.5
GOM15_20	339	1.02	4.6350	0.0940	0.3114	0.0077	0.6388	1755.0	17.0	1747.0	38.0	1764	38	1764.0	38.0	1.0
GOM15_82	235.6	1.63	4.6520	0.0680	0.3077	0.0062	0.6444	1758.0	12.0	1729.0	30.0	1772	29	1772.0	29.0	2.4
GOM15_108	599	2.37	4.7700	0.1100	0.3111	0.0066	0.7201	1780.0	18.0	1744.0	32.0	1791	29	1791.0	29.0	2.6
GOM15_22	141.6	0.69	4.4600	0.1600	0.2940	0.0110	0.8034	1727.0	31.0	1668.0	58.0	1812	38	1812.0	38.0	7.9
GOM15_62	159.3	1.09	4.9060	0.0740	0.3170	0.0054	0.5886	1804.0	12.0	1774.0	26.0	1838	26	1838.0	26.0	3.5
GOM15_96	254.1	2.75	4.6100	0.0550	0.2989	0.0038	0.4928	1750.9	9.9	1686.0	19.0	1842	20	1842.0	20.0	8.5
GOM15_38	222.9	0.89	4.8000	0.0690	0.3101	0.0052	0.5875	1784.0	12.0	1741.0	26.0	1843	26	1843.0	26.0	5.5
GOM15_102	451.7	1.25	21.3300	0.3300	0.5910	0.0120	0.6511	3153.0	15.0	2993.0	48.0	3254	23	3254.0	23.0	8.0

Sample:GOM16	Isotopic Ratios							Isotopic ages (Ma)								
Analysis	[U] ppm	U/Th	207/235	2σ err.	206/238	2σ err.	RHO	207/235	2σ err.	206/238	2σ err.	207/206	2σ err.	Best age	2σ err.	% Dis.
GOM16_51	247	0.75	0.0878	0.0035	0.0133	0.0004	0.2669	85.4	3.3	84.9	2.2	100	81	84.9	2.2	0.6
GOM16_71	291	11.12	0.3543	0.0052	0.0476	0.0006	0.1672	307.8	3.9	299.9	3.6	361	42	299.9	3.6	2.6
GOM16_32	241.9	9.49	0.3576	0.0063	0.0491	0.0006	0.1126	310.2	4.7	308.8	3.4	315	45	308.8	3.4	0.5
GOM16_48	263	0.86	0.3843	0.0064	0.0519	0.0005	0.0992	330.0	4.7	326.4	3.3	356	39	326.4	3.3	1.1
GOM16_116	450	6.34	0.3899	0.0056	0.0534	0.0006	0.4104	334.2	4.1	335.4	3.4	326	31	335.4	3.4	0.4
GOM16_87	573	52.00	0.4040	0.0360	0.0540	0.0024	0.9312	344.0	26.0	339.0	15.0	325	83	339.0	15.0	1.5
GOM16_62	238.4	12.25	0.4320	0.0062	0.0585	0.0007	0.2807	364.4	4.4	366.5	4.2	363	38	366.5	4.2	0.6
GOM16_102	151	1.95	0.4510	0.0150	0.0603	0.0014	0.7158	377.0	10.0	377.3	8.6	401	47	377.3	8.6	0.1
GOM16_42	127.1	3.78	0.5100	0.0120	0.0660	0.0010	0.2691	418.0	8.0	412.1	5.8	456	47	412.1	5.8	1.4
GOM16_94	85.4	0.88	0.4970	0.0140	0.0662	0.0013	0.0791	408.7	9.9	413.3	7.6	399	70	413.3	7.6	1.1
GOM16_26	173.9	1.24	0.5250	0.0200	0.0680	0.0015	0.5048	428.0	13.0	423.8	9.2	440	56	423.8	9.2	1.0
GOM16_22	119	0.87	0.5170	0.0110	0.0681	0.0011	0.0798	422.9	7.4	424.7	6.8	421	56	424.7	6.8	0.4
GOM16_43	507	0.92	0.5260	0.0071	0.0684	0.0006	0.4845	428.9	4.7	426.7	3.5	456	27	426.7	3.5	0.5
GOM16_7	296	3.01	0.5260	0.0200	0.0688	0.0021	0.8659	429.0	13.0	429.0	13.0	442	34	429.0	13.0	0.0
GOM16_38	60	1.30	0.5290	0.0200	0.0696	0.0014	0.4182	430.0	13.0	433.4	8.4	420	74	433.4	8.4	0.8
GOM16_6	97	1.30	0.5350	0.0140	0.0697	0.0011	0.3931	434.5	9.5	434.2	6.6	412	58	434.2	6.6	0.1
GOM16_65	594	1.03	0.5369	0.0063	0.0697	0.0007	0.5804	437.1	4.4	434.6	4.4	444	23	434.6	4.4	0.6

GOM16_113	21.76	1.50	0.5500	0.0460	0.0718	0.0044	0.1442	443.0	30.0	447.0	26.0	430	210	447.0	26.0	0.9
GOM16_100	131.2	1.39	0.5660	0.0120	0.0732	0.0009	0.1520	455.1	7.7	455.1	5.1	466	50	455.1	5.1	0.0
GOM16_54	353.4	14.03	0.5704	0.0084	0.0734	0.0007	0.3886	458.0	5.4	456.7	3.9	474	30	456.7	3.9	0.3
GOM16_30	170.3	0.63	0.5650	0.0120	0.0739	0.0018	0.1485	454.5	7.8	459.0	11.0	467	78	459.0	11.0	1.0
GOM16_23	49	0.66	0.6180	0.0200	0.0797	0.0017	0.0917	489.0	12.0	494.0	10.0	459	83	494.0	10.0	1.0
GOM16_85	649	32.00	0.6740	0.0660	0.0835	0.0058	0.9261	521.0	40.0	517.0	34.0	551	99	517.0	34.0	0.8
GOM16_97	272	1.32	0.8650	0.0140	0.1032	0.0009	0.5055	632.2	7.7	633.1	5.4	655	32	633.1	5.4	0.1
GOM16_66	253.3	1.44	1.0200	0.0140	0.1150	0.0014	0.6781	714.6	7.3	701.4	8.2	740	28	701.4	8.2	1.8
GOM16_25	46	2.57	1.0970	0.0400	0.1224	0.0029	0.5788	754.0	19.0	744.0	17.0	788	55	744.0	17.0	1.3
GOM16_101	14	0.73	1.4740	0.0590	0.1486	0.0047	0.5440	924.0	26.0	892.0	27.0	980	71	892.0	27.0	3.5
GOM16_110	15.22	1.33	1.4440	0.0610	0.1511	0.0045	0.1568	904.0	26.0	907.0	25.0	910	120	907.0	25.0	0.3
GOM16_15	45	5.90	1.4900	0.0390	0.1515	0.0031	0.1868	924.0	16.0	912.0	18.0	969	54	912.0	18.0	1.3
GOM16_11	51.2	1.27	1.4990	0.0320	0.1525	0.0022	0.0979	929.0	13.0	915.0	12.0	971	55	915.0	12.0	1.5
GOM16_123	238.7	3.88	1.6040	0.0280	0.1528	0.0030	0.6999	971.0	11.0	916.0	17.0	1084	27	916.0	17.0	5.7
GOM16_8	48.02	0.94	1.5350	0.0580	0.1530	0.0040	0.0500	943.0	23.0	917.0	23.0	990	120	917.0	23.0	2.8
GOM16_64	140.1	0.52	1.5910	0.0220	0.1561	0.0016	0.5266	966.3	8.6	935.1	9.1	1015	30	935.1	9.1	3.2
GOM16_10	82	1.38	1.5760	0.0270	0.1573	0.0015	0.2765	960.0	11.0	941.7	8.2	993	37	941.7	8.2	1.9
GOM16_44	113.7	1.52	1.5390	0.0240	0.1583	0.0014	0.0926	945.3	9.5	947.2	7.7	965	35	947.2	7.7	0.2
GOM16_63	66.1	0.66	1.5730	0.0290	0.1585	0.0018	0.1474	958.0	11.0	948.0	10.0	987	43	948.0	10.0	1.0
GOM16_53	39.7	1.43	1.5570	0.0760	0.1587	0.0095	0.0320	952.0	30.0	949.0	53.0	910	180	949.0	53.0	0.3
GOM16_37	34.14	0.71	1.6040	0.0650	0.1589	0.0040	0.0340	980.0	25.0	950.0	22.0	1044	98	950.0	22.0	3.1
GOM16_57	28.6	1.29	1.5950	0.0460	0.1593	0.0030	0.2575	966.0	18.0	952.0	16.0	1007	60	952.0	16.0	1.4
GOM16_92	62.1	0.81	1.5880	0.0280	0.1603	0.0024	0.1771	966.0	11.0	958.0	13.0	997	37	958.0	13.0	0.8
GOM16_58	74.7	2.12	1.6100	0.0210	0.1605	0.0018	0.2809	973.6	8.1	959.6	9.9	1010	34	959.6	9.9	1.4
GOM16_52	56.1	1.59	1.6510	0.0260	0.1611	0.0020	0.3136	990.0	10.0	963.0	11.0	1049	34	963.0	11.0	2.7
GOM16_19	42.2	1.15	1.6110	0.0320	0.1620	0.0020	0.3277	977.0	13.0	968.0	11.0	994	42	968.0	11.0	0.9
GOM16_49	57.2	1.64	1.6270	0.0300	0.1627	0.0022	0.4049	979.0	12.0	971.0	12.0	1013	36	971.0	12.0	0.8
GOM16_73	239	1.26	1.6420	0.0200	0.1626	0.0012	0.1821	987.5	7.4	971.3	6.8	1012	27	971.3	6.8	1.6
GOM16_35	12.77	1.73	1.5940	0.0600	0.1631	0.0039	0.0742	972.0	23.0	973.0	21.0	937	88	973.0	21.0	0.1
GOM16_112	34.5	2.03	1.6070	0.0430	0.1628	0.0023	0.0903	973.0	17.0	974.0	13.0	969	57	974.0	13.0	0.1
GOM16_115	161	1.28	1.6370	0.0180	0.1632	0.0018	0.3910	985.1	6.8	974.7	9.8	1011	27	974.7	9.8	1.1
GOM16_4	116.5	2.27	1.6890	0.0210	0.1645	0.0018	0.2957	1003.8	8.0	982.0	10.0	1056	29	982.0	10.0	2.2
GOM16_87	228	2.40	1.6610	0.0180	0.1653	0.0016	0.3316	993.5	6.8	986.3	9.0	1027	25	986.3	9.0	0.7

GOM16_2	196.9	1.88	1.6910	0.0160	0.1660	0.0016	0.5815	1005.7	6.0	990.0	8.7	1041	15	990.0	8.7	1.6
GOM16_45	479	3.45	1.6860	0.0150	0.1662	0.0012	0.7140	1003.1	5.5	990.9	6.6	1038	14	990.9	6.6	1.2
GOM16_3	34.4	1.25	1.6650	0.0380	0.1674	0.0029	0.2818	996.0	14.0	997.0	16.0	1008	56	997.0	16.0	0.1
GOM16_109	88.2	0.94	1.6970	0.0250	0.1682	0.0017	0.3264	1007.9	9.5	1001.8	9.6	1007	32	1007.0	32.0	0.5
GOM16_76	141	1.83	1.7550	0.0210	0.1740	0.0017	0.3871	1029.5	7.9	1034.2	9.4	1013	23	1013.0	23.0	2.1
GOM16_95	314	1.55	1.6990	0.0200	0.1698	0.0018	0.5565	1007.8	7.3	1011.0	10.0	1017	20	1017.0	20.0	0.6
GOM16_17	197	2.77	1.7250	0.0180	0.1696	0.0020	0.0707	1018.5	6.8	1010.0	11.0	1026	21	1026.0	21.0	1.6
GOM16_72	118.1	3.32	1.7510	0.0240	0.1713	0.0017	0.3641	1027.0	8.7	1020.1	9.8	1028	30	1028.0	30.0	0.8
GOM16_5	116	1.68	1.7130	0.0240	0.1685	0.0017	0.6155	1014.2	9.4	1003.8	9.2	1029	27	1029.0	27.0	2.4
GOM16_93	190	1.28	1.7480	0.0180	0.1733	0.0013	0.1602	1026.9	6.7	1030.4	7.2	1029	26	1029.0	26.0	0.1
GOM16_46	70.7	1.30	1.7140	0.0330	0.1697	0.0022	0.2402	1013.0	12.0	1010.0	12.0	1032	38	1032.0	38.0	2.1
GOM16_20	256	3.19	1.7190	0.0120	0.1693	0.0010	0.1833	1015.5	4.5	1008.3	5.7	1035	16	1035.0	16.0	2.6
GOM16_67	167.7	1.78	1.7970	0.0190	0.1770	0.0015	0.2870	1044.0	6.8	1050.2	8.0	1036	24	1036.0	24.0	1.4
GOM16_119	105.9	1.67	1.7580	0.0250	0.1726	0.0016	0.3454	1029.3	9.2	1026.2	9.0	1036	30	1036.0	30.0	0.9
GOM16_13	320	2.01	1.7160	0.0170	0.1682	0.0017	0.5185	1014.4	6.2	1001.8	9.5	1043	20	1043.0	20.0	4.0
GOM16_74	230	6.64	1.8170	0.0290	0.1774	0.0019	0.7412	1051.0	10.0	1053.0	10.0	1044	20	1044.0	20.0	0.9
GOM16_114	458	1.27	1.8100	0.0120	0.1771	0.0009	0.3503	1049.0	4.2	1051.0	5.0	1045	14	1045.0	14.0	0.6
GOM16_55	215.4	2.07	1.8130	0.0180	0.1777	0.0013	0.2306	1049.8	6.4	1054.5	7.2	1046	23	1046.0	23.0	0.8
GOM16_84	102.8	2.33	1.7220	0.0240	0.1679	0.0017	0.3560	1015.9	9.0	1001.4	9.4	1051	29	1051.0	29.0	4.7
GOM16_18	395	2.66	1.7660	0.0140	0.1717	0.0014	0.4628	1032.8	5.1	1022.2	7.4	1052	16	1052.0	16.0	2.8
GOM16_85	109.8	1.01	1.7730	0.0300	0.1734	0.0021	0.2809	1037.0	11.0	1031.0	12.0	1052	29	1052.0	29.0	2.0
GOM16_128	165	1.89	1.7720	0.0180	0.1710	0.0015	0.1325	1034.7	6.7	1017.7	8.0	1052	23	1052.0	23.0	3.3
GOM16_39	175	1.33	1.8040	0.0260	0.1750	0.0019	0.5641	1046.1	9.2	1039.0	10.0	1064	23	1064.0	23.0	2.3
GOM16_125	69	1.35	1.8360	0.0270	0.1753	0.0018	0.1183	1057.6	9.5	1041.0	10.0	1068	34	1068.0	34.0	2.5
GOM16_60	179	9.40	1.7800	0.0350	0.1720	0.0026	0.7374	1037.0	13.0	1023.0	14.0	1074	24	1074.0	24.0	4.7
GOM16_111	138	1.13	1.8680	0.0280	0.1787	0.0022	0.2559	1068.8	9.8	1060.0	12.0	1079	32	1079.0	32.0	1.8
GOM16_12	29.4	1.15	1.7480	0.0590	0.1683	0.0042	0.4453	1024.0	22.0	1002.0	23.0	1084	65	1084.0	65.0	7.6
GOM16_14	363	13.50	1.7700	0.0570	0.1690	0.0044	0.8170	1032.0	20.0	1006.0	24.0	1086	32	1086.0	32.0	7.4
GOM16_86	39.8	1.13	1.7700	0.0390	0.1709	0.0028	0.1851	1038.0	14.0	1019.0	16.0	1087	49	1087.0	49.0	6.3
GOM16_90	485	6.18	1.7730	0.0180	0.1700	0.0017	0.7016	1036.0	6.6	1012.2	9.1	1092	16	1092.0	16.0	7.3
GOM16_121	103	1.75	2.0230	0.0360	0.1906	0.0027	0.6832	1122.0	12.0	1124.0	14.0	1105	24	1105.0	24.0	1.7
GOM16_27	126	0.99	1.9070	0.0230	0.1803	0.0018	0.2902	1084.1	8.0	1068.3	9.7	1109	26	1109.0	26.0	3.7
GOM16_9	114	1.85	1.9860	0.0210	0.1893	0.0019	0.3223	1112.3	7.5	1117.0	10.0	1110	23	1110.0	23.0	0.6

GOM16_24	250	3.02	1.9690	0.0380	0.1862	0.0025	0.7571	1107.0	13.0	1101.0	14.0	1117	23	1117.0	23.0	1.4
GOM16_70	39.8	2.71	2.0340	0.0550	0.1930	0.0034	0.3016	1127.0	19.0	1137.0	18.0	1127	57	1127.0	57.0	0.9
GOM16_41	143	1.72	1.9560	0.0220	0.1837	0.0016	0.3311	1101.2	7.8	1087.3	8.9	1128	23	1128.0	23.0	3.6
GOM16_79	120.7	2.24	1.9610	0.0260	0.1845	0.0021	0.4250	1101.6	8.9	1091.0	12.0	1137	28	1137.0	28.0	4.0
GOM16_118	46.2	1.90	2.0760	0.0340	0.1933	0.0026	0.5254	1140.0	11.0	1139.0	14.0	1141	31	1141.0	31.0	0.2
GOM16_1	33.7	0.40	1.9220	0.0410	0.1782	0.0025	0.3828	1087.0	14.0	1057.0	13.0	1143	42	1143.0	42.0	7.5
GOM16_40	27.64	1.66	1.9290	0.0440	0.1785	0.0033	0.2899	1089.0	15.0	1059.0	18.0	1143	49	1143.0	49.0	7.3
GOM16_75	30.6	2.44	1.9360	0.0660	0.1820	0.0053	0.7680	1089.0	22.0	1077.0	29.0	1144	47	1144.0	47.0	5.9
GOM16_82	406	1.59	1.9160	0.0250	0.1781	0.0022	0.7024	1086.3	8.6	1057.0	12.0	1153	18	1153.0	18.0	8.3
GOM16_103	173	2.07	2.1200	0.0230	0.1971	0.0015	0.4702	1155.7	7.6	1159.4	8.0	1154	22	1154.0	22.0	0.5
GOM16_83	260	1.10	2.0570	0.0210	0.1915	0.0018	0.4442	1134.2	7.1	1129.3	9.8	1156	19	1156.0	19.0	2.3
GOM16_105	26.3	0.69	2.1500	0.0590	0.1998	0.0031	0.3071	1162.0	19.0	1174.0	17.0	1157	52	1157.0	52.0	1.5
GOM16_78	122.8	1.28	2.0800	0.0300	0.1934	0.0019	0.3733	1141.6	9.7	1140.0	10.0	1158	27	1158.0	27.0	1.6
GOM16_47	218	1.84	1.9630	0.0280	0.1814	0.0023	0.7272	1102.3	9.6	1075.0	13.0	1159	20	1159.0	20.0	7.2
GOM16_21	199	2.78	2.1300	0.0210	0.1948	0.0017	0.4839	1158.2	6.7	1147.3	9.3	1165	18	1165.0	18.0	1.5
GOM16_122	131.2	1.60	2.0800	0.0210	0.1901	0.0016	0.4271	1141.7	7.1	1121.6	8.7	1166	21	1166.0	21.0	3.8
GOM16_106	69.3	1.20	2.0310	0.0340	0.1883	0.0026	0.2425	1125.0	11.0	1112.0	14.0	1178	36	1178.0	36.0	5.6
GOM16_107	37.6	0.76	2.1360	0.0400	0.1943	0.0026	0.0222	1161.0	13.0	1144.0	14.0	1179	45	1179.0	45.0	3.0
GOM16_126	15.07	1.29	2.2390	0.0920	0.2024	0.0053	0.3202	1192.0	28.0	1197.0	29.0	1185	83	1185.0	83.0	1.0
GOM16_108	223	1.17	2.2490	0.0370	0.2055	0.0029	0.8299	1198.0	12.0	1205.0	15.0	1192	27	1192.0	27.0	1.1
GOM16_16	328.1	2.31	2.1320	0.0170	0.1932	0.0011	0.4958	1159.9	5.2	1138.8	6.0	1193	15	1193.0	15.0	4.5
GOM16_99	149.1	4.69	2.2750	0.0360	0.2065	0.0033	0.8237	1204.0	11.0	1210.0	17.0	1200	21	1200.0	21.0	0.8
GOM16_91	38.3	2.30	2.0950	0.0610	0.1891	0.0061	0.6546	1147.0	21.0	1115.0	33.0	1202	53	1202.0	53.0	7.2
GOM16_31	54.9	1.29	2.1550	0.0380	0.1938	0.0029	0.1763	1167.0	12.0	1141.0	16.0	1203	42	1203.0	42.0	5.2
GOM16_34	143.1	1.12	1.9590	0.0640	0.1780	0.0032	0.3212	1101.0	22.0	1056.0	18.0	1204	66	1204.0	66.0	12.3
GOM16_68	91.1	1.45	2.3110	0.0350	0.2071	0.0023	0.1740	1215.0	11.0	1213.0	12.0	1213	37	1213.0	37.0	0.0
GOM16_80	310	0.83	2.1350	0.0290	0.1925	0.0017	0.6917	1159.9	9.5	1135.0	9.4	1213	19	1213.0	19.0	6.4
GOM16_96	49.3	1.47	2.2260	0.0350	0.2022	0.0025	0.2423	1190.0	11.0	1187.0	14.0	1214	36	1214.0	36.0	2.2
GOM16_89	57.4	2.49	2.1820	0.0310	0.1964	0.0027	0.2505	1174.0	10.0	1156.0	14.0	1223	33	1223.0	33.0	5.5
GOM16_81	113.8	1.58	2.3400	0.0260	0.2101	0.0019	0.3084	1226.3	7.5	1229.4	9.9	1224	23	1224.0	23.0	0.4
GOM16_104	160.8	4.12	2.3690	0.0290	0.2131	0.0021	0.4875	1232.6	8.7	1245.0	11.0	1224	21	1224.0	21.0	1.7
GOM16_50	172	2.39	2.2660	0.0280	0.2019	0.0020	0.4761	1201.1	8.7	1186.0	11.0	1234	23	1234.0	23.0	3.9
GOM16_28	120	1.35	2.2140	0.0310	0.1955	0.0023	0.4810	1184.9	9.9	1151.0	13.0	1250	29	1250.0	29.0	7.9

GOM16_88	70	1.53	2.2210	0.0460	0.1973	0.0033	0.3929	1188.0	15.0	1161.0	18.0	1252	40	1252.0	40.0	7.3
GOM16_69	131.1	1.47	2.3970	0.0410	0.2075	0.0032	0.5751	1243.0	13.0	1215.0	17.0	1284	32	1284.0	32.0	5.4
GOM16_127	83.3	0.48	2.6620	0.0380	0.2288	0.0026	0.2352	1317.0	11.0	1330.0	14.0	1285	30	1285.0	30.0	3.5
GOM16_116	146.3	2.66	2.3700	0.1500	0.2060	0.0094	0.7535	1229.0	46.0	1207.0	50.0	1302	61	1302.0	61.0	7.3
GOM16_36	95.3	1.99	2.2150	0.0590	0.1873	0.0037	0.7047	1185.0	19.0	1106.0	20.0	1355	48	1355.0	48.0	18.4
GOM16_59	127.9	1.80	2.8220	0.0270	0.2326	0.0020	0.4947	1361.0	7.0	1348.0	10.0	1383	18	1383.0	18.0	2.5
GOM16_120	14.5	0.63	3.0140	0.0780	0.2415	0.0052	0.2902	1410.0	20.0	1393.0	27.0	1438	56	1438.0	56.0	3.1
GOM16_33	165.8	1.65	3.1280	0.0390	0.2453	0.0025	0.6711	1438.8	9.6	1416.0	13.0	1477	18	1477.0	18.0	4.1
GOM16_124	155.8	0.71	3.2530	0.0300	0.2535	0.0021	0.5532	1469.4	7.2	1457.0	11.0	1479	17	1479.0	17.0	1.5

Sample:GOM17	Isotopic Ratios							Isotopic ages (Ma)								
Analysis	[U] ppm	U/Th	207/235	2σ err.	206/238	2σ err.	RHO	207/235	2σ err.	206/238	2σ err.	207/206	2σ err.	Best age	2σ err.	% Dis.
GOM17_11	449.1	1.86	0.0216	0.0011	0.0031	0.0001	0.0442	21.7	1.1	19.8	0.5	240	120	19.8	0.5	8.9
GOM17_70	139.5	1.11	0.2036	0.0077	0.0295	0.0007	0.3298	189.1	6.7	187.1	4.4	183	77	187.1	4.4	1.1
GOM17_63	197.5	31.20	0.3910	0.0170	0.0516	0.0037	0.6097	335.0	12.0	324.0	23.0	360	230	324.0	23.0	3.3
GOM17_85	598	16.60	0.3890	0.0300	0.0518	0.0010	0.0285	334.0	22.0	325.4	5.9	370	200	325.4	5.9	2.6
GOM17_114	369	97.00	0.3860	0.0140	0.0520	0.0010	0.6291	331.0	10.0	326.7	6.1	349	70	326.7	6.1	1.3
GOM17_84	318	6.07	0.3870	0.0150	0.0523	0.0008	0.0047	332.0	11.0	328.3	4.7	326	98	328.3	4.7	1.1
GOM17_107	326.3	47.00	0.4460	0.0460	0.0555	0.0040	0.8707	373.0	32.0	348.0	24.0	490	120	348.0	24.0	6.7
GOM17_115	71.7	1.52	0.4210	0.0130	0.0557	0.0009	0.0307	356.4	9.5	349.5	5.6	365	81	349.5	5.6	1.9
GOM17_92	135.6	0.60	0.4190	0.0120	0.0563	0.0010	0.5095	355.1	8.3	352.8	6.1	369	54	352.8	6.1	0.6
GOM17_41	344.5	3.05	0.4193	0.0056	0.0565	0.0006	0.3856	356.0	3.9	354.3	3.7	350	26	354.3	3.7	0.5
GOM17_64	1030	238.40	0.4260	0.0051	0.0569	0.0006	0.5756	360.2	3.7	356.7	3.9	367	24	356.7	3.9	1.0
GOM17_71	139	3.53	0.4196	0.0084	0.0569	0.0006	0.0868	355.5	6.0	356.8	3.8	346	55	356.8	3.8	0.4
GOM17_12	89.5	1.03	0.4170	0.0097	0.0571	0.0009	0.2615	354.6	7.2	357.6	5.3	337	52	357.6	5.3	0.8
GOM17_111	193.4	3.75	0.4190	0.0078	0.0571	0.0006	0.1685	355.9	5.4	357.7	3.5	352	42	357.7	3.5	0.5
GOM17_65	133.6	1.01	0.4200	0.0110	0.0575	0.0010	0.2318	355.5	7.6	360.1	5.8	341	61	360.1	5.8	1.3
GOM17_30	343	18.60	0.4370	0.0210	0.0576	0.0025	0.2694	368.0	15.0	361.0	15.0	370	130	361.0	15.0	1.9
GOM17_7	482	8.82	0.4336	0.0043	0.0577	0.0005	0.4121	365.6	3.0	361.3	3.2	382	23	361.3	3.2	1.2
GOM17_118	167.7	22.70	0.4590	0.0530	0.0599	0.0045	0.9010	382.0	37.0	375.0	27.0	410	130	375.0	27.0	1.8
GOM17_52	219	68.40	0.4750	0.0130	0.0627	0.0011	0.5750	394.7	9.0	392.1	6.8	406	64	392.1	6.8	0.7

GOM17_60	163	2.62	0.4850	0.0130	0.0637	0.0014	0.5683	400.9	8.9	397.8	8.7	435	46	397.8	8.7	0.8
GOM17_103	22.15	0.51	0.4920	0.0340	0.0641	0.0037	0.0772	404.0	23.0	400.0	22.0	430	170	400.0	22.0	1.0
GOM17_44	78.6	0.62	0.5000	0.0120	0.0653	0.0009	0.1067	412.1	8.5	407.6	5.5	411	65	407.6	5.5	1.1
GOM17_87	222	7.20	0.5170	0.0150	0.0685	0.0018	0.7495	422.0	10.0	427.0	11.0	403	35	427.0	11.0	1.2
GOM17_22	122.8	0.71	0.5340	0.0086	0.0687	0.0008	0.0114	434.2	5.7	428.1	5.1	460	46	428.1	5.1	1.4
GOM17_10	81.1	1.22	0.5300	0.0210	0.0694	0.0015	0.2480	431.0	14.0	432.2	9.0	410	100	432.2	9.0	0.3
GOM17_50	65.3	0.95	0.5410	0.0280	0.0695	0.0018	0.1733	438.0	18.0	433.0	11.0	440	140	433.0	11.0	1.1
GOM17_53	329.9	11.31	0.5420	0.0110	0.0698	0.0012	0.1266	439.9	7.3	434.9	7.0	473	76	434.9	7.0	1.1
GOM17_9	251	1.24	0.5410	0.0120	0.0699	0.0013	0.6189	439.1	7.8	435.7	7.8	454	42	435.7	7.8	0.8
GOM17_76	395	0.97	0.5407	0.0072	0.0703	0.0007	0.3702	438.7	4.8	438.1	3.9	430	33	438.1	3.9	0.1
GOM17_67	215	1.05	0.5458	0.0090	0.0706	0.0010	0.2631	441.9	5.9	440.0	6.0	466	39	440.0	6.0	0.4
GOM17_17	189	0.86	0.5481	0.0081	0.0713	0.0007	0.1859	443.5	5.3	443.8	4.2	450	37	443.8	4.2	0.1
GOM17_105	387	2.31	0.5560	0.0120	0.0714	0.0008	0.0518	448.4	7.7	444.7	4.9	463	51	444.7	4.9	0.8
GOM17_91	455	11.50	0.5510	0.0150	0.0718	0.0029	0.6806	445.7	9.8	447.0	17.0	482	58	447.0	17.0	0.3
GOM17_82	689	51.40	0.5700	0.0330	0.0721	0.0022	0.1517	458.0	21.0	449.0	13.0	450	130	449.0	13.0	2.0
GOM17_61	80.4	0.50	0.5570	0.0140	0.0723	0.0010	0.1477	448.8	9.2	449.7	6.0	449	67	449.7	6.0	0.2
GOM17_46	152	1.77	0.5680	0.0130	0.0726	0.0012	0.4070	456.3	8.2	451.9	7.3	481	44	451.9	7.3	1.0
GOM17_57	61.7	2.59	0.5630	0.0170	0.0732	0.0011	0.1960	454.0	10.0	455.4	6.8	452	69	455.4	6.8	0.3
GOM17_77	55.4	3.14	0.5700	0.0160	0.0734	0.0013	0.1756	459.0	10.0	456.4	8.0	461	71	456.4	8.0	0.6
GOM17_3	222.9	23.90	0.5850	0.0200	0.0742	0.0016	0.0473	470.0	13.0	461.4	9.8	482	65	461.4	9.8	1.8
GOM17_120	141.1	1.81	0.5720	0.0110	0.0747	0.0010	0.3785	460.1	7.6	464.4	6.1	439	42	464.4	6.1	0.9
GOM17_37	183.7	2.18	0.5870	0.0280	0.0750	0.0020	0.2586	468.0	18.0	466.0	12.0	434	95	466.0	12.0	0.4
GOM17_100	296	45.10	0.6090	0.0140	0.0772	0.0019	0.2957	482.6	8.9	480.0	11.0	454	52	480.0	11.0	0.5
GOM17_94	466	31.50	0.6390	0.0290	0.0805	0.0047	0.7587	501.0	18.0	499.0	28.0	528	92	499.0	28.0	0.4
GOM17_93	690	31.50	0.6700	0.1000	0.0811	0.0073	0.9555	519.0	60.0	502.0	44.0	540	140	502.0	44.0	3.3
GOM17_27	960	31.50	0.6580	0.0320	0.0811	0.0038	0.9109	513.0	19.0	503.0	23.0	527	33	503.0	23.0	1.9
GOM17_124	451	24.20	0.6640	0.0330	0.0828	0.0041	0.7763	517.0	20.0	513.0	24.0	560	130	513.0	24.0	0.8
GOM17_99	811	12.20	0.6840	0.0160	0.0835	0.0014	0.5342	529.1	9.8	517.1	8.6	523	81	517.1	8.6	2.3
GOM17_119	145.1	0.61	0.6880	0.0120	0.0850	0.0009	0.1554	530.9	7.0	525.9	5.6	541	41	525.9	5.6	0.9
GOM17_13	86	0.83	0.7310	0.0240	0.0873	0.0013	0.4924	556.0	14.0	539.4	7.7	596	54	539.4	7.7	3.0
GOM17_75	108.1	0.97	0.8070	0.0200	0.0983	0.0015	0.0634	602.0	11.0	604.7	8.6	580	57	604.7	8.6	0.4
GOM17_91	38	0.93	1.3300	0.0990	0.1423	0.0030	0.1296	857.0	44.0	858.0	17.0	880	130	858.0	17.0	0.1
GOM17_47	16.77	0.87	1.6240	0.0590	0.1660	0.0039	0.2639	980.0	22.0	990.0	21.0	929	77	990.0	21.0	1.0

GOM17_19	33.8	1.03	1.5510	0.0400	0.1607	0.0026	0.2497	954.0	16.0	961.0	14.0	932	59	961.0	14.0	0.7
GOM17_21	49.7	1.42	1.5240	0.0470	0.1543	0.0035	0.1381	939.0	19.0	925.0	19.0	944	61	925.0	19.0	1.5
GOM17_101	100.7	1.33	1.6120	0.0250	0.1620	0.0017	0.3872	974.3	9.5	967.8	9.3	985	29	967.8	9.3	0.7
GOM17_74	72.6	1.14	1.6150	0.0200	0.1647	0.0017	0.1959	975.7	7.7	982.6	9.3	987	35	982.6	9.3	0.7
GOM17_6	56.6	1.33	1.6280	0.0280	0.1632	0.0022	0.0910	983.0	11.0	974.0	12.0	989	45	974.0	12.0	0.9
GOM17_25	199	2.50	1.5170	0.0310	0.1519	0.0030	0.5891	940.0	13.0	911.0	17.0	996	31	911.0	17.0	3.1
GOM17_81	48.1	2.13	1.5850	0.0290	0.1599	0.0022	0.2806	963.0	11.0	956.0	12.0	1003	39	956.0	12.0	0.7
GOM17_78	158	2.01	1.6910	0.0170	0.1691	0.0016	0.3179	1005.7	6.4	1006.9	8.9	1007	22	1007.0	22.0	0.0
GOM17_106	62.1	1.60	1.7190	0.0310	0.1703	0.0020	0.4074	1016.0	11.0	1014.0	11.0	1012	32	1012.0	32.0	0.2
GOM17_109	28.6	1.52	1.7230	0.0400	0.1725	0.0032	0.2618	1015.0	15.0	1028.0	18.0	1012	50	1012.0	50.0	1.6
GOM17_40	33.3	2.27	1.5930	0.0390	0.1580	0.0028	0.3020	966.0	15.0	945.0	16.0	1018	49	945.0	16.0	2.2
GOM17_117	93.8	6.95	1.7440	0.0300	0.1741	0.0024	0.6838	1024.0	11.0	1035.0	13.0	1020	28	1020.0	28.0	1.5
GOM17_79	156.2	1.66	1.7440	0.0160	0.1720	0.0013	0.2307	1024.7	6.1	1023.2	7.4	1027	24	1027.0	24.0	0.4
GOM17_5	73.6	2.45	1.6640	0.0350	0.1636	0.0019	0.4719	993.0	13.0	976.0	11.0	1033	40	976.0	11.0	1.7
GOM17_24	188	2.17	1.7270	0.0220	0.1711	0.0020	0.5704	1019.2	7.9	1019.0	11.0	1033	22	1033.0	22.0	1.4
GOM17_27	193	1.68	1.7230	0.0270	0.1701	0.0023	0.7003	1017.7	9.7	1012.0	13.0	1034	26	1034.0	26.0	2.1
GOM17_16	128.7	1.91	1.6620	0.0240	0.1642	0.0021	0.6331	994.6	8.8	980.0	12.0	1035	22	980.0	12.0	1.5
GOM17_29	436	1.82	1.7280	0.0170	0.1696	0.0015	0.5696	1018.7	6.4	1009.8	8.1	1038	16	1038.0	16.0	2.7
GOM17_28	110.5	0.69	1.7800	0.0230	0.1739	0.0015	0.1902	1037.7	8.2	1033.3	8.1	1045	29	1045.0	29.0	1.1
GOM17_95	70.9	2.48	1.7820	0.0310	0.1744	0.0025	0.5492	1039.0	11.0	1036.0	13.0	1045	33	1045.0	33.0	0.9
GOM17_110	172	1.84	1.7440	0.0230	0.1723	0.0021	0.5884	1024.5	8.7	1025.0	12.0	1045	25	1045.0	25.0	1.9
GOM17_51	186	3.25	1.7710	0.0170	0.1741	0.0016	0.4132	1035.5	6.1	1034.6	8.7	1046	19	1046.0	19.0	1.1
GOM17_118	171.6	1.69	1.7720	0.0250	0.1733	0.0021	0.6206	1034.9	9.0	1030.0	12.0	1047	25	1047.0	25.0	1.6
GOM17_43	127.2	1.86	1.7820	0.0230	0.1738	0.0018	0.4424	1040.7	8.2	1032.7	9.9	1050	26	1050.0	26.0	1.6
GOM17_31	152.8	2.41	1.7660	0.0250	0.1724	0.0024	0.5841	1033.4	9.3	1025.0	13.0	1051	25	1051.0	25.0	2.5
GOM17_66	393	5.52	1.7310	0.0160	0.1706	0.0015	0.6379	1019.7	5.9	1015.5	8.4	1051	16	1051.0	16.0	3.4
GOM17_32	216	1.66	1.7930	0.0190	0.1725	0.0017	0.5657	1042.4	7.0	1025.5	9.4	1062	21	1062.0	21.0	3.4
GOM17_23	53	0.66	1.8240	0.0430	0.1756	0.0032	0.4759	1052.0	15.0	1042.0	17.0	1064	41	1064.0	41.0	2.1
GOM17_90	121	1.83	1.7500	0.0250	0.1687	0.0017	0.2823	1026.4	9.1	1004.9	9.3	1065	30	1065.0	30.0	5.6
GOM17_86	136	1.03	1.9050	0.0230	0.1844	0.0020	0.4976	1082.4	8.2	1093.0	11.0	1070	22	1070.0	22.0	2.1
GOM17_45	176	1.25	1.8760	0.0280	0.1804	0.0025	0.7756	1074.3	9.2	1069.0	14.0	1077	21	1077.0	21.0	0.7
GOM17_88	128.3	1.68	1.8500	0.0260	0.1775	0.0018	0.4465	1062.5	9.1	1053.0	10.0	1091	28	1091.0	28.0	3.5
GOM17_104	42.52	1.01	1.7750	0.0630	0.1713	0.0055	0.2883	1035.0	23.0	1019.0	30.0	1091	84	1091.0	84.0	6.6

GOM17_108	219	1.95	1.9050	0.0230	0.1835	0.0017	0.4901	1082.5	7.9	1085.7	9.0	1092	20	1092.0	20.0	0.6
GOM17_15	71.2	2.01	1.9300	0.0280	0.1832	0.0020	0.4193	1090.9	9.5	1084.0	11.0	1093	28	1093.0	28.0	0.8
GOM17_72	34.3	1.16	1.9130	0.0380	0.1802	0.0026	0.0497	1086.0	14.0	1070.0	14.0	1102	49	1102.0	49.0	2.9
GOM17_35	27.8	1.11	1.8570	0.0450	0.1755	0.0030	0.3318	1066.0	16.0	1042.0	17.0	1109	53	1109.0	53.0	6.0
GOM17_68	183	2.10	1.8830	0.0180	0.1792	0.0019	0.3750	1076.1	5.9	1062.0	10.0	1111	25	1111.0	25.0	4.4
GOM17_73	64.4	1.51	2.0520	0.0470	0.1924	0.0025	0.5113	1131.0	16.0	1134.0	14.0	1138	38	1138.0	38.0	0.4
GOM17_56	71.7	1.43	1.9550	0.0750	0.1759	0.0046	0.2998	1099.0	26.0	1044.0	25.0	1143	94	1143.0	94.0	8.7
GOM17_83	126	2.80	2.1120	0.0450	0.1954	0.0028	0.7766	1151.0	15.0	1150.0	15.0	1143	30	1143.0	30.0	0.6
GOM17_2	136.8	1.61	2.1170	0.0310	0.1967	0.0019	0.5812	1153.5	9.9	1157.0	10.0	1144	24	1144.0	24.0	1.1
GOM17_30	99.2	1.43	1.8190	0.0460	0.1681	0.0034	0.3024	1052.0	17.0	1001.0	19.0	1145	58	1145.0	58.0	12.6
GOM17_99	257.7	1.82	2.0660	0.0280	0.1931	0.0022	0.4966	1141.0	8.4	1138.0	12.0	1147	25	1147.0	25.0	0.8
GOM17_69	85.2	2.24	2.0130	0.0300	0.1871	0.0023	0.3243	1119.0	10.0	1105.0	13.0	1149	33	1149.0	33.0	3.8
GOM17_80	58.8	1.74	2.1110	0.0410	0.1941	0.0027	0.4053	1151.0	13.0	1143.0	14.0	1150	35	1150.0	35.0	0.6
GOM17_55	65.6	2.50	2.1390	0.0270	0.1970	0.0024	0.3910	1163.5	8.6	1159.0	13.0	1151	26	1151.0	26.0	0.7
GOM17_18	75	1.77	2.1360	0.0320	0.1961	0.0021	0.1762	1160.0	10.0	1154.0	12.0	1154	33	1154.0	33.0	0.0
GOM17_124	84.1	1.70	1.9560	0.0320	0.1807	0.0033	0.6190	1100.0	11.0	1070.0	18.0	1158	28	1158.0	28.0	7.6
GOM17_36	91.1	2.09	2.0720	0.0240	0.1899	0.0023	0.5099	1140.1	8.1	1121.0	13.0	1166	26	1166.0	26.0	3.9
GOM17_42	42.3	2.36	2.1090	0.0380	0.1914	0.0022	0.2706	1151.0	12.0	1129.0	12.0	1172	31	1172.0	31.0	3.7
GOM17_97	351	5.33	2.1090	0.0190	0.1943	0.0013	0.3791	1151.4	6.2	1144.6	6.9	1173	16	1173.0	16.0	2.4
GOM17_85	191	1.94	2.0580	0.0360	0.1878	0.0019	0.5461	1134.0	12.0	1110.0	10.0	1174	28	1174.0	28.0	5.5
GOM17_94	298.7	4.85	1.9900	0.0230	0.1830	0.0020	0.5925	1111.6	7.8	1083.0	11.0	1176	22	1176.0	22.0	7.9
GOM17_123	136.3	1.74	2.0960	0.0270	0.1926	0.0023	0.4751	1148.2	8.6	1135.0	12.0	1177	22	1177.0	22.0	3.6
GOM17_3	90.9	1.98	1.9680	0.0480	0.1805	0.0024	0.5250	1104.0	17.0	1073.0	14.0	1178	47	1178.0	47.0	8.9
GOM17_58	73	1.10	2.2880	0.0640	0.2079	0.0043	0.4507	1207.0	20.0	1217.0	23.0	1178	58	1178.0	58.0	3.3
GOM17_113	220	1.74	2.2260	0.0250	0.2032	0.0018	0.5202	1189.7	8.0	1192.6	9.7	1178	19	1178.0	19.0	1.2
GOM17_33	195.3	2.76	2.1170	0.0280	0.1919	0.0021	0.0824	1153.6	9.1	1131.0	11.0	1181	20	1181.0	20.0	4.2
GOM17_122	263	7.10	2.1590	0.0240	0.1978	0.0022	0.6607	1167.4	7.7	1165.0	12.0	1183	19	1183.0	19.0	1.5
GOM17_54	227	1.74	2.2750	0.0270	0.2055	0.0024	0.6055	1205.2	8.6	1204.0	13.0	1204	22	1204.0	22.0	0.0
GOM17_114	187.8	1.33	2.2050	0.0240	0.1990	0.0020	0.4311	1182.2	7.8	1170.0	11.0	1212	23	1212.0	23.0	3.5
GOM17_4	261	2.64	2.2930	0.0360	0.2051	0.0022	0.9277	1210.0	11.0	1202.0	12.0	1215	25	1215.0	25.0	1.1
GOM17_82	95	0.99	2.2990	0.0290	0.2036	0.0023	0.4075	1211.5	8.8	1195.0	12.0	1229	28	1229.0	28.0	2.8
GOM17_48	46.69	1.10	2.1880	0.0620	0.1951	0.0050	0.3436	1176.0	20.0	1149.0	27.0	1239	49	1239.0	49.0	7.3
GOM17_121	164	11.60	2.4800	0.0250	0.2184	0.0022	0.5206	1266.7	7.1	1273.0	12.0	1244	19	1244.0	19.0	2.3

GOM17_1	356	1.75	2.2520	0.0280	0.2003	0.0024	0.7123	1197.2	8.6	1177.0	13.0	1246	21	1246.0	21.0	5.5
GOM17_116	287.7	3.68	2.2440	0.0400	0.1985	0.0039	0.5500	1195.0	12.0	1167.0	21.0	1247	33	1247.0	33.0	6.4
GOM17_52	284.6	4.91	1.9970	0.0410	0.1762	0.0024	0.8229	1114.0	14.0	1046.0	13.0	1249	26	1249.0	26.0	16.3
GOM17_26	101.8	0.95	2.5300	0.0340	0.2187	0.0025	0.3371	1281.3	9.4	1275.0	13.0	1288	28	1288.0	28.0	1.0
GOM17_49	237	1.13	2.5540	0.0710	0.2157	0.0069	0.7182	1287.0	20.0	1259.0	37.0	1301	51	1301.0	51.0	3.2
GOM17_8	138.5	1.37	2.6600	0.0270	0.2265	0.0026	0.4612	1318.3	7.8	1316.0	13.0	1331	22	1331.0	22.0	1.1
GOM17_39	289.2	1.84	2.6980	0.0180	0.2277	0.0016	0.5377	1327.7	5.0	1322.3	8.5	1339	15	1339.0	15.0	1.2
GOM17_20	93.2	1.78	2.7070	0.0370	0.2267	0.0028	0.6101	1331.0	10.0	1317.0	15.0	1345	26	1345.0	26.0	2.1
GOM17_102	119	1.68	2.8000	0.0420	0.2287	0.0025	0.5493	1355.0	11.0	1327.0	13.0	1406	22	1406.0	22.0	5.6
GOM17_93	152.8	1.18	2.9800	0.0340	0.2422	0.0027	0.5458	1402.1	8.7	1398.0	14.0	1414	23	1414.0	23.0	1.1
GOM17_96	110.4	0.95	3.1050	0.0330	0.2458	0.0037	0.2957	1433.7	8.1	1416.0	19.0	1456	33	1456.0	33.0	2.7
GOM17_112	71.3	1.36	3.1370	0.0420	0.2466	0.0033	0.6177	1441.0	10.0	1421.0	17.0	1471	22	1471.0	22.0	3.4
GOM17_63	141.8	0.86	3.1800	0.1900	0.2486	0.0065	0.4554	1452.0	47.0	1431.0	34.0	1478	99	1478.0	99.0	3.2
GOM17_98	73.5	0.72	3.9300	0.0510	0.2796	0.0028	0.5755	1619.0	10.0	1589.0	14.0	1637	25	1637.0	25.0	2.9
GOM17_107	109.1	0.90	3.9070	0.0500	0.2785	0.0027	0.5217	1616.5	9.9	1584.0	13.0	1657	24	1657.0	24.0	4.4

Sample:GOM18	Isotopic Ratios							Isotopic ages (Ma)								
Analysis	[U] ppm	U/Th	207/235	2σ err.	206/238	2σ err.	RHO	207/235	2σ err.	206/238	2σ err.	207/206	2σ err.	Best age	2σ err.	% Dis.
GOM18_94	721	183.00	0.3701	0.0053	0.0506	0.0005	0.5714	319.6	4.0	318.0	3.2	330	30	318.0	3.2	0.5
GOM18_99	890	146.00	0.3746	0.0050	0.0513	0.0009	0.0691	323.1	3.7	322.3	5.3	340	52	322.3	5.3	0.2
GOM18_15	624	9.74	0.3756	0.0087	0.0514	0.0016	0.3890	323.7	6.4	323.3	9.5	337	70	323.3	9.5	0.1
GOM18_84	268	70.00	0.4290	0.0180	0.0522	0.0018	0.4821	362.0	13.0	328.0	11.0	580	90	328.0	11.0	9.4
GOM18_89	732	9.11	0.3921	0.0057	0.0529	0.0008	0.4112	335.9	4.2	332.1	4.7	335	39	332.1	4.7	1.1
GOM18_85	433	97.00	0.4180	0.0340	0.0534	0.0034	0.7461	354.0	25.0	335.0	21.0	371	69	335.0	21.0	5.4
GOM18_60	630	81.80	0.4110	0.0230	0.0539	0.0019	0.7383	349.0	16.0	339.0	12.0	405	87	339.0	12.0	2.9
GOM18_64	745	3.72	0.3984	0.0050	0.0541	0.0005	0.5655	340.4	3.6	339.6	2.7	340	25	339.6	2.7	0.2
GOM18_124	507	102.20	0.4004	0.0042	0.0542	0.0006	0.3695	341.9	3.0	340.2	3.6	345	27	340.2	3.6	0.5
GOM18_117	527	94.00	0.4030	0.0100	0.0545	0.0009	0.2772	344.0	7.4	342.3	5.4	338	70	342.3	5.4	0.5
GOM18_30	139.9	0.63	0.4073	0.0086	0.0558	0.0007	0.0604	347.7	6.0	349.9	4.3	335	53	349.9	4.3	0.6
GOM18_36	319	4.07	0.4195	0.0057	0.0564	0.0004	0.2211	355.5	4.0	353.8	2.7	363	33	353.8	2.7	0.5
GOM18_119	700	280.00	0.4239	0.0062	0.0567	0.0008	0.6055	358.6	4.4	355.7	4.6	383	28	355.7	4.6	0.8

GOM18_39	183	3.63	0.4244	0.0084	0.0571	0.0007	0.0995	358.9	6.0	358.0	4.0	375	43	358.0	4.0	0.3
GOM18_120	614	2.25	0.4323	0.0052	0.0577	0.0005	0.3013	364.7	3.7	361.4	3.0	379	27	361.4	3.0	0.9
GOM18_24	37.7	1.90	0.4290	0.0210	0.0578	0.0014	0.1023	366.0	15.0	362.4	8.5	370	110	362.4	8.5	1.0
GOM18_67	1490	68.00	0.4270	0.0330	0.0579	0.0057	0.9475	360.0	23.0	363.0	35.0	367	63	363.0	35.0	0.8
GOM18_110	236	14.70	0.4396	0.0075	0.0587	0.0007	0.4290	369.8	5.3	367.9	4.3	368	38	367.9	4.3	0.5
GOM18_95	440	29.00	0.4590	0.0310	0.0592	0.0017	0.6723	383.0	21.0	371.0	10.0	400	120	371.0	10.0	3.1
GOM18_115	182	1.54	0.4640	0.0120	0.0611	0.0013	0.6543	387.7	7.9	382.4	8.0	388	44	382.4	8.0	1.4
GOM18_25	193.7	2.52	0.4670	0.0130	0.0620	0.0016	0.8465	388.7	9.3	387.6	9.5	380	32	387.6	9.5	0.3
GOM18_114	238.9	0.43	0.4990	0.0110	0.0648	0.0009	0.0338	411.0	7.5	404.4	5.5	424	58	404.4	5.5	1.6
GOM18_65	79.3	1.39	0.5200	0.0200	0.0673	0.0016	0.0734	424.0	13.0	419.8	9.4	460	87	419.8	9.4	1.0
GOM18_32	186.8	0.47	0.5170	0.0140	0.0674	0.0013	0.3338	424.4	9.3	420.3	7.7	452	66	420.3	7.7	1.0
GOM18_21	158	1.28	0.5250	0.0130	0.0675	0.0013	0.2306	428.2	8.8	420.8	7.7	475	59	420.8	7.7	1.7
GOM18_42	76.7	0.87	0.5290	0.0150	0.0688	0.0011	0.2305	430.4	9.7	428.6	6.6	400	64	428.6	6.6	0.4
GOM18_86	248	0.43	0.5390	0.0100	0.0688	0.0010	0.3784	437.3	6.9	428.9	6.0	461	49	428.9	6.0	1.9
GOM18_88	421	1.28	0.5278	0.0073	0.0689	0.0009	0.5132	430.2	4.8	429.3	5.3	429	28	429.3	5.3	0.2
GOM18_3	434	0.88	0.5411	0.0099	0.0698	0.0007	0.1706	439.7	6.3	434.9	4.1	465	44	434.9	4.1	1.1
GOM18_63	82.4	1.56	0.5490	0.0110	0.0712	0.0011	0.3408	443.8	7.5	443.3	6.4	437	55	443.3	6.4	0.1
GOM18_4	586	65.00	0.5560	0.0340	0.0713	0.0023	0.5748	448.0	22.0	444.0	14.0	450	110	444.0	14.0	0.9
GOM18_98	147	16.60	0.5740	0.0180	0.0719	0.0031	0.6015	460.0	12.0	448.0	18.0	466	98	448.0	18.0	2.6
GOM18_1	3730	75.90	0.5630	0.0170	0.0722	0.0020	0.2053	454.0	11.0	449.0	12.0	478	97	449.0	12.0	1.1
GOM18_113	147	1.15	0.5590	0.0100	0.0730	0.0009	0.1611	450.8	6.5	454.0	5.5	444	45	454.0	5.5	0.7
GOM18_57	67	1.34	0.5650	0.0180	0.0732	0.0030	0.1314	454.0	12.0	455.0	18.0	430	91	455.0	18.0	0.2
GOM18_62	680	1.38	0.5782	0.0063	0.0741	0.0005	0.4151	463.1	4.0	460.7	3.2	447	23	460.7	3.2	0.5
GOM18_74	355	91.90	0.5830	0.0100	0.0742	0.0013	0.2899	466.2	6.6	461.1	7.7	506	50	461.1	7.7	1.1
GOM18_72	36.3	0.64	0.5910	0.0180	0.0753	0.0017	0.3507	472.0	12.0	468.0	10.0	479	76	468.0	10.0	0.8
GOM18_41	305	0.92	0.6120	0.0160	0.0755	0.0014	0.6843	483.9	9.9	469.2	8.2	550	36	469.2	8.2	3.0
GOM18_66	518	17.80	0.6360	0.0200	0.0808	0.0020	0.2714	500.0	12.0	501.0	12.0	480	100	501.0	12.0	0.2
GOM18_100	420.2	25.70	0.6610	0.0290	0.0809	0.0027	1.0000	515.0	18.0	502.0	16.0	513	18	502.0	16.0	2.5
GOM18_116	576	2.81	0.7970	0.0170	0.0862	0.0013	0.0417	594.7	9.5	532.8	7.5	823	48	532.8	7.5	10.4
GOM18_27	91.2	2.40	0.7690	0.0150	0.0932	0.0015	0.2839	579.6	8.2	574.0	8.6	611	48	574.0	8.6	1.0
GJ1_25	83.1	9.58	1.0940	0.0450	0.1094	0.0035	0.9087	687.0	21.0	660.0	20.0	767	22	660.0	20.0	3.9
GOM18_90	151	4.67	1.0400	0.0500	0.1085	0.0039	0.5253	718.0	25.0	663.0	23.0	845	40	663.0	23.0	7.7
GOM18_19	60.4	1.22	1.0160	0.0250	0.1151	0.0022	0.3861	711.0	13.0	702.0	13.0	757	52	702.0	13.0	1.3

GOM18_31	271	1.92	1.3930	0.0180	0.1379	0.0017	0.7882	885.8	7.5	832.5	9.5	1005	21	832.5	9.5	6.0
GOM18_23	25.42	0.80	1.6200	0.0480	0.1631	0.0028	0.0404	975.0	18.0	976.0	16.0	943	60	976.0	16.0	0.1
GOM18_7	80.4	1.76	1.5030	0.0450	0.1507	0.0026	0.3544	924.0	15.0	904.0	14.0	965	42	904.0	14.0	2.2
GOM18_105	127.3	1.34	1.5190	0.0440	0.1527	0.0030	0.5524	938.0	18.0	916.0	17.0	978	60	916.0	17.0	2.3
GOM18_103	30.8	1.53	1.6050	0.0460	0.1608	0.0034	0.1713	970.0	18.0	961.0	19.0	987	73	961.0	19.0	0.9
GOM18_69	34.8	0.96	1.5900	0.0400	0.1585	0.0030	0.1158	965.0	16.0	948.0	17.0	999	59	948.0	17.0	1.8
GOM18_14	200.9	2.29	1.6770	0.0210	0.1662	0.0019	0.5000	999.1	8.0	991.0	10.0	1004	24	991.0	10.0	0.8
GOM18_76	112.9	1.21	1.7020	0.0220	0.1691	0.0025	0.3639	1008.6	8.3	1007.0	14.0	1004	32	1004.0	32.0	0.3
GOM18_77	228.4	3.07	1.6120	0.0270	0.1601	0.0018	0.6561	976.0	11.0	957.4	9.7	1004	27	957.4	9.7	1.9
GOM18_11	286	4.33	1.6230	0.0260	0.1626	0.0022	0.5879	981.0	10.0	971.0	12.0	1010	27	971.0	12.0	1.0
GOM18_93	23.71	0.59	1.7180	0.0420	0.1689	0.0029	0.2405	1018.0	16.0	1006.0	16.0	1010	53	1010.0	53.0	0.4
GOM18_118	106	1.15	1.6980	0.0230	0.1657	0.0024	0.3450	1007.1	8.6	988.0	13.0	1028	32	988.0	13.0	1.9
GOM18_71	368	1.32	1.7260	0.0140	0.1692	0.0014	0.5243	1019.4	5.2	1007.6	7.5	1029	15	1029.0	15.0	2.1
GOM18_116	233	1.80	1.4540	0.0350	0.1422	0.0026	0.6915	911.0	14.0	857.0	14.0	1033	43	857.0	14.0	5.9
GOM18_18	70.2	0.62	1.6500	0.0310	0.1639	0.0028	0.0872	991.0	11.0	978.0	15.0	1034	48	978.0	15.0	1.3
GOM18_45	59.9	1.37	1.7060	0.0380	0.1650	0.0024	0.2727	1010.0	14.0	984.0	13.0	1035	47	984.0	13.0	2.6
GOM18_123	77.2	2.12	1.6970	0.0380	0.1663	0.0030	0.3831	1006.0	14.0	991.0	16.0	1038	42	991.0	16.0	1.5
GOM18_5	103	0.54	1.7860	0.0310	0.1743	0.0019	0.2298	1039.0	11.0	1035.0	11.0	1039	39	1039.0	39.0	0.4
GOM18_9	187	0.51	1.6950	0.0190	0.1665	0.0015	0.4289	1007.2	7.5	992.9	8.1	1042	24	992.9	8.1	1.4
GOM18_87	402	2.51	1.7970	0.0150	0.1748	0.0013	0.5754	1045.1	5.6	1038.3	7.1	1044	16	1044.0	16.0	0.5
GOM18_107	58.4	1.21	1.6940	0.0300	0.1633	0.0028	0.5690	1006.0	12.0	975.0	15.0	1044	29	975.0	15.0	3.1
GOM18_55	539	0.73	1.8260	0.0220	0.1766	0.0024	0.7783	1054.3	7.8	1048.0	13.0	1050	17	1050.0	17.0	0.2
GOM18_68	113.9	1.71	1.7350	0.0210	0.1703	0.0018	0.2465	1021.1	7.8	1013.9	9.8	1050	27	1050.0	27.0	3.4
GOM18_81	250	1.36	1.8070	0.0180	0.1749	0.0013	0.2381	1047.7	6.4	1039.0	7.2	1051	23	1051.0	23.0	1.1
GOM18_96	256	1.44	1.8130	0.0170	0.1757	0.0015	0.2576	1050.0	6.1	1043.2	8.1	1053	22	1053.0	22.0	0.9
GOM18_79	780	2.58	1.6890	0.0160	0.1611	0.0019	0.8043	1004.4	6.0	963.0	11.0	1054	15	963.0	11.0	4.1
GOM18_101	451	3.36	1.8730	0.0160	0.1813	0.0016	0.6452	1072.2	5.5	1074.2	8.7	1058	14	1058.0	14.0	1.5
GOM18_2	195	1.32	1.8090	0.0440	0.1777	0.0035	0.4696	1047.0	16.0	1054.0	19.0	1062	47	1062.0	47.0	0.8
GOM18_95	30.04	2.33	1.7820	0.0470	0.1697	0.0032	0.2111	1037.0	17.0	1010.0	18.0	1070	58	1070.0	58.0	5.6
GOM18_102	251	1.74	1.7820	0.0150	0.1708	0.0010	0.4692	1039.2	5.3	1017.2	5.8	1076	16	1076.0	16.0	5.5
GOM18_84	82.6	1.74	1.7730	0.0480	0.1662	0.0024	0.2594	1035.0	18.0	991.0	13.0	1079	51	991.0	13.0	4.3
GOM18_121	168	0.94	1.8460	0.0210	0.1778	0.0017	0.2320	1063.6	7.6	1054.8	9.4	1079	25	1079.0	25.0	2.2
GOM18_33	76	1.36	1.8920	0.0660	0.1832	0.0042	0.6138	1077.0	23.0	1084.0	23.0	1081	53	1081.0	53.0	0.3

GOM18_38	414	1.74	1.9070	0.0170	0.1828	0.0018	0.9119	1083.3	6.0	1082.2	9.6	1082	13	1082.0	13.0	0.0
GOM18_40	375	10.30	1.9610	0.0490	0.1861	0.0035	0.9440	1100.0	16.0	1100.0	19.0	1087	20	1087.0	20.0	1.2
GOM18_78	31.3	1.10	1.8660	0.0420	0.1782	0.0030	0.3473	1069.0	15.0	1059.0	17.0	1089	45	1089.0	45.0	2.8
GOM18_37	285	5.48	1.9380	0.0200	0.1840	0.0020	0.6390	1093.8	6.8	1090.0	11.0	1095	19	1095.0	19.0	0.5
GOM18_15	144	2.21	1.8200	0.1000	0.1734	0.0087	0.9325	1049.0	37.0	1030.0	48.0	1097	42	1097.0	42.0	6.1
GOM18_80	309	1.41	1.7280	0.0290	0.1637	0.0019	0.0673	1018.0	11.0	977.0	10.0	1098	31	977.0	10.0	4.0
GOM18_82	36.6	1.26	1.8510	0.0360	0.1758	0.0023	0.0198	1064.0	12.0	1045.0	13.0	1106	46	1106.0	46.0	5.5
GOM18_4	457	1.11	1.8030	0.0350	0.1728	0.0031	0.7964	1049.0	12.0	1027.0	17.0	1109	25	1109.0	25.0	7.4
GOM18_13	150.9	1.95	1.9760	0.0240	0.1862	0.0016	0.1585	1108.2	8.4	1100.9	8.5	1122	28	1122.0	28.0	1.9
GOM18_99	17.08	8.60	2.0300	0.1400	0.1862	0.0078	0.4114	1121.0	45.0	1110.0	45.0	1126	87	1126.0	87.0	1.4
GOM18_28	145.6	7.95	2.0380	0.0260	0.1905	0.0026	0.5872	1127.7	8.8	1124.0	14.0	1136	24	1136.0	24.0	1.1
GOM18_20	444	3.16	1.9940	0.0230	0.1865	0.0018	0.7021	1113.0	7.7	1102.0	10.0	1145	17	1145.0	17.0	3.8
GOM18_108	40	1.43	2.1010	0.0420	0.1956	0.0025	0.1090	1148.0	14.0	1151.0	13.0	1150	43	1150.0	43.0	0.1
GOM18_34	77.2	1.79	2.1350	0.0260	0.1966	0.0020	0.1666	1159.5	8.5	1157.0	11.0	1151	30	1151.0	30.0	0.5
GOM18_83	257	7.92	2.1000	0.0200	0.1936	0.0019	0.6667	1148.4	6.5	1141.0	10.0	1151	16	1151.0	16.0	0.9
GOM18_117	112	1.20	2.0020	0.0240	0.1853	0.0020	0.4757	1116.0	8.0	1096.0	11.0	1152	24	1152.0	24.0	4.9
GOM18_8	548	4.28	1.9820	0.0850	0.1851	0.0055	0.6110	1108.0	29.0	1095.0	30.0	1153	98	1153.0	98.0	5.0
GOM18_111	177	1.58	2.1210	0.0240	0.1957	0.0022	0.6316	1155.1	7.7	1152.0	12.0	1153	19	1153.0	19.0	0.1
GOM18_10	122	2.17	2.0150	0.0340	0.1864	0.0023	0.4376	1119.0	11.0	1102.0	13.0	1154	32	1154.0	32.0	4.5
GOM18_85	117	1.27	2.1430	0.0290	0.1976	0.0021	0.4703	1162.0	9.5	1162.0	11.0	1159	27	1159.0	27.0	0.3
GOM18_59	27.11	1.96	1.9900	0.1200	0.1808	0.0052	0.3479	1109.0	40.0	1071.0	28.0	1160	150	1160.0	150.0	7.7
GOM18_100	79.7	1.84	2.0970	0.0320	0.1930	0.0019	0.1215	1147.0	11.0	1138.0	10.0	1160	32	1160.0	32.0	1.9
GOM18_22	363	1.70	1.9500	0.0330	0.1789	0.0023	0.4637	1098.0	11.0	1064.0	14.0	1161	35	1161.0	35.0	8.4
GOM18_29	94	2.26	1.9670	0.0320	0.1812	0.0039	0.4597	1104.0	11.0	1073.0	21.0	1162	41	1162.0	41.0	7.7
GOM18_53	315.6	1.09	1.9020	0.0230	0.1744	0.0019	0.5189	1081.6	8.1	1036.0	10.0	1164	23	1164.0	23.0	11.0
GOM18_46	202.9	1.71	2.0670	0.0220	0.1911	0.0015	0.5794	1139.7	7.4	1127.5	8.4	1167	17	1167.0	17.0	3.4
GOM18_74	234	2.35	2.1190	0.0390	0.1920	0.0022	0.6285	1155.0	13.0	1132.0	12.0	1168	35	1168.0	35.0	3.1
GOM18_91	536.7	1.07	2.0410	0.0140	0.1870	0.0012	0.5578	1129.1	4.7	1104.9	6.3	1172	12	1172.0	12.0	5.7
GOM18_97	25.5	0.63	2.1200	0.0470	0.1945	0.0029	0.3292	1155.0	15.0	1145.0	16.0	1173	49	1173.0	49.0	2.4
GOM18_26	66.1	0.82	2.0280	0.0360	0.1869	0.0025	0.3929	1128.0	12.0	1104.0	13.0	1176	30	1176.0	30.0	6.1
GOM18_61	234	2.34	2.1250	0.0220	0.1933	0.0017	0.5236	1156.6	7.1	1139.1	9.4	1178	20	1178.0	20.0	3.3
GOM18_60	74.3	2.69	2.1240	0.0360	0.1937	0.0022	0.5555	1156.0	12.0	1141.0	12.0	1183	29	1183.0	29.0	3.6
GOM18_66	37.1	2.11	2.1980	0.0420	0.1993	0.0025	0.0104	1182.0	13.0	1172.0	13.0	1185	49	1185.0	49.0	1.1

GOM18_70	180	9.90	2.1860	0.0470	0.1950	0.0030	0.7406	1177.0	15.0	1148.0	16.0	1201	24	1201.0	24.0	4.4
GOM18_104	102	1.17	2.2550	0.0300	0.2026	0.0022	0.3601	1197.6	9.3	1189.0	12.0	1210	25	1210.0	25.0	1.7
GOM18_12	115	1.05	2.1990	0.0470	0.1975	0.0037	0.5832	1181.0	15.0	1161.0	20.0	1211	35	1211.0	35.0	4.1
GOM18_51	70.5	1.01	2.2780	0.0320	0.2035	0.0016	0.2755	1204.8	9.8	1194.1	8.4	1214	27	1214.0	27.0	1.6
GOM18_17	170	2.05	2.2030	0.0300	0.1982	0.0023	0.6955	1181.2	9.5	1166.0	12.0	1216	20	1216.0	20.0	4.1
GOM18_50	78	1.35	2.4150	0.0550	0.2136	0.0049	0.7012	1245.0	16.0	1247.0	26.0	1220	32	1220.0	32.0	2.2
GOM18_47	30	1.86	2.2960	0.0490	0.2004	0.0027	0.0500	1210.0	15.0	1177.0	15.0	1249	52	1249.0	52.0	5.8
GOM18_43	20.26	4.20	2.2510	0.0490	0.1971	0.0032	0.2098	1203.0	16.0	1159.0	17.0	1250	49	1250.0	49.0	7.3
GOM18_1	385	3.55	2.3170	0.0330	0.2048	0.0019	0.3959	1217.0	10.0	1201.0	10.0	1255	27	1255.0	27.0	4.3
GOM18_58	135.9	1.25	2.4210	0.0240	0.2123	0.0020	0.3865	1248.3	7.2	1241.0	11.0	1255	21	1255.0	21.0	1.1
GOM18_67	94.4	2.80	2.4280	0.0310	0.2084	0.0020	0.3339	1250.2	9.2	1220.0	10.0	1295	28	1295.0	28.0	5.8
GOM18_106	31.39	0.43	2.4060	0.0540	0.2047	0.0033	0.1018	1245.0	16.0	1202.0	17.0	1320	44	1320.0	44.0	8.9
GOM18_98	179.6	2.28	2.6510	0.0490	0.2141	0.0048	0.7434	1320.6	7.5	1251.0	26.0	1412	42	1412.0	42.0	11.4
GOM18_16	394	4.21	2.8340	0.0240	0.2286	0.0019	0.6542	1364.3	6.2	1327.0	10.0	1418	13	1418.0	13.0	6.4
GOM18_112	63	0.69	3.0800	0.0430	0.2460	0.0031	0.3920	1427.0	11.0	1418.0	16.0	1441	27	1441.0	27.0	1.6
GOM18_73	82.9	1.52	3.0030	0.0370	0.2384	0.0022	0.2372	1407.9	9.4	1378.0	11.0	1449	24	1449.0	24.0	4.9
GOM18_92	267	1.50	3.0670	0.0310	0.2399	0.0028	0.5473	1424.0	7.6	1386.0	15.0	1469	19	1469.0	19.0	5.7
GOM18_8	442	1.58	10.1850	0.0990	0.4408	0.0048	0.7035	2451.4	9.0	2354.0	21.0	2537	10	2537.0	10.0	7.2

Sample:GOM19	Isotopic Ratios							Isotopic ages (Ma)								
Analysis	[U] ppm	U/Th	207/235	2σ err.	206/238	2σ err.	RHO	207/235	2σ err.	206/238	2σ err.	207/206	2σ err.	Best age	2σ err.	% Dis.
GOM19_70	849	1.23	0.3390	0.0042	0.0460	0.0006	0.5584	296.3	3.1	289.7	3.8	354	27	289.7	3.8	2.2
GOM19_58	772	2.58	0.3433	0.0055	0.0462	0.0009	0.6119	299.6	4.1	291.1	5.7	337	41	291.1	5.7	2.8
GOM19_104	1286	106.00	0.3550	0.0120	0.0462	0.0011	0.3808	308.1	8.9	291.4	6.7	376	82	291.4	6.7	5.4
GOM19_59	1810	4.34	0.3900	0.0056	0.0476	0.0008	0.6883	334.3	4.0	299.8	4.7	568	29	299.8	4.7	10.3
GOM19_86	347	3.44	0.3552	0.0066	0.0486	0.0006	-0.0601	308.4	4.9	306.0	3.7	320	44	306.0	3.7	0.8
GOM19_46	378	1.02	0.3632	0.0049	0.0494	0.0006	0.1783	314.5	3.7	311.1	3.8	310	35	311.1	3.8	1.1
GOM19_1	1690	4.88	0.3743	0.0093	0.0519	0.0020	0.7354	322.4	6.8	326.0	12.0	294	52	326.0	12.0	1.1
GOM19_75	363.9	43.10	0.4059	0.0078	0.0528	0.0011	0.3351	345.8	5.6	331.4	6.7	377	50	331.4	6.7	4.2
GOM19_107	1218	12.37	0.3926	0.0073	0.0532	0.0013	0.4981	336.2	5.3	334.2	8.2	352	55	334.2	8.2	0.6
GOM19_63	436	11.89	0.3947	0.0088	0.0534	0.0010	0.5668	337.6	6.4	335.1	6.3	361	41	335.1	6.3	0.7

GOM19_81	359	69.10	0.4080	0.0130	0.0537	0.0016	0.4490	346.9	9.1	337.2	9.5	357	63	337.2	9.5	2.8
GOM19_22	404	7.90	0.4520	0.0170	0.0580	0.0019	0.6729	378.0	12.0	363.0	11.0	396	57	363.0	11.0	4.0
GOM19_12	560	7.30	0.4680	0.0110	0.0600	0.0011	0.6929	389.3	7.8	375.7	6.6	456	42	375.7	6.6	3.5
GOM19_124	605	1.54	0.4570	0.0230	0.0611	0.0034	0.0549	382.0	16.0	382.0	20.0	410	150	382.0	20.0	0.0
GOM19_92	356	0.73	0.4936	0.0084	0.0645	0.0010	0.4954	407.1	5.7	402.9	5.9	437	38	402.9	5.9	1.0
GOM19_36	529	4.60	0.5090	0.0130	0.0651	0.0016	0.8701	418.1	8.9	406.1	9.7	444	31	406.1	9.7	2.9
GOM19_103	1158	2.65	0.5314	0.0078	0.0657	0.0008	0.7775	432.5	5.2	410.0	5.1	531	22	410.0	5.1	5.2
GOM19_64	156	2.65	0.4940	0.0130	0.0657	0.0015	0.3914	408.2	8.6	410.2	9.1	413	62	410.2	9.1	0.5
GOM19_62	111	2.81	0.5060	0.0130	0.0658	0.0011	0.1926	415.3	8.8	411.0	6.5	403	56	411.0	6.5	1.0
GOM19_65	432.9	1.28	0.5017	0.0083	0.0660	0.0011	0.4935	412.7	5.6	411.9	6.6	437	35	411.9	6.6	0.2
GOM19_117	462	2.04	0.5234	0.0096	0.0678	0.0012	0.4781	428.0	6.5	423.1	7.0	446	38	423.1	7.0	1.1
GOM19_116	332.2	1.16	0.5310	0.0130	0.0695	0.0021	0.6265	432.0	8.4	433.0	13.0	429	50	433.0	13.0	0.2
GOM19_114	431.6	0.41	0.5280	0.0100	0.0699	0.0012	0.6213	430.4	6.6	435.4	7.5	441	33	435.4	7.5	1.2
GOM19_25	104.4	1.09	0.5540	0.0170	0.0707	0.0012	0.0173	449.0	11.0	440.1	7.3	442	78	440.1	7.3	2.0
GOM19_99	437	0.68	0.5637	0.0097	0.0716	0.0012	0.3649	453.8	6.3	445.5	7.3	479	43	445.5	7.3	1.8
GOM19_71	60.9	0.89	0.5900	0.0370	0.0727	0.0047	0.3791	470.0	23.0	452.0	29.0	490	180	452.0	29.0	3.8
GOM19_118	265.5	25.90	0.6100	0.0560	0.0730	0.0043	0.9242	482.0	35.0	454.0	26.0	551	67	454.0	26.0	5.8
GOM19_4	973	11.00	0.6220	0.0380	0.0736	0.0034	0.8516	490.0	24.0	458.0	21.0	653	65	458.0	21.0	6.5
GOM19_119	207	1.81	0.6100	0.0110	0.0783	0.0011	0.3783	484.1	7.0	486.1	6.6	484	38	486.1	6.6	0.4
GOM19_21	399	1.15	0.6721	0.0094	0.0829	0.0010	0.3641	521.8	5.7	513.2	6.1	539	34	513.2	6.1	1.6
GOM19_88	615	25.80	0.7590	0.0300	0.0913	0.0029	0.9002	572.0	17.0	563.0	17.0	597	39	563.0	17.0	1.6
GOM19_94	375	0.74	0.7690	0.0150	0.0932	0.0018	0.7064	578.8	8.4	575.0	11.0	583	38	575.0	11.0	0.7
GOM19_73	124	1.25	0.8120	0.0140	0.0962	0.0015	0.5216	603.0	7.9	592.3	8.9	628	40	592.3	8.9	1.8
GOM19_54	141.5	10.20	1.1950	0.0200	0.1229	0.0015	0.7909	773.3	9.0	744.4	8.7	831	10	744.4	8.7	3.7
GOM19_53	60.3	0.65	1.1330	0.0410	0.1264	0.0026	0.2324	767.0	20.0	767.0	15.0	788	73	767.0	15.0	0.0
GOM19_113	2358	6.24	1.2910	0.0260	0.1285	0.0021	0.8252	841.0	11.0	779.0	12.0	1007	23	779.0	12.0	7.4
GOM19_2	260.2	1.25	1.2780	0.0430	0.1301	0.0040	0.6779	835.0	19.0	788.0	23.0	992	47	788.0	23.0	5.6
GOM19_68	161.1	1.51	1.4090	0.0170	0.1409	0.0014	0.1771	892.5	7.3	849.5	8.1	998	26	849.5	8.1	4.8
GOM19_81	198	1.85	1.3820	0.0400	0.1412	0.0038	0.7726	880.0	17.0	851.0	21.0	972	45	851.0	21.0	3.3
GOM19_108	206.2	2.58	1.3910	0.0320	0.1433	0.0043	0.5125	885.0	14.0	863.0	24.0	946	59	863.0	24.0	2.5
GOM19_124	365.7	1.61	1.5280	0.0460	0.1478	0.0046	0.8353	941.0	19.0	889.0	26.0	1161	47	889.0	26.0	5.5
GOM19_60	215.5	1.09	1.4520	0.0340	0.1487	0.0039	0.3895	910.0	14.0	894.0	22.0	963	58	894.0	22.0	1.8
GOM19_85	401	3.80	1.5140	0.0400	0.1501	0.0041	0.4232	936.0	16.0	901.0	23.0	969	49	901.0	23.0	3.7

GOM19_83	277	3.49	1.5470	0.0220	0.1539	0.0030	0.5802	949.8	9.0	922.0	17.0	1005	26	922.0	17.0	2.9
GOM19_82	227.1	2.48	1.5630	0.0300	0.1548	0.0033	0.6193	955.0	12.0	927.0	18.0	1000	35	927.0	18.0	2.9
GOM19_79	110.4	0.70	1.5370	0.0530	0.1558	0.0036	0.7413	948.0	20.0	933.0	20.0	980	44	933.0	20.0	1.6
GOM19_67	156.9	0.89	1.5570	0.0480	0.1573	0.0056	0.4124	952.0	19.0	941.0	31.0	1013	82	941.0	31.0	1.2
GOM19_49	511	2.32	1.5850	0.0180	0.1576	0.0023	0.7326	964.1	6.9	943.0	13.0	1014	20	943.0	13.0	2.2
GOM19_38	724	1.60	1.6180	0.0290	0.1580	0.0030	0.7654	976.0	11.0	948.0	18.0	1039	28	948.0	18.0	2.9
GOM19_100	521	2.22	1.6420	0.0260	0.1589	0.0031	0.7907	986.0	9.8	950.0	17.0	1057	23	950.0	17.0	3.7
GOM19_8	309	4.44	1.5980	0.0180	0.1601	0.0015	0.7424	969.0	6.9	957.2	8.2	995	16	957.2	8.2	1.2
GOM19_19	272	0.82	1.6160	0.0320	0.1616	0.0027	0.6372	976.0	13.0	966.0	15.0	995	33	966.0	15.0	1.0
GOM19_102	403	2.40	1.6350	0.0390	0.1624	0.0047	0.7235	983.0	15.0	969.0	26.0	1013	40	969.0	26.0	1.4
GOM19_78	514	2.17	1.6550	0.0350	0.1641	0.0038	0.7387	993.0	14.0	979.0	21.0	1023	34	979.0	21.0	1.4
GOM19_15	431	0.83	1.6460	0.0280	0.1643	0.0038	0.6406	987.0	11.0	980.0	21.0	1003	33	980.0	21.0	0.7
GOM19_104	85	1.09	1.6460	0.0480	0.1649	0.0039	0.5281	987.0	18.0	984.0	22.0	991	48	984.0	22.0	0.3
GOM19_41	186.4	1.76	1.7660	0.0270	0.1650	0.0031	0.6790	1033.9	9.6	984.0	17.0	1127	27	984.0	17.0	4.8
GOM19_47	947	2.10	1.7460	0.0380	0.1673	0.0046	0.7806	1026.0	14.0	996.0	25.0	1064	32	996.0	25.0	2.9
GOM19_26	38.4	1.76	1.6820	0.0390	0.1679	0.0031	0.1977	1003.0	14.0	1000.0	17.0	997	54	997.0	17.0	0.3
GOM19_80	28.6	1.04	1.7360	0.0670	0.1774	0.0059	0.6966	1024.0	26.0	1052.0	32.0	1001	55	1001.0	55.0	5.1
GOM19_35	51.7	1.14	1.7900	0.0500	0.1727	0.0036	0.1870	1041.0	18.0	1027.0	20.0	1010	66	1010.0	66.0	1.7
GOM19_55	40.5	0.82	1.7040	0.0510	0.1689	0.0031	0.0649	1013.0	19.0	1006.0	17.0	1034	68	1034.0	68.0	2.7
GOM19_14	139	1.72	1.7110	0.0370	0.1692	0.0034	0.4905	1012.0	14.0	1007.0	19.0	1035	49	1035.0	49.0	2.7
GOM19_118	83.7	1.15	1.7280	0.0330	0.1711	0.0031	0.3086	1018.0	12.0	1018.0	17.0	1055	41	1055.0	41.0	3.5
GOM19_4	112.3	1.47	2.0100	0.1200	0.1970	0.0097	0.7887	1117.0	40.0	1159.0	52.0	1057	77	1057.0	77.0	9.6
GOM19_74	285	1.07	1.7660	0.0220	0.1717	0.0018	0.4645	1032.6	8.1	1021.6	9.8	1076	23	1076.0	23.0	5.1
GOM19_18	67.9	0.71	1.8240	0.0370	0.1724	0.0024	0.4831	1053.0	13.0	1025.0	13.0	1091	35	1091.0	35.0	6.0
GOM19_121	280	1.49	1.7980	0.0470	0.1696	0.0045	0.7578	1043.0	17.0	1010.0	25.0	1095	32	1095.0	32.0	7.8
GOM19_23	496	6.16	1.7970	0.0320	0.1716	0.0026	0.7953	1044.0	11.0	1021.0	14.0	1098	26	1098.0	26.0	7.0
GOM19_10	721	2.35	1.7830	0.0260	0.1686	0.0026	0.7767	1038.9	9.6	1004.0	14.0	1099	20	1099.0	20.0	8.6
GOM19_50	449	3.70	1.8320	0.0350	0.1747	0.0031	0.7550	1057.0	13.0	1038.0	17.0	1105	29	1105.0	29.0	6.1
GOM19_93	403	3.02	1.8000	0.0290	0.1708	0.0030	0.8284	1047.0	10.0	1016.0	17.0	1105	20	1105.0	20.0	8.1
GOM19_77	59.3	0.56	1.7760	0.0900	0.1705	0.0053	0.6297	1035.0	33.0	1014.0	29.0	1110	67	1110.0	67.0	8.6
GOM19_57	97	1.29	2.0190	0.0510	0.1935	0.0042	0.6573	1129.0	15.0	1139.0	23.0	1111	31	1111.0	31.0	2.5
GOM19_69	286	1.72	1.8130	0.0190	0.1707	0.0019	0.5136	1050.0	6.7	1016.0	11.0	1111	22	1111.0	22.0	8.6
GOM19_37	171.2	0.99	1.8930	0.0260	0.1763	0.0023	0.6659	1077.9	9.3	1048.0	12.0	1112	23	1112.0	23.0	5.8

GOM19_13	494	1.94	1.9790	0.0290	0.1855	0.0037	0.6300	1108.1	9.8	1097.0	20.0	1123	34	1123.0	34.0	2.3
GOM19_105	180	2.99	1.8730	0.0310	0.1760	0.0029	0.5262	1073.0	11.0	1045.0	16.0	1123	31	1123.0	31.0	6.9
GOM19_16	97	1.36	2.0680	0.0390	0.1902	0.0036	0.5064	1137.0	13.0	1122.0	19.0	1126	34	1126.0	34.0	0.4
GOM19_87	217	0.81	2.0360	0.0290	0.1888	0.0031	0.5975	1128.3	9.4	1115.0	17.0	1129	27	1129.0	27.0	1.2
GOM19_45	84.7	1.26	1.9970	0.0360	0.1858	0.0026	0.3345	1116.0	12.0	1099.0	14.0	1134	39	1134.0	39.0	3.1
GOM19_106	117	1.54	1.8690	0.0370	0.1753	0.0056	0.3944	1070.0	13.0	1041.0	31.0	1139	52	1139.0	52.0	8.6
GOM19_101	336	1.46	1.9250	0.0330	0.1776	0.0029	0.7673	1089.0	12.0	1053.0	16.0	1145	24	1145.0	24.0	8.0
GOM19_76	265.9	2.67	1.9520	0.0260	0.1809	0.0025	0.4465	1098.6	8.8	1072.0	14.0	1148	30	1148.0	30.0	6.6
GOM19_48	766	4.61	1.9160	0.0610	0.1776	0.0046	0.8759	1086.0	21.0	1054.0	25.0	1153	33	1153.0	33.0	8.6
GOM19_52	203	2.43	2.1110	0.0270	0.1947	0.0021	0.5923	1153.3	8.6	1147.0	12.0	1155	26	1155.0	26.0	0.7
GOM19_20	219.2	1.87	1.9290	0.0230	0.1771	0.0024	0.5547	1092.6	8.1	1051.0	13.0	1157	25	1157.0	25.0	9.2
GOM19_122	453	2.29	2.0860	0.0260	0.1943	0.0025	0.7353	1145.6	8.2	1145.0	13.0	1168	19	1168.0	19.0	2.0
GOM19_123	258	1.17	2.0200	0.0270	0.1855	0.0027	0.6147	1121.5	9.0	1097.0	15.0	1168	26	1168.0	26.0	6.1
GOM19_9	370	2.02	2.0660	0.0350	0.1891	0.0034	0.7006	1137.0	12.0	1116.0	19.0	1174	27	1174.0	27.0	4.9
GOM19_61	857	3.11	1.8930	0.0220	0.1708	0.0018	0.6366	1078.5	7.6	1016.5	9.8	1174	19	1174.0	19.0	13.4
GOM19_120	1037	2.08	1.8910	0.0240	0.1751	0.0028	0.7805	1077.9	8.5	1040.0	16.0	1175	23	1175.0	23.0	11.5
GOM19_91	81.7	1.39	2.1440	0.0340	0.1939	0.0028	0.5192	1162.0	11.0	1142.0	15.0	1181	31	1181.0	31.0	3.3
GOM19_116	205	1.47	2.1620	0.0800	0.2006	0.0076	0.7348	1175.0	23.0	1189.0	37.0	1185	52	1185.0	52.0	0.3
GOM19_54	148.9	2.15	2.2470	0.0400	0.2006	0.0028	0.4781	1196.0	12.0	1178.0	15.0	1190	32	1190.0	32.0	1.0
GOM19_115	106.7	3.40	2.0910	0.0960	0.1884	0.0068	0.5882	1144.0	32.0	1113.0	37.0	1197	64	1197.0	64.0	7.0
GOM19_95	404	2.04	2.2430	0.0520	0.2027	0.0041	0.6831	1196.0	16.0	1189.0	22.0	1198	34	1198.0	34.0	0.8
GOM19_33	70.3	2.03	2.1220	0.0370	0.1901	0.0032	0.3859	1157.0	12.0	1121.0	17.0	1205	36	1205.0	36.0	7.0
GOM19_34	182	2.85	2.1580	0.0490	0.1924	0.0046	0.8001	1166.0	16.0	1134.0	25.0	1206	28	1206.0	28.0	6.0
GOM19_90	217	2.62	2.3150	0.0530	0.2087	0.0045	0.8927	1218.0	16.0	1221.0	24.0	1208	22	1208.0	22.0	1.1
GOM19_96	184	1.60	2.1740	0.0300	0.1928	0.0037	0.6602	1174.0	10.0	1136.0	20.0	1215	26	1215.0	26.0	6.5
GOM19_56	373	1.15	2.2840	0.0310	0.2029	0.0031	0.7851	1206.5	9.7	1190.0	16.0	1220	23	1220.0	23.0	2.5
GOM19_3	100	2.42	2.4020	0.0540	0.2137	0.0065	0.2083	1243.0	16.0	1248.0	34.0	1224	71	1224.0	71.0	2.0
GOM19_6	267.2	2.16	2.0330	0.0370	0.1808	0.0040	0.5284	1126.0	12.0	1071.0	22.0	1225	38	1225.0	38.0	12.6
GOM19_5	684	0.68	2.1150	0.0380	0.1879	0.0027	0.6976	1153.0	12.0	1110.0	15.0	1226	20	1226.0	20.0	9.5
GOM19_84	486	1.54	2.1570	0.0420	0.1910	0.0038	0.8173	1169.0	13.0	1126.0	20.0	1228	23	1228.0	23.0	8.3
GOM19_97	667	2.28	2.0360	0.0290	0.1769	0.0025	0.6307	1127.2	9.7	1050.0	14.0	1249	24	1249.0	24.0	15.9
GOM19_89	143.9	1.22	2.2700	0.0360	0.1990	0.0028	0.5030	1204.0	11.0	1170.0	15.0	1254	29	1254.0	29.0	6.7
GOM19_17	1032	2.10	2.3810	0.0460	0.2024	0.0052	0.7791	1236.0	14.0	1193.0	29.0	1296	33	1296.0	33.0	7.9

GOM19_43	305	2.85	2.4590	0.0470	0.2093	0.0044	0.6416	1259.0	14.0	1225.0	23.0	1309	33	1309.0	33.0	6.4
GOM19_112	381.2	0.69	2.4690	0.0310	0.2099	0.0027	0.7606	1262.4	9.2	1228.0	14.0	1319	17	1319.0	17.0	6.9
GOM19_109	176.3	2.00	2.5390	0.0400	0.2126	0.0038	0.6579	1284.0	12.0	1242.0	20.0	1358	23	1358.0	23.0	8.5
GOM19_11	344.5	2.09	2.8140	0.0410	0.2278	0.0036	0.6336	1362.0	11.0	1322.0	19.0	1405	27	1405.0	27.0	5.9
GOM19_39	119.7	2.35	2.7840	0.0520	0.2216	0.0051	0.5303	1350.0	14.0	1290.0	27.0	1425	39	1425.0	39.0	9.5
GOM19_29	268	1.20	3.0500	0.0360	0.2437	0.0026	0.6007	1419.8	8.9	1406.0	14.0	1429	20	1429.0	20.0	1.6
GOM19_7	379	1.91	2.8330	0.0240	0.2237	0.0016	0.5019	1364.1	6.3	1301.5	8.6	1455	15	1455.0	15.0	10.5
GOM19_72	683	2.54	2.8960	0.0370	0.2285	0.0033	0.7077	1380.2	9.6	1326.0	17.0	1458	22	1458.0	22.0	9.1
GOM19_98	209.2	0.78	2.9770	0.0500	0.2349	0.0032	0.3301	1401.0	13.0	1360.0	17.0	1459	33	1459.0	33.0	6.8
GOM19_24	435	0.69	3.2110	0.0760	0.2488	0.0066	0.7178	1459.0	18.0	1431.0	34.0	1473	38	1473.0	38.0	2.9
GOM19_30	638	0.84	4.2840	0.0390	0.2878	0.0033	0.7203	1690.0	7.4	1630.0	16.0	1747	14	1747.0	14.0	6.7

Table A3: Detrital zircon U-Pb Geochronologic analyses of lower Miocene sandstones by LA-ICP-MS.

APPENDIX B: SUPPLEMENTARY FILE FOR CHAPTER 3

Appendix B1 U-Pb age data

Sample Name: GOM20

Location: Latitude 29.2569 Longitude -93.3323

			Isotopic Ratios					Isotopic ages (Ma)							
Grain #	**[U] ppm**	**U/Th**	**207/235**	**2σ error**	**206/238**	**2σ error**	**RHO**	**207/235**	**2σ error**	**206/238**	**2σ error**	**207/206**	**2σ error**	**Best age**	**2σ error**	**%Disc.**
GOM20_95	323	0.90	0.0238	0.0021	0.0037	0.0002	0.0078	23.9	2.0	23.5	1.0	160	190	23.5	1.0	1.6
GOM20_97	645	0.68	0.0256	0.0019	0.0040	0.0002	0.1089	25.6	1.9	26.0	1.0	30	150	26.0	1.0	1.6
GOM20_9	313	0.67	0.0267	0.0018	0.0042	0.0002	0.0349	26.8	1.8	27.0	1.1	150	180	27.0	1.1	0.7
GOM20_34	315.7	0.85	0.0303	0.0024	0.0045	0.0002	0.1136	30.3	2.3	28.8	1.6	120	230	28.8	1.6	5.0
GOM20_29	73	0.62	0.0372	0.0038	0.0059	0.0002	0.0791	37.0	3.7	37.7	1.5	50	190	37.7	1.5	1.9
GOM20_3	197	1.89	0.0463	0.0025	0.0070	0.0002	0.0956	45.9	2.4	45.1	1.2	110	100	45.1	1.2	1.7
GOM20_91	291	1.39	0.0934	0.0026	0.0141	0.0003	0.2477	90.6	2.4	90.2	1.7	113	66	90.2	1.7	0.4
GOM20_96	324	1.32	0.1074	0.0026	0.0155	0.0003	0.2310	103.5	2.4	99.4	1.9	209	59	99.4	1.9	4.0
GOM20_23	610	1.11	0.1720	0.0032	0.0252	0.0003	0.2329	161.1	2.7	160.2	1.9	176	43	160.2	1.9	0.6
GOM20_13	164	1.50	0.5130	0.0210	0.0644	0.0025	0.2449	420.0	14.0	402.0	15.0	510	140	402.0	15.0	4.3
GOM20_46	197	0.61	0.5090	0.0100	0.0662	0.0009	0.2960	417.4	6.9	413.2	5.2	431	43	413.2	5.2	1.0
GOM20_53	522	2.61	0.5176	0.0067	0.0680	0.0009	0.5965	423.4	4.5	424.1	5.4	410	27	424.1	5.4	0.2
GOM20_43	64.6	0.49	0.6130	0.0350	0.0751	0.0027	0.7947	485.0	22.0	467.0	16.0	560	190	467.0	16.0	3.7
GOM20_11	99.4	0.84	0.6010	0.0190	0.0753	0.0020	0.1745	478.0	12.0	468.0	12.0	498	89	468.0	12.0	2.1
GOM20_101	250.5	1.35	0.6060	0.0210	0.0760	0.0015	0.3875	481.0	13.0	472.0	8.8	514	69	472.0	8.8	1.9
GOM20_54	245	0.91	0.8450	0.0160	0.0980	0.0021	0.4572	621.7	9.1	603.0	12.0	669	51	603.0	12.0	3.0
GOM20_99	455	3.38	1.5300	0.0360	0.1519	0.0033	0.5750	944.0	15.0	911.0	18.0	987	45	911.0	18.0	3.5
GOM20_33	45.7	1.38	1.6330	0.0350	0.1602	0.0029	0.0589	982.0	14.0	958.0	16.0	1001	63	958.0	16.0	2.4

GOM20_28	26.7	0.35	1.5900	0.0680	0.1598	0.0044	0.0006	964.0	27.0	962.0	26.0	960	110	962.0	26.0	0.2
GOM20_19	446	1.15	1.6060	0.0250	0.1611	0.0019	0.6229	972.3	9.7	963.0	10.0	976	24	963.0	10.0	1.0
GOM20_64	34.3	0.75	1.6510	0.0510	0.1635	0.0041	0.3948	992.0	20.0	976.0	23.0	1028	60	976.0	23.0	1.6
GOM20_44	215	2.39	1.6560	0.0290	0.1647	0.0027	0.5702	991.0	11.0	983.0	15.0	1006	36	983.0	15.0	0.8
GOM20_83	78.7	2.18	1.6940	0.0240	0.1677	0.0019	0.3960	1005.4	9.2	999.0	11.0	1035	27	999.0	11.0	0.6
GOM20_42	142.9	4.90	1.7290	0.0390	0.1712	0.0040	0.6183	1019.0	14.0	1019.0	22.0	1005	37	1005.0	37.0	1.4
GOM20_59	215	4.52	1.7020	0.0180	0.1696	0.0018	0.4768	1008.7	6.6	1009.9	9.7	1021	23	1021.0	23.0	1.1
GOM20_7	191	1.32	1.7070	0.0320	0.1700	0.0031	0.6407	1011.0	12.0	1012.0	17.0	1025	35	1025.0	35.0	1.3
GOM20_81	68.1	1.02	1.7100	0.0370	0.1689	0.0027	0.1769	1011.0	14.0	1006.0	15.0	1025	46	1025.0	46.0	1.9
GOM20_27	65.8	0.74	1.7900	0.0290	0.1753	0.0028	0.5568	1044.0	10.0	1041.0	15.0	1026	32	1026.0	32.0	1.5
GOM20_82	20.2	1.41	1.7220	0.0750	0.1686	0.0030	0.4698	1023.0	26.0	1004.0	17.0	1032	70	1032.0	70.0	2.7
GOM20_105	19.4	1.16	1.7410	0.0560	0.1687	0.0037	0.2024	1020.0	21.0	1008.0	20.0	1032	74	1032.0	74.0	2.3
GOM20_76	185	1.18	1.7220	0.0300	0.1690	0.0030	0.5117	1016.0	11.0	1007.0	16.0	1041	34	1041.0	34.0	3.3
GOM20_8	43.9	1.19	1.8010	0.0490	0.1751	0.0046	0.2543	1045.0	18.0	1040.0	25.0	1043	49	1043.0	49.0	0.3
GOM20_40	29.6	0.82	1.8090	0.0540	0.1735	0.0048	0.1093	1047.0	20.0	1031.0	26.0	1056	86	1056.0	86.0	2.4
GOM20_30	63.9	0.82	1.7830	0.0580	0.1710	0.0032	0.1010	1038.0	21.0	1018.0	17.0	1057	55	1057.0	55.0	3.7
GOM20_94	310	1.99	1.7580	0.0330	0.1723	0.0029	0.5992	1030.0	12.0	1025.0	16.0	1058	34	1058.0	34.0	3.1
GOM20_120	100.4	1.44	1.7710	0.0330	0.1733	0.0030	0.4882	1034.0	12.0	1030.0	16.0	1058	38	1058.0	38.0	2.6
GOM20_52	201	2.41	1.7190	0.0230	0.1686	0.0027	0.5928	1016.1	8.5	1004.0	15.0	1060	28	1060.0	28.0	5.3
GOM20_87	171	1.69	1.8310	0.0280	0.1773	0.0023	0.5144	1056.0	10.0	1052.0	12.0	1060	30	1060.0	30.0	0.8
GOM20_35	238.8	5.70	1.8120	0.0230	0.1749	0.0021	0.4961	1052.4	8.5	1039.0	12.0	1061	24	1061.0	24.0	2.1
GOM20_121	178.8	1.78	1.8520	0.0230	0.1793	0.0022	0.1510	1063.8	8.1	1063.0	12.0	1062	31	1062.0	31.0	0.1
GOM20_109	61.3	3.75	1.8060	0.0570	0.1711	0.0040	0.1552	1050.0	20.0	1018.0	22.0	1063	77	1063.0	77.0	4.2
GOM20_1	48.6	0.98	1.7550	0.0350	0.1712	0.0025	0.1197	1028.0	13.0	1018.0	14.0	1072	42	1072.0	42.0	5.0
GOM20_116	75.2	0.56	1.9070	0.0290	0.1818	0.0026	0.4745	1083.0	10.0	1076.0	14.0	1079	29	1079.0	29.0	0.3
GOM20_108	395	27.10	1.7990	0.0540	0.1712	0.0037	0.7286	1044.0	20.0	1018.0	20.0	1085	55	1085.0	55.0	6.2
GOM20_110	111.1	1.03	1.8700	0.0350	0.1789	0.0027	0.3538	1069.0	12.0	1061.0	15.0	1087	32	1087.0	32.0	2.4
GOM20_104	105.7	2.62	1.8260	0.0280	0.1752	0.0021	0.6302	1054.0	10.0	1041.0	12.0	1090	23	1090.0	23.0	4.5

GOM20_51	125.3	1.49	1.8360	0.0230	0.1780	0.0021	0.4779	1057.9	8.3	1056.0	11.0	1091	23	1091.0	23.0	3.2
GOM20_48	91.2	0.93	1.8660	0.0350	0.1782	0.0026	0.1794	1068.0	12.0	1057.0	14.0	1095	42	1095.0	42.0	3.5
GOM20_84	184	1.63	1.9680	0.0730	0.1879	0.0053	0.4433	1104.0	25.0	1110.0	29.0	1099	71	1099.0	71.0	1.0
GOM20_73	140	2.48	1.8290	0.0430	0.1731	0.0030	0.5800	1055.0	16.0	1029.0	16.0	1100	45	1100.0	45.0	6.5
GOM20_93	47.4	0.90	2.0050	0.0360	0.1897	0.0035	0.4550	1118.0	12.0	1120.0	19.0	1103	38	1103.0	38.0	1.5
GOM20_14	111.45	0.85	1.9470	0.0610	0.1838	0.0043	0.5056	1097.0	21.0	1088.0	23.0	1109	52	1109.0	52.0	1.9
GOM20_123	106	1.54	1.9700	0.0350	0.1861	0.0022	0.6423	1104.0	12.0	1102.0	12.0	1110	29	1110.0	29.0	0.7
GOM20_74	116.1	1.13	1.9670	0.0430	0.1851	0.0043	0.5578	1106.0	15.0	1094.0	23.0	1111	43	1111.0	43.0	1.5
GOM20_80	58.1	1.52	1.9940	0.0310	0.1899	0.0026	0.4520	1113.0	10.0	1120.0	14.0	1117	30	1117.0	30.0	0.3
GOM20_111	150.7	0.83	2.0540	0.0280	0.1910	0.0022	0.3750	1133.1	9.4	1126.0	12.0	1132	28	1132.0	28.0	0.5
GOM20_88	505	5.14	1.8680	0.0210	0.1755	0.0019	0.7499	1069.5	7.6	1042.0	10.0	1135	15	1135.0	15.0	8.2
GOM20_78	112	0.71	2.0130	0.0350	0.1891	0.0026	0.0177	1119.0	11.0	1116.0	14.0	1139	37	1139.0	37.0	2.0
GOM20_2	54	0.43	2.1020	0.0620	0.1981	0.0051	0.5996	1147.0	20.0	1164.0	28.0	1140	46	1140.0	46.0	2.1
GOM20_60	113.2	1.01	2.0350	0.0370	0.1892	0.0027	0.3852	1127.0	12.0	1117.0	14.0	1141	37	1141.0	37.0	2.1
GOM20_119	112.2	35.00	1.9910	0.0310	0.1840	0.0031	0.4714	1112.0	11.0	1089.0	17.0	1145	38	1145.0	38.0	4.9
GOM20_66	21.56	0.74	1.9650	0.0610	0.1828	0.0058	0.1184	1102.0	21.0	1082.0	32.0	1148	90	1148.0	90.0	5.7
GOM20_36	214.8	2.11	2.0680	0.0420	0.1920	0.0037	0.6433	1141.0	13.0	1132.0	20.0	1149	35	1149.0	35.0	1.5
GOM20_47	97	0.89	1.9720	0.0340	0.1825	0.0020	0.5082	1105.0	12.0	1080.0	11.0	1151	32	1151.0	32.0	6.2
GOM20_77	198.7	2.59	2.0350	0.0230	0.1886	0.0025	0.6555	1126.8	7.7	1114.0	13.0	1158	20	1158.0	20.0	3.8
GOM20_4	112.8	1.16	2.1590	0.0260	0.1976	0.0029	0.4312	1168.4	8.5	1164.0	16.0	1164	27	1164.0	27.0	0.0
GOM20_118	222	1.52	2.0800	0.0210	0.1918	0.0018	0.5820	1141.8	7.0	1131.1	9.6	1164	18	1164.0	18.0	2.8
GOM20_17	166.9	1.52	2.1050	0.0220	0.1925	0.0014	0.4149	1152.0	7.3	1135.0	7.6	1182	21	1182.0	21.0	4.0
GOM20_106	74.3	2.00	2.0700	0.0420	0.1868	0.0037	0.3036	1138.0	14.0	1104.0	20.0	1195	36	1195.0	36.0	7.6
GOM20_71	92	1.08	2.2960	0.0390	0.2044	0.0033	0.4790	1210.0	12.0	1198.0	18.0	1218	34	1218.0	34.0	1.6
GOM20_18	454.7	6.28	2.0290	0.0390	0.1795	0.0048	0.6929	1125.0	13.0	1064.0	26.0	1221	36	1221.0	36.0	12.9
GOM20_113	159	3.11	2.3920	0.0290	0.2120	0.0023	0.5541	1240.5	8.4	1239.0	12.0	1225	21	1225.0	21.0	1.1
GOM20_61	139	1.43	2.2830	0.0310	0.2039	0.0032	0.4957	1206.2	9.4	1196.0	17.0	1236	28	1236.0	28.0	3.2
GOM20_112	26.9	1.09	2.4550	0.0630	0.2132	0.0038	0.4223	1256.0	19.0	1245.0	20.0	1254	51	1254.0	51.0	0.7

GOM20_68	59.8	2.05	2.3430	0.0410	0.2055	0.0036	0.4067	1224.0	13.0	1204.0	19.0	1257	36	1257.0	36.0	4.2
GOM20_56	151	2.17	2.5470	0.0360	0.2190	0.0024	0.6174	1288.0	11.0	1278.0	13.0	1296	23	1296.0	23.0	1.4
GOM20_16	60.3	1.37	2.4110	0.0590	0.2085	0.0040	0.5231	1244.0	18.0	1220.0	21.0	1298	42	1298.0	42.0	6.0
GOM20_107	187.3	1.89	2.5430	0.0290	0.2181	0.0021	0.3337	1284.1	8.3	1272.0	11.0	1306	24	1306.0	24.0	2.6
GOM20_98	112.3	1.25	2.4530	0.0800	0.2086	0.0049	0.8384	1257.0	24.0	1220.0	26.0	1308	37	1308.0	37.0	6.7
GOM20_89	62.2	0.90	2.4820	0.0630	0.2100	0.0039	0.3016	1266.0	18.0	1229.0	21.0	1313	46	1313.0	46.0	6.4
GOM20_42	44.26	0.89	2.6260	0.0580	0.2212	0.0040	0.1947	1307.0	16.0	1288.0	21.0	1343	47	1343.0	47.0	4.1
GOM20_72	83.3	1.73	2.7110	0.0350	0.2277	0.0028	0.4727	1330.5	9.5	1322.0	15.0	1355	27	1355.0	27.0	2.4
GOM20_117	62.5	1.23	2.7400	0.0780	0.2265	0.0043	0.7175	1338.0	21.0	1316.0	23.0	1372	37	1372.0	37.0	4.1
GOM20_102	271	1.48	2.9090	0.0370	0.2382	0.0034	0.6780	1383.5	9.5	1377.0	18.0	1384	20	1384.0	20.0	0.5
GOM20_114	195	1.98	2.8320	0.0470	0.2349	0.0047	0.2511	1364.0	12.0	1360.0	25.0	1407	53	1407.0	53.0	3.3
GOM20_103	38.75	1.69	2.4700	0.1200	0.2050	0.0130	0.2481	1263.0	33.0	1200.0	70.0	1417	63	1417.0	63.0	15.3
GOM20_49	64.4	2.49	2.9390	0.0660	0.2406	0.0036	0.4328	1391.0	17.0	1390.0	19.0	1423	35	1423.0	35.0	2.3
GOM20_86	306	1.10	3.0830	0.0250	0.2509	0.0019	0.5973	1428.0	6.3	1443.1	9.9	1426	15	1426.0	15.0	1.2
GOM20_21	176	1.62	3.0250	0.0490	0.2436	0.0041	0.5087	1413.0	12.0	1405.0	21.0	1437	31	1437.0	31.0	2.2
GOM20_58	344	1.01	3.0990	0.0380	0.2477	0.0023	0.2336	1429.4	8.2	1426.0	12.0	1445	17	1445.0	17.0	1.3
GOM20_70	52.4	1.05	3.0810	0.0550	0.2470	0.0035	0.3439	1429.0	14.0	1423.0	18.0	1458	37	1458.0	37.0	2.4
GOM20_122	70.1	1.57	3.1670	0.0550	0.2527	0.0038	0.7166	1448.0	14.0	1452.0	19.0	1462	24	1462.0	24.0	0.7
GOM20_26	64.7	0.64	3.2820	0.0840	0.2517	0.0046	0.7515	1480.0	20.0	1446.0	24.0	1520	32	1520.0	32.0	4.9
GOM20_69	112	0.54	3.9630	0.0460	0.2878	0.0031	0.5953	1627.1	9.2	1630.0	15.0	1622	18	1622.0	18.0	0.5
GOM20_37	200	2.14	4.1720	0.0660	0.2947	0.0047	0.8129	1669.0	13.0	1664.0	24.0	1650	19	1650.0	19.0	0.8
GOM20_20	61.1	2.20	4.3240	0.0720	0.3006	0.0054	0.7572	1696.0	14.0	1693.0	27.0	1675	30	1675.0	30.0	1.1
GOM20_5	72.2	0.45	4.2330	0.0780	0.2966	0.0078	0.8059	1680.0	15.0	1674.0	39.0	1690	27	1690.0	27.0	0.9
GOM20_79	43.2	0.73	4.3930	0.0960	0.3021	0.0063	0.3334	1712.0	19.0	1701.0	31.0	1726	45	1726.0	45.0	1.4
GOM20_32	139	0.76	4.5150	0.0650	0.3043	0.0053	0.5472	1735.0	11.0	1712.0	26.0	1743	29	1743.0	29.0	1.8
GOM20_63	187.2	0.69	4.1270	0.0730	0.2823	0.0060	0.7355	1658.0	14.0	1602.0	30.0	1751	29	1751.0	29.0	8.5
GOM20_50	250	1.18	4.5460	0.0530	0.3085	0.0034	0.7557	1740.3	9.6	1733.0	17.0	1753	14	1753.0	14.0	1.1
GOM20_124	273	0.56	4.1900	0.0700	0.2835	0.0062	0.7922	1671.0	14.0	1608.0	31.0	1757	23	1757.0	23.0	8.5

GOM20_67	171.3	2.63	4.5800	0.2100	0.3060	0.0150	0.7785	1743.0	38.0	1719.0	75.0	1758	41	1758.0	41.0	2.2
GOM20_22	249	1.02	4.6240	0.0700	0.3105	0.0048	0.7537	1756.0	12.0	1743.0	24.0	1767	19	1767.0	19.0	1.4
GOM20_90	51.7	0.45	4.6250	0.0760	0.3114	0.0052	0.3295	1753.0	14.0	1747.0	25.0	1773	42	1773.0	42.0	1.5
GOM20_38	129.5	1.37	4.0200	0.1000	0.2630	0.0071	0.6039	1637.0	21.0	1505.0	36.0	1792	39	1792.0	39.0	16.0
GOM20_24	87	1.05	5.1560	0.0880	0.3278	0.0053	0.2624	1848.0	15.0	1828.0	26.0	1878	38	1878.0	38.0	2.7
GOM20_85	104	1.21	7.0500	0.1800	0.3915	0.0083	0.7917	2123.0	22.0	2134.0	37.0	2079	24	2079.0	24.0	2.6
GOM20_55	75.4	0.75	13.0440	0.0930	0.5156	0.0038	0.4902	2682.4	6.7	2680.0	16.0	2685	12	2685.0	12.0	0.2
GOM20_12	62.4	1.04	13.6600	0.2300	0.5280	0.0100	0.8497	2725.0	16.0	2733.0	44.0	2728	17	2728.0	17.0	0.2
GOM20_100	78.9	1.67	27.8500	0.4000	0.6970	0.0130	0.7698	3415.0	14.0	3407.0	49.0	3417	18	3417.0	18.0	0.3

Table B1: Detrital zircon U-Pb age data of sample GOM20.

Appendix B2 Double-dated zircon U-Pb and ZHe ages

Sample	U-Pb age (Ma)	±2σ (Ma)	(U-Th)/He age (Ma)	±2σ (Ma)	U (ppm)	Th (ppm)	147Sm (ppm)	[U]e	Th/U	He (nmol/g)	mass (ug)	Ft	ESR
GOM1-6	641	10	254.1	20.33	50.4	22.5	3.6	55.6	0.45	56.9	3.20	0.73	43.40
GOM1-15	1690	18	188.5	15.08	440.7	181.3	6.9	482.5	0.41	361.4	3.23	0.73	42.17
GOM1-23	1017	51	364.5	29.16	18.6	8.0	1.3	20.5	0.43	30.4	3.26	0.74	43.72
GOM1-27	1671	19	207.3	16.58	85.2	46.7	2.2	95.9	0.55	86.4	8.46	0.79	57.19
GOM1-36	1073	30	396.5	31.72	38.9	26.2	1.9	44.9	0.67	72.0	3.30	0.73	43.00
GOM1-42	1233	42	803.0	64.24	81.2	17.3	1.3	85.2	0.21	289.8	3.33	0.74	43.52
GOM1-67	533	9.5	373.5	29.88	40.6	28.7	2.3	47.3	0.71	74.7	5.11	0.76	50.01
GOM1-71	1360	30	133.2	10.66	57.3	24.2	0.9	62.8	0.42	35.9	6.93	0.79	55.28
GOM1-109	1372	34	389.1	31.13	24.7	15.9	8.1	28.4	0.65	44.8	3.54	0.73	43.30
GOM1-115	1612	22	83.7	6.69	215.0	20.1	1.5	219.6	0.09	75.0	4.11	0.75	45.98
GOM1-116	1106	27	959.1	76.73	96.1	43.6	9.4	106.2	0.45	506.8	17.47	0.84	76.66
GOM1-123	1412	22	215.8	17.26	82.5	36.7	3.0	90.9	0.45	85.6	9.99	0.80	57.84
GOM2-10	1422	10	45.4	3.63	51.1	39.2	0.5	60.1	0.77	12.1	16.79	0.82	66.52
GOM2-104	1102	20	372.9	29.83	63.7	27.1	0.6	69.9	0.43	106.6	3.30	0.74	44.20
GOM2-12	37.1	2.5	37.2	2.98	718.3	411.2	2.6	813.0	0.57	132.5	13.79	0.81	62.30
GOM2-25	1670	13	624.4	49.95	105.9	65.3	1.4	120.9	0.62	350.3	10.89	0.82	65.65
GOM2-26	152.2	2.8	95.1	7.61	56.0	56.5	0.6	69.0	1.01	30.5	23.42	0.85	84.13
GOM2-33	58.8	1	64.3	5.14	161.4	99.0	0.2	184.1	0.61	54.0	20.01	0.84	75.90
GOM2-34	33.2	1.5	32.6	2.61	47.1	109.3	0.3	72.3	2.32	10.8	20.14	0.84	77.45
GOM2-4	172.7	2.1	160.8	12.86	163.2	147.3	0.7	197.1	0.90	146.9	20.40	0.85	79.95
GOM2-41	1636	8.5	366.8	29.34	95.6	44.1	0.3	105.8	0.46	172.5	8.10	0.80	59.59
GOM2-52	74.2	1.3	78.6	6.29	39.1	10.8	0.2	41.6	0.28	15.6	38.46	0.88	98.67
GOM2-56	1663	14	70.4	5.64	131.4	45.6	0.4	141.9	0.35	46.6	25.14	0.86	85.43
GOM2-69	91.7	2.1	86.1	6.89	120.7	67.9	0.4	136.3	0.56	54.7	22.86	0.86	84.75
GOM2-7	229.1	2	148.0	11.84	240.2	68.2	0.3	255.9	0.28	177.7	25.28	0.86	85.39

GOM2-85	198	2.3	151.3	12.10	113.6	36.1	0.1	121.9	0.32	87.1	30.11	0.86	88.50
GOM2-93	1218	12	62.8	5.02	150.5	74.0	1.6	167.5	0.49	42.9	4.22	0.75	47.28
GOM2-97	72.4	1.8	62.8	5.03	29.1	28.4	0.5	35.6	0.98	10.0	13.13	0.82	67.98
GOM2-62	1019	13	73.0	5.84	304.5	144.4	1.5	337.7	0.47	98.2	3.92	0.73	43.61
GOM4-69	1152.1	7	125.7	10.06	249.3	25.7	0.8	255.2	0.10	134.4	5.31	0.77	49.82
GOM4-70	1134	19	1241.2	99.30	75.5	34.2	10.9	83.4	0.45	432.1	2.52	0.70	38.14
GOM4-72	1036	23	837.6	67.01	11.1	7.2	3.1	12.8	0.65	47.6	5.85	0.77	51.69
GOM4-108	1090.4	7	264.5	21.16	78.1	47.6	9.6	89.1	0.61	101.5	7.33	0.78	54.49
GOM7-108	1459	16	665.7	53.26	69.8	33.1	2.4	77.5	0.47	244.0	15.33	0.83	70.00
GOM7-652	1689.1	6	61.6	4.92	217.8	65.5	1.2	232.9	0.30	61.4	7.37	0.79	55.77
GOM7-602	1675.3	8.4	127.2	10.17	187.8	39.3	1.2	196.9	0.21	104.3	4.97	0.77	49.16
GOM7-648	1421	10	181.0	14.48	73.9	26.5	0.5	80.0	0.36	66.6	17.34	0.84	74.99
GOM7-106	1017	13	407.0	32.56	70.1	31.3	0.8	77.3	0.45	139.4	7.43	0.80	58.23
GOM7-1	56.38	0.74	63.2	5.05	151.2	67.4	0.2	166.8	0.45	49.1	33.93	0.86	85.58
GOM7-4	56.79	0.84	55.8	4.46	133.8	73.4	0.2	150.7	0.55	38.1	17.62	0.84	73.24
GOM7-606	167.8	1.6	156.0	12.48	302.4	216.4	0.9	352.2	0.72	234.0	7.00	0.78	54.03
GOM7-621	93.5	2.7	65.9	5.27	66.9	27.2	0.3	73.2	0.41	21.9	15.62	0.84	73.57
GOM7-634	1711	12	86.5	6.92	302.5	212.0	2.8	351.4	0.70	127.7	6.02	0.77	52.18
GOM7-653	1158	14	118.7	9.50	33.0	17.9	1.0	37.2	0.54	19.7	13.52	0.82	66.71
GOM7-654	1003	21	54.1	4.33	26.7	17.5	0.7	30.7	0.66	6.9	5.34	0.76	50.18
GOM7-658	74.2	1.6	53.2	4.26	245.1	105.1	0.5	269.3	0.43	61.0	7.51	0.79	55.06
GOM7-659	1693.4	6.1	127.1	10.16	132.5	30.1	0.8	139.4	0.23	78.0	9.77	0.81	61.46
GOM7-78	1136	13	203.4	16.27	202.4	53.1	0.6	214.6	0.26	188.6	6.88	0.79	55.41
GOM7-92	98.8	1.1	76.5	6.12	327.5	156.2	1.3	363.5	0.48	117.9	8.67	0.78	53.74
GOM7-98	1410.4	7.8	139.8	11.18	91.3	27.7	0.4	97.6	0.30	62.3	17.86	0.84	73.26
GOM8-2	1069	19	322.7	25.81	320.7	116.2	4.9	347.5	0.36	503.5	10.75	0.81	62.98
GOM8-27	1394	18	94.0	7.52	145.3	75.7	3.3	162.7	0.52	71.6	25.88	0.86	87.11
GOM8-45	1714	21	117.7	9.42	79.6	39.2	3.1	88.7	0.49	46.7	11.79	0.82	66.78
GOM8-60	1184	65	213.4	17.08	100.3	71.0	17.6	116.7	0.71	112.7	14.40	0.82	68.66

GOM8-90	1430	41	98.8	7.90	88.0	46.9	2.5	98.8	0.53	44.7	18.18	0.84	76.33
GOM8-95	1711	18	184.8	14.79	181.1	99.9	4.6	204.1	0.55	163.3	7.39	0.79	56.79
GOM8-108	1455	39	40.8	3.27	75.9	50.3	1.4	87.5	0.66	16.3	23.59	0.84	77.44
GOM8-120	1729	17	102.7	8.21	153.2	73.2	3.7	170.1	0.48	74.7	7.48	0.79	55.22
GOM8-122	40.3	1.8	47.0	3.76	109.2	66.3	1.5	124.5	0.61	26.8	20.70	0.84	77.55
GOM10-81	1175.3	7.9	339.1	27.12	176.2	41.7	0.5	185.7	0.24	293.5	15.64	0.84	74.50
GOM10-124	1513	10	217.0	17.36	46.5	37.1	0.5	55.0	0.80	51.4	6.43	0.78	55.51
GOM10-25	1457.7	6.3	139.2	11.14	120.9	44.4	0.7	131.1	0.37	81.6	11.45	0.82	66.04
GOM10-94	1450.6	7.2	259.0	20.72	44.0	22.1	0.4	49.1	0.50	60.2	25.40	0.86	86.34
GOM10-95	1692.4	6.3	74.0	5.92	304.7	113.4	4.9	330.8	0.37	103.9	6.22	0.78	53.97
GOM10-38	1701.8	7.9	742.9	59.43	55.4	33.7	0.9	63.2	0.61	210.1	6.12	0.78	54.42
GOM10-31	1708.7	7.1	114.9	9.19	95.7	55.8	0.5	108.5	0.58	55.4	11.25	0.82	65.19
GOM10-9	1460	7.1	267.3	21.38	203.8	87.2	3.0	223.9	0.43	250.2	4.84	0.76	48.68
GOM10-117	81.8	4.1	66.4	5.31	208.9	94.3	0.6	230.6	0.45	64.6	6.77	0.78	52.80
GOM10-119	46.42	0.73	49.0	3.92	263.3	154.4	1.2	298.8	0.59	63.1	12.05	0.80	58.32
GOM10-19	61.4	1.6	46.8	3.75	173.5	85.5	19.0	193.3	0.49	38.9	8.43	0.79	57.11
GOM10-21	36.4	1.2	37.3	2.98	152.7	91.1	1.1	173.7	0.60	26.8	8.07	0.76	49.79
GOM10-22	1144	18	817.8	65.42	20.2	10.4	0.4	22.6	0.51	87.6	13.39	0.82	66.25
GOM10-3	164.5	2.6	84.6	6.77	61.0	37.1	0.4	69.5	0.61	25.4	7.20	0.79	57.55
GOM10-64	33.9	1.3	31.1	2.48	71.9	78.7	0.6	90.0	1.09	10.5	2.52	0.69	37.61
GOM10-80	1703.8	5.9	55.5	4.44	219.9	48.6	1.0	231.1	0.22	50.0	3.04	0.72	40.38
GOM10-84	78.3	1.2	66.5	5.32	194.0	67.9	0.4	209.6	0.35	60.8	9.67	0.80	60.41
GOM10-93	1275	27	358.1	28.65	47.5	33.6	0.5	55.2	0.71	83.4	4.98	0.76	49.60
GOM13-10	1754.8	5.9	962.7	77.01	86.4	24.8	0.3	92.1	0.29	421.6	8.93	0.81	61.22
GOM13-106	366	3.7	196.6	15.73	177.1	80.8	0.9	195.7	0.46	152.2	2.95	0.72	41.68
GOM13-118	1430	16	868.2	69.45	47.9	27.6	1.0	54.3	0.58	212.6	6.01	0.78	53.57
GOM13-120	80.7	1.3	92.0	7.36	104.3	73.7	0.7	121.2	0.71	49.5	12.96	0.82	65.49
GOM13-23	77.8	2.2	54.0	4.32	223.3	63.1	0.4	237.8	0.28	56.7	10.62	0.82	64.33
GOM13-24	56.66	0.83	60.3	4.82	290.6	169.0	0.4	329.5	0.58	86.1	9.33	0.80	59.25

GOM13-36	1824.5	6.7	186.7	14.94	58.7	68.7	2.8	74.6	1.17	56.6	3.82	0.74	46.08
GOM13-48	1716.4	7.7	127.7	10.22	110.9	51.6	0.7	122.8	0.47	62.2	3.03	0.73	42.53
GOM13-49	1687.3	4.4	91.7	7.34	127.3	23.6	0.4	132.7	0.19	53.5	9.43	0.81	61.12
GOM13-5	208.9	1.9	183.0	14.64	654.5	126.3	3.5	683.6	0.19	512.0	3.88	0.75	45.68
GOM13-52	163.6	2.6	117.0	9.36	271.9	244.2	0.9	328.1	0.90	157.2	4.81	0.75	47.68
GOM13-54	987	16	354.5	28.36	16.2	16.6	0.5	20.0	1.03	30.1	5.14	0.76	50.81
GOM13-61	189	1.5	219.8	17.59	109.6	44.2	0.1	119.8	0.40	120.2	14.11	0.83	71.10
GOM13-63	1069.4	9.8	390.4	31.23	46.5	36.5	0.7	54.9	0.78	87.4	3.43	0.73	44.26
GOM13-67	39.16	0.97	35.4	2.83	51.5	37.2	0.3	60.1	0.72	9.5	14.13	0.82	68.50
GOM13-90	1085	17	288.0	23.04	22.1	15.2	0.6	25.6	0.69	30.5	4.04	0.75	47.05
GOM13-92	36.77	0.6	37.5	3.00	210.8	143.4	0.5	243.8	0.68	39.4	7.65	0.80	58.43
GOM14-101	425.1	4.5	217.8	17.42	229.0	86.6	1.2	248.9	0.38	228.3	5.15	0.77	50.34
GOM14-12	1183	21	323.3	25.86	128.9	43.8	2.2	139.0	0.34	200.0	9.02	0.80	60.29
GOM14-20	1183	32	214.9	17.20	71.8	44.0	2.6	81.9	0.61	80.3	14.37	0.83	71.12
GOM14-26	986	27	104.9	8.39	112.6	41.4	1.1	122.1	0.37	54.1	6.11	0.78	52.46
GOM14-27	1394	25	53.8	4.31	141.5	69.1	0.7	157.4	0.49	38.2	14.34	0.83	70.95
GOM14-38	1651	20	267.9	21.43	139.5	48.5	3.6	150.6	0.35	172.7	6.11	0.78	52.60
GOM14-40	1381	21	75.5	6.04	237.8	72.2	1.5	254.5	0.30	80.7	7.54	0.77	51.65
GOM14-42	1047	31	363.0	29.04	77.2	333.1	27.6	154.0	4.32	243.1	7.28	0.78	56.87
GOM14-45	1686	23	64.6	5.17	368.6	94.3	1.5	390.3	0.26	108.8	7.42	0.80	57.49
GOM14-47	1039	27	395.9	31.67	91.8	38.1	1.9	100.5	0.42	171.7	6.26	0.78	52.43
GOM14-5	1185	16	264.8	21.18	158.1	25.8	1.1	164.0	0.16	183.7	5.65	0.77	49.89
GOM14-54	432.1	7.6	320.7	25.65	296.8	131.5	2.6	327.0	0.44	423.8	3.46	0.73	43.20
GOM14-68	1078	34	276.2	22.09	44.2	20.9	0.3	49.0	0.47	61.9	14.91	0.83	70.20
GOM14-74	1202	34	306.9	24.56	54.6	48.3	1.4	65.7	0.89	82.7	4.28	0.74	45.94
GOM14-75	1688	20	110.5	8.84	135.5	80.8	8.2	154.1	0.60	73.6	8.29	0.79	57.57
GOM14-8	1790	9.7	84.7	6.77	238.7	46.0	1.0	249.3	0.19	91.4	7.79	0.80	57.78
GOM14-9	1443	22	1100.1	88.01	48.1	25.0	1.9	53.8	0.52	282.6	11.10	0.80	59.56
GOM14-97	1038	17	361.8	28.94	264.0	125.0	4.2	292.8	0.47	440.0	4.07	0.75	46.64

GOM19-101	1145	24	127.8	10.22	202.9	32.3	1.2	210.3	0.16	115.5	8.10	0.79	55.10
GOM19-103	410	5.1	213.9	17.11	208.6	82.6	1.1	227.6	0.40	211.6	7.15	0.79	56.91
GOM19-104	291.4	6.7	152.6	12.21	115.4	29.9	0.8	122.2	0.26	83.1	10.49	0.82	64.22
GOM19-107	334.2	8.2	240.4	19.23	477.8	79.2	4.9	496.0	0.17	515.1	8.03	0.79	54.38
GOM19-118	454	26	47.3	3.78	185.4	53.2	1.6	197.6	0.29	38.5	5.02	0.76	48.45
GOM19-14	1035	49	124.5	9.96	54.3	18.0	1.1	58.4	0.33	30.5	5.42	0.77	50.81
GOM19-34	1206	28	224.4	17.95	97.8	20.9	0.3	102.7	0.21	97.3	5.71	0.77	50.44
GOM19-36	406.1	9.7	217.5	17.40	167.3	71.0	1.5	183.7	0.42	177.3	9.83	0.81	62.08
GOM19-37	1112	23	161.9	12.95	74.3	31.8	1.4	81.7	0.43	56.1	10.02	0.78	52.72
GOM19-39	1425	39	145.6	11.65	47.0	12.0	0.7	49.8	0.26	27.6	2.98	0.70	37.37
GOM19-46	311.1	3.8	206.2	16.49	128.8	137.3	1.3	160.4	1.07	124.2	3.71	0.69	36.95
GOM19-48	1153	33	170.8	13.67	333.4	37.2	0.7	342.0	0.11	233.9	3.69	0.73	42.48
GOM19-50	1105	29	143.6	11.49	195.8	31.9	0.5	203.1	0.16	121.7	5.06	0.77	49.15
GOM19-70	289.7	3.8	200.2	16.01	230.9	142.3	1.1	263.6	0.62	220.8	6.02	0.76	49.96
GOM19-71	452	29	121.0	9.68	32.6	11.0	0.4	35.2	0.34	17.2	3.67	0.74	44.99
GOM19-84	1228	23	215.0	17.20	135.5	46.5	0.4	146.2	0.34	126.7	3.80	0.74	43.64
GOM19-98	1459	33	206.9	16.56	91.2	30.3	0.2	98.2	0.33	91.0	11.21	0.82	64.77
GOM19-99	445.5	7.3	137.4	10.99	332.0	224.0	3.0	383.6	0.67	194.8	2.32	0.68	35.61
GOM20-11	468	12	259.0	20.72	61.0	17.9	1.3	65.2	0.29	71.4	5.80	0.77	50.50
GOM20-14	1109	52	363.7	29.10	112.5	87.3	9.8	132.7	0.78	194.7	3.11	0.73	43.18
GOM20-27	1026	32	297.3	23.79	64.7	47.6	3.1	75.7	0.74	97.9	7.87	0.79	56.45
GOM20-33	958	16	343.7	27.50	73.2	31.3	6.4	80.4	0.43	122.9	10.39	0.80	59.96
GOM20-37	1650	19	116.3	9.30	214.3	55.4	2.1	227.1	0.26	105.3	3.47	0.73	42.88
GOM20-47	1151	32	261.5	20.92	92.8	50.3	4.5	104.4	0.54	122.1	11.56	0.81	63.74
GOM20-53	424.1	5.4	327.5	26.20	302.0	95.1	55.3	324.2	0.31	445.7	4.62	0.76	48.18
GOM20-58	1445	17	91.8	7.35	94.9	61.6	2.2	109.1	0.65	40.8	4.29	0.75	46.66
GOM20-79	1726	45	63.3	5.06	126.1	36.1	6.4	134.5	0.29	35.4	4.81	0.77	49.84
GOM20-86	1426	15	79.1	6.33	289.6	96.2	17.7	311.8	0.33	101.9	5.78	0.76	48.69
GOM20-107	1306	24	366.2	29.30	145.8	52.8	4.2	157.9	0.36	255.6	7.62	0.80	57.81

GOM20-116	1079	29	658.3	52.66	45.4	36.2	3.3	53.7	0.80	163.2	10.07	0.81	63.75
GOM20-123	1110	29	379.3	30.34	67.2	27.0	11.2	73.4	0.40	124.2	8.64	0.80	59.88
GOM20-124	1757	23	337.4	26.99	124.2	88.5	4.8	144.7	0.71	211.7	6.60	0.78	55.05

Table B2: Double-dated zircon U-Pb and ZHe ages.

APPENDIX C: SUPPLEMENTARY FILE FOR CHAPTER 4

Appendix C1 Well log database

Well ID	Well API	Latitude	Longitude	Paleo-river system	Data Source
Dip_12_4	422853272900	29.445	-96.783	Guadalupe	Young et al. (2010)
Dip_12_5	422853117200	29.426	-96.710	Guadalupe	Young et al. (2010)
Dip_12_6	422850032600	29.377	-96.685	Guadalupe	Young et al. (2010)
Dip_12_7	420893160400	29.297	-96.601	Guadalupe	Young et al. (2010)
Dip_12_9	424810169500	29.152	-96.498	Guadalupe	Young et al. (2010)
Dip_12_10	424810177000	29.066	-96.384	Guadalupe	Young et al. (2010)
Dip_13_2	422850035800	29.279	-97.048	Guadalupe	Young et al. (2010)
Dip_13_4	422853176200	29.127	-96.862	Guadalupe	Young et al. (2010)
Dip_13_5	424693243200	28.975	-96.861	Guadalupe	Young et al. (2010)
Dip_13_6	422390004700	29.010	-96.785	Guadalupe	Young et al. (2010)
Dip_13_7	422390155600	28.956	-96.711	Guadalupe	Young et al. (2010)
Dip_14_2	421230087000	29.098	-97.401	Guadalupe	Young et al. (2010)
Dip_14_3	421230029000	29.101	-97.264	Guadalupe	Young et al. (2010)
Dip_14_5	424693155300	28.947	-97.150	Guadalupe	Young et al. (2010)
Dip_14_6	424690093400	28.869	-97.086	Guadalupe	Young et al. (2010)
Dip_14_8	424690162400	28.756	-96.960	Guadalupe	Young et al. (2010)
Dip_14_10	424693189700	28.638	-96.868	Guadalupe	Young et al. (2010)
Grimes_26	4218500000	30.269	-96.015	Houston-Brazos	Spradin (1980)
Harris_1149	4220100000	30.028	-95.749	Houston-Brazos	Spradin (1980)
Harris_1165	4220100000	29.948	-95.738	Houston-Brazos	Spradin (1980)
Harris_1490	4220100000	30.084	-95.887	Houston-Brazos	Spradin (1980)
Liberty_152	4229100000	30.210	-95.062	Houston-Brazos	Spradin (1980)
Liberty_781	4229100000	30.333	-95.058	Houston-Brazos	Spradin (1980)
Liberty_131	4229100000	30.203	-94.960	Houston-Brazos	Spradin (1980)
San_Jacinto_8	4240700000	30.406	-95.106	Houston-Brazos	Spradin (1980)
San_Jacinto_28	4240700000	30.435	-95.104	Houston-Brazos	Spradin (1980)
San_Jacinto_55	4240700000	30.676	-95.185	Houston-Brazos	Spradin (1980)
San_Jacinto_65	4240700000	30.548	-95.220	Houston-Brazos	Spradin (1980)
San_Jacinto_89	4240700000	30.519	-95.112	Houston-Brazos	Spradin (1980)
San_Jacinto_94	4240700000	30.530	-95.160	Houston-Brazos	Spradin (1980)
San_Jacinto_132	4240700000	30.723	-95.283	Houston-Brazos	Spradin (1980)
Waller_132	4247300000	30.183	-95.996	Houston-Brazos	Spradin (1980)

GBDS_5259	422910501800	30.249	-95.042	Houston-Brazos	Dodge (1981)
GBDS_5417	424733097800	29.793	-95.965	Houston-Brazos	Dodge (1981)
Dip_7_3A	421853032100	30.348	-95.958	Houston-Brazos	Young et al. (2012)
Dip_7_6	423390101400	30.133	-95.751	Houston-Brazos	Young et al. (2012)
Dip_7_7	423393085200	30.109	-95.704	Houston-Brazos	Young et al. (2012)
Dip_7_9	422010010400	30.066	-95.679	Houston-Brazos	Young et al. (2012)
Dip_7_9.7	422013167000	29.922	-95.577	Houston-Brazos	Young et al. (2012)
Dip_8_5	420150023000	30.010	-96.129	Houston-Brazos	Young et al. (2012)
GBDS_2507	170390000700	30.904	-92.447	Mississippi	Eversull (1984)
GBDS_2509	170392006300	30.699	-92.521	Mississippi	Eversull (1984)
GBDS_2510	170392014700	30.607	-92.424	Mississippi	Eversull (1984)
GBDS_5609	170972037300	30.653	-91.982	Mississippi	Eversull (1984)
GBDS_5610	170972039600	30.785	-91.872	Mississippi	Eversull (1984)
GBDS_5617	170030032800	30.499	-92.896	Mississippi	Eversull (1984)
GBDS_5619	170032010800	30.724	-92.911	Mississippi	Eversull (1984)
GBDS_1012	422410017800	30.470	-94.008	Red	Eversull (1984)
GBDS_1013	422413004100	30.389	-94.010	Red	Eversull (1984)
GBDS_1014	422441002130	30.290	-94.049	Red	Eversull (1984)
GBDS_1015	423613039200	30.197	-93.902	Red	Eversull (1984)
GBDS_1016	423610022500	30.132	-93.927	Red	Eversull (1984)
GBDS_1017	423640024800	30.078	-93.911	Red	Eversull (1984)
GBDS_1018	423613031700	30.045	-93.876	Red	Eversull (1984)
GBDS_5444	423613069000	30.213	-93.825	Red	Gulf of Mexico Basin Depositional Synthesis Project
GBDS_5582	170110095900	30.521	-93.393	Red	Bebout (1982)
GBDS_5583	170192003200	30.369	-93.417	Red	Bebout (1982)
GBDS_5703	170190003900	30.279	-93.645	Red	Bebout (1982)
GBDS_5711	170190116300	30.328	-93.237	Red	Bebout (1982)
Newton_218	4235100000	30.704	-93.667	Red	Spradin (1980)
Jasper_1	4224100000	30.443	-94.091	Red	Galloway et al. (1986)
Jasper_2	4224100000	30.345	-93.999	Red	Galloway et al. (1986)
Jasper_3	4224100000	30.272	-93.985	Red	Galloway et al. (1986)
Orange_1	4236130085	30.187	-93.983	Red	Galloway et al. (1986)
Orange_2	4236100000	30.131	-93.956	Red	Galloway et al. (1986)
Orange_3	4236100471	30.035	-93.990	Red	Galloway et al. (1986)
Dip_21_3	421313760200	27.824	-98.312	Rio Grande	Young et al. (2010)
Dip_21_4	422493205300	27.782	-98.195	Rio Grande	Young et al. (2010)
Dip_21_5	422493192300	27.655	-98.112	Rio Grande	Young et al. (2010)
Dip_21_6	422730000300	27.634	-98.016	Rio Grande	Young et al. (2010)
Dip_21_7	422730031600	27.578	-97.920	Rio Grande	Young et al. (2010)

Dip_22_3	421313519700	27.619	-98.601	Rio Grande	Young et al. (2010)
Dip_22_5	421313726100	27.565	-98.427	Rio Grande	Young et al. (2010)
Dip_22_6	421313234100	27.507	-98.293	Rio Grande	Young et al. (2010)
Dip_22_7	422493086800	27.533	-98.121	Rio Grande	Young et al. (2010)
Dip_22_8	422733233600	27.421	-97.964	Rio Grande	Young et al. (2010)
Dip_23_4	421310996700	27.364	-98.615	Rio Grande	Young et al. (2010)
Dip_23_5	422473177300	27.331	-98.544	Rio Grande	Young et al. (2010)
Dip_23_6	421313634000	27.390	-98.479	Rio Grande	Young et al. (2010)
Dip_23_7	421310980400	27.325	-98.410	Rio Grande	Young et al. (2010)
Dip_23_9	422490351400	27.305	-98.100	Rio Grande	Young et al. (2010)
Dip_23_10	422730124200	27.275	-97.941	Rio Grande	Young et al. (2010)
Dip_25_6	422473199500	27.127	-98.623	Rio Grande	Young et al. (2010)
Dip_25_7	422473225400	27.111	-98.566	Rio Grande	Young et al. (2010)
Dip_25_9	420473155200	27.090	-98.430	Rio Grande	Young et al. (2010)
Dip_25_10	420473206500	27.021	-98.330	Rio Grande	Young et al. (2010)
Dip_25_11	420470069400	26.990	-98.280	Rio Grande	Young et al. (2010)
Dip_25_12	420473001700	27.043	-98.192	Rio Grande	Young et al. (2010)
Dip_25_13	420470124900	26.979	-98.087	Rio Grande	Young et al. (2010)
Section_C_9	4225500000	28.727	-97.774	Rio Grande	Baker (1995)
Section_C_10	4217500000	28.688	-97.670	Rio Grande	Baker (1995)
Section_D_16	4213100000	27.608	-98.420	Rio Grande	Baker (1995)
Section_D_17	4213100000	27.594	-98.246	Rio Grande	Baker (1995)
Section_D_18	4224900000	27.429	-98.193	Rio Grande	Baker (1995)

Table C1: Information of well logs used in this study.

Appendix C2 Example of the Channel-belt thickness measurement from well log

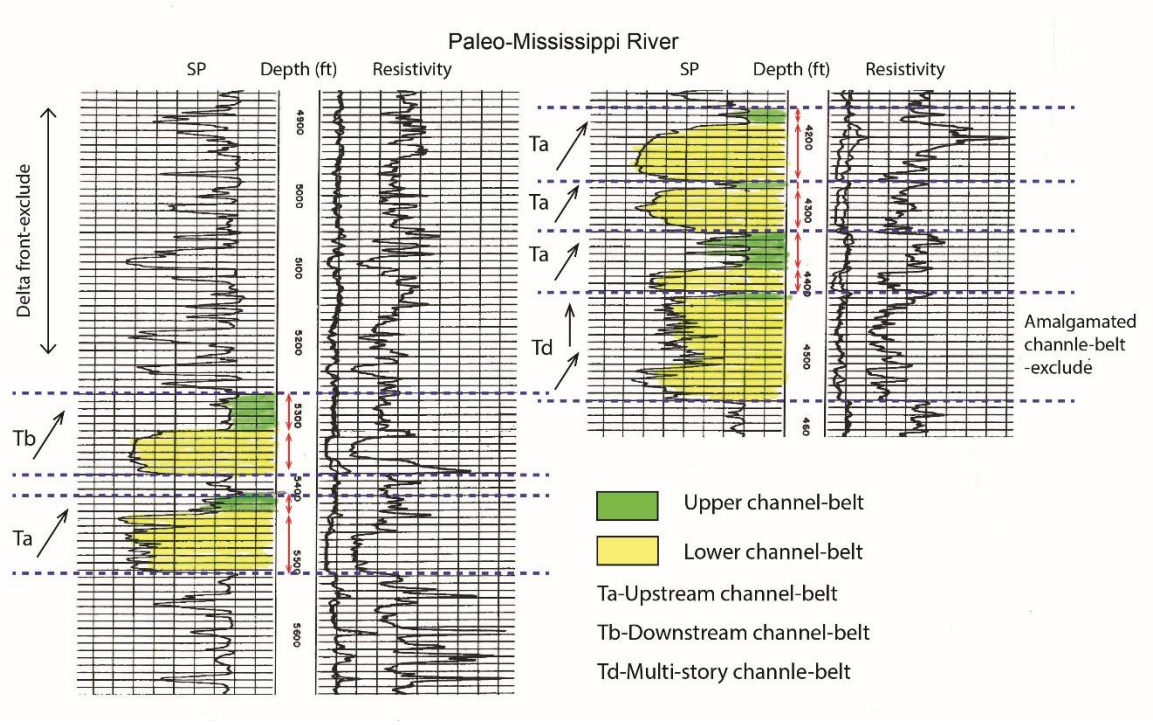

Figure C1: Measurement of Paleo-Mississippi River channel-belt thickness from well log data

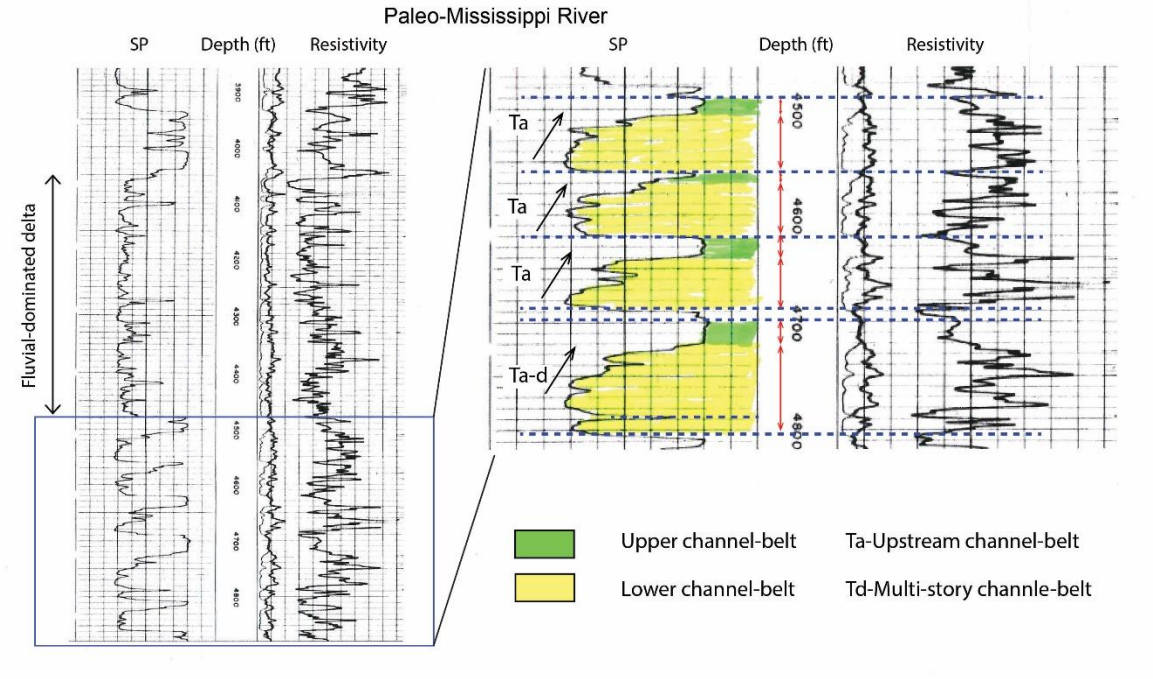

Figure C2: Measurement of Paleo-Red River channel-belt thickness from well log data

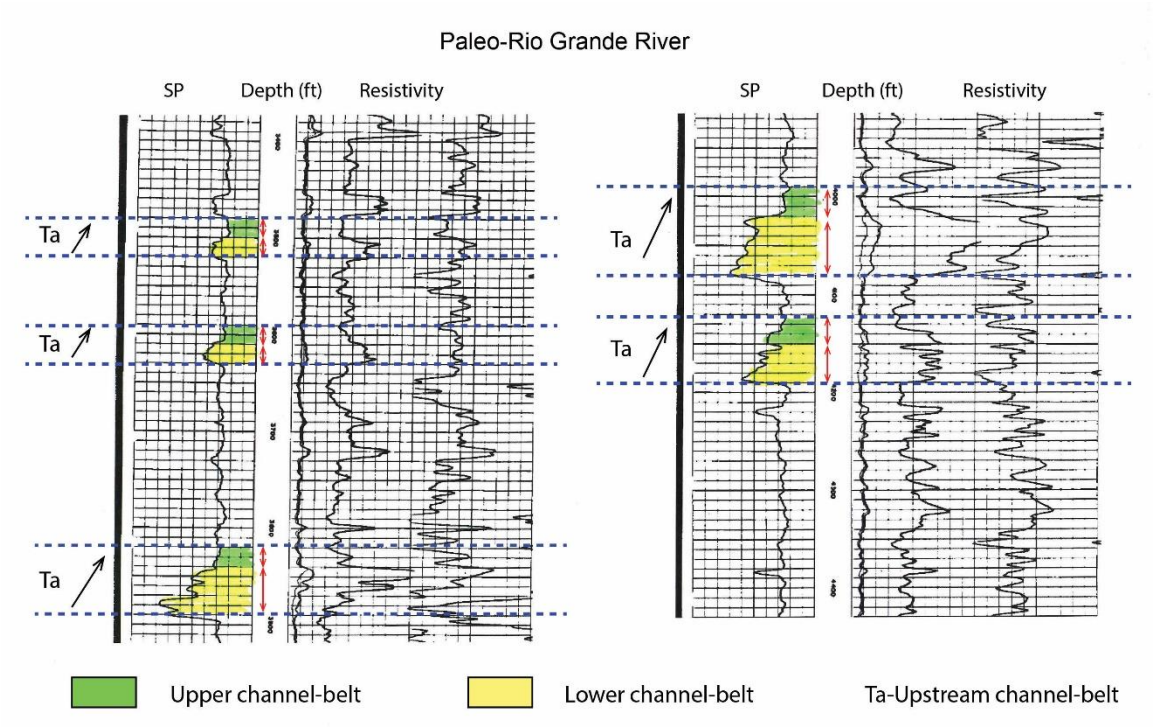

Figure C3: Measurement of Paleo-Rio Grande River channel-belt thickness from well log data

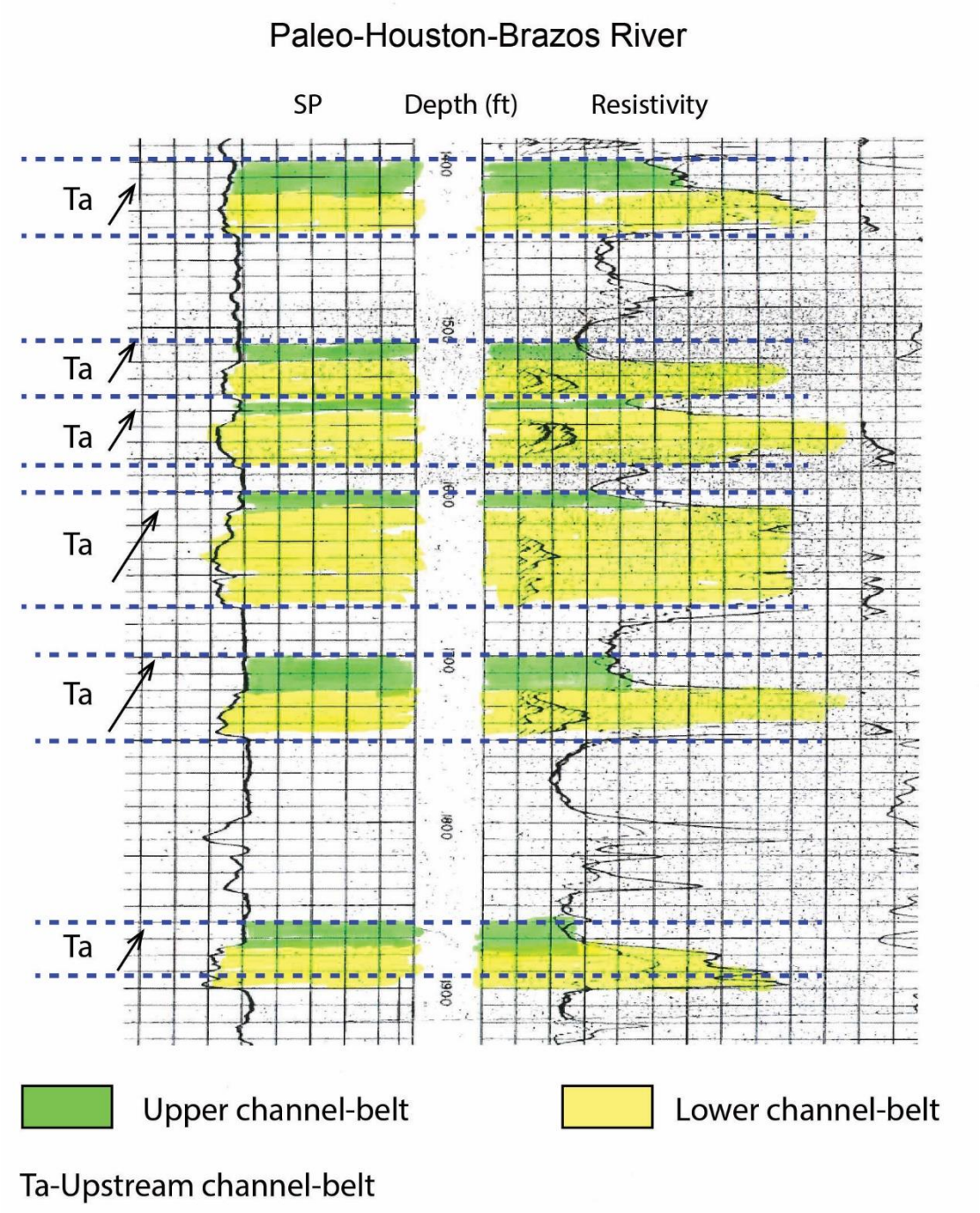

Figure C4: Measurement of Paleo-Houston-Brazos River channel-belt thickness from well log data

Appendix C3 Channel-belt thickness data of five early Miocene rivers

Well ID	Channel deposit type	Lower Channel-belt thickness (m)	Bankfull thickness (m)
Mississippi River system			
GBDS2507	A	13.7	18.3
GBDS2507	C	22.9	24.4
GBDS2507	C	9.1	15.2
GBDS2507	C	9.1	15.2
GBDS2507	C	9.1	15.2
GBDS2507	D	51.8	56.4
GBDS2507	D	36.6	41.1
GBDS2509	A	27.4	27.4
GBDS2509	C	21.3	30.5
GBDS2509	C	39.6	42.7
GBDS2509	C	12.2	21.3
GBDS2509	C	15.2	22.9
GBDS2509	D	68.6	77.7
GBDS2509	D	76.2	79.2
GBDS2509	D	42.7	51.8
GBDS2510	A	21.3	25.9
GBDS2510	A	9.1	12.2
GBDS2510	C	15.2	21.3
GBDS2510	C	32.0	32.0
GBDS2510	C	13.7	18.3
GBDS2510	D	70.1	79.2
GBDS5552	A	16.8	24.4
GBDS5552	A	39.6	41.1
GBDS5552	A	12.2	16.8
GBDS5552	A	16.8	19.8
GBDS5552	A	16.8	19.8
GBDS5552	A	13.7	18.3
GBDS5552	A	12.2	15.2
GBDS5552	A	18.3	21.3
GBDS5552	B	15.2	22.9
GBDS5552	C	27.4	39.6
GBDS5552	C	19.8	27.4
GBDS5552	D	67.1	79.2
GBDS5552	D	64.0	85.3
GBDS5552	D	45.7	51.8
GBDS5609	A	15.2	25.9
GBDS5609	A	35.1	39.6
GBDS5609	A	16.8	19.8
GBDS5609	A	30.5	33.5
GBDS5609	A	30.5	45.7
GBDS5609	B	7.6	19.8
GBDS5609	B	9.1	18.3
GBDS5609	D	61.0	64.0
GBDS5609	D	64.0	79.2
GBDS5609	D	91.4	103.6
GBDS5609	D	61.0	64.0
GBDS5610	A	12.2	16.8

GBDS5610	A	13.7	15.2
GBDS5610	A	18.3	30.5
GBDS5610	A	18.3	32.0
GBDS5610	A	18.3	24.4
GBDS5610	D	42.7	51.8
GBDS5610	D	42.7	51.8
GBDS5610	D	41.1	50.3
GBDS5617	A	24.4	33.5
GBDS5617	A	9.1	12.2
GBDS5617	A	10.7	15.2
GBDS5617	A	18.3	21.3
GBDS5617	A	24.4	24.4
GBDS5617	A	24.4	30.5
GBDS5617	A	24.4	30.5
GBDS5617	A	21.3	32.0
GBDS5617	A	13.7	19.8
GBDS5617	B	18.3	33.5
GBDS5617	B	9.1	18.3
GBDS5617	B	7.6	22.9
GBDS5617	C	9.1	24.4
GBDS5617	C	12.2	22.9
GBDS5617	C	24.4	39.6
GBDS5617	D	42.7	45.7
GBDS5617	D	64.0	79.2
GBDS5617	D	41.1	48.8
GBDS5619	A	24.4	30.5
GBDS5619	A	18.3	22.9
GBDS5619	D	64.0	70.1
GBDS5718	A	30.5	42.7
GBDS5718	C	36.6	51.8
GBDS5719	A	39.6	42.7
GBDS5719	D	42.7	61.0
GBDS5719	D	39.6	51.8
GBDS5719	D	45.7	51.8
GBDS5719	D	85.3	97.5
Red River system			
GBDS1012	A	7.6	13.7
GBDS1012	A	7.6	13.7
GBDS1012	A	9.1	15.2
GBDS1012	A	18.3	19.8
GBDS1012	A	25.9	30.5
GBDS1012	B	6.1	15.2
GBDS1012	D	48.8	54.9
GBDS1012	D	50.3	53.3
GBDS1012	D	24.4	30.5
GBDS1012	D	42.7	44.2
GBDS1012	D	36.6	39.6
GBDS1013	A	7.6	12.2
GBDS1013	A	16.8	21.3
GBDS1013	A	7.6	12.2
GBDS1013	A	25.9	29.0
GBDS1013	C	12.2	19.8

GBDS1013	D	29.0	41.1
GBDS1013	D	57.9	64.0
GBDS1013	D	30.5	36.6
GBDS1014	A	24.4	30.5
GBDS1014	A	12.2	15.2
GBDS1014	A	12.2	15.2
GBDS1014	A	15.2	22.9
GBDS1014	A	24.4	30.5
GBDS1014	A	21.3	27.4
GBDS1014	B	9.1	19.8
GBDS1014	C	22.9	30.5
GBDS1014	D	44.2	50.3
GBDS1014	D	25.9	30.5
GBDS1014	D	82.3	86.9
GBDS1014	D	30.5	45.7
GBDS1015	A	12.2	15.2
GBDS1015	A	9.1	13.7
GBDS1015	A	25.9	29.0
GBDS1015	A	22.3	25.3
GBDS1015	A	9.1	16.8
GBDS1015	A	10.7	16.8
GBDS1015	A	24.4	25.9
GBDS1015	A	13.7	18.3
GBDS1015	A	19.8	25.9
GBDS1015	A	10.7	18.3
GBDS1015	D	27.4	38.1
GBDS1015	D	29.0	32.0
GBDS1015	D	45.7	53.3
GBDS1015	D	61.0	64.0
GBDS1015	D	41.1	44.2
GBDS1016	A	24.4	30.5
GBDS1016	A	6.1	12.2
GBDS1016	A	18.3	22.9
GBDS1016	A	21.3	24.4
GBDS1016	A	10.7	15.2
GBDS1016	A	10.7	19.8
GBDS1016	A	25.9	29.0
GBDS1016	A	9.1	16.8
GBDS1016	A	22.9	24.4
GBDS1016	A	15.2	22.9
GBDS1016	A	19.8	24.4
GBDS1016	D	83.8	93.0
GBDS1016	D	30.5	35.1
GBDS1016	D	30.5	35.1
GBDS1016	D	22.9	25.9
GBDS1016	D	67.1	70.1
GBDS1016	D	47.2	56.4
GBDS1016	D	35.1	45.7
GBDS1018	A	10.7	18.3
GBDS1018	A	13.7	16.8
GBDS1018	A	21.3	25.9
GBDS1018	A	9.1	15.2
GBDS1018	A	9.1	15.2

GBDS1018	A	27.4	27.4
GBDS1018	D	29.0	30.5
GBDS1018	D	30.5	45.7
GBDS1018	D	42.7	48.8
GBDS5444	A	27.4	32.0
GBDS5444	A	18.9	21.3
GBDS5444	A	14.0	17.7
GBDS5444	A	37.5	42.1
GBDS5444	A	11.6	17.4
GBDS5444	A	16.5	25.9
GBDS5444	A	16.5	23.5
GBDS5444	A	21.0	26.8
GBDS5444	A	15.2	22.3
GBDS5444	A	24.7	28.3
GBDS5444	A	16.5	18.9
GBDS5444	C	17.7	24.1
GBDS5444	D	29.3	33.8
GBDS5444	D	42.1	42.1
GBDS5444	D	31.7	36.3
GBDS5444	D	53.6	58.2
GBDS5444	D	45.7	52.7
GBDS5582	A	21.3	27.4
GBDS5582	A	24.4	27.4
GBDS5582	A	19.8	29.0
GBDS5582	B	9.1	27.4
GBDS5583	A	27.4	27.4
GBDS5583	A	13.7	15.2
GBDS5583	A	39.6	45.7
GBDS5583	B	9.1	22.9
GBDS5583	D	30.5	42.7
GBDS5703	A	14.1	17.6
GBDS5703	A	18.2	22.3
GBDS5703	A	9.4	11.7
GBDS5703	A	17.6	24.6
GBDS5703	A	15.2	17.6
GBDS5703	A	17.6	21.1
GBDS5703	B	14.1	25.8
GBDS5703	B	15.8	24.6
GBDS5711	A	18.3	22.9
GBDS5711	A	18.3	24.4
GBDS5711	A	22.9	24.4
GBDS5711	B	6.1	16.8
GBDS5711	C	16.8	18.3
GBDS5711	D	39.6	39.6
GBDS5711	D	32.0	44.2
Newton_218	A	8.5	11.6
Newton_218	A	9.8	11.6
Newton_218	D	36.0	36.6
Newton_218	A	9.1	10.7
Newton_218	A	12.8	18.9
Newton_218	A	22.9	27.4
Newton_218	A	24.4	27.4
Newton_84	A	12.2	18.3

Newton_84	A	16.8	22.9
Newton_84	A	36.6	36.6
Newton_84	A	24.4	30.5
Newton_84	A	12.2	18.3
Orange_3	A	19.8	21.3
Orange_3	A	12.2	13.7
Orange_3	C	9.1	16.8
Orange_3	A	25.9	27.4
Orange_3	D	27.4	30.5
Orange_3	A	9.1	13.7
Orange_3	D	42.7	51.8
Orange_3	D	29.0	30.5
Orange_3	D	32.0	39.6
Orange_3	A	27.4	29.0
Orange_2	D	24.4	38.1
Orange_2	A	18.3	21.3
Orange_2	A	19.8	24.4
Orange_2	A	12.2	15.2
Orange_2	D	22.9	32.0
Orange_2	A	15.2	21.3
Orange_2	A	12.2	18.3
Orange_2	A	15.2	21.3
Orange_2	D	35.1	41.1
Orange_2	A	12.2	18.3
Orange_2	A	19.8	25.9
Orange_2	C	13.7	19.8
Orange_2	A	9.1	12.2
Orange_2	B	6.1	13.7
Orange_1	A	16.8	22.9
Orange_1	A	10.7	18.3
Orange_1	A	18.3	27.4
Orange_1	A	19.8	27.4
Orange_1	D	33.5	35.1
Orange_1	A	10.7	13.7
Orange_1	C	16.8	21.3
Orange_1	A	9.1	12.2
Orange_1	C	7.6	13.7
Orange_1	A	27.4	29.0
Orange_1	A	16.8	18.3
Orange_1	A	13.7	15.2
Orange_1	A	16.8	21.3
Orange_1	A	18.3	21.3
Orange_1	C	9.1	13.7
Orange_1	A	19.8	25.9
Jasper_3	A	24.4	30.5
Jasper_3	D	51.8	57.9
Jasper_3	A	9.1	15.2
Jasper_3	A	22.9	24.4
Jasper_3	A	10.7	15.2
Jasper_3	A	19.8	24.4
Jasper_3	A	12.2	16.8
Jasper_3	A	10.7	12.2
Jasper_3	D	70.1	73.2

Jasper_3	D	70.1	76.2
Jasper_3	D	57.9	64.0
Jasper_3	D	39.6	50.3
Jasper_3	D	45.7	48.8
Jasper_3	A	21.3	24.4
Jasper_3	A	16.8	27.4
Jasper_3	A	10.7	13.7
Jasper_3	A	18.3	25.9
Jasper_1	A	18.3	24.4
Jasper_1	A	15.2	24.4
Jasper_1	C	27.4	30.5
Jasper_1	A	29.0	33.5
Jasper_1	A	7.6	10.7
Jasper_1	A	9.1	13.7
Jasper_1	A	27.4	27.4
Jasper_1	A	10.7	13.7
Jasper_1	A	12.2	13.7
Jasper_1	D	27.4	29.0
Jasper_1	A	19.8	19.8
Jasper_1	C	27.4	29.0
Jasper_1	D	41.1	47.2
Jasper_1	B	4.6	10.7
GBDS_1017	A	16.8	21.3
GBDS_1017	D	76.2	80.8
GBDS_1017	A	7.6	12.2
GBDS_1017	D	27.4	33.5
GBDS_1017	A	16.8	18.3
GBDS_1017	A	9.1	16.8
GBDS_1017	D	25.9	33.5
GBDS_1017	A	7.6	9.1
GBDS_1017	A	21.3	24.4
GBDS_1017	A	13.7	21.3
GBDS_1017	A	35.1	41.1
GBDS_1017	A	13.7	16.8
GBDS_1017	A	15.2	21.3
GBDS_1017	D	32.0	38.1
GBDS_1017	A	10.7	13.7
GBDS_1017	A	4.6	9.1
GBDS_1017	C	6.1	12.2
GBDS_1017	D	22.9	25.9
GBDS_1017	D	83.8	85.3
GBDS_1017	D	45.7	51.8
GBDS_1017	A	24.4	29.0
GBDS_1017	A	12.2	18.3
GBDS_1017	A	12.2	21.3
GBDS_1017	A	12.2	16.8
GBDS_1017	A	15.2	21.3
Jasper_2	B	12.2	27.4
Jasper_2	A	21.3	24.4
Jasper_2	D	39.6	42.7
Jasper_2	D	61.0	68.6
Jasper_2	A	39.6	45.7
Jasper_2	A	15.2	24.4

Jasper_2	A	27.4	29.0
Jasper_2	D	44.2	47.2
Rio Grande River system			
Dip_23_10	A	9.1	15.2
Dip_23_10	A	4.6	9.1
Dip_23_10	A	9.1	18.3
Dip_23_10	A	22.9	25.9
Dip_23_10	A	12.2	18.3
Dip_23_10	A	18.3	27.4
Dip_23_10	A	7.6	12.2
Dip_22_7	A	6.1	12.2
Dip_22_7	A	19.8	24.4
Dip_22_7	A	22.9	24.4
Dip_22_7	A	13.7	16.8
Dip_22_6	A	6.1	12.2
Dip_22_6	A	10.7	13.7
Dip_22_6	A	4.6	9.1
Dip_22_6	A	7.6	15.2
Dip_22_6	A	6.1	15.2
Dip_22_6	A	9.1	21.3
Dip_22_6	A	13.7	18.3
Dip_22_8	A	9.1	18.3
Dip_22_8	A	9.1	18.3
Dip_22_8	A	9.1	15.2
Dip_22_8	A	12.2	15.2
Dip_22_8	A	6.1	12.2
Dip_22_8	A	9.1	12.2
Dip_22_8	A	15.2	33.5
Dip_22_8	A	12.2	21.3
Dip_23_9	A	6.1	10.7
Dip_23_9	A	16.8	25.9
Dip_23_9	A	18.3	21.3
Dip_23_9	A	9.1	15.2
Dip_23_9	A	13.7	18.3
Dip_23_9	A	9.1	10.7
Dip_23_9	A	12.2	18.3
Dip_23_9	A	7.6	12.2
Dip_23_9	A	12.2	21.3
Dip_23_9	A	15.2	24.4
Dip_23_6	A	21.3	30.5
Dip_23_6	A	9.1	18.3
Dip_23_6	A	7.6	10.7
Dip_23_6	A	15.2	18.3
Dip_23_6	A	9.1	13.7
Dip_23_6	A	18.3	21.3
Dip_23_6	A	18.3	30.5
Dip_21_6	A	6.1	12.2
Dip_21_6	A	9.1	15.2
Dip_21_6	A	12.2	15.2
Dip_21_6	A	10.7	13.7
Dip_21_6	A	16.8	22.9
Dip_21_5	A	7.6	12.2

Dip_21_5	A	6.1	12.2
Dip_21_3	A	9.1	12.2
Dip_21_3	A	15.2	18.3
Dip_21_4	A	12.8	21.3
Dip_21_4	A	11.6	14.0
Dip_22_3	A	9.1	12.2
Dip_22_5	A	12.2	21.3
Dip_22_5	A	6.1	12.2
Dip_22_5	A	6.1	12.2
Dip_22_5	A	15.2	18.3
Dip_22_5	A	12.2	15.2
Dip_25_12	A	4.6	9.1
Dip_25_12	A	4.6	6.1
Dip_25_12	A	18.3	27.4
Dip_25_12	A	12.2	13.7
Dip_25_12	A	15.2	21.3
Dip_25_13	A	10.7	12.2
Dip_25_13	A	12.2	21.3
Dip_25_13	A	13.7	21.3
Dip_25_13	A	6.1	7.6
Dip_25_13	A	9.1	12.2
Baker_Section_9	A	9.1	15.2
Baker_Section_9	A	9.1	15.2
Baker_Section_9	A	10.7	18.3
Baker_Section_10	A	6.1	10.7
Baker_Section_10	A	6.1	9.1
Baker_Section_10	A	4.6	9.1
Baker_Section_10	A	12.2	13.7
Baker_Section_18	A	10.7	16.8
Baker_Section_18	A	6.1	13.7
Baker_Section_18	A	9.1	13.7
Baker_Section_17	A	7.6	13.7
Dip_25_11	A	12.2	18.3
Dip_25_11	A	13.7	15.2
Dip_25_11	A	16.8	18.3
Dip_25_11	A	10.7	13.7
Dip_25_11	A	16.8	22.9
Dip_25_11	A	15.2	21.3
Dip_23_7	A	10.7	13.7
Dip_23_7	A	9.1	12.2
Dip_23_7	A	9.1	12.2
Dip_23_7	A	15.2	24.4
Dip_23_7	A	13.7	22.9
Dip_23_7	A	18.3	29.0
Dip_23_7	A	16.8	21.3
Dip_23_7	A	21.3	24.4
Dip_23_7	A	6.1	9.1
Dip_23_7	A	18.3	24.4
Dip_23_5	A	15.2	18.3
Dip_23_5	A	13.7	15.2
Dip_23_5	A	9.1	15.2
Dip_21_7	A	6.1	12.2
Dip_21_7	A	6.1	12.2

Dip_21_7	A	10.7	15.2
Dip_21_7	A	9.1	13.7
Dip_21_7	A	9.1	15.2
Dip_22_7	B	3.0	10.7
Dip_22_7	B	7.6	16.8
Dip_22_7	B	6.1	16.8
Dip_22_8	B	7.6	22.9
Dip_22_8	B	15.2	33.5
Dip_22_5	B	7.6	19.8
Dip_25_13	B	9.1	24.4
Baker_Section_16	B	7.6	19.8
Baker_Section_16	B	7.6	16.8
Dip_25_11	B	10.7	22.9
Dip_23_7	B	7.6	16.8
Dip_21_7	B	6.1	19.8
Dip_23_10	C	12.2	15.2
Dip_23_10	C	12.2	19.8
Dip_23_10	C	15.2	19.8
Dip_21_6	C	16.8	21.3
Dip_21_5	C	10.7	13.7
Dip_21_5	C	13.7	22.9
Dip_25_12	C	9.1	13.7
Dip_25_13	C	6.1	15.2
Dip_25_13	C	15.2	21.3
Dip_25_11	C	15.2	24.4
Dip_21_7	C	12.2	19.8
Dip_21_7	C	18.3	27.4
Dip_21_7	C	15.2	21.3
Dip_22_7	D	35.1	36.6
Dip_22_6	D	22.9	33.5
Dip_22_8	D	27.4	36.6
Dip_23_9	D	24.4	30.5
Dip_23_9	D	32.0	35.1
Dip_21_6	D	21.3	24.4
Dip_22_5	D	36.6	39.6
Dip_25_13	D	25.9	29.0
Baker_Section_9	D	21.3	24.4
Baker_Section_18	D	29.0	30.5
Dip_25_11	D	30.5	35.1
Dip_25_11	D	33.5	42.7
Dip_25_11	D	22.9	30.5
Dip_23_7	D	25.9	30.5
Dip_23_7	D	15.2	24.4
Dip_23_7	D	12.2	24.4
Dip_23_7	D	22.9	25.9
Dip_23_5	D	24.4	32.0
Houston-Brazos River system			
Dip_7_3A	D	16.8	22.9
Dip_7_3A	C	7.6	12.2
Dip_7_3A	A	4.6	9.1
Dip_7_3A	A	7.6	10.7
Dip_7_3A	A	3.0	6.1

Dip_7_6	A	7.6	12.2
Dip_7_6	A	8.5	14.6
Dip_7_6	A	19.8	22.9
Dip_7_6	A	9.1	12.2
Dip_7_6	A	7.6	10.7
Dip_7_6	A	7.6	13.7
Dip_7_6	A	6.1	12.2
Dip_7_6	D	22.9	25.9
Dip_7_6	A	7.6	10.7
Dip_7_6	A	18.3	19.8
Dip_7_6	A	12.2	18.3
Dip_7_7	A	6.1	9.1
Dip_7_7	A	12.2	15.2
Dip_7_7	C	7.6	15.2
Dip_7_7	D	15.2	21.3
Dip_7_7	D	19.8	25.9
Dip_7_9.7	D	29.0	30.5
Dip_7_9.7	A	9.1	16.8
Dip_7_9.7	B	7.6	16.8
Dip_7_9.7	A	15.2	18.3
Dip_7_9.7	A	12.2	16.8
Dip_7_9.7	A	9.1	15.2
Dip_8_5	A	18.3	21.3
Dip_8_5	A	6.1	12.2
Dip_8_5	C	19.8	22.9
Dip_8_5	A	6.1	12.2
Dip_8_5	D	27.4	39.6
Grimes_26	A	7.6	9.1
Grimes_26	A	9.1	15.2
Grimes_26	A	9.1	15.2
Grimes_26	A	21.3	24.4
Grimes_26	A	7.6	10.7
Harris_1149	A	10.1	12.8
Harris_1149	A	7.9	13.1
Harris_1149	A	10.4	11.9
Harris_1149	A	11.6	15.8
Harris_1165	A	10.7	18.3
Harris_1165	A	7.0	14.0
Harris_1165	A	7.6	9.1
Harris_1165	A	16.8	21.3
Harris_1165	A	9.1	15.2
Harris_1490	A	16.8	19.8
Harris_1490	A	12.2	16.8
Harris_1490	A	7.6	10.7
Harris_1490	A	6.1	7.6
Harris_1490	A	7.6	10.7
Harris_1490	A	7.6	12.2
Harris_1490	D	39.6	45.7
Harris_1490	A	6.1	9.1
Harris_1490	B	4.6	10.7
Liberty_131	D	18.3	38.1
Liberty_131	C	12.2	18.3
Liberty_131	A	10.7	15.2

Liberty_152	A	6.1	10.7
Liberty_152	A	15.2	19.8
Liberty_781	B	4.0	13.1
Liberty_781	D	12.5	18.0
Liberty_781	B	4.0	7.9
Liberty_781	A	9.8	15.5
San_Jacinto_132	A	7.6	13.7
San_Jacinto_132	A	9.1	12.2
San_Jacinto_132	A	12.2	15.2
San_Jacinto_132	A	9.1	12.2
San_Jacinto_132	A	7.6	9.1
San_Jacinto_132	B	3.0	10.7
San_Jacinto_132	A	6.1	12.2
San_Jacinto_28	A	6.1	9.1
San_Jacinto_28	A	9.1	12.2
San_Jacinto_28	A	6.1	9.1
San_Jacinto_28	A	6.1	9.1
San_Jacinto_28	A	6.1	9.1
San_Jacinto_55	A	10.7	12.2
San_Jacinto_55	A	6.1	9.1
San_Jacinto_55	A	6.1	9.1
San_Jacinto_55	B	4.6	10.7
San_Jacinto_55	A	6.1	12.2
San_Jacinto_55	B	3.0	12.2
San_Jacinto_55	A	6.1	9.1
San_Jacinto_55	B	4.6	10.7
San_Jacinto_55	A	10.7	13.7
San_Jacinto_65	A	12.2	18.3
San_Jacinto_8	A	9.1	13.7
San_Jacinto_8	A	7.6	12.2
San_Jacinto_8	A	7.6	12.2
San_Jacinto_8	C	12.2	18.3
San_Jacinto_8	B	4.6	10.7
San_Jacinto_89	A	21.3	27.4
San_Jacinto_94	A	9.1	10.7
Waller_132	A	10.7	12.2
Waller_132	A	12.2	13.7
Waller_132	A	3.0	6.1
Waller_132	B	3.0	7.6
Waller_132	A	15.2	18.3
Waller_132	A	7.6	9.1
Waller_132	A	7.6	10.7
Waller_132	A	10.7	13.7
Waller_136	A	10.7	16.2
Guadalupe River system			
Dip_13_2	C	9.1	15.2
Dip_13_4	D	15.2	24.4
Dip_13_4	C	22.9	29.0
Dip_13_4	A	21.3	24.4
Dip_13_4	A	6.1	9.1
Dip_13_4	A	4.6	7.6
Dip_13_4	B	6.1	12.2

Dip_13_4	B	3.0	9.1
Dip_13_5	A	9.1	12.2
Dip_13_5	D	15.2	25.9
Dip_13_5	A	6.1	12.2
Dip_13_5	A	6.1	12.2
Dip_13_6	A	15.2	18.3
Dip_13_6	A	4.6	9.1
Dip_13_6	A	4.6	7.6
Dip_13_6	A	6.1	12.2
Dip_13_6	D	36.6	44.2
Dip_13_7	A	10.7	13.7
Dip_13_7	A	9.1	15.2
Dip_14_1	A	12.2	15.2
Dip_14_1	A	10.7	13.7
Dip_14_1	A	4.6	9.1
Dip_14_1	A	7.6	13.7
Dip_14_1	B	3.0	13.7
Dip_14_1	A	9.1	21.3
Dip_14_2	B	4.6	12.2
Dip_14_2	B	3.0	9.1
Dip_14_2	A	5.5	9.1
Dip_14_2	A	6.1	12.2
Dip_14_2	A	10.7	16.8
Dip_14_2	A	11.3	14.3
Dip_14_2	A	6.1	9.1
Dip_14_2	A	9.8	12.8
Dip_14_2	A	12.2	15.2
Dip_14_2	A	12.2	13.7
Dip_14_2	A	7.6	10.7
Dip_14_2	A	7.6	10.7
Dip_14_3	B	6.1	13.7
Dip_14_3	D	27.4	36.6
Dip_14_3	A	12.2	15.2
Dip_14_3	A	18.3	24.4
Dip_14_6	A	9.1	15.2
Dip_14_6	A	9.1	16.8
Dip_14_6	A	15.2	18.3
Dip_14_6	B	4.6	12.2
Dip_14_6	A	12.2	15.2
Dip_14_6	A	6.1	10.7
Dip_12_4	A	7.6	13.7
Dip_12_4	A	6.1	12.2
Dip_12_4	A	6.1	12.2
Dip_12_4	A	12.2	19.8
Dip_12_4	B	6.1	18.3
Dip_12_5	C	10.7	21.3
Dip_12_5	A	9.1	15.2
Dip_12_5	A	6.1	12.2
Dip_12_5	A	7.6	10.7
Dip_12_6	B	9.1	21.3
Dip_12_6	A	6.1	12.2
Dip_12_6	A	10.7	18.3
Dip_12_6	B	3.0	9.1

Dip_12_6	A	6.1	12.2
Dip_12_6	A	7.6	13.7
Dip_12_7	B	3.0	9.1
Dip_12_7	B	3.0	9.1
Dip_12_7	B	3.0	9.1
Dip_12_7	B	6.1	15.2
Dip_12_7	A	15.2	19.8
Dip_12_9	A	8.8	10.1
Dip_12_9	C	8.2	13.7
Dip_12_9	A	5.5	11.9
Dip_12_9	A	6.7	12.2
Dip_12_10	A	3.0	6.1
Dip_12_10	B	3.0	7.6
Dip_12_10	A	8.5	11.6
Dip_12_10	A	4.6	7.6
Dip_12_10	C	6.1	12.2
Dip_12_10	A	6.1	9.1

Note: A-Upstream Channel-belt; B-Abandoned channel fill; C-Downstream channel-belt; D-Multi-storey channel-belt

Table C2: Lower channel-belt and bankfull thickness measured from well logs on early Miocene coastal plain of the Gulf of Mexico.

References

Allen, D.R., and Chilingarian, G.V., 1975, Mechanics of sand compaction, in Chilingarian, G. V., and Wolf, K.H., eds., Compaction of coarse-grained sediments I: New York, Elsevier, p. 43–77.

Allen, P.A., 2008a, From landscapes into geological history: Nature, v. 451, p. 274–276.

Allen, P.A., 2008b, Time scales of tectonic landscapes and their sediment routing systems, in Gallagher, K., Jones, S.J., and Wainwright, J., eds., Landscape Evolution: Denudation, Climate and Tectonics Over Different Time and Space Scales: Geological Society of London Special Publication 296, p. 7–28.

Amato, J.M., and Mack, G.H., 2012, Detrital zircon geochronology from the Cambrian-Ordovician Bliss Sandstone, New Mexico: Evidence for contrasting Grenville-age and Cambrian sources on opposite sides of the Transcontinental Arch: Geological Society of America Bulletin, v. 124, p. 1826-1840, doi: 10.1130/B30657.1.

Ambrose, W.A., Hentz, T.F., Bonnaffé, F., Loucks, R.G., Brown, L.F., Jr., Wang, F.P., and Potter, E.C., 2009, Sequence-stratigraphic controls on complex reservoir architecture of highstand fluvial-dominated deltaic and lowstand valley-fill deposits in the Upper Cretaceous (Cenomanian) Woodbine Group, East Texas field: regional and local perspectives: American Association of Petroleum Geologists Bulletin, v. 93, no.2, p. 231–269.

Anderson, J.B., Rodriguez, A., Abdulah, K.C., Fillon, R.H., Banfield, L.A., McKeown, H.A., and Wellner, J.S., 2004, Late Quaternary stratigraphic evolution of the northern Gulf of Mexico margin: a synthesis, in Anderson, J.B., and Fillon, R.H., eds., Late Quaternary Stratigraphic Evolution of the Northern Gulf of Mexico Margin: SEPM, Special Publication 79, p. 1–23.

Anderson, J.B., Wallace, D.J., Simms, A.R., Rodriguez, A.B., and Milliken, K.T., 2014, Variable response of coastal environments of the northwestern Gulf of Mexico to sea-level rise and climate change: Implications for future change: Marine Geology, v. 352, p.348-366.

Anderson, J.B., Wallace, D.J., Simms, A.R., Rodriguez, A.B., Weight, R.W. and Taha, Z.P., 2016, Recycling sediments between source and sink during a eustatic cycle: Systems of late Quaternary northwestern Gulf of Mexico Basin: Earth-Science Reviews, v.153, p.111-138.

Baker, E.T., Jr., 1995, Stratigraphic Nomenclature and Geologic Sections of the Gulf Coastal Plain of Texas: U.S. Geological Survey Open-File Report 94–461, 34 p.

Barra, F., Ruiz, J., Valencia, V.A., Ochoa–Landín, L., Chesley, J.T., and Zürcher, L., 2005, Laramide porphyry Cu–Mo mineralization in northern Mexico: Age constraints

from Re–Os geochronology in molybdenites: Economic Geology and the Bulletin of the Society of Economic Geologists, v. 100, p. 1605–1616.

Bart, H.A., 1975, Miocene sediment dispersal for western Nebraska and south-eastern Wyoming: Contributions to Geology (Copenhagen), v. 14, p. 27-39.

Bebout, D.G., and Gutierrez, D.R., 1983, Regional cross sections, Louisiana Gulf Coast: Baton Rouge, Louisiana Geological Survey Folio Series 6, 10 p.

Bentley, S.J., Blum, M.D., Maloney, J., Pond, L., and Paulsell, R., 2016, The Mississippi River source-to-sink system: Perspectives on tectonic, climatic, and anthropogenic influences, Miocene to Anthropocene: Earth-Science Reviews, v. 153, p. 139–174, doi: 10 .1016 /j .earscirev .2015 .11 .001.

Benyon, C., Leier, A., Leckie, D.A., Webb, A., Hubbard, S.M., and Gehrels, G.E., 2014, Provenance of the Cretaceous Athabasca Oil Sands, Canada: Implications for continental-scale sediment transport: Journal of Sedimentary Research, v. 84, p. 136-143, doi:10.2110/jsr.2014.16.

Bernard, H.A., Major, C.F., Parrot, B.F., and LeBlanc, R.J., Sr., 1970, Recent Sediments of Southeast Texas: A Field Guide to the Brazos Alluvial and Deltaic Plains and the Galveston Barrier Island Complex: The University of Texas at Austin, Bureau of Economic Geology, 140 p.

Bhattacharya, J.P., and Tye, R.S., 2004, Searching for Modern Ferron Analogs and Application to Subsurface Interpretation, in Chidsey, T. C. Jr., Adams, R. D., and Morris, T. H., eds., The fluvial-deltaic Ferron Sandstone: regional to wellbore-scale outcrop analog studies and application to reservoir modeling. AAPG Studies in Geology 50, p. 39–57.

Bhattacharya, J.P., Copeland, P., Lawton, T.F., and Holbrook, J.H., 2016, Estimation of source area, river paleo-discharge, paleoslope, and sediment budgets of linked deep-time depositional systems and implications for hydrocarbon potential: Earth Science Reviews, v. 153, p. 77–110.

Bickford, M.E., Van Schmus, W.R., and Zietz, I., 1986, Proterozoic history of the midcontinent region of North America: Geology, v. 14, p. 492–496, doi: 10.1130 /0091–7613(1986)14<492:PHOTMR>2.0.CO;2.

Blum, M., and Pecha, M., 2014, Mid–Cretaceous to Paleocene North American drainage reorganization from detrital zircons: Geology, v. 42, p. 607–610, doi: 10.1130/G35513.1.

Blum, M., Martin, B.J., Milliken, K., and Garvin, M., 2013, Paleovalley systems: insights from quaternary analogs and experiments: Earth Science Reviews, v. 116, p. 128–169.

Blum, M.D., and Roberts, H.H., 2012, The Mississippi delta region, past, present, and future: Annual Review of Earth and Planetary Sciences, v. 40, p. 655–683.

Blum, M.D., and Törnqvist, T.E., 2000, Fluvial responses to climate and sea-level change: a review and look forward: Sedimentology 47, p. 2–48.

Blum, M.D., and Womack, J.H., 2009, Climate change, sea-level change, and fluvial sediment supply to deepwater systems, in Kneller, B., Martinsen, O.J., and McCaffrey, B., eds., External Controls on Deep Water Depositional Systems: Climate, Sea-Level, and Sediment Flux: SEPM Special Publication, 92, p. 15–39.

Boettcher, S.S., and Milliken, K.L., 1994, Mesozoic–Cenozoic unroofing of the southern Appalachian Basin: Apatite fission track evidence from Middle Pennsylvanian Sandstones: Journal of Geology, v. 102, p. 655-668, doi: 10.1086 /629710.

Bridge, J.S., 2003, Rivers and Floodplains: Forms, Processes, and Sedimentary Record: Blackwell Science Ltd, Oxford, UK, 504 p.

Bridge, J.S., and Tye, R.S., 2000, Interpreting the dimensions of ancient fluvial channel bars, channels, and channel belts from wireline logs and cores: AAPG Bulletin, v. 84, p. 1205–1228.

Bryant, J.D., MacFadden, B.J., and Mueller, P.A., 1992, Improved chronologic resolution of the Hawthorn and Alum Bluff groups in northern Florida: Geological Society of America Bulletin, v.104, p. 208-218.

Campbell, I.H., Reiners, P.W., Allen, C.M., Nicolescu, S., and Upadhyay, R., 2005, He–Pb double dating of detrital zircons from the Ganges and Indus Rivers: Implications for sediment recycling and provenance studies: Earth and Planetary Science Letters, v. 237, p. 402–432, doi: 10.1016/j.epsl.2005.06.043.

Carrapa, B., 2010, Resolving tectonic problems by dating detrital minerals: Geology, v. 38, No. 2, p. 191-192.

Carroll, A.R., Chetel, L.M., and Smith, M.E., 2006, Feast to famine: Sediment supply control on Laramide basin fi ll: Geology, v. 34, p. 197–200, doi: 10.1130/G22148.1.

Cather, S.M., 2011, Late Oligocene–early Miocene deep erosion on the southern Colorado Plateau and the southern Great Plains, in Beard, L.S., et al., eds., CREvolution 2—Origin and evolution of the Colorado River system, workshop abstracts: U.S. Geological Survey Open-File Report 2011-1210, p. 46-54, http://pubs.usgs.gov/of/2011/1210/.

Cather, S.M., Chamberlin, R.M., Chapin, C.E., and McIntosh, W.C., 1994, Stratigraphic consequences of episodic extension in the Lemitar Mountains, central Rio Grande rift, in Keller, G.R., and Cather, S.M., eds., Basins of the Rio Grande Rift: Structure, stratigraphy, and tectonic setting: Boulder, Colorado, Geological Society of America Special Paper 291, p.157–169.

Cather, S.M., Chapin, C.E., and Kelley, S.A., 2012, Diachronous episodes of Cenozoic erosion in southwestern North America and their relationship to surface uplift,

paleoclimate, paleodrainage, and paleoaltimetry: Geosphere, v. 8, no. 6, p. 1177–1206.

Cather, S.M., Connell, S.D., Chamberlin, R.M., McIntosh, W.C., Jones, G.E., Potochnik, A.R., Lucas, S.G., and Johnson, P.S., 2008, The Chuska erg: Paleogeomorphic and paleoclimatic implications of an Oligocene sand sea on the Colorado Plateau: Geological Society of America Bulletin, v. 120, p. 13-33, doi:10.1130/B26081.1.

Chapin, C.E., 2008, Interplay of oceanographic and paleoclimate events with tectonism during middle to late Miocene sedimentation across the southwestern USA: Geosphere, v. 4, p. 976-991, doi:10.1130/GES00171.1.

Chapin, C.E., 2012, Origin of the Colorado Mineral Belt: Geosphere, v. 8, p. 28–43, doi:10.1130/GES00694.1.

Chapin, C.E., and Cather, S.M., 1994, Tectonic setting of the axial basins of the northern and central Rio Grande rift, in Keller, G.R., and Cather, S.M., eds., Basins of the Rio Grande rift; Structure, stratigraphy, and tectonic setting: Geological Society of America Special Paper 291, p. 5–25.

Chapin, C.E., Wilks, M., and McIntosh, W.C., 2004, Space–time patterns of late Cretaceous to present magmatism in New Mexico—Comparison with Andean volcanism and potential for future volcanism: Socorro: New Mexico Bureau of Geology and Mineral Resources Bulletin, v. 160, p. 13–40.

Chen, J.H., and Moore, J. G., 1982, Uranium–lead isotopic ages from the Sierra Nevada Batholith, California: Journal of Geophysical Research, v. 87, no. B6, p. 4761–4784, doi:10.1029/JB087iB06p04761.

Clements, B., Sevastjanova, I., Hall, R., Belousova, E.A., Griffin, W.L., and Pearson, N., 2012, Detrital zircon U–Pb age and Hf–isotope perspective on sediment provenance and tectonic models in SE Asia, in Rasbury, E.T., Hemming, S.R., and Riggs, N.R., eds., Mineralogical and Geochemical Approaches to Provenance: Geological Society of America Special Paper 487, p. 37–61, doi:10.1130/2012.2487(03).

Condon S.M., 2005, Geological studies of the Platte River, south-central Nebraska and adjacent areas—geologic maps, subsurface study, and geologic history: Geological Survey Professional Paper 1706, 63p.

Connell, S.D., 2004, Geology of the Albuquerque Basin and tectonic development of the Rio Grande rift, north-central New Mexico, in Mack, G.H., and Giles, K.J., eds., The geology of New Mexico, A geologic history: New Mexico Geological Society, Special Publication 11, p. 359–388.

Corrigan, J., Cervany, P.F., Donelick, R., and Bergman, S.C., 1998, Postorogenic denudation along the late Paleozoic Ouachita trend, south central United States of America: magnitude and timing constraints from apatite fission track data: Tectonics, v. 17, 587–603.

Covault, J.A., Romans, B.W., Fildani, A., McGann, M., and Graham, S.A., 2010, Rapid Climatic Signal Propagation from Source to Sink in a Southern California Sediment-Routing System: The Journal of Geology, v. 118, no,3, p. 247-259.

Covault, J.A., Romans, B.W., Graham, S.A., Fildani, A., And Hilley, G.E., 2011, Terrestrial source to deep-sea sink sediment budgets at high and low sea levels: insights from tectonically active Southern California: Geology, v. 39, p. 619–622.

Covault, J.A., Shelef, E., Traer, M., Hubbard, S.M., Romans, B.W., and Fildani, A., 2012, Deep-water channel run-out length: insights from seafloor geomorphology: Journal of Sedimentary Research, v.82, no.1, p.25–40.

Cox, R.T., Lumsden, D.N., and Van Arsdale, R.B., 2014, Possible relict meanders of the Pliocene Mississippi River and their Implications: The Journal of Geology, v. 122, no. 5, p. 609-622.

Craddock, W.H., and Kylander–Clark, A.R.C., 2013, U–Pb ages of detrital zircons from the Tertiary Mississippi River Delta in central Louisiana: Insights into sediment provenance: Geosphere, v. 9, p. 1832–1851, doi:10.1130/GES00917.1.

Cunningham, C.G., Naeser, C.W., Marvin, R.F., Luedke, R.G., and Wallace, A.R., 1994, Ages of selected intrusive rocks and associated ore deposits in the Colorado mineral belt: U.S. Geological Survey Bulletin 2109, 31 p.

Davidson, S.K., and Hartley, A.J., 2014, A quantitative approach to linking drainage area and distributive-fluvial-system area in modern and ancient endorheic basins: Journal of Sedimentary Research, v. 84, p. 1005–1020.

Davidson, S.K., and North, C.P., 2009, Geomorphological regional curves for prediction of drainage area and screening modern analogues for rivers in the rock record: Journal of Sedimentary Research, v. 79, p. 773–792.

Davies, D.K., Williams, B.P.J., and Vessell, R.K., 1993, Dimensions and quality of reservoirs originating in low and high sinuosity channel systems, Lower Cretaceous Travis Peak Formation, east Texas, USA, in C. P. North and D. J. Prosser, eds., Characterization of fluvial and aeolian reservoirs: London Geological Society Special Publication no. 73, p. 95–121.

DeCelles, P.G., 2004, Late Jurassic to Eocene evolution of the Cordilleran thrust belt and foreland basin system, western USA: American Journal of Science, v. 304, p. 105–168, doi:10.2475/ajs.304.2.105.

DeCelles, P.G., Ducea, M. N., Kapp, P., and Zandt, G., 2009, Cyclicity in Cordilleran orogenic systems: Nature Geoscience, v.2, no. 4, p. 251–257.

DeWitt, D., Lawn, A., Means, H., and Kincaid, T., 2010, Alum bluff, in Southeastern Geological Society fall meeting and field trip, Guidebook No. 51, p.1-19.

Dickinson W.R., Gehrels, G.E., and Stern R. J., 2010, Late Triassic Texas uplift preceding Jurassic opening of the Gulf of Mexico: Evidence from U-Pb ages of detrital zircons: Geosphere, v. 6, no. 5, p. 641-662, doi: 10.1130/GES00532.1.

Dickinson, W.R., 2008, Impact of differential zircon fertility of granitoid basement rocks in North America on age populations of detrital zircons and implications for granite petrogenesis: Earth and Planetary Science Letters, v. 275, p. 80–92, doi:10.1016/j.epsl.2008.08.003.

Dickinson, W.R., and Gehrels, G.E., 2003, U–Pb ages of detrital zircons from Permian and Jurassic eolian sandstones of the Colorado Plateau, USA: Paleogeographic implications: Sedimentary Geology, v. 163, p. 29–66, doi:10.1016/S0037–0738(03)00158–1.

Dickinson, W.R., and Gehrels, G.E., 2009, U–Pb ages of detrital zircons in Jurassic eolian and associated sandstones of the Colorado Plateau: Evidence for transcontinental dispersal and intraregional recycling of sediment: Geological Society of America Bulletin, v. 121, p. 408–433, doi:10.1130/B26406.1.

Dickinson, W.R., and Lawton, T.F., 2001, Carboniferous to Cretaceous assembly and fragmentation of Mexico: Geological Society of America Bulletin, v. 113, p. 1142–1160, doi:10.1130/0016-7606(2001)113<1142:CTCAAF>2.0.CO;2.

Dickinson, W.R., and Suczek, C.A., 1979, Plate tectonics and sandstone compositions: The American Association of Petroleum Geologists Bulletin, v. 63, p. 2164-2182.

Dickinson, W.R., Klute, M.A., Hayes, M.J., Janecke, S.U., Lundin, E.R., McKittrick, M.A., and Olivares, M.D., 1988, Paleogeographic and paleotectonic setting of Laramide sedimentary basins in the central Rocky Mountain region: Geological Society of America Bulletin, v. 100, p. 1023-1039, doi: 10.1130/0016-7606(1988)100<1023:PAPSOL>2.3 .CO;2.

Dickinson, W.R., Lawton, T.F., and Gehrels, G.E., 2009, Recycling detrital zircons: A case study from the Cretaceous Bisbee Group of southern Arizona: Geology, v. 37, p. 503–506, doi: 10.1130/G25646A.1.

Dockery, D.T., III, and May, J.H., 1981, Detailed mid-Tertiary stratigraphy along the Chickasawhay River, east-central Mississippi; Field trip 3, in Field trip guidebook for southern Mississippi: Southern Geological Society Publication, no. 3, p. 3.1-3.59.

Dodge, M.M., and Posey, J.S., 1981, Structural cross sections, Tertiary Formations, Texas Gulf Coast: The University of Texas at Austin, Bureau of Economic Geology, 6 p.

Ducea, M., 2001, The California arc: Thick granitic batholiths, eclogitic residues, lithospheric–scale thrusting and magmatic flare–ups: GSA Today, v. 11, no. 11, p. 4–10, doi: 10.1130/1052–5173(2001)011 <0004:TCATGB>2.0.CO;2.

Durkin, P.R., Hubbard, S.M., Boyd, R.L., and Leckie, D.A., 2015, Stratigraphic expression of intra-point-bar erosion and rotation: Journal of Sedimentary Research, v. 85, p. 1238–1257.

Dutton S.P., Loucks, R.G., and Day-Stirrat R.J., 2012, Impact of regional variation in detrital mineral composition on reservoir quality in deep to ultradeep lower Miocene sandstones, western Gulf of Mexico: Marine and Petroleum Geology, v. 35, p. 139-153.

Eaton, G.P., 2008, Epeirogeny in the southern Rocky Mountains region: Evidence and origin: Geosphere, v. 4, p. 764-784, doi: 10.1130/GES00149.1.

Eriksson, K.A., Campbell, I.H., Palin, J.M., Allen, C.M., and Bock, B., 2004, Evidence for multiple recycling in Neoproterozoic through Pennsylvanian sedimentary rocks of the central Appalachian basin: Journal of Geology, v. 112, p. 261-276, doi: 10.1086 /382758.

Eriksson, K.A., Campbell, I.H., Palin, J.M., and Allen, C.M., 2003, Predominance of Grenvillian magmatism recorded in detrital zircons from modern Appalachian rivers: The Journal of Geology, v. 111, p. 707-717, doi:10.1086/378338.

Ethridge, F.G., and Schumm, S.A., 1977, Reconstructing paleochannel morphologic and flow characteristics: methodology, limitations and assessment, in Miall, A.D., ed., Fluvial Sedimentology: Canadian Society of Petroleum Geology Memoir 5, p. 703–721.

Eversull, L.G., 1984, Regional cross sections - North Louisiana: Louisiana Geological Survey, Folio Series no. 7.

Ewing, T.E., 2005, Phanerozoic development of the Llano Uplift: South Texas Geological Society Bulletin, v. 45, p. 15–25.

Fallin, J.A.T., 1988, Hydrogeology of Lower Cretaceous strata under the southern High Plains of New Mexico: New Mexico Geology, v. 10, p. 6-9.

Fan, M., DeCelles, P.G., Gehrels, G.E., Dettman, D.L., Quade, J., and Peyton, S.L., 2011, Sedimentology, detrital zircon geochronology, and stable isotope geochemistry of the lower Eocene strata in the Wind River Basin, central Wyoming: Geological Society of America Bulletin, v. 123, p. 979-996, doi: 10.1130 /B30235.1.

Fan, M., Heller, P., Allen, S. D., and Hough, B. J., 2014, Middle Cenozoic Uplift and Concomitant Drying in the Central Rocky Mountains and Adjacent Great Plains: Geology, v. 42, n. 6, p. 547–550

Feldman, H.R., Franseen, E.K., Joeckel, R.M., and Heckel, P.H., 2005, Impact of longer-term modest climate shifts on architecture of high-frequency sequences (cyclothems), Pennsylvanian of mid-continent U.S.A.: Journal of Sedimentary Research, v. 75, p. 350–368.

Ferrari, L., Lopez-Martinez, M., Aguirre-Diaz, G., and Carrasco-Nunez, G., 1999, Space-time patterns of Cenozoic arc volcanism in central Mexico: From the Sierra Madre Occidental to the Mexican Volcanic Belt: Geology, v. 27, p. 303–306, doi: 10.1130/0091-7613(1999)027<0303:STPOCA>2.3 .CO;2.

Ferrari, L., Valencia-Moreno, M., and Bryan, S., 2007, Magmatism and tectonics of the Sierra Madre Occidental and its relation with the evolution of the western margin of North America, in Alaniz-Álvarez, S.A., and Nieto-Samaniego, Á.F., eds., Geology of México: Celebrating the Centenary of the Geological Society of México: Geological Society of America Special Paper 422, p. 1–39, doi: 10.1130/2007.2422(01).

Fielding, C.R., and Crane, R.C., 1987, An application of statistical modelling to the prediction of hydrocarbon recovery factors in fluvial reservoir sequences, in Ethridge, F.G., Flores, R.M., and Harvey, M.D., eds., Recent Developments in Fluvial Sedimentology: SEPM, Special Publication 39, p. 321–327.

Fildani, A., McKay, M.P., Stockli, D., Clark, J., Dykstra, M.L., Stockli, L., and Hessler, A.M., 2016, The ancestral Mississippi drainage archived in the late Wisconsin Mississippi deep–sea fan: Geology, v. 44, no. 6, p. 479–482.

Filleaudeau, P.Y., Mouthereau, F., and Pik, R., 2012, Thermotectonic evolution of the south–central Pyrenees from rifting to orogeny: Insights from detrital zircon U/Pb and (U–Th)/He thermochronometry: Basin Research, v. 24, p. 401–417, doi: 10.1111 /j.1365 –2117 .2011 .00535.x.

Finzel, E. S., 2014, Detrital zircons from Cretaceous midcontinent strata reveal an Appalachian Mountains–Cordilleran foreland basin connection: Lithosphere, v. 6, p. 378–382, doi:10.1130/L400.1.

Fisk, H.N., 1944, Geological Investigation of the Alluvial Valley of the Lower Mississippi River: U.S. Army Corps of Engineers Mississippi River Commission, 78 p.

Foote, R.Q, Stoudt, D.L., Hutchinson, P.J., and Gordon, P.T., 1990, Gulf Coast regional cross section, east Texas-Texas coastal plain sector: Tulsa, Oklahoma, American Association of Petroleum Geologists, 3 sheets.

Frazier, D.E., and Osanik, A., 1961, Point-bar deposits, Old River Locksite, Louisiana: Gulf Coast Association of Geological Societies Transactions, v. 11, p. 121–137.

Frost, B.R., Chamberlain, K.R., Swapp, S., Frost, C.D., and Hulsebosch, T.P., 2000, Late Archean structural and metamorphic history of the Wind River Range: Evidence for a long-lived active margin on the Archean Wyoming craton: Geological Society of America Bulletin, v. 112, p. 564-578, doi: 10.1130/0016-7606(2000)112<564:LASAMH>2.0.CO;2.

Gallen, S.F., Wegmann, K.W., and Bohnenstieh, D.R., 2013, Miocene rejuvenation of topographic relief in the southern Appalachians: GSA Today, v. 23, no. 2, p. 4-10, doi: 10.1130 /GSATG163A.1.

Galloway, W.E., 1977, Catahoula Formation of the Texas coastal plain: Depositional systems, composition, structural development, ground–water flow history, and uranium distribution: The University of Texas at Austin, Bureau of Economic Geology, Report of Investigations No. 87, 59 p.

Galloway, W.E., 1981, Depositional architecture of Cenozoic Gulf Coastal Plain fluvial systems: Society of Economic Paleontologists and Mineralogists Special Publication No. 31, p. 127–155.

Galloway, W.E., 1998, Siliciclastic slope and base-of-slope depositional systems: component facies, stratigraphic architecture, and classification: AAPG Bulletin, v. 82, p. 569–595.

Galloway, W.E., 2005, Cenozoic evolution of the northern Gulf of Mexico continental margin, in Gulf Coast Section SEPM 25th Annual Research Conference Proceedings, p. 1–15.

Galloway, W.E., 2008, Depositional evolution of the Gulf of Mexico sedimentary basin, in Miall, A.D., ed., Sedimentary Basins of the World: Volume 5, The Sedimentary Basins of the United States and Canada: Amsterdam, The Netherlands, Elsevier, p. 505–549.

Galloway, W.E., and Hobday, D.K., 1996, Terrigenous Clastic Depositional Systems, Springer-Verlag, Heidelberg, 489 pp.

Galloway, W.E., Ganey-Curry, P.E., Li, X., and Buffler, R.T., 2000, Cenozoic depositional history of the Gulf of Mexico Basin: AAPG Bulletin, v. 84, p. 1743–1774.

Galloway, W.E., Henry C.D., and Smith, G.E., 1982, Depositional framework, hydrostratigraphy, and uranium mineralization of the Oakville Sandstone (Miocene), Texas coastal plain: The University of Texas at Austin, Bureau of Economic Geology, Report of Investigations No. 113, 51 p.

Galloway, W.E., Jirik, L.A., Morton, R.A., and Dubar J.R., 1986, Lower Miocene (Fleming) depositional episode of the Texas Coastal Plain and Continental Shelf: structural framework, facies, and hydrocarbon resources: The University of Texas at Austin, Bureau of Economic Geology, Report of Investigations No. 150, 50 p.

Galloway, W.E., Whiteaker, T.L., and Ganey-Curry, P., 2011, History of Cenozoic North American drainage basin evolution, sediment yield, and accumulation in the Gulf of Mexico basin: Geosphere, v. 7, p. 938–973.

Garrity, C.P., and Soller, D.R., 2009, Database of the Geologic Map of North America; adapted from the map by J.C. Reed, Jr. and others (2005): U.S. Geological Survey Data Series 424.

Gehrels, G., 2011, Detrital zircon U–Pb geochronology: Current methods and new opportunities, in Busby, C., and Azor, A., eds., Recent Advances in Tectonics of Sedimentary Basins: Hoboken, New Jersey, Blackwell Publishing, p.47–62. Gehrels, G., 2014, Detrital zircon U–Pb geochronology applied to tectonics: Annual Review of Earth and Planetary Sciences, v. 42, no. 1, p. 127–149.

Gehrels, G., 2014, Detrital Zircon U-Pb Geochronology Applied to Tectonics: Annual Review of Earth and Planetary Sciences, v. 42, no.1, p. 127-149.

Gehrels, G., and Pecha, M., 2014, Detrital zircon U–Pb geochronology and Hf isotope geochemistry of Paleozoic and Triassic passive margin strata of western North America: Geosphere, v. 10, no. 1, p. 49–65, doi:10.1130 /GES00889.1.

Gerdes, A., and Zeh, A., 2006, Combined U–Pb and Hf isotope LA–(MC–)ICP–MS analyses of detrital zircons: Comparison with SHRIMP and new constraints for the provenance and age of an Armorican metasediment in Central Germany: Earth and Planetary Science Letters, v. 249, no. 47–61.

Ghinassi, M., and Ielpi, A., 2015, Stratal architecture and morphodynamics of downstream migrating fluvial point bars (Jurassic Scalby Formation, UK): Journal of Sedimentary Research 85, p. 1123–1137.

Ghinassi, M., and Ielpi, A., 2016, Downstream-migrating fluvial point bars in the rock record: Sedimentary Geology, v. 334, p. 66–96.

Gibling, M.R., 2006, Width and thickness of fluvial channel bodies and valley fills in the geological record: a literature compilation and classification: Journal of Sedimentary Research, v. 76, p. 731–770.

Gleason, J.D., Gehrels, G.E., Dickinson, W.R., Patchett, P.J., and Kring, D.A., 2007, Laurentian sources for detrital zircon grains in turbidite and deltaic sandstones of the Pennsylvanian Haymond Formation, Marathon assemblage, west Texas, U.S.A.: Journal of Sedimentary Research, v. 77, p. 888-890, doi: 10.2110/ jsr.2007.084.

Hatcher, R.D., Jr., 1987, Tectonic of the southern and central Appalachian trends: Annual Review of Earth and Planetary Sciences, v.15, p. 337-362.

Hatcher, R.D., Jr., 2010, The Appalachian orogen: A brief summary, in Tollo, R.P., Bartholomew, M.J., Hibbard, J.P., and Karabinos, P.M., eds., From Rodinia to Pangea: The Lithotectonic Record of the Appalachian Region: Geological Society of America Memoir 206, p. 1–19, doi: 10.1130/2010.1206(01).

Hoagstrom, C.W., Ung, V., and Taylor, K., 2014, Miocene rivers and taxon cycles clarify the comparative biogeography of North American highland fishes: Journal of Biogeography, v. 41, p. 644–658.

Hoffman, P.F., 1988, United plates of America, the birth of a craton: Early Proterozoic assembly and growth of Laurentia: Annual Review of Earth and Planetary Sciences, v. 16, p. 543–603, doi:10.1146/annurev.ea.16.050188.002551.

Hoffman, P.F., 1989, Precambrian geology and tectonic history of North America, in Bally, A.W., and Palmer, A.R., eds., The Geology of North America—An Overview: Boulder, Colorado, Geological Society of America, The Geology of North America, v. A, p. 447–512.

Holbrook, J., and Wanas, H., 2014, A fulcrum approach to assessing source-to-sink mass balance using channel paleohydrologic parameters derivable from common fluvial data sets with an example from the Cretaceous of Egypt: Journal of Sedimentary Research, v. 84, p. 349–372.

Hovius, N., 1998, Controls on sediment supply by large rivers, in Shanley, K.W., McCabe, P.J. eds., Relative Role of Eustasy, Climate, and Tectonism in Continental Rocks: SEPM Special Publication, 59, p. 3–16.

Hovius, N., and Leeder, M., 1998, Clastic sediment supply to basins: Basin Research, v. 10, p. 1–5.

Howard, A.D., 1958, Drainage evolution in northeastern Montana and northwestern North Dakota: Geological Society of America Bulletin, v. 69, p. 575-588, doi:10.1130/0016-7606(1958)69 [575:DEINMA]2.0.CO;2.

Hubbard, S.M., Smith, D.G., Nielsen, H., Leckie, D.A., Fustic, M., Spencer, R.J., and Bloom, L., 2011, Seismic geomorphology and sedimentology of a tidally influenced river deposit, Lower Cretaceous Athabasca oil sands, Alberta, Canada: AAPG Bulletin, v. 65/7, p. 1123–1145.

Hudec, M.R., Norton, I.O., Jackson, M.P.A., and Peel, F.J., 2013, Jurassic evolution of the Gulf of Mexico salt basin: American Association of Petroleum Geologists Bulletin, v. 97, p. 1683–1710, doi:10.1306/04011312073.

Hutto, A.P., Yancey, T.E., and Miller, B.V., 2009, Provenance of Paleocene–Eocene Wilcox Group sediments in Texas: The evidence from detrital zircons: Gulf Coast Association of Geological Societies Transactions, v. 59, p. 357-362.

Iizuka, T., Campbell, I.H., Allen, C.M., Gill, J.B., Maruyama, S., Makoka, F., 2013, Evolution of the African continental crust as recorded by U–Pb, Lu–Hf and O isotopes in detrital zircons from modern rivers: Geochimica et Cosmochimica Acta, v.107, p.96–120.

Iizuka, T., Hirata, T., Komiya, T., Rino, S., Katayama, I., Motoki, A., and Maruyama, S., 2005, U-Pb and Lu-Hf isotope systematics of zircons from the Mississippi River sand: Implications for reworking and growth of continental crust: Geology, v. 33, p. 485-488, doi: 10.1130 /G21427.1.

Jackson, S.E., Pearson, N.J., Griffin, W.L., and Belousova, E.A., 2004, The application of laser ablation-inductively coupled plasma-mass spectrometry to in situ U–Pb zircon geochronology: Chemical Geology, v. 211, no. 1-2, p. 47–69.

Johnston J. E., Heinrich P. V., Lovelace J. K., McCulloh R. P., and Zimmerman R. K., 2000. Stratigraphic Charts of Louisiana: Louisiana Geological Survey Folio Series No. 8.

Karlstrom, K.E., Amato, J.M., Williams, M.L., Heizler, M.T., Shaw, C.A., Read, A.S., and Bauer, P., 2004, Proterozoic tectonic evolution of the New Mexico region: A synthesis, in Mack, G.H., and Giles, K.A., eds., The Geology of New Mexico; A Geologic History: New Mexico Geological Society Special Publication 11, p. 1-34.

Karlstrom, K.E., Dallmeyer, R.D., and Grambling, J.A., 1997, 40Ar/39Ar evidence for 1.4 Ga regional metamorphism in New Mexico: Implications for thermal evolution of lithosphere in the southwestern USA: The Journal of Geology, v. 105, p. 205-224, doi:10.1086/515912.

Kelley, S.A., and Chapin, C.E., 1995, Apatite fission-track thermochronology of southern Rocky Mountain–Rio Grande rift–western High Plains provinces, in Bauer, P.W., et al., eds., Geology of the Santa Fe region: New Mexico Geological Society Field Conference Guidebook 46, p. 87-96.

Kluth, C.F., 1986, Plate tectonics of the Ancestral Rocky Mountains, in Peterson, J.A., ed., Paleotectonics and sedimentation in the Rocky Mountain region, United States: American Association of Petroleum Geologists Memoir 41, p. 353–369.

Kluth, C.F., and Coney, P.J., 1981, Plate tectonics of the Ancestral Rocky Mountains: Geology, v. 9, p. 10–15.

Kolb, C.R., and Durham C.O., Jr., 1967, Lower Mississippi alluvial valley and terraces, in Geological Society of America annual meeting, Field Trip Guidebook Part A: New Orleans, Louisiana, 14 p.

Labrecque, P.A., Jensen, J.L., and Hubbard, S.M., 2011, Cyclicity in Lower Cretaceous point bar deposits with implications for reservoir characterization, Athabasca Oil Sands, Alberta, Canada: Sedimentary Geology, v. 242, p. 18–33.

Larsen, E.E., and Evanoff, E., 1998, Tephrostratigraphy and source of the tuffs of the White River sequence, in Terry, D.O., Jr., LaGarry, H.E., and Hunt, R.M., Jr., Depositional environments, lithostratigraphy, and biostratigraphy of the White River and Arikaree Groups (Late Eocene to Early Miocene, North America): Boulder, Colorado, Geological Society of America Special Paper 325, p. 1–14.Laskowski A. K., DeCelles, P.G., and Gehrels, G. E., 2013, Detrital zircon geochronology of Cordilleran retroarc foreland basin strata, western North America: Tectonics, v.32: p. 1027-1048.

Laskowski, A.K., DeCelles, P.G., and Gehrels, G.E., 2013, Detrital zircon geochronology of Cordilleran retroarc foreland basin strata, western North America: Tectonics, v. 32, p. 1027–1048, doi: 10 .1002 /tect .20065.

Lawton, T.F., 2008, Laramide sedimentary basins, in Hsü, K.J., ed., Sedimentary basins of the world, Volume 5, The sedimentary basins of the United States and Canada, Miall, A.D., ed.: The Netherlands, Elsevier, p. 429–450.

Lawton, T. F., 2014, Small grains, big rivers, continental concepts: Geology, v. 42, no. 7, p. 639–640, doi:10.1130/focus072014.1.

Lawton, T.F., Bradford, I.A., Vega, F.J., Gehrels, G.E., and Amato, J.M., 2009, Provenance of Upper Cretaceous–Paleogene sandstones in the foreland basin system of the Sierra Madre Oriental, northeastern Mexico, and its bearing on fluvial dispersal systems of the Mexican Laramide Province: Geological Society of America Bulletin, v. 121, p. 820–836, doi:10.1130/B26450.1.

Leeder, M.R., 1973, Fluviatile fining-upward cycles and the magnitude of paleochannels: Geological Magazine, v. 110, no. 3, p. 265–276.

Leier, A.L., and Gehrels, G.E., 2011, Continental–scale detrital zircon provenance signatures in Lower Cretaceous strata, western North America: Geology, v. 39, p. 399–402, doi:10.1130/G31762.1.

Leithold, E.L., Blair, N.E., and Wegmann, K.W., 2016, Source-to-Sink sedimentary systems and global carbon burial: A river runs through it: Earth–Science Reviews, v.153, p.30–42.

Leopold, L.B., and Maddock, T., 1953, The Hydraulic Geometry of Stream Channels and Some Physiographic Implications: USGS Professional Paper 252, 57 p.

Liu, L., 2014, Rejuvenation of Appalachian topography caused by subsidence–induced differential erosion: Nature Geoscience, v. 7, p. 518–523, doi:10.1038/ngeo2187.

Lorenz, J.C., Heinze, D.M., Clark, J.A., and Searls, C.A., 1985, Determination of widths of meander-belt sandstone reservoirs from vertical downhole data, Mesaverde Group, Piceance Creek Basin, Colorado: AAPG Bulletin, v. 69, no. 5, p. 710–721.

Loucks, R.G., Moore, B.T., and Zeng, H., 2011, On-shelf lower Miocene Oakville sediment dispersal patterns within a three-dimensional sequence-stratigraphic architectural framework and implications for deep-water reservoirs in the central coastal area of Texas: The American Association of Petroleum Geologists Bulletin, v. 95, no. 10, p. 1795-1817.

Mack, G.H., 2004, Middle and Late Cenozoic crustal extension, sedimentation, and volcanism in the southern Rio Grande Rift, Basin and Range, and southern transition zone of southwestern New Mexico, in Mack, G.H., and Giles, K.A., eds., The geology of New Mexico: A geologic history: New Mexico Geologic Society Special Publication 11, p. 389–406.

Mackey, G.N., Horton, B.K., and Milliken, K.L., 2012, Provenance of the Paleocene–Eocene Wilcox Group, western Gulf of Mexico basin: Evidence for integrated drainage of the southern Laramide Rocky Mountains and Cordilleran arc: Geological Society of America Bulletin, v. 124, p. 1007–1024, doi: 10.1130 /B30458.1.

Manning, E., 1990, The early Miocene Sabine River: Gulf Coast Association of Geological Societies Transactions, v. 40, p. 531–549.

Matthai, H. F., 1990, Floods, in Woolman, M.G., and Riggs, H.C., eds., The Geology of North America: Vol. O-1, Surface Water Hydrology: The Geological Society of America, Boulder, Colorado, p. 97–120.

McBride, E.F., Land, L.S., Diggs, T.N., and Mack, L.E., 1988, Petrography, stable isotope geochemistry and diagenesis of Miocene sandstones, Vermillion block 31, offshore Louisiana: Gulf Coast Association of Geological Societies Transactions, v. 38, p. 513-523.

McKeon, R.E., Zeitler, P.K., Pazzaglia, F.J., Idleman, B.D., and Enkelmann, E., 2014, Decay of an old orogen: Inferences about Appalachian landscape evolution from low temperature thermochronology: Geological Society of America Bulletin, v. 126, p. 31–46, doi:10.1130/B30808.1.

Metcalf, C., 2004, Regional Channel Characteristics for Maintaining Natural Fluvial Geomorphology in Florida Streams: U.S. Fish and Wildlife Service, Panama City Fisheries Resource Office.

Miall, A.D., 2006, How do we identify big rivers? And how big is big? : Sedimentary Geology, v. 186, p. 39–50.

Miall, A.D., 2010, Alluvial deposits, in James, N.P., and Dalrymple, R.W., eds., Facies Models 4, Geological Association of Canada, St. John's, Newfoundland, Geo text 6, p. 105–137.

Miall, A. D., 2014, Large rivers and their depositional systems, in Miall, A.D., ed., Fluvial Depositional Systems: Springer, p. 273–294.

Miller, S.R., Sak, P.B., Kirby, E., and Bierman, P.R., 2013, Neogene rejuvenation of central Appalachian topography: Evidence for differential rock uplift from stream profiles and erosion rates: Earth and Planetary Science Letters, v. 369-370, p. 1-12, doi: 10.1016 /j.epsl .2013.04.007.

Milliken, K.L., 1988, Loss of provenance information through subsurface diagenesis in Plio-Pleistocene sandstones, northern Gulf of Mexico: Journal of Sedimentary Petrology, v. 58, p. 992–1002, doi: 10.1306 /212F8EE0 -2B24 -11D7-8648000102C1865D.

Milliken, K.L., 2007, Provenance and diagenesis of heavy minerals, Cenozoic units of the northwestern Gulf of Mexico sedimentary basin, in Mange, M.A., and Wright,

D.T., eds., Heavy minerals in use: Developments in Sedimentology Volume 58: Amsterdam, Elsevier, p. 247-261, doi.10.1016/S0070-4571(07)58008-8.

Milliman, J.D., and Syvitski, J.P.M., 1992, Geomorphic tectonic control of sediment discharge to the ocean: the importance of small mountainous rivers: The Journal of Geology, v. 100, p. 525–544.

Moecher, D.P., and Samson, S.D., 2006, Differential zircon fertility of source terranes and natural bias in the detrital zircon record: Implications for sedimentary provenance analysis: Earth and Planetary Science Letters, v. 247, p. 252–266, doi:10.1016/j.epsl.2006.04.035.

Moody, T., Wirtanen, M., and Yard, S.N., 2003, Regional Relationships for Bankfull Stage in Natural Channels of the Arid Southwest: Flagstaff, AZ, U.S.A., Natural Channel Design Inc.

Mosher, S., 1998, Tectonic evolution of the southern Laurentian Grenville orogenic belt: Geological Society of America Bulletin, v. 110, p. 1357–1375, doi:10.1130/0016–7606(1998)110<1357:TEOTSL> 2.3.CO;2.

Mulder, T., and Syvitski, J.P.M., 1995, Turbidity currents generated at river mouths during exceptional discharges to the world oceans: Journal of Geology, v. 103, p. 285–299.

Nicholas, A.P., Smith, G.H.S., Amsler, M.L., Ashworth, P.J., Best, J.L., Hardy, R.J., Lane, S.N., Orfeo, O., Parsons, D.R., Reesink, A.J.H., Sandbach, S.D., Simpson, C.J., and Szupiany, R.N., 2016, The role of discharge variability in determining alluvial stratigraphy: Geology: v. 44, p. 3–6, doi: 10.1130/G37215.1.

Olariu, C., and Bhattacharya, J.P., 2006, Terminal distributary channels and delta front architecture of river-dominated delta systems: Journal of Sedimentary Research, v. 76, p. 212–233.

Painter, C.S., Carrapa, B., DeCelles, P.G., Gehrels, G.E., and Thomson, S.N., 2014, Exhumation of the North American Cordillera revealed by multi–dating of Upper Jurassic–Upper Cretaceous foreland basin deposits: GSA Bulletin, v.126, no.11/12, p. 1439–1464.

Park, H., Barbeau, D.L., Jr., Rickenbaker, A., Bachmann–Krug, D., and Gehrels, G., 2010, Application of foreland basin detrital–zircon geochronology to the reconstruction of the Southern and Central Appalachian orogen: Journal of Geology, v. 118, no. 1, p. 23–44, doi: 10.1086/648400.

Patchett, P.J., Ross, G.M., and Gleason, J.D., 1999, Continental drainage in North America during the Phanerozoic from Nd isotopes: Science, v. 283, p. 671–673.

Paterson, S.R., Okaya, D., Memeti, V., Economos, R., and Miller, R.B., 2011, Magma addition and flux calculations of incrementally constructed magma chambers in

continental margin arcs: Combined field, geochronologic, and thermal modeling studies: Geosphere, v. 7, p. 1439–1468, doi:10.1130/GES00696.1.

Pazzaglia, F.J., and Kelley, S.A., 1998, Large-scale geomorphology and fission-track thermochronology in topographic and exhumation reconstructions of the Southern Rocky Mountains: Rocky Mountain Geology, v. 33, p. 229-257.

Pindell, J.L., 1985, Alleghenian reconstruction and subsequent evolution of the Gulf of Mexico, Bahamas, and proto–Caribbean: Tectonics, v. 4, p. 1–39.

Poag, C.W., and Sevon, W.D., 1989, A record of Appalachian denudation in post–rift Mesozoic and Cenozoic sedimentary deposits of the U.S. middle Atlantic continental margin: Geomorphology, v. 2, p. 119–157, doi:10.1016/0169–555X(89)90009–3.

Pullen, A., Ibanez-Mejia, M., Gehrels, G.E., Ibanez-Mejia, J.C., and Pecha, M., 2014, What happens when n=1000? Creating large-n geochronological datasets with LA-ICP-MS for geologic investigations: Journal of Analytical Atomic Spectrometry, v. 29, p. 971–980, doi:10.1039 /c4ja00024b.

Rahl, J.M., Reiners, P.W., Campbell, I.H., Nicolescu, S., and Allen, C.M., 2003, Combined single–grain (U–Th)/He and U/Pb dating of detrital zircons from the Navajo Sandstone, Utah: Geology, v. 31, p. 761–764, doi: 10.1130/G19653.1.

Rainbird, R.H., Heaman, L.M., and Young, G., 1992, Sampling Laurentia: Detrital zircon geochronology offers evidence for an extensive Neoproterozoic river system originating from the Grenville orogen: Geology, v. 20, p. 351–354.

Reiners, P.W., Campbell, I.H., Nicolescu, S., Allen, C.M., Hourigan, J.K., Garver, J.I., Mattinson, J.M., and Cowan, D.S., 2005, (U–Th)/(He–Pb) double dating of detrital zircons: American Journal of Science, v. 305, no. 4, p. 259–311,

Riggs, N.R., Lehman, T.M., Gehrels, G.E., and Dickinson, W.R., 1996. Detrital zircon link between headwaters and terminus of the Upper Triassic Chinle – Dockum paleoriver system: Science, v. 273, p. 97-100.

Rino, S., Kon, Y., Sato, W., Maruyama, S., Santosh, M., and Zhao, D., 2008, The Grenvillian and Pan–African orogens: world's largest orogenies through geologic time, and their implications on the origin of superplume: Gondwana Research, v.14, p.51–72.

Rivers, T., 2008, Assembly and preservation of lower, mid, and upper orogenic crust in the Grenville Province—Implications for the evolution of large hot long-duration orogens: Precambrian Research, v.167, p. 237-259, doi:10.1016/j.precamres.2008.08.005.

Rivers, T., Ketchum, J., Indares, A., and Hynes, A., 2002. The High Pressure belt in the Grenville Province: architecture, timing and exhumation: Canadian Journal of Earth Sciences, v.39, no. 5, p. 867-893, doi: 10.1139/E02-025.

Romans, B.W., and Graham, S.A., 2013, A deep-time perspective of land-ocean linkages in the sedimentary record: Annual review of marine science, v.5, p.69-94.

Romans, B.W., Castelltort, S., Covault, J.A., Fildani, A., and Walsh, J.P., 2016, Environmental signal propagation in sedimentary systems across timescales: Earth-Science Reviews, v.153, p.7-29.

Roy, M., Kelley, S., Pazzaglia, F.J., Cather, S., and House, M.A., 2004, Middle Tertiary buoyancy modification and its relationship to rock exhumation, cooling, and subsequent extension at the eastern margin of the Colorado Plateau: Geology, v. 32, p. 925-928, doi:10.1130/G20561.1.

Sadler, P.M., and Jerolmack, D.J., 2015, Scaling laws for aggradation, denudation and progradation rates: the case for time-scale invariance at sediment sources and sinks: Geological Society of London Special Paper, v. 404, p. 69–88.

Saucier, R.T., 1994, Geomorphology and Quaternary Geologic History of the Lower Mississippi Valley: Mississippi River Commission, Vicksburg, 205 p.

Saylor, J.E., Stockli, D.F., Horton, B.K., Nie, J., and Mora, A., 2012, Discriminating rapid exhumation from syndepositional volcanism using detrital zircon double dating: Implications for the tectonic history of the Eastern Cordillera, Colombia: Geological Society of America Bulletin, v. 154, no. 5/6, p.762–779, doi:10.1130/B30534.1.

Scott, G.R., 1975, Cenozoic surfaces and deposits in the southern Rocky Mountains, in Curtis, F.B., ed., Cenozoic history of the southern Rocky Mountains: Boulder, Colorado, Geological Society of America Memoir 144, p. 227–248.

Scott, T.M., Campbell, K.M., Rupert, F.R., Arthur, J.D., Missimer, T.M., Lloyd, J.M., Yon, J.W., and Duncan, J.G. 2001, Geologic Map of the State of Florida: Florida Geological Survey.

Sears, J.W., 2013, Late Oligocene–early Miocene Grand Canyon: A Canadian connection? : GSA Today, v. 23, no. 11, p. 4–10, doi:10.1130/GSATG178A.1.

Singleton, S.W., 2008, Petrified Wood in the Miocene Fleming Formation, Jasper County, Texas: Gulf Coast Association of Geological Societies Transactions, v. 58, p. 797-814.

Smith, D.G., Hubbard, S., Leckie, D., and Fustic, M., 2009, Counter point bars in modern meandering rivers: recognition of morphology, lithofacies and reservoir significance, examples from Peace River, AB, Canada: Sedimentology, v. 56, p. 1655–1669.

Smith, D.G., Hubbard, S.M., Lavigne, J.R., Leckie, D.A., and Fustic, M., 2011, Stratigraphy of counter-point bar and eddy-accretion deposits in low energy meander belts of the Peace–Athabasca delta, northeast Alberta, Canada, in Davidson, S.K., Leleu, S., and North, C.P., eds., From River to Rock Record: The

Preservation of Fluvial Sediments and Their Subsequent Interpretation: SEPM Special Publication 97, p. 143–152.

Snedden, J.W., 1984, Validity of the Use of the Spontaneous Potential Curve Shape in the Interpretation of Sandstone Depositional Environments, Gulf Coast Association of Geological Societies Transactions, v. 34, p. 255-263.

Snedden, J.W., Galloway, W.E., Whiteaker, T.L., and Ganey-Curry, P.E., 2012, Eastward shift of deepwater fan axes during the Miocene in the Gulf of Mexico: Possible causes and models: Gulf Coast Association of Geological Societies Journal, v. 1, p. 131–144.

Snedden, J.W., Virdell, J, Whiteaker, T.L., and Ganey–Curry, P., 2016, A basin–scale perspective on Cenomanian–Turonian (Cretaceous) depositional systems, greater Gulf of Mexico (USA): Interpretation, v. 4, no. 1, p. 1–22.

Sømme, T.O., Helland-Hansen, W., Martinsen, O.J., and Thurmond, J.B., 2009a, Relationships between morphological and sedimentological parameters in source-to-sink systems: a basis for predicting semi-quantitative characteristics in subsurface systems: Basin Research, v. 21, p. 361–387.

Sømme, T.O., Martinsen, O.J., and Thurmond, J.B., 2009b, Reconstructing morphological and depositional characteristics in subsurface sedimentary systems: an example from the Maastrichtian-Danian Ormen Lange system, Møre Basin, Norwegian Sea: AAPG Bulletin, v. 93, p. 1347–1377.

Sømme, T.O., Martinsen, O.J., and Lunt, I., 2013, Linking offshore stratigraphy to onshore paleotopography: the Late Jurassic–Paleocene evolution of the south Norwegian margin: Geological Society of America, Bulletin, v. 125, p. 1164–1186.

Spencer, J.E., Smith, G.R., and Dowling, T.E., 2008, Middle to late Cenozoic geology, hydrography, and fish evolution in the American Southwest, in Reheis, M.C., et al., eds., Late Cenozoic drainage history of the southwestern Great Basin and lower Colorado River region: Geologic and biotic perspectives: Geological Society of America Special Paper 439, p. 279-299, doi:10.1130/2008.2439(12).

Spradlin, S.D., 1980, Miocene fluvial systems: southeast Texas [M.S. Thesis]: Austin, Texas, University of Texas at Austin, 139 p.

Stern, R.J., and Dickinson, W.R., 2010, The Gulf of Mexico is a Jurassic backarc basin: Geosphere, v. 6, p. 739–754, doi: 10.1130/GES00585.1.

Stewart, J.H., 1998, Regional characteristics, tilt domains, and extensional history of the later Cenozoic Basin and Range province, western North America, in Faulds, J.E., and Stewart, J.H., eds., Accommodation zones and transfer zones: The regional segmentation of the Basin and Range province: Geological Society of America Special Paper 323, p. 47–74.

Stockli, D.F., and Stockli, L.D., 2013, Unlocking provenance secrets from single detrital zircons by U-Pb and trace-element depth-profile laser-ablation-split-stream ICP-MS analysis and (U-Th)/He double dating: Geological Society of America Abstracts with Programs. Vol. 45, No. 7, p.744. Thomas, W.A., Becker, T.P., Samson, S.D., and Hamilton, M.A., 2004, Detrital zircon evidence of a recycled orogenic foreland provenance for Alleghanian clastic-wedge sediments: The Journal of Geology, v.112, p. 23-37.

Strauss, D., and Sadler, P.M., 1989, Stochastic models for the completeness of stratigraphic sections: Journal of the International Association for Mathematical Geology, v. 21, p. 37–59.

Syvitski, J.P.M., and Milliman, J.D., 2007, Geology, geography, and humans battle for dominance over the delivery of fluvial sediment to the coastal ocean: Journal of Geology, v. 115, p. 1–19.

Thomas, W.A., 2011, Detrital–zircon geochronology and sedimentary provenance: Lithosphere, v. 3, p. 304–308, doi:10.1130/RF.L001.1.

Thomas, W.A., Becker, T.P., Samson, S.D., and Hamilton, M.A., 2004, Detrital zircon evidence of a recycled orogenic foreland provenance for Alleghanian clastic–wedge sandstones: Journal of Geology, v. 112, p. 23–37.

Torres, R., Ruiz, J., Patchett, P. J., and Grajales, J. M., 1999, Permo-Triassic continental arc in eastern Mexico: Tectonic implications for reconstructions of southern North America, in Bartolini, C., Wilson, J. L., and Lawton, T. F., eds., Mesozoic Sedimentary and Tectonic History of North-Central Mexico: Boulder, Colorado, Geological Society of America Special Paper 340.

Tweto, O., 1975, Laramide (late Cretaceous–early Tertiary) orogeny in the southern Rocky Mountains, in Curtis, F.B., ed., Cenozoic history of the southern Rocky Mountains: Boulder, Colorado, Geological Society of America Memoir 144, p. 1–44.

Tweto, O., 1980, Summary of Laramide orogeny, in Kent, H.C., and Porter, K.W., eds., Colorado geology: Denver, Colorado, Rocky Mountain Association of Geologists, Symposium on Colorado Geology, p. 129–134.

Tweto, O., and Sims, P.K., 1963, Precambrian ancestry of the Colorado mineral belt: Geological Society of America Bulletin, v. 74, p. 991-1014.

Tye, R.S., 1991, Fluvial-sandstone reservoirs of the Travis Peak Formation, East Texas basin, in Miall, A.D., and Tyler, Noel, eds., The three-dimensional facies architecture of terrigenous clastic sediments and its implications for hydrocarbon discovery and recovery: SEPM Concepts in Sedimentology and Paleontology, v. 3, p. 172–188.

Van Avendonk, H.J.A., Christeson, G.L., Norton, I.O., and Eddy, D.R., 2015, Continental rifting and sediment infill in the northwestern Gulf of Mexico: Geology, v. 43, no. 7, p. 631-634, doi:10.1130/G36798.1

Van Schmus, W.R., Bickford, M.E., and Turek, A., 1996. Proterozoic geology of the east–central midcontinent basement, in van der Pluijm, B.A., and Catacosinos, P. (Eds.), Basement and Basins of Eastern North America: Geological Society of America Special Paper 308, p. 7–32.

Vermeesch, P., 2004, How many grains are needed for a provenance study?: Earth and Planetary Science Letters, v. 224, p. 441–451, doi: 10.1016/j.epsl.2004.05.037.

Vermeesch, P., 2012, On the visualization of detrital age distributions: Chemical Geology, v. 312–313, p. 190–194, doi:10.1016/j.chemgeo.2012.04.021.

Vermeesch, P., 2013, Multi-sample comparison of detrital age distributions: Chemical Geology, v. 341, p. 140–146, doi:10.1016/j.chemgeo.2013.01.010.

Walsh, J.P., Wiberg, P.L., Aalto, R., Nittrouer, C.A., and Kuehl, S.A., 2016, Source-to-Sink research: economy of the Earth's surface and its strata: Earth Science Reviews, v.153, p. 1–6.

Weeks, J.B., and Gutentag, E.D., 1981, Bedrock geology, altitude at base, and 1980 saturated thickness of the High Plains aquifer in parts of Colorado, Kansas, Nebraska, New Mexico, Oklahoma, South Dakota, Texas, and Wyoming: U.S. Geological Survey Hydrologic Investigations Atlas HA-648, 2 sheets, scale 1:250,000.

Weislogel, A.L., Hunt, B., Lisi, A., Lovell, T., and Robinson, D.M., 2015, Detrital zircon provenance of the eastern Gulf of Mexico subsurface: Constraints on Late Jurassic paleogeography and sediment dispersal of North America, in Anderson, T.H., Didenko, A.N., Johnson, C.L., Khanchuk, A.I., and MacDonald, J.H., Jr., eds., Late Jurassic Margin of Laurasia—A Record of Faulting Accommodating Plate Rotation: Geological Society of America Special Paper 513, doi:10.1130/2015.2513(02).

Wetzel, A., 1993, The transfer of river load to deep-sea fans: a quantitative approach: AAPG Bulletin, v. 77, p. 1679–1692.

Whitmeyer, S.J., and Karlstrom, K.E., 2007, Tectonic model for the Proterozoic growth of North America: Geosphere, v. 3, p. 220–259, doi: 10.1130 /GES00055.1.

Willis, B.J., 1989, Paleochannel reconstructions from point bar deposits: a three-dimensional perspective: Sedimentology, v. 36, no. 5, p. 757–766.

Willis, B.J., and Tang, H., 2010, Three-dimensional connectivity of point-bar deposits: Journal of Sedimentary Research, v. 80, p. 440–454.

Winker, C.D., 1982, Cenozoic shelf margins, northwestern Gulf of Mexico: Gulf Coast Association of Geological Societies Transactions, v. 32, p. 427–448.

Wolfe, M., and Stockli, D.F., 2010, Zircon (U–Th)/ He thermochronometry in the KTB drill hole, Germany, and its implications for bulk He diffusion kinetics in zircon:

Earth and Planetary Science Letters, v. 295, p. 69–82, doi:10.1016/j .epsl.2010.03.025.

Wolman, M.G., and Leopold, L.B., 1957, River Floodplains: Some Observations on their Formation: U.S. Geological Survey, USGS Professional Paper 282-C, Washington, DC.

Wolman, M.G., and Miller, J.P., 1960, Magnitude and frequency of forces in geomorphic processes: Journal of Geology, v. 68, p. 54-74.

Xu, J., Snedden J.W., Stockli, D.F., Fulthorpe, C.S., Galloway, W.E., 2016, Early Miocene continental–scale sediment supply to the Gulf of Mexico Basin based on detrital zircon analysis: Geological Society of America Bulletin.

Young, S.C., Budge, T., Knox, P.R., Kalbouss, R., Baker, E.T., Jr., Hamlin, H.S., Galloway, W.E., and Deeds, N., 2010, Hydrostratigraphy of the Gulf Coast Aquifer from the Brazos River to the Rio Grande: Final report prepared for Texas Water Development Board, Austin, TX, 231 p.

Young, S.C., Ewing, T., Hamlin, S., Baker, E., and Lupton, D., 2012, Final report updating the hydrogeologic framework for the northern portion of the Gulf Coast aquifer: Texas Water Development Board, Austin, TX: 285 p.

Zeng, H., and Hentz, T.F., 2004, High-frequency sequence stratigraphy from seismic sedimentology: Applied to Miocene, Vermilion Block 50, Tiger Shoal area, offshore Louisiana: The American Association of Petroleum Geologists Bulletin, v. 88, no. 2, p. 153-174, doi:10.1306/10060303018.

Vita

Jie Xu was born in Wenling, Zhejiang province, China. He received his Bachelor degree in Petroleum Engineering and Master degree in Geology from the China University of Geosciences (Beijing) in June 2007 and 2010, respectively. He joined the Graduate School at the University of Texas at Austin in August 2012. During his study in the University of Texas at Austin, he met his wife, Ruohan Gao and got married in December 2015.

His research interests focus on sedimentary geology, sequence stratigraphy, geochronology and basin analysis.

Permanent email: jiexu@utexas.edu

This dissertation was typed by Jie Xu.